

Archive ouverte UNIGE

https://archive-ouverte.unige.ch

	Thèse	2021
These 2021	Thàsa	2024
	rnese	2021

Open Access

This version of the publication is provided by the author(s) and made available in accordance with the copyright holder(s).

Total synthesis of furanoheliangolides, hunting druggability of the nuclear transport protein importin-5

Patouret, Rémi

How to cite

PATOURET, Rémi. Total synthesis of furanoheliangolides, hunting druggability of the nuclear transport protein importin-5. Doctoral Thesis, 2021. doi: 10.13097/archive-ouverte/unige:156506

This publication URL: https://archive-ouverte.unige.ch/unige:156506

Publication DOI: 10.13097/archive-ouverte/unige:156506

© This document is protected by copyright. Please refer to copyright holder(s) for terms of use.

Section de chimie et biochimie Département de chimie organique Professeur N. Winssinger

TOTAL SYNTHESIS OF FURANOHELIANGOLIDES, HUNTING DRUGGABILITY OF THE NUCLEAR TRANSPORT PROTEIN IMPORTIN-5

THÈSE

présentée à la Faculté des sciences de l'Université de Genève pour obtenir le grade de Docteur ès sciences, mention chimie

par

Rémi PATOURET

de

Etrée (France)

Thèse N° 5611

GENÈVE

Nom de l'atelier d'impression

2021



DOCTORAT ÈS SCIENCES, MENTION CHIMIE

Thèse de Monsieur Rémi PATOURET

intitulée :

«Total Synthesis of Furanoheliangolides, Hunting Druggability of the Nuclear Transport Protein Importin-5»

La Faculté des sciences, sur le préavis de Monsieur N. WINSSINGER, professeur ordinaire et directeur de thèse (Département de chimie organique), Madame S. HOOGENDOORN, professeure assistante (Département de chimie organique), Monsieur K. GADEMANN, professeur (Department of Chemistry, University of Zurich, Zurich), autorise l'impression de la présente thèse, sans exprimer d'opinion sur les propositions qui y sont énoncées.

Genève, le 9 novembre 2021

Thèse - 5611 -

Le Doyen

PhD Director:

Professor Nicolas Winssinger

University of Geneva

Department of Organic Chemistry

Quai Ernest-Ansermet 30

CH-1211 Geneva 4 Switzerland

Internal jury member:

Professor Sascha Hoogendoorn

University of Geneva

Department of Organic Chemistry

Quai Ernest-Ansermet 30

CH-1211 Geneva 4 Switzerland

External jury member:

Professor Karl Gademann

University of Zurich

Department of Chemistry

Wintherthurerstrasse 190

CH-8057 Zurich Switzerland

Résumé

Cette thèse est composée d'une première partie sur la synthèse, l'identification de cibles et l'activité biologique du produit naturel goyazensolide. La seconde partie évalue les protéines ciblées par le produit naturel withaferin A et contribuant à un effet antiviral sur H5N1.

La première partie commence par la synthèse totale de la sesquiterpène lactone goyazensolide via le premier exemple d'une allylation de Barbier faisant émerger la formation d'une α -méthylène- γ -butyrolactone et la formation du macrocycle germacrène de manière concomitante. La synthèse d'un analogue, 5-epiisogoyazensolide, a ensuite été achevé afin de valider la stratégie. L'obtention d'une sonde avec un groupement alcyne greffé sur la structure permettra par la suite l'identification d'une protéine nommée importin-5 (IPO5) en tant que cible covalente. Cette protéine ayant des propriétés intéressantes dans le domaine du cancer, il a été démontré que l'incubation de goyazensolide in-cellulo inhibe la translocation du cargo RASAL2 dans le noyau et ainsi, décroît drastiquement la phosphorylation de AKT, marqueur de la prolifération cellulaire. De plus, le traitement de goyazensolide sur un lysate montre la perturbation du binding entre IPO5 et deux « nuclear localization sequence » NLS provenant de protéines virales appartenant à influenza A et au VIH. Ces expériences démontrent la découverte du premier inhibiteur d'IPO5. Une étude de relation structure activité a ensuite montré que seuls goyazensolide et atripliciolide, contrairement aux analogues de la famille des furanohéliangolides, possèdent la capacité à binder IPO5.

La seconde partie concerne une étude sur l'activité anti-influenza de la lactone stéroïdale withaferin A. De manière surprenante, withaferin A interagit également de manière covalente avec importin-5 malgré sa différence structurale significative et aucune référence ne mentionnant cette interaction malgré plus de deux décennies d'investigations sur cette molécule. Une diminution significative de la réplication d'influenza A a été démontré lorsque les cellules sont traitées avec withaferin A ainsi que les sondes WAPs alors qu'un effet modéré est observé avec goyazensolide. Les premières conclusions ont finalement exclu IPO5 en tant que cible unique dans l'activité anti-influenza A de withaferin A. Une recherche bibliographique a montré que withaferin A ciblait plusieurs protéines impliquées dans la réplication d'influenza A. Ces

composés sont ainsi appelés « multi-target ». Withaferin A cible, entre autres, la protéine Keap1, induisant l'expression de Heme Oxygenase 1 (HO-1) puis l'induction des interferons-stimulated genes (ISGs) qui ont un effet significatif sur l'inhibition de la réplication virale. Cette hypothèse a été testé avec succès en utilisant un inhibiteur de Keap1: bardoxolone methyl. Cependant, la multitude de cascades biologiques durant le cycle de vie d'influenza A combinée à l'utilisation de composés multi-target complexifie drastiquement la détermination du mécanisme d'action globale inhibant la réplication virale. Malgré le très grand potentiel anti-influenza A de withaferin A en ciblant *a minima* huit protéines impliquées dans la réplication virale, la rationalisation globale de son mécanisme d'action demeure un énorme défi.

Summary

This thesis is composed of two parts: the first is about goyazensolide and second part about Withaferin A.

The first part started with the total synthesis of the sesquiterpene lactone goyazensolide via the first example of a Barbier allylation / lactonization merging an α -methylene- γ -butyrolactone with the closure of a 10-membered germacrene in one step. An analog, 5-epi-isogoyazensolide, was also synthesized to validate the strategy. Synthesis of a goyazensolide probe with an alkyne tag allowed the identification of importin-5 (IPO5) as a covalent target of goyazensolide. As this protein has interesting anti-cancer activities, we have demonstrated that goyazensolide inhibits *in cellulo* the translocation of RASAL2, a negative regulator of RasGAP, causing a drastic decrease in the level of p-AKT, a marker of cell proliferation. Moreover, incubation of goyazensolide with a cell lysate indicated a perturbation in the pull-down of IPO5 with two nuclear localization sequence (NLS) of viral proteins belong to influenza and HIV. A structure activity relationship study of related furanoheliangolides demonstrated that only goyazensolide and atripliciolide were able to bind IPO5.

The second part was focused on the study of the anti-influenza A activity by withaferin A. Surprisingly, withaferin A also binds IPO5 while its structure is significantly different to goyazensolide. A drastic reduction in the rate of influenza replication was observed when cells were treated with withaferin A and the probes WAPs, while a moderate effect was observed in the presence of goyazensolide. Literature reported that withaferin A targets several proteins related to influenza A. This compound can be also called "multi-target compound". Keap1 is one of the targets of withaferin A and its inhibition induced heme oxygenase 1 (HO-1) expression, promoting the interferonstimulated genes (ISGs) induction which inhibits the influenza A replication. While the prediction of the anti-IAV activity from the Keap1 inhibitor bardoxolone methyl was successful, the myriad of biological pathways during the influenza A life cycle combined to the use of non-selective compounds drastically increase the difficulty to determine the whole mode of action. Natural products as goyazensolide and withaferin A are typically multi-target compounds and, despite their tremendous therapeutic potential, their rational development still represent a formidable challenge.

Table of Contents

CHAPTE	R 1. Introduction & Literature	10
I. Na	tural products as an important source of drugs	10
II. E	Electrophilic molecules "Michael acceptors" type	11
II.1.	"Michael acceptor": definition	12
II.2.	Chemical reactivity	14
II.3.	Biological reactivity	16
II.4.	"Michael acceptors" biological targets	17
II.5.	Partial conclusion	21
III. T	The sesquiterpene lactone family	22
III.1.	Structure	22
III.2.	Historical milestones	25
III.3.	Biogenesis	27
III.4.	Biological and therapeutic properties of the sesquiterpene lactones.	29
III.5.	Partial conclusion	31
IV. T	The natural product goyazensolide	32
IV.1.	Structure	32
IV.2.	Biological properties	34
CHAPTE	R 2. Total synthesis	36
I. Tot	tal synthesis of goyazensolide: strategy 1	36
I.1.	Ring closing metathesis strategy	36
I.2.	The tetrahydrofuranol scaffold	39
I.3.	Partial conclusion	41
II. T	Total synthesis of goyazensolide: strategy 2	41
II.1.	$\textit{Trans}\text{-disubstituted }\alpha\text{-exo-methylene-}\gamma\text{-butyrolactone synthesis}$	41
II.2.	Racemic route validation	43
II.3.	Acetate protecting group	45

II.4.	Stereoselective route of the alkyne moiety	47
II.5.	En route to goyazensolide	48
II.6.	Partial conclusion	49
III. Sy	nthesis of 5-epi-isogoyazensolide	49
III.1.	Retrosynthetic route	49
III.2.	Synthesis of the chiral lactone 67	50
III.3.	Access to 5- <i>epi</i> -isogoyazensolide	51
IV. Co	onclusion	51
CHAPTER	3. Target identification	53
I. Natu	ıral products alkyne tagged as probes for target identification	53
I.1.	Proteome labeling	53
I.2 .	Probe design	54
II. Pr	otein of interest determination	60
II.1.	Target enrichment	60
II.2.	Pull-down experiment with desthiobiotin	60
II.3.	Pull-down experiment with DTB-Cy3	61
II.4.	InGel digestion	63
II.5.	MS/MS analysis	63
II.6.	Target confirmation by antibody	64
II.7.	Selectivity versus other importins	65
III. Co	onclusion	65
CHAPTER	4. Biological activity	66
I. The	nuclear transport protein Importin-5	66
I.1.	Presentation	66
I.2 .	RASAL-2 translocation	67
I.3 .	Impact of goyazensolide on RASAL-2 translocation	67
I.4.	Downstream effect of RASAL-2 translocation inhibition	68

I. 5 .	Pulldown of IPO5 by the NLSs immobilized on beads	69
II. C	Conclusion	70
CHAPTE	R 5. Binding mode	71
I. Bin	ding mode	71
I.1.	Synthesis/Competition with truncated Michael acceptors analogs	71
1.2.	Competition with other natural products	72
I.3.	Synthesis and comparison of various natural products probes	74
1.4.	Competition of analogs versus GOYA-2	74
I. 5 .	Comparison between goyazensolide, atripliciolide and deoxygoyazenso	olide
I.6.	Cysteine determination	83
II. C	Conclusion	83
CHAPTE	R 6. Anti-influenza A activity of withaferin A	87
I. Intr	oduction	87
II. V	Vithaferin A targets IPO5 and possesses anti-influenza activity	88
II.1. targe	Dose dependent competition and pull-down experiment with GOYA-	
II.2.	Probe synthesis and pull-down experiments	89
II.3.	Cell viability assay	90
II.4.	Plaque assay	91
II.5.	Partial conclusion	92
III. V	Vithaferin A targets multiple proteins related to influenza A	93
III.1.	Literature search	93
III.2.	Target identification by gel-based assay and chemical proteomics	94
III.3.	Plaque assay using the selective vimentin inhibitor FiVe1	97
III.4.	Withaferin A, WAPs and BXM induce HO-1 in A549 cells	98
III.5.	Plaque assay using the Keap1 inhibitor Bardoxolone methyl (BXM)	102

III.6.	Labeling competitions experiments on Keap1Error! Bookn	nark	not
defir			
	Conclusion		
General (conclusion	•••••	. 107
Referenc	es		. 109
Experime	ental section		. 126
I. Su	oplementary synthetic routes and strategies		. 126
I.1.	Synthesis of intermediate 3		. 126
I.2.	Synthesis of the dinitrophenyl derivate		. 126
I.3.	Coupling between 30 and 8		. 127
1.4.	Synthesis of the alkyne intermediate <i>via</i> a Wittig / Wittig-Horn 128	ner stra	ategy
I.5.	Synthesis of goyazensolide diastereoisomer		. 129
I.6.	Synthesis of the « primary cyclized scaffold »		. 130
I.7.	Synthesis of FiVe1		130
II. S	Supplementary proteomic experiments		. 131
II.1.	Click reaction in blank conditions.		. 131
II.2.	Investigations of the band at 38 kDa in A549 cells		. 132
III. E	xperimental procedures		. 134
III.1.	General information for the chemistry part		. 134
III.2.	Protocols		. 135
III.3.	Computational study (Performed by Dr. Romain Pertschi)		. 196
III.4.	General information for proteomic/biological part		. 197
III.5.	Experimental procedures for confocal microscopy		. 199
III.6.	Experimental procedures for pAKT assay and NLS pull-down.		. 205
III.7.	Preparation of NLS-1 and NLS-2		. 207
III.8.	Quantification of fluorescent bands		210

		Reaction between goyazensolide / atripliciolide / 15-deoxygoyazenso	
W	ith git	utathione	212
III	l.10.	Synthesis of desthiobiotinylated lodoacetamide	213
III	l.11.	Cell viability / cytotoxicity assays	215
III	l.12.	Procedure viral nucleoprotein quantification	216
Ш	l.13.	Procedure plaque assay	217
IV.	NM	IR spectrum	222

CHAPTER 1. Introduction & Literature

I. Natural products as an important source of drugs

It is likely that humans have used plants as medicine for as long as we have existed. The earliest historical records of herbs are found from the Sumerian civilization, where medications with plants are listed on clay tablets (Figure 1). Humans have experimented with plants to learn how they can help us cure diseases or pain. In other words, humans have been involved for dozen of centuries in a huge clinical trial with medicinal plants. Early therapeutics have combined these ingredients with mysticism, astrology or religion, and the treatments that were effective were recorded and documented leading to the early herbal remedies. As chemical techniques improved, the active constituents were

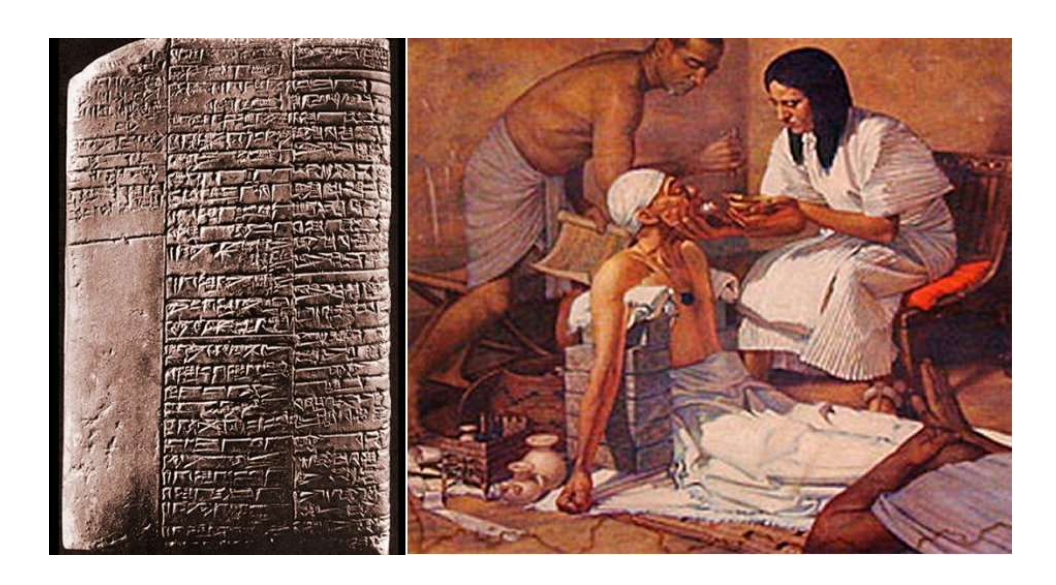


Figure 1: (Left) Sumerian medical clay tablet (2200 BC); (Right) treatment of a patient

isolated from plants, characterized and were synthesized in a laboratory. Sometimes, chemical modifications (semi-synthesis) could enhance the activity or drugs were better tolerated. Gradually, synthetic compounds replaced many of the plant active constituents, though certain plant derived agents were never surpassed and remain as valued medicines to this day. The molecules shown below (Figure 2) are some of the natural product-derived medicinal compounds from past to present.

Figure 2: Examples of natural products-based drugs from past to present

There is currently a renewed interest in active natural products from plants, animals, or microorganisms, in the drug discovery *continuum*. This is clearly observable in the areas of cancer and infectious diseases. National Cancer Institute conducted a survey and, among the new 877 small-molecule authorized as drugs worldwide between 1981 and 2002, 61% were inspired by natural products.³ The biological activity of natural products has been rationalized by the fact that during biosynthesis, they interact with multiple proteins as substrates and targets, so called "multi-target drugs".⁴ Therefore, they are capable of penetrating biological barriers and exert their effect. Thus, most natural products are biologically validated to target specific proteins and triggered various biological cascades. In the plant itself, natural products as secondary metabolites and often serve to protect against predators. In humans, these chemical entities are used to protect or treat some of our diseases often by acting as specific toxins against aberrant cells or deregulating physiology.

II. Electrophilic molecules "Michael acceptors" type

An electrophilic molecule is a compound having one or more electron deficient atoms. It is able to form a bond with a compound called "nucleophile" which will share its electron doublet. Electrophiles are species which will be able to modulate certain biological functions by interacting with nucleophilic macromolecules. These

interactions lead to various biological activities of interest in therapy. There are a myriad of electrophilic molecules or patterns, but the subject of this research work focused on a particularly promising class of therapeutic agents: "Michael acceptors".

After defining the concept of "Michael acceptor", explaining the chemical and biological reactivities of these compounds, this first part will describe different identified biological targets. Their clinical significance will, when possible, be illustrated by molecules currently on the market, or under development.

II.1. "Michael acceptor": definition

The so-called "Michael" addition reaction is a conjugated nucleophilic addition between a "Michael donor", nucleophile, and an α,β -unsaturated electrophile or "Michael acceptor". Michael donors are heteroatoms carrying a free doublet (Figure 3) such as thiols, anions, or amines. Michael acceptors (MA), on the other hand, are patterns with a double bond, or an alkyne function, in the α and β position of an electron-withdrawing group (EWG) such as carbonyl functions, amides or nitriles.

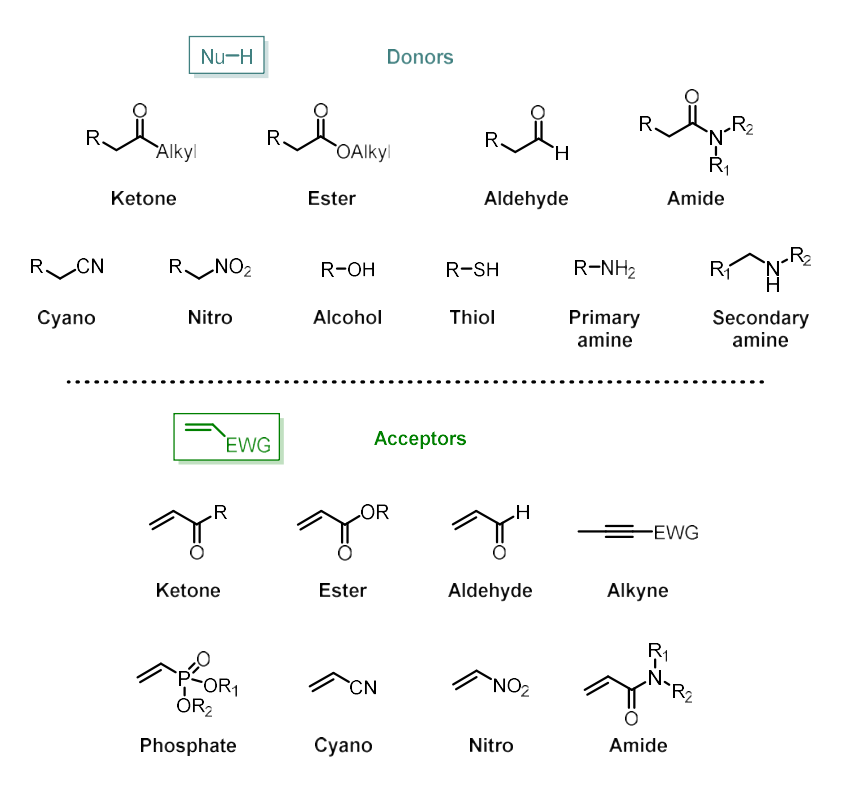


Figure 3: List of Michael donors and acceptors

Michael reaction is a case of vinylogy, the premise of which is that "the property of a functional group is expressed (or is relayed) through one (or more) double bond(s), that is to say vinyl(s)".

In the case of Michael acceptors, this principle can be visualized in Figure 4 representing an α,β -unsaturated carbonyl system, motif regularly used to illustrate Michael acceptors. The figure shows the polarization of the carbonyl function relayed along the double bond by resonance. In the case of α,β -ethylenic carbonyl derivatives, there are therefore two electrophilic sites within the molecule which can rise two addition reactions in competition.

$$\begin{bmatrix} \delta + & \delta - & & \\ \beta & \alpha & & \beta & \alpha \end{bmatrix}$$

Figure 4: Representation of the vinylogy principle applicated to a α,β -unsaturated ketone

In theory, a nucleophile can either directly attack the carbon of the carbonyl, or attack the β -carbon, which is electrophilic by mesomerism. The carbonyl attack is a direct addition of type 1,2 (reaction 1, Figure 5), while the addition taking place at the level of β -carbon is a conjugated addition, known as 1,4 addition or Michael addition (reaction 2, Figure 5). Depending on the conditions, either of the additions may be favored.

1 Nu-H
$$\xrightarrow{B}$$
 \xrightarrow{Nu} $\xrightarrow{\beta}$ \xrightarrow{Nu} \xrightarrow{Nu} \xrightarrow{Nu} \xrightarrow{Nu} \xrightarrow{Nu} 1,2 addition

Figure 5: Nucleophilic addition on conjugated systems

II.2. Chemical reactivity

From a chemical point of view, the preferential position of the nucleophilic addition depends on three elements⁵:

- the nature of the nucleophile
- the nature of the electron-withdrawing group and the steric hindrance generated
- the reaction conditions

The first major principle explaining the selectivity of nucleophilic addition is the HSAB (Hard and Soft Acids and Bases) theory or Pearson concept, which is based on the characters "soft" or "hard" of the nucleophile and the electrophile involved in the reaction. The HSAB principle explains that the addition of a hard nucleophile to a hard electrophile, or a soft nucleophile with a soft electrophile, will be faster than those between species of opposite characters. They will therefore be favored. An electrophile or nucleophile is said "Soft" when it is bulky, neutral, or weakly charged, and easily polarizable, that is, their charge is dispersed. Conversely, a nucleophile or an electrophile is said "Hard" when it is small, has a high load and is weakly polarizable, i.e. the charge is very localized (Figure 6).6

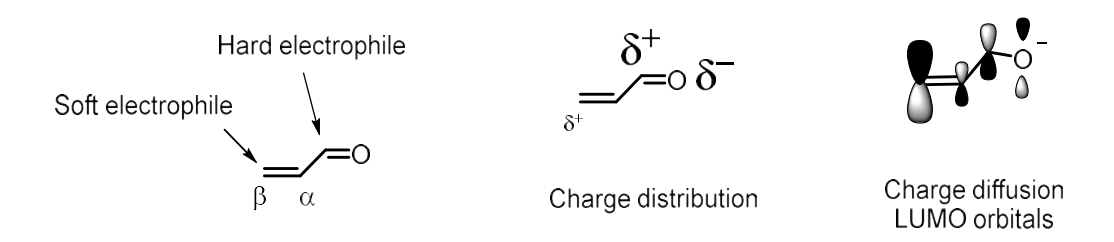


Figure 6 : Charges and polarization of an α,β -unsaturated carbonyl system. In this case, the carbon atom of the carbonyl is a hard electrophile due to its strong charge and its poor polarizability. The β -carbon is a soft electrophile due to it low and diffuse charge

The hard interactions therefore involve the charges and the electrostatic characteristics of the species concerned, while the soft interactions are orbital interactions. 5,7 Since β -carbon is a soft electrophile (Figure 7), the Michael addition or addition 1,4 is defined as a soft interaction thus involving the orbitals. It is favored when the difference in energy levels between the orbitals LUMO of the electrophile and HOMO of the

nucleophile is low.⁷ The soft nucleophile has a high energy HOMO and the soft electrophile has a low energy LUMO.

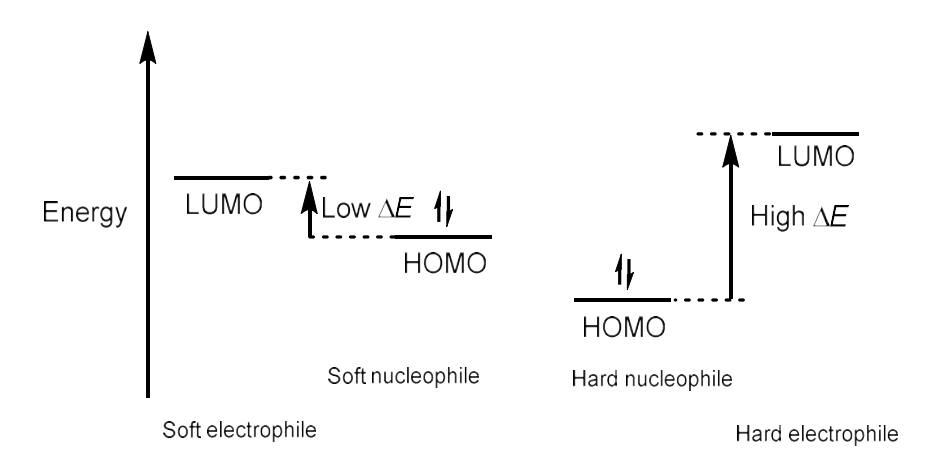


Figure 7: Orbital interaction levels between hard and soft species (HSAB principle)

These rules govern the reactivities of soft and hard species excluding all considerations of size, competition and other physicochemical phenomena that can be involved between two molecules. A classic example of the regioselectivity of the attack on an α,β -unsaturated ketone, conditioned by the hard or soft nature of the electrophilic, is the difference in reactivity of an organolithium (hard) and a cuprate (soft). In practice, this is more complex. The reactivity of the α,β -unsaturated electrophile will depend on the nature of the nucleophile present as well as the nature of the electron-withdrawing group, but also the steric hindrance generated. The carbon of the carbonyl, being a hard electrophile (Figure 7), is capable of reacting in presence of a hard nucleophile by a 1,2 addition. The nature of the EWG and the steric size may in some cases promote a 1,2 addition.

The reactivity also depends on the reaction conditions and on the presence of several nucleophiles in competition. Thus, the selectivity of the 1,2 or 1,4 addition depends on the kinetic or thermodynamic control of the reaction. Under kinetic control, the favored addition is the fastest kinetic constant. 1,2 addition is often faster but giving a less stable product. Kinetic control takes place at low temperature, with short reaction times, in an aprotic medium and in the presence of a strong base. If the nucleophile is a good leaving group, the 1,2 addition may be reversible. Nevertheless, the conjugate adduct is also formed, in parallel, but no longer slowly. It becomes the persistent species at the end of the reaction.^{5, 9} Thus, thermodynamic control favors the conjugate addition,

which is slower, but generally a more stable β -adduct is obtained. Conditions involving a thermodynamic control are so-called balancing conditions: a high temperature, the presence of a weak base and a long reaction time. In these conditions, all stages of Michael addition are potentially reversible; the nucleophile can be removed, regenerating the acceptor. The product may be stabilized by external factors and persist. Although the nucleophilic character of the Michael donor is improved in basic medium, it has been shown that the conjugate addition can also occurs in acidic catalysis. The reaction rate is then significantly increased. 10

II.3. Biological reactivity

Although it is difficult to generalize, the HSAB principle makes it possible to understand and predict, to some extent, the privileged responsiveness of Michael acceptor systems to many nucleophilic biological molecules. In fact, many proteins are likely to interact with Michael acceptors at the level of their nucleophilic amines. This is particularly the case with sulfhydryl groups of cysteine residues (Figure 8), the primary amine and the ε -amino group of lysine, or even the amine of histidine imidazole.¹¹

Figure 8: Structure of cysteine. The soft nucleophilic character is due to the terminal thiol function

Michael acceptors have been shown to be more prone to react with sulfhydryl groups molecules than with amine groups (Figure 9). This is explained by the fact that the thiols are softer nucleophiles than amine groups.¹¹ Cysteine residues are therefore important targets of Michael acceptors.

Figure 9: Addition between a biological macromolecule and a Michael acceptor via the thiol group

The reaction with biomolecules can also, in some cases, be stabilized by external factors,⁷ such as intermolecular hydrogen bonds between Michael acceptor and cysteine,¹² and become irreversible. Some Michael acceptors were identified as potentially genotoxic acting as alkylating agents of DNA.

However, many molecules, for whom a Michael addition corresponds to the mechanism of action, have already been shown to have a medicinal benefit, or are undergoing clinical trials. The interactions, irreversible or not, with cysteine residues, particularly at the enzymatic sites, are responsible for many therapeutic effects.

II.4. "Michael acceptors" biological targets

II.4.1. Cysteine proteases

Some Michael acceptors are irreversible inhibitors of enzymes bearing cysteine residues. These enzymes have a cysteine residue within their active site and are therefore good nucleophiles. They constitute interesting therapeutic targets due to their ubiquitous presence within protozoa, helminths, viruses, bacteria, but also mammals.^{13, 14} In humans, their deregulation is linked to many cardiovascular, inflammatory, neurological and immunological diseases.¹³ The mechanism of action is through Michael addition at the cysteine active site of the enzyme.¹⁵

Cysteine proteases may serve as preferred targets in the development of human rhinoviruses. ¹⁶ Rupintrivir (AG7088) is an example of an antiviral protease inhibitor C3 (Figure 10). The molecule acts by a Michael addition to a cysteine residue of the protease. ¹⁶ Development of Rupintrivir stopped in phase II due to its limited effectiveness in the prevention and treatment of the common cold but investigations are still ongoing. ¹⁷ More recently, the molecule has been repositioned as a potential SARS-CoV-2 treatment. ¹⁸

Figure 10: Structure of Rupintrivir, recently repositioned as potential SARS-CoV-2 treatment

Certain cysteine proteases are also essential for the survival of pathogens and are excellent targets for the treatment of malaria agent Plasmodium falciparum and Trypanosomes. Among these are cruzaïne from Trypanosoma cruzi, which causes Chagas disease; falcipain present in P. falciparum; or rhodesaine, present in Trypanosoma brucei, the agent of sleeping sickness. 15, 19 Compound K11777 or K777, containing a vinyl sulfone, is one example to illustrate this case (Figure 11). This molecule was identified at the University of California, San Francisco and is in clinical trials in the United States for the treatment of Chagas disease. 20 This molecule has been shown to be effective against different strains of Trypanosoma cruzi, including strains resistant to current treatment, benznidazole and nifurtimox. Compound K777 inhibits selectively cruzaïne by binding irreversibly to the thiol residue Cys25 of the enzyme by Michael addition. 21, 22 This molecule is also being investigated to fight SARS-CoV-2 as it inhibits infection of human cells. 23

Figure 11: Structure of K777, a cruzaïne selective inhibitor

Numerous peptide and peptidomimetic derivatives possessing a Michael acceptor function were therefore developed in therapy as inhibitors of cysteine proteases.¹³

II.4.2. Kinases

Michael acceptors are also of great interest as irreversible inhibitors of another type of enzyme, protein kinases and more particularly tyrosine kinases. Proteins are involved in many physiological mechanisms, and their dysfunction can lead to pathologies ranging from inflammation to cancer.^{24, 25} Michael acceptors have the ability to covalently bind with cysteine residues at the non-catalytic site of the enzyme. Currently this mechanism of action is the subject of renewed interest in therapeutic, more particularly in cancerology and it leads not only to the discovery of original Michael acceptor structural patterns, but also new potential targets, among the kinases. This keen interest for kinase inhibitors has also led to the discovery of a new class of potential anti-parasite compounds since many kinases have been identified in the Plasmodium²⁶ and the family of Trypanosomatids genus Trypanosoma)²⁷. A natural polyketide derived from a fungus, hypothemycin (Figure 12), showed excellent activity against the agent T. brucei, in which it inhibits 10 of the 21 CDXG3 identified kinases.²⁷⁻²⁹ This molecule acts by Michael addition at the cysteine from CDXG kinases.²⁵ It has also been observed to possess immunosuppressive activity against concanavalin A-induced T cell proliferation.³⁰

Figure 12: Structure of hypothemycin, a kinase inhibitor of *Trypanosoma brucei*

Many other kinases have been identified in humans as therapeutic targets. The kinases involved in the vital regulatory pathways of MAPs (Mitogen-Activated Protein)³¹ can be inhibited at several levels of the signaling.^{25, 32} AKT Kinase B is another example.³³

The compound E6201 has successfully passed a Phase 1 clinical trial in the treatment of solid tumors³⁴ and Phase 2 in psoriasis (Figure 13).³⁵ It acts as a competitive inhibitor at the level of MEK kinase ATP binding site by Michael addition. E6201 is derived from a natural compound.^{36, 37}

Figure 13: Structure of E6201, a MEK kinase inhibitor

These tyrosine kinases, intracellular or intramembrane, catalyze the phosphorylation of proteins by transferring an ATP molecule to protein effectors. Thus, they play a major role in cell signaling.³⁸ The development of irreversible tyrosine kinase inhibitors is currently one of the avenues of research in the fight against cancer.³⁹ For instance, Michael acceptors can bind irreversibly to a cysteine residue nucleophile of the epidermal growth factor receptor (EGFR) protein.³⁸ Many molecules possessing this mechanism of action are currently in development or already on the market (Dacomitinib, PF-00299804, Neratinib, HKI-272, BIBW-2992)³⁸. One of them, Afatinib (Giotrif®, Boehringer Ingelheim International Gmbh®), is currently on the market for the treatment of non-small cell bronchial cancer. Within its structure, it possesses an acrylamide motif and covalently binds to EGFR through a Michael addition.²⁴ An another molecule, Neratinib (Puma Biotechnology, Inc.®), is a selective inhibitor indicated in HER2-positive breast cancer.²⁴ He is currently at different stages of clinical development, alone or in combination with other anticancer agents.^{40, 41}

II.4.3. Other enzymatic targets

There are many other potential targets of Michael acceptors at the enzymatic level. Finasteride, a 5-α-reductase inhibitor used in the treatment of benign prostatic hyperplasia has a mechanism of action involving a Michael addition.⁴² Selegiline, used in the treatment of Parkinson's disease irreversibly inhibits MAO-B (Monoamine Oxidase type B), thus making it possible to block its dopamine degradation function and therefore regulating its rate. Two mechanisms of action have been proposed and both involve Michael adducts.⁴² Monoglyceride lipase (MGL) is also efficiently and selectively inhibited by N-substituted maleimide Michael acceptors.⁴³ It has been reported that transportins can be targeted by Michael acceptors. One example is leptomycin (Figure 14), through covalent modification of Cys529 of exportin-1 (XPO1),

a protein which transport cargos from the nucleus to the cytosol.^{44, 45} Significant efforts in medicinal chemistry led to the development of Selinexor, a covalent inhibitor which is FDA approved for multiple myeloma and diffuse large B-cell lymphoma.

Figure 14: Structures of leptomycin (left) and selinexor, FDA approved (right)

II.5. Partial conclusion

Until very recently, electrophilic compounds, including Michael acceptors, were often neglected, and even denigrated in the discovery of new therapeutics. This was mainly due to the lack of selectivity of their mechanism of action and the non reversible nature of the bonds.^{7, 46} Michael acceptors are often associated with a risk of high toxicity, including risks of immunogenicity, carcinogenicity and contact dermatitis.^{10, 11}

Recently, the discovery and the development of promising new molecules, some of which are selective (Neratinib, K777), aroused keen interest in this class of compounds.

The formation of adducts with sulfhydryl groups of macromolecules has appeared as an important mechanism, selectivity constitutes a challenge for the development of future treatments. New studies to investigate the structure activity relationships as well as the role played by various factors (reversibility, pH, competition of nucleophiles) in the reactivity of Michael acceptors and their toxicity have emerged.^{7,8} While waiting to better understand these relationships, the bioguiding is an essential avenue of discovery for the identification of new molecules. This also makes it possible to feed the structural databases of this class, important treatment and ultimately, perhaps, to better understand their mechanism of action and identify new biological targets. The plant world has always been and continues to be a considerable source of inspiration in the development of new therapeutic molecules. Plants produce, for their survival and protection, a certain number of secondary metabolites having within their Michael

acceptor structures: aldehydes-, amides-, ketones-, γ -lactones-, δ -lactones- or nitrones- α,β -unsaturated and vinylsufone giving them interesting biological activities. Among the major families of secondary metabolites exhibiting Michael acceptor, can be mentioned phenolic compounds such as cinnamates, coumarins, chalcones, curcuminoids N-alkylamides or even the well known, sesquiterpene lactones. This last class of metabolites includes many bioactive molecules and is particularly represented within the Asteraceae plant family.

III. The sesquiterpene lactone family

Sesquiterpene lactones are secondary metabolites with a 15 carbon sesquiterpene skeleton, which have subsequently undergone structural modifications by cyclization and oxidation.⁴⁹⁻⁵¹

They represent an important class of secondary metabolites due to their high number of compounds and their great structural diversity. These molecules are present in fungi, bryophytes, and plants. It is within the Asteraceae family that they are found for the most part.

The great interest in the study of these compounds comes from their strong therapeutic potential. Many plants containing sesquiterpene lactones are frequently used in traditional medicine⁵² and these compounds have been widely studied for many years for their broad spectrum of biological activities, such as antibacterial, antifungal, antiprotozoal⁵³ and more importantly anti-inflammatory and anti-tumor. They are therefore very promising compounds for the development of new anti-inflammatory and anti-cancer therapeutic molecules.⁵⁴ From a physico-chemical point of view, they are lipophilic, weakly volatile, colorless, bitter and often thermolabile compounds.⁵⁵

III.1. Structure

Sesquiterpene lactones are divided based on the structure of carbon skeletons, to which is added the suffix "olide" indicating the presence of a lactone function (Figure 15).

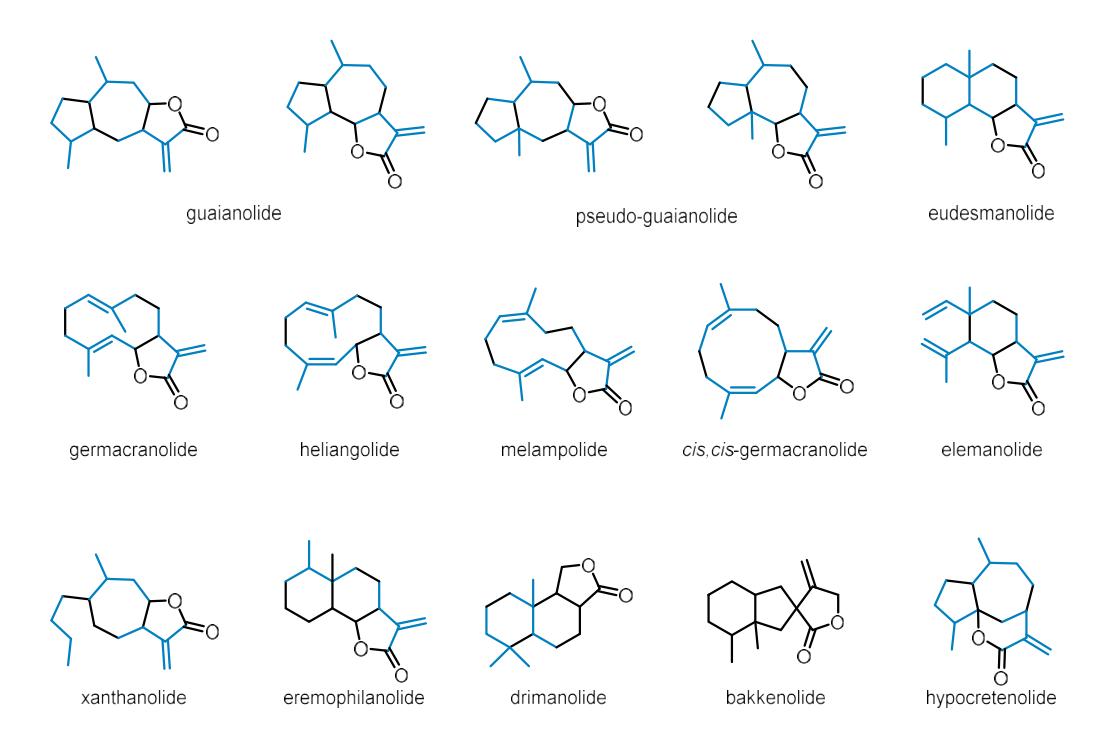


Figure 15: Examples of sesquiterpene lactones structures

By 2015, more than 6000 sesquiterpene lactones had been discovered.⁵⁶ According to Schmidt, there are 100 different sesquiterpene groups in the Dictionary of Natural Products and more than 300 according to certain authors, but 87% of the structures identified would derive from seven main groups.^{57, 58} These seven major groups are the germacranolides group, as well as 6 groups deriving from the germacranolides precursor type: guaianolides, pseudoguaianolides, eudesmanolides, eremophilanolides, elemanolides and xanthans (Figure 16).

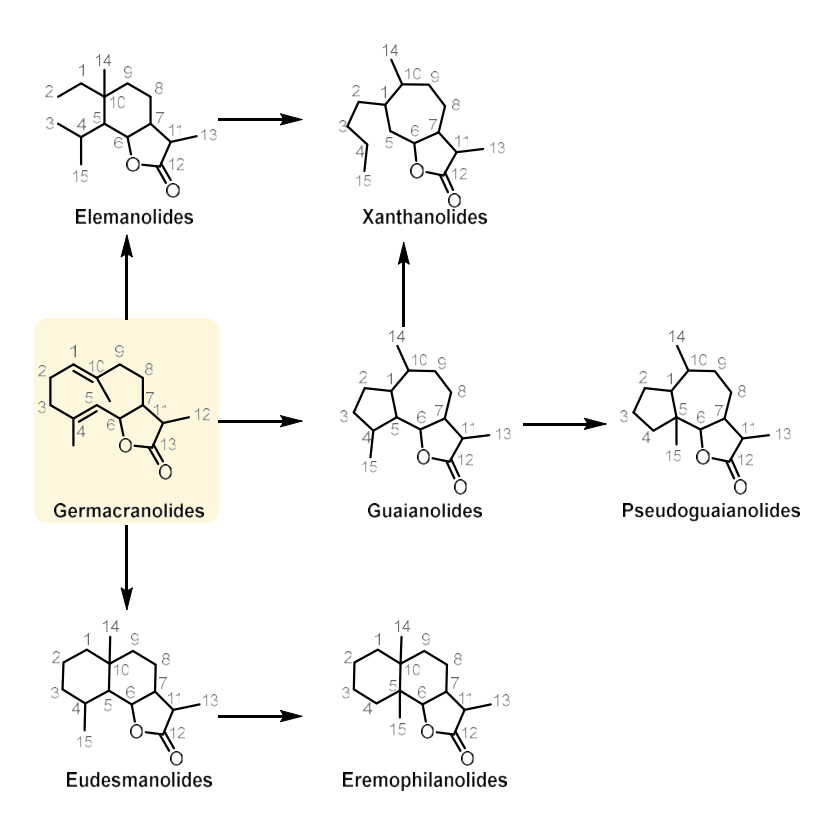


Figure 16: The seven main groups of sesquiterpene lactones according to Schmidt (2006) and their relationships according to Fischer *et al.* (1979)

The group of germacranolides is the predominant group in terms of number of compounds and it is itself divided into subgroups according to the configuration of the two double bonds of the cyclodecadiene skeleton (Figure 17): the germacrolide (E,E), heliangolides (1-10-E, 4-Z), melampolide (1-10-Z, 4-E) and Z,Z-germacranolides.⁵⁹ The subgroup of germacranolides is the most represented.

Natural Germacrane Lactones

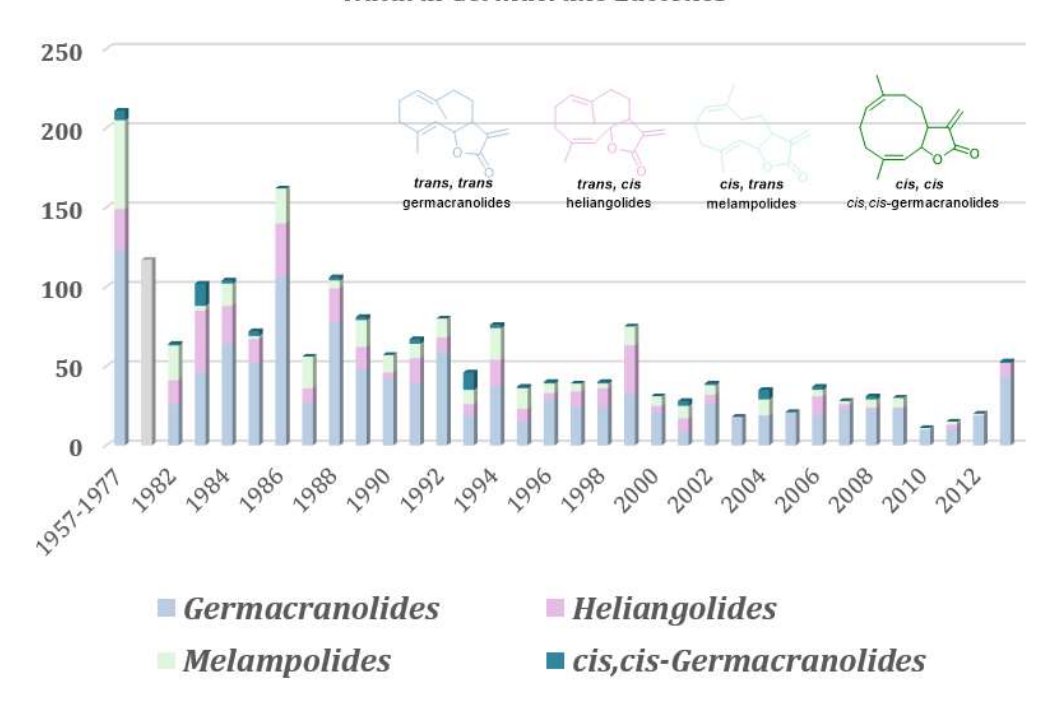


Figure 17: Number of germacranes lactones discovered in function of their respective subgroup from 1957 to 2013.

III.2. Historical milestones

Since 1957, important steps have been reached in the knowledge of the sesquiterpene lactones family, from the first structural elucidation of Pyrethrosin to the total synthesis of (+)-diversifolin.⁵⁹⁻⁷¹

- **1957** The first structural elucidation of Germacrane Lactones-Pyrethrosin was performed.
- **1958** Simplest representative, costunolide, was isolated.
- 1970 Nobilin was isolated.

The structure of costunolide was confirmed with the use of X-ray.

- **1971** First review of Germacrane Sesquiterpenoids. Various natural sources especially in Compositae. Fused α-methylene-γ-lactone moiety and variegated oxygen containing groups.
- **1976** The isolation and structure determination of goyazensolide responsible for the schistosomicidal properties. Pycnolide, the first seco-germacranolide found in nature.
- **1979** A very comprehensive review of all sesquiterpenoid lactones reported. At the end of 1977, nearly 950 sesquiterpene lactones were known, including G 123, M 26, H 56, CC 6. Liverworts tends to produce sesquiterpenoids enantiomeric to those found in higher plants.
- 1980 Newest additions -allenic germacranolides-vernonallenolides.
- **1983** Professors Herz and Bohlmann. Search for biologically active compounds and the chemotaxonomic classification. Tagitinin C was transformed to Tagitinin F.
- **1990** Bisparthenolidine an unusual new germacranolide alkaloid with antitumour properties.
- **1991** Cronquistiolide, a new carbon skeleton with 1,3-cyclopropane.

First stereoselective total synthesis of eremantholide A.

- **1994** New skeleton with 1,4-cyclobutane.
- **2009** The first total synthesis of the bioactive lactone (+)-diversifolin. Except for the isolation, chemical (cationic or radical, total synthesis) and biological transformations were reported. More and more different activities were reported.

anti-inflammatory activities, anti-cancer agents, antiplasmodial activity, antibacterial and antifungal activities, antifeedant, phytotoxic activity, inhibitor of tumour necrosis and interleukin-6, NF-κB inhibitors, inhibitors of germination and seedling growth in plant species and other various biological activities.

III.3. Biogenesis

There are quite a few studies on the biogenetic origins of sesquiterpene lactones. They originate, within higher organisms, from two biosynthetic pathways of terpenoids: the mevalonate pathway (MVA) located in the cytosol and the methylerythritol phosphate pathway (MEP) located in the plastid. These two pathways lead, either from acetyl-CoA (MVA), or from pyruvate (MEP) to the formation of a C₅ unit, isopentenyl pyrophosphate (IPP). IPP is a key intermediate in the biosynthesis of terpenes. The methylerythritol phosphate pathway was discovered more recently, in the 1980s. It has been shown that the IPP behind the biosynthesis of sesquiterpene lactones could originate from these two pathways and that exchanges were possible between the plastid.⁷² **IPP** cytoplasm and the The is then isomerized into dimethylallylpyrophosphate (DMAPP) by the enzymatic route. The two intermediates IPP and DMAPP subsequently condense into geranylpyrophosphate (GPP), precursor of the chemical group of monoterpenes (Figure 18). The following series derive from successive condensations: farnesyl PP (FPP), geranyl-geranylPP (GGPP), geranylfarnesylPP (GFPP), squalene and Z-phytoene, which are the precursors of the various classes of terpenes.⁷³

The precursor of sesquiterpenes is farnesylpyrophosphate (FPP), a linear unit in C_{15} , and it is generally accepted that the main skeletons of the sesquiterpene lactones are derived from the cyclization of the conformer 2E, 6E-farnesylPP by ionization of C_2 and elimination of pyrophosphate OPP forming the precursor of all the sesquiterpene lactones: the cation germacradiene, a cyclodecadiene.⁴⁹ This germacrene intermediate is oxidized to a carboxylic function at the level of C_{12} , a double bond is created at C_{11} , constituting the germacranic acid. This acid will then be hydroxylated in position C_6 or C_8 , in α or in β of the cycle, allowing the formation of an ester bond between the hydroxyl and the carbonyl leading to lactonization. The hydroxyl leading to this lactonization (whether in position C_6 or C_8). Lactonization most often leads to a five-membered ring, called γ -lactone.^{49, 74, 75} The six-cyclizations, cycle breaks, migration of methyl functions then take place, even before the formation of the lactone, δ -lactone cycles are very rare.⁴⁹ The diagram representing the biosynthetic pathway of the main sesquiterpene lactone groups is presented in Figure 18.⁷⁶

The synthesis of sesquiterpene lactones in plants mainly takes place at the level of the leaves, bracts, inflorescences, as well as at the level of achenes. These compounds are sequestered in specialized organs such as secretory hairs and may be present in an exudate covering the surface of the organs mentioned above. This main localization in the aerial parts is explained by the main function of these secondary metabolites which is the chemical protection of the plant against its predators.

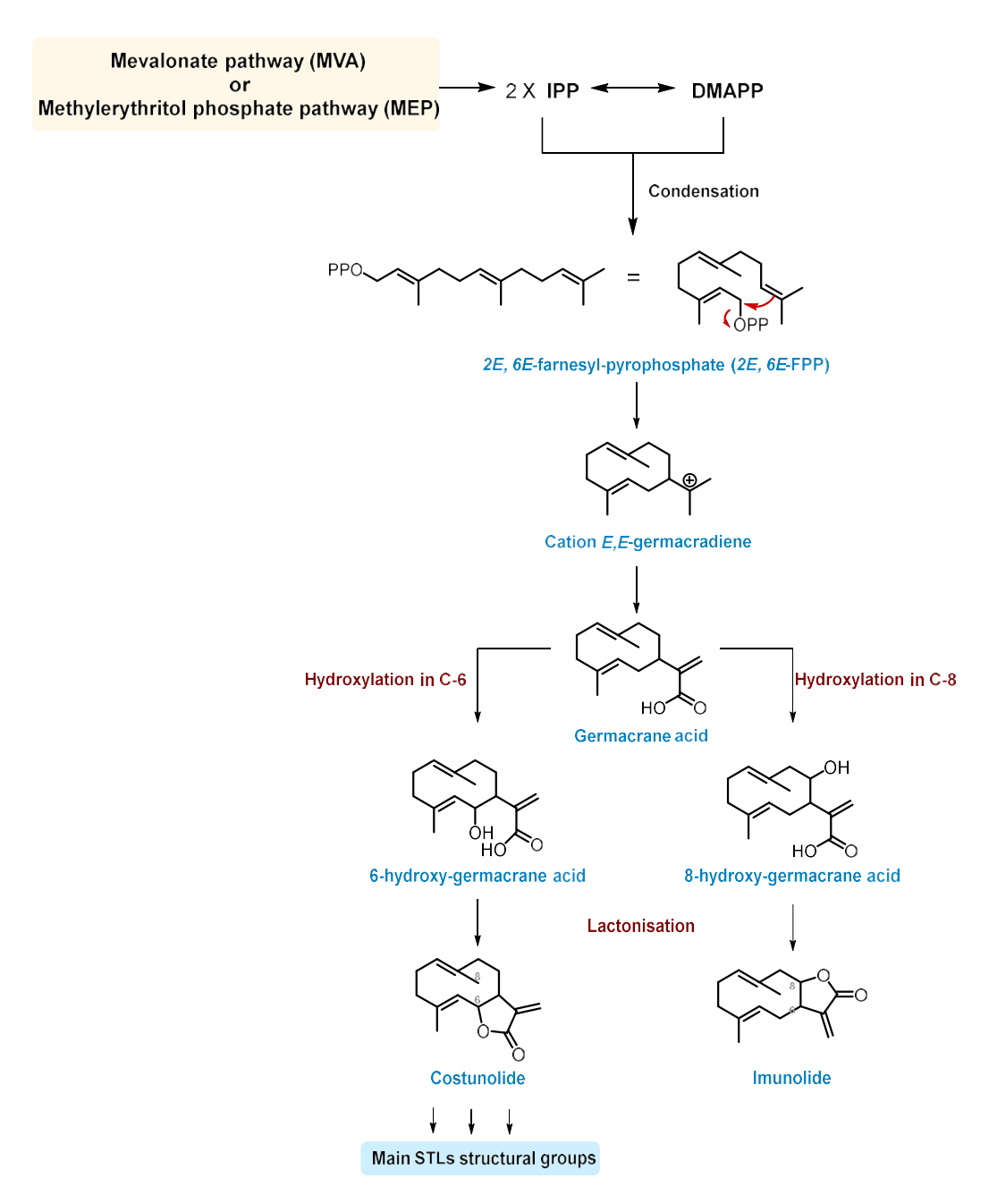


Figure 18: Schematic representation of the STLs biogenesis

III.4. Biological and therapeutic properties of the sesquiterpene lactones

One of the first biological properties attributed to sesquiterpene lactones is their cytotoxicity, undoubtedly linked to their protective role within the plant.79 They also have a strong propensity to induce allergies or contact dermatitis.⁵³ Beyond this cytotoxicity, sesquiterpene lactones have a very wide range of biological activities, generally exercising at very low concentrations, between nanomolar and micromolar, or even lower.⁷⁹ Antitumor, antibacterial, antifungal and antiparasitic properties have been reported, which were compiled in 1986 by Picman.⁵³ In 2012, Schmidt et al. have identified promising secondary metabolites in the treatment of neglected tropical parasitic diseases.80 More than 80 sesquiterpene lactones are among these compounds, in particular several germacranolides. Parthenolide, costunolide and eupatoriopicrin are some examples. Most of the biological properties of these molecules which have antiparasitic properties but also cytotoxicity, are most often correlated with the presence of the same structural patterns: the α,β -unsaturated group.81 Michael acceptor motifs are particularly represented in sesquiterpene lactones compared to other classes of molecules and are involved in addition reactions with biological nucleophilic molecules, particularly cysteine residues.^{58, 82} The Michael addition is not the sole mechanism responsible for the biological activity of this class of secondary metabolites. This is the case, for instance, of artemisinin, a sesquiterpene lactone with antimalarial properties⁸³, initially isolated from the plant Artemisia annua L., a species of Asteraceae used in traditional Chinese medicine for the same indication.^{84, 85} Artemisinin's activity comes from the endoperoxide motif of the 1,2,4trioxane cycle present within its structure (Figure 19 Left). Its mechanism of action is still the subject of debate, but it would act as a prodrug, undergoing a reduction via the Fe²⁺ of the heme leading to the homolytic cleavage of endoperoxide, leading to the release of radical species. The antiparasitic effect is thought to result from the reaction of these species with various proteins of the parasite, inducing cellular damage.86

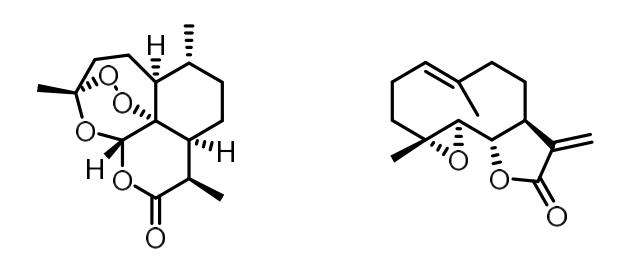


Figure 19: (Left) Structure of Artemisinine, (Right) structure of parthenolide

Perhaps one of the most representative example of the therapeutic potential of this class of compounds is parthenolide (Figure 19).87 Parthenolide is a germacranolide mainly isolated from Chamomile, Tanacetum parthenium (Asteraceae), and possesses an α-methylene-y-butyrolactone motif within its structure. This molecule is particularly interesting for its anticancer and anti-inflammatory properties, which is the case for the large group of sesquiterpene lactones more generally. 54, 55, 88 Mathema et al. published in 2011 an article summarizing its different biological targets justifying a promising future in these two fields which have been shown to be closely linked.^{89, 90} Parthenolide first acts as an anti-inflammatory by inhibiting the NF-κB pathway at several levels.90 Its anticancer properties come from this inhibition but also from its ability to increase the production of ROS (Reactive Oxygen Species) within cancer cells and to inactivate the STAT pathway, transcription factors involved in cell proliferation. Parthenolide also has interesting antiparasitic properties. It has been shown to selectively inhibit the parasites Leishmania amazonensis and Trypanosoma cruzi in vitro. 91, 92 Parthenolide is capable of activating the Keap1 / Nrf2 / ARE pathway93, 94 in the same way as other molecules with an α-methylene-γ-butyrolactone motif.95

Cynaropicrin is a natural molecule isolated from Centaurea salmantica L. (Asteraceae) inhibiting the growth of T. brucei rhodesiense *in vitro* and *in vivo*. ⁹⁶ This sesquiterpene lactone has been shown to be able to block the parasite's redox trypanothione system by binding to reduced trypanothione. The molecule binds via these two Michael acceptor motifs at the level of the two sulfhydryl functions of the molecule (Figure 20). ⁹⁷ This reaction may explain the trypanocidal activity of the molecule.

Figure 20: Formation of a bis-adduct between cynaropicrin and trypanothione

III.5. Partial conclusion

Trypanothione

The great structural diversity of sesquiterpene lactones and their numerous therapeutic properties continue to arouse interest within the scientific community. The fact that the cytotoxicity and the biological properties of these compounds are carried by the same pharmacophores makes it difficult to predict selectivity. Like reactivity, it seems to be modulated by other factors, in particular by the lipophilicity, the geometry and the electronic environment of these molecules. Discovery efforts for new sesquiterpene lactones by bio-guidance therefore continues to be a privileged access route in the search for new active compounds which may ultimately lead to the development of therapeutic agents.

IV. The natural product goyazensolide

Goyazensolide is a natural product discovered from plants of the family Asteraceae (Figure 21). The compound was first isolated from *Eremanthus Goyazensis* during a research program to find schistosomicidal agents.⁹⁸ This compound has also been extracted from *Erementhus mattogrossensis*,⁹⁹ *Lychnofora granmongolense*,¹⁰⁰ *Lychnofora pohlii*,¹⁰¹ *Camchaia calcarea*,¹⁰² *Centraterum Punctatum*,¹⁰³ and *Piptocoma* rufescens,¹⁰⁴ but essentially from *Eremanthus goyazensis*. This plant is an Asteraceae specie endemic of quartzite rupestrian fields. This ecosystem emerges at the top of Brazilian savannas ("Cerrado") located in central Brazil within the states of Minas Gerais, São Paulo, Bahia, and Goiás.¹⁰⁵ In these areas, the specie is known as "candeia".



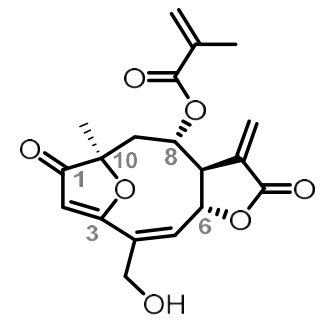


Figure 21: (Left) Erementhus goyazensis plant; (Right) Structure of goyazensolide

IV.1. Structure

Goyazensolide is a sesquiterpene lactone belonging to the furanoheliangolide subfamily. Furanoheliangolides is a highly oxidized subgroup of germacranolides with C_3 and C_{10} bridged furan ring that are mainly present in plants. From a structural point of view, furanoheliangolides can be divided into two subsets-8 α -OR and 8 β -OR (Figure 22). The diverse members exhibit a broad range of bioactivity ranging from antiparasitic, anti-cancer, anti-inflammatory activity to plant defensive functions.¹⁰⁶

$$\begin{array}{c} OR_2 \\ R_1 \\ \hline \\ Furanoheliangolide-8\alpha-OR \end{array}$$
 Furanoheliangolide-8 β -OR

Figure 22: Structure of furanoheliangolides pointing α/β configuration on C₈

The first investigation on furanoheliangolides can be traced back to 1970, zexbrevin was isolated and named by de Vivar *et al.*. ¹⁰⁷ In 1982, Herz *et al.* published the first X-ray structure of goyazensolide (Figure 23). ¹⁰⁸

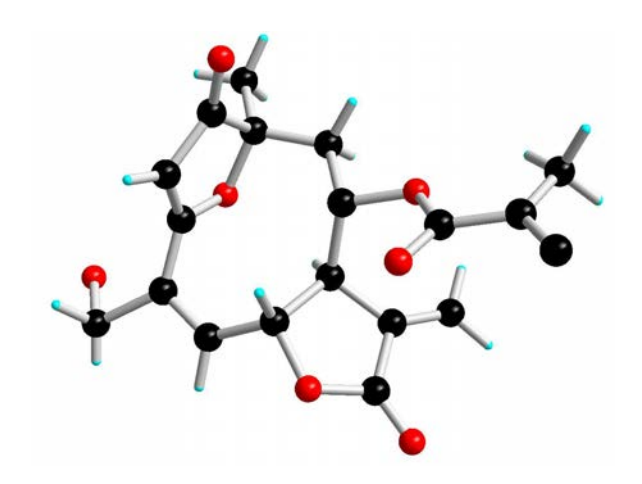


Figure 23: X-Ray structure of goyazensolide CCDC number 1111128

Despite the intriguing architecture as well as diverse activities, there are very few reports on their synthetic studies and total synthesis. 109 Presented by eremantholide A and diversifolin (Figure 24), the furan-fused 10-membered ring can be constructed by Ramberg–Bäcklund reaction, vinylogous aldol reaction or ring-closing metathesis (RCM) reaction. $^{68, 71, 110-112}$ However, the formation of α -methylene- γ -butyrolactone or its C_8 side chain hybrid version as shown in eremantholide A is strategically inefficient as it requires multiple steps.

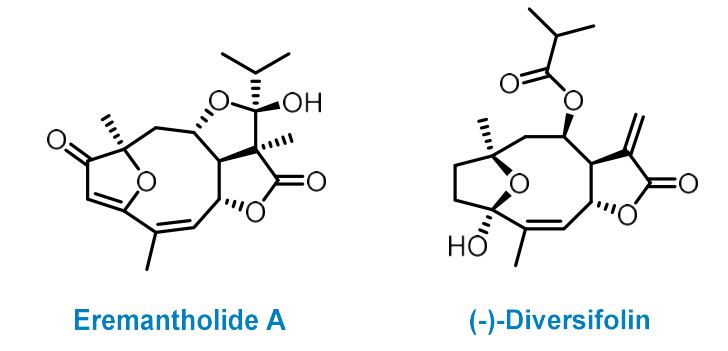


Figure 24: Structure of Eremantholide A and (-)-Diversifolin

Biogenetically, furanoheliangolides are originally derived from universal isoprenoid precursor as shown previously. This ionization–recombination–reionization sequence followed by oxidation and cyclization cascade affords structural diverse furanoheliangolides.^{113, 114}

IV.2. Biological properties

Goyazensolide possesses various bioactivities such as schistosomicidal, trypadocinal^{101, 115}, antimicobacterial¹⁰², cytotoxic^{102, 104, 116} and genotoxic¹¹⁷ effects. This compound exhibits nuclear factor kappa B (NF-kB)^{104, 118, 119} and C-*myb*-dependent gene expression inhibitory activity.¹²⁰ Goyazensolide induces aptoptosis in cancer cells *in vitro* and *in vivo*.¹²¹ More recently, the first *in vivo* experiments demonstrated an anti-hyperuricemic activity and a potential trypanocidal activity for Chagas disease.¹²²

While goyazensolide shows various biological activities, its mode of action remains to be defined.

V. Objective

While goyazensolide properties remains largely unstudied, it has been shown to be an interesting compound in the treatment of an animal model bearing colon tumors. The objective of this work consisted of establishing a rationalization of its anti-cancer activity.

As goyazensolide is not commercially available, the first step will be its total synthesis via the design of a novel synthetic route as goyazensolide or close analogs have never been synthesized.

Having access to the natural product, design and synthesis of a goyazensolide probe will be performed with the intention of preparing an activity-base probe for a proteomewide target screen. With this in mind, the structure of goyazensolide indicates a quick and easy incorporation of the tag on the allylic alcohol through an acylation with 4-pentynoyl chloride.

The alkyne tag probe incubated in a cell lysate followed by reaction with a fluorophore will revealed specific targets of goyazensolide. Once localized, targets of interest will be enriched, digested and analyzed via MS/MS. Identification of the target will be confirm by the use of a specific antibody.

Moreover, MS/MS analysis would also detect the probe adduct and, thus, provide the exact localization of the covalent interaction.

The identification of the target will let us interrogate its functions in the presence or in the absence of goyazensolide. Biological cascades trigger various protein modulations and will be monitored by the use of specific antibodies. In consequence, its anti-cancer activity will be rationalized.

CHAPTER 2. Total synthesis

I. Total synthesis of goyazensolide: strategy 1

I.1. Ring closing metathesis strategy

The retrosynthetic route was composed of two key steps: a ring closing metathesis (RCM) and a Barbier allylation (Figure 25). To simplify the synthesis and validate the strategy, the allylic alcohol of the south part (C₄) and the methyl group at the C₁₀ have been removed.

Figure 25: Retrosynthetic route of goyazensolide 1 and its analog 2.

I.1.1. Synthesis of bromolactone 3

Figure 26: Structure of bromolactone 3

The synthesis of **3** was already performed in the laboratory and described in the literature (See experimental section).¹²³

I.1.2. Synthesis of aldehyde 4

Figure 27: Retrosynthetic route of synthon 4

Intermediate **7** was obtained from Malic acid according to the literature (Figure 28).¹²⁴, Weinreb amide **8** is obtained after the cleavage of the acetonide by trimethylaluminium and the Weinreb salt. An alkynylation of **8** gave the ynone **10** which require two equivalents of alkyne **9** due to the free alcohol present on the weinreb amide. The 3-(2H)-furanone **11** was accessed by an intramolecular cyclization with HgO in acidic conditions. Dess-Martin oxidation afforded aldehyde **13** followed by a second oxidation with H₂O₂ to obtain the corresponding sulfoxide, but the harsh thermolysis conditions under microwave irradiation (MW) did not afford **4**. This "masked alkene" deprotection was also tested on the alcohol **11** but a decomposition was observed. Thus, the thermolysis will be applied after the Barbier reaction.

Figure 28: Synthetic route of the synthon 13 precursor

I.1.3. Synthons 3 and 13 coupling

Figure 29: Last part of the synthetic route

Intermediates **3** and **13** reacted in the presence of Zinc and ammonium chloride to provide **14** *via* a Barbier allylation (Figure 29).^{128, 129} Analysis of the Barbier products indicated the presence of several non-separable compounds by NMR with the correct mass (LC-MS) suspecting a possible racemization at the 3-(2H)-furanone position during the Barbier reaction or during the previous steps. Oxidation with one equivalent of H₂O₂ gave the sulfoxide **15**, which should be eliminate by thermolysis.¹³⁰ Although the reaction was clean arising a single compound, the obtained product didn't correspond to the expected dienone **16**. After full analysis, the elimination reaction occurred but the intermediate **16**, which already bears a dienophile, can revealed by prototropy a diene furan scaffold **17** and reacts in an intra Diels Alder reaction to give a single polycyclic compound **18** (Figure 30). NMR analysis did not allow the determination of the exact stereochemistry.

Figure 30: Intra Diels Alder during the thermolysis reaction

Several tests to crystallize the compound were unsuccessful, even with the incorporation of a 3,5-dinitrobenzoyl on the secondary alcohol. DFT calculations were performed and indicated that only the stereoisomer **18a endo** should be formed during the intramolecular Diels-Alder reaction (Computational study was performed by Dr. Romain Pertschi, see experimental section). The scaffold of this unexpected product didn't correspond to any structure in the literature and further investigations might be done for a potential utility.

I.2. The tetrahydrofuranol scaffold

$$\begin{array}{c} \text{OTBS} \\ \text{OTBS} \\$$

Figure 31: *(Top)* Retrosynthetic route of the tetrahydrofuranol strategy. *(Bottom)* Strategy from tetrahydrofuranol to 3-(2H)-furanone synthesis

As the 3-(2H)-furanone scaffold was highly sensitive, this moiety will be constructed later in the synthetic route, *via* double oxidation of the tetrahydrofuranol starting with a first oxidation to give the tetrahydrofuranone followed by the formation of the

conjugated double bond using DDQ oxidation (Figure 31 bottom). In this case, chemical transformations should be cleaner and more robust due to the higher stability of the protected tetrahydrofuranol compared to the conjugated 3-(2H)-furanone.

Figure 32: Synthetic route of the tetrahydrofuranol strategy

Intermediate **11** was reduced by NaBH₄ to give the diol **19** (Figure 32). Both alcohol were protected using TBSOTf then a mono-deprotection of the primary alcohol gave **21**.¹³¹ DMP oxidation afforded the aldehyde **22** followed by the Barbier allylation. By using this tetrahydrofuranol scaffold, the elimination of the bromohydrin to give the alkene during the Barbier allylation was efficient as well as the thermolysis to obtain **24** in good yields. To facilitate investigations on the RCM, the methacrylate ester was substituted by an acetyl, which is represented by the intermediate **25**. The ring closing metathesis step gave a single macrocyclized compound.¹³² Nevertheless, NOESY analysis of the macrocycle **26** has indicated clear correlations and revealed the wrong configuration obtained at the fused five membered ring position (Figure 33).

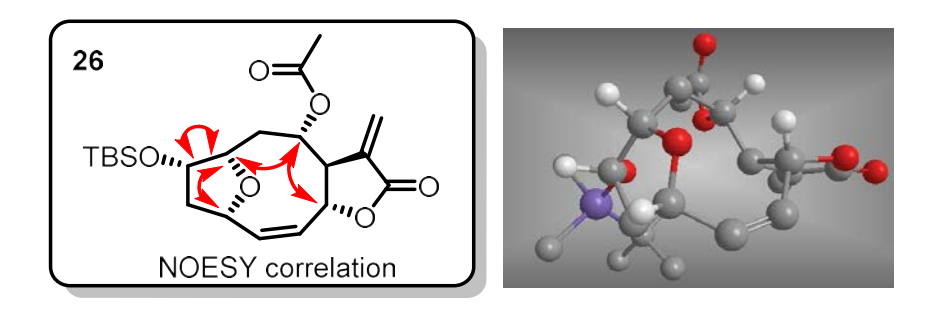


Figure 33: (Left) NOESY correlation of intermediate 26; (Right) 3D representation

I.3. Partial conclusion

While the ring closing metathesis with the analog **26** successfully occurred, only the stereoisomer with the wrong configuration has cyclized. Furthermore, problems of racemization have been observed underlining the acidic character of the proton localized in α -position of the carbonyl within the 3-(2H)-furanone. In consequence, a new approach is required to synthesize goyazensolide.

II. Total synthesis of goyazensolide: strategy 2

II.1. Trans-disubstituted α -exo-methylene- γ -butyrolactone synthesis

A strategy has been performed within the laboratory to synthesize chiral disubstituted α -exo-methylene- γ -butyrolactone scaffold from bromolactones (like bromolactone 3) but the major bottleneck is number of steps to obtain the bromolactone (8 steps) and using harsh conditions (HBr aq.48%) non compatible with sensitive chemical moieties (See experimental section). A potential strategy to build a *trans*-disubstituted α -exomethylene- γ -butyrolactone scaffold would be to, first synthesize the monosubstituted α -exo-methylene- γ -butyrolactone (Figure 34), followed by a Riley oxidation α -exo-methylene- α -butyrolactone (Figure 34), a bromination in smooth conditions α -methylene- α -butyrolactone.

$$R_1$$
-CHO $\frac{1}{Z_{II}}$ $\frac{CO_2Et}{Z_{II}}$ $\frac{1}{Z_{II}}$ $\frac{1}$

Figure 34: Strategy to obtain the trans-disubstituted- α -methylene- γ -butyrolactone

From a mechanistic point of view, the intermediate passed by a Zimmerman-Traxler transition state and gives the *trans-trans*-configuration (Figure 35). 138, 139

Figure 35: Formation of the α -exo-methylene- γ -butyrolactone with a *trans-trans*-configuration *via* a Barbier allylation.

It is interesting to note that the strategy uses two aldehydes R_1 and R_2 (Figure 34). If R_1 and R_2 are on the same molecule, it could be possible to perform a macrocyclization with a concomitant formation of the α -exo-methylene- γ -butyrolactone (Figure 36).

Figure 36: Schematic representation of the macrocyclization strategy.

The retrosynthetic route possesses 3 key steps: a gold catalyzed transannulation, a Barbier allylation and a Sonogashira coupling (Figure 37).

Figure 37: Retrosynthetic route of the second synthetic strategy

II.2. Racemic route validation

To validate the route as soon as possible, the design of the synthetic route will be racemic. Other unsuccessful routes have been tested to obtain the racemic "coupled intermediate" (Figure 37) and are described in the experimental section.

The intermediate **31** was prepared from the commercially available diol **27** through a monoprotection with TBDPSCI followed by a bromination in the presence of Red-Al to give **29** (Figure 38). After a Dess Martin oxidation, a Barbier allylation/lactonization with ethyl 2-(bromomethyl) acrylate afforded **31**.

Figure 38: Scheme of the racemic synthetic route

With **31** in hand, the commercially available compound **32** has been protected with TESCI and deprotonation of **33** with *t*-BuLi allowed the attack of the 1,1-dimethoxy-3-butanone to form **34** in a mixture of diastereoisomers (Figure 38). Desilylation of TMS and TES with TBAF afforded **35**. The Sonogashira coupling gave a mixture of diastereoisomers in good yield. At this stage, LC-MS monitoring and analysis will take a higher consideration in the compound characterizations as the complexity of the NMRs has increased. Some diastereoisomers are separable by flash chromatography but they are collected all together to avoid any loss of diastereoisomer. Propargyl alcohol oxidation with Parikh-Doering reaction gave good yield and gold catalyzed cyclization afforded **38**. Allylic oxidation step increased the number of

diastereoisomers due the formation of a new chiral center and, moreover, was not clean due to the partial acetal deprotection. A bromination screening did not afford the expected compound but a mixture of by-products.^{137, 142-145}

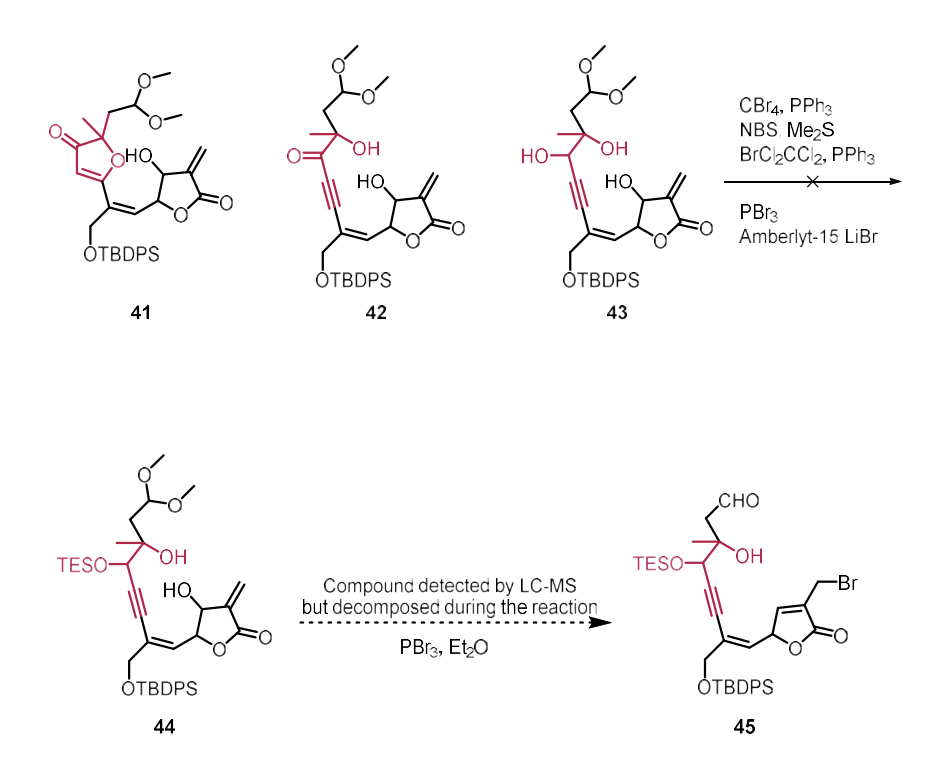


Figure 39: Screening of bromination with different intermediates

Allylic alcohols have been synthesized on previous intermediate to screen the bromination step but failed (Figure 39). Interestingly, the expected compound during the bromination of intermediate **44** has been clearly detected (LC-MS) but disappeared during the reaction. It has been explained by, once **45** was formed, desilylation due to the acidic conditions decomposed the structure. The next step was to incorporate a protecting group resistant to acidic conditions.

II.3. Acetate protecting group

In order to avoid any deprotection of the propargyl alcohol **35** in acidic conditions (as observed with the TES protecting group), the acetate group would be an appropriate protecting group (Figure 40).¹³¹ As the allylic oxidation step was not clean enough (partial deprotection of acetal), the incorporation of the allylic alcohol has been shifted before the Sonogashira coupling.

Figure 40: Racemic synthetic route with the propargyl alcohol acetate protection

Propargyl alcohol **35** was acetylated with acetic anhydride then coupled with the vinyl bromide **37**. Sonogashira coupling between **36** and **37** gave intermediate **46** in low yield. This drastic decreased of yield may be due to a potential chelation of the palladium to the allylic alcohol and thus block the reaction. Bromination converted the allylic alcohol into the bromide (SN2') with concomitant deprotection of the dimethylacetal to afford the cyclization precursor **47**. A screening of different metals (Zn, CrCl₂, In, SnCl₂)¹⁴⁶⁻¹⁴⁹ indicated that only CrCl₂ afforded the macrocyclization. The use of DMF increased the yield compared to THF. At this stage, proper separation of each spots became too complicated due to the formation of a high number of diastereoisomers but analysis by LC-MS have shown several peaks corresponding to the expected mass. Replacing the racemic alkyne **36** by the chiral one will reduce the number of diastereoisomers.

II.4. Stereoselective route of the alkyne moiety

Figure 41: Synthetic route of the chiral alkyne intermediate

The route started with a carboalumination of the homopropargylalcohol **49** followed by a quenching with iodine to afford the vinyl iodide **50** (Figure 41).^{150, 151} A one pot oxidation / acetal protection followed by a Sonogashira coupling with trimethylsilylacetylene gave the enyne **52**. A Sharpless dihydroxylation with the ligand (DHQD)PYR afforded the diol **53** in good yield and enantiomeric excess.¹⁵² The enantiomeric excess was evaluated by the formation of the Mosher esters and gave ee = 94% (Figure 42).¹⁵³ Indeed, the poor UV absorption of the structure did not allow any analysis by chiral chromatography. The propargyl alcohol of the diol **53** was then acylated followed by a desilylation with TBAF to give **55**.

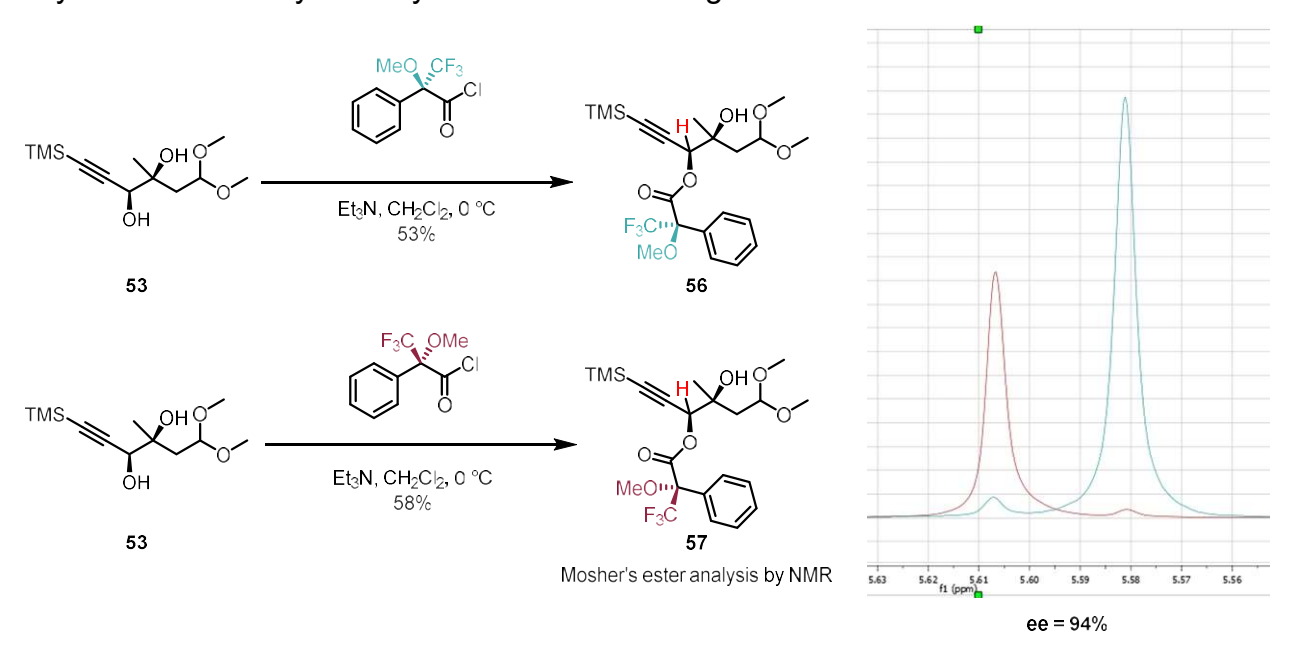


Figure 42: Mosher ester synthesis and NMR analysis

II.5. En route to goyazensolide

Figure 43: En route to goyazensolide

With the vinyl bromide **37** and the alkyne **55** in hand, Sonogashira coupling was performed followed by a treatment with PBr₃ to obtain the cyclization precursor **59** (Figure 43). Treatment of **59** with CrCl₂ in DMF afforded a clean transformation to the desired germacrene framework as a separable mixture of diastereoisomers (**60** and **61**) arising from the undefined stereocenter at C₆. Full NMR analysis didn't give clear conclusions on the stereochemistry of the two diastereoisomers, thus the two diastereoisomers were pushed until the last step (Synthesis with the diastereoisomer **60** described in the experimental section). Macrocycle **61** was treated with methacrylic anhydride followed by a selective deprotection of the propargyl acetate gave **63**. MnO₂ oxidation followed by a gold catalyzed transannulation gave the strained bicyclic framework **65**. Finally, deprotection of the TBDPS occurred smoothly in the presence

of HF/Pyr to obtain the single diastereoisomer (-)-goyazensolide **1.** The structure was confirmed by NMR and by optical activity found from the literature.

II.6. Partial conclusion

While the access of the sesquiterpene lactone goyazensolide is now available, this build-couple-pair strategy could be generalized and thus gave an opportunity to access to various furanoheliangolides. 5-*epi*-isogoyazensolide has been selected for its easy and quick accessibility.

III. Synthesis of 5-epi-isogoyazensolide

III.1. Retrosynthetic route

Figure 44: Retrosynthetic route of 5-epi-isogoyazensolide

To generalize the strategy, a second natural product, 5-*epi*-isogoyazensolide, was synthesized (Figure 44). It is interesting to note that intermediate **67** without the allylic alcohol was already described in the literature¹⁵⁴ and intermediate **55** was already used for the total synthesis of goyazensolide.

III.2. Synthesis of the chiral lactone 67

Figure 45: Synthetic route of intermediate 67

The route started by a treatment of the commercially available alcohol **68** with triethyl orthoacetate in acidic conditions to afford the diene **69** (Figure 45). ¹⁵⁵ A Sharpless dihydroxylation followed by the protection of the allylic alcohol with the trichloroacetamide **71** gave the lactone **72**. ¹³⁵ Bromination followed by treatment of Eschenmoser salt gave the α -exo-methylene- γ -butyrolactone **74**. ¹⁵⁴, ¹⁵⁶, ¹⁵⁷ Finally, the allylic oxidation afforded **67**.

III.3. Access to 5-epi-isogoyazensolide

Figure 46: End of 5-epi-isogoyazensolide synthetic route

With **55** and **67** in hand, Sonogashira coupling was performed to obtain **75** (Figure 46). The route continued as described for goyazensolide to finish by a deprotection of the *p*-methoxybenzyl alcohol **81** with DDQ to afford 5-*epi*-isogoyazensolide **66**. The access of 5-*epi*-isogoyazensolide is entirely stereoselective.

IV.Conclusion

A novel strategy was designed for the synthesis of furanoheliangolides. Most of the furanoheliangolides possess a methyl group in the south part of the structure (C₄ position) and an ideal starting point would be the "Primary cyclized intermediate" with

a methyl group in the south part of the structure (Figure 47).¹⁵⁹ It is interesting to note that modulations of the "primary cyclized intermediate" **82**, such as a chiral inversion at C₈ position and Meyer-Schuster type rearrangement at C₁₋₃ position would increase structural diversity (Synthesis of the "Primary cyclized intermediate described in the experimental section).

Figure 47: Structure of the « Primary cyclized intermediate » and the hot spots modulations 160, 161

Investigations continued in the laboratory and led to the optimization of the route (Sonogashira coupling, propargyl alcohol oxidation,...) and the synthesis of a significative number of other natural products (Figure 48). None of which had been previously synthesized.

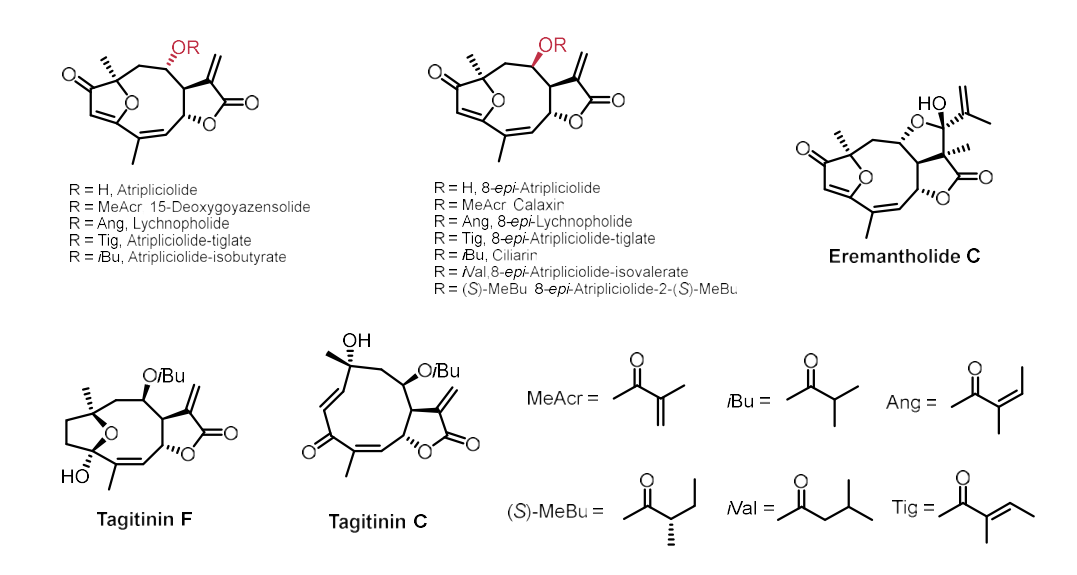


Figure 48: Non exhaustive list of natural products synthesized in the laboratory.

CHAPTER 3. Target identification

I. Natural products alkyne tagged as probes for target identification

The identification of small molecule-protein interactions is one of the main goals of chemical biology. There are several methods to identify the protein targets of bioactive compounds, such as chemical proteomics, haploinsufficiency profiling or resistance profiling. The incorporation of an alkyne on the natural product allows chemical modifications within the biological matrix, such as clicking a fluorophore or a biotinylated probe and thus, discriminating proteins of interest.

I.1. Proteome labeling

With the natural product goyazensolide in hand, it was then possible to synthesize a probe to target proteins. The alkyne tagged natural product was incubated in a lysate, clicked to a fluorophore and proteins were separated *via* SDS Page (Figure 49).

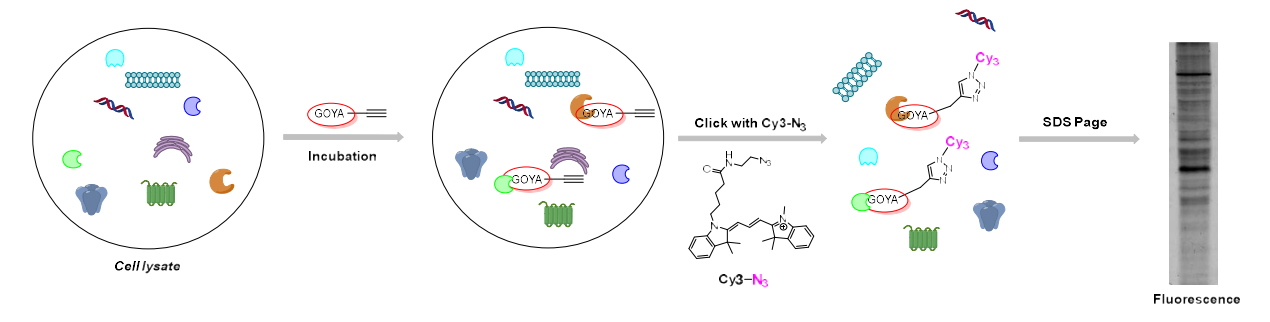


Figure 49: Schematic representation of the proteome labeling experiment with the alkyne tagged of goyazensolide

I.2. Probe design

I.2.1. Synthesis of the probe GOYA-1

Goyazensolide possesses a free primary allylic alcohol on the southern part of the structure. The alkyne was incorporated by reacting the natural product with pent-4-ynoyl chloride (Figure 50).

Figure 50: Synthesis of GOYA-1

I.2.2. Gel base assay with GOYA-1

The labeling experiment used Helenalin probe as control (already synthesized in the laboratory).

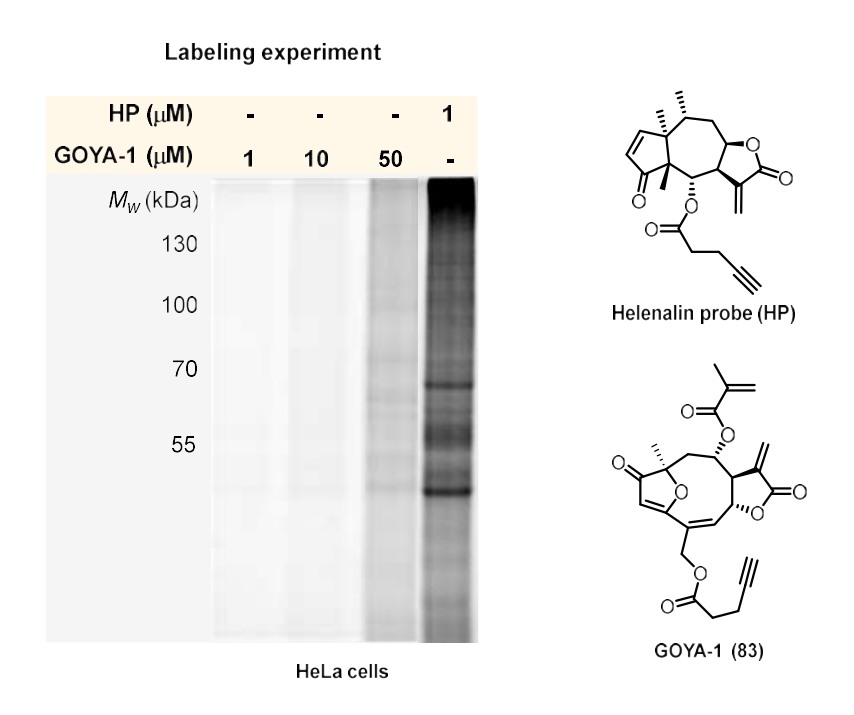


Figure 51: Proteome labeling with an increasing concentration of GOYA-1

A range of concentrations of GOYA-1 was used and incubated in a HeLa cell lysate. Then, Cy3-N₃ with the click reagents were added and incubated, followed by a SDS Page. Even at high concentration the signal is extremely low (Figure 51). With this disappointing result in hand, a click reaction in blank conditions (without the lysate) was tested and confirmed that the probe reacted correctly with Cy3-N₃ to give the click product GOYA-1-Cy3 (See experimental section). Temperature and incubation time were then screened but no improvement was observed (Figure 52).

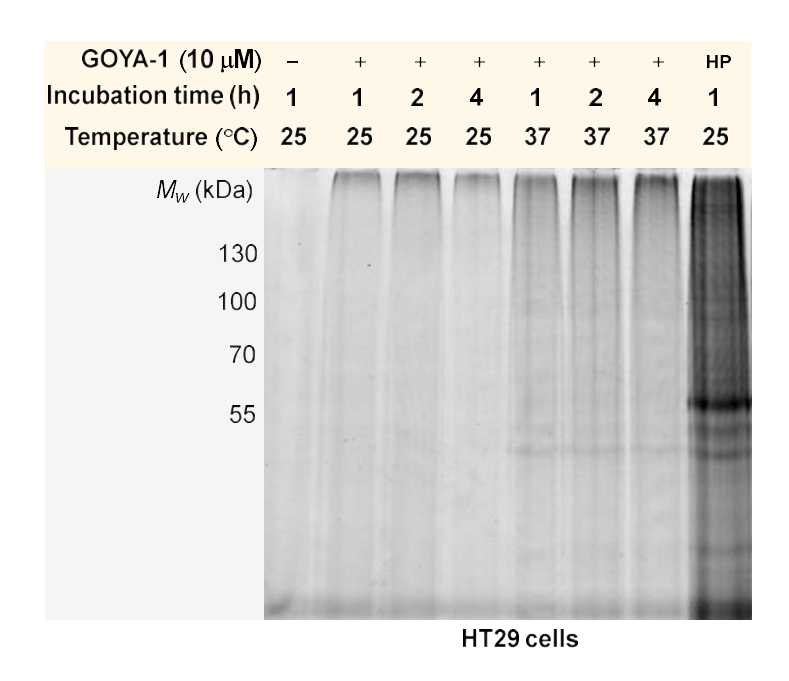


Figure 52: Temperature and incubation time screening

These results demonstrated that the probe had problems labeling proteins for unknown reasons (hydrolysis of the ester?). The next step was the substitution of the allylic alcohol of goyazensolide to an azide to obtain GOYA-N₃.

I.2.3. Synthesis of the probe GOYA-N₃

Figure 53: Synthesis of GOYA-N₃

The synthesis of GOYA-N₃ started with the activation of the allylic alcohol by tosyl chloride followed by a nucleophilic substitution of the azide group. Unfortunately, the nucleophilic substitution gave a single compound which was the isogoyazensolide scaffold through a SN2' reaction (Figure 54). The stereochemistry was determined by NOESY.

Figure 54: Unexpected synthesis of ISOGOYA-N₃

This result could explain the loss of signal from GOYA-1. Indeed, if a protein attacked the 1,6-dienone at the C_6 position, it may remove the alkyne by elimination of the ester and thus, eliminate the possibility to incorporate the fluorophore. The obtention of the compound **85** is not the best-case scenario to continue the target identification. This scaffold would allow the detection of false positive results due to the structural differences with goyazensolide **1**. Furthermore, a secondary azide will be more difficult to react compared to a primary azide. Finally, the choice was prioritised to incorporate the alkyne on the side chain of the natural product.

I.2.4. Synthesis of the probe GOYA-2

Figure 55: Synthetic route of GOYA-2

To synthesize GOYA-2, a methacrylate side chain analog must be designed with an alkyne tag to react with the secondary alcohol of the macrocycle **61** (Figure 55). The anhydride **87** has been synthesized from the nucleophilic substitution of propargyl alcohol with the allyl bromide followed by HCI treatment to give the carboxylic acid **86**. A Yamaguchi esterification didn't afford the formation of the asymmetric but the symmetric anhydride **87**. The next steps were the same as goyazensolide synthetic route previously described.

I.2.5. Gel base assay with GOYA-2

With GOYA-2 in hand, the proteome labeling experiment was performed. The labeling with GOYA-2 and Cy3 as fluorophore revealed a strong band at around 120 kDa and was selectively competed in the presence of the natural product as the competitor (Figure 56).

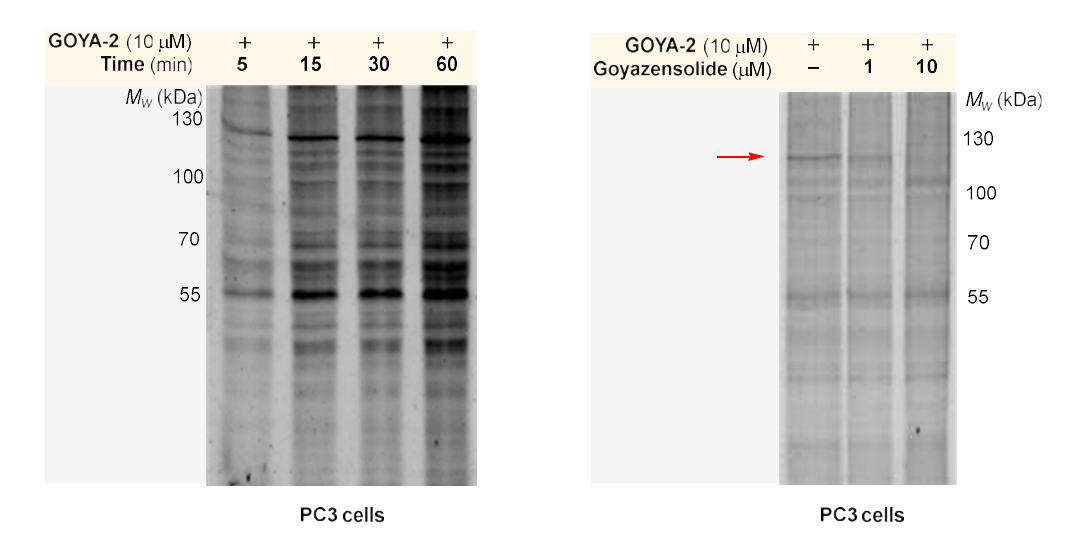


Figure 56: Proteome labeling with GOYA-2 and Cy3-N₃. (*Left*) Labeling with different incubation times; (*Right*) Labeling competition experiment showing the disappearance of a specific band in the presence of goyazensolide

Five other cancer cell lines were tested and showed the same profile (Figure 57).

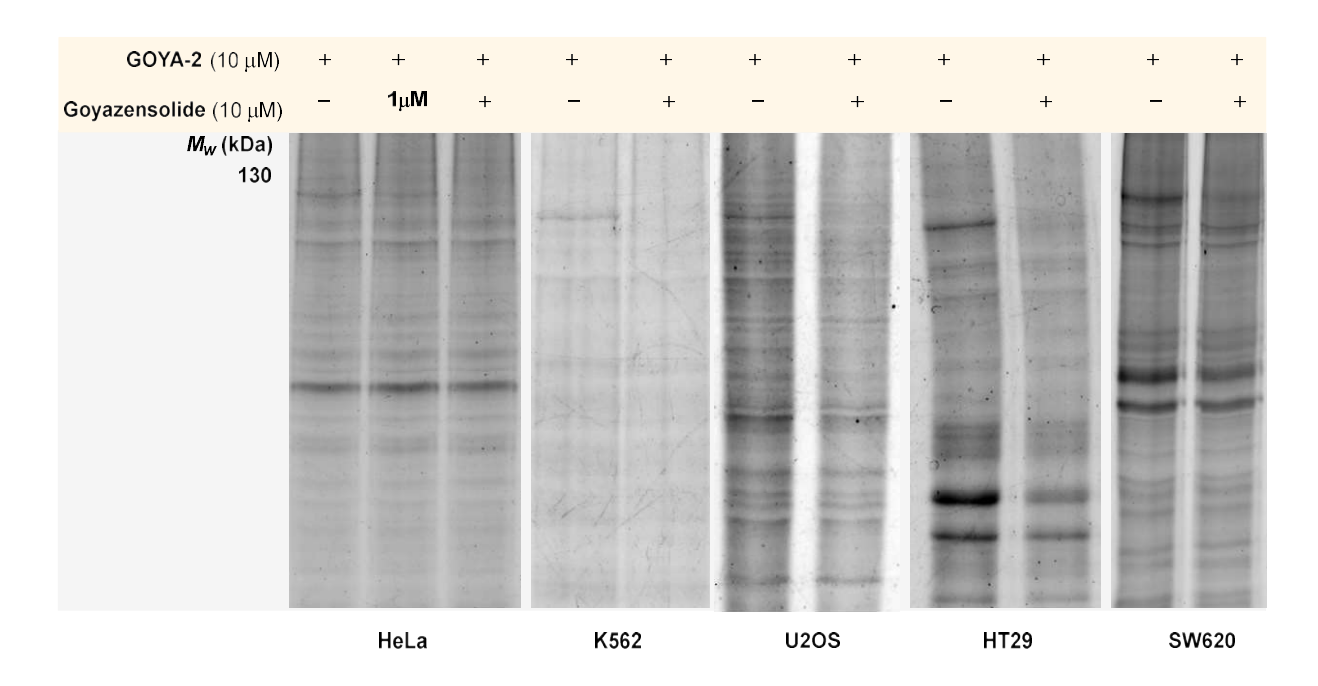


Figure 57: Labeling competition experiment on 5 different cancer cell lines

I.2.6. A second band at 38kDa in A549 cells

A strong and specific band at around 38 kDa was observed with A549 cell line for the labeling/competition with goyazensolide (Figure 58).

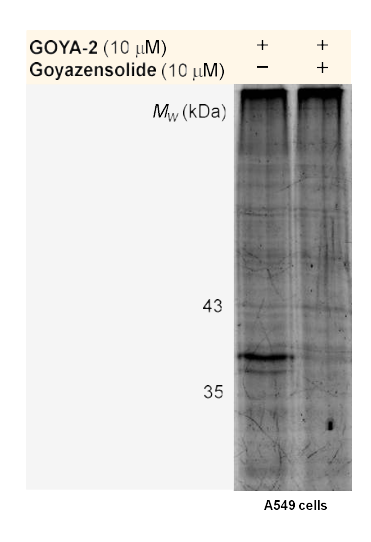


Figure 58: Labeling competition experiment on A549 cell line revealed a second specific band at 38 kDa

After a pulldown experiment, the band was cut and digested. MS/MS analysis has detected **Annexin A2** as the major protein. Further investigations have shown a competition with other sesquiterpene lactones (Helenalin, deoxyelephantopin). In consequence, this target is not specific to goyazensolide and investigations will be focused on the specific band at around 120 kDa. Details of these investigations are described in the experimental section.

II. Protein of interest determination

II.1. Target enrichment

As indicated in Figure 59, targets of interest can be enriched by immobilization on streptavidin beads *via* a biotin/desthiobiotin tag.

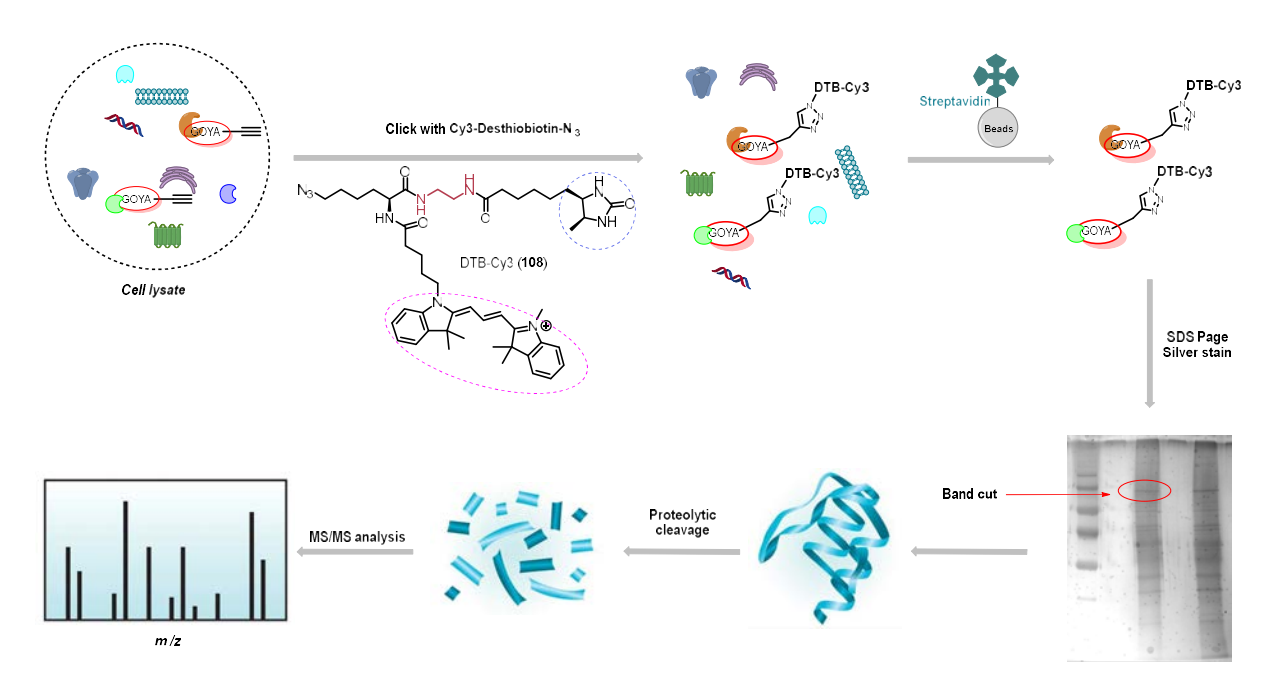


Figure 59: Schematic representation of the target identification process

II.2. Pull-down experiment with desthiobiotin

Investigations started by incubating a cell lysate with GOYA-2 prior to clicking a desthiobiotin with a fluorophore incorporated *via* a CuAAC reaction (preincubation with goyazensolide for the competition experiment). Proteins were precipitated, washed to remove excess of desthiobiotin and resolubilized to perform immobilization on streptavidin beads. Proteins were separated by SDS Page and silver stain gel revealed a band at around 120 kDa as observed in the labeling by fluorescence (Figure 60). Surprisingly, the band was observed in the pull-down labeling as well as in the pull-down competition. Does the band observed by fluorescence was the same as observed by silver stain? The band was cut, digested, and analyzed by MS/MS.

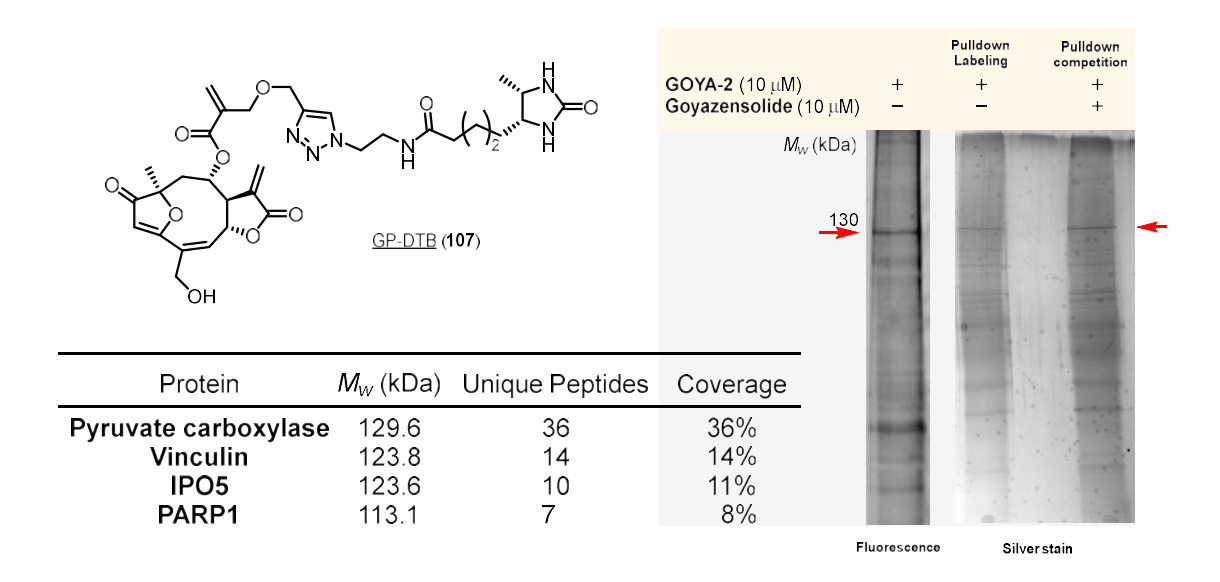


Figure 60: Pull-down experiment with desthiobiotin (Fluorescence gel as a reference).

Data processing was performed by Maxquant software, and the protein selection method was based on the number of unique peptides, molecular weight and intensity. The major protein detected was pyruvate carboxylase: a protein which naturally possesses a biotin, which represented a typical false positive. This result was consistent as the protein of interest shouldn't be detected in the pull-down competition experiment.

In order to cut the band observed by fluorescence after the pull-down, a new chemical entity which possesses a desthiobiotin as well as a fluorophore Cy3 has been synthesized.

II.3. Pull-down experiment with DTB-Cy3

The desthiobiotin moiety and the Cy3 motif were incorporated on a lysine azide (Figure 61) to afford desthiobiotin-Cy3 azide (DTB-Cy3).

Figure 61: Structure of the three generations of DTB-Cy3

Three generations of DTB-Cy3 have been designed and tested during the pull-down optimization sequence. The different lengths of the linker did not show any difference.

Cell lysate was incubated with GOYA-2 and then clicked with DTB-Cy3. Tagged proteins were immobilized on streptavidin beads. After elution, proteins were separated by SDS Page, and the band of interest was determined by fluorescence (Figure 62).

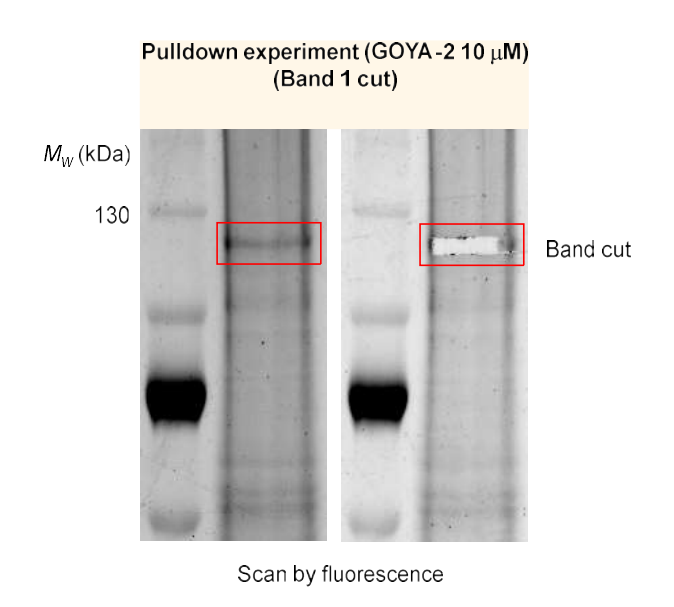


Figure 62: Pull-down labeling experiment with DTB-Cy3 followed by the band cut

II.4. InGel digestion

Once the band of interest was cut (Figure 62) in small pieces, treatment with DTT followed by iodoacetamide was performed to avoid any formation of disulfide bond. Optimized digestion conditions were obtained with a triple digestion by trypsin, chymotrypsin and GluC.

II.5. MS/MS analysis

The band of interest localized at around 120 kDa detected Importin-5 (IPO5) as the major protein. A triple digestion trypsin/GluC/chymotrypsin is required. Indeed, simple digestion gave a very poor coverage of IPO5 and was detected as a minor protein. Other proteins were detected with lower number of unique peptides, sequence coverage and intensity (Table 1). Within the top 4 proteins, pyruvate carboxylase has been detected followed by ubiquitin-like modifier-activating enzyme 1 (UBA1) and ATP-citrate synthase (ACLY). These two other remaining proteins were then tested by a specific antibody.

Table 1: Raw data of top 8 protein list. Selection by number of unique peptides, molecular weight and intensity

	Description	Coverage	Unique peptides	MW [kDa]
1	Importin-5 OS=Homo sapiens	40.65634	63	123.55
2	Pyruvate carboxylase, mitoch OS	32.85229	52	129.55
3	Heterog. nuclear ribonucleoprotein U OS	28.84848	33	90.528
4	Acetyl-CoA carboxylase 1 OS	10.99744	27	265.39
5	Keratin, type II cytoskeletal 1 OS	36.3354	26	65.999
6	Ubiquitin-like modifier-activ. Enzyme 1 OS	17.76938	19	117.77
7	AlaninetRNA ligase, cytoplasmic OS	17.56198	19	106.74
8	ATP-citrate synthase OS=Homo sapiens	13.44233	18	120.76

II.6. Target confirmation by antibody

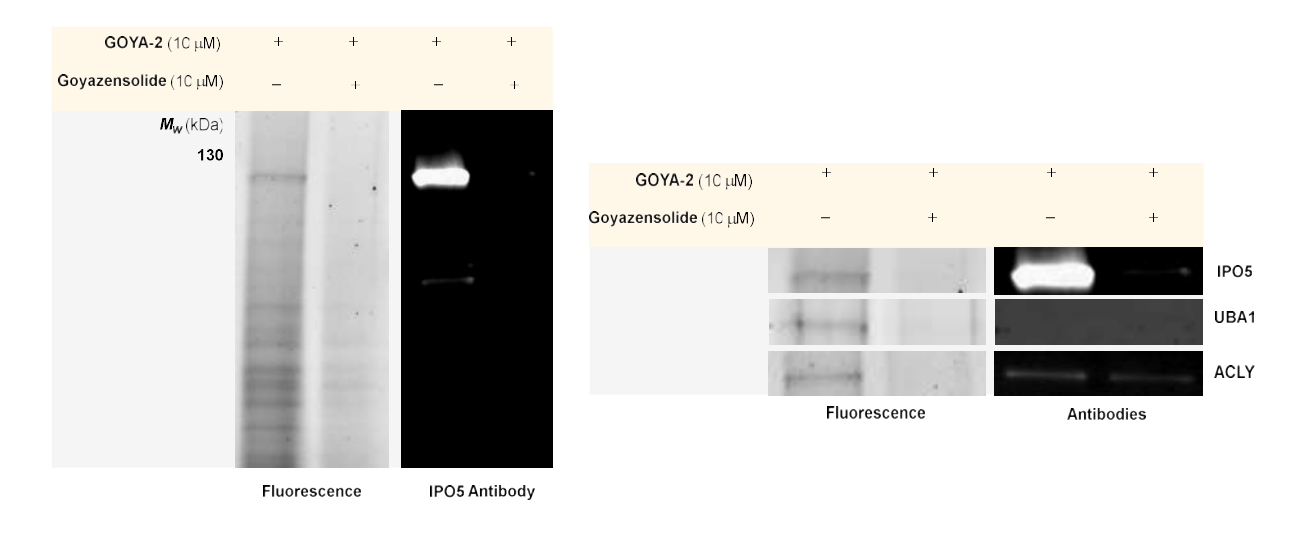


Figure 63: Immunoblot of competitive pull-down labeling experiment with DTB-Cy3 followed by the use of specific antibodies

The positive result by a specific antibody for IPO5 confirmed the identity of the target (Figure 63). Moreover, the use of UBA1 and ACLY antibodies didn't reveal any signal.

II.7. Selectivity versus other importins

Once IPO5 was confirmed as goyazensolide's target, the selectivity versus other importins was tested. Several pull-down experiments have been carried out followed by the use of KPNB1, KPNB2, IPO7, IPO8 and IPO12 antibodies as shown in Figure 64. None of the five other importins were targeted by goyazensolide.

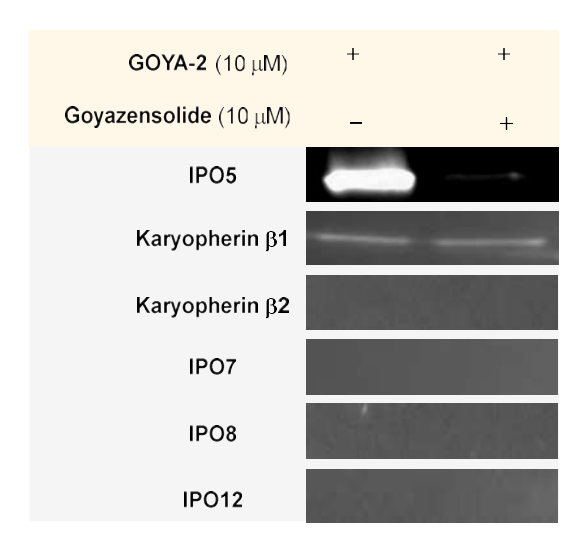


Figure 64: Immunoblots of competitive pull-down labeling experiments with DTB-Cy3 which demonstrates the selectivity of goyazensolide versus other importins

III. Conclusion

The target identification process afforded the discovery of IPO5 as the target of goyazensolide and confers a particular interest due to its selectivity. To the best of our knowledge, no pharmacological modulators of IPO5 have been reported to date. In consequence, goyazensolide is a tool of choice to investigate potential modulations of IPO5 activities.

CHAPTER 4. Biological activity

I. The nuclear transport protein Importin-5

I.1. Presentation

In 1997, a 124 kDa protein was identified and characterized as a novel Ran binding protein and named RanBP5. 166 This protein is related to importin β family, a part of the karyopherin superfamily. 167 Thus, RanBP5 can be called IPO5, importin-5, importin β -3, karyopherin β 3 or KPNB3. In these initial reports, IPO5/RanBP5 (hereafter referred to as IPO5) was found to bind short amino acid sequences called nuclear localization sequences (NLSs) in proteins that were actively imported to the nucleus from the cytosol. IPO5 has been shown to mediate the nuclear import of not only cellular proteins, but also viral proteins. $^{168-170}$ In fact, crucial signaling pathways, such as the RAS pathway and viral replication processes, involve IPO5-dependent nuclear import steps. $^{171-173}$ The constant and increasing number of publications demonstrates an interest as a potential therapeutic target due its crucial role in protein trafficking. 174

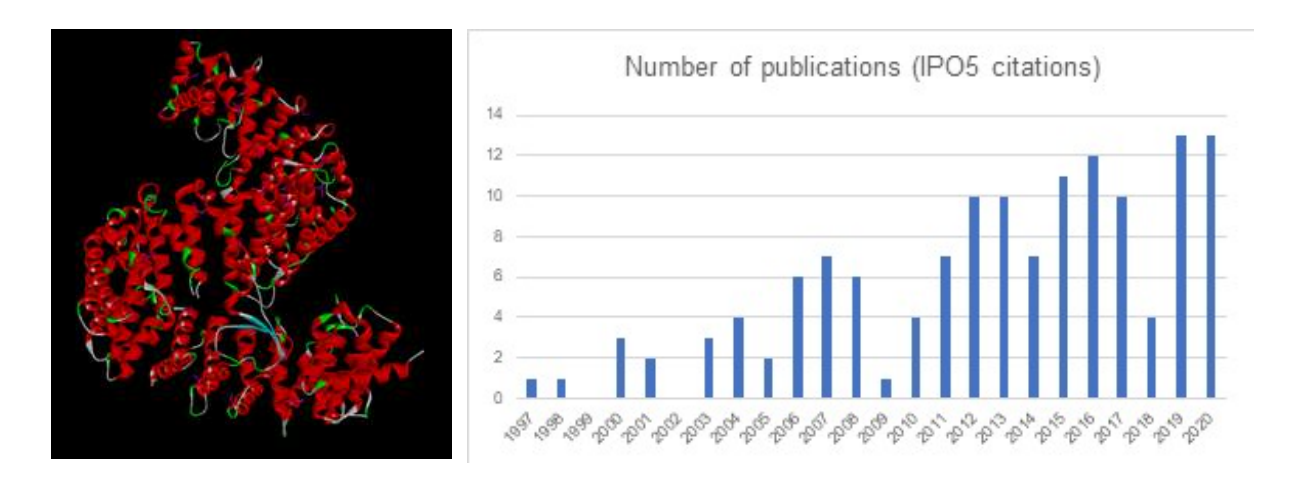


Figure 65: (Left) Crystal structure of IPO5 (6xte). (Right) Number of publications per year in which IPO5 is mentioned

I.2. RASAL-2 translocation

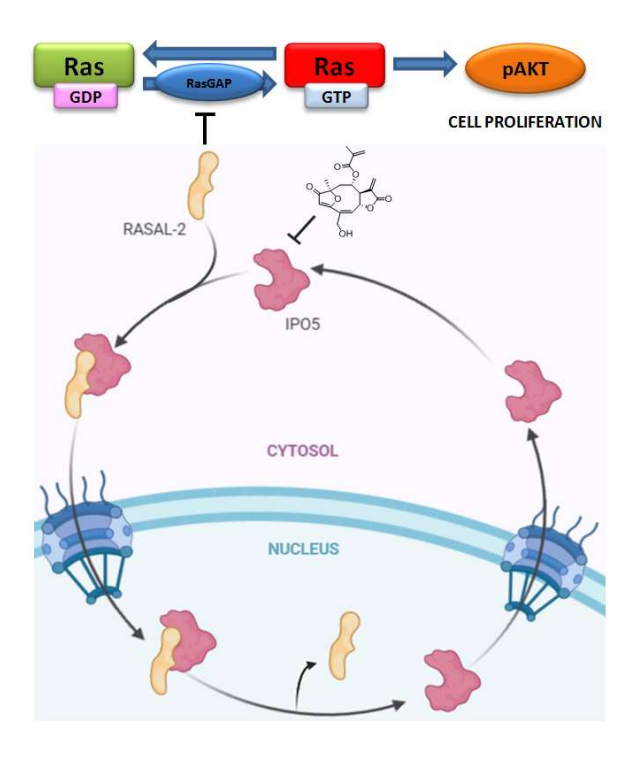


Figure 66: Illustrative overview of the IPO5 nuclear import cycle. Nuclear import of a cargo protein bearing a NLS mediated by IPO5. This illustration was created with Biorender (http://biorender.com)

IPO5 has been shown to be involved in the transport of RAS protein activator-like 2 (RASAL2) to the nucleus, a negative regulator of RasGAP (Figure 66). Thus, nuclear translocation of RASAL2 frees RasGAP to convert inactive Ras-GDP to active Ras-GTP.¹⁷³ It is interesting to note that the RAS pathway induces phosphorylation of protein kinase B (AKT).

I.3. Impact of goyazensolide on RASAL-2 translocation

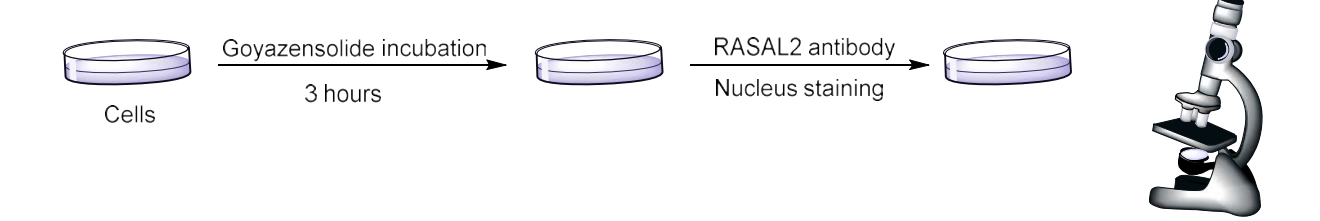


Figure 67: Illustrative representation of the RASAL2 cytosolic/nuclear ratio measurement.

Zhang et al. has demonstrated that the ratio of cytosolic RASAL2 was clearly shown to depend on IPO5 using siRNA silencing of IPO5 (increased cytosolic concentration of RASAL2) and IPO5 overexpression (decreased cytosolic concentration of RASAL2). In order to understand if goyazensolide could phenocopy the silencing activity of siRNA targeting IPO5, a SW620 colon cancer cell line was used to measure the RASAL2 ratio in the cytosol versus the nucleus in the presence and the absence of goyazensolide (Figure 67). In the absence of treatment, the cytosolic/nuclear ratio of RASAL2 is 1.2 (Figure 68). Upon treatment with 1.0 or 2.5 μ M of goyazensolide for 3 hours, the ratio increased to 1.8 and 2.0 respectively. Thus, goyazensolide treatment led to an increased cytosolic/nuclear ratio of RASAL2 in a dose dependent manner.

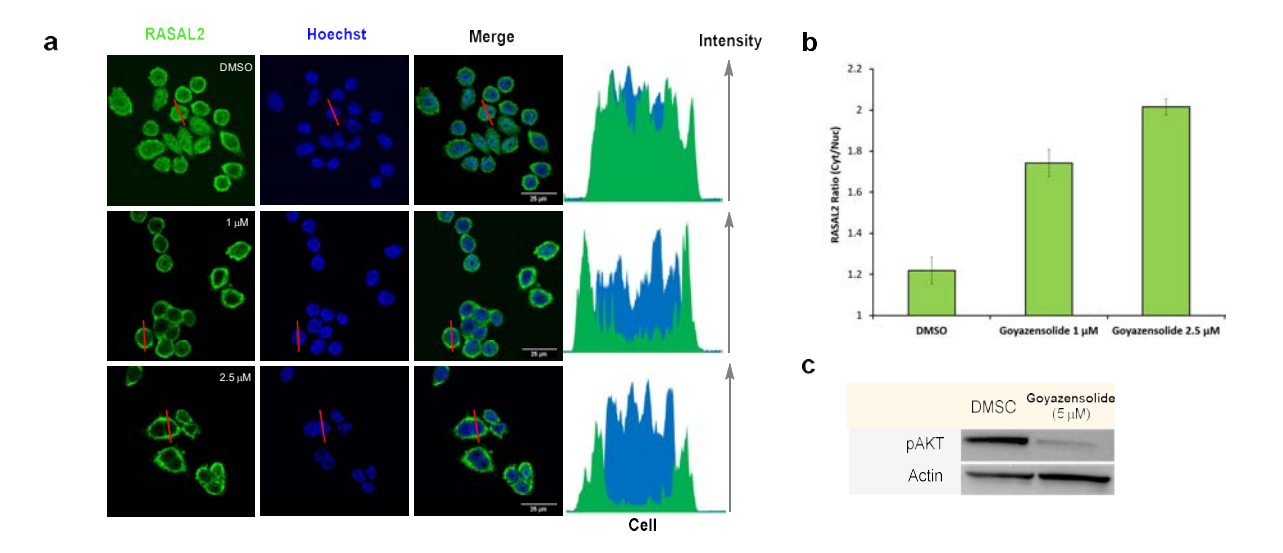


Figure 68: *(a)* Confocal microscopy images of SW620 cells treated with DMSO or 1 or 2.5 mM goyazensolide for 3 h, imaging of localization of RASAL2 using a RASAL2 primary antibody followed by an Alexa fluor488 secondary antibody (green), nuclear stain with Hoescht (blue), and fluorescence quantification of the images. Fluorescence intensity profile across the red line is shown on the right. *(b)* Ratio of fluorescence in cytosol versus nucleus (number of cells > 15). *(c)* Immunoblot of pAKT (pAKT Ser473) expression upon treatment of SW620 cells with DMSO or goyazensolide (5 μM, 4 h)

I.4. Downstream effect of RASAL-2 translocation inhibition

Since the inhibition of RASAL2 translocation to the nucleus should have a downstream effect on the amount of pAKT, level of pAKT (Ser473) was also monitored in the presence or absence of drug. As shown in Figure 68c and in Figure 69, treatment with 5 μ M of goyazensolide led to a dramatic reduction of pAKT. Collectively, these

experiments demonstrate that IPO5 is the target of goyazensolide and that covalent engagement of IPO5 inhibits its transport activity *in-cellulo*.

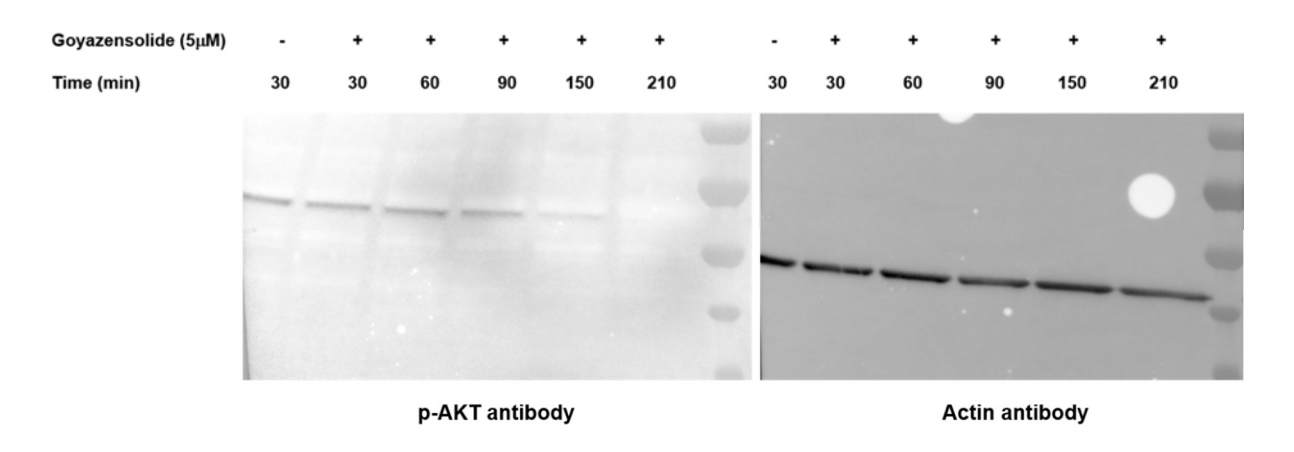


Figure 69: Time-/Dose-dependent manner of pAKT assay. Immunoblot of p-AKT (p-AKT Ser473 antibody) expression upon treatment of SW620 cells with DMSO or goyazensolide (5 μM)

I.5. Pulldown of IPO5 by the NLSs immobilized on beads

IPO5 has been shown to be recruited by influenza A to transport essential cargo to the nucleus, and disruption of the interaction between the NLS of the influenza A protein PB1 and IPO5 inhibits viral replication. IPO5 is also important for the transport of viral proteins of HCV and HIV. IPO5 To test whether goyazensolide was effective at inhibiting the interaction between IPO5 and the NLSs of viral proteins, the sequences NLS-1 (NLS of Rev; HIV) and NLS-2 (NLS of PB1; influenza A) were coupled to biotin tags and loaded on magnetic beads for pull-down experiments with IPO5 (Figure 70, see Supporting information for the NLSs synthesis).

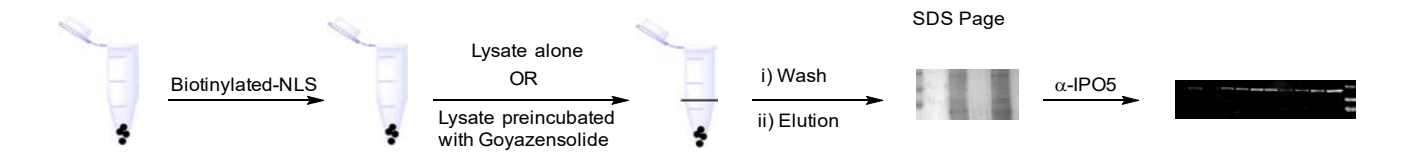


Figure 70: Illustrative representation of the NLS pull-down experiment

In the absence of an inhibitor, both NLS sequences effectively pulled-down IPO5, as observed in a Western blot of the elution fraction (Figure 71). Addition of goyazensolide (10 μ M) to the cell lysates prior to the addition of the beads inhibits the pull-down of IPO5. Thus, the covalent interaction between goyazensolide and IPO5 inhibits its interaction with these two NLSs.

NLS-1 = TRQARRNRRRRWRERQR-DAP-Biotin
NLS-2 = FQRKRRVRDNMTKKMVTQRTIGKRKQRLN-DAP-Biotin



Figure 71: Immunoblot of the NLS pull-down experiment

II. Conclusion

The fact that a small molecule can outcompete a high affinity interaction with larger molecular entities such as the interaction of transportin with a NLS sequence of a protein underpins the unique features of covalent inhibitors. Transport of cargo between the cytoplasm and nucleus is a highly regulated process with the nuclear pore complex acting as a molecular sieve restricting diffusion. Translocation thus requires active transport leveraged on the action of a superfamily of karyopherin (importin and exportin). The ability to modulate this traffic with small molecules is empowering, but there are only few examples thus far. The finding that goyazensolide selectively engages IPO5 covalently and inhibits its interaction with cargo rationalizes its anticancer activity and points to potential antiviral applications.

CHAPTER 5. Binding mode

I. Binding mode

I.1. Synthesis/Competition with truncated Michael acceptors analogs

In order to determine which Michael acceptor of goyazensolide reacts with IPO5, several compounds with truncated Michael acceptors were synthesized (Figure 72).

Figure 72: Synthetic route of the truncated Michael acceptors analogs

To obtain the truncated Michael acceptor 1 (MA1), the methacrylate side chain was replaced by an isobutyl side chain to obtain **93**. MA2 required the use of the Stryker reagent¹⁸¹ to selectively reduced the exo-methylene and gave the exo-methyl intermediate **98**. The fastest and easiest way to obtain an analog with the truncated

1,6 dienone was to deprotect the intermediate **64** (from goyazensolide's route). Competitions were performed with these analogs and the unexpectedly synthesized ISOGOYA-N₃.

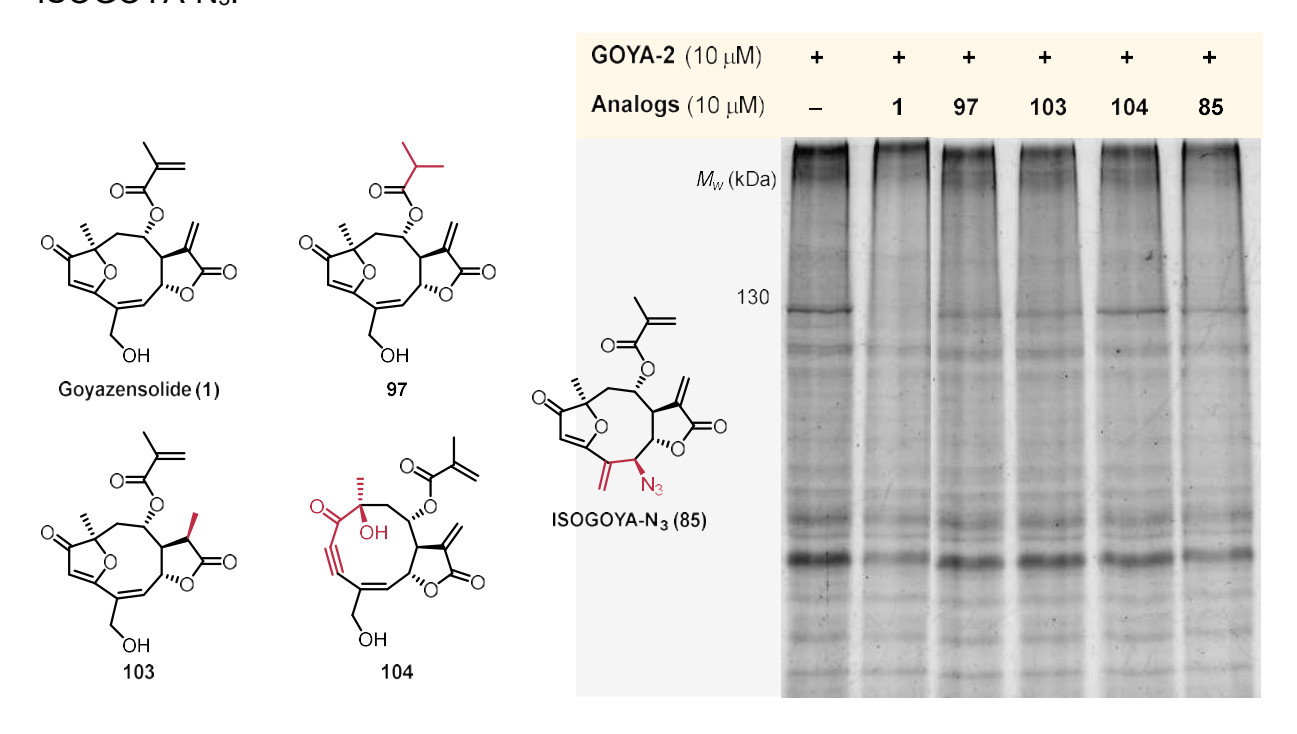


Figure 73: Competition with truncated Michael acceptors analogs (Cy3 used as fluorophore).

As observed in Figure 73, the complete competition with goyazensolide slightly differs with the partial competition with analogs **97**, **103** and ISOGOYA-N₃ (**85**). Nevertheless, no competition was observed with analogs **104**. No definitive conclusions can be drawn as analog **104** scaffold is too different from goyazensolide scaffold and the other analogs didn't completely compete with the natural product.

I.2. Competition with other natural products

Competitions with various sesquiterpene lactones versus GOYA-2 were performed. A series of natural products were selected with identical or similar Michael acceptors such as deoxyelephantopin, helenalin, cnicin, cynaropicrin and lactucin. Two other natural products were included bearing different Michael acceptors: thapsigargin and withaferin A (Figure 74).

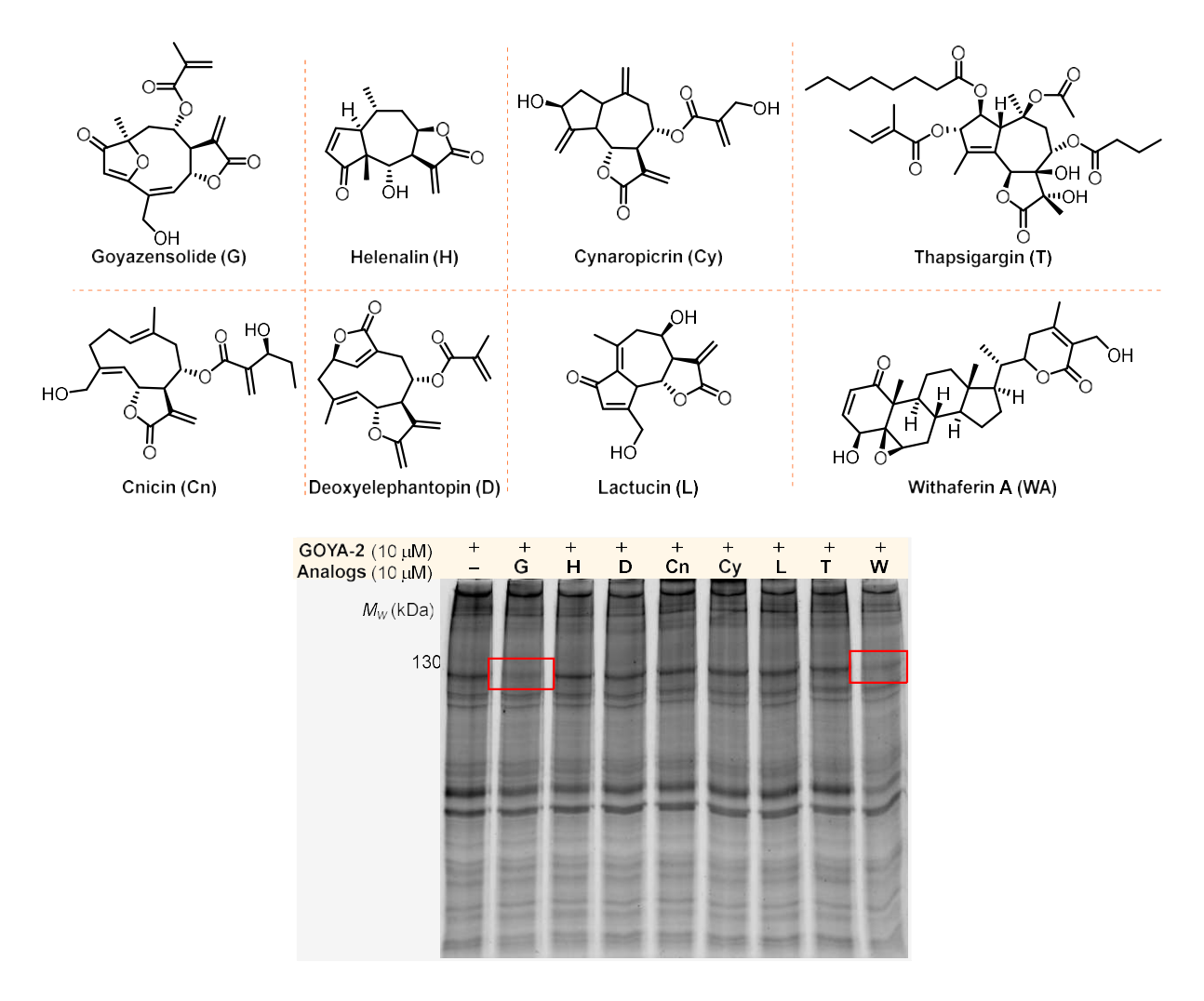


Figure 74: Competition experiment of GOYA-2 with various natural products (Cy3 used as fluorophore).

The competition of GOYA-2 with various sesquiterpene lactones indicated that none of them binds to the same target as goyazensolide (Figure 74). Surprisingly, the steroidal lactone withaferin A binds IPO5. Further investigations of withaferin A were described in Chapter 6.

I.3. Synthesis and comparison of various natural products probes

Additional probes from natural sesquiterpene lactones have been synthesized and tested to investigate the selectivity of goyazensolide (Figure 75).

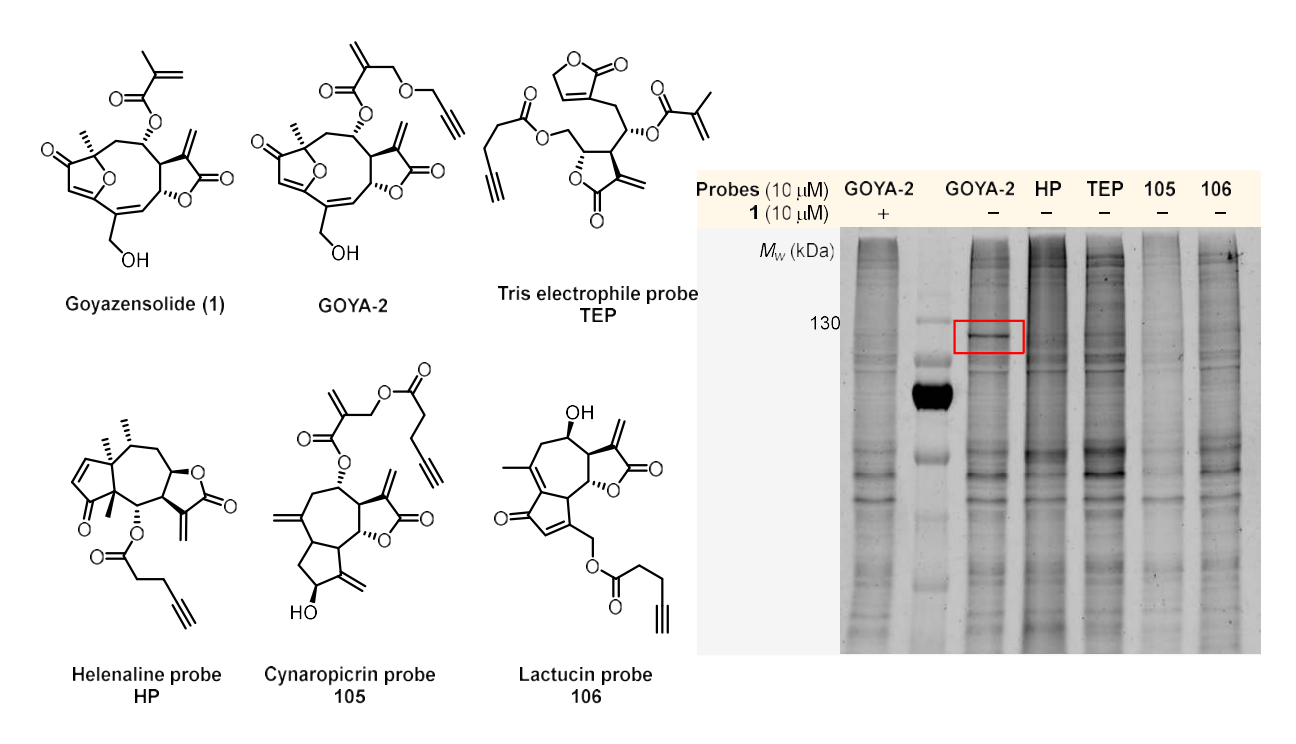


Figure 75: Labeling experiment comparison of GOYA-2 with various probes (Cy3 used as fluorophore)

No strong band at around 120 kDa was observed for the other probes, which confirms the selective nature of goyazensolide.

I.4. Competition of analogs versus GOYA-2

A collection of furanoheliangolides and analogs were synthesized in the laboratory and have been tested to evaluate a potential binding with IPO5.

The experiment used GOYA-2 in competition with a series of natural products (Figure 76). The assay revealed that only atripliciolide was as effective as goyazensolide, suggesting that the interaction of goyazensolide with IPO5 may not require the acrylate side chain at C₈. However, the C₈ stereochemistry has an impact on the binding efficiency as shown by the difference of competition between a-e versus f-I (Figure 77).

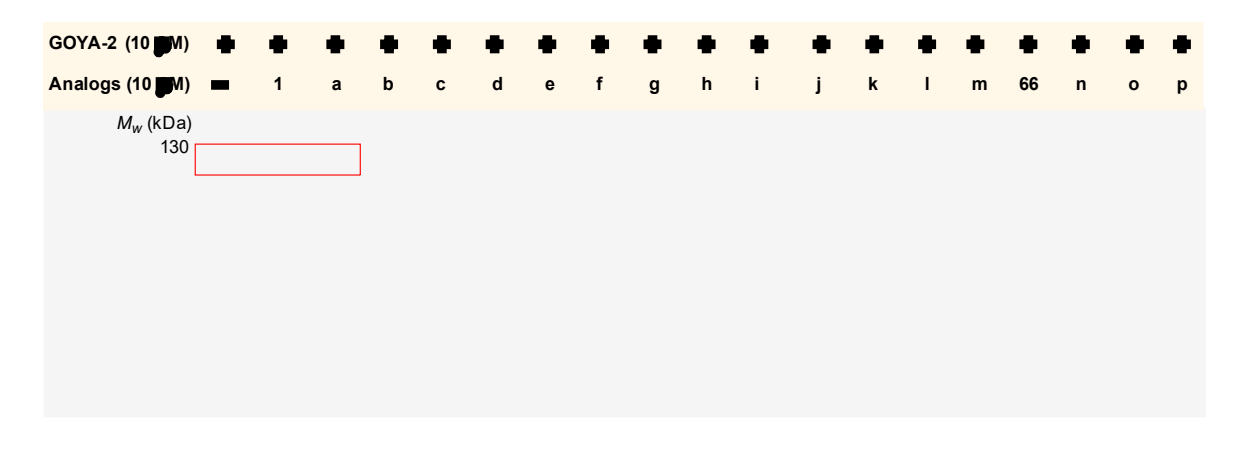


Figure 76: Competition experiment of GOYA-2 with various synthesized natural products (p is 15-deoxygoyazensolide stereoisomer, Cy3 used as fluorophore)

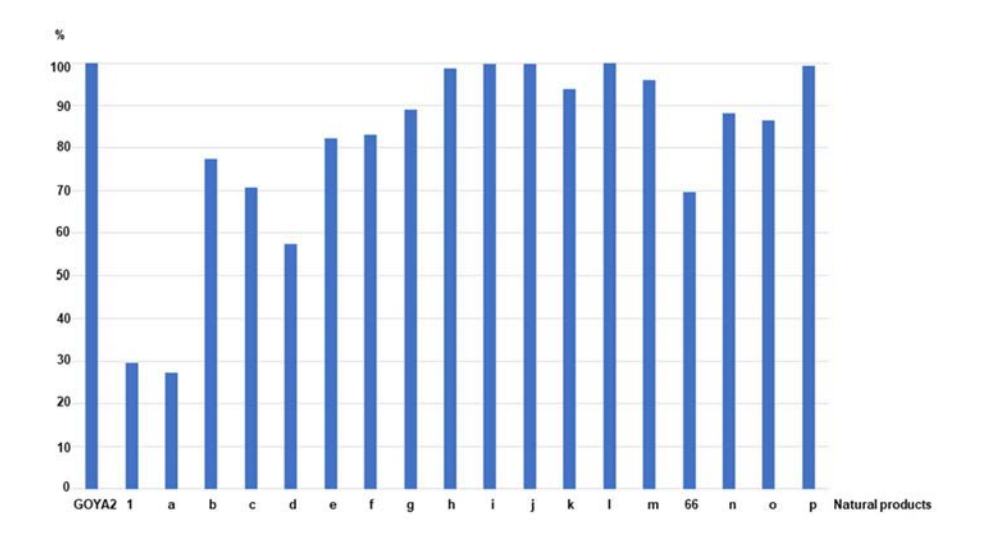


Figure 77: Binding efficiency. Difference of binding efficiency by comparison of compounds a-e versus f-l is observed. The C₈ stereochemistry plays a role in the binding efficiency

I.5. Comparison between goyazensolide, atripliciolide and deoxygoyazensolide

I.5.1. IPO5 binding capacity

A competition in a dose dependent manner has been investigated between the two IPO5 binders (goyazensolide and atripliciolide) and the very similar non-binder 15-deoxygoyazensolide (Figure 78).

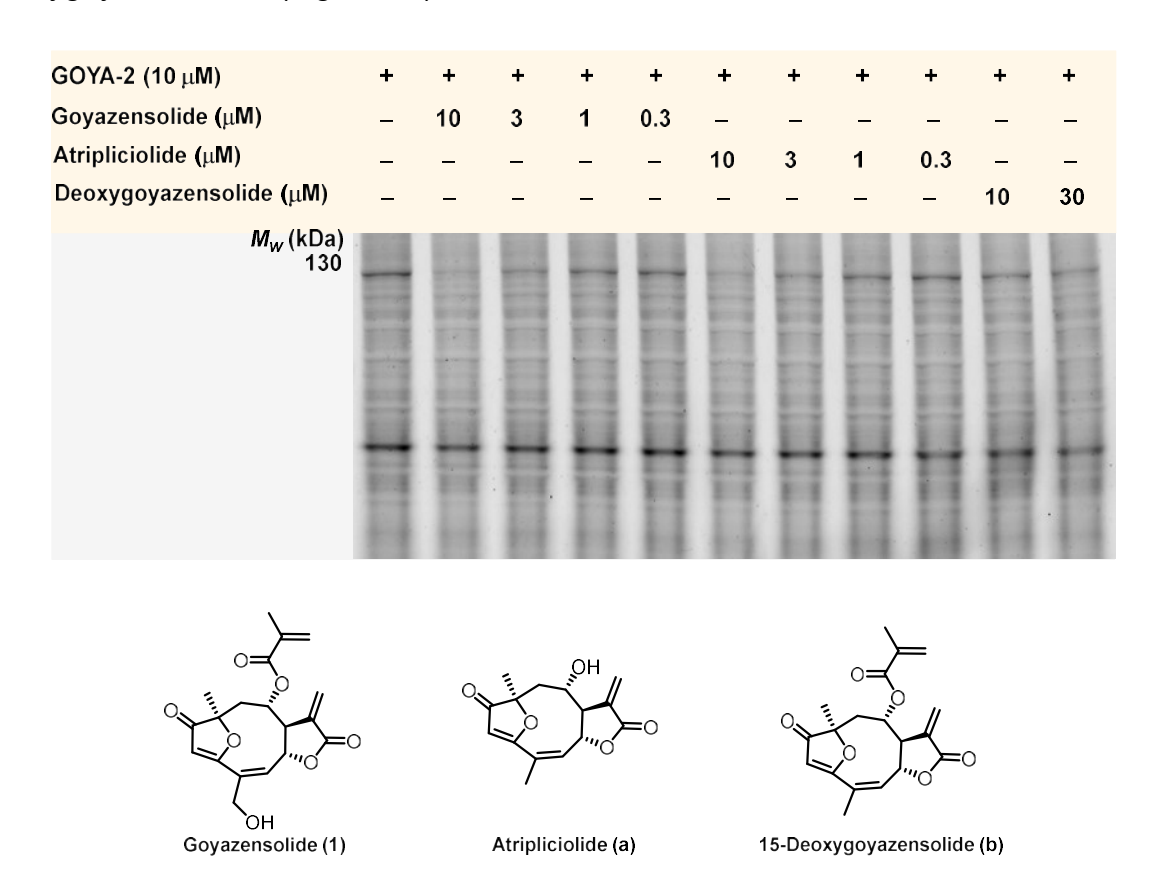


Figure 78: Dose response of GOYA-2 in competition with goyazensolide, atripliciolide or 15-deoxygoyazensolide (Cy3 used as fluorophore)

It is clear that goyazensolide and atripliciolide react in a dose dependent manner while 15-deoxygoyazensolide does not compete. As the global morphology seems similar, the Michael acceptors reactivity is expected to be similar. Nevertheless, experimental observations demonstrated a clear difference.

I.5.2. Reaction with glutathione monitored by LC-MS

Natural products were incubated with an excess of glutathione (GSH) in order to determine the number of reactive Michael acceptors.

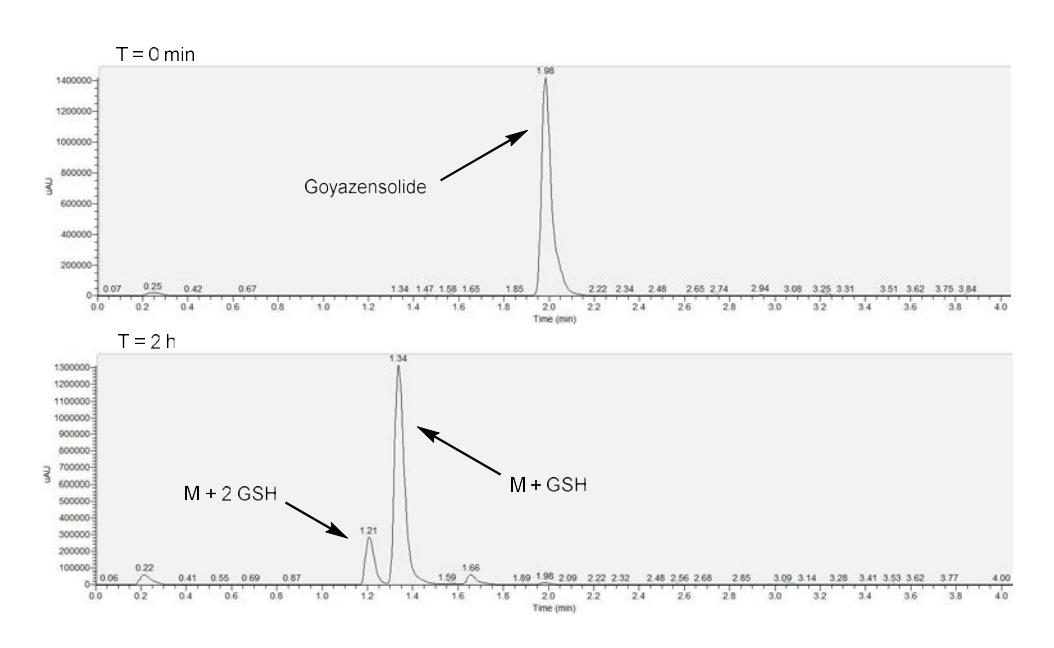
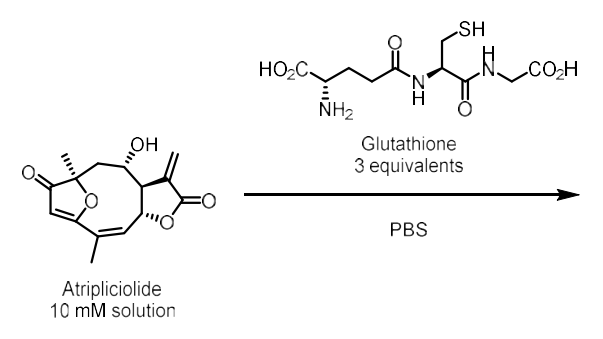


Figure 79: LC-MS monitoring of the reaction between goyazensolide and glutathione



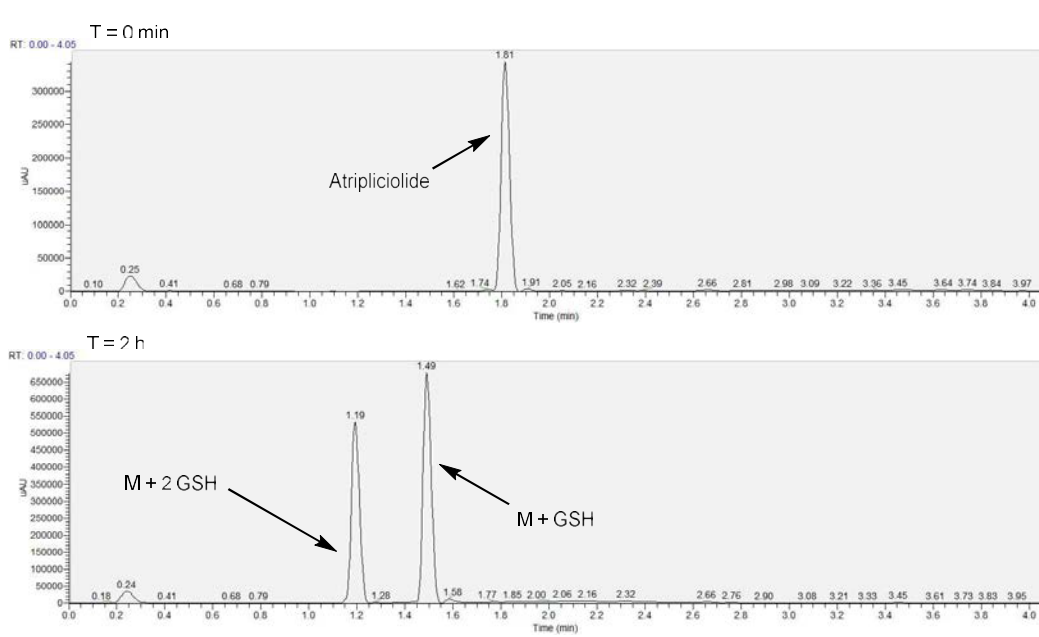


Figure 80: LC-MS monitoring of the reaction between atripliciolide and glutathione

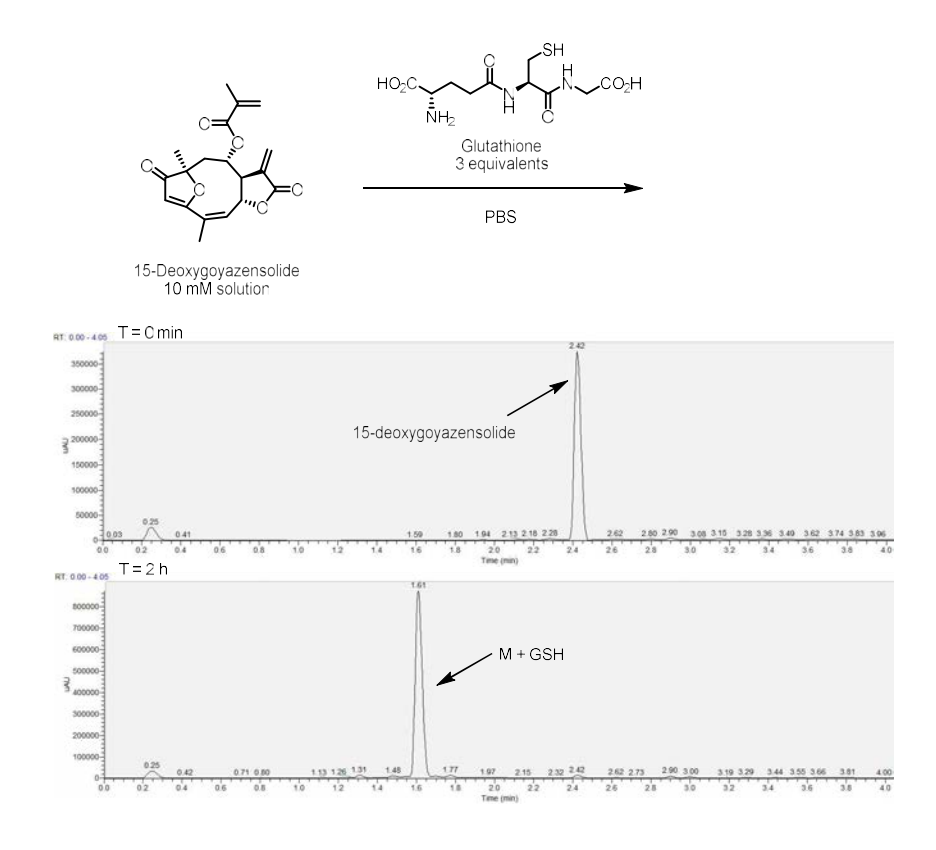


Figure 81: LC-MS monitoring of the reaction between 15-deoxygoyazensolide and glutathione

LC-MS monitoring of goyazensolide indicated a quasi-exclusive mono-addition of glutathione and 15-deoxygoyazensolide gave an exclusive mono-addition while atripliciolide is able to react with two glutathiones (Figure 79, Figure 80, Figure 81).

I.5.3. Reaction with glutathione monitored by NMR

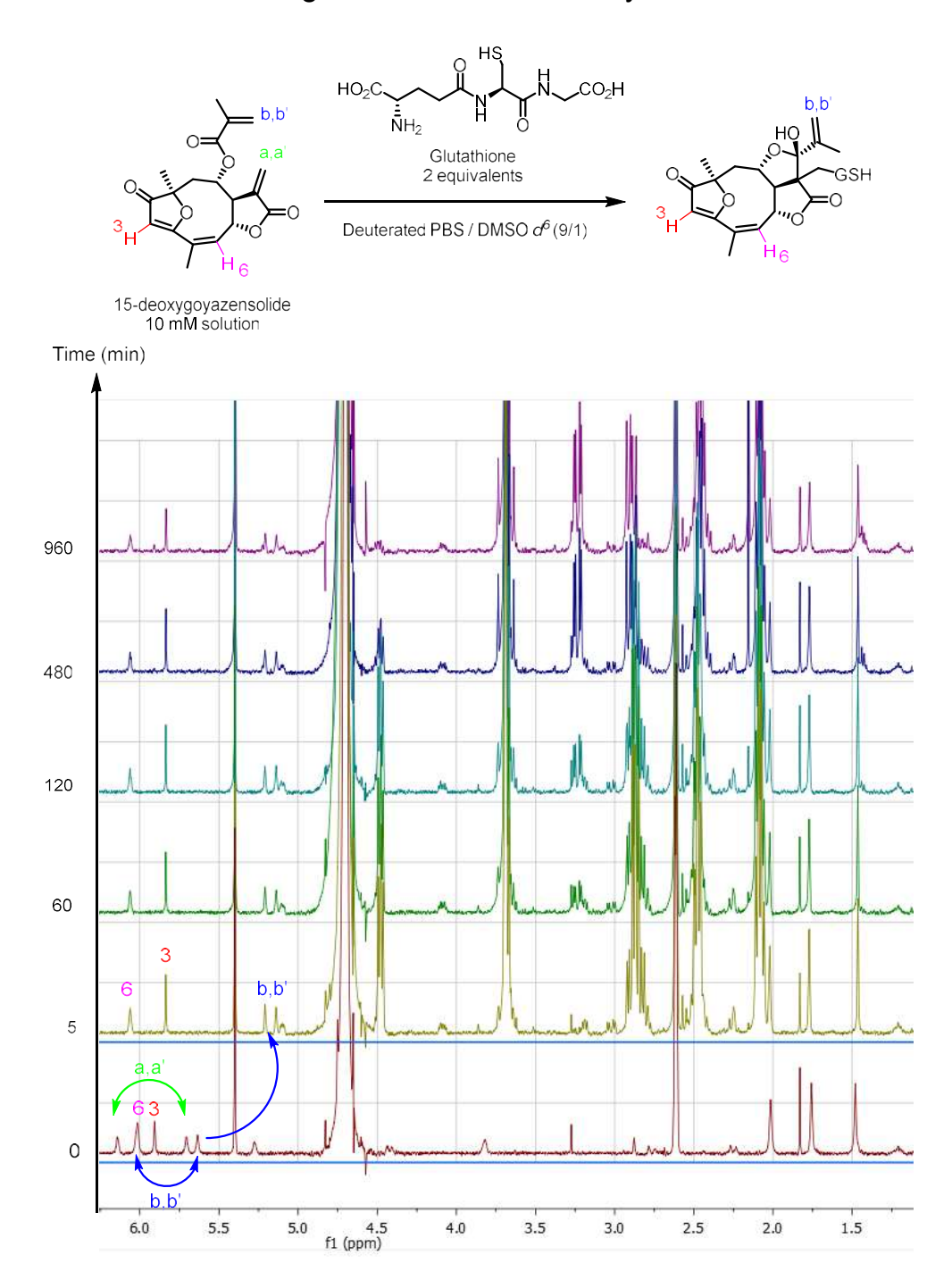


Figure 82: NMR monitoring of the reaction between 15-deoxygoyazensolide and glutathione

Experiment realized by Dr. Weilong Liu

Reaction between 15-deoxygoyazensolide and glutathione gave an adduct in which glutathione attacked the Michael acceptor localized on the α -methylene- γ -butyrolactone. But surprisingly, a cyclization occurred to give the eremantholide

scaffold. No other attack from glutathione was observed, even after 16 hours (Figure 82).

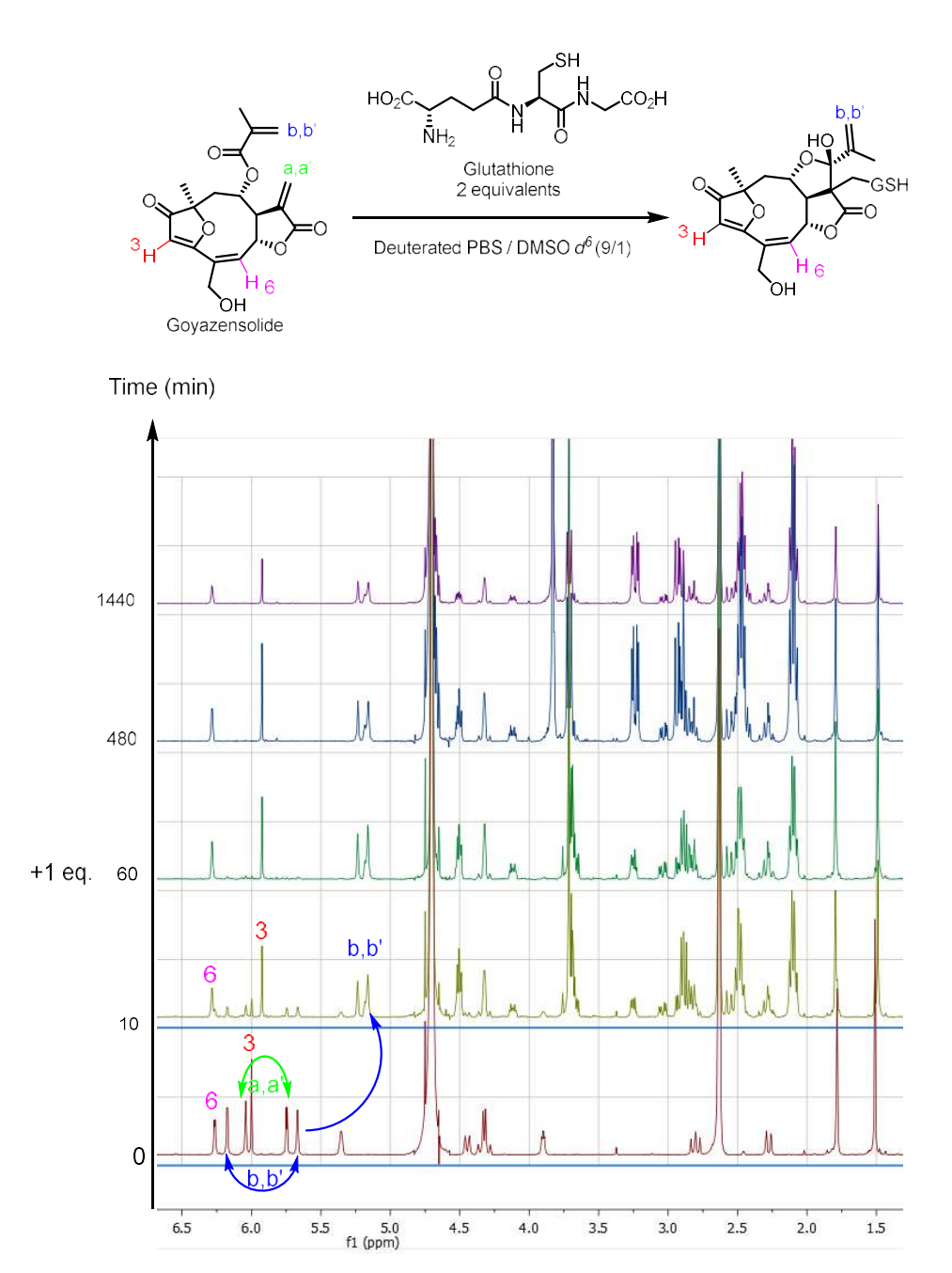


Figure 83: NMR monitoring of the reaction between goyazensolide and glutathione

The reaction between goyazensolide and glutathione gave the same result as 15-deoxygoyazensolide. No bis-adduct was observed, even after 16 hours (Figure 83).

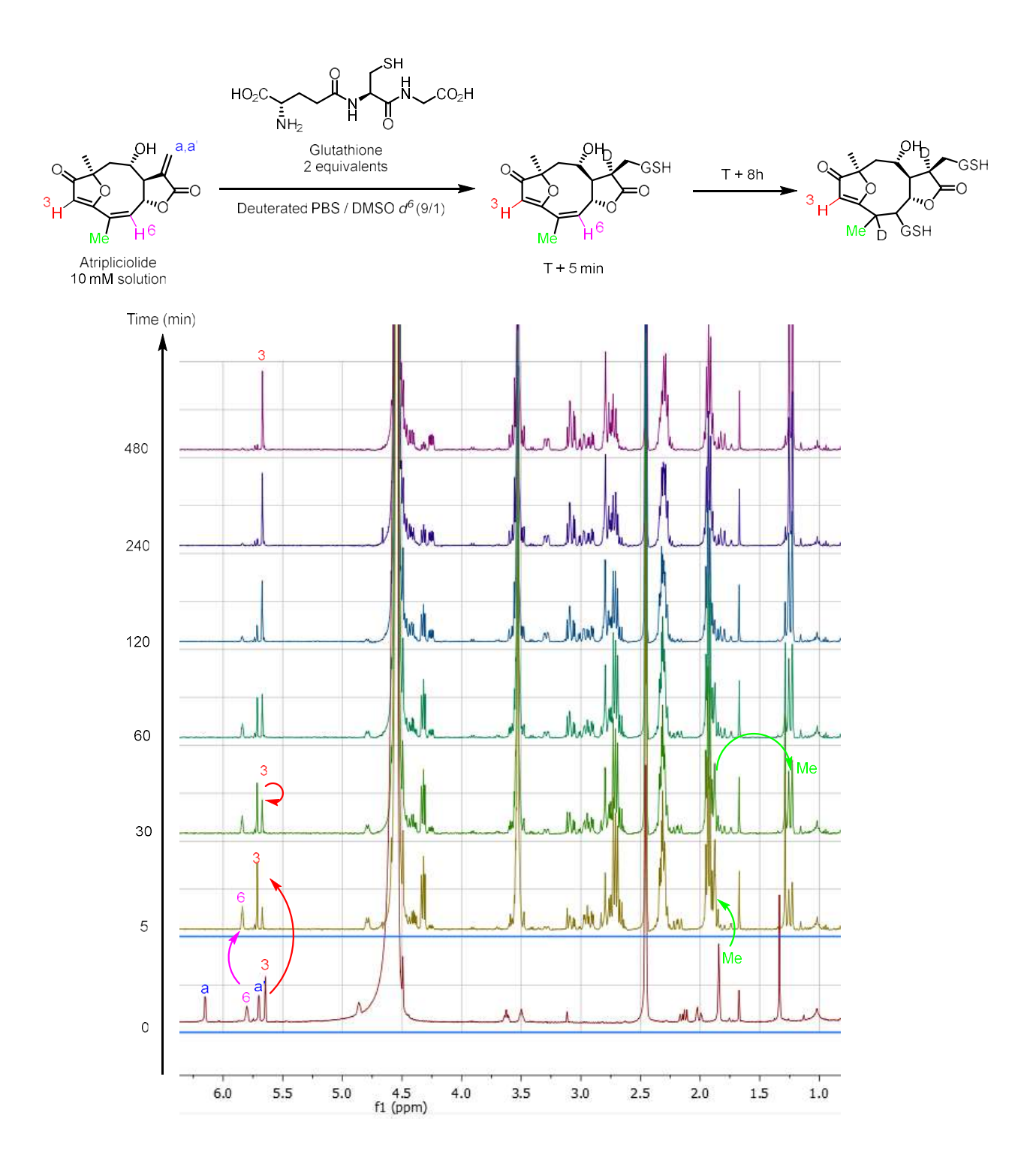


Figure 84: NMR monitoring of the reaction between atripliciolide and glutathione

Reaction between atripliciolide and glutathione clearly indicated the first glutathione attack localized on the α -methylene- γ -butyrolactone within the five first minutes characterized by the disappearance of protons (a,a') and then a slow Michael addition on the $\Delta^{4,5}$ double bond of atripliciolide (Figure 84). The second Michael addition was characterized by the disappearance of the proton 6, the shift of the methyl group (still

a singlet after the shift) and the correlation by HMBC between proton 3 and carbon C₃ of the macrocycle (See experimental section).

The reaction on the 1,6-dienone of goyazensolide with glutathione was not clearly characterized. Nevertheless, nucleophilic attack by NaN₃ on the 1,6-dienone was previously demonstrated and Le Quesne *et al.* observed that propanethiol reacts on the $\Delta^{4,5}$ double bond of eremantholide A, indicating that the reactivity depends on the type of nucleophile and the pH (Figure 85).¹⁸²

Figure 85: Nucleophilic attack on the 1,6-dienone of eremantholide (Le Quesne et al.)

I.6. Cysteine determination

Various labeling / pull-down experiments with goyazensolide / biotinylated probe / biotinylated iodoacetamide and pure IPO5 (expressed in the laboratory) followed by tryptic digestion and LC-MS/MS analysis didn't give a clear adduct. A deeper proteomic analysis within the laboratory found Cys563 as the potential reactive cysteine (Elsa Peev's investigations).

II. Conclusion

The difference of binding properties between goyazensolide / atripliciolide and other furanoheliangolides was unexpected. The specific micro-environment in protein binding pockets modulates the nucleophilic and electrophilic properties of species. The system "natural product, PBS, glutathione" is clearly too reductive. This modulation of reactivity due to the microenvironment can dramatically change the binding mode of these compounds and are extremely difficult to predict. For instance, Schmidt demonstrated that glutathione reacts with the cyclopentenone of helenalin whilst cysteine reacts with the α -methylene- γ -butyrolactone of helenalin (Figure 86). ¹⁸³ As a possible reason for the dramatic increase in reactivity of the exomethylene group towards free cysteine; an electrostatic interaction of the ammonium group of cysteine

with the lactone carbonyl (carbonyl and double bond in a cisoid orientation) of helenalin might stabilize the transition state and product, while a similar interaction would not occur in case of the cyclopentenone.

Figure 86: Chemoselectivity of glutathione and cysteine addition to helenalin

As atripliciolide effectively binds IPO5, the methacrylate on the side chain is not essential for the binding. The first Michael addition occurred for all three compounds on the α -methylene- γ -butyrolactone. The formation of the eremantholide scaffold seems to desactivate the 1,6-dienone of goyazensolide and 15-deoxygoyazensolide. Nevertheless, the allylic alcohol in the southern part of the structure has a role in the binding as its analog, 15-deoxygoyazensolide, doesn't bind IPO5. This allylic alcohol could interact or stabilize the complex molecule-protein and help the binding of IPO5 (Figure 87).

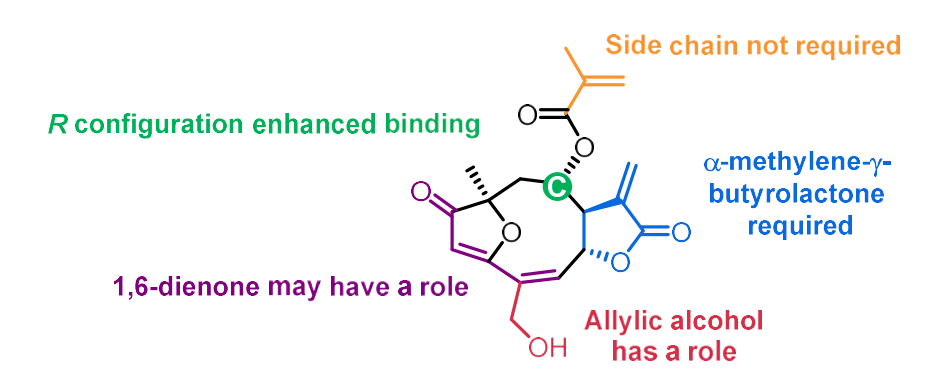


Figure 87: Structural SAR

Finally, both Michael acceptors, α -methylene- γ -butyrolactone and the 1,6-dienone may have a role in the binding. One hypothesis is a double binding with two cysteines: the

three compounds are able to react with the first cysteine as a reversible Michael addition. The formation of the eremantholide scaffold desactivates the 1,6-dienone but the allylic alcohol of goyazensolide has a probable role of assistance and thus the 1,6-dienone would be able to react with a second cysteine (or a lysine) in an irreversible reaction (Figure 88).

Figure 88: Hypothesis of the binding mode with importin-5

X-ray co-cristallization experiments are on-going and may provide insights on the binding mode.

Perspectives

Competition experiments with various natural products (Figure 74) indicated that withaferin A competed GOYA-2 for IPO5. The discovery that withaferin A targets IPO5 was unexpected. While this natural product has a wide range of pharmacological activities, including antiviral activities, no one demonstrated any anti-influenza activity.

Recruitment of IPO5 by influenza A to translocate essential viral proteins has been reported. As now we know that withaferin A targets IPO5, this is an ideal starting point to investigate a potential anti-influenza activity of withaferin A. We will also include goyazensolide during the investigations.

CHAPTER 6. Anti-influenza A activity of withaferin A

I. Introduction

Figure 89: Structure of withaferin A

Withaferin A (WA) is a steroidal lactone found in the medicinal plant *Withania somnifera* used in Ayurvedic medicine for over 3000 years (Figure 89). This natural product has wide a range of pharmacological activities and recently, WA passed a phase I clinical trial in advanced stage high grade osteosarcoma. ^{184, 185} It has anticancer activity in breast cancer, ¹⁸⁶⁻¹⁹² ovarian cancer, ¹⁹³⁻¹⁹⁸ prostate cancer, ¹⁹⁹⁻²⁰⁵ colorectal cancer, ²⁰⁶⁻²⁰⁹ and lung cancer. ²¹⁰ In addition, it's therapeutic potential includes anti-diabetic activity, ²¹¹⁻²¹⁵ neuroprotective activity, ²¹⁶⁻²²⁰, cardioprotective activity, ^{221, 222} anti-osteoporosis, ²²³ anti-hepatitis activity ²²⁴ and anti-SarS CoV2 activity. ^{225, 226} Only a single reference has mentioned, by a computational studies, the neuraminidase of H1N1 influenza as a potential target of WA. ²²⁷ However, this was not supported by experimental evidence. Additionally, whilst several proteomic characterizations of withaferin A have been published, it has never been mentioned that withaferin A targets IPO5. ²²⁸⁻²³⁰

II. Withaferin A targets IPO5 and possesses anti-influenza activity

II.1. Dose dependent competition and pull-down experiment with GOYA-2 for target confirmation

A competition assay was performed at a range of concentrations. It was discovered that WA competed with GOYA-2 for IPO5 in a dose dependent manner (Figure 90). Moreover, IPO5 was not pulled-down by GOYA-2 when the lysate was preincubated with WA.

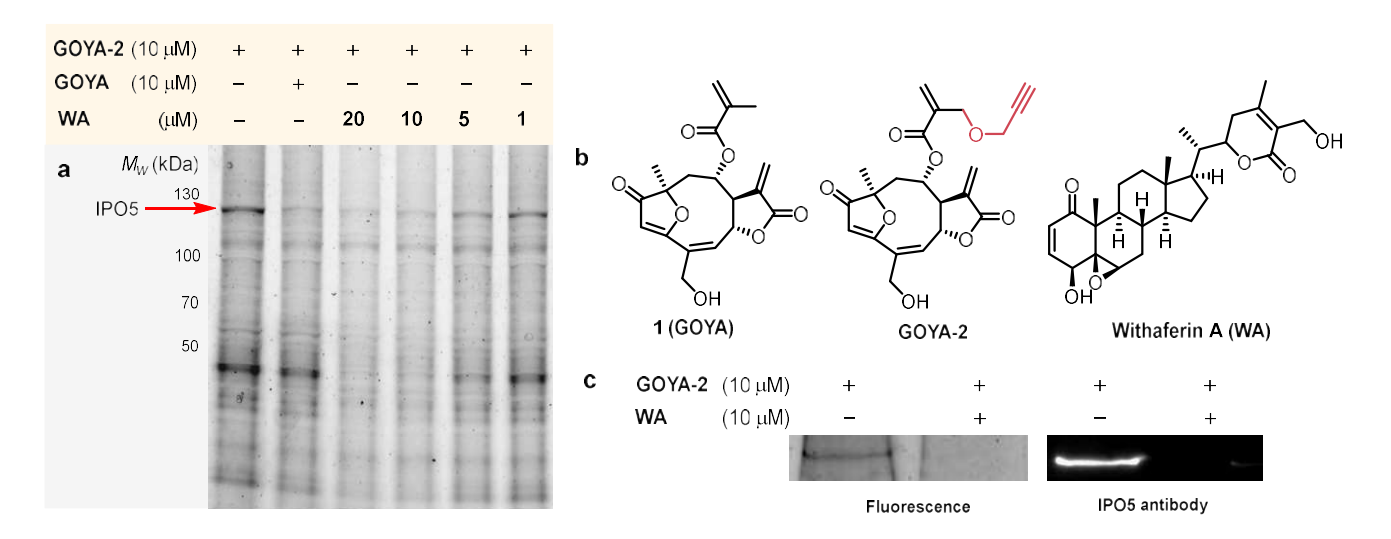


Figure 90: (a) proteomic profile and competition with goyazensolide or withaferin A in PC3 cells using GOYA-2 probe at 10 μ M followed by CuAAC reaction with Cy3-N₃ 1 hour at room temperature in the dark, then proteins were separated by SDS-PAGE. (b) Structures of withaferin A, goyazensolide and GOYA-2. (c) Immunoblot of competitive pull-down upon treatment of HT29 cell lysate with withaferin A or goyazensolide (10 μ M, 30 min) followed by GOYA-2 (10 μ M, 30 min), CuAAC reaction with biotinylated fluorophore and streptavidin enrichment.

This result was remarkable in two ways: from a structural point of view, goyazensolide selectively binds IPO5, whilst other close structural furanoheliangolides do not. WA, a steroidal lactone, has a significantly different shape. The second point is that WA has been studied for more than twenty years, with several proteomic studies and none of them mentioned any interaction between WA and IPO5.²²⁸⁻²³¹

II.2. Probe synthesis and pull-down experiments

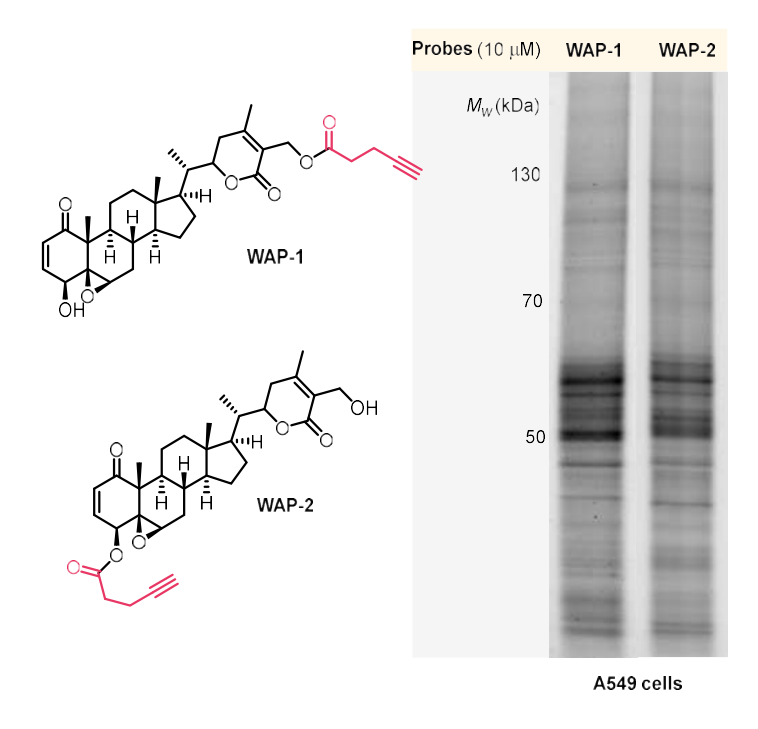


Figure 91: (Left) Structure of WAPs. (Right) Proteome profile of WAPs in A549 cells

Probes WAP-1 and WAP-2 (Figure 91) were obtained by acylation with the corresponding acyl chloride. A gel base assay indicated highly close proteome profile between the two probes (Cy3 used as fluorophore).

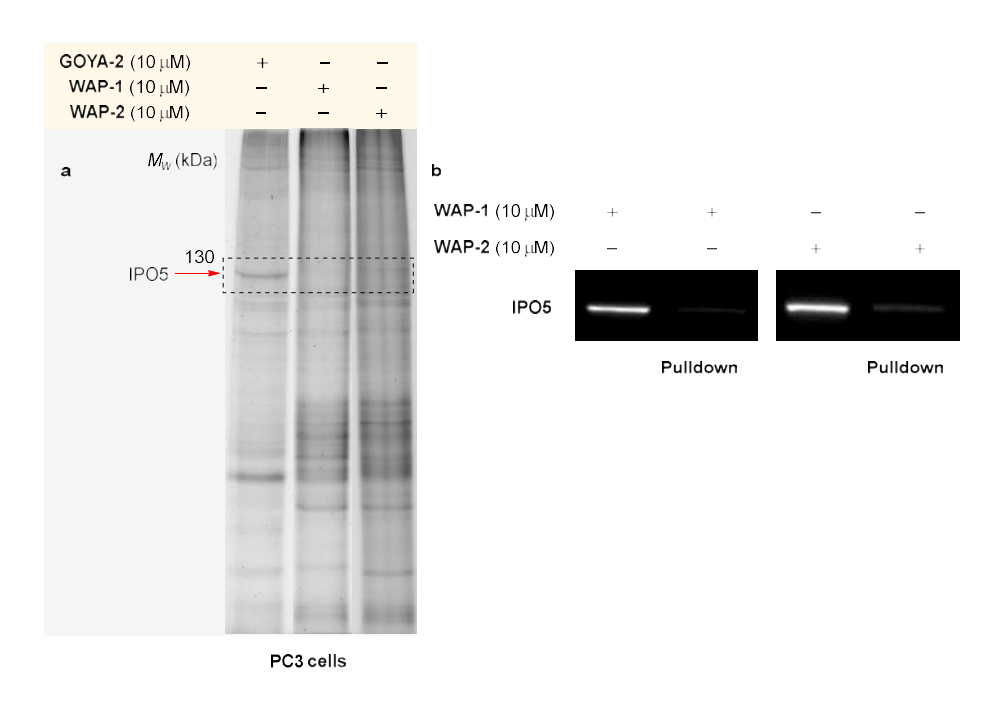


Figure 92: (a) proteomic profile in PC3 cells using GOYA-2 or WAP-1 or WAP-2 probes at 10 μ M followed by CuAAC reaction with Cy3-N₃ 1 hour at room temperature in the dark, then proteins were

separated by SDS-PAGE. (b) Immunoblot of pull-down upon treatment of PC3 cell lysate with WAP-1 or WAP-2 (10 µM, 30 min), CuAAC reaction with biotinylated fluorophore and streptavidin enrichment.

Surprisingly, neither WAP-1 or WAP-2 exhibited a fluorescent band at the same position as GOYA-2 (Figure 92). Moreover, IPO5 was not pulled down by these probes. It could be explained by the fact that the alkyne moieties hinder the binding between IPO5 and WAPs, or that the individual alcohols play a role in the binding.

Both goyazensolide and withaferin A will be tested, and WAP-1/2 will be used as negative controls due to their absence of covalent interaction with IPO5.

II.3. Cell viability assay

As withaferin A and goyazensolide are known to be cytotoxic, a cell viability assay was measured by microscopy (cell counting) to exclude any bioactivity resulting from the cytotoxicity of goyazensolide, WA or WAPs. $^{232, 233}$ Incubation in A549 cells for plaque assay experiments was performed with a total exposure time of 10 hours with the compounds. The maximum concentration was fixed at 1 μ M.

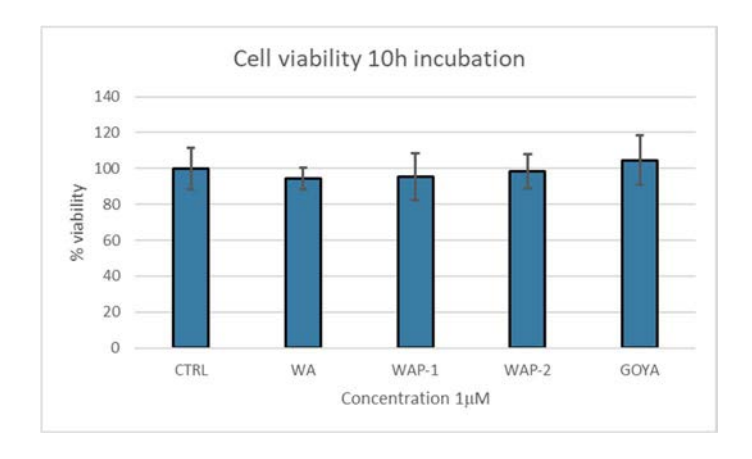


Figure 93: Cell viability assay with 10 h incubation of compounds (1 μ M) on A549 cells

The cell viability assay indicated that cells were not affected in the presence of the compounds at 1 μ M for 10 hours (Figure 93).

II.4. Plaque assay

A plaque assay consists of infecting cells with influenza A and removing a sample of the supernatant at a desired time point. A serie of dilutions is then performed and MDCK cells are then infected followed by addition of an agar layer. Thus, virions can only infect the neighbouring cells. The advantage of using a plaque assay is the direct quantification of infectious virions through the counting of discrete plaques (infectious units or cell dead zone) in cell culture (Figure 94).

The replication cycle of influenza viruses, from the time of entry to the production of new virus, is very quick, with shedding of the first influenza viruses from infected cells occurring after only 6 hours.

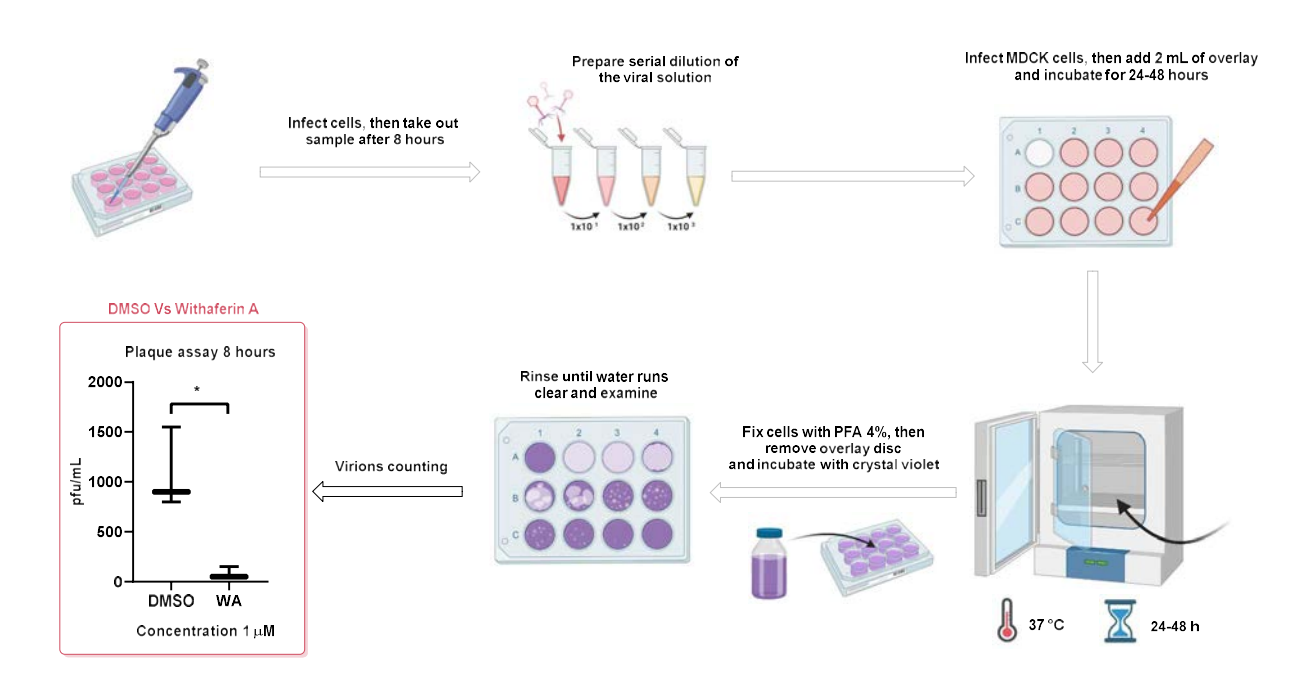


Figure 94: Schematic representation of a plaque assay experiment, alongside the first result comparing DMSO and withaferin A

A first experiment, comparing DMSO and withaferin A at 0.01 MOI (corresponding to 1 virion for 100 cells), indicated a strong inhibition in the viral replication when cells were incubated with withaferin A (Figure 94). Encouraged by this first result, plaque assays were performed with goyazensolide and the WAPs. The results indicated a strong inhibition in the viral replication with the WAPs, on par with withaferin A (Figure 95). Goyazensolide exhibited a moderate inhibition of influenza replication but was less effective than WA.

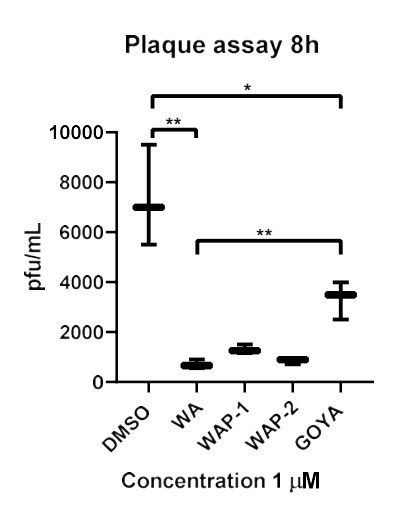


Figure 95: Results of the plaque assays (0.2 MOI) with goyazensolide, WA and the WAPs

II.5. Partial conclusion

While both goyazensolide and withaferin A bind IPO5, the difference of anti-IAV activity is significant and presumes another mechanism of action. Moreover, the fact that the WAPs exhibited a strong inhibition while they don't bind IPO5 suggests a minor role in the inhibition of IAV replication by the covalent interaction of goyazensolide and withaferin A with IPO5. Additional plaque assays indicated a complete loss of activity at 500 nM with goyazensolide while WA and WAPs still exhibited a moderate activity (See experimental section). A complete loss of activity was observed at 250 nM for WA and WAPs. Puzzled by these results, a literature search was performed to explore other mode of actions.

III. Withaferin A targets multiple proteins related to influenza A

III.1. Literature search

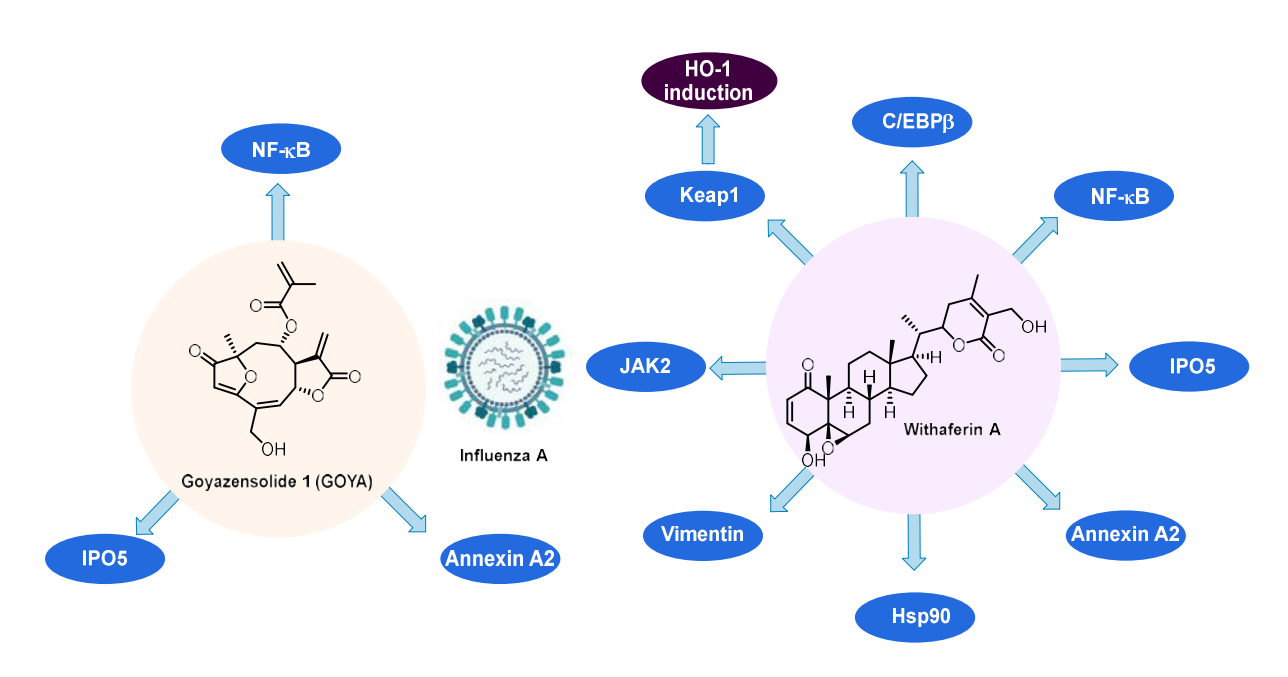


Figure 96: List of targets related to influenza A replication for each compound

Literature searching indicated that withaferin A covalently targets multiple proteins related to IAV replication (Figure 96). Similar to goyazensolide, withaferin A covalently binds IPO5, Annexin A2, and inhibits the NF-kB pathway.^{200, 201, 234-250}. However, NF-kB inhibition could be detrimental rather than beneficial to influenza A inhibition.

Additionally, WA covalently binds the cellular chaperone Hsp90, a protein which plays a role in nuclear import by translocating the viral protein PB1 and PB2 to the nucleus.^{245, 246}

WA also covalently binds vimentin, a protein that plays a role in the release of IA viral genome, and the knockout of vimentin inhibited IAV replication.^{200, 240}

It is also known that WA covalently binds C/EBP β , a transcription factor that forms a complex with the viral protein NS1.²⁵¹⁻²⁵³ This complex inhibits retinoic acid inducible gene 1 (RIG-1) transcription, a pathogen sensor indispensable for protection against many viruses including influenza A.

Additionally, WA covalently binds Kelch Like ECH Associated Protein 1 (Keap1) and induces expression of Heme oxygenase 1 (HO-1) through Nrf2 pathway activation. Three examples in the literature report the suppression of IAV replication by the use of HO-1 inducers.²⁵⁴⁻²⁵⁷

Finally, WA inhibits JAK/STAT signaling by suppressing the phosphorylation of JAK2 and STAT3.²⁵⁸ Wang *et al.* reported anti-IAV activity by JAK/STAT inhibitors Gingerenone A and ruxolitinib, as well as teriflunomide (anti-rheumatoid arthritis) by suppressing the phosphorylation of JAKs and STAT3.^{258, 259}

Based on the different target engagement of withaferin A versus WAP-1/2 relative to IPO5, we asked if other targets of withaferin A would also be affected and could inform on the crucial target(s) for IAV replication.

III.2. Target identification by gel-based assay and chemical proteomics

III.2.1. Hsp90

WA covalently binds the cellular chaperone Hsp90, a protein which translocates influenza polymerases PB1 and PB2 to the nucleus (Figure 97).^{245, 246} Additionally, Hsp90 directly interacts with the viral protein NS1 and mediates apoptosis induced by influenza A.²⁶⁰

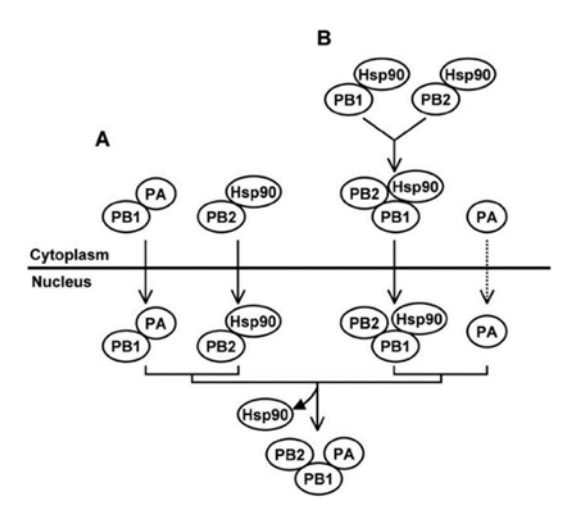


Figure 97: A model for Hsp90-related nuclear import and assembly of the influenza virus polymerases. (A) PB1 and PA interact with each other in the cytoplasm and translocate into the nucleus as a complex. PB2 is transported into the the nucleus with Hsp90. (B) Hsp90 interacts with PB1, PB2, and a PB1-PB2 subcomplex, and then a PB1-PB2-Hsp90 complex is formed and translocated into the nucleus. The ternary polymerase complex is assembled with nuclear transported viral polymerase subunits and/or subcomplexes, and concomitantly Hsp90 is released from subunits and/or subcomplexes (Scheme from Naito *et al.*, licence number 1150112-1).²⁴⁶

A pulldown experiment was performed with the probes WAP-1 and WAP-2 followed by a treatment with a specific Hsp90 antibody.

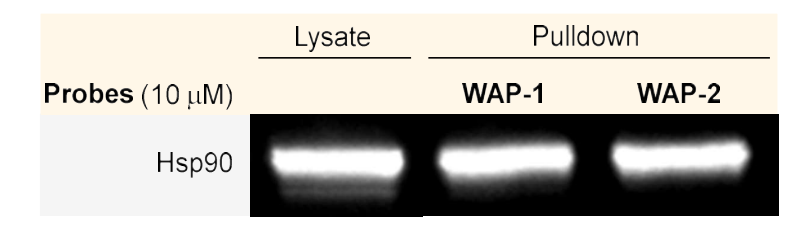


Figure 98: Immunoblot of pulldown experiment of Hsp90 with WAP-1 and WAP-2

Immunoblot revealed that all probes effectively pulled-down Hsp90 (Figure 98).

III.2.2. Annexin A2

Involvement of annexin A2 in the replication of influenza virus was characterized by the fact that activation of plasminogen, mediated by annexin A2, promotes the replication of IAV.²³⁸ The inhibition of the conversion of plasminogen into plasmin blocked influenza virus replication.²³⁸ Moreover, Ma *et al.* demonstrated an interaction between the viral protein NS1 and annexin A2.²⁴² Overexpression of annexin A2 significantly increased the concentration of IAV, whereas siRNA-mediated knockdown of annexin A2 inhibited the expression of viral proteins and reduced the virus concentration.

Gel based assays using WAP-1 indicated that a protein was specifically competed by WA in A549 cells (Figure 99a). This band was pulled-down and MS/MS analysis detected Annexin A2, in line with the literature.²³⁴ As annexin A2 is now localized by WAPs, competition experiments with withaferin A / goyazensolide were performed.

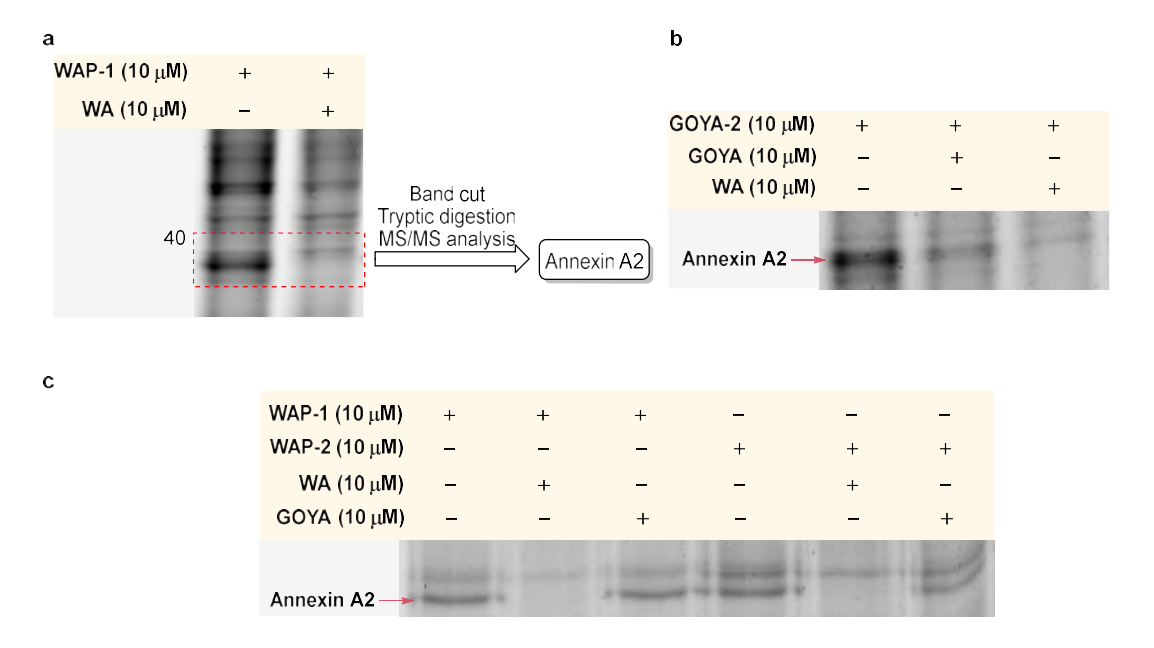


Figure 99: Proteomic profiling, competitions and pull-downs in A549 cells. (a) Target identification of a specific competitive band in A549 cells using WAP-1 probe at 10 μM followed by CuAAC reaction with DTB-Cy3-N₃ 1 hour at room temperature in the dark. Band of interest was pulled-down, cut, digested with trypsin and analyzed by MS/MS. (b)(c) Labeling/competition using GOYA-2, WAP-1 and WAP-2 probes at 10 μM followed by CuAAC reaction with Cy3-N₃ 1 hour at room temperature in the dark, then samples were analyzed by SDS-PAGE.

Competition experiments indicated that both withaferin A and goyazensolide competed with GOYA-2 (Figure 99b). WA competed with WAPs but, surprisingly, goyazensolide didn't compete with WAPs for annexin A2 (Figure 99c). This unexpected result could be explained by the fact that withaferin A reacts with two reactive cysteines whereas goyazensolide binds with only one reactive cysteine or WAPs labeled a protein at the same molecular weight while goyazensolide did not.

III.2.3. Vimentin

WA covalently binds vimentin, a protein which plays a role in the release of IA viral genome, and knockout of vimentin inhibited IAV replication.^{200, 240}

A second competitive band was observed in PC3 cells, and the identification process was similar to annexin A2 (Figure 100a). This specific band corresponded to vimentin, in line with the literature.

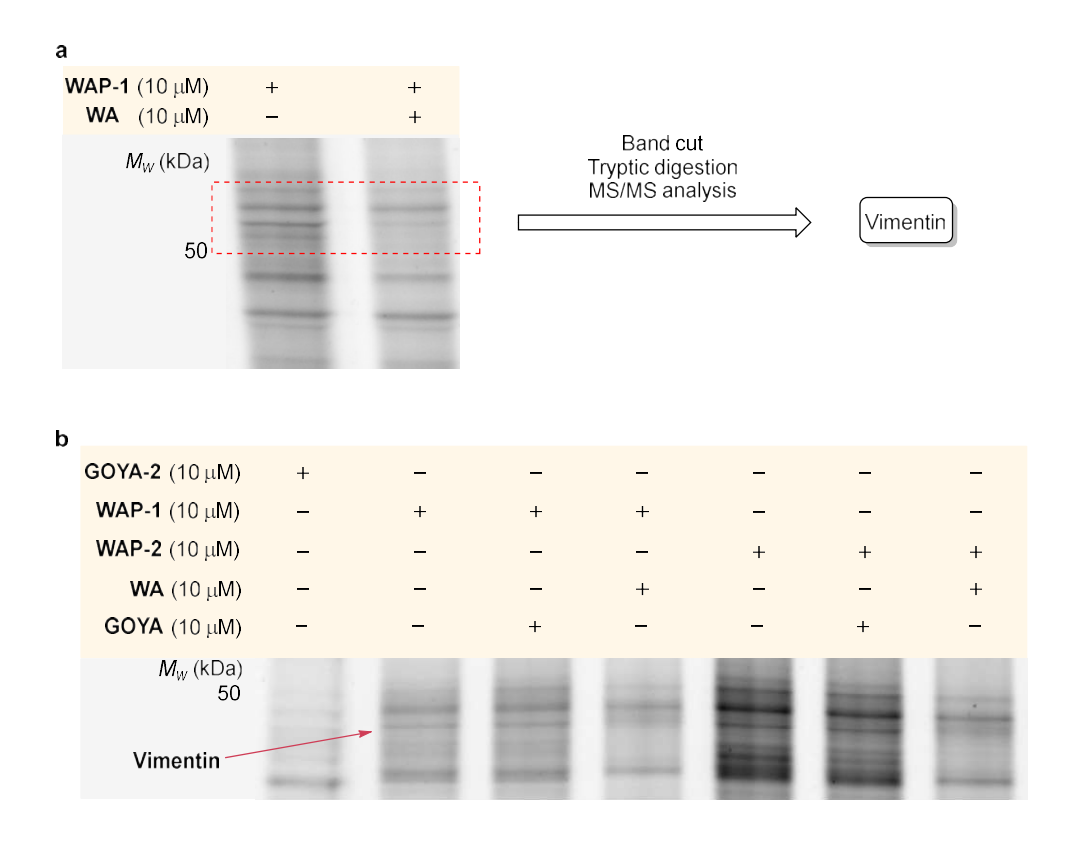


Figure 100: Proteomic profiling, competitions and pull-downs in PC3 cells. (a) Target identification of a specific competitive band in PC3 cells using WAP-1 probe at 10 μM followed by CuAAC reaction with DTB-Cy3-N₃ 1 hour at room temperature in the dark. Band of interest was pulled-down, cut, digested with trypsin and analyzed by MS/MS. (b) Labeling/competition using GOYA-2, WAP-1 and WAP-2 probes at 10 μM followed by CuAAC reaction with Cy3-N₃ 1 hour at room temperature in the dark, then samples were analyzed by SDS-PAGE

A labeling/competition assay was performed and indicated that GOYA-2 didn't label vimentin (Figure 100b). Moreover, goyazensolide didn't compete with WAPs for vimentin. The lack of binding of goyazensolide to vimentin could explain the difference of anti-IAV activity as vimentin plays a role in the replication of influenza.

III.2.4. Plaque assay using the selective vimentin inhibitor FiVe1.

In order to investigate if vimentin has a role in anti-IAV activity, a plaque assay was performed with the selective inhibitor FiVe1 (Synthesis of the compound described in the experimental section).²⁶¹

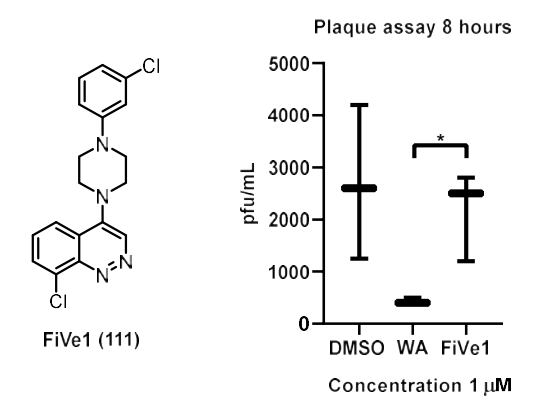


Figure 101: (Left) structure of FiVe1. (Right) Plaque assay with FiVe1

Results of the plaque assay (0.2 MOI) in Figure 101 indicated that selectively targeting vimentin is not sufficient to obtain an anti-IAV activity.

III.3. Withaferin A, WAPs and BXM induce HO-1 in A549 cells

The modulator effects of heme oxygenase-1 (HO-1) on the immune response as well as the antiviral activity mediated by HO-1 induction is well known and several examples reported suppression of IAV replication using HO-1 inducers (Figure 103a).^{254-257, 262} HO-1 induction is triggered by three major transcription factors: NF-κB, AP-1, and Nrf2 (Figure 102b). Interestingly, withaferin A inhibits both NF-κB and AP-1.^{236, 263} Nevertheless, the detrimental impact of these inhibition could be rescued by Nrf2.

Heyninck *et al.* demonstrated that withaferin A induces heme oxygenase 1 (HO-1) expression *via* activation of the Keap1/Nrf2 pathway in HUVEC cells by covalent interaction of Kelch Like ECH Associated Protein 1 (Keap1) (Figure 102a).²⁵⁴ Moreover, this induction triggered by withaferin A was observed in 3 other cancer cell lines (EA.hy926, Ca9-22 and MMR1).^{228, 264}

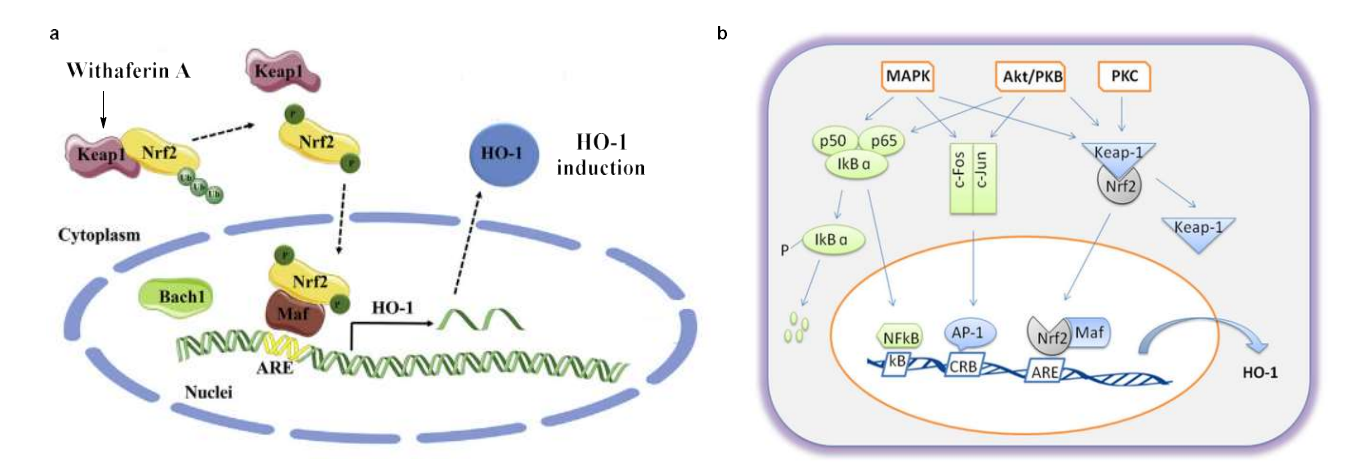


Figure 102: (a) Induction of HO-1 mediated by withaferin A that produces the dissociation of Keap1 and Nrf2. Then Nrf2 is phosphorylated, translocated, and promotes *in fine* the induction of HO-1. (Figure modified from Espinoza *et al.*, Licence number 5150710269283).²⁶² (b) Schematic representation showing different HO-1 induction pathways. Under external stimuli, transcription factors NF-kB, AP-1, and Nrf2 are translocated and lead to the HO-1 induction. (Figure modified from Waza *et al.*, Licence number 5156390802945).

Nrf2 can be activated by inhibiting Keap1 or by activating phosphorylation of p38/ERK (MAPK pathway) as indicated in Figure 103b. Surprisingly, WA inhibits phosphorylation of p38/ERK and thus, confirms that HO-1 induction exclusively comes from the Keap1/Nrf2 pathway.²⁶⁵

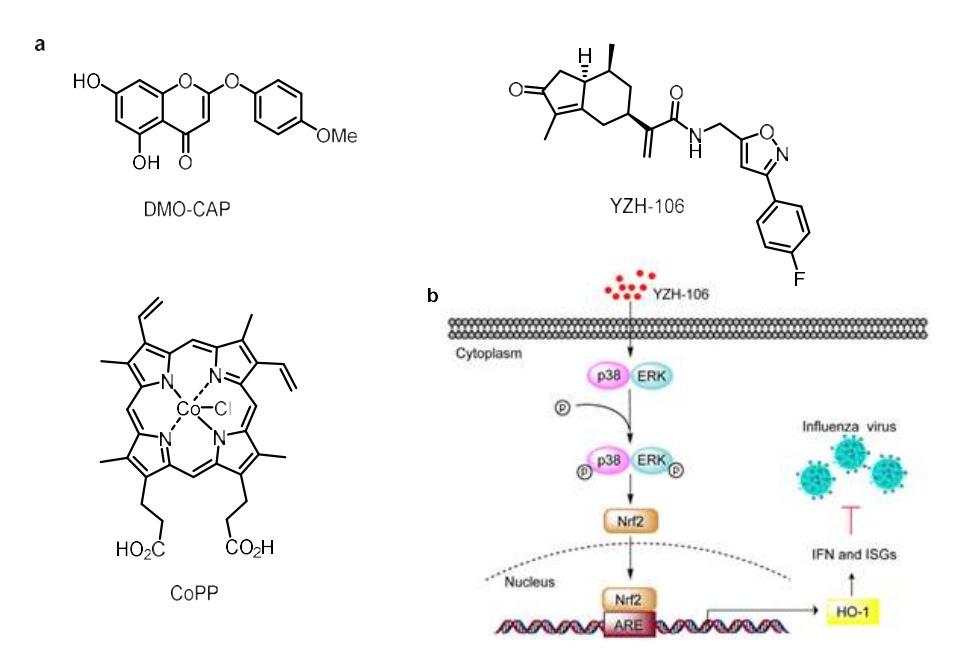


Figure 103: (a) Structures of the three compounds inducing HO-1 expression.

(b) Schematic showing that YZH-106 (a rupestonic acid derivate) inhibits influenza virus replication. YZH106 induces p38 MAPK and ERK1/2 phosphorylation, which subsequently leads to nuclear translocation of Nrf2. Next, Nrf2 binding to ARE increases HO-1 expression. HO-1 up-regulation enhances type I IFN expression and subsequent induction of ISGs, which finally leads to inhibition of influenza virus replication (Figure from Ma et al., Licence number 5150710751748).²⁵⁶

Additionally, Dai *et al.* discovered that curcumin exhibited an anti-IAV activity by modulating several pathways including Nrf2 activation, and Shin *et al.* demonstrated that curcumin covalently binds Keap1.^{266, 267}

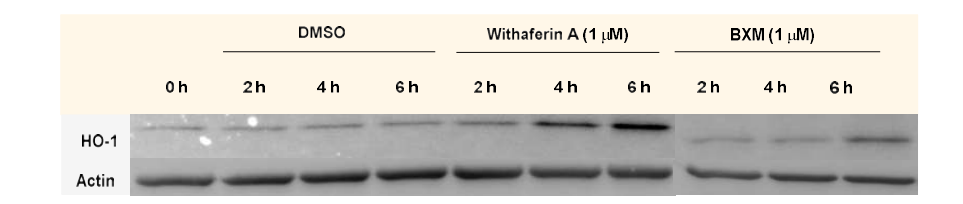
In a second aspect, WA also inhibits the JAK/STAT signaling by suppressing the phosphorylation of JAK2 and STAT3. Involvement of JAK inhibitors in anti-IAV activity was clearly demonstrated whereas the mechanism of action is not completely understood. ^{268, 269} Han *et al.* reported that JAK2 silencing leads to the increased expression of antiviral genes such as IFN-β, MxA, IFIT1, RIG-1, and ISG15, suggesting that the inhibition of JAK2 may enhance the antiviral defense activity of host cells. ²⁷⁰ On the other hand, Du *et al.* reported that JAK1 was ubiquitinated and degraded in infected cells, resulting in inhibition of IFN responses, demonstrating that IAV antagonizes the IFN-activated JAK/STAT signaling pathway by inducing the degradation of JAK1. Their findings suggest that IAV infection induces SOCS1 expression to promote JAK1 degradation, which in turn inhibits host innate immune responses. ²⁷¹

Thus, the specific choice to include the compound bardoxolone-methyl (BXM) in the next experiments was motivated by its capacity to covalently bind Keap1 and selectively inhibit JAK1 but not JAK2 (Figure 104). Conversely, WA covalently targets Keap1 and inhibits JAK2. This difference may show the contribution of JAK2 inhibition in anti-IAV activity. BXM also interacts with Hsp90, and inhibits NF- κ B pathway by targeting Cys179 of IKK β like withaferin A. 273, 274

Bardoxolone methyl (BXM)

Figure 104: Structure of BXM, a covalent Keap1/JAK1 inhibitor

Investigations started by the demonstration of HO-1 induction in A549 cells. BXM (Phase III clinical trial, renal disease, oral administration) was included in these investigations.²⁷⁵⁻²⁷⁷ Interestingly, it was reported that BXM induces HO-1 expression in U937 cells.^{278, 279}



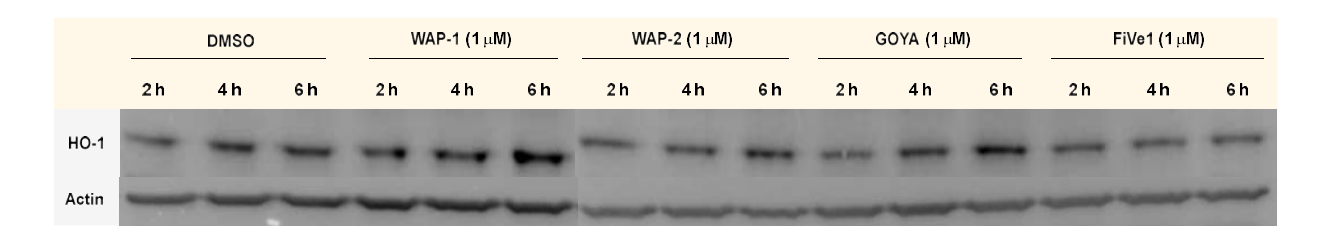


Figure 105: Immunoblot of A549 cell lysate incubated with DMSO or compound (1 μ M) then treated with a specific HO-1 antibody. Actin antibody was used as control.

Treatment of A549 cells with DMSO or compounds indicated an induction of HO-1 with WA, WAPs, BXM, and goyazensolide (Figure 105). No HO-1 induction was observed with FiVe1.

III.4. Plaque assay using the Keap1 inhibitor Bardoxolone methyl (BXM).

A plaque assay was performed to evaluate a potential anti-IAV activity of BXM.

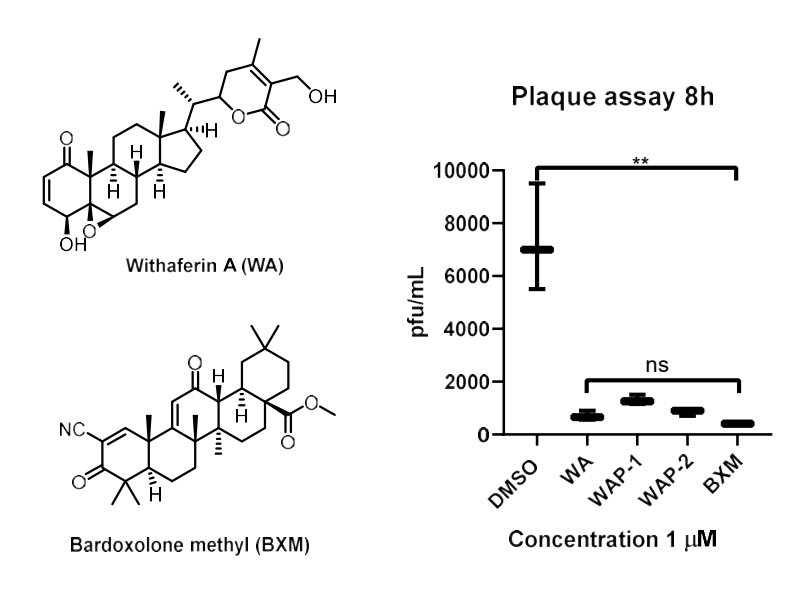


Figure 106: (Left) Structure of withaferin A and bardoxolone methyl. (Right) Plaque assay result

A plaque assay with BXM revealed a strong inhibition of the viral replication, as with withaferin A (Figure 106). Since BXM does not inhibit JAK2, the major anti-IAV activity does not come from JAK2 inhibition. Moreover, we expected a lower anti-IAV activity as JAK1 inhibition upregulates IAV infection.

Next results from BXM were used to validate or exclude previously discussed targets. While BXM exhibited similar anti-IAV activity to withaferin A, it didn't compete with GOYA-2 for IPO5, nor did it compete WAP-1 for both annexin A2 or vimentin, and a pull-down experiment indicated that WAP-1 still pulled-down Hsp90 with a lysate preincubated with BXM.

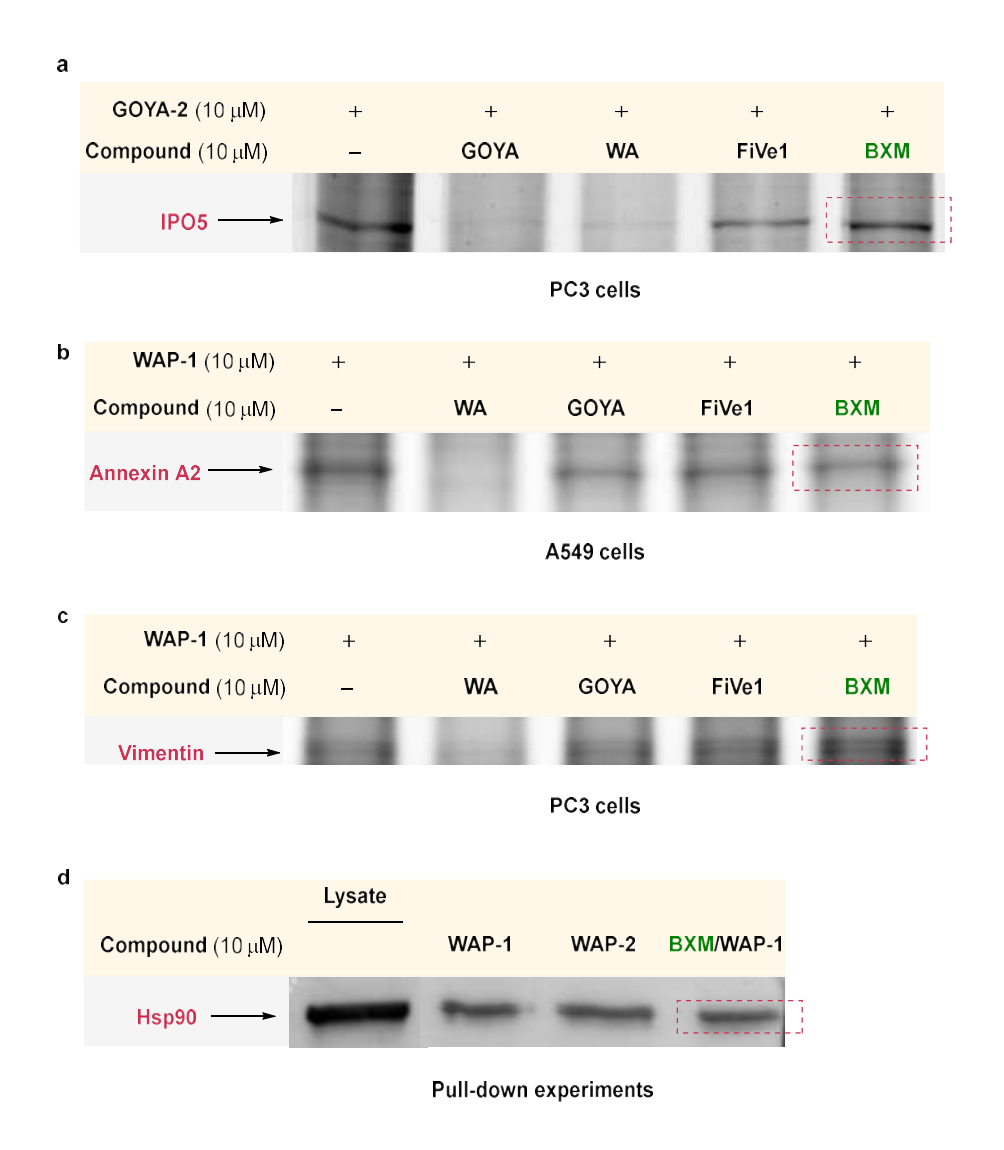


Figure 107: Labeling/competition experiments and pulldown experiment for BXM target characterization (DTB-Cy3 used as fluorophore).

This series of results showed several clear differences between BXM and withaferin A while their anti-IAV activities are similar. BXM didn't compete with WAP-1 for Hsp90, although the interaction between BXM and Hsp90 was reported and indicated a covalent binding.²⁷⁴ The fact that BXM didn't compete with WAP-1 for Hsp90 underlines a possible covalent interaction to a different cysteine residue targeted by withaferin A. This result indicated that the biological modulation of Hsp90 activity may be different between withaferin A and BXM, pointing out, once more, the difficulty to validate or exclude involvement of a target in the global anti-IAV activity. Zhang *et al.* reported a protein-protein interaction between Hsp90 and the viral protein NS1.²⁶⁰ Investigating the disruption of this interaction with withaferin A and BXM could reveal some difference if their binding sites are different.

III.5. Future experiments

To confirm the covalent binding between WAPs and Keap1, fluorescent probes will be synthesized and tested, followed by competition experiments with goyazensolide and JAK inhibitor teriflunomide. These investigations are currently on-going.

The signal transducer and activator of transcription 1 (STAT1) is a cytoplasmic protein and, once activated, is translocated to the nucleus and acts as part of a protein complex to activate transcription from IFN-regulated genes (Figure 108). In the absence of STAT1, IFN-mediated gene induction does not occur and anti-IAV response is inhibited. Plaque assays with WA, WAPs, GOYA, and BXM will be performed using A549 cells (STAT1 -/-) to validate the mechanism of action.

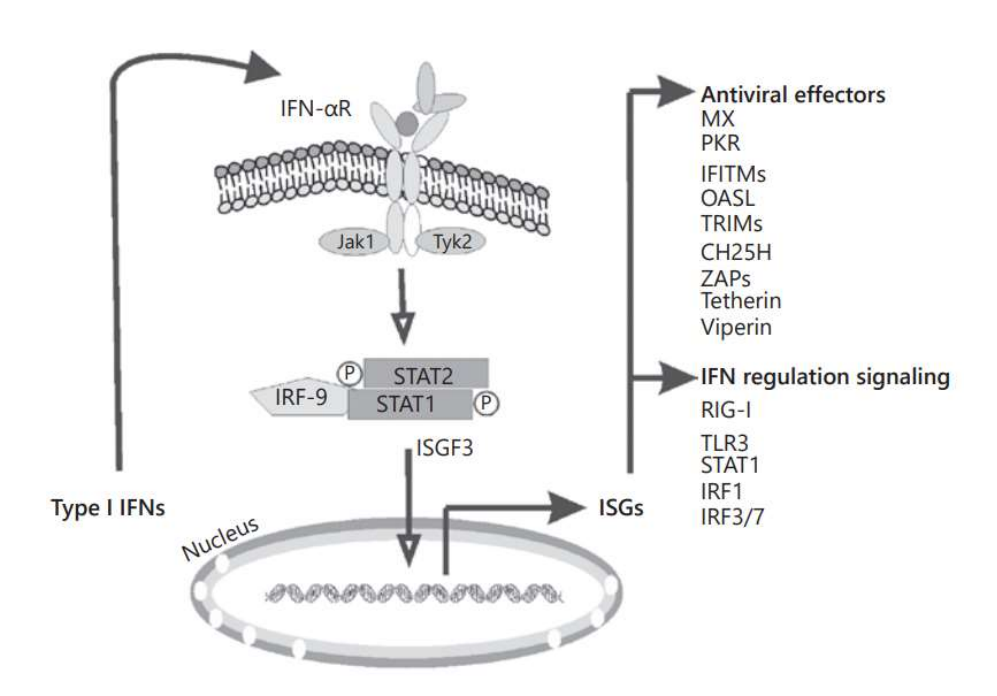


Figure 108: Induction of type I IFNs and ISGs by influenza virus. Innate immune cells, such as macrophages and lung epithelial cells, produce type I IFNs after sensing IAV genomic RNA using various PRRs. In infected and neighboring cells, type I IFN signaling activates the JAK-STAT pathway, leading to transcription of ISGs, the products of which initiate intracellular antiviral effectors that limit the spread of the viruses. (Figure modified from Wu and Metcalft, Licence creative Commons CC-BY-NC-ND).²⁸⁰

IV.Conclusion

Withaferin A targets multiple proteins involved in the influenza A life cycle. But which are more important? It is not known to date. To answer this question, several investigations were performed to compare the anti-IAV activity of compounds, and the different targets involved.

The difference of anti-IAV activity between goyazensolide and withaferin A pushed us to investigate specific targets of withaferin A, such as vimentin. WA covalently bind Keap1, activates the Nrf2 pathway and induces HO-1. Nevertheless, WA inhibits the MAPK pathway and desactivates the translocation of Nrf2 into the nucleus.²⁶⁵ Sun *et al.* demonstrated that phosphorylation of Nrf2 by MAP kinases has a limited contribution in modulating Nrf2-dependent antioxidant response, which is consistent since withaferin A clearly induces HO-1.²⁸¹ As withaferin A inhibits NF-κB, it confirms that HO-1 induction comes from the Keap1/Nrf2 pathway.

The similar effect between the Keap1/JAK1 inhibitor BXM and withaferin A underlines the fact that monitoring inhibition of JAK2/STAT3 phosphorylation may be not sufficient to explain the biological effect of compounds described as anti-IAV agents (gingerenone, ...). Moreover, literature reported that the anti-IAV JAK inhibibitor teriflunomide also induced HO-1.^{282, 283}

Withaferin A and BXM both inhibit replication of influenza A and both covalently interact with Keap1.

Future investigations using selective Keap1, NF-κB or JAK inhibitors would highlight the relative contributions of Keap1/Nrf2, NF-κB and JAK/STAT pathways, respectively. Nevertheless, designing selective covalent inhibitors is challenging, and targeting several proteins related to influenza A by a single compound may have some advantages, such as a synergistic effect. Research for anti-IAV compounds has been first focused on Neuraminidase (NA) inhibitors, M2 channel ion blockers, followed by influenza RNA polymerase as specific drug targets. The limited efficiency from anti-IAV compounds demonstrated the drawback of the "one drug-one target" paradigm by especially when targeting the complex influenza life cycle which involves more than 900 biological factors.²⁸⁴⁻²⁸⁹ The challenge also comes from the high rate of mutation and evolves resistance against drugs. Combination of natural extracts from medicinal

plants with empirical knowledge has provided a new platform for the development of new therapeutics.²⁹⁰ The use of natural products in traditional medicine gives them the benefit of a preliminary toxicology profile in human and their high reactivity allowing the targeting of several proteins and modulating various biological pathways through the new paradigm "target network" or "multi-component therapeutics".²⁹¹

General conclusion

The work presented in this manuscript focuses on the total synthesis of furanoheliangolides, the target identification of goyazensolide and its mode of action. Further investigations have been performed to elucidate the anti-influenza activity of the steroidal lactone withaferin A.

Regarding the total synthesis of goyazensolide, the route includes the first example merging the α -methylene- γ -butyrolactone formation with the closure of a 10-membered germacrene framework via a Barbier allylation. This synthetic strategy allowed the access of various furanoheliangolides and sesquiterpene lactones never synthesized. It is interesting to note that this Barbier allylation might be applied to the synthesis of diverse sesquiterpene lactone families, such as germacranolides or even the more famous guaianolides which may benefit from merging the α -methylene- γ -butyrolactone formation with the easier closure of a 7-membered ring.

The total synthesis of goyazensolide enabled access to its alkyne tagged probe, required for investigations of protein targeting. The design of a fluorophore with a desthiobiotin incorporated enabled the monitoring of the labeling as well as an efficient method to discriminate enriched proteins. The study of the covalent interactome of goyazensolide, revealed IPO5 as its molecular target.

In the case of goyazensolide, there was clear evidence of anticancer activity from mouse xenografts and cellular assays, but the mode of action remained unknown. The finding that goyazensolide selectively engages IPO5 covalently and inhibits its interaction with RASAL2 rationalizes its anticancer activity.

The unexpected covalent interaction of IPO5 by withaferin A pushed to investigate the potential anti-influenza activity for both natural products. The multi-target properties and the strong anti-IAV activities of withaferin A and WAPs lead to the conclusion that IPO5 is not the major target responsible for this biological effect. While the prediction of the anti-IAV activity from bardoxolone methyl was successful, the myriad of biological pathways involved in the influenza A life cycle combined with the use of non-selective compounds drastically increased the difficulty to determine the complete mode of action. Nevertheless, research has focused on the paradigm "one drug-one

target" for decades and the complexity of this disease has clearly demonstrated that such single-target drugs are inadequate to achieve an efficient therapeutic effect. Natural products, such as goyazensolide and withaferin A are typically multi-target compounds and, despite their tremendous therapeutic potential, their rationalised development still represents a formidable challenge.

References

- 1. Petrovska, B. B., Historical review of medicinal plants' usage. *Pharmacogn Rev* **2012**, *6* (11), 1-5.
- 2. Newman, D. J.; Cragg, G. M., Natural products as sources of new drugs over the last 25 years. *J Nat Prod* **2007**, *70* (3), 461-77.
- 3. Newman, D. J.; Cragg, G. M.; Snader, K. M., Natural products as sources of new drugs over the period 1981-2002. *J Nat Prod* **2003**, *66* (7), 1022-37.
- 4. Koch, M. A.; Schuffenhauer, A.; Scheck, M.; Wetzel, S.; Casaulta, M.; Odermatt, A.; Ertl, P.; Waldmann, H., Charting biologically relevant chemical space: a structural classification of natural products (SCONP). *Proc Natl Acad Sci U S A* **2005**, *102* (48), 17272-7.
- 5. Clayden, J.; Greeves, N.; Warren, S.; Wothers, P., Organic chemistry. Oxford university press Oxford: 2001.
- 6. Fleming, I., Molecular orbitals and organic chemical reactions. John Wiley & Sons: 2011.
- 7. H Johansson, M., Reversible Michael additions: covalent inhibitors and prodrugs. *Mini reviews in medicinal chemistry* **2012**, *12* (13), 1330-1344.
- 8. Amslinger, S., The tunable functionality of α , β -unsaturated carbonyl compounds enables their differential application in biological systems. *ChemMedChem* **2010**, *5* (3), 351-356.
- 9. Brown, W. H.; Poon, T., Introduction to organic chemistry. John Wiley & Sons: 2016.
- 10. Mulliner, D.; Wondrousch, D.; Schüürmann, G., Predicting Michael-acceptor reactivity and toxicity through quantum chemical transition-state calculations. *Organic & biomolecular chemistry* **2011,** *9* (24), 8400-8412.
- 11. LoPachin, R. M.; Gavin, T.; DeCaprio, A.; Barber, D. S., Application of the hard and soft, acids and bases (HSAB) theory to toxicant—target interactions. *Chemical research in toxicology* **2012**, *25* (2), 239-251.
- 12. Amorim, M. H. R.; Gil da Costa, R. M.; Lopes, C.; Bastos, M. M., Sesquiterpene lactones: adverse health effects and toxicity mechanisms. *Critical reviews in toxicology* **2013**, *43* (7), 559-579.
- 13. Ghosh, A. K.; Gemma, S., *Structure-based design of drugs and other bioactive molecules: tools and strategies.* John Wiley & Sons: 2014.
- 14. Sajid, M.; McKerrow, J. H., Cysteine proteases of parasitic organisms. *Molecular and biochemical parasitology* **2002**, *120* (1), 1-21.
- 15. Santos, M.; Moreira, R., Michael acceptors as cysteine protease inhibitors. *Mini reviews in medicinal chemistry* **2007**, *7* (10), 1040-1050.
- 16. Tan, J.; George, S.; Kusov, Y.; Perbandt, M.; Anemüller, S.; Mesters, J. R.; Norder, H.; Coutard, B.; Lacroix, C.; Leyssen, P., 3C protease of enterovirus 68: structure-based design of Michael acceptor inhibitors and their broad-spectrum antiviral effects against picornaviruses. *Journal of virology* **2013**, *87* (8), 4339-4351.
- 17. Danov, O.; Lasswitz, L.; Obernolte, H.; Hesse, C.; Braun, A.; Wronski, S.; Sewald, K., Rupintrivir reduces RV-induced TH-2 cytokine IL-4 in precision-cut lung slices (PCLS) of HDM-sensitized mice ex vivo. *Respiratory research* **2019**, *20* (1), 1-9.
- 18. Zhang, L.; Liu, J.; Cao, R.; Xu, M.; Wu, Y.; Shang, W.; Wang, X.; Zhang, H.; Jiang, X.; Sun, Y.; Hu, H.; Li, Y.; Zou, G.; Zhang, M.; Zhao, L.; Li, W.; Guo, X.; Zhuang, X.; Yang, X. L.; Shi, Z. L.; Deng, F.; Hu, Z.; Xiao, G.; Wang, M.; Zhong, W., Comparative Antiviral Efficacy of Viral Protease Inhibitors against the Novel SARS-CoV-2 In Vitro. *Virol Sin* **2020**, *35* (6), 776-784.
- 19. Breuning, A.; Degel, B. r.; Schulz, F.; Büchold, C.; Stempka, M.; Machon, U.; Heppner, S.; Gelhaus, C.; Leippe, M.; Leyh, M., Michael acceptor based antiplasmodial and antitrypanosomal cysteine protease inhibitors with unusual amino acids. *Journal of medicinal chemistry* **2010**, *53* (5), 1951-1963.

- 20. Jäger, T.; Koch, O.; Flohé, L., Trypanosomatid diseases: molecular routes to drug discovery. *Trypanosomatid diseases: molecular routes to drug discovery.* **2013**.
- 21. Götz, M. G.; James, K. E.; Hansell, E.; Dvorák, J.; Seshaadri, A.; Sojka, D.; Kopácek, P.; McKerrow, J. H.; Caffrey, C. R.; Powers, J. C., Aza-peptidyl Michael acceptors. A new class of potent and selective inhibitors of asparaginyl endopeptidases (legumains) from evolutionarily diverse pathogens. *Journal of medicinal chemistry* **2008**, *51* (9), 2816-2832.
- 22. Lee, G. M.; Balouch, E.; Goetz, D. H.; Lazic, A.; McKerrow, J. H.; Craik, C. S., Mapping inhibitor binding modes on an active cysteine protease via nuclear magnetic resonance spectroscopy. *Biochemistry* **2012**, *51* (50), 10087-10098.
- 23. Mellott, D.; Tseng, C.-T.; Drelich, A.; Fajtova, P.; Chenna, B. C.; Kostomiris, D.; Hsu, J. C.; Zhu, J.; Taylor, Z.; Tat, V., A cysteine protease inhibitor blocks SARS-CoV-2 infection of human and monkey cells. *bioRxiv* **2020**.
- 24. Carmi, C.; Mor, M.; Petronini, P. G.; Alfieri, R. R., Clinical perspectives for irreversible tyrosine kinase inhibitors in cancer. *Biochemical pharmacology* **2012**, *84* (11), 1388-1399.
- 25. Schirmer, A.; Kennedy, J.; Murli, S.; Reid, R.; Santi, D. V., Targeted covalent inactivation of protein kinases by resorcylic acid lactone polyketides. *Proceedings of the National Academy of Sciences* **2006**, *103* (11), 4234-4239.
- 26. Artz, J. D.; Wernimont, A. K.; Lin, L. Y.; Amani, M.; Neculai, M.; Hills, T.; Hui, R., Selective Inhibition of Parasite Protein Kinases. *Protein Phosphorylation in Parasites* **2013**, 235-260.
- 27. Miller, R. M.; Taunton, J., Targeting protein kinases with selective and semipromiscuous covalent inhibitors. *Methods in enzymology* **2014**, *548*, 93-116.
- 28. Merritt, C.; Silva, L. E.; Tanner, A. L.; Stuart, K.; Pollastri, M. P., Kinases as druggable targets in trypanosomatid protozoan parasites. *Chemical reviews* **2014**, *114* (22), 11280-11304.
- 29. Nishino, M.; Choy, J. W.; Gushwa, N. N.; Oses-Prieto, J. A.; Koupparis, K.; Burlingame, A. L.; Renslo, A. R.; McKerrow, J. H.; Taunton, J., Hypothemycin, a fungal natural product, identifies therapeutic targets in Trypanosoma brucei. *Elife* **2013**, *2*, e00712.
- 30. Gao, Y.; Duan, F.-F.; Liu, L.; Peng, X.-G.; Meng, X.-G.; Ruan, H.-L., Hypothemycin-Type Resorcylic Acid Lactones with Immunosuppressive Activities from a Podospora sp. *Journal of Natural Products* **2021**, *84* (2), 483-494.
- 31. Morrison, D. K., MAP kinase pathways. *Cold Spring Harbor perspectives in biology* **2012**, *4* (11), a011254.
- 32. Xu, J.; Chen, A.; Joy, J.; Xavier, V. J.; Ong, E. H.; Hill, J.; Chai, C. L., Rational design of resorcylic acid lactone analogues as covalent MNK1/2 kinase inhibitors by tuning the reactivity of an enamide Michael acceptor. **2013**.
- 33. Nguyen, T.; Coover, R. A.; Verghese, J.; Moran, R. G.; Ellis, K. C., Phenylalanine-based inactivator of AKT kinase: design, synthesis, and biological evaluation. *ACS medicinal chemistry letters* **2014**, *5* (5), 462-467.
- 34. Tibes, R.; Borad, M. J.; Dutcus, C. E.; Reyderman, L.; Feit, K.; Eisen, A.; Verbel, D. A.; Von Hoff, D. D., Safety, pharmacokinetics, and preliminary efficacy of E6201 in patients with advanced solid tumours, including melanoma: results of a phase 1 study. *British journal of cancer* **2018**, *118* (12), 1580-1585.
- 35. Chiricozzi, A.; Pitocco, R.; Saraceno, R.; Nistico, S. P.; Giunta, A.; Chimenti, S., New topical treatments for psoriasis. *Expert opinion on pharmacotherapy* **2014**, *15* (4), 461-470.
- 36. Shen, Y.; Boivin, R.; Yoneda, N.; Du, H.; Schiller, S.; Matsushima, T.; Goto, M.; Shirota, H.; Gusovsky, F.; Lemelin, C., Discovery of anti-inflammatory clinical candidate E6201, inspired from resorcylic lactone LL-Z1640-2, III. *Bioorganic & medicinal chemistry letters* **2010**, *20* (10), 3155-3157.
- 37. Narita, Y.; Okamoto, K.; Kawada, M. I.; Takase, K.; Minoshima, Y.; Kodama, K.; Iwata, M.; Miyamoto, N.; Sawada, K., Novel ATP-competitive MEK inhibitor E6201 is effective against vemurafenib-resistant melanoma harboring the MEK1-C121S mutation in a preclinical model. *Molecular cancer therapeutics* **2014**, *13* (4), 823-832.
- 38. Schwartz, P. A.; Kuzmic, P.; Solowiej, J.; Bergqvist, S.; Bolanos, B.; Almaden, C.; Nagata, A.; Ryan, K.; Feng, J.; Dalvie, D., Covalent EGFR inhibitor analysis reveals importance of reversible

- interactions to potency and mechanisms of drug resistance. *Proceedings of the National Academy of Sciences* **2014**, *111* (1), 173-178.
- 39. Merlin, J.-L., Les inhibiteurs de tyrosine kinase en oncologie. *Lett. pharmacol* **2008**, *22* (2), 51-62.
- 40. Lavaud, P.; Andre, F., Strategies to overcome trastuzumab resistance in HER2-overexpressing breast cancers: focus on new data from clinical trials. *BMC medicine* **2014**, *12* (1), 1-10.
- 41. Martin, M.; Holmes, F. A.; Ejlertsen, B.; Delaloge, S.; Moy, B.; Iwata, H.; von Minckwitz, G.; Chia, S. K.; Mansi, J.; Barrios, C. H., Neratinib after trastuzumab-based adjuvant therapy in HER2-positive breast cancer (ExteNET): 5-year analysis of a randomised, double-blind, placebo-controlled, phase 3 trial. *The lancet oncology* **2017**, *18* (12), 1688-1700.
- 42. Potashman, M. H.; Duggan, M. E., Covalent modifiers: an orthogonal approach to drug design. *Journal of medicinal chemistry* **2009**, *52* (5), 1231-1246.
- 43. Matuszak, N.; Muccioli, G. G.; Labar, G.; Lambert, D. M., Synthesis and in vitro evaluation of N-substituted maleimide derivatives as selective monoglyceride lipase inhibitors. *Journal of medicinal chemistry* **2009**, *52* (23), 7410-7420.
- 44. Kudo, N.; Matsumori, N.; Taoka, H.; Fujiwara, D.; Schreiner, E. P.; Wolff, B.; Yoshida, M.; Horinouchi, S., Leptomycin B inactivates CRM1/exportin 1 by covalent modification at a cysteine residue in the central conserved region. *Proc Natl Acad Sci U S A* **1999**, *96* (16), 9112-7.
- 45. Nachmias, B.; Schimmer, A. D., Targeting nuclear import and export in hematological malignancies. *Leukemia* **2020**, *34* (11), 2875-2886.
- 46. Krishnan, S.; Miller, R. M.; Tian, B.; Mullins, R. D.; Jacobson, M. P.; Taunton, J., Design of reversible, cysteine-targeted Michael acceptors guided by kinetic and computational analysis. *Journal of the American Chemical Society* **2014**, *136* (36), 12624-12630.
- 47. Gersch, M.; Kreuzer, J.; Sieber, S. A., Electrophilic natural products and their biological targets. *Natural product reports* **2012**, *29* (6), 659-682.
- 48. Dinkova-Kostova, A. T.; Massiah, M. A.; Bozak, R. E.; Hicks, R. J.; Talalay, P., Potency of Michael reaction acceptors as inducers of enzymes that protect against carcinogenesis depends on their reactivity with sulfhydryl groups. *Proceedings of the National Academy of Sciences* **2001**, *98* (6), 3404-3409.
- 49. Seaman, F. C., Sesquiterpene lactones as taxonomic characters in the Asteraceae. *The botanical review* **1982**, *48* (2), 121-594.
- 50. Moujir, L.; Callies, O.; Sousa, P.; Sharopov, F.; Seca, A. M., Applications of sesquiterpene lactones: a review of some potential success cases. *Applied Sciences* **2020**, *10* (9), 3001.
- 51. Jean, B., *Pharmacognosie, phytochimie, plantes médicinales (4e éd.)*. Lavoisier: 2009.
- 52. Duraipandiyan, V.; Al-Harbi, N. A.; Ignacimuthu, S.; Muthukumar, C., Antimicrobial activity of sesquiterpene lactones isolated from traditional medicinal plant, Costus speciosus (Koen ex. Retz.) Sm. *BMC complementary and alternative medicine* **2012**, *12* (1), 1-6.
- 53. Picman, A. K., Biological activities of sesquiterpene lactones. *Biochemical systematics and Ecology* **1986**, *14* (3), 255-281.
- 54. Merfort, I., Review of the analytical techniques for sesquiterpenes and sesquiterpene lactones. *Journal of Chromatography A* **2002**, *967* (1), 115-130.
- 55. Ghantous, A.; Gali-Muhtasib, H.; Vuorela, H.; Saliba, N. A.; Darwiche, N., What made sesquiterpene lactones reach cancer clinical trials? *Drug discovery today* **2010**, *15* (15-16), 668-678.
- 56. Adekenov, S., Sesquiterpene lactones with unusual structure. Their biogenesis and biological activity. *Fitoterapia* **2017**, *121*, 16-30.
- 57. Lesburg, C. A.; Caruthers, J. M.; Paschall, C. M.; Christianson, D. W., Managing and manipulating carbocations in biology: terpenoid cyclase structure and mechanism. *Current opinion in structural biology* **1998**, *8* (6), 695-703.
- 58. Schmidt, T. J., Structure-activity relationships of sesquiterpene lactones. In *Studies in natural products chemistry*, Elsevier: 2006; Vol. 33, pp 309-392.

- 59. Fischer, N.; Olivier, E.; Fischer, H., The biogenesis and chemistry of sesquiterpene lactones. In Fortschritte der chemie organischer naturstoffe/progress in the chemistry of organic natural products, Springer: 1979; pp 47-320.
- 60. Barton, D.; De Mayo, P., 25. Sesquiterpenoids. Part VIII. The constitution of pyrethrosin. *Journal of the Chemical Society (Resumed)* **1957**, 150-158.
- 61. Šorm, F.; Suchý, M.; Holub, M.; Linek, A.; Hadinec, I.; Novak, C., Crystalline structure of the addition compound of costunolide with silver nitrate. *Tetrahedron Letters* **1970**, *11* (22), 1893-1896.
- 62. Benešová, V.; Samek, Z.; Herout, V.; Šorm, F., The structure of nobilin. *Tetrahedron Letters* **1970,** *11* (57), 5017-5020.
- 63. Sorm, F., Sesquiterpenes wth ten-membered carbon rings. Review. *Journal of Agricultural and Food Chemistry* **1971,** *19* (6), 1081-1087.
- 64. Herz, W.; Sharma, R. P., Constituents of Liatris species. XI. Pycnolide, a seco-germacradienolide from Liatris pycnostachya, and other antitumor constituents of Liatris species. *The Journal of organic chemistry* **1976**, *41* (7), 1248-1253.
- 65. Bohlmann, F.; Gupta, R.; Jakupovic, J., Naturally occurring terpene derivatives, 292. The first sesquiterpene lactone with an allenic group [Vernonia cotoneaster]. *Liebigs Annalen der Chemie (Germany, FR)* **1980**.
- 66. Sarma, J.; Sharma, R.; De Jong, R.; Stam, C., Absolute stereochemistry of tagitinin A. *Phytochemistry* **1987**, *26* (8), 2406-2407.
- 67. Fraga, B. M., Natural sesquiterpenoids. *Natural product reports* **2012**, *29* (11), 1334-1366.
- 68. Boeckman Jr, R. K.; Yoon, S. K.; Heckendorn, D. K., Synthetic studies directed toward the eremantholides. 2. A novel application of the Ramberg-Baecklund rearrangement to a highly stereoselective synthesis of (+)-eremantholide A. *Journal of the American Chemical Society* **1991**, *113* (25), 9682-9684.
- 69. Sakamoto, S.; Tsuchiya, N.; Kuroyanagi, M.; Ueno, A., Biotransformation of germacrone by suspension cultured cells. *Phytochemistry* **1994**, *35* (5), 1215-1219.
- 70. Quijano, L.; Trejo, R. I.; Collera, O.; Ríos, T., Sesquiterpene lactones from Montanoa leucantha subsp. Leucantha. *Phytochemistry* **1994**, *36* (6), 1443-1448.
- 71. Nakamura, T.; Tsuboi, K.; Oshida, M.; Nomura, T.; Nakazaki, A.; Kobayashi, S., Total synthesis of (–)-diversifolin. *Tetrahedron Letters* **2009**, *50* (23), 2835-2839.
- 72. van Klink, J.; Becker, H.; Andersson, S.; Boland, W., Biosynthesis of anthecotuloide, an irregular sesquiterpene lactone from Anthemis cotula L.(Asteraceae) via a non-farnesyl diphosphate route. *Organic & biomolecular chemistry* **2003**, *1* (9), 1503-1508.
- 73. Lamarti, A.; Badoc, A.; Deffieux, G.; Carde, J., Biogénèse des Monoterpènes–II–La chaîne isoprénique. *Bull. Soc. Pharm. Bordeaux* **1994,** *133*, 79-99.
- 74. De Kraker, J.-W.; Franssen, M. C.; Joerink, M.; De Groot, A.; Bouwmeester, H. J., Biosynthesis of costunolide, dihydrocostunolide, and leucodin. Demonstration of cytochrome P450-catalyzed formation of the lactone ring present in sesquiterpene lactones of chicory. *Plant physiology* **2002**, *129* (1), 257-268.
- 75. Ramirez, A. M.; Saillard, N.; Yang, T.; Franssen, M. C.; Bouwmeester, H. J.; Jongsma, M. A., Biosynthesis of sesquiterpene lactones in pyrethrum (Tanacetum cinerariifolium). *PloS one* **2013**, *8* (5), e65030.
- 76. Perassolo, M.; Cardillo, A. B.; Busto, V. D.; Giulietti, A. M.; Talou, J. R., Biosynthesis of sesquiterpene lactones in plants and metabolic engineering for their biotechnological production. In *Sesquiterpene Lactones*, Springer: 2018; pp 47-91.
- 77. Yin, H.; Zhuang, Y.-b.; Li, E.; Bi, H.-p.; Zhou, W.; Liu, T., Heterologous biosynthesis of costunolide in Escherichia coli and yield improvement. *Biotechnology letters* **2015**, *37* (6), 1249-1255.
- 78. Chadwick, M.; Trewin, H.; Gawthrop, F.; Wagstaff, C., Sesquiterpenoids lactones: benefits to plants and people. *International journal of molecular sciences* **2013**, *14* (6), 12780-12805.
- 79. Schmidt, T. J., Toxic activities of sesquiterpene lactones: structural and biochemical aspects. *Curr Org Chem* **1999**, *3* (6), 577-608.

- 80. J Schmidt, T.; A Khalid, S.; J Romanha, A.; Ma Alves, T.; W Biavatti, M.; Brun, R.; B Da Costa, F.; L de Castro, S.; F Ferreira, V.; VG de Lacerda, M., The potential of secondary metabolites from plants as drugs or leads against protozoan neglected diseases-part II. *Current medicinal chemistry* **2012**, *19* (14), 2176-2228.
- 81. Schmidt, T. J.; Heilmann, J., Quantitative Structure-Cytotoxicity Relationships of Sesquiterpene Lactones derived from partial charge (Q)-based fr actional A ccessible S urface A rea Descriptors (Q frASAs). *Quantitative Structure-Activity Relationships* **2002**, *21* (3), 276-287.
- 82. Kupchan, S. M.; Fessler, D. C.; Eakin, M. A.; Giacobbe, T. J., Reactions of alpha methylene lactone tumor inhibitors with model biological nucleophiles. *Science* **1970**, *168* (3929), 376-378.
- 83. Bridgford, J. L.; Xie, S. C.; Cobbold, S. A.; Pasaje, C. F. A.; Herrmann, S.; Yang, T.; Gillett, D. L.; Dick, L. R.; Ralph, S. A.; Dogovski, C., Artemisinin kills malaria parasites by damaging proteins and inhibiting the proteasome. *Nature communications* **2018**, *9* (1), 1-9.
- 84. Graziose, R.; Ann Lila, M.; Raskin, I., Merging traditional Chinese medicine with modern drug discovery technologies to find novel drugs and functional foods. *Current drug discovery technologies* **2010**, *7* (1), 2-12.
- 85. Lu, F.; He, X.-L.; Richard, C.; Cao, J., A brief history of artemisinin: Modes of action and mechanisms of resistance. *Chin J Nat Med* **2019**, *17* (5), 331-336.
- 86. Klonis, N.; Creek, D. J.; Tilley, L., Iron and heme metabolism in Plasmodium falciparum and the mechanism of action of artemisinins. *Current opinion in microbiology* **2013**, *16* (6), 722-727.
- 87. Freund, R. R.; Gobrecht, P.; Fischer, D.; Arndt, H.-D., Advances in chemistry and bioactivity of parthenolide. *Natural product reports* **2020**, *37* (4), 541-565.
- 88. Zhang, S.; Won, Y.-K.; Ong, C.-N.; Shen, H.-M., Anti-cancer potential of sesquiterpene lactones: bioactivity and molecular mechanisms. *Current Medicinal Chemistry-Anti-Cancer Agents* **2005**, *5* (3), 239-249.
- 89. Perwez Hussain, S.; Harris, C. C., Inflammation and cancer: an ancient link with novel potentials. *International journal of cancer* **2007**, *121* (11), 2373-2380.
- 90. Mathema, V. B.; Koh, Y.-S.; Thakuri, B. C.; Sillanpää, M., Parthenolide, a sesquiterpene lactone, expresses multiple anti-cancer and anti-inflammatory activities. *Inflammation* **2012**, *35* (2), 560-565.
- 91. Tiuman, T. S.; Ueda-Nakamura, T.; Cortez, D. A. G.; Dias Filho, B. P.; Morgado-Díaz, J. A.; de Souza, W.; Nakamura, C. V., Antileishmanial activity of parthenolide, a sesquiterpene lactone isolated from Tanacetum parthenium. *Antimicrobial agents and Chemotherapy* **2005**, *49* (1), 176-182.
- 92. Izumi, E.; Morello, L. G.; Ueda-Nakamura, T.; Yamada-Ogatta, S. F.; Dias Filho, B. P.; Cortez, D. A. G.; Ferreira, I. C. P.; Morgado-Díaz, J. A.; Nakamura, C. V., Trypanosoma cruzi: antiprotozoal activity of parthenolide obtained from Tanacetum parthenium (L.) Schultz Bip.(Asteraceae, Compositae) against epimastigote and amastigote forms. *Experimental Parasitology* **2008**, *118* (3), 324-330.
- 93. Uruno, A.; Furusawa, Y.; Yagishita, Y.; Fukutomi, T.; Muramatsu, H.; Negishi, T.; Sugawara, A.; Kensler, T. W.; Yamamoto, M., The Keap1-Nrf2 system prevents onset of diabetes mellitus. *Molecular and cellular biology* **2013**, *33* (15), 2996-3010.
- 94. Wu, R. P.; Hayashi, T.; Cottam, H. B.; Jin, G.; Yao, S.; Wu, C. C.; Rosenbach, M. D.; Corr, M.; Schwab, R. B.; Carson, D. A., Nrf2 responses and the therapeutic selectivity of electrophilic compounds in chronic lymphocytic leukemia. *Proceedings of the National Academy of Sciences* **2010**, *107* (16), 7479-7484.
- 95. Le Lamer, A.-C.; Authier, H.; Rouaud, I.; Coste, A.; Boustie, J.; Pipy, B.; Gouault, N., Protolichesterinic acid derivatives: α -Methylene- γ -lactones as potent dual activators of PPAR γ and Nrf2 transcriptional factors. *Bioorganic & medicinal chemistry letters* **2014**, *24* (16), 3819-3822.
- 96. Zimmermann, S.; Kaiser, M.; Brun, R.; Hamburger, M.; Adams, M.; Tropical, S., bIntroduction. *Planta Med* **2012**, *78*, 553-556.
- 97. Zimmermann, S.; Oufir, M.; Leroux, A.; Krauth-Siegel, R. L.; Becker, K.; Kaiser, M.; Brun, R.; Hamburger, M.; Adams, M., Cynaropicrin targets the trypanothione redox system in Trypanosoma brucei. *Bioorganic & medicinal chemistry* **2013**, *21* (22), 7202-7209.

- 98. Vichnewski, W.; Sarti, S. J.; Gilbert, B.; Herz, W., Goyazensolide, a schistosomicidal heliangolide from Eremanthus goyazensis. *Phytochemistry* **1976**, *15* (1), 191-193.
- 99. Lunardello, M. A.; Tomaz, J. C.; Vichnewski, W.; Lopes, J. L. C.; Gutierrez, A. B.; Diaz, J. G.; Herz, W., Sesquiterpene Lactones and Flavonoids from Eremanthus-Mattogrossensis and Eremanthus-Eriopus. *J Brazil Chem Soc* **1995**, *6* (3), 307-311.
- 100. Grael, C. F. F.; Vichnewski, W.; de Souza, G. E. P.; Lopes, J. L. C.; Albuquerque, S.; Cunha, W. R., A study of the trypanocidal and analgesic properties from Lychnophora granmongolense (Duarte) Semir & Leitao Filho. *Phytother Res* **2000**, *14* (3), 203-206.
- 101. Grael, C. F. F.; Albuquerque, S.; Lopes, J. L. C., Chemical constituents of Lychnophora pohlii and trypanocidal activity of crude plant extracts and of isolated compounds. *Fitoterapia* **2005**, *76* (1), 73-82.
- 102. Vongvanich, N.; Kittakoop, P.; Charoenchai, P.; Intamas, S.; Sriklung, K.; Thebtaranonth, Y., Antiplasmodial, antimycobacterial, and cytotoxic principles from Camchaya calcarea. *Planta Med* **2006**, *72* (15), 1427-1430.
- 103. Valdes, D. A.; Bardon, A.; Catalan, C. A. N.; Gedris, T. E.; Herz, W., Goyazensolides and isogoyazensolides from Argentine Centratherum punctatum ssp. punctatum. *Biochem Syst Ecol* **1998**, *26* (7), 805-808.
- 104. Ren, Y.; Acuna, U. M.; Jimenez, F.; Garcia, R.; Mejia, M.; Chai, H.; Gallucci, J. C.; Farnsworth, N. R.; Soejarto, D. D.; de Blanco, E. J. C.; Kinghorn, A. D., Cytotoxic and NF-kappa B inhibitory sesquiterpene lactones from Piptocoma rufescens. *Tetrahedron* **2012**, *68* (12), 2671-2678.
- 105. de Menezes, N. L.; Semir, J., Burlemarxia, a new genus of Velloziaceae. *Taxon* **1991**, 413-426.
- 106. Liu, Y.; Jing, S.-X.; Luo, S.-H.; Li, S.-H., Non-volatile natural products in plant glandular trichomes: chemistry, biological activities and biosynthesis. *Natural product reports* **2019**, *36* (4), 626-665.
- 107. De Vivar, A. R.; Guerrero, C.; Diaz, E.; Ortega, A., Structure and stereochemistry of zexbrevin, A 3 (2H) furanone germacranolide. *Tetrahedron* **1970**, *26* (7), 1657-1664.
- 108. Herz, W.; Goedken, V. L., Structure of goyazensolide and its congeners. *The Journal of Organic Chemistry* **1982**, *47* (14), 2798-2800.
- 109. Brown, D. S.; Paquette, L. A., Synthetic studies on furanoheliangolides. Stereocontrolled construction of the oxygen-bridged tricyclic framework. *The Journal of Organic Chemistry* **1992,** *57* (16), 4512-4521.
- 110. Takao, K.-i.; Ochiai, H.; Yoshida, K.-i.; Hashizuka, T.; Koshimura, H.; Tadano, K.-i.; Ogawa, S., Novel total synthesis of (+)-eremantholide A. *The Journal of Organic Chemistry* **1995**, *60* (25), 8179-8193.
- 111. Li, Y.; Hale, K. J., Asymmetric total synthesis and formal total synthesis of the antitumor sesquiterpenoid (+)-eremantholide A. *Organic letters* **2007**, *9* (7), 1267-1270.
- 112. Tsuboi, K.; Nakamura, T.; Suzuki, T.; Nakazaki, A.; Kobayashi, S., Second-generation total synthesis of (–)-diversifolin. *Tetrahedron Letters* **2010**, *51* (14), 1876-1879.
- 113. Christianson, D. W., Structural and chemical biology of terpenoid cyclases. *Chemical reviews* **2017**, *117* (17), 11570-11648.
- 114. Miller, D. J.; Allemann, R. K., Sesquiterpene synthases: passive catalysts or active players? *Natural product reports* **2012**, *29* (1), 60-71.
- 115. Vichnewski, W.; Sarti, S. J.; Gilbert, B.; Herz, W., Goyazensolide, a Schistosomicidal Heliangolide from Eremanthus-Goyazensis. *Phytochemistry* **1976**, *15* (1), 191-193.
- 116. dos Santos, P. A.; Amarante, M. F. C.; Pereira, A. M. S.; Bertoni, B.; Franca, S. C.; Pessoa, C.; de Moraes, M. O.; Costa-Lotufo, L. V.; Pereira, M. R. P.; Lopes, N. P., Production of an antiproliferative furanoheliangolide by Lychnophora ericoides cell culture. *Chem Pharm Bull* **2004**, *52* (12), 1433-1435.
- 117. Mantovani, M. S.; Takahashi, C. S.; Vichnewski, W., Evaluation of the Genotoxic Activity of the Sesquiterpene Lactone Goyazensolide in Mammalian Systems in-Vitro Amd in-Vivo. *Rev Bras Genet* **1993**, *16* (4), 967-975.

- 118. Rungeler, P.; Castro, V.; Mora, G.; Goren, N.; Vichnewski, W.; Pahl, H. L.; Merfort, I.; Schmidt, T. J., Inhibition of transcription factor NF-kappa B by sesquiterpene lactones: a proposed molecular mechanism of action. *Bioorgan Med Chem* **1999**, *7* (11), 2343-2352.
- 119. Wagner, S.; Hofmann, A.; Siedle, B.; Terfloth, L.; Merfort, I.; Gasteiger, J., Development of a structural model for NF-kappa B inhibition of sesquiterpene lactones using self-organizing neural networks. *Journal of Medicinal Chemistry* **2006**, *49* (7), 2241-2252.
- 120. Schomburg, C.; Schuehly, W.; Da Costa, F. B.; Klempnauer, K. H.; Schmidt, T. J., Natural sesquiterpene lactones as inhibitors of Myb-dependent gene expression: Structure-activity relationships. *Eur J Med Chem* **2013**, *63*, 313-320.
- 121. Acuna, U. M.; Shen, Q.; Ren, Y.; Lantvit, D. D.; Wittwer, J. A.; Kinghorn, A. D.; Swanson, S. M.; de Blanco, E. J., Goyazensolide Induces Apoptosis in Cancer Cells in vitro and in vivo. *Int J Cancer Res* **2013**, *9* (2), 36-53.
- 122. Milagre, M. M.; Branquinho, R. T.; Goncalves, M. F.; de Assis, G. M. P.; de Oliveira, M. T.; Reis, L. E. S.; Saude-Guimaraes, D. A.; de Lana, M., Activity of the sesquiterpene lactone goyazensolide against Trypanosoma cruzi in vitro and in vivo. *Parasitology* **2020**, *147* (1), 108-119.
- 123. Lagoutte, R.; Pastor, M.; Berthet, M.; Winssinger, N., Rapid and scalable synthesis of chiral bromolactones as precursors to α -exo-methylene- γ -butyrolactone-containing sesquiterpene lactones. *Tetrahedron* **2018**, *74* (41), 6012-6021.
- 124. Banville, J.; Bouthillier, G.; Plamondon, S.; Remillard, R.; Meanwell, N. A.; Martel, A.; Walker, M. A., (Z)-2, 2-Dimethyl-5-carboxymethylene-1, 3-dioxolan-4-one: a new synthon for the synthesis of α , γ -diketoacid derivatives. *Tetrahedron Letters* **2010**, *51* (24), 3170-3173.
- 125. Ohira, S.; Yokogawa, Y.; Tsuji, S.; Mitsui, T.; Fukukawa, T.; Hayashi, K.-i.; Kuboki, A.; Matsuura, N.; Iinuma, M.; Nozaki, H., New naphthoquinone and monoterpenoid from Plumbago zeylanica. *Tetrahedron Letters* **2014**, *55* (48), 6554-6556.
- 126. Sun, W. C.; Ng, C. S.; Prestwich, G. D., Synthesis of partially fluorinated analogs of (Z)-5-decenyl acetate: probes for hydrophobic interaction in pheromone reception. *The Journal of Organic Chemistry* **1992,** *57* (1), 132-137.
- 127. Marson, C. M.; Edaan, E.; Morrell, J. M.; Coles, S. J.; Hursthouse, M. B.; Davies, D. T., A catalytic asymmetric protocol for the enantioselective synthesis of 3 (2 H)-furanones. *Chemical communications* **2007**, (24), 2494-2496.
- 128. Lagoutte, R.; Serba, C.; Abegg, D.; Hoch, D. G.; Adibekian, A.; Winssinger, N., Divergent synthesis and identification of the cellular targets of deoxyelephantopins. *Nature communications* **2016.** *7* (1), 1-11.
- 129. Gao, Y.; Wang, X.; Sun, L.; Xie, L.; Xu, X., Zinc or indium-mediated Barbier-type allylation of aldehydes with 3-bromomethyl-5H-furan-2-one in aqueous media: an efficient synthesis method for α -methylene- γ -butyrolactone. *Organic & biomolecular chemistry* **2012**, *10* (20), 3991-3998.
- 130. Cubbage, J.; Guo, Y.; McCulla, R.; Jenks, W., Thermolysis of alkyl sulfoxides and derivatives: a comparison of experiment and theory. *The Journal of organic chemistry* **2001**, *66* 26, 8722-36.
- 131. Wuts, P. G.; Greene, T. W., *Greene's protective groups in organic synthesis*. John Wiley & Sons: 2006.
- 132. Grubbs, R. H.; Miller, S. J.; Fu, G. C., Ring-closing metathesis and related processes in organic synthesis. *Accounts of chemical research* **1995**, *28* (11), 446-452.
- 133. Riley, H. L.; Morley, J. F.; Friend, N. A. C., 255. Selenium dioxide, a new oxidising agent. Part I. Its reaction with aldehydes and ketones. *Journal of the Chemical Society (Resumed)* **1932**, 1875-1883.
- 134. Mendgen, T.; Scholz, T.; Klein, C. D., Structure—activity relationships of tulipalines, tuliposides, and related compounds as inhibitors of MurA. *Bioorganic & medicinal chemistry letters* **2010**, *20* (19), 5757-5762.
- 135. Fürstner, A.; Nagano, T.; Müller, C.; Seidel, G.; Müller, O., Total Synthesis and Evaluation of the Actin-Binding Properties of Microcarpalide and a Focused Library of Analogues. *Chemistry—A European Journal* **2007**, *13* (5), 1452-1462.

- 136. Ramachandran, P. V.; Helppi, M. A.; Lehmkuhler, A. L.; Marchi, J. M.; Schmidt, C. M.; Yip-Schneider, M. T., Factors influencing the cytotoxicity of α -methylene- γ -hydroxy esters against pancreatic cancer. *Bioorganic & medicinal chemistry letters* **2015**, *25* (19), 4270-4273.
- 137. Ferreira, M.; Assunção, L. S.; Silva, A. H.; Filippin-Monteiro, F. B.; Creczynski-Pasa, T. B.; Sá, M. M., Allylic isothiouronium salts: The discovery of a novel class of thiourea analogues with antitumor activity. *European journal of medicinal chemistry* **2017**, *129*, 151-158.
- 138. Liu, W.; Yu, Z.; Winssinger, N., Total Syntheses of Paraconic Acids and 1, 10-seco-Guaianolides via a Barbier Allylation/Translactonization Cascade of 3-(Bromomethyl)-2 (5 H)-furanone. *Organic Letters* **2021**, *23* (3), 969-973.
- 139. Hodgson, D. M.; Talbot, E. P.; Clark, B. P., Synthesis of the anti-trypanosomal agent (±)-hydroxyanthecotulide by Cr (ii)-catalysed allylation and Meyer–Schuster rearrangement. *Chemical Communications* **2012**, *48* (51), 6349-6350.
- 140. Liu, W.-T.; Xu, Z.-L.; Mou, X.-Q.; Zhang, B.-H.; Bao, W.; Wang, S.-H.; Lee, D.; Lei, L.-S.; Zhang, K., The synthesis of cycloalka [b] furans via an Au (i)-catalyzed tandem reaction of 3-yne-1, 2-diols. *Organic & biomolecular chemistry* **2017**, *15* (30), 6333-6337.
- 141. Parikh, J. R.; Doering, W. v. E., Sulfur trioxide in the oxidation of alcohols by dimethyl sulfoxide. *Journal of the American Chemical Society* **1967**, *89* (21), 5505-5507.
- 142. Basavaiah, D.; Hyma, R. S.; Padmaja, K.; Krishnamacharyulu, M., The Baylis-Hillman reaction: An expedient synthesis of (Z)-keto allyl bromides and chlorides. *Tetrahedron* **1999**, *55* (22), 6971-6976.
- 143. Lima, S. R.; Coelho, F., Synthesis of 1, 4, 6-Tricarbonyl Compounds via Regioselective Gold (I)-Catalyzed Alkyne Hydration and Their Application in the Synthesis of α -Arylidene-butyrolactones. *ACS omega* **2020**, *5* (14), 8032-8045.
- 144. Lim, C. H.; Kim, S. H.; Lee, H. J.; Kim, H. J.; Kim, J. N., An Expedient Synthesis of Cinnamyl Fluorides from Morita-Baylis-Hillman Adducts. *Bulletin of the Korean Chemical Society* **2013**, *34* (3), 993-996.
- 145. Charette, A. B.; Cote, B.; Monroc, S.; Prescott, S., Synthesis of Monoprotected 2-Alkylidene-1, 3-propanediols by an Unusual SN2'Mitsunobu Reaction. *The Journal of Organic Chemistry* **1995**, *60* (21), 6888-6894.
- 146. Gil, A.; Albericio, F.; Álvarez, M., Role of the Nozaki–Hiyama–Takai–Kishi reaction in the synthesis of natural products. *Chemical reviews* **2017**, *117* (12), 8420-8446.
- 147. Marshall, J. A.; Griot, C. A.; Chobanian, H. R.; Myers, W. H., Synthesis of a Lactone Diastereomer of the Cembranolide Uprolide D. *Organic letters* **2010**, *12* (19), 4328-4331.
- 148. Chen, W.; Yang, Q.; Zhou, T.; Tian, Q.; Zhang, G., Enantioselective synthesis of α -exomethylene γ -butyrolactones via chromium catalysis. *Organic letters* **2015**, *17* (21), 5236-5239.
- 149. Hu, X.; Xu, S.; Maimone, T. J., A Double Allylation Strategy for Gram-Scale Guaianolide Production: Total Synthesis of (+)-Mikanokryptin. *Angewandte Chemie International Edition* **2017**, *56* (6), 1624-1628.
- 150. Gund, M.; Déry, M.; Amzallag, V. r.; Spino, C., Dialkoxycarbenes in (4+ 1) Cycloadditions: Application to the Synthesis of Carotol. *Organic letters* **2016**, *18* (17), 4280-4283.
- 151. Penner, M.; Rauniyar, V.; Kaspar, L. T.; Hall, D. G., Catalytic asymmetric synthesis of palmerolide A via organoboron methodology. *Journal of the American Chemical Society* **2009**, *131* (40), 14216-14217.
- 152. Brummond, K. M.; Lu, J.; Petersen, J., A rapid synthesis of hydroxymethylacylfulvene (HMAF) using the allenic Pauson– Khand reaction. A synthetic approach to either enantiomer of this illudane structure. *Journal of the American Chemical Society* **2000**, *122* (20), 4915-4920.
- 153. Hoye, T. R.; Jeffrey, C. S.; Shao, F., Mosher ester analysis for the determination of absolute configuration of stereogenic (chiral) carbinol carbons. *Nature protocols* **2007**, *2* (10), 2451-2458.
- 154. Kutsumura, N.; Kiriseko, A.; Saito, T., TOTAL SYNTHESIS OF (+)-HETEROPLEXISOLIDE E (Dedicated to Professor Dr. Ei-ichi Negishi on the occasion of his 77th birthday). *Heterocycles: an international journal for reviews and communications in heterocyclic chemistry* **2012**, *86* (2), 1367-1378.

- 155. Ghosh, A. K.; Gong, G., Total synthesis and revision of C6 stereochemistry of (+)-amphidinolide W. *The Journal of organic chemistry* **2006**, *71* (3), 1085-1093.
- 156. Kutsumura, N.; Niwa, K.; Saito, T., Novel One-Pot Method for Chemoselective Bromination and Sequential Sonogashira Coupling. *Organic letters* **2010**, *12* (15), 3316-3319.
- 157. Kutsumura, N.; Yokoyama, T.; Ohgiya, T.; Nishiyama, S., 1, 2-Dibromoalkanes into alkynes by elimination reaction under DBU conditions and their application to total synthesis of sapinofuranone B. *Tetrahedron letters* **2006**, *47* (25), 4133-4136.
- 158. Wright, J. A.; Yu, J.; Spencer, J. B., Sequential removal of the benzyl-type protecting groups PMB and NAP by oxidative cleavage using CAN and DDQ. *Tetrahedron Letters* **2001**, *42* (24), 4033-4036.
- 159. Siedle, B.; García-Piñeres, A. J.; Murillo, R.; Schulte-Mönting, J.; Castro, V.; Rüngeler, P.; Klaas, C. A.; Da Costa, F. B.; Kisiel, W.; Merfort, I., Quantitative structure– activity relationship of sesquiterpene lactones as inhibitors of the transcription Factor NF-κB. *Journal of medicinal chemistry* **2004**, *47* (24), 6042-6054.
- 160. Engel, D. A.; Dudley, G. B., The Meyer–Schuster rearrangement for the synthesis of α , β -unsaturated carbonyl compounds. *Organic & biomolecular chemistry* **2009**, *7* (20), 4149-4158.
- 161. Roy, D.; Tharra, P.; Baire, B., Intercepted Meyer–Schuster Rearrangements in Organic Synthesis. *Asian Journal of Organic Chemistry* **2018**, *7* (6), 1015-1032.
- 162. Schmitt, E. K.; Hoepfner, D.; Krastel, P., Natural products as probes in pharmaceutical research. *Journal of Industrial Microbiology and Biotechnology* **2016**, *43* (2-3), 249-260.
- 163. Chemla, F.; Dulong, F.; Ferreira, F.; Pérez-Luna, A., Radical zinc-atom-transfer-based carbozincation of haloalkynes with dialkylzincs. *Beilstein journal of organic chemistry* **2013**, *9* (1), 236-245.
- 164. Inanaga, J.; Hirata, K.; Saeki, H.; Katsuki, T.; Yamaguchi, M., A rapid esterification by means of mixed anhydride and its application to large-ring lactonization. *Bulletin of the chemical society of Japan* **1979**, *52* (7), 1989-1993.
- 165. Jitrapakdee, S.; St Maurice, M.; Rayment, I.; Cleland, W. W.; Wallace, J. C.; Attwood, P. V., Structure, mechanism and regulation of pyruvate carboxylase. *Biochemical journal* **2008**, *413* (3), 369-387.
- 166. Deane, R.; Schäfer, W.; Zimmermann, H.-P.; Mueller, L.; Görlich, D.; Prehn, S.; Ponstingl, H.; Bischoff, F. R., Ran-binding protein 5 (RanBP5) is related to the nuclear transport factor importin-beta but interacts differently with RanBP1. *Molecular and cellular biology* **1997**, *17* (9), 5087-5096.
- 167. Ström, A.-C.; Weis, K., Importin-beta-like nuclear transport receptors. *Genome biology* **2001**, *2* (6), 1-9.
- 168. Arnold, M.; Nath, A.; Hauber, J.; Kehlenbach, R. H., Multiple importins function as nuclear transport receptors for the Rev protein of human immunodeficiency virus type 1. *Journal of Biological Chemistry* **2006**, *281* (30), 20883-20890.
- 169. Hutchinson, E. C.; Orr, O. E.; Liu, S. M.; Engelhardt, O. G.; Fodor, E., Characterization of the interaction between the influenza A virus polymerase subunit PB1 and the host nuclear import factor Ran-binding protein 5. *Journal of general virology* **2011**, *92* (8), 1859-1869.
- 170. Krawczyk, E.; Hanover, J. A.; Schlegel, R.; Suprynowicz, F. A., Karyopherin β3: a new cellular target for the HPV-16 E5 oncoprotein. *Biochemical and biophysical research communications* **2008**, *371* (4), 684-688.
- 171. Hutchinson, E. C.; Denham, E. M.; Thomas, B.; Trudgian, D. C.; Hester, S. S.; Ridlova, G.; York, A.; Turrell, L.; Fodor, E., Mapping the phosphoproteome of influenza A and B viruses by mass spectrometry. *PLoS pathogens* **2012**, *8* (11), e1002993.
- 172. Li, X.; Aierken, A.; Shen, L., IPO5 promotes malignant progression of esophageal cancer through activating MMP7. *European review for medical and pharmacological sciences* **2020**, *24* (8), 4246-4254.
- 173. Zhang, W.; Lu, Y.; Li, X.; Zhang, J.; Lin, W.; Zhang, W.; Zheng, L.; Li, X., IPO5 promotes the proliferation and tumourigenicity of colorectal cancer cells by mediating RASAL2 nuclear transportation. *Journal of Experimental & Clinical Cancer Research* **2019**, *38* (1), 1-14.

- 174. Patouret, R., The Nuclear Transport Protein Importin-5: A Promising Target in Oncology and Virology. *Chimia* **2021**, *75* (4), 319-322.
- 175. Levin, A.; Neufeldt, C. J.; Pang, D.; Wilson, K.; Loewen-Dobler, D.; Joyce, M. A.; Wozniak, R. W.; Tyrrell, D. L. J., Functional characterization of nuclear localization and export signals in hepatitis C virus proteins and their role in the membranous web. *PloS one* **2014**, *9* (12), e114629.
- 176. Görlich, D.; Kutay, U., Transport between the cell nucleus and the cytoplasm. *Annual review of cell and developmental biology* **1999**, *15* (1), 607-660.
- 177. Kudo, N.; Matsumori, N.; Taoka, H.; Fujiwara, D.; Schreiner, E. P.; Wolff, B.; Yoshida, M.; Horinouchi, S., Leptomycin B inactivates CRM1/exportin 1 by covalent modification at a cysteine residue in the central conserved region. *Proceedings of the National Academy of Sciences* **1999**, *96* (16), 9112-9117.
- 178. Wagstaff, K. M.; Sivakumaran, H.; Heaton, S. M.; Harrich, D.; Jans, D. A., Ivermectin is a specific inhibitor of importin α/β -mediated nuclear import able to inhibit replication of HIV-1 and dengue virus. *Biochemical Journal* **2012**, *443* (3), 851-856.
- 179. Mahipal, A.; Malafa, M., Importins and exportins as therapeutic targets in cancer. *Pharmacology & therapeutics* **2016**, *164*, 135-143.
- 180. Kosyna, F. K.; Depping, R., Controlling the gatekeeper: therapeutic targeting of nuclear transport. *Cells* **2018**, *7* (11), 221.
- 181. Dorel, R.; Echavarren, A. M., Gold (I)-catalyzed activation of alkynes for the construction of molecular complexity. *Chemical reviews* **2015**, *115* (17), 9028-9072.
- 182. Le Quesne, P. W.; Levery, S. B.; Menachery, M. D.; Brennan, T. F.; Raffauf, R. F., Antitumour plants. Part 6. Novel modified germacranolides and other constituents of Eremanthus elaeagnus Schultz-Bip (Compositae). *Journal of the Chemical Society, Perkin Transactions 1* **1978,** (12), 1572-1580.
- 183. Schmidt, T. J., Helenanolide-type sesquiterpene lactones—III. Rates and stereochemistry in the reaction of helenalin and related helenanolides with sulfhydryl containing biomolecules. *Bioorganic & medicinal chemistry* **1997**, *5* (4), 645-653.
- 184. Kupchan, S. M.; Anderson, W. K.; Bollinger, P.; Doskotch, R. W.; Smith, R. M.; Saenz-Renauld, J. A.; Schnoes, H. K.; Burlingame, A. L.; Smith, D. H., Tumor inhibitors. XXXIX. Active principles of Acnistur arborescens. Isolation and structural and spectral studies of withaferin a and withacnistin. *The Journal of organic chemistry* **1969**, *34* (12), 3858-3866.
- 185. Pires, N.; Gota, V.; Gulia, A.; Hingorani, L.; Agarwal, M.; Puri, A., Safety and pharmacokinetics of Withaferin-A in advanced stage high grade osteosarcoma: A phase I trial. *Journal of Ayurveda and integrative medicine* **2020**, *11* (1), 68-72.
- 186. Stan, S. D.; Hahm, E.-R.; Warin, R.; Singh, S. V., Withaferin A causes FOXO3a-and Bimdependent apoptosis and inhibits growth of human breast cancer cells in vivo. *Cancer research* **2008**, *68* (18), 7661-7669.
- 187. Lee, J.; Hahm, E.-R.; Singh, S. V., Withaferin A inhibits activation of signal transducer and activator of transcription 3 in human breast cancer cells. *Carcinogenesis* **2010**, *31* (11), 1991-1998.
- 188. Hahm, E.-R.; Moura, M. B.; Kelley, E. E.; Van Houten, B.; Shiva, S.; Singh, S. V., Withaferin A-induced apoptosis in human breast cancer cells is mediated by reactive oxygen species. *PloS one* **2011**, *6* (8), e23354.
- 189. Stan, S. D.; Zeng, Y.; Singh, S. V., Ayurvedic medicine constituent withaferin a causes G2 and M phase cell cycle arrest in human breast cancer cells. *Nutrition and cancer* **2008**, *60* (S1), 51-60.
- 190. Thaiparambil, J. T.; Bender, L.; Ganesh, T.; Kline, E.; Patel, P.; Liu, Y.; Tighiouart, M.; Vertino, P. M.; Harvey, R. D.; Garcia, A., Withaferin A inhibits breast cancer invasion and metastasis at subcytotoxic doses by inducing vimentin disassembly and serine 56 phosphorylation. *International journal of cancer* **2011**, *129* (11), 2744-2755.
- 191. Liu, W.; Wang, G.; Palovcak, A.; Li, Y.; Hao, S.; Liu, Z.-J.; Landgraf, R.; Yuan, F.; Zhang, Y., Impeding the single-strand annealing pathway of DNA double-strand break repair by withaferin A-mediated FANCA degradation. *DNA repair* **2019**, *77*, 10-17.

- 192. Muniraj, N.; Siddharth, S.; Nagalingam, A.; Walker, A.; Woo, J.; Győrffy, B.; Gabrielson, E.; Saxena, N. K.; Sharma, D., Withaferin A inhibits lysosomal activity to block autophagic flux and induces apoptosis via energetic impairment in breast cancer cells. *Carcinogenesis* **2019**, *40* (9), 1110-1120.
- 193. Kakar, S. S.; Jala, V. R.; Fong, M. Y., Synergistic cytotoxic action of cisplatin and withaferin A on ovarian cancer cell lines. *Biochemical and biophysical research communications* **2012**, *423* (4), 819-825.
- 194. Devi, P. U.; Kamath, R.; Rao, B., Radiosensitization of a mouse melanoma by withaferin A: in vivo studies. **2000**.
- 195. Zhang, X.; Samadi, A. K.; Roby, K. F.; Timmermann, B.; Cohen, M. S., Inhibition of cell growth and induction of apoptosis in ovarian carcinoma cell lines CaOV3 and SKOV3 by natural withanolide Withaferin A. *Gynecologic oncology* **2012**, *124* (3), 606-612.
- 196. Straughn, A. R.; Kakar, S. S., Withaferin A ameliorates ovarian cancer-induced cachexia and proinflammatory signaling. *Journal of ovarian research* **2019**, *12* (1), 1-14.
- 197. Kelm, N. Q.; Straughn, A. R.; Kakar, S. S., Withaferin A attenuates ovarian cancer-induced cardiac cachexia. *Plos one* **2020**, *15* (7), e0236680.
- 198. Kakar, S. S.; Parte, S.; Kelsey Carter, I. G. J.; Worth, C.; Rameshwar, P.; Ratajczak, M. Z., Withaferin A (WFA) inhibits tumor growth and metastasis by targeting ovarian cancer stem cells. *Oncotarget* **2017**, *8* (43), 74494.
- 199. Bargagna-Mohan, P.; Deokule, S. P.; Thompson, K.; Wizeman, J.; Srinivasan, C.; Vooturi, S.; Kompella, U. B.; Mohan, R., Withaferin A effectively targets soluble vimentin in the glaucoma filtration surgical model of fibrosis. *PLoS One* **2013**, *8* (5), e63881.
- 200. Bargagna-Mohan, P.; Hamza, A.; Kim, Y.-e.; Ho, Y. K. A.; Mor-Vaknin, N.; Wendschlag, N.; Liu, J.; Evans, R. M.; Markovitz, D. M.; Zhan, C.-G., The tumor inhibitor and antiangiogenic agent withaferin A targets the intermediate filament protein vimentin. *Chemistry & biology* **2007**, *14* (6), 623-634.
- 201. Grin, B.; Mahammad, S.; Wedig, T.; Cleland, M. M.; Tsai, L.; Herrmann, H.; Goldman, R. D., Withaferin a alters intermediate filament organization, cell shape and behavior. *PloS one* **2012**, *7* (6), e39065.
- 202. Moselhy, J.; Suman, S.; Alghamdi, M.; Chandarasekharan, B.; Das, T. P.; Houda, A.; Ankem, M.; Damodaran, C., Withaferin A inhibits prostate carcinogenesis in a PTEN-deficient mouse model of prostate cancer. *Neoplasia* **2017**, *19* (6), 451-459.
- 203. Suman, S.; Das, T. P.; Moselhy, J.; Pal, D.; Kolluru, V.; Alatassi, H.; Ankem, M. K.; Damodaran, C., Oral administration of withaferin A inhibits carcinogenesis of prostate in TRAMP model. *Oncotarget* **2016**, *7* (33), 53751.
- 204. Srinivasan, S.; Ranga, R. S.; Burikhanov, R.; Han, S.-S.; Chendil, D., Par-4-dependent apoptosis by the dietary compound withaferin A in prostate cancer cells. *Cancer research* **2007**, *67* (1), 246-253.
- 205. Kim, S.-H.; Hahm, E.-R.; Singh, K. B.; Shiva, S.; Stewart-Ornstein, J.; Singh, S. V., RNA-seq reveals novel mechanistic targets of withaferin A in prostate cancer cells. *Carcinogenesis* **2020**, *41* (6), 778-789.
- 206. Das, T.; Roy, K. S.; Chakrabarti, T.; Mukhopadhyay, S.; Roychoudhury, S., Withaferin A modulates the Spindle Assembly Checkpoint by degradation of Mad2–Cdc20 complex in colorectal cancer cell lines. *Biochemical pharmacology* **2014**, *91* (1), 31-39.
- 207. Koduru, S.; Kumar, R.; Srinivasan, S.; Evers, M. B.; Damodaran, C., Notch-1 inhibition by Withaferin-A: a therapeutic target against colon carcinogenesis. *Molecular cancer therapeutics* **2010**, *9* (1), 202-210.
- 208. Pal, D.; Tyagi, A.; Chandrasekaran, B.; Alattasi, H.; Ankem, M. K.; Sharma, A. K.; Damodaran, C., Suppression of Notch1 and AKT mediated epithelial to mesenchymal transition by Verrucarin J in metastatic colon cancer. *Cell death & disease* **2018**, *9* (8), 1-11.
- 209. Chandrasekaran, B.; Pal, D.; Kolluru, V.; Tyagi, A.; Baby, B.; Dahiya, N. R.; Youssef, K.; Alatassi, H.; Ankem, M. K.; Sharma, A. K., The chemopreventive effect of withaferin A on spontaneous and inflammation-associated colon carcinogenesis models. *Carcinogenesis* **2018**, *39* (12), 1537-1547.
- 210. Kyakulaga, A. H.; Aqil, F.; Munagala, R.; Gupta, R. C., Withaferin a inhibits epithelial to mesenchymal transition in non-small cell lung cancer cells. *Scientific reports* **2018**, *8* (1), 1-14.

- 211. Khalilpourfarshbafi, M.; Devi Murugan, D.; Abdul Sattar, M. Z.; Sucedaram, Y.; Abdullah, N. A., Withaferin A inhibits adipogenesis in 3T3-F442A cell line, improves insulin sensitivity and promotes weight loss in high fat diet-induced obese mice. *PloS one* **2019**, *14* (6), e0218792.
- 212. Riboulet-Chavey, A.; Diraison, F.; Siew, L. K.; Wong, F. S.; Rutter, G. A., Inhibition of AMP-activated protein kinase protects pancreatic β -cells from cytokine-mediated apoptosis and CD8+ T-cell-induced cytotoxicity. *Diabetes* **2008**, *57* (2), 415-423.
- 213. Vesa, C. M.; Popa, A. R.; Bungau, S.; Daina, L. G.; Buhas, C.; Judea-Pusta, C. T.; Pasca, B.; Dimulescu, I. A.; Zaha, D. C., Exploration of insulin sensitivity, insulin resistance, early insulin secretion and β -cell function, and their relationship with glycated hemoglobin level in normal weight patients with newly diagnosed type 2 diabetes mellitus. *Rev Chim* **2019**, *70*, 4217-4223.
- 214. Tekula, S.; Khurana, A.; Anchi, P.; Godugu, C., Withaferin-A attenuates multiple low doses of Streptozotocin (MLD-STZ) induced type 1 diabetes. *Biomedicine & Pharmacotherapy* **2018**, *106*, 1428-1440.
- 215. Batumalaie, K.; Amin, M. A.; Murugan, D. D.; Sattar, M. Z. A.; Abdullah, N. A., Withaferin A protects against palmitic acid-induced endothelial insulin resistance and dysfunction through suppression of oxidative stress and inflammation. *Scientific reports* **2016**, *6* (1), 1-11.
- 216. Tiwari, S.; Atluri, V. S. R.; Yndart Arias, A.; Jayant, R. D.; Kaushik, A.; Geiger, J.; Nair, M. N., Withaferin a suppresses beta amyloid in APP expressing cells: studies for tat and cocaine associated neurological dysfunctions. *Frontiers in aging neuroscience* **2018**, *10*, 291.
- 217. Choudhary, M. I.; Yousuf, S.; Nawaz, S. A.; Ahmed, S., Cholinesterase inhibiting withanolides from Withania somnifera. *Chemical and pharmaceutical bulletin* **2004**, *52* (11), 1358-1361.
- 218. Banu, M. R.; Ibrahim, M.; Prabhu, K.; Rajasankar, S., Withaferin-A protects the nigral dopamine neuron and recovers motor activity in aged rats. *Cells Tissues Organs* **2019**, *208* (1-2), 59-65.
- 219. Zhou, Z.; Xiang, W.; Jiang, Y.; Tian, N.; Wei, Z.; Wen, X.; Wang, W.; Liao, W.; Xia, X.; Li, Q., Withaferin A alleviates traumatic brain injury induced secondary brain injury via suppressing apoptosis in endothelia cells and modulating activation in the microglia. *European journal of pharmacology* **2020**, *874*. 172988.
- 220. Khan, Z. A.; Ghosh, A. R., Withaferin-A displays enhanced anxiolytic efficacy without tolerance in rats following sub chronic administration. *African Journal of Biotechnology* **2011**, *10* (60), 12973-12978.
- 221. Guo, R.; Gan, L.; Lau, W. B.; Yan, Z.; Xie, D.; Gao, E.; Christopher, T. A.; Lopez, B. L.; Ma, X.; Wang, Y., Withaferin A Prevents Myocardial Ischemia/Reperfusion Injury by Upregulating AMP-Activated Protein Kinase-Dependent B-Cell Lymphoma2 Signaling. *Circulation Journal* **2019**, *83* (8), 1726-1736.
- 222. Ku, S.-K.; Bae, J.-S., Antiplatelet, anticoagulant, and profibrinolytic activities of withaferin A. *Vascular pharmacology* **2014**, *60* (3), 120-126.
- 223. Khedgikar, V.; Kushwaha, P.; Gautam, J.; Verma, A.; Changkija, B.; Kumar, A.; Sharma, S.; Nagar, G.; Singh, D.; Trivedi, P., Withaferin A: a proteasomal inhibitor promotes healing after injury and exerts anabolic effect on osteoporotic bone. *Cell death & disease* **2013**, *4* (8), e778-e778.
- 224. Patel, D. P.; Yan, T.; Kim, D.; Dias, H. B.; Krausz, K. W.; Kimura, S.; Gonzalez, F. J., Withaferin A improves nonalcoholic steatohepatitis in mice. *Journal of Pharmacology and Experimental Therapeutics* **2019**, *371* (2), 360-374.
- 225. Kumar, V.; Dhanjal, J. K.; Kaul, S. C.; Wadhwa, R.; Sundar, D., Withanone and caffeic acid phenethyl ester are predicted to interact with main protease (Mpro) of SARS-CoV-2 and inhibit its activity. *Journal of Biomolecular Structure and Dynamics* **2020**, 1-13.
- 226. Straughn, A. R.; Kakar, S. S., Withaferin A: a potential therapeutic agent against COVID-19 infection. *Journal of Ovarian Research* **2020**, *13* (1), 1-5.
- 227. Cai, Z.; Zhang, G.; Tang, B.; Liu, Y.; Fu, X.; Zhang, X., Promising anti-influenza properties of active constituent of Withania somnifera ayurvedic herb in targeting neuraminidase of H1N1 influenza: Computational study. *Cell biochemistry and biophysics* **2015**, *72* (3), 727-739.

- 228. Dom, M.; Offner, F.; Berghe, W. V.; Van Ostade, X., Proteomic characterization of Withaferin A-targeted protein networks for the treatment of monoclonal myeloma gammopathies. *Journal of proteomics* **2018**, *179*, 17-29.
- 229. Grossman, E. A.; Ward, C. C.; Spradlin, J. N.; Bateman, L. A.; Huffman, T. R.; Miyamoto, D. K.; Kleinman, J. I.; Nomura, D. K., Covalent ligand discovery against druggable hotspots targeted by anticancer natural products. *Cell chemical biology* **2017**, *24* (11), 1368-1376. e4.
- 230. Narayan, M.; Seeley, K. W.; Jinwal, U. K., Identification and quantitative analysis of cellular proteins affected by treatment with withaferin a using a SILAC-based proteomics approach. *Journal of ethnopharmacology* **2015**, *175*, 86-92.
- 231. Dom, M.; Berghe, W. V.; Van Ostade, X., Broad-spectrum antitumor properties of Withaferin A: A proteomic perspective. *RSC Medicinal Chemistry* **2020**, *11* (1), 30-50.
- 232. Liu, X.; Chen, L.; Liang, T.; Tian, X.-d.; Liu, Y.; Zhang, T., Withaferin A induces mitochondrial-dependent apoptosis in non-small cell lung cancer cells via generation of reactive oxygen species. *J BUON* **2017**, *22* (1), 244-250.
- 233. Cai, Y.; Sheng, Z.-Y.; Chen, Y.; Bai, C., Effect of Withaferin A on A549 cellular proliferation and apoptosis in non-small cell lung cancer. *Asian Pacific Journal of Cancer Prevention* **2014**, *15* (4), 1711-1714.
- 234. Ozorowski, G.; Ryan, C. M.; Whitelegge, J. P.; Luecke, H., Withaferin A binds covalently to the N-terminal domain of annexin A2. *Biological chemistry* **2012**, *393* (10), 1151-1163.
- 235. Yu, Y.; Hamza, A.; Zhang, T.; Gu, M.; Zou, P.; Newman, B.; Li, Y.; Gunatilaka, A. L.; Zhan, C.-G.; Sun, D., Withaferin A targets heat shock protein 90 in pancreatic cancer cells. *Biochemical pharmacology* **2010**, *79* (4), 542-551.
- 236. Singh, D.; Aggarwal, A.; Maurya, R.; Naik, S., Withania somnifera inhibits NF-κB and AP-1 transcription factors in human peripheral blood and synovial fluid mononuclear cells. *Phytotherapy Research* **2007**, *21* (10), 905-913.
- 237. Heyninck, K.; Lahtela-Kakkonen, M.; Van der Veken, P.; Haegeman, G.; Berghe, W. V., Withaferin A inhibits NF-kappaB activation by targeting cysteine 179 in IKKβ. *Biochemical pharmacology* **2014**, *91* (4), 501-509.
- 238. LeBouder, F.; Morello, E.; Rimmelzwaan, G. F.; Bosse, F.; Péchoux, C.; Delmas, B.; Riteau, B., Annexin II incorporated into influenza virus particles supports virus replication by converting plasminogen into plasmin. *Journal of virology* **2008**, *82* (14), 6820-6828.
- 239. LeBouder, F.; Lina, B.; Rimmelzwaan, G. F.; Riteau, B., Plasminogen promotes influenza A virus replication through an annexin 2-dependent pathway in the absence of neuraminidase. *Journal of general virology* **2010**, *91* (11), 2753-2761.
- 240. Wu, W.; Panté, N., Vimentin plays a role in the release of the influenza A viral genome from endosomes. *Virology* **2016**, *497*, 41-52.
- 241. Ramos, I.; Stamatakis, K.; Oeste, C. L.; Pérez-Sala, D., Vimentin as a multifaceted player and potential therapeutic target in viral infections. *International journal of molecular sciences* **2020**, *21* (13), 4675.
- 242. Ma, Y.; Sun, J.; Gu, L.; Bao, H.; Zhao, Y.; Shi, L.; Yao, W.; Tian, G.; Wang, X.; Chen, H., Annexin A2 (ANXA2) interacts with nonstructural protein 1 and promotes the replication of highly pathogenic H5N1 avian influenza virus. *BMC microbiology* **2017**, *17* (1), 1-9.
- 243. Zhang, Y.; Wen, Z.; Shi, X.; Liu, Y.-J.; Eriksson, J. E.; Jiu, Y., The diverse roles and dynamic rearrangement of vimentin during viral infection. *Journal of Cell Science* **2021**, *134* (5), jcs250597.
- 244. Momose, F.; Naito, T.; Yano, K.; Sugimoto, S.; Morikawa, Y.; Nagata, K., Identification of Hsp90 as a stimulatory host factor involved in influenza virus RNA synthesis. *Journal of Biological Chemistry* **2002**, *277* (47), 45306-45314.
- 245. Chase, G.; Deng, T.; Fodor, E.; Leung, B. W.; Mayer, D.; Schwemmle, M.; Brownlee, G., Hsp90 inhibitors reduce influenza virus replication in cell culture. *Virology* **2008**, *377* (2), 431-439.
- 246. Naito, T.; Momose, F.; Kawaguchi, A.; Nagata, K., Involvement of Hsp90 in assembly and nuclear import of influenza virus RNA polymerase subunits. *Journal of virology* **2007**, *81* (3), 1339-1349.

- 247. Momose, F.; Kikuchi, Y.; Komase, K.; Morikawa, Y., Visualization of microtubule-mediated transport of influenza viral progeny ribonucleoprotein. *Microbes and infection* **2007**, *9* (12-13), 1422-1433.
- 248. Bernasconi, D.; Amici, C.; La Frazia, S.; Ianaro, A.; Santoro, M. G., The IkB kinase is a key factor in triggering influenza A virus-induced inflammatory cytokine production in airway epithelial cells. *Journal of Biological Chemistry* **2005**, *280* (25), 24127-24134.
- 249. Ehrhardt, C.; Rückle, A.; Hrincius, E. R.; Haasbach, E.; Anhlan, D.; Ahmann, K.; Banning, C.; Reiling, S. J.; Kühn, J.; Strobl, S., The NF-κ B inhibitor SC 75741 efficiently blocks influenza virus propagation and confers a high barrier for development of viral resistance. *Cellular microbiology* **2013**, *15* (7), 1198-1211.
- 250. Yan, H.; Wang, H.; Ma, L.; Ma, X.; Yin, J.; Wu, S.; Huang, H.; Li, Y., Cirsimaritin inhibits influenza A virus replication by downregulating the NF-κB signal transduction pathway. *Virology journal* **2018**, *15* (1), 1-9.
- 251. Falkenberg, K. D.; Jakobs, A.; Matern, J. C.; Dörner, W.; Uttarkar, S.; Trentmann, A.; Steinmann, S.; Coulibaly, A.; Schomburg, C.; Mootz, H. D., Withaferin A, a natural compound with anti-tumor activity, is a potent inhibitor of transcription factor C/EBPβ. *Biochimica et Biophysica Acta (BBA)-Molecular Cell Research* **2017**, *1864* (7), 1349-1358.
- 252. Kumari, R.; Guo, Z.; Kumar, A.; Wiens, M.; Gangappa, S.; Katz, J. M.; Cox, N. J.; Lal, R. B.; Sarkar, D.; Fisher, P. B., Influenza virus NS1-C/EBPβ gene regulatory complex inhibits RIG-I transcription. *Antiviral research* **2020**, *176*, 104747.
- 253. Ranjan, P.; Jayashankar, L.; Deyde, V.; Zeng, H.; Davis, W. G.; Pearce, M. B.; Bowzard, J. B.; Hoelscher, M. A.; Jeisy-Scott, V.; Wiens, M. E., 5'PPP-RNA induced RIG-I activation inhibits drugresistant avian H5N1 as well as 1918 and 2009 pandemic influenza virus replication. *Virology journal* **2010**, *7* (1), 1-11.
- 254. Heyninck, K.; Sabbe, L.; Chirumamilla, C. S.; vel Szic, K. S.; Vander Veken, P.; Lemmens, K. J.; Lahtela-Kakkonen, M.; Naulaerts, S.; de Beeck, K. O.; Laukens, K., Withaferin A induces heme oxygenase (HO-1) expression in endothelial cells via activation of the Keap1/Nrf2 pathway. *Biochemical pharmacology* **2016**, *109*, 48-61.
- 255. Zhong, M.; Wang, H.; Ma, L.; Yan, H.; Wu, S.; Gu, Z.; Li, Y., DMO-CAP inhibits influenza virus replication by activating heme oxygenase-1-mediated IFN response. *Virology journal* **2019**, *16* (1), 1-9. 256. Ma, L.-L.; Wang, H.-Q.; Wu, P.; Hu, J.; Yin, J.-Q.; Wu, S.; Ge, M.; Sun, W.-F.; Zhao, J.-Y.; Aisa, H. A., Rupestonic acid derivative YZH-106 suppresses influenza virus replication by activation of heme oxygenase-1-mediated interferon response. *Free Radical Biology and Medicine* **2016**, *96*, 347-361.
- 257. Ma, L.-L.; Zhang, P.; Wang, H.-Q.; Li, Y.-F.; Hu, J.; Jiang, J.-D.; Li, Y.-H., heme oxygenase-1 agonist CoPP suppresses influenza virus replication through IRF3-mediated generation of IFN- α/β . *Virology* **2019**, *528*, 80-88.
- 258. Um, H. J.; Min, K.-j.; Kim, D. E.; Kwon, T. K., Withaferin A inhibits JAK/STAT3 signaling and induces apoptosis of human renal carcinoma Caki cells. *Biochemical and biophysical research communications* **2012**, *427* (1), 24-29.
- 259. Wang, J.; Prinz, R. A.; Liu, X.; Xu, X., In vitro and in vivo antiviral activity of gingerenone A on influenza A virus is mediated by targeting janus kinase 2. *Viruses* **2020**, *12* (10), 1141.
- 260. Zhang, C.; Yang, Y.; Zhou, X.; Yang, Z.; Liu, X.; Cao, Z.; Song, H.; He, Y.; Huang, P., The NS1 protein of influenza A virus interacts with heat shock protein Hsp90 in human alveolar basal epithelial cells: implication for virus-induced apoptosis. *Virology journal* **2011**, *8* (1), 1-9.
- 261. Bollong, M. J.; Pietilä, M.; Pearson, A. D.; Sarkar, T. R.; Ahmad, I.; Soundararajan, R.; Lyssiotis, C. A.; Mani, S. A.; Schultz, P. G.; Lairson, L. L., A vimentin binding small molecule leads to mitotic disruption in mesenchymal cancers. *Proceedings of the National Academy of Sciences* **2017**, *114* (46), E9903-E9912.
- 262. Espinoza, J. A.; Gonzalez, P. A.; Kalergis, A. M., Modulation of antiviral immunity by heme oxygenase-1. *The American journal of pathology* **2017**, *187* (3), 487-493.
- 263. Ndlovu, M. N.; Van Lint, C.; Van Wesemael, K.; Callebert, P.; Chalbos, D.; Haegeman, G.; Vanden Berghe, W., Hyperactivated NF-κB and AP-1 transcription factors promote highly accessible

- chromatin and constitutive transcription across the interleukin-6 gene promoter in metastatic breast cancer cells. *Molecular and cellular biology* **2009**, *29* (20), 5488-5504.
- 264. Yu, T.-J.; Tang, J.-Y.; Ou-Yang, F.; Wang, Y.-Y.; Yuan, S.-S. F.; Tseng, K.; Lin, L.-C.; Chang, H.-W., Low concentration of withaferin A inhibits oxidative stress-mediated migration and invasion in oral cancer cells. *Biomolecules* **2020**, *10* (5), 777.
- 265. Ku, S.-K.; Han, M.-S.; Bae, J.-S., Withaferin A is an inhibitor of endothelial protein C receptor shedding in vitro and in vivo. *Food and chemical toxicology* **2014**, *68*, 23-29.
- 266. Dai, J.; Gu, L.; Su, Y.; Wang, Q.; Zhao, Y.; Chen, X.; Deng, H.; Li, W.; Wang, G.; Li, K., Inhibition of curcumin on influenza A virus infection and influenzal pneumonia via oxidative stress, TLR2/4, p38/JNK MAPK and NF-κB pathways. *International immunopharmacology* **2018**, *54*, 177-187.
- 267. Shin, J. W.; Chun, K.-S.; Kim, D.-H.; Kim, S.-J.; Kim, S. H.; Cho, N.-C.; Na, H.-K.; Surh, Y.-J., Curcumin induces stabilization of Nrf2 protein through Keap1 cysteine modification. *Biochemical pharmacology* **2020**, *173*, 113820.
- 268. Perwitasari, O.; Yan, X.; O'Donnell, J.; Johnson, S.; Tripp, R. A., Repurposing kinase inhibitors as antiviral agents to control influenza A virus replication. *Assay and drug development technologies* **2015**, *13* (10), 638-649.
- 269. Watanabe, T.; Kawakami, E.; Shoemaker, J. E.; Lopes, T. J.; Matsuoka, Y.; Tomita, Y.; Kozuka-Hata, H.; Gorai, T.; Kuwahara, T.; Takeda, E., Influenza virus-host interactome screen as a platform for antiviral drug development. *Cell host & microbe* **2014**, *16* (6), 795-805.
- 270. Han, J.; Perez, J. T.; Chen, C.; Li, Y.; Benitez, A.; Kandasamy, M.; Lee, Y.; Andrade, J.; Manicassamy, B., Genome-wide CRISPR/Cas9 screen identifies host factors essential for influenza virus replication. *Cell reports* **2018**, *23* (2), 596-607.
- 271. Du, Y.; Yang, F.; Wang, Q.; Xu, N.; Xie, Y.; Chen, S.; Qin, T.; Peng, D., Influenza a virus antagonizes type I and type II interferon responses via SOCS1-dependent ubiquitination and degradation of JAK1. *Virology Journal* **2020**, *17* (1), 1-10.
- 272. Ahmad, R.; Raina, D.; Meyer, C.; Kufe, D., Triterpenoid CDDO-methyl ester inhibits the Janus-activated kinase-1 (JAK1)→ signal transducer and activator of transcription-3 (STAT3) pathway by direct inhibition of JAK1 and STAT3. *Cancer research* **2008**, *68* (8), 2920-2926.
- 273. Ahmad, R.; Raina, D.; Meyer, C.; Kharbanda, S.; Kufe, D., Triterpenoid CDDO-Me blocks the NF-κB pathway by direct inhibition of IKKβ on Cys-179. *Journal of Biological Chemistry* **2006**, *281* (47), 35764-35769.
- 274. Qin, D.-J.; Tang, C.-X.; Yang, L.; Lei, H.; Wei, W.; Wang, Y.-Y.; Ma, C.-M.; Gao, F.-H.; Xu, H.-Z.; Wu, Y.-L., Hsp90 is a novel target molecule of CDDO-Me in inhibiting proliferation of ovarian cancer cells. *PLoS One* **2015**, *10* (7), e0132337.
- 275. Couch, R. D.; Browning, R. G.; Honda, T.; Gribble, G. W.; Wright, D. L.; Sporn, M. B.; Anderson, A. C., Studies on the reactivity of CDDO, a promising new chemopreventive and chemotherapeutic agent: implications for a molecular mechanism of action. *Bioorganic & medicinal chemistry letters* **2005**, *15* (9), 2215-2219.
- 276. Thimmulappa, R. K.; Fuchs, R. J.; Malhotra, D.; Scollick, C.; Traore, K.; Bream, J. H.; Trush, M. A.; Liby, K. T.; Sporn, M. B.; Kensler, T. W., Preclinical evaluation of targeting the Nrf2 pathway by triterpenoids (CDDO-Im and CDDO-Me) for protection from LPS-induced inflammatory response and reactive oxygen species in human peripheral blood mononuclear cells and neutrophils. *Antioxidants & redox signaling* **2007**, *9* (11), 1963-1970.
- 277. Kostov, R. V.; Knatko, E. V.; McLaughlin, L. A.; Henderson, C. J.; Zheng, S.; Huang, J. T.-J.; Honda, T.; Dinkova-Kostova, A. T., Pharmacokinetics and pharmacodynamics of orally administered acetylenic tricyclic bis (cyanoenone), a highly potent Nrf2 activator with a reversible covalent mode of action. *Biochemical and biophysical research communications* **2015**, *465* (3), 402-407.
- 278. Wu, Q. Q.; Wang, Y.; Senitko, M.; Meyer, C.; Wigley, W. C.; Ferguson, D. A.; Grossman, E.; Chen, J.; Zhou, X. J.; Hartono, J., Bardoxolone methyl (BARD) ameliorates ischemic AKI and increases expression of protective genes Nrf2, PPARγ, and HO-1. *American Journal of Physiology-Renal Physiology* **2011**, *300* (5), F1180-F1192.

- 279. Liby, K.; Hock, T.; Yore, M. M.; Suh, N.; Place, A. E.; Risingsong, R.; Williams, C. R.; Royce, D. B.; Honda, T.; Honda, Y., The synthetic triterpenoids, CDDO and CDDO-imidazolide, are potent inducers of heme oxygenase-1 and Nrf2/ARE signaling. *Cancer research* **2005**, *65* (11), 4789-4798.
- 280. Wu, W.; Metcalf, J. P., The role of type i ifns in influenza: antiviral superheroes or immunopathogenic villains? *Journal of innate immunity* **2020,** *12* (6), 437-447.
- 281. Sun, Z.; Huang, Z.; Zhang, D. D., Phosphorylation of Nrf2 at multiple sites by MAP kinases has a limited contribution in modulating the Nrf2-dependent antioxidant response. *PloS one* **2009**, *4* (8), e6588.
- 282. Wang, J.; Sun, J.; Hu, J.; Wang, C.; Prinz, R. A.; Peng, D.; Liu, X.; Xu, X., A77 1726, the active metabolite of the anti-rheumatoid arthritis drug leflunomide, inhibits influenza A virus replication in vitro and in vivo by inhibiting the activity of Janus kinases. *The FASEB Journal* **2020**, *34* (8), 10132-10145.
- 283. Moon, S.-J.; Kim, E.-K.; Jhun, J. Y.; Lee, H. J.; Lee, W. S.; Park, S.-H.; Cho, M.-L.; Min, J.-K., The active metabolite of leflunomide, A77 1726, attenuates inflammatory arthritis in mice with spontaneous arthritis via induction of heme oxygenase-1. *Journal of translational medicine* **2017**, *15* (1), 1-12.
- 284. Shen, Z.; Lou, K.; Wang, W., New small-molecule drug design strategies for fighting resistant influenza A. *Acta Pharmaceutica Sinica B* **2015**, *5* (5), 419-430.
- 285. Yen, H.-L., Current and novel antiviral strategies for influenza infection. *Current opinion in virology* **2016**, *18*, 126-134.
- 286. Müller, K. H.; Kakkola, L.; Nagaraj, A. S.; Cheltsov, A. V.; Anastasina, M.; Kainov, D. E., Emerging cellular targets for influenza antiviral agents. *Trends in pharmacological sciences* **2012**, *33* (2), 89-99.
- 287. Ilyushina, N. A.; Yilmaz, N.; Boon, A. C.; Webster, R. G.; Govorkova, E. A., Oseltamivirribavirin combination therapy for highly pathogenic H5N1 influenza virus infection in mice. *Antimicrobial agents and chemotherapy* **2008**, *52* (11), 3889-3897.
- 288. Jordan, P. C.; Stevens, S. K.; Deval, J., Nucleosides for the treatment of respiratory RNA virus infections. *Antiviral Chemistry and Chemotherapy* **2018**, *26*, 2040206618764483.
- 289. Matsuoka, Y.; Matsumae, H.; Katoh, M.; Eisfeld, A. J.; Neumann, G.; Hase, T.; Ghosh, S.; Shoemaker, J. E.; Lopes, T. J.; Watanabe, T., A comprehensive map of the influenza A virus replication cycle. *BMC systems biology* **2013**, *7* (1), 1-18.
- 290. Rajasekaran, D.; Palombo, E. A.; Chia Yeo, T.; Lim Siok Ley, D.; Lee Tu, C.; Malherbe, F.; Grollo, L., Identification of traditional medicinal plant extracts with novel anti-influenza activity. *PloS one* **2013**, *8* (11), e79293.
- 291. Rai, A.; Kumar, V.; Jerath, G.; Kartha, C.; Ramakrishnan, V., Mapping drug-target interactions and synergy in multi-molecular therapeutics for pressure-overload cardiac hypertrophy. *NPJ systems biology and applications* **2021**, *7* (1), 1-11.
- 292. Fung, D. S.; Doscher, M. S., Preparation and crystallization of 41-dinitrophenyl ribonuclease S. *Biochemistry* **1971**, *10* (22), 4099-4104.
- 293. Carson, J.; WONG, F. F., Isolation of (+) S-methyl-L-cysteine sulfoxide and of (+) Sn-propyl-L-cysteine sulfoxide from onions as their N-2, 4-dinitrophenyl derivatives. *The Journal of Organic Chemistry* **1961**, *26* (12), 4997-5000.
- 294. Woodham, A. W.; Taylor, J. R.; Jimenez, A. I.; Skeate, J. G.; Schmidt, T.; Brand, H. E.; Da Silva, D. M.; Kast, W. M., Small molecule inhibitors of the annexin A2 heterotetramer prevent human papillomavirus type 16 infection. *Journal of Antimicrobial Chemotherapy* **2015**, *70* (6), 1686-1690.
- 295. Valapala, M.; Thamake, S. I.; Vishwanatha, J. K., A competitive hexapeptide inhibitor of annexin A2 prevents hypoxia-induced angiogenic events. *Journal of cell science* **2011**, *124* (9), 1453-1464.
- 296. Gaussian09, R. A., 1, mj frisch, gw trucks, hb schlegel, ge scuseria, ma robb, jr cheeseman, g. Scalmani, v. Barone, b. Mennucci, ga petersson et al., gaussian. *Inc., Wallingford CT* **2009**, *121*, 150-166.

- 297. Beck, A. D., Density-functional thermochemistry. III. The role of exact exchange. *J. Chem. Phys* **1993,** *98* (7), 5648-6.
- 298. Lee, C.; Yang, W.; Parr, R. G., Development of the Colle-Salvetti correlation-energy formula into a functional of the electron density. *Physical review B* **1988**, *37* (2), 785.
- 299. Stephens, P. J.; Devlin, F. J.; Chabalowski, C. F.; Frisch, M. J., Ab initio calculation of vibrational absorption and circular dichroism spectra using density functional force fields. *The Journal of physical chemistry* **1994**, *98* (45), 11623-11627.
- 300. Grimme, S.; Antony, J.; Ehrlich, S.; Krieg, H., A consistent and accurate ab initio parametrization of density functional dispersion correction (DFT-D) for the 94 elements H-Pu. *The Journal of chemical physics* **2010**, *132* (15), 154104.
- 301. Frisch, M. J.; Pople, J. A.; Binkley, J. S., Self-consistent molecular orbital methods 25. Supplementary functions for Gaussian basis sets. *The Journal of chemical physics* **1984**, *80* (7), 3265-3269.
- 302. Hariharan, P. C.; Pople, J. A., The influence of polarization functions on molecular orbital hydrogenation energies. *Theoretica chimica acta* **1973**, *28* (3), 213-222.
- 303. Hehre, W. J.; Ditchfield, R.; Pople, J. A., Self—consistent molecular orbital methods. XII. Further extensions of Gaussian—type basis sets for use in molecular orbital studies of organic molecules. *The Journal of Chemical Physics* **1972**, *56* (5), 2257-2261.
- 304. Marenich, A. V.; Cramer, C. J.; Truhlar, D. G., Universal solvation model based on solute electron density and on a continuum model of the solvent defined by the bulk dielectric constant and atomic surface tensions. *The Journal of Physical Chemistry B* **2009**, *113* (18), 6378-6396.

Experimental section

I. Supplementary synthetic routes and strategies

I.1. Synthesis of intermediate 3

The synthetic route starts by the esterification of the commercially available (+)-Tartaric acid followed by the protection of the diol **112** (Figure 109). Treatment with LiAlH₄ reduced both esters and monoactivation by Tosyl chloride afforded the nucleophilic substitution with LiBr to give **116**. A Swern oxidation, followed by a Morita-Baylis-Hillman reaction and HBr treatment gave the first synthon **3**.

Procedures and characterizations are available in the literature. 123

Figure 109: Synthetic route of intermediate 3.

I.2. Synthesis of the dinitrophenyl derivate

In order to cristallize compound **18a**, a solvent screening was performed (CH₂Cl₂/Pentane, Et₂O/Pentane, *i*-Pr₂O/Pentane, EtOH) but no crystals have been obtained. The secondary alcohol localized on the structure was an opportunity to incorporate a dinitrophenyl moiety to help for the crystallization.^{292, 293}

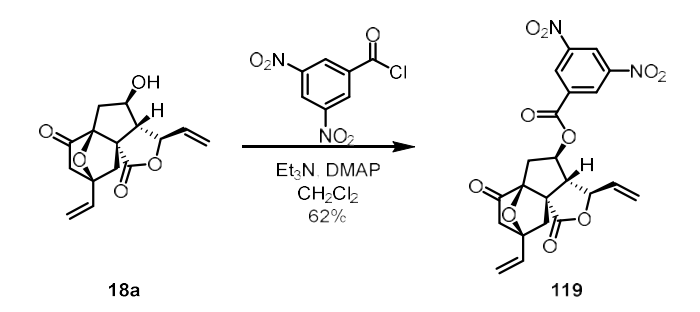


Figure 110: Synthesis of the dinitrophenyl derivate

I.3. Coupling between 30 and 8

The first investigation indicated that early formation of the conjugated furanone conducts to very sensitive intermediates. Indeed, deprotection of the dimethyl acetal to access to the furanone conjugated aldehyde failed in all the conditions tested (Figure 111A) due to its probable instability. While the access of the enyne conjugated aldehyde was possible, lactonization or furanone synthesis didn't give any expected product. Also, coupling reaction with the iodoalkyne and the aldehyde was a failure (Figure 111B).

Figure 111: First investigation of the « coupled intermediate » synthesis

I.4. Synthesis of the alkyne intermediate *via* a Wittig / Wittig-Horner strategy

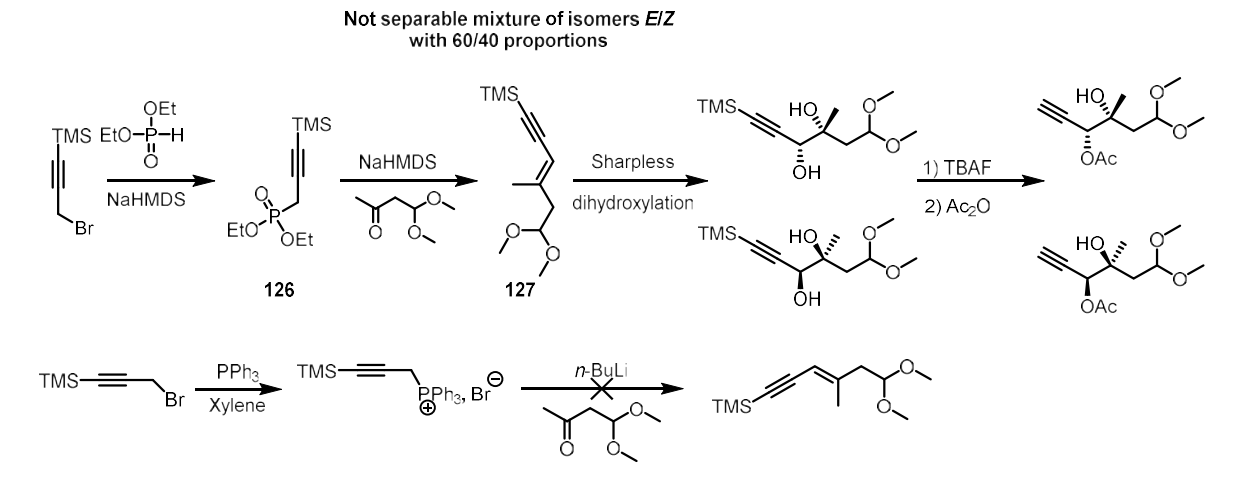


Figure 112: First Investigations on the racemic/chiral alkyne intermediate

Synthesis of alkyne intermediate via a Wittig-Horner strategy was limited due to the lack of E/Z stereoselectivity of the enyne (Figure 112).

I.5. Synthesis of goyazensolide diastereoisomer

Figure 113: Synthetic pathway to obtain the diastereoisomer of goyazensolide

Synthesis of the goyazensolide diastereoisomer **131** was performed in similar conditions than goyazensolide.

I.6. Synthesis of the « primary cyclized scaffold »

Figure 114: Synthetic route of the "primary cyclized scaffold"

Synthesis of the « Primary cyclized scaffold » was performed in similar conditions than goyazensolide unless the use of iodine in the carboalumination step.

I.7. Synthesis of FiVe1

The synthetic route of FiVe1 starts with the formation of acyl chloride **140** from the commercially available acid. Attack of the magnesium diethyl malonate on the acyl chloride followed by a decarboxylation in strong acidic conditions gave the acetophenone derivative **141**. Once the nitro reduced, the formation of the electrophilic diazonium species allowed an intracyclization by its enol form to give the cinnoline **143**. Treatment with POBr₃ followed by a SNAr with the piperidine derivative **145** allowed the access of FiVe1 (**146**).²⁶¹

Figure 115: Synthetic route for the preparation of FiVe1

II. Supplementary proteomic experiments

II.1. Click reaction in blank conditions.

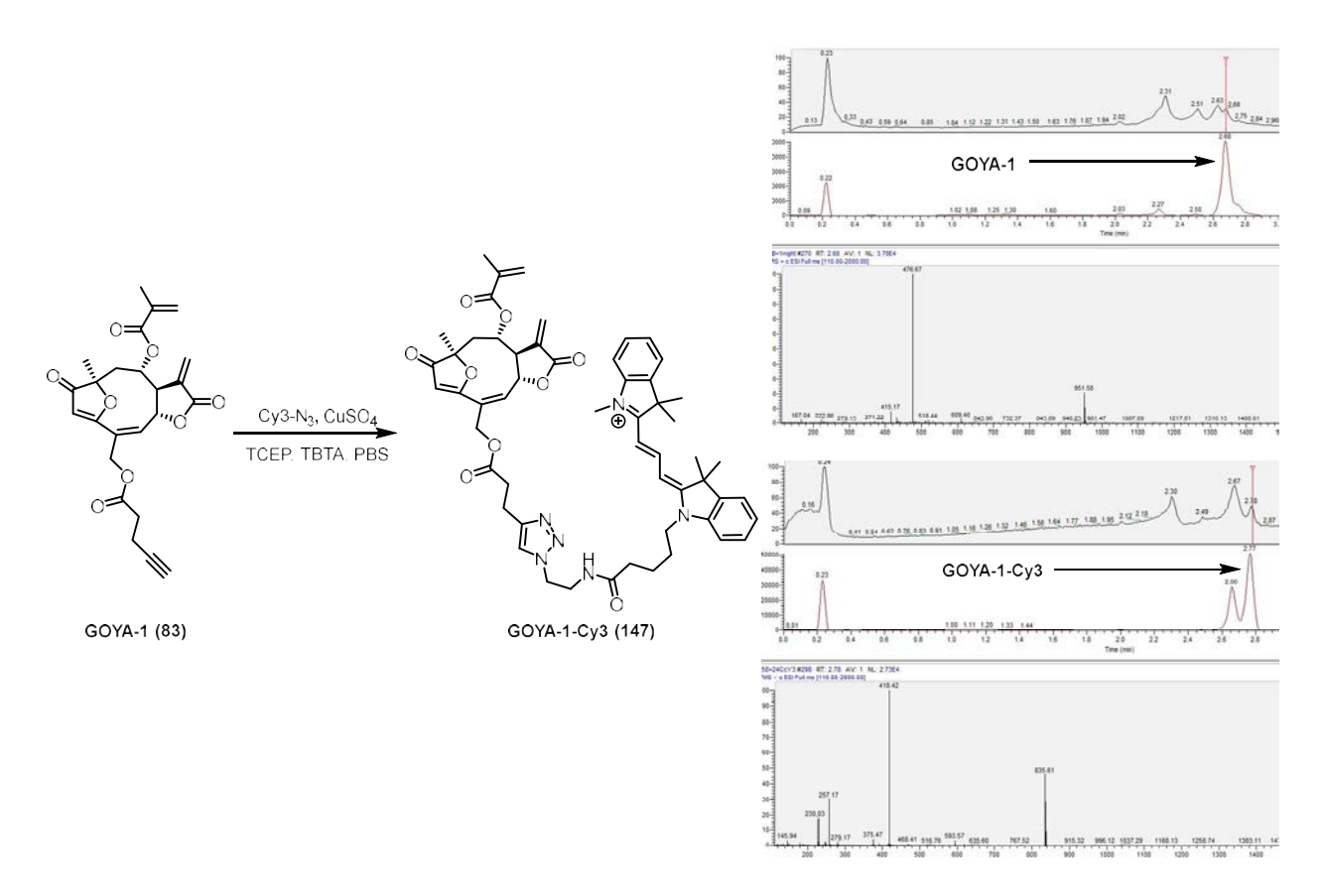


Figure 116: (*Left*) Click reaction of GOYA-1. (*Right*) LC-MS analysis indicating the presence of the major compound as GOYA-1-Cy3

II.2. Investigations of the band at 38 kDa in A549 cells

1. Investigations on selectivity

To determine the selectivity of goyazensolide, competition with other natural products have been applied.

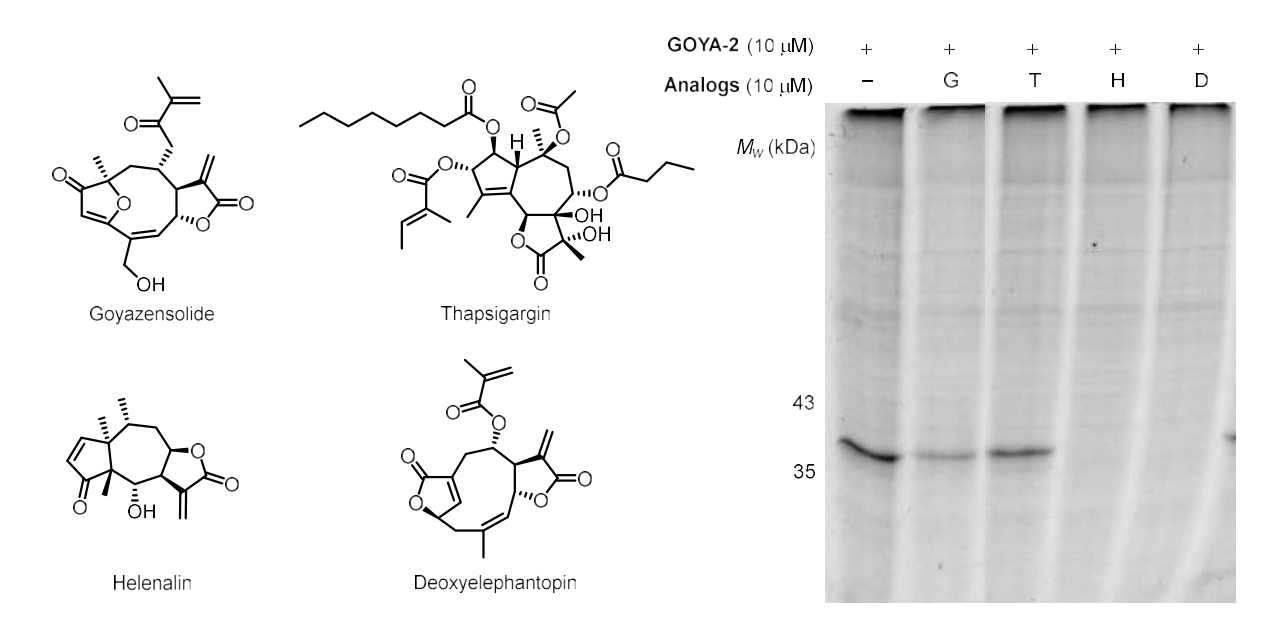


Figure 117: Labeling/competition experiment of the 38 kDa band with various natural products

The 38 kDa band is competed by Helenalin as well as Deoxyelephantopin, indicated that the binding of this band is not specific to goyazensolide.

2. Protein identification

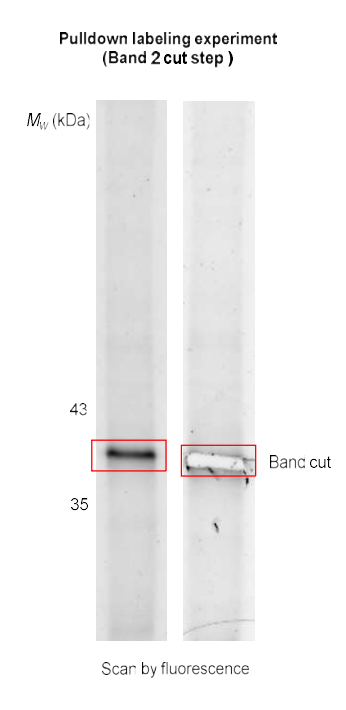


Figure 118: Pulldown experiment followed by a band cut

A pulldown labeling experiment followed by a band cut and a tryptic digestion gave a mixture of peptides ready to be analyzed by MS/MS.

3. MS/MS analysis

MS/MS analysis for the second band indicated the characterization of the protein **Annexin A2** as the major protein. Nevertheless, it has been previously demonstrated that the target is not selective to other sesquiterpene lactones. Moreover, the natural product withaferin A has been described as covalent binder of annexin A2 and several inhibitors are described in the literature.^{234, 294, 295}

III. Experimental procedures

III.1. General information for the chemistry part

NMR spectra were recorded on AMX-300, AMX-400 and AMX-500 Bruker Advance spectrometers at 298 K with CDCl₃ as the solvent unless otherwise stated. Chemical shifts are reported in parts per million, relative to chloroform (¹H, δ 7.26; ¹³C, δ 77.16) unless otherwise stated. Data for ¹H NMR are reported as follows: chemical shift, multiplicity (s = singlet, d = doublet, t = triplet, q = quartet, quint = quintuple, sept. = septuplet, m = multiplet), coupling constants and integration. Infrared spectra (IR) were recorded on a Perkin-Elmer 1650 FT-IR spectrometer using neat samples on a diamond ATR Golden Gate sampler. High-resolution mass spectra (HRMS) were obtained on a Xevo G2 Tof spectrometer (Ionization mode: ESI positive polarity; Mobile phase: MeOH 100 µL/min). Optical rotations were recorded on OMNI Lab JASCO P-1030 polarimeter at 589 nm and are recorded as [α]^T (concentration in grams/100 mL solvent). Analytical thin layer chromatography (TLC) was performed using 0.25 mm silica gel 60-F₂₅₄ plates from *Merck*, using 250 nm UV light as the visualizing agent and a solution of phosphomolybdic acid or potassium permangante and heat as developing agents. Flash chromatography was performed using 200-400 mesh silica gel. Yields refer to chromatographically and spectroscopically pure materials, unless otherwise stated. Reverse phase column chromatography was performed using Isolera Biotage using SNAP Cartridge KP-C18-HS of 60 g or 12 g. The X-ray diffraction data were

collected on an Agilent Supernova diffractometer equipped with an ATLAS CCD detector using CuK α (λ = 1.54184 Å) radiation. The enantiomeric excess (ee) were determined by HPLC analysis. Chiral HPLC analysis was performed on Waters Acquity UPC2 with column OJ-H. All reagents were used as supplied by Aldrich, Fluka, Acros or Strem and used without purification unless otherwise stated. All reactions were carried out in oven-dried glassware under nitrogen atmosphere unless otherwise stated.

III.2. Protocols

III.2.1. Synthesis of synthon 13

Step 1:

$$\begin{array}{c} OH \\ HO_2C (R) \\ \hline D-Malic Acid \end{array} \qquad \begin{array}{c} O \\ PTSA \\ 76\% \\ \end{array} \qquad \begin{array}{c} CO_2H \\ \hline \end{array}$$

In a 1 L flask under N₂, D-malic acid (25 g, 182 mmol) was charged followed by 2,2-dimethoxypropane (150 mL). PTSA was added (350 mg, 2.03 mmol) and the mixture was stirred 4 h at room temperature. After completion, the crude mixture was diluted with 400 mL EtOAc and 400 mL HCl 0.1 M. The organic phase was washed with brine, dried over Na₂SO₄ and concentrated under vacuo. Compound **5** (24.2g, 76%) was used without further purification.

¹H NMR (300 MHz, CDCl₃) δ 4.73 (dd, J = 6.5, 3.9 Hz, 1H), 3.09 – 2.79 (m, 2H), 1.62 (d, J = 15.6 Hz, 6H).

Step 2:

In a 500 mL flask under N₂ was added dropwise BH₃.Me₂S (45 mL 2 M in THF, 91 mmol) to the mixture of acid **5** (12.2 g, 70.1 mmol) in THF (120 mL) at 0 °C. The mixture was allowed to warm at room temperature and stirred one night at this temperature. After completion, the crude mixture was quenched with MeOH (40 mL) at 0 °C and the solvent was removed. MeOH was added again and the solvent was removed. Oil **6** was obtained (10.8 g, 96%) and used without further purification.

¹H NMR (300 MHz, CDCl₃) δ 4.58 (dd, J = 7.1, 5.0 Hz, 1H), 3.84 (ddd, J = 8.1, 6.7, 4.9 Hz, 2H), 2.24 – 1.92 (m, 2H), 1.65 – 1.56 (m, 6H).

Step 3:

In a 500 mL flask under N_2 , TBDMSCI (3.5 g, 23.2 mmol) was added by portions to the mixture of alcohol **6** (3.4 g, 21.2 mmol), imidazole (3.75 g, 52 mmol) in DMF (20 mL) and stirred 2 h at room temperature. Dilution with 250 mL Et₂O and 200 mL water. Organic layer was washed with water, brine, dried over Na_2SO_4 and concentrated under vacuo. Flash chromatography (Pentane/EtOAc 8/2 as eluent) gave **7** as a yellow oil (4.5 g, 78%).

¹H NMR (300 MHz, CDCl₃) δ 4.55 (dd, J = 7.9, 4.3 Hz, 1H), 3.92 – 3.73 (m, 2H), 2.15 – 2.05 (m, 1H), 2.00 – 1.82 (m, 1H), 1.59 (dd, J = 19.4, 0.8 Hz, 6H), 0.91 (s, 9H), 0.08 (s, 6H).

<u>Step 4:</u>

In a 250 mL flask under N_2 , AIMe₃ (27 mL, 54.7 mmol) was added dropwise to the Weinreb salt (5.3 g, 54.7 mmol) in CH_2Cl_2 (100 mL) at 0 °C. The mixture was allowed

to warm at room temperature and stirred 45 min. The mixture was cooled to 0 $^{\circ}$ C and acetonide **7** (5 g, 18.2 mmol) was added dropwise. The mixture was stirred 2 h at 0 $^{\circ}$ C and carefully quenched with HCl 0.1 M. The mixture was diluted with 200 mL CH₂Cl₂ and 200 mL HCl 0.1 M. The organic layer was washed with water, brine and dried over Na₂SO₄. Flash chromatography (Pentane/EtOAc 1/1 as eluent) gave **8** as a yellow oil (3.2 g, 63%).

¹H NMR (300 MHz, CDCl₃) δ 4.57 (t, J = 8.3 Hz, 1H), 3.87 (s, 2H), 3.73 (s, 3H), 3.25 (s, 4H), 1.99 (dd, J = 8.2, 5.6 Hz, 1H), 1.66 (dd, J = 9.1, 4.6 Hz, 1H), 0.91 (s, 9H), 0.08 (d, J = 2.9 Hz, 6H). Step 5:

In a 250 mL flask under N₂, *n*-BuLi (8.7 mL, 2.5 M in hexane, 21.6 mmol) was added dropwise to a solution of alkyne **9** (3.5 g, 21.6 mmol) in THF (50 mL) at -78 °C and stirred 1 h. The deprotonated alkyne mixture was added in portions by cannula to the solution of Weinreb amide **8** (2.4 g, 8.64 mmol) in THF (60 mL) at -78 °C. The mixture was allowed to warm at 0 °C and stirred 30 min. The mixture was cooled to -78 °C and quenched with saturated NH₄Cl. The mixture was diluted with 200 mL Et₂O and 100 mL water. The organic layer was washed with brine and dried over Na₂SO₄. Flash chromatography (Pentane/EtOAc 7/3 as eluent) gave **10** as a yellow oil (2.65 g, 81%). **1H NMR (300 MHz, CDCl₃) δ** 7.36 – 7.18 (m, 6H), 4.27 (dt, J = 6.9, 4.2 Hz, 1H), 3.74 (ddd, J = 10.4, 6.6, 4.9 Hz, 2H), 3.53 (d, J = 4.4 Hz, 1H), 3.04 (t, J = 7.3 Hz, 2H), 2.63 (t, J = 7.3 Hz, 2H), 2.20 – 2.07 (m, 1H), 2.00 – 1.85 (m, 1H), 0.83 (s, 9H), -0.00 (d, J = 1.8 Hz, 6H).

Step 6:

OTBS
$$\frac{\text{HgO. dil. H}_2\text{SO}_4}{\text{Acetone}}$$
 OH

In a 500 mL flask under N₂, mercuric solution (2.76 mL, 0.1 M in 2.5% H₂SO₄) was added dropwise to the solution of ynone **10** (2.65 g, 7 mmol) in dry acetone (250 mL) and stirred 2 h at room temperature. The reaction was quenched with NaHCO₃, stirred 1h30 at room temperature, filtered and the solvent was removed *in vacuo*. Flash chromatography (Pentane/EtOAc 3/7 as eluent) gave **11** as a yellow oil (1.4 g, 76%). **1H NMR (300 MHz, CDCl₃) δ** 7.35 – 7.18 (m, 5H), 5.45 (s, 1H), 4.52 (dd, J = 7.6, 5.9 Hz, 1H), 3.78 (d, J = 5.4 Hz, 2H), 3.13 (t, J = 7.4 Hz, 2H), 2.76 (t, J = 7.2 Hz, 2H), 2.02 (d, J = 1.8 Hz, 1H), 1.97 – 1.87 (m, 1H).

1. **MS(ESI)** [M + H]⁺ calculated for C₁₄H₁₆O₃S: 265.08, found 265.21.

Step 7:

In a 50 mL flask under N₂, DMP (385 mg, 0.91 mmol) was added by portions to the mixture of alcohol **11** (200 mg, 0.76 mmol) in CH₂Cl₂ (8 mL) at 0 °C. Mixture was allowed to warm at room temperature and stirred 40 min. The reaction was quenched with Na₂CO₃ saturated, 15 mL of Et₂O and 10 mL of NaHCO₃ saturated. The organic layer was washed with NaHCO₃, water, brine and dried over Na₂SO₄. Aldehyde **13** was obtained as a yellow oil (154 mg, 77%).

¹H NMR (300 MHz, CDCl₃) δ 9.72 (s, 1H), 7.33 – 7.18 (m, 5H), 5.47 (s, 1H), 4.77 (dd, J = 8.8, 3.2 Hz, 1H), 3.15 – 2.95 (m, 3H), 2.80 – 2.65 (m, 3H).

MS(ESI) [M + H]⁺ calculated for C₁₄H₁₄O₃S: 263.07, found 263.28.

III.2.2. Coupling between intermediates 3 and 10

Step 1:

In a 100 mL flask under N_2 , Zinc (186 mg, 2.86 mmol) was added by portions to the cold mixture of aldehyde **13** (150 mg, 0.572 mmol), bromolactone **3** (189 mg, 0.63 mmol) in THF/NH₄Cl saturated water 2/1 (6 mL). The mixture was stirred 30 min at 0 °C and then heated to 70 °C for 1 h. The mixture was diluted with EtOAc (40 mL) and Brine (20 mL). The aqueous phase extracted with EtOAc (10 mL) and the combined organic layers were dried over Na_2SO_4 . The solvent was removed under *vacuo* and the crude was purified by flash chromatography (Pentane/EtOAc 4/6 as eluent) gave **14** as a yellow oil (94 mg, 43%).

¹H NMR (300 MHz, CDCl₃) δ 7.38 (d, J = 1.4 Hz, 5H), 6.42 (d, J = 2.3 Hz, 1H), 5.87 – 5.78 (m, 2H), 5.56 (s, 1H), 5.40 (d, J = 1.2 Hz, 1H), 5.27 (s, 1H), 4.96 – 4.85 (m, 1H), 4.65 (d, J = 3.2 Hz, 1H), 4.06 (dd, J = 8.7, 3.4 Hz, 1H), 3.20 (s, 2H), 2.97 – 2.85 (m, 4H).

MS(ESI) [M + H]⁺ calculated for $C_{21}H_{22}O_5S$: 387.12, found 387.18.

Step 2:

In a 50 mL flask under N_2 , H_2O_2 (14 mL, 0.227 mmol) was added to the mixture of sulfide **14** (80 mg, 0.206 mmol) in HFIP (500 mL) at 0 °C and stirred for 30 min. The reaction was quenched with $Na_2S_2O_3$ and the mixture was diluted with CH_2Cl_2 (10 mL) and $NaHCO_3$ saturated (10 mL). The organic layer was washed with $NaHCO_3$, brine and dried over Na_2SO_4 . The solvent was removed under *vacuo*. Sulfoxide **15** was obtained (78 mg, 94%) as a yellow oil and used without further purification. **MS(ESI) [M + H]**⁺ calculated for $C_{21}H_{22}O_6S$: 403.11, found 403.18.

Step 3:

In a sealed tube under N_2 , the sulfoxide **15** (20 mg, 0.05 mmol) was irradiated under microwave in toluene (2 mL) at 180 °C for 10 min. The solvent was removed under *vacuo*. The crude was purified by flash chromatography (Pentane/EtOAc 1/1 as eluent) gave **18a** as a light yellow solid (8 mg, 58%).

¹H NMR (500 MHz, CDCl₃) δ 6.16 (d, J = 10.9 Hz, 1H, Ha), 5.88 (ddd, J = 17.0, 10.6, 5.6 Hz, 1H, Hf), 5.40 – 5.39 (m, 1H, Hc1), 5.38 – 5.36 (m, 2H, Hc2+Hg1), 5.35 (d, J = 0.8 Hz, 1H, Hg2), 5.24 (d, J = 10.6 Hz, 1H, He), 5.02 – 4.98 (m, 1H, Hi), 2.93 – 2.80 (d, 1H, OH), 2.79 (s, 1H, Ha1), 2.71 – 2.68 (m, 1H, Hh), 2.61 (s, 1H, Hd1), 2.49 (d, J = 2.5 Hz, 1H, Ha2), 2.36 (t, J = 6.1 Hz, 1H, Hk1), 2.19 – 2.16 (m, 1H, Hd2), 2.12 – 2.09 (m, 1H, Hk2).

¹³C NMR (126 MHz, CDCI₃) δ 200.70(C1), 174.46(C8), 136.76(C10), 134.31(C4), 115.24(C5-C11), 114.07(C9), 70.71(C13), 52.47(C12), 46.41(C6), 43.82(C2), 30.18(C14).

2D NMR correlations			
	¹ H- ¹ H COSY	НМВС	NOESY
18a	OH OH	OH OH	OH C

MS(ESI) [M + H]⁺ calculated for $C_{15}H_{16}O_{5}$: 277.10, found. 277.22.

$$\begin{array}{c} O_2N \\ O_$$

In a 5 mL flask under N_2 , acyl chloride (6.2 mg, 0.027 mmol) was added dropwise at 0 °C in a mixture of alcohol **18a** (5 mg, 0.018 mmol), Et₃N (7.5 μ L,0.054 mmol), DMAP (0.2 mg, 0.002 mmol) in CH₂Cl₂ (1 mL). The resulting mixture was allowed to warm at room temperature and stirred for 18 h. The crude mixture was directly purified on PTLC (Pentane/EtOAc 7/3 as eluent) to give **26** as a yellow oil (5.2 mg, 62%).

¹H NMR (400 MHz, CDCI₃) δ 9.29 (t, J = 2.1 Hz, 1H), 9.15 (d, J = 2.1 Hz, 2H), 6.19 (dd, J = 17.5, 11.0 Hz, 1H), 6.02 – 5.77 (m, 2H), 5.49 – 5.38 (m, 2H), 5.36 – 5.26 (m, 2H), 5.06 (d, J = 1.5 Hz, 1H), 3.16 (dd, J = 7.7, 4.3 Hz, 1H), 2.84 (d, J = 17.6 Hz, 1H), 2.67 (d, J = 12.5 Hz, 1H), 2.59 – 2.42 (m, 2H), 2.31 (dd, J = 12.6, 2.4 Hz, 1H). **MS(ESI)** [**M + H**]⁺ calculated for C₂₂H₁₈N₂O₁₀: 471.10, found. 471.19.

III.2.3. The tetrahydrofuranol scaffold

Step 1:

In a 250 mL flask under N_2 , NaBH₄ (220 mg, 5.7 mmol) was added by portions to the mixture of furanone **11** (1.5 g, 5.7 mmol) in THF (30 mL) at 0 °C. The mixture was allowed to warm at room temperature and stirred 3 h. The mixture was quenched with HCl 0.5 M at 0 °C and diluted with Et₂O (100 mL) and HCl 0.1 M (50 mL). The aqueous phase was extracted with Et₂O (50 mL) and the combined organic layers were washed with Brine and dried over Na₂SO₄. The solvent was removed under *vacuo*. Diol **19** was obtained as a yellow oil (1.5 g, 98%). The compound was used without further purification. NMR gave acomplex mixture of diastereoisomers **19**.

¹H NMR (300 MHz, CDCl₃) δ 7.36 - 7.27 (m, 5H), 4.37 - 4.17 (m, 1H), 4.08 (d, J = 6.8 Hz, 1H), 3.92 - 3.74 (m, 3H), 3.16 - 2.91 (m, 2H), 2.43 (dd, J = 12.4, 5.4 Hz, 1H), 2.12 - 1.91 (m, 2H), 1.90 - 1.80 (m, 2H), 1.72 - 1.59 (m, 1H).

MS(ESI) [M + H]⁺ calculated for $C_{14}H_{20}O_3S$: 269.11, found. 269.08.

<u>Step 2:</u>

In a 250 mL flask under N₂, TBSOTf (7 mL, 3.04 mmol) was added dropwise to the mixture of diol **19** (370 mg, 1.38 mmol), 2,6-lutidine (513 mL, 4.42 mmol) in CH₂Cl₂ (15 mL) at 0 °C. Mixture stirred 1 h at 0 °C, then quenched with NaHCO₃ saturated and diluted with Et₂O (50 mL) and NaHCO₃ 10%. The organic layer was washed with HCl 0.1 M, water, brine and dried over Na₂SO₄. The solvent was removed under *vacuo*. A filtration on silica gel (Pentane/EtOAc 9/1 as eluent) gave **20** as a yellow oil (424 mg, 62%). NMR gave complex mixture of diastereoisomers.

¹H NMR (300 MHz, CDCI₃) δ 7.40 – 7.13 (m, 5H), 4.33 - 4.09 (m, 1H), 4.09 - 3.89 (m, 1H), 3.77 (dddd, J = 12.7, 7.5, 5.9, 2.9 Hz, 3H), 3.22 - 2.83 (m, 2H), 2.38 - 2.17 (m, 1H), 2.14 - 1.95 (m, 1H), 1.95 - 1.69 (m, 3H), 1.67 - 1.50 (m, 2H), 0.92 - 0.89 (m, 18H), 0.07 (dt, J = 5.0, 1.1 Hz, 12H).

MS(ESI) [M + H]⁺ calculated for C₂₆H₄₈O₃SSi: 497.29, found. 497.18.

<u>Step 3:</u>

In a 100 mL flask under N₂, CHCl₃ (10 mL, pretreated with HCl 1 M, shaken in a separating funnel) was added to the disilylated product **20** (160 mg, 0.322 mmol). The mixture was stirred one night at room temperature, diluted with Et₂O (50 mL) and brine (30 mL). The organic layer was dried over Na₂SO₄ and the solvent was removed under *vacuo*. Flash chromatography (Pentane/EtOAc 8/2 as eluent) gave **21** as a yellow oil (90 mg, 73%). NMR gave complex mixture of diastereoisomers.

¹H NMR (300 MHz, CDCl₃) δ 7.25 (dd, J = 15.0, 1.5 Hz, 5H), 4.20 (dd, J = 3.7, 2.5 Hz, 1H), 3.97 (dd, J = 6.4, 4.5 Hz, 1H), 3.86 – 3.68 (m, 3H), 2.97 (ddd, J = 20.5, 8.6, 6.2 Hz, 2H), 2.32 – 2.13 (m, 1H), 2.06 – 1.80 (m, 3H), 1.74 – 1.43 (m, 3H), 0.83 (s, 9H), 0.00 (s, 6H).

MS(ESI) [M + H]⁺ calculated for C₂₀H₃₄O₃SSi: 383.20, found. 383.12.

Step 4:

In a 50 mL flask under N₂, DMP (72 mg, 0.17 mmol) was added by portions to the alcohol **21** (50 mg, 0.131 mmol) in CH₂Cl₂ (2 mL) at 0 °C. The mixture was allowed to warm at room temperature and stirred 40 min. The reaction was quenched with Na₂CO₃ saturated, diluted with 25 mL Et₂O and 10 mL NaHCO₃ saturated. The organic layer was washed with NaHCO₃, water, brine and dried over Na₂SO₄. The solvent was removed under *vacuo*. A yellow oil of **22** was obtained (39 mg, 79%). NMR gave complex mixture of diastereoisomers.

¹H NMR (300 MHz, CDCl₃) δ 9.83 - 9.59 (m, 1H), 7.49 - 7.06 (m, 5H), 4.36 - 3.94 (m, 3H), 3.08 - 2.84 (m, 2H), 2.68 - 2.45 (m, 2H), 2.25 (s, 1H), 1.97 (d, J = 8.5 Hz, 1H), 1.78 (s, 1H), 1.61 - 1.47 (m, 1H).

MS(ESI) [M + H]⁺ calculated for $C_{20}H_{32}O_3SSi$: 381.18, found. 381.24.

Step 5:

In a 50 mL flask under N₂, Zinc (33 mg, 0.51 mmol) was added by portions to the cold mixture of aldehyde **22** (39 mg, 0.102 mmol), bromolactone **3** (42 mg, 0.143 mmol) in 2/1 THF/NH₄Cl saturated water (3 mL). The mixture was stirred 30 min at 0 °C and then heated to 70 °C 1 h. The crude mixture was diluted with EtOAc (10 mL) and Brine (10 mL). The aqueous phase was extracted with EtOAc (5 mL) and combined organic layers were dried over Na₂SO₄. The solvent was removed under *vacuo*. A flash chromatography (Pentane/EtOAc 1/1 as eluent) gave **23** as a yellow oil (38 mg, 73%). NMR gave complex mixture of diastereoisomers ¹H NMR (300 MHz, CDCl₃) δ 7.29 – 7.19 (m, 7H), 6.34 (s, 1H), 5.71 (d, J = 2.1 Hz, 1H), 5.40 (d, J = 17.1 Hz, 1H), 5.28 (s, 1H), 4.95 – 4.77 (m, 1H), 4.19 (d, J = 1.9 Hz, 2H), 3.97 (d, J = 5.5 Hz, 1H), 3.74 (s, 1H), 2.91 (d, J = 7.5 Hz, 2H), 2.31 – 2.21 (m, 1H), 2.02 – 1.93 (m, 1H), 1.79 (dd, J = 6.3, 2.8 Hz, 2H), 1.55 (d, J = 7.7 Hz, 2H), 0.83 – 0.80 (m, 10H), -0.00 (s, 7H). **MS(ESI)** [M + H]⁺ calculated for C₂₇H₄₀O₅SSi: 505.24, found. 505.32.

Step 6:

In a 10 mL flask under N_2 , H_2O_2 (3.1 mL, 0.09 mmol) was added to the mixture of sulfide **23** (38 mg, 0.075 mmol) in HFIP (200 mL) at 0 °C and stirred 30 min. The reaction was quenched with $Na_2S_2O_3$ and diluted with CH_2Cl_2 (3 mL) and $NaHCO_3$ saturated (3 mL). The organic layer was washed with $NaHCO_3$, brine and dried over Na_2SO_4 . The solvent was removed under *vacuo*. Sulfoxide **24** was obtained as a yellow oil (38 mg, 99%). The compound used without further purification.

Step 7:

In a sealed tube under N_2 , the sulfoxide (38 mg, 0.073 mmol) was heated in toluene (2 mL) at 180 °C 4 h. The solvent was removed under *vacuo*. A flash chromatography (Pentane/EtOAc 1/1 as eluent) gave a light yellow solid **24** (16 mg, 55%). NMR gave complex mixture of diastereoisomers.

¹H NMR (300 MHz, CDCl₃) δ 6.32 (d, J = 2.4 Hz, 1H), 5.84 (d, J = 7.5 Hz, 1H), 5.77 – 5.69 (m, 1H), 5.37 – 5.17 (m, 3H), 5.15 – 4.98 (m, 2H), 4.96 – 4.74 (m, 1H), 4.43 (dd,

J = 6.8, 1.1 Hz, 1H), 4.04 – 3.97 (m, 1H), 3.83 – 3.72 (m, 1H), 2.92 (dd, J = 3.6, 2.1 Hz, 1H), 2.28 (d, J = 1.4 Hz, 1H), 1.94 (s, 1H), 1.84 – 1.75 (m, 1H), 1.61 (d, J = 12.4 Hz, 1H), 1.49 – 1.38 (m, 1H), 0.83 – 0.77 (m, 12H), 0.03 – -0.07 (m, 8H). **MS(ESI)** [M + H]⁺ calculated for $C_{21}H_{34}O_5Si$: 395.22, found. 395.31.

Step 8:

In a 5 mL flask under N_2 , Acetic anhydride (5.7 mL, 0.06 mmol) was added to the mixture of alkene **24** (16 mg, 0.04 mmol), pyridine (6.6 mL, 0.08 mmol), DMAP (0.48 mg, 0.004 mmol) in CH₂Cl₂ (500 mL) at 0 °C. The mixture was allowed to warm at room temperature and stirred for 1 h. The mixture was diluted with Et₂O (5 mL) and HCl 0.1 M (5 mL). The aquous phase was extracted with Et₂O (5 mL), and the combined organic layers were washed with Brine and dried over Na_2SO_4 . The solvent removed under vacuo. A flash chromatography (Pentane/EtOAc 7/3 as eluent) gave **25** as a yellow oil (12 mg, 68%). NMR gave complex mixture of diastereoisomers.

¹H NMR (300 MHz, CDCI₃) δ 6.35 (d, J = 1.6 Hz, 1H), 5.93 – 5.66 (m, 3H), 5.34 – 5.11 (m, 4H), 5.04 (s, 1H), 4.81 (dd, J = 2.9, 1.5 Hz, 1H), 4.51 – 4.27 (m, 1H), 3.88 (dd, J = 6.8, 4.2 Hz, 1H), 3.81 – 3.58 (m, 1H), 3.30 – 3.06 (m, 1H), 2.35 – 2.16 (m, 1H), 1.98 (d, J = 5.2 Hz, 3H), 1.91 – 1.72 (m, 2H), 1.67 – 1.56 (m, 1H), 0.84 – 0.80 (m, 9H), 0.02 – -0.04 (m, 6H).

MS(ESI) [M + H]⁺ calculated for C₂₃H₃₆O₆Si: 437.23, found. 437.13.

Step 9:

In a 25 mL flask under N_2 , the alkene **25** (12 mg, 0.027 mmol), Hoveyda-Grubbs II (3.4 mg, 0.005 mmol) in toluene (20 mL) were stirred 2 h at 100 °C under N_2 . The crude mixture was quenched with silica and the solvent was removed under *vacuo*. The crude was purified by PTLC (Pentane/EtOAc 7/3 as eluent) and gave **26** as a yellow oil (2 mg, 18%).

¹H NMR (500 MHz, CDCI₃) δ 6.33 (dd, J = 3.3, 0.8 Hz, 1H, h1), 6.11 – 6.01 (m, 1H, f), 5.81 (dd, J = 3.0, 0.9 Hz, 1H, h2), 5.68 – 5.58 (m, 1H, d), 5.50 (ddd, J = 11.6, 7.7, 2.5 Hz, 1H, e), 5.11 – 4.95 (m, 2H, c+i), 4.39 (dd, J = 12.4, 3.0 Hz, 1H, k), 4.10 (d, J = 5.4 Hz, 1H, a), 2.97 (dd, J = 10.2, 9.0 Hz, 1H, g), 2.32 – 2.17 (m, 1H, b1), 2.14 (s, 3H, I), 1.98 (dd, J = 6.9, 1.3 Hz, 1H, b2), 1.90 – 1.81 (m, 1H, j1), 1.68-1.64 (dd, 1H, j2), 0.91 (s, 9H, t-Bu), 0.09 (s, 6H, 2 CH₃).

¹³C NMR (126 MHz, CDCI₃) δ 136.76 (C10), 136.00 (C6), 125.93 (C7), 124.37 (C11), 85.74 (C17), 77.44 (C5), 76.68 (C8), 76.09 (C3), 75.19 (C13), 49.44 (C12), 41.47 (C4), 40.16 (C16), 25.80 (C1), 21.17 (C15), 1.04 (C2).

2D NMR correlations						
	¹ H- ¹ H COSY	НМВС	NOESY			
26	TBSO, H _a H _b	TBSO, TBSO TBSO	TBSC III			

MS(ESI) [M + H]⁺ calculated for $C_{21}H_{32}O_6Si$: 409.20, found. 409.32.

III.2.4. Total synthesis of goyazensolide: Strategy 2

Step 1:

28 was prepared from 27 according to the reported procedure.1

Step 2:

To a solution of **28** (38 g, 104 mmol) in THF (400 mL) in a 1000 mL flask under N_2 , was added vitride (53 mL, 3.5 M in toluene, 185 mmol) at 0 °C. The mixture was stirred at 0 °C for 15 minutes, and then Br_2 (6.96 mL, 135 mmol) was added dropwise over 5 minutes. After 15 minutes, saturated aqueous $Na_2S_2O_3$ (100 mL) and saturated aqueous Rochelle's salt (100 mL) were added at room temperature, and the mixture was stirred for 30 minutes. The mixture was then extracted with ethyl acetate (3 x 100 mL), and the combined organic layers were washed with brine (200 mL), dried over MgSO₄, and concentrated to give the crude alcohol **29** as a colorless oil (28 g, 67%). Colorless oil.

¹H NMR (400 MHz, CDCl₃) δ 7.69 (dd, J = 7.9, 1.5 Hz, 4H), 7.44 (ddd, J = 18.9, 7.6, 6.1 Hz, 6H), 6.39 (tt, J = 6.1, 1.6 Hz, 1H), 4.34 (d, J = 6.1 Hz, 2H), 4.30 (d, J = 1.5 Hz, 2H), 1.11 (s, 9H) ppm;

¹³C NMR (101 MHz, CDCI₃) δ 135.5, 132.9, 129.9, 127.8, 126.8, 126.6, 68.0, 61.8, 26.7, 19.2 ppm; TLC: Rf = 0.4 (Pentane/Ethyl acetate = 3/1).

Step 3:

OTBDPS

Br

CH2Cl2

OTBDPS

OTBDPS

30

To a solution of **29** (25 g, 61.7 mmol) in CH₂Cl₂ (300 mL) was added DMP (31.3 g, 74 mmol) in portions at 0 °C. The mixture was stirred at 0 °C for 15 minutes, and the mixture was allowed to warm to room temperature. After 30 minutes, saturated aqueous Na₂S₂O3 (50 mL) and saturated aqueous NaHCO₃ (50 mL) were added at room temperature, and the mixture was stirred for 10 more minutes. The whole was extracted with Et₂O (3 x 150 mL), and the combined organic layers were washed with brine (200 mL) dried over MgSO₄, and concentrated to give crude aldehyde **30** as a paled yellow oil (20.3 g, yield 82%).

¹H NMR (400 MHz, CDCl₃) δ 10.00 (d, J = 6.9 Hz, 1H), 7.67 (d, J = 8.0 Hz, 4H), 7.47 (dd, J = 15.8, 6.0 Hz, 6H), 6.93 (d, J = 6.9 Hz, 1H), 4.43 (s, 2H), 1.11 (s, 9H) ppm. ¹³C NMR (101 MHz, CDCl₃) δ 192.5, 147.3, 135.1, 131.8, 129.9, 127.7, 125.2, 68.1, 26.4, 18.9 ppm; TLC: Rf = 0.6 (Pentane/Ethyl acetate = 8/2).

¹ Koura, M., Yamaguchi, Y., Kurobuchi, S., Sumida, H., Watanabe, Y., Enomoto, T., Matsuda, T., Koshizawa, T., Matsumoto, Y., Shibuya, K. *Bioorg. Med. Chem.* **2016**, *24*, 3436-3446.

Step 4:

To a mixture of **30** (8.5 g, 21.2 mmol), allyl bromide (6.13 g, 31.8 mmol) in THF/water (6/1, 140 mL) at 0 °C under a vigorous stirring was added Zn (2.48 g, 38.2 mmol) in portions. The mixture was allowed to warm to room temperature for 1 hour. The reaction mixture was then diluted with Et₂O (200 mL) and water (150 mL). The organic phase was washed with Brine (100 mL), dried over Na₂SO₄ and volatiles were evaporated in vacuo. The crude was diluted in CH₂Cl₂ (150 mL) and to the solution was added p-toluene sulfonic acid (0.86 g, 5.0 mmol). Then the mixture was stirred for 4 hours at room temperature. The reaction was then diluted with HCI (0.1M, 100 mL). the organic phase was then washed with H₂O (100 mL) and Brine (100 mL), dried over Na₂SO₄ and the solvent was removed in vacuo. Chromatography on silica gel (pentane/ethyl acetate 8/2 as eluent) gave **31** as a pale-yellow oil (8.1 g, yield 81%). ¹H NMR (400 MHz, CDCl₃) δ 7.67 (dd, J = 8.7, 3.8 Hz,4H), 7.50–7.39 (m, 6H), 6.36 (dt, J = 7.6, 1.7 Hz, 1H), 6.30 (t, J = 2.8 Hz, 1H), 5.70 (t, J = 2.5 Hz, 1H), 5.37 (dd, J = 2.8 Hz, 1Hz), 5.37 (dd, J = 2.8 Hz, 1Hz14.6. 7.6 Hz. 1H), 4.36-4.24 (m. 2H), 3.30 (dd, J = 17.1, 7.9 Hz. 1H), 2.66 (dd, J = 17.1), 3.30 (dd, J =17.1, 6.7 Hz, 1H), 1.10 (s, 9H) ppm; 13 C NMR (101 MHz, CDCl₃) δ 170.0, 135.4, 135.4, 133.7, 132.7, 132.5, 130.0, 130.0, 128.9, 127.9, 127.8, 126.1, 122.5, 76.0, 67.8, 33.8, 26.7, 19.2;

HRMS(ESI) [M + H]⁺ calculated for C₂₄H₂₇BrO₃Si: 471.0913, found 471.1007;

Step 5:

To a stirred solution of lactone **31** (2,0 g, 4.2 mmol) in dioxane (20 mL) was added SeO₂ (2.8 g, 25.2 mmol) in 3 portions at 95 °C within 1.5 hours. After the addition, the reaction mixture was stirred at the same temperature for another 30 minutes and then cooled down to room temperature. Then dioxane was evaporated and Et₂O (80 mL) was added, stirred for 30 minutes, filtered and the solution was washed with saturated aqueous NaHCO₃ (20 mL), diluted Na₂S (10 mL) and brine (20 mL). The organic phase was dried over Na₂SO₄, then filterred and concentrated *in vacuo*. The residue was purified on silica gel chromatography (Pentane/Ethyl acetate = $10/1 \sim 1/1$ as eluent) to provide **37** as a light yellow oil (860 mg, 42%). A mixture of diastereomers was obtained (dr = 2:1 as determined by ¹H NMR);

¹H NMR (400 MHz, CDCl₃) δ 7.66 (td, J = 7.2, 1.5 Hz, 4H), 7.48–7.39 (m, 6H), 6.51 (d, J = 1.7 Hz, 0.33H), 6.49 (d, J = 2.4 Hz, 0.66H), 6.40 (dt, J = 7.6, 1.7 Hz, 0.33H), 6.26 (dt, J = 8.0, 1.7 Hz, 0.66H), 6.06 (d, J = 1.5 Hz, 0.33H), 6.02 (d, J = 2.1 Hz, 0.66H), 5.35 (dd, J = 7.5, 5.6 Hz, 0.33H), 5.14 (dd, J = 8.0, 4.7 Hz, 0.66H), 5.01 (dt, J = 5.6,

1.6 Hz, 0.33H), 4.63 (dt, J = 4.6, 2.3 Hz, 0.66H), 4.36 (d, J = 5.0 Hz, 0.66H), 4.34 (s, 1.32H), 1.10 (s, 9H) ppm;

¹³C NMR (101 MHz, CDCI₃) δ 167.9, 137.4, 135.5, 132.7, 132.4, 131.0, 130.1, 130.0, 127.9, 126.1, 123.5, 121.1, 83.4, 81.0, 73.8, 69.1, 67.9, 26.7, 26.7, 19.2 ppm; HRMS(ESI) [M + Na]⁺ calculated for $C_{24}H_{27}BrO_4Si$: 509.0862, found 509.0772;

Step 1:

33 was prepared from 32 according to the reported procedure.²

<u>Step 2:</u>

-

² Koura, M., Yamaguchi, Y., Kurobuchi, S., Sumida, H., Watanabe, Y., Enomoto, T., Matsuda, T., Koshizawa, T., Matsumoto, Y., Shibuya, K. *Bioorg. Med. Chem.* **2016**, *24*, 3436-3446.

In a 500 mL flask under N₂, *t*-BuLi (15.7 mL, 26.78 mmol) was added dropwise to a solution of alkyne **33** (5 g, 20.6 mmol) in THF (100 mL) at -78 °C. The mixture was stirred 30 min at -78 °C, the commercial methylketone (3.26 mL, 24.7 mmol) was added dropwise and reaction stirred 1 h at -78 °C. The reaction was quenched with NH₄Cl saturated, diluted with EtOAc (150 mL) and HCl 0.05 M (100 mL). The aquous phase was extracted with EtOAc (80 mL) and the combined organic layers were washed with brine and dried over Na₂SO₄. The solvent was removed in *vacuo* and the crude was purified by flash chromatography (Pentane/EtOAc 7/3 as eluent) to give **34** as a yellow oil (5.2 g, 65%).

¹H NMR (400 MHz, CDCl₃) δ 4.85 - 4.74 (m, 1H), 4.22 (d, J = 26.1 Hz, 1H), 3.43 - 3.32 (m, 6H), 2.08 - 1.98 (m, 1H), 1.88 (ddd, J = 14.4, 11.4, 6.2 Hz, 1H), 1.27 (d, J = 2.5 Hz, 3H), 1.04 - 1.00 (m, 6H), 0.78 - 0.61 (m, 9H), 0.18 (d, J = 0.7 Hz, 9H).

<u>Step 3:</u>

In a 250 mL flask under N₂, K₂CO₃ (810 mg, 5.87 mmol) was added by portions to the mixture of silylated alkyne **34** (2.2 g, 5.87 mmol) in MeOH (45 mL) and stirred one night at room temperature. The mixture was quenched with HCl 0.05 M dropwise at 4°C and diluted with EtOAc (50 mL) and HCl 0.05 M (10 mL). The organic phase was extracted 2 times with EtOAc (80 mL), and the combined organic layers were washed with brine and dried over Na₂SO₄. The solvent was removed under *vacuo* and the crude was purified by flash chromatography (Pentane/EtOAc 7/3 as eluent) to give **35** as a yellow oil (590 mg, 54%).

¹H NMR (400 MHz, CDCl₃) δ 4.86 - 4.67 (m, 1H), 4.24 (d, J = 9.4 Hz, 1H), 3.86 - 3.51 (m, 1H), 3.51 - 3.34 (m, 6H), 2.98 (d, J = 131.3 Hz, 1H), 2.50 (d, J = 2.3 Hz, 1H), 2.21 - 1.85 (m, 2H), 1.34 (d, J = 10.2 Hz, 3H).

Step 4:

To a stirred solution of alkyne **35** (550 mg, 2.92 mmol), vinyl bromide **31** (1.15 g, 1.76 mmol), PdCl₂(PPh₃)₂ (280 mg, 0.244 mmol), CuI (93 mg, 0.488 mmol) in degassed THF (21 mL) was added dropwise degassed Et₃N (3 mL)) at 4°C under N₂ atmosphere. The resulted mixture was allowed to warm at room temperature and stirred for 2 hours. The reaction was quenched by NH₄Cl saturated (15 mL) and extracted with ethyl acetate (3 x 20 mL). The combined organic layers were dried over Na₂SO₄, filterred and concentrated *in vacuo*. The residue was purified on silica gel chromatography (CH₂Cl₂/EtOAc = 3/7 as eluent) to provide enyne **36** as mixture of diastereomers as a yellow oil (807 mg, 79%).

¹H NMR (300 MHz, CDCl₃) δ 7.66 (d, J = 7.9 Hz, 4H), 7.51 – 7.39 (m, 6H), 6.29 (t, J = 2.8 Hz, 1H), 6.26 – 6.16 (m, 1H), 5.68 (s, 1H), 5.47 (d, J = 7.7 Hz, 1H), 4.78 – 4.65 (m, 1H), 4.39 – 4.29 (m, 1H), 4.21 (d, J = 1.9 Hz, 2H), 3.43 – 3.33 (m, 6H), 3.31 – 3.19 (m, 1H), 3.13 (t, J = 5.6 Hz, 1H), 2.74 – 2.61 (m, 1H), 2.20 – 2.09 (m, 1H), 2.03 – 1.77 (m, 1H), 1.25 (s, 3H), 1.08 (s, 9H).

MS(ESI) [M + H]⁺ calculated for $C_{33}H_{42}O_7Si$: 579.27, found. 579.41.

Step 5:

To a stirred solution of propargyl alcohol **36** (750 mg, 1.30 mmol), Et₃N (1.8 mL, 13 mmol) in CH₂Cl₂/DMSO (10 mL/5 mL) was added SO₃.Pyridine complex (2.06 g, 13 mmol) by portions at 4 °C. The mixture was allowed to warm at room temperature and stirred for 1 h. The mixture was diluted with CH₂Cl₂ (100 mL) and HCl 0.05 M (100 mL) and extracted 2 times with CH₂Cl₂ (50 mL). The combined organic layers were washed 2 times with water, brine and dried over Na₂SO₄. The solvent was removed under vacuo and the crude was purified by flash chromatography (CH₂Cl₂/EtOAc 1/1 as eluent) to give **37** as a yellow oil (532 mg, 71%).

¹H NMR (400 MHz, CDCI₃) δ 7.72 – 7.61 (m, 4H), 7.50 – 7.39 (m, 6H), 6.51 – 6.37 (m, 1H), 6.31 (t, J = 2.8 Hz, 1H), 5.71 (t, J = 2.5 Hz, 1H), 5.49 (s, 1H), 4.47 (dd, J = 7.0, 4.3 Hz, 1H), 4.28 (dq, J = 2.1, 1.0 Hz, 2H), 3.97 (d, J = 12.0 Hz, 1H), 3.30 (dd, J = 12.7, 2.4 Hz, 7H), 2.67 (ddd, J = 17.2, 5.1, 2.1 Hz, 1H), 2.39 – 2.25 (m, 1H), 2.07 – 1.97 (m, 2H), 1.38 (s, 3H), 1.09 (s, 9H).

MS(ESI) [M + H]⁺ calculated for C₃₃H₄₀O₇Si: 577.25, found. 577.32.

<u>Step 6:</u>

To a stirred solution of ynone **37** (550 mg, 0.954 mmol) in THF (50 mL) was added dropwise a premixed solution of AuClPPh₃ (9.4 mg, 0.019 mmol) and AgSbF₆ (6.5 mg, 0.019 mmol) in THF (5 mL). The mixture was stirred 15 min at room temperature and diluted with Et₂O (100 mL) and HCl 0.05 M (50 mL). The aqueous phase was extracted with Et₂O and the combined organic layers were washed with brine and dried over Na₂SO₄. The crude was purified by flash chromatography (CH₂Cl₂/EtOAc 1/1 as eluent) to give **38** as a yellow oil (397 mg, 72%).

¹H NMR (400 MHz, CDCl₃) δ 7.65 (ddd, J = 6.6, 2.8, 1.4 Hz, 4H), 7.52 – 7.40 (m, 6H), 6.31 (td, J = 2.9, 1.0 Hz, 1H), 6.20 (dd, J = 8.0, 4.6 Hz, 1H), 5.84 – 5.74 (m, 1H), 5.58 (d, J = 5.2 Hz, 1H), 4.45 – 4.32 (m, 3H), 3.98 (dd, J = 7.4, 5.5 Hz, 1H), 3.45 – 3.15 (m, 7H), 2.63 (d, J = 17.3 Hz, 1H), 2.15 (ddd, J = 14.7, 6.0, 3.4 Hz, 1H), 1.87 – 1.83 (m, 1H), 1.41 (d, J = 2.2 Hz, 3H), 1.08 (d, J = 1.2 Hz, 9H).

MS(ESI) [M + H]⁺ calculated for $C_{33}H_{40}O_7Si$: 577.25, found. 577.32.

Step 7:

To a stirred solution of lactone **38** (200 mg, 0.347 mmol) in dioxane (8 mL) was added SeO₂ (192 mg, 1.73 mmol) in 3 portions at 95 °C within 1.5 hours. After the addition, the reaction mixture was stirred at the same temperature for another 30 minutes and then cooled down to room temperature. Then dioxane was evaporated and Et₂O (80 mL) was added, stirred for 5 minutes, filtered and the solution was washed with saturated aqueous NaHCO₃ (20 mL), diluted Na₂S (10 mL) and brine (20 mL). The organic phase was dried over Na₂SO₄, then filterred and concentrated *in vacuo*. The residue was purified on silica gel chromatography (CH₂Cl₂/EtOAc = $1/1 \sim 1/4$ as eluent) to provide **39** as a yellow oil (43 mg, 21%).

¹H NMR (400 MHz, CDCl₃) δ 7.70 – 7.64 (m, 4H), 7.50 – 7.41 (m, 6H), 6.50 (dd, J = 4.8, 1.8 Hz, 1H), 6.16 – 5.98 (m, 2H), 5.79 – 5.45 (m, 2H), 4.57 – 4.47 (m, 2H), 4.37 (q, J = 1.3 Hz, 2H), 3.34 – 3.24 (m, 6H), 2.25 – 2.09 (m, 2H), 1.43 (d, J = 3.8 Hz, 3H), 1.08 (d, J = 3.4 Hz, 9H).

MS(ESI) [M + H]⁺ calculated for $C_{33}H_{40}O_7Si$: 577.25, found. 577.18.

Step 1:

Vinyl iodide **50** was prepared from commercially available 3-butyn-1-ol using a carboalumination /iodination according to the literature.³

Step 2:

To a 0 °C solution of alcohol **50** (132 mmol) in CH₂Cl₂ (250 mL) Dess–Martin periodinane (DMP, 56 g, 132 mmol) was slowly added by portions. The mixture was stirred at room temperature for 3 hours, until TLC analysis showed disappearance of starting material (aldehyde, Rf = 0.60, Pentane/Ethyl acetate = 5/1). Then, the mixture was cooled down again to 0 °C and a catalytic amount of *p*-TsOH•H₂O (1.0 g) was added, followed by addition of CH(OMe)₃ (21.6 mL, 198 mmol). The reaction mixture was allowed to warm to room temperature and stirred for 30 minutes. the mixture was then quenched with saturated aqueous NH₄Cl and Na₂SO₃(v/v = 1:1, 500 mL) and extracted with CH₂Cl₂ (3 × 500 mL). The combined organic layers were washed with brine (500 mL), dried over Na₂SO₄, then filtered and concentrated *in vacuo*. The residue was purified on silica gel chromatography (Pentane/Ethyl acetate = 30/1 as eluent) to provide **51** as yellow oil (26.4 g, 78%).

¹H NMR (400 MHz, CDCl₃) δ 6.02 (m, 1H, H_1), 4.47 (t, J = 5.7 Hz, 1H, H_4), 3.32 (s, 6H, -OMe), 2.50 (dd, J = 5.7, 1.0 Hz, 2H, H_3), 1.88 (d, J = 1.1 Hz, 3H, H_5) ppm;

_

³ Prasad, K. R., Pawar, A. B. *Org Lett.*, **2011**, *13*, 4252-4255.

¹³C NMR (100 MHz, CDCl₃) δ 143.4 (C_2), 102.9 (C_4 H), 77.8 (C_7 H), 53.1 (-OMe), 42.5 (C_3 H₂), 24.6 (C_5 H₃) ppm;

<u>Step 3:</u>

To a stirred solution of vinyl iodide **51** (20.8 g, 81 mmol) in THF/*i*-Pr₂NH (150 mL/50 mL) was added trimethylsilyl acetylene (13.5 mL, 97.5 mmol) at 0 °C. Then Pd(PPh₃)₂Cl₂ (2.8 g, 4.05 mmol) and CuI (1.54 g, 8.1 mmol) were added at the same temperature. The reaction mixture was allowed to reach room temperature and stirred for 1 hour until TLC analysis showed disappearance of starting material. Then, pentane (800 mL) was added to the reaction mixture, stirred for 30 minutes, the mixture was filterred and the solution washed with saturated aqueous NH₄Cl (200 mL). The aqueous phase was extracted with CH₂Cl₂ (2 × 100 mL). The combined organic layers were dried over Na₂SO₄, then filtered and concentrated *in vacuo*. The residue was purified on silica gel chromatography (Pentane/Ethyl acetate = 50/1 ~ 25/1 as eluent) to provide the **52** as light-yellow oil (13.3 g, 72%).

¹H NMR (400 MHz, CDCl₃) δ 5.38 (m, 1H, H_3), 4.47 (t, J = 5.7 Hz, 1H, H_6), 3.30 (s, 6H, -OMe), 2.37 (d, J = 5.8 Hz, 2H, H_5), 1.94 (d, J = 0.8 Hz, 3H, H_7), 0.18 (s, 9H, -TMS) ppm;

¹³C NMR (100 MHz, CDCl₃) δ 148.9 (C_4), 107.9 (C_6 H), 103.2 (C_2), 103.1 (C_3 H), 97.6 (C_1), 52.9 (-OMe), 41.8 (C_5 H₂), 20.2 (C_7 H₃), 0.2 (-TMS) ppm;

HRMS(ESI) [M + H]⁺ calculated for $C_{12}H_{23}O_2Si$: 227.1467, found: 227.1250; TLC: Rf = 0.30 (Pentane/Ethyl acetate = 25/1).

Step 4:

A 500 mL round bottom flask equipped with a magnetic stir bar was charged with $K_2OsO_2(OH)_2 \cdot 2H_2O$ (320 mg, 0.9 mmol), (DHQD)₂PYR (1.2 g, 1.36 mmol), $K_3Fe(CN)_6$ (44.6 g, 136 mmol), K_2CO_3 (18.8 g, 136 mmol) and t-BuOH/H₂O (100 mL/100 mL). The bi-phasic mixture was stirred at room temperature for 30 minutes, then MeSO₂NH₂ (4.8 g, 50.5 mmol) was added and the mixture was stirred for another 30 minutes. Enyne **52** (10.2 g, 45 mmol) was added to the AD-mix- β mixture and stirred at room temperature for 1 night. The reaction was followed by NMR analysis till disappearance of the starting material. The reaction slurry was filtered and the filtrate was extrated

with CH₂Cl₂ (4 × 100 mL). The combined organic layers were dried over Na₂SO₄, filtered, concentrated *in vacuo* to obtain **53** a yellow oil (13.4 g, 51.5 mmol). The compound was used without further purification. $[\alpha]_D^{20}$ -34 (c 0.3, CHCl₃).

¹H NMR (400 MHz, CDCl₃) δ 4.70 (t, J = 5.8 Hz, 1H), 4.23 (s, 1H), 3.38 (d, J = 3.6 Hz, 6H), 2.03 (dd, J = 14.5, 5.9 Hz, 1H), 1.90 (dd, J = 14.6, 5.7 Hz, 1H), 1.32 (s, 3H), 0.18 (s, 10H).

Step 5:

To a mixture of compound **53** (13.4 g, 51.5 mmol), acetic anhydride (5.84 mL, 61.85 mmol) and DMAP (628 mg, 5.15 mmol) in CH₂Cl₂ (200 mL) was added dropwise Et₃N (17.8 mL, 129 mmol) at 4 °C. Mixture allowed to warm at room temperature and stirred 1 hour. Mixture diluted with CH₂Cl₂ (20 mL) and HCl 0.1M (100 mL). Organic phase washed with H₂O and Brine then dried over sodium sulfate. Solvent removed and **54** was obtained as a pale-yellow oil (15.5 g, yield 99%). [α]_D²⁰ -34 (c 0.3, CHCl₃).

¹H NMR (400 MHz, CDCl₃) δ 5.42 (s, 1H), 4.73 (dd, J = 6.4, 5.3 Hz,1H), 3.40 (d, J = 9.9 Hz, 6H), 2.15 (s, 3H), 2.09 (dd, J = 14.6, 5.3 Hz, 1H), 1.91 (dd, J = 14.6, 6.5 Hz, 1H), 0.19 (s, 9H).

¹³C NMR (101 MHz, CDCl₃) δ 169.96, 102.34, 100.46, 92.03, 72.79, 69.77, 53.57, 53.22, 39.89, 23.08, 21.02, -0.29.

HRMS(ESI) [M + Na]⁺ calculated for C₁₄H₂₆O₅SiNa: 325.15, found: 325.1437

Step 6:

To a solution of **54** (15.5 g, 51.5 mmol) in THF (170 mL) was added dropwise TBAF (51.5 mL, 1M in THF, mmol) at 4 °C. The mixture was stirred 15 minutes and quenched with NH₄Cl saturated (50 mL). The mixture was diluted with Et₂O (200 mL) and HCl 0.1M (100 mL). The organic phase was washed with H₂O and Brine then dried over Na₂SO₄. A flash chromatography on silica gel (pentane/EtOAc 7/3 as eluent) gave **55** as a yellow pale oil (9.75g, yield 82%).[α]_D²⁰ -19.4 (c 0.1, CHCl₃).

¹H NMR (400 MHz, CDCl₃) δ 5.38 (d, J = 2.2 Hz, 1H), 4.74 (t, J = 5.8 Hz, 1H), 3.40 (d, J = 4.4 Hz, 6H), 2.50 (d, J = 2.2 Hz, 1H), 2.15 (s, 3H), 2.11 (dd, J = 14.6, 5.6 Hz, 1H), 1.93 (dd, J = 14.6, 6.0 Hz, 1H).

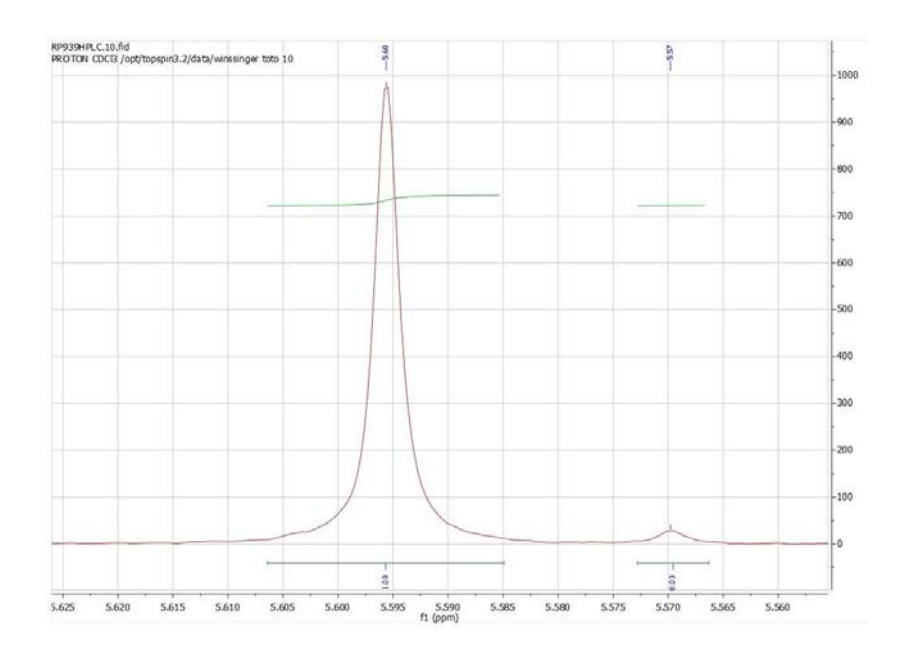
¹³C NMR (101 MHz, CDCl₃) δ 169.89, 102.20, 79.08, 74.87, 72.52, 69.39, 53.43, 53.24, 39.59, 23.22, 20.91.

HRMS(ESI) [M + H]⁺ calculated for $C_{20}H_{28}O$: 230.12, not found.

Mosher ester 1 (56)

To a mixture of diol **53** (5 mg, 0.019 mmol), Et₃N (6.6 μ L, 0.047 mmol) in CH₂Cl₂ (200 mL) was added (R)-(-)- α -methoxy- α -trifluoromethylphenylacetyl chloride (4.3 mL, 0.023 mmol) at 0 °C. The mixture was allowed to warm at room temperature and stirred for 30 min. The mixture was directly purified by PTLC (Pentane/EtOAc 1/1 as eluent) to give **56** as a yellow oil 4.8 mg (yield 53%).

¹H NMR (400 MHz, CDCl₃) δ 7.65 – 7.56 (m, 2H), 7.45 – 7.38 (m, 3H), 5.60 (s, 1H), 4.70 (t, J = 5.7 Hz, 1H), 3.61 (d, J = 1.1 Hz, 3H), 3.37 (d, J = 9.9 Hz, 6H), 2.07 (dd, J = 14.6, 5.6 Hz, 1H), 1.85 (dd, J = 14.5, 5.9 Hz, 1H), 1.23 (s, 3H), 0.19 (s, 9H). Enantiomeric excess: 94%

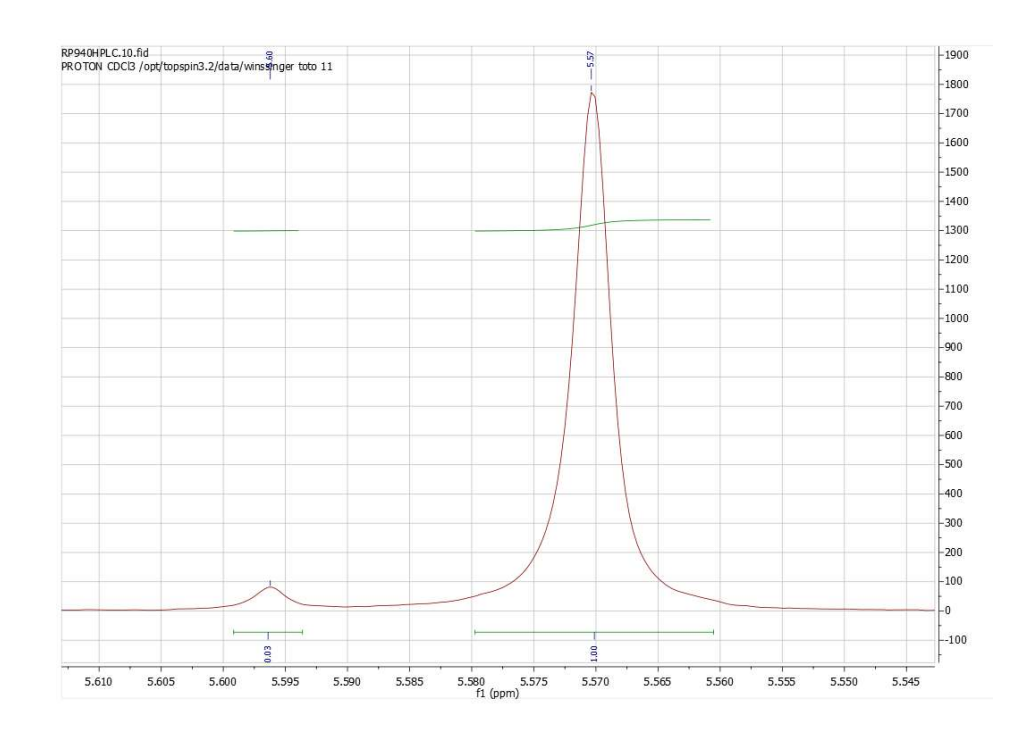


Mosher ester 2 (57)

To a mixture of diol **53** (5 mg, 0.019 mmol), Et₃N (6.6 μ L, 0.047 mmol) in CH₂Cl₂ (200 mL) was added (S)-(+)- α -methoxy- α -trifluoromethylphenylacetyl chloride (4.3 mL, 0.023 mmol) at 0 °C. The mixture was allowed to warm at room temperature and stirred for 30 min. The mixture was directly purified by PTLC (Pentane/EtOAc 1/1 as eluent) to give **57** as a yellow oil 5.3 mg (yield 58%).

¹H NMR (400 MHz, CDCI₃) δ 7.59 (d, J = 3.6 Hz, 2H), 7.44 – 7.39 (m, 3H), 5.57 (s, 1H), 4.72 (dd, J = 6.2, 5.3 Hz, 1H), 3.61 (d, J = 1.2 Hz, 3H), 3.40 (d, J = 12.5 Hz, 6H), 2.09 (dd, J = 14.6, 5.3 Hz, 1H), 1.93 (dd, J = 14.6, 6.3 Hz, 1H), 1.30 (s, 3H), 0.16 (s, 9H).

Enantiomeric excess: 94%



<u>Step 1:</u>

To a stirred solution of alkyne **55** (269 mg, 1.17 mmol) and vinyl bromide **37** (860 mg, 1.76 mmol) in DMF/Et₃N (6.0 mL/2.0 mL) was added PPh₃ (60 mg, 0.23 mmol) at room temperature, under N₂. Then Pd₂dba₃ (109 mg, 0.12 mmol) and Cul (11 mg, 0.06 mmol) were added to the reaction. The resulted mixture was stirred at the same temperature for 3 hours or until the TLC analysis showed disappearance of starting material. The reaction was quenched by sat. aq. NH₄Cl (5.0 mL) and extracted with ethyl acetate (3 x 20 mL). The combined organic layers were dried over Na₂SO₄, filtered and concentrated *in vacuo*. The residue was purified on silica gel chromatography (CH₂Cl₂/ethyl acetate = 1/1 as eluent) to provide enyne **58** as a mixture of diastereomers as a yellow oil (402 mg, 54%).

1H NMR (400 MHz, CDCI₃) δ 7.66 (m, 4H), 7.42 (m, 6H), 6.47 (m, 1H), 6.22 (m, 1H), 6.01 (m, 1H), 5.51–5.33 (m, 1H), 5.30–4.97 (m, 1H), 4.77–4.55 (m, 2H), 4.23 (m, 2H), 3.45–3.24 (m, 6H), 2.18–1.98 (m, 4H), 1.96–1.79 (m, 1H), 1.33 (t, 3H), 1.08 (s, 9H) ppm;

¹³C NMR (101 MHz, CDCI₃) δ 170.2, 168.4, 137.9, 137.6, 135.5, 133.4, 133.0, 132.8, 132.8, 132.7, 132.7, 129.9, 129.8, 128.0, 127.8, 126.3, 126.1, 126.0, 126.0, 102.3, 102.1, 102.0, 92.4, 92.4, 84.0, 83.9, 81.6, 80.1, 74.1, 74.1, 72.8, 72.7, 72.7, 70.5, 70.4, 70.2, 69.8, 65.0, 64.7, 64.7, 53.6, 53.5, 53.4, 53.3, 53.2, 53.2, 39.4, 39.4, 39.3, 26.7, 26.7, 23.9, 23.8, 23.7, 20.9, 20.9, 19.2 ppm;

HRMS(ESI) [M + Na]⁺ calculated for C₃₅H₄₄O₉Si: 659.2755, found 659.2652;

Step 2:

AcO
$$\xrightarrow{\text{OH}}_{\text{HO}}$$
 $\xrightarrow{\text{PBr}_3}$ $\xrightarrow{\text{AcO}}$ $\xrightarrow{\text{OH}}_{\text{OH}}$ $\xrightarrow{\text{Br}}_{\text{O}}$ $\xrightarrow{\text{OTBDPS}}$ $\xrightarrow{\text{S8}}$ $\xrightarrow{\text{59}}$

To a solution of **58** (402 mg, 0.63 mmol) in Et_2O (20 mL) at -25 °C, was added dropwise a solution of PBr_3 (1.2 mL, 1M in Et_2O). After 30 minutes, the mixture was quenched

with cold H_2O (1 mL) and allowed to warm to room temperature. Then the reaction was extracted with CH_2CI_2 (50 mL), and the organic layer was dried over Na_2SO_4 and concentrated. The residue was purified on silica gel chromatography (Pentane/Ethyl acetate = $7/3 \sim 3/7$) to give a yellow solid corresponding to **59** as a mixture of inseparable 1:1 diasteroisomers (213 mg, yield 52%). Yellow solid;

¹H NMR (400 MHz, CDCl₃) δ 9.85 (t, J = 3.8 Hz, 1H), 7.71–7.60 (m, 4H), 7.52–7.37 (m, 7H), 7.35 (d, J = 1.2 Hz, 1H), 5.96 – 5.81 (m, 2H), 5.48 (d, J = 2.6 Hz, 1H), 4.21 (d, J = 0.7 Hz, 2H), 4.14 (d, J = 0.8 Hz, 2H), 2.70 (ddd, J = 29.0, 15.2, 9.3 Hz, 2H), 2.13 (s, 3H), 1.41 (s, 3H), 1.07 (s, 9H) ppm;

¹³C NMR (101 MHz, CDCl₃) δ 201.30, 201.28, 170.98, 170.95, 169.66, 169.64, 150.55, 135.68, 135.66, 135.63, 135.61, 132.85, 132.74, 131.53, 131.51, 130.18, 129.33, 129.32, 128.04, 127.88, 92.58, 92.52, 81.81, 81.79, 79.31, 79.28, 77.41, 77.16, 76.91, 73.45, 70.19, 70.17, 65.17, 50.65, 50.60, 26.91, 24.18, 24.16, 20.98, 20.96, 19.38 ppm;

HRMS(ESI) [M + Na]⁺ calculated for $C_{33}H_{37}BrO_7Si$: 675.1492, found 675.1390;

<u>Step 3:</u>

A 10 mL round bottom flask equipped with a magnetic stir bar was charged with bromolactone **59** (213 mg, 0.33 mmol) and DMF (10 mL). The reaction mixture was cooled down to -30 °C and CrCl₂ (405 mg, 3.3 mmol) was added. The temperature was allowed to rise to room temperature and stirred for 30 minutes till the TLC analysis showed disappearance of the starting material. Then the reaction was quenched with sat. aq. NH₄Cl (50 mL) and extracted with ethyl acetate (3 × 25 mL). The combined organic layers were dried over Na₂SO₄, then filtered and concentrated *in vacuo*. The residue was purified on silica gel chromatography (CH₂Cl₂/Ethyl acetate = 1/1 as eluent) to provide **61** as a yellow solid (72 mg, 38%). Yellow solid; $[\alpha]_D^{20}$ -108 (c 0.25, CHCl₃).

¹H NMR (500 MHz, CDCI₃) δ 7.64 (dd, J = 6.5, 5.0 Hz, 4H, Ph), 7.48–7.36 (m, 6H, Ph), 6.46 (s, 1H, g1), 6.41 (s, 1H, d)), 5.81 (s, 1H, g2), 5.20 (s, 1H, e), 5.16 (s, 1H, b), 4.15 (s, 2H, c), 4.10 (s, 1H, h), 3.98 (s, 1H, f), 2.63 (d, J = 14.0 Hz, 1H, i1), 2.16–2.09 (m, 4H, a+i2), 1.42 (s, 3H, j), 1.07 (s, 9H, tBu) ppm;

¹³C NMR (126 MHz, CDCI₃) δ 169.7, 169.3, 139.2, 135.5, 135.5, 132.8, 132.8, 129.9, 129.9, 127.8, 125.7, 70.8, 70.4, 63.9, 29.7, 26.8, 20.8, 19.2 ppm;

	2D NMR correlations					
	¹H-¹H COSY		NOESY			
61	AcO OH OH OH OTBDPS		Acc OH OH OH OH OTBDPS			

HRMS(ESI) [M + Na]⁺ calculated for C₃₃H₃₈O₇Si: 597.2387, found 597.2284;

Diasteroisomer 60

¹H NMR (400 MHz, CDCl₃) δ 7.68 – 7.63 (m, 4H, Ph), 7.46 – 7.38 (m, 6H, Ph), 6.54 (d, J = 2.2 Hz, 1H, d), 6.48 (d, J = 3.4 Hz, 1H, g1), 5.75 (d, J = 2.9 Hz, 1H, g2), 5.25 (s, 1H, b), 5.12 – 5.03 (m, 1H, e), 4.80 (s, 1H, h), 4.17 (s, 2H, c), 3.97 – 3.87 (m, 1H, f), 2.50 (dd, J = 15.2, 6.3 Hz, 1H, i1), 2.10 (s, 3H, a), 2.04 – 1.99 (m, 1H, i2), 1.37 (s, 3H, j), 1.08 (s, 9H, tBu).

¹³C NMR (101 MHz, CDCI₃) δ 169.29 (C2), 169.17 (C12), 135.57 (C10+Ph), 129.95 (Ph), 127.84 (Ph), 123.22 (C14), 80.15 (C11), 69.05 (C3), 67.26 (C16), 64.65 (C7), 49.75 (C15), 47.46 (C17), 26.80 (C19+tBu), 20.85 (C1).

MS(ESI) [M + H]⁺ calculated for $C_{33}H_{38}O_7Si$: 575.24, found. 575.31.

	2D NMR correlations					
	¹H-¹H COSY	NOESY				
60	AcO OH OH OH OTBDPS	AcC OH				

Step 4:

To a solution of **61** (50 mg, 0.087 mmol), methacrylic anhydride (20 μ L, 0.13 mmol) and DMAP (1.0 mg, 9.0 μ mol) in CH₂Cl₂ (1.0 mL) at 0 °C, was added dropwise a solution of Et₃N (30 μ L, 0.22 mmol) in CH₂Cl₂ (0.5 mL). The mixture was allowed to warm at room temperature for 4 h. The mixture was quenched with HCl 0.1M (1.0 mL) and the aqueous phase was extracted with CH₂Cl₂ (2 x 2.0 mL), and the combined organic layers were washed with brine (1.0 mL), dried over MgSO₄, and purified by silica gel chromatography (pentane/ethyl acetate = 6/4 as eluent) to give **62** as a yellow oil (27.5 mg, yield 49%). Yellow oil; $[\alpha]_{20}^{10}$ -61 (c 0.15, CHCl₃);

¹H NMR (400 MHz, CDCI₃) δ 7.67–7.64 (m, 4H), 7.45–7.38 (m, 6H), 6.50 (d, J = 2.4 Hz, 1H), 6.43 (d, J = 2.8 Hz, 1H), 6.04 (s, 1H), 5.86 (s, 1H), 5.84 (d, J = 2.3 Hz, 1H), 5.59 (s, 1H), 5.02 (dd, J = 5.1, 2.6 Hz, 1H), 4.53 (dd, J = 5.1, 2.5 Hz, 1H), 4.20–4.12 (m, 2H), 2.39 (dd, J = 14.8, 3.6 Hz, 1H), 2.20 (t, J = 8.3 Hz, 4H), 1.91 (s, 3H), 1.39 (s, 3H), 1.09 (s, 9H) ppm;

¹³C NMR (101 MHz, CDCI₃) δ 169.7, 166.2, 138.5, 135.8, 135.5, 134.8, 132.8, 129.9, 127.8, 126.4, 124.0, 122.7, 95.9, 80.4, 74.7, 72.6, 69.4, 64.2, 46.2, 29.6, 26.8, 20.8, 19.2, 18.2 ppm;

HRMS(ESI) [M + H]⁺ calculated for $C_{37}H_{42}O_8Si$: 643.2649, found 643.2888; TLC: Rf = 0.25 (Pentane/Ethyl acetate = 2/1).

Step 5:

To a solution of **62** (27.5 mg, 0.043 mmol) in MeOH (2.0 mL) at 0 °C, was added dropwise a solution of K_2CO_3 (27 μ L, 1M in H_2O). The mixture was stirred 20 minutes at 0 °C and quenched with a cold mixture of CH_2Cl_2/H_2O (10mL). The reaction was then extracted with CH_2Cl_2 (5.0 mL), and the combined organic layers were washed with brine (5.0 mL), dried over MgSO₄, concentrated and purified by PTLC (pentane/ethyl acetate = 1/1 as eluent) to give the propargyl alcohol **63** as a yellow oil (24 mg, yield 92%). Yellow oil; $[\alpha]_D^{20}$ -48 (c 0.12, CHCl₃);

¹H NMR (400 MHz, CDCl₃) δ 7.66 (dd, J = 7.9, 1.5 Hz, 4H), 7.47–7.37 (m, 6H), 6.46 (dd, J = 6.5, 2.6 Hz, 2H), 6.06 (s, 1H), 5.92 (d, J = 9.4 Hz, 1H), 5.86 (d, J = 2.5 Hz, 1H), 5.63–5.58 (m, 1H), 4.95 (dd, J = 5.6, 2.6 Hz, 1H), 4.43 (td, J = 4.6, 2.5 Hz, 1H), 4.26 (s, 1H), 4.23–4.16 (m, 2H), 4.14 (d, J = 7.1 Hz, 1H), 2.29 (dd, J = 15.0, 3.3 Hz, 1H), 2.19–2.10 (m, 1H), 1.90 (s, 3H), 1.45 (s, 3H), 1.09 (s, 9H) ppm;

¹³C NMR (101 MHz, CDCI₃) δ 169.4, 166.9, 137.7, 135.6, 135.5, 134.6, 132.8, 129.9, 127.8, 126.9, 123.8, 122.6, 98.7, 84.5, 80.3, 75.7, 72.5, 69.6, 64.4, 60.4, 53.4, 46.0, 39.8, 29.0, 26.8, 21.0, 19.2, 18.0, 14.2 ppm;

HRMS(ESI) [M + H]⁺ calculated for $C_{35}H_{40}O_7Si$: 601.2543, found 601.2622; TLC: Rf = 0.25 (Pentane/Ethyl acetate = 2/1).

Steps 6/7:

To a stirred solution of **63** (24 mg, 40 μ mol) in CH₂Cl₂ (5.0 mL) was added MnO₂ (35 mg, 0.4 mmol) and the solution was stirred at room temperature for 2 hours, till the TLC analysis showed disappearance of the starting material. The crude mixture was filterred and a trace of tBu_3 PAuNTf₂ was added and the solution was stirred for 10 more minutes till the TLC analysis showed disappearance of the starting material. The resulted solution was concentrated *in vacuo* and the residue was purified on silica gel chromatography (Pentane/Ethyl acetate = 3/1 as eluent) to provide **65** as a white solid (19 mg, 82%).

Analysis of 64

White solid; $[\alpha]_{D}^{20}$ -36 (c 0.12, CHCl₃);

¹H NMR (400 MHz, CDCl₃) δ 7.70–7.62 (m, 4H), 7.51–7.39 (m, 6H), 6.80 (q, J = 2.0 Hz, 1H), 6.49 (d, J = 3.3 Hz, 1H), 6.09 (s, 1H), 5.84 (t, J = 4.5 Hz, 1H), 5.81 (d, J = 2.9 Hz, 1H), 5.66–5.59 (m, 1H), 5.28 (dq, J = 7.3, 2.5 Hz, 1H), 4.32–4.25 (m, 2H), 4.01 (dt, J = 6.0, 2.8 Hz, 1H), 2.51 (dd, J = 15.5, 5.7 Hz, 1H), 2.36 (dt, J = 6.4, 2.9 Hz, 1H), 1.92 (s, 3H), 1.47 (s, 3H), 1.10 (d, J = 6.4 Hz, 9H) ppm;

¹³C NMR (101 MHz, CDCI₃) δ 190.0, 169.0, 167.0, 143.8, 136.1, 135.9, 133.5, 133.0, 130.7, 128.5, 127.7, 125.1, 121.4, 96.0, 94.4, 80.3, 80.2, 71.2, 64.8, 50.9, 44.4, 27.3, 25.6, 19.8, 18.7 ppm;

HRMS(ESI) [M + H]⁺ calculated for $C_{35}H_{38}O_7Si$: 599.2387, found 599.2465; TLC: Rf = 0.3 (Pentane/Ethyl acetate = 2/1).

Analysis of 65

 $[\alpha]_{D}^{20}$ -2 (c 0.1, CHCl₃);

¹H NMR (400 MHz, CDCl₃) δ 7.69–7.65 (m, 4H), 7.50–7.38 (m, 6H), 6.26 (d, J = 3.2 Hz, 1H), 6.14 (d, J = 2.9 Hz, 1H), 6.03 (s, 1H), 5.68 (s, 1H), 5.58–5.54 (m, 1H), 5.48 (d, J = 2.7 Hz, 1H), 5.30 (td, J = 5.0, 2.3 Hz, 1H), 4.53 (d, J = 11.8 Hz, 1H), 4.40 (dd, J = 34.3, 13.9 Hz, 2H), 3.77–3.72 (m, 1H), 2.49 (dd, J = 13.8, 11.8 Hz, 1H), 2.32 (d, J = 11.9 Hz, 1H), 1.85 (s, 3H), 1.51 (s, 3H), 1.09 (s, 9H) ppm;

¹³C NMR (101 MHz, CDCl₃) δ 204.6, 184.7, 168.7, 166.7, 135.6, 135.5, 135.4, 134.3, 133.9, 133.3, 132.6, 130.1, 127.8, 127.8, 126.4, 124.3, 106.4, 89.6, 81.5, 73.1, 64.1, 50.8, 43.9, 29.6, 26.7, 20.6, 19.2, 17.9 ppm;

HRMS(ESI) [M + H]⁺ calculated for C₃₅H₃₈O7Si: 599.2387, found 599.2450;

TLC: Rf = 0.25 (Pentane/Ethyl acetate = 2/1).

Step 8:

To a solution of **65** (17 mg, 0.029 mmol) in THF (2.0 mL) at 0 °C, was added dropwise a solution of HF·pyridine 70% (85 μ L) in THF (1.0 mL). The mixture was stirred 4 hours at 0 °C and quenched with saturated NaHCO₃ (2.0 mL). The quenched mixture was then extracted with Et₂O (5.0 mL × 2), and the combined organic layers were washed with brine (5.0 mL), dried over MgSO₄, and purified by PTLC (Pentane/Ethyl acetate = 2/8 as eluent) to give (-)-Goyazensolide **1** (8.5 mg, yield 82%). Waxy solid.

 $[\alpha]_{D}^{20}$ -19 (c 0.1, CHCl₃);

¹H NMR (500 MHz, CDCl₃) δ 6.30 (dt, J = 3.0, 1.5 Hz, 1H), 6.25 (d, J = 3.1 Hz, 1H), 6.03 (s, 1H), 5.82 (s, 1H), 5.59–5.54 (m, 1H), 5.49 (d, J = 2.7 Hz, 1H), 5.36 (dd, J = 2.7 H

4.9, 2.7 Hz, 1H), 4.57 (dt, J = 11.7, 2.2 Hz, 1H), 4.42 (dt, J = 3.1, 1.7 Hz, 2H), 3.82 (t, J = 5.3 Hz, 1H), 2.56–2.48 (m, 1H), 1.85 (s, 3H), 1.56 (s, 3H) ppm;

¹³C NMR (126 MHz, CDCI₃) δ 204.6, 184.2, 166.8, 135.5, 135.3, 134.2, 133.1, 126.6, 124.6, 106.6, 89.8, 81.5, 73.2, 63.2, 50.9, 43.9, 20.7, 18.0 ppm;

HRMS (ESI) [M + H]⁺ calculated for $C_{19}H_{20}O_7$: 361.1209, found 361.1392; TLC: Rf = 0.2 (CH₂CI₂/Ethyl acetate = 1/2).

III.2.5. Total synthesis of 5-epi-isogoyazensolide

Step 1:

To a stirred solution of alkyne **55** (210 mg, 0.913 mmol), $PdCl_2(PPh_3)_2$ (21 mg, 0.03 mmol) and CuI (11.6 mg, 0.061 mmol) in THF/TEA (3 mL/1 mL) was added dropwise vinyl bromide **67** (225 mg, 0.609 mmol). The mixture was then stirred for 2 hours and the reaction was quenched by addition of *sat. aq.* NH₄Cl (10 mL) and extracted with ethyl acetate (3 × 20 mL). The combined organic layers were dried over Na₂SO₄, then filtered and concentrated *in vacuo*. The residue was purified on silica gel chromatography (Pentane/Ethyl acetate = 3/1 as eluent) to provide enyne **75** as a yellow oil (57 mg, 18%).

¹H NMR (400 MHz, CDCI₃) δ 7.25 (d, J = 8.6 Hz, 2H), 6.89 (d, J = 8.6 Hz, 2H), 6.40 (d, J = 2.4 Hz, 1H), 5.94 (d, J = 2.1 Hz, 1H), 5.83 – 5.77 (m, 1H), 5.71 (t, J = 1.2 Hz, 1H), 5.44 (s, 1H), 4.73 (s, 1H), 4.65 (d, J = 11.6 Hz, 1H), 4.48 – 4.40 (m, 1H), 4.34 (d, J = 11.5 Hz, 1H), 4.00 (d, J = 5.1 Hz, 1H), 3.83 (s, 3H), 3.38 (d, J = 6.1 Hz, 7H), 2.16 (s, 4H), 1.92 (dd, J = 14.6, 5.8 Hz, 2H), 1.35 (s, 3H).

¹³C NMR (101 MHz, CDCl₃) δ 132.14, 132.04, 129.61, 128.59, 128.47, 113.89, 102.21, 102.15, 84.98, 79.67, 72.90, 72.84, 70.76, 70.26, 69.80, 69.37, 55.28, 53.58, 53.51, 53.09, 39.72, 39.64, 23.61, 23.57, 20.96, 20.82.

MS(ESI) [M + H]⁺ calculated for $C_{27}H_{34}O_{10}$: 519.22, found. 519.28.

Step 2:

Enyne **75** (30 mg, 0.058 mmol) was dissolved in Et_2O (3.0 mL). The reaction was cooled down to -30 °C and PBr₃ (5.5 μ L, 0.058 mmol) was added. The mixture was allowed to warm slowly to -10 °C in 45 min then the reaction was quenched with water (5.0 mL) and extracted with Et_2O (10 mL). The combined organic layers were dried over Na₂SO₄, then filtered and concentrated *in vacuo*. The residue was purified on silica gel chromatography (Pentane/Ethyl acetate = 3/1 as eluent) to provide bromolactone **76** as a colorless oil (14 mg, 58%).

¹H NMR (300 MHz, CDCl₃) δ 9.95 – 9.79 (m, 1H), 7.51 – 7.37 (m, 1H), 7.30 – 7.22 (m, 2H), 6.95 – 6.84 (m, 2H), 5.86 – 5.73 (m, 1H), 5.70 – 5.62 (m, 1H), 5.49 – 5.40 (m, 1H), 5.17 – 5.05 (m, 1H), 4.69 – 4.57 (m, 1H), 4.45 – 4.32 (m, 1H), 4.14 – 4.06 (m, 2H), 3.83 (s, 3H), 2.88 – 2.59 (m, 2H), 2.14 (d, J = 2.6 Hz, 3H), 1.43 (s, 3H). ¹³C NMR (75 MHz,) δ 201.66, 169.61, 159.63, 149.74, 132.31, 129.68, 128.74, 127.84, 125.48, 113.99, 87.04, 84.48, 81.38, 79.70, 73.41, 71.09, 70.25, 55.33, 50.61, 24.01, 20.89, 20.72.

MS(ESI) [M + H]⁺ calculated for $C_{25}H_{27}BrO_8$: 535.09, found. 535.27.

Step 3:

Bromolactone **76** (14 mg, 0.026 mmol) was dissolved in DMF (1 mL). The reaction mixture was cooled down by a mixture of ice + NaCl and $CrCl_2$ (6.2 mg, 0.5 mmol) was added to the mixture. The temperature was allowed to warm at room temperature and stirred for 30 minutes. Reaction was quenched with NH₄Cl saturated (5.0 mL) and extracted with ethyl acetate (3 × 5.0 mL). The combined organic layers were dried over Na₂SO₄, then filtered and concentrated *in vacuo*. The residue was purified on silica gel chromatography (Pentane/Ethyl acetate = 2/1 as eluent) to provide **77** as a waxy solid (5 mg, 42%).

¹H NMR (400 MHz, CDCI₃) δ 7.37 – 7.29 (m, 2H), 6.96 – 6.85 (m, 2H), 6.49 – 6.37 (m, 1H), 5.88 – 5.80 (m, 2H), 5.74 (t, J = 1.5 Hz, 1H), 5.23 (s, 1H), 4.66 – 4.56 (m, 2H), 4.47 (dd, J = 8.8, 3.7 Hz, 1H), 4.26 (d, J = 4.1 Hz, 1H), 4.10 (d, J = 7.4 Hz, 1H), 3.96 – 3.88 (m, 1H), 3.81 (s, 3H), 2.32 (dd, J = 15.2, 3.1 Hz, 1H), 2.15 (d, J = 1.4 Hz, 3H), 2.13 – 2.08 (m, 1H), 1.40 (s, 3H).

¹³C NMR (101 MHz, CDCl₃) δ 169.62, 134.91, 129.78, 129.31, 126.57, 125.55, 124.87, 113.92, 90.80, 83.56, 81.63, 72.69, 70.07, 69.89, 60.40, 55.29, 47.62, 29.35, 20.88. **MS(ESI)** [**M** + **H**]⁺ calculated for $C_{25}H_{28}O_{8}$: 457.18, found. 457.24.

Step 4:

To a stirred solution of alcohol **77** (5 mg, 0.011 mmol) in CH_2CI_2 (1.0 mL) was added Et_3N (4.5 μ L, 0.033 mmol) and methacrylic anhydride (2.5 μ L, 0.016 mmol) followed by a trace of DMAP at 0 °C. The reaction mixture was allowed to warm at room temperature and stirred for 1 h. Reaction was then quenched with *sat. aq.* NaHCO₃ (2.0 mL), the mixture was extracted with ethyl acetate (5.0 mL), the combined organic layers were dried over Na₂SO₄, then filtered and concentrated *in vacuo*. The residue was purified by PTLC (Pentane/Ethyl acetate = 2/1 as eluent) to provide the **78** as a waxy solid (4 mg, 69%).

¹H NMR (500 MHz, CDCI₃) δ 7.34 – 7.28 (m, 2H), 6.94 – 6.81 (m, 2H), 6.46 (d, J = 2.8 Hz, 1H), 6.01 (dt, J = 9.1, 1.6 Hz, 2H), 5.94 – 5.89 (m, 1H), 5.83 – 5.77 (m, 1H), 5.75 (t, J = 1.8 Hz, 1H), 5.56 (p, J = 1.5 Hz, 1H), 5.26 (s, 1H), 4.70 (d, J = 11.1 Hz, 1H), 4.58 (d, J = 11.0 Hz, 1H), 4.48 (dd, J = 5.2, 2.7 Hz, 1H), 4.25 (dd, J = 9.3, 5.0 Hz, 1H), 3.98

(dt, J = 9.3, 2.0 Hz, 1H), 3.82 (s, 3H), 2.29 (dd, J = 14.7, 4.0 Hz, 1H), 2.18 – 2.11 (m, 1H), 2.06 (s, 2H), 1.42 (s, 3H).

¹³C NMR (126 MHz, CDCl₃) δ 134.38, 129.70, 126.49, 125.99, 125.35, 124.00, 113.90, 90.50, 86.54, 84.03, 81.41, 74.37, 73.66, 72.65, 69.17, 55.29, 45.78, 40.62, 29.71, 28.53, 20.90, 18.14.

MS(ESI) [M + H]⁺ calculated for $C_{29}H_{32}O_{9}$: 525.20, found. 525.31.

Step 5:

To a solution of **78** (4 mg, 7.6 μ mol) in MeOH (0.5 mL) at 0 °C, was added dropwise a solution of K₂CO₃ (3.8 μ L, 1M in H₂O, 0.0038 mmol). The mixture was stirred 20 minutes at 0 °C and quenched with a cold mixture of CH₂Cl₂/H₂O (10mL). The reaction was then extracted with CH₂Cl₂ (5.0 mL), and the combined organic layers were washed with brine (5.0 mL), dried over MgSO₄, concentrated and purified by PTLC (pentane/ethyl acetate = 1/1 as eluent) to give propargyl alcohol **79** as a yellow oil (3.4 mg, yield 92%).

¹H NMR (500 MHz, CDCI₃) δ 7.35 – 7.30 (m, 2H), 6.93 – 6.83 (m, 2H), 6.46 (d, J = 2.9 Hz, 1H), 6.01 (q, J = 1.6 Hz, 2H), 5.92 (d, J = 2.5 Hz, 1H), 5.85 – 5.77 (m, 1H), 5.73 (t, J = 1.8 Hz, 1H), 5.57 (p, J = 1.5 Hz, 1H), 4.74 – 4.57 (m, 2H), 4.40 (dt, J = 5.7, 2.7 Hz, 1H), 4.27 (s, 1H), 4.22 (dd, J = 9.1, 5.4 Hz, 1H), 3.99 (dt, J = 9.2, 1.9 Hz, 1H), 3.82 (s, 3H), 2.25 (dd, J = 14.8, 3.6 Hz, 1H), 2.15 – 2.05 (m, 2H), 1.94 – 1.81 (m, 3H).

¹³C NMR (126 MHz, CDCI₃) δ 135.69, 134.29, 129.69, 126.71, 125.54, 125.47, 123.87, 83.96, 81.49, 75.42, 73.64, 72.44, 69.47, 55.30, 45.83, 40.30, 29.71, 27.83, 18.06.

MS(ESI) [M + H]⁺ calculated for C₂₇H₃₀O₈: 483.19, found. 483.24.

Step 6:

To a stirred solution of **79** (2 mg, $4.0 \mu mol$) and NaHCO₃ (2 mg, $0.024 \mu mol$) in CH₂Cl₂ (1 mL) was added DMP (3.5 mg, $80 \mu mol$) and the solution was stirred at room temperature for one night. Reaction diluted with Et₂O and water (10 mL). The organic layer was washed with brine, dried over Na₂SO₄, concentrated and purified by PTLC (pentane/ethyl acetate = 7/3 as eluent) to give ynone **80** as a yellow oil (1.5 mg, yield 75%).

¹H NMR (500 MHz, CDCl₃) δ 7.32 (t, J = 2.0 Hz, 2H), 6.94 – 6.84 (m, 2H), 6.46 (dd, J = 3.2, 1.8 Hz, 1H), 6.26 (q, J = 1.6 Hz, 1H), 6.14 – 6.08 (m, 1H), 6.08 – 5.98 (m, 1H),

5.88 (t, J = 2.3 Hz, 1H), 5.75 (d, J = 8.6 Hz, 1H), 5.60 (q, J = 1.8 Hz, 1H), 5.32 (d, J = 1.8 Hz, 1H), 4.74 – 4.58 (m, 2H), 4.31 (td, J = 7.2, 1.7 Hz, 1H), 4.13 (ddd, J = 9.1, 6.2, 1.9 Hz, 2H), 3.83 (t, J = 1.7 Hz, 3H), 2.45 – 2.33 (m, 1H), 2.26 – 2.16 (m, 1H), 1.95 – 1.87 (m, 3H), 1.33 – 1.28 (m, 3H).

¹³C NMR (126 MHz, CDCl₃) δ 132.35, 129.74, 126.85, 124.33, 123.89, 114.00, 98.07, 82.43, 80.43, 73.17, 70.13, 55.31, 47.70, 44.05, 25.28, 18.14.

MS(ESI) [M + H]⁺ calculated for $C_{27}H_{28}O_8$: 481.18, found. 481.22.

Step 7:

To a stirred solution of **80** (1.5 mg, 3.1 μ mol) in THF (1 mL) was added a premix AuClPPh₃ (0.15 mg, 3.1 μ mol) / AgSbF₆ (0.1 mg, 3.1 μ mol) in THF (0.3 mL). Reaction was stirred at room temperature for 15 min diluted with Et₂O and water (10 mL). The organic layer was washed with brine, dried over Na₂SO₄, concentrated and purified by PTLC (pentane/ethyl acetate = 7/3 as eluent) to give furanone **81** as a yellow oil (1.1 mg, yield 73%).

¹H NMR (500 MHz, CDCI₃) δ 7.41 – 7.33 (m, 2H), 6.96 – 6.88 (m, 2H), 6.29 (d, J = 3.4 Hz, 1H), 6.22 (dd, J = 2.2, 1.0 Hz, 1H), 6.05 – 5.95 (m, 3H), 5.59 – 5.50 (m, 2H), 4.87 (d, J = 11.1 Hz, 1H), 4.69 (dd, J = 9.4, 5.8 Hz, 1H), 4.61 (d, J = 11.2 Hz, 1H), 4.39 (ddt, J = 9.5, 6.1, 1.9 Hz, 2H), 3.83 (s, 3H), 3.69 – 3.63 (m, 1H), 2.50 (dd, J = 13.7, 11.9 Hz, 1H), 2.45 – 2.33 (m, 1H), 1.87 – 1.79 (m, 3H), 1.34 – 1.29 (m, 3H).

¹³C NMR (126 MHz, CDCl₃) δ 129.78, 126.50, 124.14, 123.70, 113.93, 106.81, 85.49, 80.72, 74.67, 70.65, 55.31, 51.74, 45.38, 29.72, 21.08, 17.99.

MS(ESI) [M + H]⁺ calculated for C₂₇H₃₄₂₈O₈: 481.18, found. 481.24.

Step 8:

To a stirred solution of protected alcohol **81** (1.1 mg, 2.2 μ mol) in CH₂Cl₂/water 10/1 (1.1 mL) was added DDQ (1.5 mg, 6.9 μ mol) and the mixture was stirred at room temperature for 24 h. The mixture was quenched by NaHCO₃ saturated (1 mL) and extracted with CH₂Cl₂ (2 x 5 mL). The combined layers were dried over Na₂SO₄, filtered, concentrated *in vacuo* and purified by PTLC (Pentane/EtOAc 2/1 as eluent) to provide 5-*epi*-isogoyazenslide **66** (0.4 mg, 56%).

¹H NMR (500 MHz, CDCl₃) δ 6.29 (d, J = 3.5 Hz, 1H), 6.26 (dd, J = 2.2, 0.9 Hz, 1H), 6.03 – 6.00 (m, 2H), 5.97 (s, 1H), 5.59 – 5.55 (m, 2H), 4.71 – 4.65 (m, 1H), 4.61 (dd, J = 9.6, 6.0 Hz, 1H), 4.42 – 4.36 (m, 1H), 3.70 – 3.65 (m, 1H), 2.50 (d, J = 12.0 Hz, 1H), 2.38 – 2.36 (m, 1H), 1.84 (d, J = 0.6 Hz, 3H).

¹³C NMR (126 MHz, CDCI₃) δ 126.70, 124.84, 123.28, 106.49, 84.97, 73.93, 70.49, 60.41, 53.42, 51.13, 45.18, 29.71, 21.18, 21.06, 14.21.

MS(ESI) [M + H]⁺ calculated for $C_{18}H_{20}O_7$: 361.12, found. 361.18.

III.2.6. « Primary cyclized scaffold »

Step 1:

Aldehyde **134** was prepared from commercially available 2-butyn-1-ol (**132**) in 2 steps using a carboalumination / iodination then modified DMP oxidation process. All spectroscopic and spectrometric analyses were in agreements with the literature accordingly for allylic alcohol (Z)-3-iodobut-2-en-1-ol (**133**)⁴ and aldehyde **134**.⁵

169

⁴ Dakoji, S.; Li, D.; Agnihotri, G.; Zhou, H.; Liu, H. J. Am. Chem. Soc. **2001**, 123, 9749-9759.

⁵ Meyer, C., Marek, I., Normant, J. F. *Synlett.* **1993**, *6*, 386-388.

Modified DMP oxidation: To a stirred solution of crude allylic alcohol **133** (\sim 42 g, 212 mmol) in CH₂Cl₂ (400 mL) was added DMP (90 g, 212 mmol) in portions at 0 °C. The reaction was monitored by TLC until no starting material remained (2 hours). Then pentane (1.2 L) was added to the reaction and stirred at room temperature for 30 minutes. The white precipitate was filtered off and the resulting colorless solution was concentrated *in vacuo* to give a yellow to brown oil **134** (\sim 42 g) which was used directly for Barbier reaction without any further purification.

Supplement. Synthesis of ethyl 2-(bromomethyl)acrylate

ethyl 2-(diethoxyphosphoryl)acetate ethyl 2-(hydroxymethyl)acrylate ethyl 2-(bromomethyl)acrylate

ethyl 2-(bromomethyl)acrylate was prepared in 2 steps including Baylis–Hillman reaction⁶ and bromination⁷ from triethyl phosphonoacetate. All spectroscopic and spectrometric analyses were in agreement with the literature.

Step 2:

A 2.5 L round bottom flask equipped with a magnetic stir bar was charged with aldehyde 134 (82 g, 418 mmol), ethyl 2-(bromomethyl)acrylate (121 g, 627 mmol), THF (800 mL) and NH₄Cl saturated solution (160 mL). The yellow bi-phasic mixture turned colorless and was cooled down to 0 °C. Then Zn (54 g, 836 mmol) was added in small portions within 30 minutes (caution the reaction is very exothermic). The reaction mixture was stirred at 0 °C for 20 minutes. The reaction mixture was filterred, the filtrate was concentrated in vacuo and redissolved in CH₂Cl₂ (800 mL). The organic layer was washed with water (200 mL) and brine (200 mL), dried over Na₂SO₄, filtered, concentrated in vacuo and used directly for cyclization without further purification. The crude product was dissolved in CH₂Cl₂ (500 mL) and a catalytic amount p-TsOH•H₂O (1.0 g) was added. The reaction mixture was stirred at room temperature until the TLC analysis showed disappearance of starting material. Then the mixture was washed with sat. aq. NaHCO₃ (100 mL), brine (100 mL), dried over Na₂SO₄, then filtered and concentrated in vacuo. The residue was purified on silica gel chromatography (Pentane/Ethyl acetate = $20/1 \sim 5/1$ as eluent) to provide the **135** as light-yellow oil (70.6 g, 64%).

170

⁶ Patil, S., Chen, L., Tanko, J. M. Eur. J. Org. Chem. **2014**, *3*, 502-505.

⁷ Li, Y., Zhang, J., Li, D., Chen, Y. Org. Lett. **2018**, 20, 3296-3299.

¹H NMR (400 MHz, CDCl₃) δ 6.25-6.20 (m, 1H), 5.71 (dt, J = 7.6, 1.8 Hz, 1H), 5.65 (q, J = 2.2 Hz, 1H), 5.04 (dt, J = 9.8, 6.8 Hz, 1H), 3.25 (ddt, J = 17.1, 7.7, 2.3 Hz, 1H), 2.64 (ddtd, J = 17.2, 6.2, 3.0, 1.3 Hz, 1H), 2.54 (d, J = 1.7 Hz, 3H) ppm;

HRMS(ESI) [M + H]⁺ calculated for C₈H₁₀IO₂: 264.9725, found: 264.9709;

<u>Step 3:</u>

To a stirred solution of lactone **135** (22 g, 83 mmol) in dioxane (500 mL) was added SeO₂ (50 g, 450 mmol) in 3 portions at 95 °C within 2 hours. The reaction mixture was stirred at the same temperature for another hour and cooled down to room temperature. Then dioxane was evaporated and Et₂O (800 mL) was added, stirred for 30 min, filtered and the solution was washed with saturated aqueous NaHCO₃ (100 mL), diluted Na₂S (50 mL) and brine (100 mL). The organic phase was dried over Na₂SO₄, then filtered and concentrated *in vacuo*. The residue was purified on silica gel chromatography (Pentane/Ethyl acetate = $10/1 \sim 1/1$ as eluent) to provide the **21** as light-yellow oil (9.8 g, 42%). Lactone **136** was obtained as a mixture of inseparable diastereomers.;

¹H NMR (300 MHz, CDCl₃) δ 6.48 (dd, J = 4.6, 2.0 Hz, 1H), 6.04 (dd, J = 10.5, 1.8 Hz, 1H), 5.76 (ddd, J = 46.7, 7.6, 1.6 Hz, 1H), 5.19 – 4.53 (m, 2H), 2.64 (ddd, J = 10.3, 1.5, 0.6 Hz, 3H).

HRMS(ESI) [M + H]⁺ calculated for $[C_8H_{10}IO_3]^+$: 280.9669, found: 280.9675

Step 4:

To a stirred solution at 4 °C and under inert atmosphere of N_2 of $Pd_2Cl_2(PPh_3)_2$ (300 mg, 0.43 mmol) CuI (40 mg, 0.21 mmol) and vinyl iodide **136** (1.20 g, 4.3 mmol) in THF/Et₃N (3/1 12 mL) was added dropwise the alkyne (1.29 g, 5.6 mmol). The resulted mixture was allowed to warm at room temperature and stirred for 3 hours. The reaction was then quenched by addition of *sat. aq.* NH₄Cl (100 mL) and extracted with ethyl acetate (3 × 200 mL). The combined organic layers were dried over Na₂SO₄, then filtered and concentrated *in vacuo*. The residue was purified on silica gel chromatography (Pentane/Ethyl acetate = 1/1 ~ 1/3 as eluent) to provide enyne **137** as yellow oil (380 mg, 23%). Enyne **137** was obtained as a complicated mixture of

diastereomers and that could not be seperated by conventional chromatographic techniques.

¹H NMR (400 MHz, CDCI₃) δ 6.45 (d, J = 2.4 Hz, 1H), 6.00 (d, J = 2.1 Hz, 1H), 5.86 – 5.66 (m, 1H), 5.43 (s, 1H), 5.06 – 4.84 (m, 1H), 4.72 (t, J = 5.7 Hz, 2H), 3.60 (s, 1H), 3.41 (d, J = 3.9 Hz, 6H), 3.37 – 3.26 (m, 1H), 2.63 (ddd, J = 13.7, 1.6, 0.6 Hz, 2H), 2.20 – 2.14 (m, 4H), 2.13 – 2.04 (m, 2H), 2.00 – 1.89 (m, 3H).

LCMS(ESI) [M + H]⁺ calculated for C₁₉H₂₆O₈: 383.16, found: 383.28;

Step 5:

A 100 mL round bottom flask equipped with a magnetic stir bar was charged with enyne 137 (100 mg, 0.26 mmol) and Et₂O (5 mL). The reaction mixture was cooled down to -30 °C and PBr₃ (25 μ L, 0.26 mmol) was added. The temperature was allowed to rise to -10 °C and stirred for 45 min. Then, the reaction was quenched with water (5 mL) and extracted with Et₂O (2 × 5 mL). The combined organic layers were dried over Na₂SO₄, then filtered and concentrated *in vacuo*. The residue was purified on silica gel chromatography (Pentane/Ethyl acetate = 3/1 ~ 1/1 as eluent) to provide bromolactone 138 as colorless oil (60 mg, 58%) as a 1:1 mixture of non seperable diastereomers.

¹H NMR (300 MHz, CDCI₃) δ 9.86 - 9.80 (m, 1H), 7.28 (s, 1H), 5.75 (t, J = 8.1 Hz, 1H), 5.51 - 5.31 (m, 2H), 4.03 (t, J = 1.4 Hz, 2H), 3.43 - 3.24 (m, 1H), 2.80 - 2.61 (m, 2H), 2.08 (d, J = 2.3 Hz, 4H), 2.04 - 1.96 (m, 1H), 1.91 - 1.87 (m, 3H), 1.38 (s, 3H).

LCMS(ESI) [M + H]⁺ calculated for C₁₇H₁₉BrO₆: 399.04, found: 595.1516;

Step 6:

A 50 mL round bottom flask equipped with a magnetic stir bar was charged with bromolactone **138** (60 mg, 0.15 mmol) and DMF (2 mL). The reaction mixture was cooled down to 0 °C and CrCl₂ (55 mg, 0.45 mmol) was added. The temperature was allowed to rise to room temperature and stirred for 1 hour. Then, the reaction was quenched with *sat. aq.* NH₄Cl (20 mL) and extracted with ethyl acetate (3 × 5 mL). The combined organic layers were dried over Na₂SO₄, then filtered and concentrated *in*

vacuo. The residue was purified on silica gel chromatography (Pentane/Ethyl acetate = $1/1 \sim 1/3$ as eluent) to provide **139** as a light yellow solid (14 mg, 30%).

¹H NMR (400 MHz, CDCl₃) δ 6.43 (d, J = 1.8 Hz, 1H), 6.02 (dd, J = 3.5, 1.8 Hz, 1H), 5.81 (dd, J = 1.6, 0.7 Hz, 1H), 5.22 (s, 1H), 5.19 – 5.12 (m, 1H), 4.08 (d, J = 9.2 Hz, 1H), 3.89 (s, 1H), 2.67 (d, J = 15.5 Hz, 1H), 2.15 (s, 4H), 1.85 (t, J = 1.8 Hz, 3H), 1.43 (s, 3H).

LCMS(ESI) [M + H]⁺ calculated for C₁₇H₂₀O₆: 321.13, found: 321.21;

III.2.7. Unexpected synthesis of ISO GOYA-N₃ (85)

<u>Step 1:</u>

To a stirred solution of goyazensolide 1 (3.0 mg, 8 μ mol) in CH₂Cl₂ (0.3 mL) was added Et₃N (2.9 μ L, 21 μ mol) and tosyl chloride (1.9 mg, 10 μ mol) at 0 °C. The reaction mixture was allowed to warm at room temperature and stirred for 1 h. Reaction was then quenched with *sat. aq.* NaHCO₃ (1.0 mL), the mixture was extracted with ethyl acetate (5.0 mL), the organic layer was dried over Na₂SO₄, then filtered and concentrated *in vacuo*. The residue was purified by PTLC (Pentane/Ethyl acetate = 2/1 as eluent) to provide the **84** as a yellow oil (3.8 mg, 88%).

¹H NMR (500 MHz, CDCl₃) δ 7.73 (d, J = 8.3 Hz, 2H), 7.30 (d, J = 8.0 Hz, 2H), 6.24 – 6.20 (m, 1H), 6.16 (d, J = 3.1 Hz, 1H), 5.93 (t, J = 1.4 Hz, 1H), 5.61 (s, 1H), 5.48 (t, J = 1.7 Hz, 1H), 5.39 (d, J = 2.7 Hz, 1H), 5.21 – 5.14 (m, 1H), 4.73 – 4.64 (m, 2H), 4.39 (d, J = 11.8 Hz, 1H), 3.61 (dd, J = 5.3, 2.7 Hz, 1H), 2.39 (s, 4H), 2.22 (dd, J = 13.9, 2.0 Hz, 1H), 1.75 (s, 3H), 1.43 (s, 3H).

¹³C NMR (126 MHz, CDCl₃) δ 204.28, 166.82, 145.63, 141.20, 132.76, 130.08, 128.09, 126.72, 124.80, 107.20, 89.92, 81.00, 73.11, 68.80, 50.55, 43.89, 21.71, 20.64, 17.97. **MS(ESI)** [**M** + **H**]⁺ calculated for $C_{26}H_{26}O_{9}S$: 515.13, found. 515.19.

Step 2:

To a stirred solution of **84** (3.8 mg, 7.4 μ mol) in DMF at 0 °C was added NaN₃ (0.48 mg, 7.4 μ mol). The mixture was stirred 10 min at 0 °C and purified by reverse HPLC (water/ACN 9/1 to 8/2 as eluent) to obtain **85** as a pale yellow oil (2.1 mg, 73%).

¹H NMR (500 MHz, CDCl₃) δ 6.26 (d, J = 3.3 Hz, 1H, f1), 6.07 (s, 1H, b1), 6.02 (q, J = 1.1 Hz, 1H, h1), 5.91 (s, 2H, a+b2), 5.56 (t, J = 1.8 Hz, 1H, h2), 5.51 (d, J = 2.9 Hz, 1H, f2), 4.82 (d, J = 5.1 Hz, 1H, d), 4.75 (s, 1H, c), 4.29 (d, J = 12.0 Hz, 1H, g), 4.06 (m, 1H, e), 2.54 (dd, J = 13.7, 12.0 Hz, 1H, j1), 2.40 – 2.34 (m, 1H, j2), 1.85 – 1.83 (m, 3H, i), 1.58 (s, 3H, k).

¹³C NMR (126 MHz, CDCI₃) δ 204.16 (C1), 184.22 (C3), 168.26 (C13), 166.99 (C9), 135.31 (C quat.), 133.62 (C quat.), 127.48 (C5), 126.71 (C14), 124.44 (C11), 107.23 (C2), 83.39 (C7), 71.93 (C12), 67.93 (C6), 46.18 (C8), 44.51 (C16), 21.27 (C18), 17.97 (C15).

	2D NMR correlations					
	¹H-¹H COSY	НМВС	NOESY			
85	N ₃	N ₃				

NOESY: Correlation beween c and d.

MS(ESI) [M + H]⁺ calculated for $C_{19}H_{19}N_3O_6$: 386.13, found. 386.22.

III.2.8. Synthesis of GOYA-1 and GOYA-2

To a solution of 1 (5.0 mg, 14 μ mol), pent-4-ynoyl chloride (2.4 mg, 21 μ mol) and DMAP (0.17 mg, 0.0014 mmol) in CH₂Cl₂ (0.3 mL) at 0 °C, was added dropwise a solution of Et₃N (6.0 μ L, 42 μ mol) in CH₂Cl₂ (0.1 mL). The mixture was allowed to warm to room temperature and after 4 hours, HCl (0.1M, 0.2 mL) was added. The solution was then extracted with CH₂Cl₂ (1.0 mL × 2), and the combined organic layers were washed with brine (1.0 mL), dried over MgSO₄, and purified by PTLC (Pentane/Ethyl acetate = 1/1) to give **GOYA-1** as a white solid (2.5 mg, yield 41%).

Data of **GOYA-1**: $[\alpha]_D^{20}$ -13 (c 0.1, CHCl₃);

¹H NMR (400 MHz, CDCI₃) δ 6.39–6.34 (m, 1H), 6.26 (d, J = 3.1 Hz, 1H), 6.03 (s, 1H), 5.83 (s, 1H), 5.57 (s, 1H), 5.49 (d, J = 2.7 Hz, 1H), 5.35 (d, J = 1.9 Hz, 1H), 4.86 (s, 2H), 4.60 – 4.51 (m, 1H), 3.80 (d, J = 2.5 Hz, 1H), 2.63 (t, J = 6.8 Hz, 2H), 2.59–2.49 (m, 3H), 2.34 (dd, J = 13.9, 1.9 Hz, 1H), 2.02 (t, J = 2.6 Hz, 1H), 1.85 (s, 3H), 1.57 (d, J = 7.8 Hz, 3H) ppm

¹³C NMR (101 MHz, CDCI₃) δ 204.4, 183.0, 170.9, 168.4, 166.8, 138.7, 135.3, 132.9, 129.5, 126.6, 124.7, 106.8, 89.8, 82.0, 81.2, 73.2, 69.5, 63.6, 50.8, 43.9, 33.1, 20.6, 17.9, 14.3 ppm

HRMS(ESI) [M + H] $^+$ calculated for C₂₄H₂₄O₈: 441.1471, found 441.1394;

Steps 1/2:

A sealed solution of propargyl alcohol (1.2 g, 21.4 mmol), ethyl 2-(bromomethyl) acrylate (5.8 g, 30 mmol), Nal (320 mg, 2.1 mmol) and Et_3N (12 mL, 85.6 mmol) in CH_2Cl_2 (80 mL) was heated overnight at 50 °C. The mixture was then diluted with CH_2Cl_2 (50 mL) and HCl (0.1 M, 100 mL). The aqueous phase was extracted with CH_2Cl_2 (100 mL), and the combined organic layers were washed with brine (200 mL), dried over MgSO₄, concentrated and purified by silica gel chromatography (Pentane/Ethyl acetate = 8/2 as eluent) to give a pale yellow oil (2.8 g, yield 78%).

¹H NMR (400 MHz, CDCI₃) δ 6.34 (s, 1H), 5.89 (s, 1H), 4.30 (s, 2H), 4.27 – 4.20 (m, 4H), 2.46 (t, J = 2.4 Hz, 1H), 1.31 (d, J = 7.1 Hz, 3H);

¹³C NMR (101 MHz, CDCl₃) δ 165.7, 136.7, 126.2, 79.3, 74.7, 67.9, 60.7, 57.8, 14.1 ppm; TLC: Rf = 0.4 (Pentane/Ethyl acetate = 4/1).

A solution of Ester (500 mg, 2.98 mmol) in 6N HCl (5.0 mL) was heated at 65 °C overnight. The mixture was then diluted with H_2O (20 mL) and CH_2Cl_2 (20 mL). The solution was then extracted with CH_2Cl_2 (10 mL × 2), and the combined organic layers

were washed with brine (10 mL), dried over MgSO₄, and concentrated to give crude acid **86** as a brownish solid (308 mg, yield 74%).

¹H NMR (400 MHz, CDCI₃) δ 6.49 (s, 1H), 6.04 (s, 1H), 4.31 (s, 2H), 4.24 (s, 2H), 2.48 (s, 1H);

¹³C NMR (101 MHz, CDCl₃) δ 170.9, 135.9, 129.0, 79.2, 74.9, 67.4, 57.9 ppm; TLC: Rf = 0.3 (Pentane/Ethyl acetate/AcOH = 1/1/0.01).

<u>Step 3:</u>

To a solution of **86** (308 mg, 2.2 mmol) and Et₃N (608 μ L, 4.4 mmol) in CH₂Cl₂ (6.0 mL) at 0 °C, was added dropwise a solution of acyl chloride (644 mg, 2.64 mmol) in CH₂Cl₂ (2.0 mL). The mixture was then allowed to warm to room temperature and after 30 minutes, HCl (0.1 M, 5 mL) was added. The solution was then extracted with CH₂Cl₂ (5.0 mL × 2) and the combined organic layers were washed with brine (5.0 mL), dried over MgSO₄, and purified by Isolera Biotage using SNAP Cartridge KP-C18-HS 12 g column (Water/acetonitrile 9/1 to 1/1) to give **87** as a yellow oil (153 mg, yield 53%). Compound unstable on silica gel;

¹H NMR (400 MHz, CDCI₃) δ 6.50 (s, 1H), 6.19 (s, 1H), 4.35 (s, 2H), 4.26 (s, 2H), 2.48 (s, 1H);

¹³C NMR (101 MHz, CDCl₃) δ 161.0, 136.0, 130.3, 75.1, 67.2, 65.8, 58.0 ppm; HRMS(ESI) [M + Na]⁺ calculated for $C_{14}H_{14}O_{5}$: 285.0841, found 285.0836.

Step 4:

To a solution of **61** (50 mg, 0.087 mmol), **87** (103 mg, 0.39 mmol) in DCE (1.0 mL) at 50 $^{\circ}$ C, was added dropwise a solution of DMAP (46 mg, 0.38 mmol) in CH₂Cl₂ (0.3 mL). The mixture was stirred 2 hours and then allowed to cool at room temperature.

HCI (0.1M, 1.0 mL) was added and the mixture was extracted with CH_2Cl_2 (5.0 mL × 2), the combined organic layers were washed with brine (5.0 mL), dried over MgSO₄, the solvent was evaporated *in vacuo* and the resulting residue was purified by silica gel chromatography (Pentane/Ethyl acetate = 7/3 as eluent) to give **88** as a yellow oil (16 mg, yield 26%).

 $[\alpha]_{D}^{20}$ -57 (c 0.1, CHCl₃);

¹H NMR (400 MHz, CDCI₃) δ 7.66–7.62 (m, 4H), 7.46–7.38 (m, 6H), 6.47 (dd, J = 3.3, 2.0 Hz, 2H), 6.42 (d, J = 2.3 Hz, 1H), 6.04 (d, J = 1.4 Hz, 1H), 5.90 (d, J = 1.2 Hz, 1H), 5.64 (s, 1H), 5.19 (s, 1H), 5.09 (s, 1H), 4.49 (d, J = 2.1 Hz, 1H), 4.36–4.30 (m, 2H), 4.25 (d, J = 2.4 Hz, 2H), 4.21 (dd, J = 5.0, 2.4 Hz, 2H), 2.49 (m, J = 3.5 Hz, 2H), 2.17 (m, 4H), 1.36 (s, 3H), 1.08 (s, 9H);

¹³C NMR (101 MHz, CDCI₃) δ 169.5, 168.4, 164.3, 138.7, 135.9, 135.5, 134.8, 132.8, 129.9, 128.8, 127.8, 127.7, 79.1, 78.9, 75.2, 74.9, 74.7, 72.8, 69.8, 68.2, 67.6, 64.0, 57.9, 57.7, 30.0, 29.7, 20.8, 19.2 ppm;

HRMS(ESI) [M + Na]⁺ calculated for $C_{40}H_{44}O_9Si$: 719.2755, found 719.2653; TLC: Rf = 0.3 (Pentane/Ethyl acetate = 2/1).

Step 5:

To a solution of **88** (8.0 mg, 11 µmol) in MeOH (1.0 mL) at 0 °C, was added dropwise a solution of K_2CO_3 (0.6 µL, 1 M in H_2O). The reaction was stirred for 20 minutes at 0 °C and quenched with a cold mixture of CH_2CI_2/H_2O (1 mL/1mL). The solution was then extracted with CH_2CI_2 (2.0 mL) and the combined organic layers were washed with brine (1.0 mL) dried over MgSO₄, concentrated and purified by PTLC (Pentane/Ethyl acetate = 1/1 as eluent) to give propargyl alcohol **89** as a pale-yellow oil (4.1 mg, yield 54%).

 $[\alpha]_{D}^{20}$ -51 (c 0.2, CHCl₃)

¹H NMR (500 MHz, CDCI₃) δ 7.66 (dd, J = 6.6, 1.3 Hz, 4H), 7.48–7.39 (m, 6H), 6.43 (d, J = 2.5 Hz, 2H), 6.33 (s, 1H), 5.92 (d, J = 1.1 Hz, 1H), 5.84 (d, J = 2.1 Hz, 1H), 5.77 (s, 1H), 5.02 (d, J = 2.1 Hz, 1H), 4.42 (s, 1H), 4.28 (s, 1H), 4.24 (s, 1H), 4.22–4.20 (m, 2H), 4.19 (d, J = 1.8 Hz, 1H), 4.17 (d, J = 2.3 Hz, 1H), 4.14 (d, J = 7.1 Hz, 1H), 2.49 (t, J = 2.3 Hz, 1H), 2.40 (d, J = 13.1 Hz, 1H), 2.15 (dd, J = 14.5, 10.5 Hz, 1H), 1.43 (s, 3H), 1.08 (s, 9H);

¹³C NMR (126 MHz, CDCI₃) δ 171.1, 170.9, 169.4, 165.0, 137.9, 135.8, 135.5, 134.7, 132.8, 129.9, 129.3, 127.8, 124.4, 123.1, 79.8, 78.9, 75.7, 75.2, 72.7, 69.8, 68.0, 64.3, 60.4, 57.77, 53.4, 46.4, 31.9, 29.7, 29.3, 26.8, 22.7, 21.0, 19.2, 14.2, 14.2, 14.1 ppm; HRMS(ESI) [M + Na]* calculated for $C_{38}H_{42}O_8Si$: 677.2649, found 677.2546; TLC: Rf = 0.3 (Pentane/Ethyl acetate = 1/1).

Steps 6/7:

To a stirred solution of **89** (4.1 mg, 6.26 μ mol) in CH₂Cl₂ (1 mL) was added MnO₂ (5.0 mg, 63 μ mol) and the solution was stirred at room temperature for 2 hours, till the TLC analysis showed disappearance of the starting material. The reaction was filtered and a trace of *t*-Bu₃PAuNTf₂ was added to the CH₂Cl₂ solution and the mixture stirred for 10 more minutes till the TLC analysis showed disappearance of the starting material. The resulted reaction was then concentrated *in vacuo*, and the residue optained was purified on a PTLC (Pentane/Ethyl acetate = 3/1 as eluent) to provide **91** as a white solid (2.7 mg, 66%).

Data analysis of **90**. $[\alpha]_D^{20}$ -56 (c 0.1, CHCl₃);

¹H NMR (500 MHz, CDCl₃) δ 7.66 (ddd, J = 8.0, 2.5, 1.4 Hz, 4H), 7.50–7.39 (m, 6H), 6.78 (d, J = 2.3 Hz, 1H), 6.49 (d, J = 3.2 Hz, 1H), 6.32 (d, J = 0.9 Hz, 1H), 5.96 (d, J = 1.3 Hz, 1H), 5.82 (d, J = 2.8 Hz, 2H), 5.27 (dd, J = 6.6, 2.6 Hz, 1H), 4.28 (dd, J = 4.0, 2.1 Hz, 2H), 4.24 (d, J = 1.0 Hz, 2H), 4.23–4.19 (m, 2H), 4.03 (d, J = 5.1 Hz, 1H), 2.50 (dt, J = 4.7, 4.1 Hz, 2H), 2.42 – 2.37 (m, 1H), 1.47 (s, 3H), 1.10 (s, 9H);

¹³C NMR (126 MHz, CDCl₃) δ 189.2, 168.3, 164.8, 143.2, 135.8, 135.5, 132.9, 132.4, 130.1, 128.7, 127.9, 124.7, 120.9, 95.3, 94.0, 79.0, 75.1, 70.9, 67.7, 64.1, 60.4, 57.8, 53.4, 50.1, 31.9, 29.7, 26.8, 25.2, 22.7, 21.0, 19.2, 14.1 ppm;

HRMS(ESI) [M + Na]⁺ calculated for $C_{38}H_{44}O_8Si$: 675.2492, found 675.2390; TLC: Rf = 0.35 (Pentane/Ethyl acetate = 2/1).

Data analysis of **91**. $[\alpha]_{D}^{20}$ -11 (c 0.1, CHCl₃);

¹H NMR (500 MHz, CDCI₃) δ 7.68–7.65 (m, 4H), 7.44–7.39 (m, 6H), 6.26 (dd, J = 3.7, 2.2 Hz, 2H), 6.15–6.12 (m, 1H), 5.91 (d, J = 1.3 Hz, 1H), 5.68 (s, 1H), 5.50 (d, J = 2.7 Hz, 1H), 5.28 (d, J = 2.3 Hz, 1H), 4.56 (d, J = 11.9 Hz, 1H), 4.46–4.33 (m, 2H), 4.18 (d, J = 2.6 Hz, 2H), 4.14 (d, J = 7.2 Hz, 2H), 3.75 (d, J = 2.6 Hz, 1H), 2.54–2.46 (m, 2H), 2.36–2.31 (m, 1H), 1.52 (s, 3H), 1.09 (s, 9H) ppm;

 13 C NMR (126 MHz, CDCI₃) δ 204.5, 168.6, 135.7, 135.6, 135.5, 134.3, 133.9, 132.6, 130.1, 127.9, 127.8, 124.7, 106.4, 89.5, 81.5, 74.9, 73.5, 67.4, 64.1, 60.4, 57.8, 50.8, 43.9, 31.9, 29.7, 29.3, 26.8, 22.7, 20.6, 19.2, 14.1 ppm;

HRMS(ESI) [M + H]⁺ calculated for C₃₈H₄₀O₈Si: 653.2492, found 653.2570;

Step 8:

To a solution of **91** (2.3 mg, 3.5 µmol) in THF (1.0 mL) at 0 °C, was added dropwise a solution of hydrogen fluoride pyridine (hydrogen fluoride ~70%, 10 µL) in THF (0.2 mL). The mixture was stirred 4 hours at 0 °C and quenched with saturated NaHCO₃ (0.5 mL). The mixture was then extracted with Et₂O (2.0 mL × 2), and the combined organic layers were washed with brine (1.0 mL), dried over MgSO₄, and purified by PTLC (Pentane/Ethyl acetate = 2/8 as eluent) to give **GOYA-2** (**92**) (0.21 mg, yield 14.5%) as a waxy solid. $[\alpha]_D^{20}$ -14 (c 0.1, CHCl₃);

¹H NMR (500 MHz, CDCI₃) δ 6.30 (s, 1H), 6.23 (s, 2H), 5.91 (s, 1H), 5.82 (s, 1H), 5.51 (s, 1H), 5.35 (s, 1H), 4.63–4.40 (m, 3H), 4.24–4.12 (m, 4H), 3.83 (d, J = 2.4 Hz, 1H), 2.58–2.48 (m, 1H), 2.47 (t, J = 2.3 Hz, 1H), 2.37 (dd, J = 15.7, 8.7 Hz, 1H), 1.32 (s, 9H) ppm;

¹³C NMR (126 MHz, CDCl₃) δ 196.2, 184.1, 135.6, 132.8, 127.9, 124.9, 106.6, 89.6, 81.0, 75.0, 73.4, 63.1, 57.6, 50.8, 43.2, 31.8, 29.3, 22.7, 20.6, 13.9 ppm; Traces of water (integration = 135.65) and grease (integration = 75.65). Purity 19%. DMSO stock solutions have been prepared by weighting residues after high vacuum evaporation.

HRMS(ESI) [M + H]⁺ calculated for C₂₂H₂₂O₈: 414.1315, found 415.1394;

III.2.9. Synthesis of goyazensolide analogs

Truncated MA1, Step 1

To a stirred solution of alcohol **61** (10 mg, 17.4 µmol) in CH₂Cl₂ (1 mL) was added DMAP (4.2 mg, 0.035 µmol) and methacrylic anhydride (3.5 µL, 21 µmol) at 0 °C. The reaction mixture was allowed to warm at room temperature and stirred for 1 h. The reaction was then quenched with NaHCO₃ saturated (2 mL), the mixture was extracted with ethyl acetate (5 mL), the combined organic layers were dried over Na₂SO₄, then filtered and concentrated *in vacuo*. The residue was purified by PTLC (Pentane/Ethyl acetate = 2/1 as eluent) to provide **93** as a waxy solid (8 mg, 71%).

¹H NMR (400 MHz, CDCl₃) δ 7.65 (dd, J = 6.5, 1.5 Hz, 4H), 7.48 – 7.38 (m, 6H), 6.50 (d, J = 2.3 Hz, 1H), 6.42 (d, J = 2.8 Hz, 1H), 5.88 – 5.72 (m, 2H), 5.01 (dd, J = 5.1, 2.6

Hz, 1H), 4.48 (dd, J = 5.0, 2.5 Hz, 1H), 4.23 – 4.14 (m, 2H), 2.70 – 2.57 (m, 1H), 2.25 (s, 1H), 2.17 – 2.09 (m, 1H), 1.38 (s, 3H), 1.17 – 1.13 (m, 6H), 1.08 (s, 9H). **MS(ESI)** [**M** + **H**]⁺ calculated for C₃₇H₄₄O₈Si: 645.28, found. 645.21.

Truncated MA1, Step 2:

To a solution of **93** (8 mg, 12.4 μ mol) in MeOH (0.5 mL) at 0 °C, was added dropwise a solution of K₂CO₃ (6.2 μ L, 1M in H₂O, 6.2 μ mol). The mixture was stirred 20 minutes at 0 °C and quenched with a cold mixture of CH₂Cl₂/H₂O (10mL). The reaction was then extracted with CH₂Cl₂ (5.0 mL), and the combined organic layers were washed with brine (5.0 mL), dried over MgSO₄, concentrated and purified by PTLC (pentane/ethyl acetate = 1/1 as eluent) to give propargyl alcohol **94** as a yellow oil (6 mg, yield 80%).

¹H NMR (400 MHz, CDCl₃) δ 7.66 (dd, J = 6.7, 1.4 Hz, 4H), 7.48 – 7.40 (m, 6H), 6.44 (dd, J = 10.7, 2.6 Hz, 2H), 5.84 (d, J = 2.5 Hz, 2H), 4.93 (dd, J = 5.6, 2.7 Hz, 1H), 4.38 (d, J = 2.9 Hz, 1H), 4.18 (d, J = 6.9 Hz, 2H), 3.75 (d, J = 5.0 Hz, 1H), 3.64 (d, J = 2.2 Hz, 1H), 2.53 (s, 1H), 2.30 – 2.19 (m, 1H), 2.12 (d, J = 10.3 Hz, 1H), 1.44 (s, 3H), 1.14 (dd, J = 7.0, 2.6 Hz, 6H), 1.09 (s, 9H).

MS(ESI) [M + H]⁺ calculated for C₃₅H₄₂O₇Si: 603.27, found. 603.22.

Truncated MA1, Step 3:

To a stirred solution of **94** (6 mg, 10 μ mol) and NaHCO₃ (25 mg, 100 μ mol) in CH₂Cl₂ (1 mL) was added DMP (12.6 mg, 30 μ mol) and the solution was stirred at room temperature for one night. The reaction was diluted with Et₂O and water (10 mL). The organic layer was washed with brine, dried over Na₂SO₄, concentrated and purified by PTLC (pentane/ethyl acetate = 7/3 as eluent) to give ynone **95** as a yellow oil (4.5 mg, yield 75%). **MS(ESI) [M + H]**⁺ calculated for C₃₅H₄₀O₇Si: 601.25, found. 601.18.

Truncated MA1, Step 4:

To a stirred solution of **95** (4.5 mg, 7.5 μ mol) in THF (1 mL) was added a premix AuClPPh₃ (0.37 mg, 0.75 μ mol) / AgSbF₆ (0.26 mg, 0.75 μ mol) in THF (0.3 mL). Reaction was stirred at room temperature for 15 min diluted with Et₂O and water (10 mL). The organic layer was washed with brine, dried over Na₂SO₄, concentrated and purified by PTLC (pentane/ethyl acetate = 7/3 as eluent) to give furanone **96** as a yellow oil (3.1 mg, yield 68%).

MS(ESI) [M + H]⁺ calculated for C₃₅H₄₀O₇Si: 601.25, found. 601.32.

Truncated MA1, Step 5:

To a solution of **96** (3.1 mg, 5.2 μ mol) in THF (1.0 mL) at 0 °C, was added dropwise a solution of hydrogen fluoride pyridine (hydrogen fluoride ~70%, 20 μ L) in THF (0.2 mL). The mixture was stirred 4 hours at 0 °C and quenched with saturated NaHCO₃ (0.5 mL). The mixture was then extracted with Et₂O (2.0 mL × 2), and the combined organic layers were washed with brine (1.0 mL), dried over MgSO₄, and purified by PTLC (Pentane/Ethyl acetate = 2/8 as eluent) to give **97** (1.1 mg, yield 58%) as a waxy solid. ¹H NMR (500 MHz, CDCl₃) δ 6.30 (dd, J = 3.1, 1.9 Hz, 2H), 5.81 (s, 1H), 5.50 (d, J = 2.7 Hz, 1H), 5.33 (dd, J = 5.0, 2.7 Hz, 1H), 4.50 – 4.39 (m, 3H), 3.80 (dd, J = 5.3, 2.6 Hz, 1H), 2.52 – 2.35 (m, 2H), 2.29 (dd, J = 13.9, 2.0 Hz, 1H), 1.27 (s, 3H), 1.08 (dd, J = 16.9, 7.0 Hz, 6H).

¹³C NMR (126 MHz, CDCl₃) δ 204.63, 184.28, 135.76, 134.13, 132.85, 124.47, 106.78, 81.61, 72.57, 63.35, 50.92, 44.07, 33.61, 29.72, 20.77, 18.76, 18.58. MS(ESI) [M + H]⁺ calculated for $C_{19}H_{22}O_7$: 363.14, found. 363.12.

Truncated MA2, Step 1:

To a stirred solution of **61** (21 mg, 36.5 μ mol) in THF (1 mL) was added Stryker reagent (36 mg, 18.3 μ mol). Mixture stirred 30 min at 0 °C quenched with saturated NH₄Cl (0.5 mL). The mixture was then extracted with Et₂O (2.0 mL × 2), and the combined organic layers were washed with brine (1.0 mL), dried over MgSO₄, and purified by PTLC (Pentane/Ethyl acetate = 2/8 as eluent) to give **98** (10 mg, yield 47%).

¹H NMR (400 MHz, CDCI₃) δ 7.68 – 7.65 (m, 4H), 7.50 – 7.41 (m, 7H), 6.60 – 6.49 (m, 1H), 5.17 (s, 2H), 5.07 (s, 1H), 4.18 – 4.13 (m, 3H), 3.31 – 3.16 (m, 1H), 3.11 (dd, J = 7.6, 5.7 Hz, 1H), 2.12 (d, J = 2.0 Hz, 3H), 2.10 – 2.08 (m, 1H), 2.03 (d, J = 7.6 Hz, 1H), 1.41 (s, 3H), 1.36 (d, J = 7.4 Hz, 3H), 1.08 (s, 9H).

MS(ESI) [M + H]⁺ calculated for C₃₃H₄₀O₇Si: 577.25, found. 577.18.

Truncated MA2, Step 2:

To a stirred solution of alcohol **98** (10 mg, 17.4 μ mol) in CH₂Cl₂ (1 mL) was added NEt₃ (7.3 μ L, 52 μ mol), DMAP (0.2 mg, 5.2 μ mol) and methacrylic anhydride (3.2 μ L, 22.5 μ mol) at 0 °C. The reaction mixture was allowed to warm at room temperature and stirred for 1 h. The reaction was then quenched with NaHCO₃ saturated (2.0 mL), the mixture was extracted with ethyl acetate (5.0 mL), the combined organic layers were dried over Na₂SO₄, then filtered and concentrated *in vacuo*. The residue was purified by PTLC (Pentane/Ethyl acetate = 2/1 as eluent) to provide the **99** as a waxy solid (8 mg, 71%).

¹H NMR (400 MHz, CDCI₃) δ 7.68 – 7.65 (m, 4H), 7.48 – 7.40 (m, 6H), 6.54 (d, J = 2.3 Hz, 1H), 6.13 (d, J = 1.2 Hz, 1H), 6.08 – 6.01 (m, 1H), 5.65 (d, J = 1.5 Hz, 1H), 5.20 (s, 1H), 4.83 (dd, J = 8.6, 2.5 Hz, 1H), 4.17 (q, J = 2.0 Hz, 3H), 3.65 (ddd, J = 9.5, 8.6, 1.1 Hz, 1H), 3.02 (dd, J = 9.4, 7.2 Hz, 1H), 2.23 (d, J = 11.2 Hz, 1H), 2.18 (s, 3H), 2.03 (d, J = 5.0 Hz, 1H), 1.99 – 1.97 (m, 3H), 1.47 (d, J = 7.3 Hz, 3H), 1.36 (s, 3H), 1.08 (d, J = 1.1 Hz, 9H).

MS(ESI) [M + H]⁺ calculated for $C_{37}H_{44}O_8Si$: 645.28, found. 645.21.

Truncated MA2, Step 3:

To a solution of **99** (8 mg, 12.4 μ mol) in MeOH (0.5 mL) at 0 °C, was added dropwise a solution of K₂CO₃ (6.2 μ L, 1M in H₂O, 6.2 μ mol). The mixture was stirred 20 minutes at 0 °C and quenched with a cold mixture of CH₂Cl₂/H₂O (10mL). The reaction was then extracted with CH₂Cl₂ (5.0 mL), and the combined organic layers were washed with brine (5.0 mL), dried over MgSO₄, concentrated and purified by PTLC (pentane/ethyl acetate = 1/1 as eluent) to give propargyl alcohol **100** as a yellow oil (5 mg, yield 67%).

¹H NMR (400 MHz, CDCI₃) δ 7.71 – 7.65 (m, 5H), 7.50 – 7.40 (m, 6H), 6.51 (d, J = 2.2 Hz, 1H), 6.19 – 6.03 (m, 2H), 5.67 (t, J = 1.5 Hz, 1H), 4.79 (dd, J = 8.9, 2.5 Hz, 1H), 4.24 – 4.16 (m, 3H), 3.56 (ddd, J = 9.7, 8.9, 0.9 Hz, 1H), 3.04 (dd, J = 9.7, 7.2 Hz, 1H), 2.20 – 2.10 (m, 1H), 2.04 – 1.95 (m, 4H), 1.49 (d, J = 7.3 Hz, 3H), 1.41 (s, 3H), 1.09 (s, 9H).

MS(ESI) [M + H]⁺ calculated for C₃₅H₄₂O₇Si: 603.27, found. 603.24.

Truncated MA2, Step 4:

To a stirred solution of **100** (5 mg, $8.3 \mu mol$) and NaHCO₃ (7 mg, $83 \mu mol$) in CH₂Cl₂ (1 mL) was added DMP (10.6 mg, 25 μmol) and the solution was stirred at room temperature for one night. The mixture was diluted with Et₂O and water (10 mL). The organic layer was washed with brine, dried over Na₂SO₄, concentrated and purified by PTLC (pentane/ethyl acetate = 7/3 as eluent) to give ynone **101** as a yellow oil (3.5 mg, yield 70%).

¹H NMR (400 MHz, CDCl₃) δ 7.69 – 7.64 (m, 4H), 7.43 (dd, J = 7.2, 5.1 Hz, 6H), 6.85 – 6.76 (m, 1H), 6.20 (t, J = 1.2 Hz, 1H), 6.14 – 6.05 (m, 1H), 5.72 (t, J = 1.5 Hz, 1H), 5.02 (dd, J = 9.3, 2.5 Hz, 1H), 4.28 (d, J = 2.2 Hz, 2H), 3.11 – 2.86 (m, 2H), 2.26 (dd, J = 10.0, 4.5 Hz, 1H), 2.01 (d, J = 0.6 Hz, 3H), 1.44 (d, J = 1.4 Hz, 3H), 1.11 (s, 9H). **MS(ESI) [M + H]**⁺ calculated for C₃₅H₄₀O₇Si: 601.25, found. 601.17.

Truncated MA2, Step 5:

To a stirred solution of **101** (3.5 mg, 5.8 μ mol) in THF (1 mL) was added a premix AuClPPh₃ (0.28 mg, 0.58 μ mol) / AgSbF₆ (0.19 mg, 0.58 μ mol) in THF (0.3 mL). The reaction was stirred at room temperature for 15 min and diluted with Et₂O and water (10 mL). The organic layer was washed with brine, dried over Na₂SO₄, concentrated and purified by PTLC (pentane/ethyl acetate = 7/3 as eluent) to give furanone **102** as a yellow oil (2.7 mg, yield 77%).

¹H NMR (500 MHz, CDCl₃) δ 7.67 (dt, J = 8.1, 1.5 Hz, 4H), 7.52 – 7.42 (m, 6H), 6.19 (d, J = 1.9 Hz, 1H), 6.10 (s, 1H), 5.70 (s, 1H), 5.65 (s, 1H), 5.08 (dd, J = 9.3, 2.3 Hz, 1H), 4.94 (dt, J = 11.7, 2.0 Hz, 1H), 4.50 – 4.29 (m, 2H), 3.06 – 2.96 (m, 1H), 2.49 – 2.33 (m, 2H), 2.23 – 2.15 (m, 1H), 1.93 (d, J = 0.7 Hz, 3H), 1.37 (d, J = 6.9 Hz, 3H), 1.09 (s, 9H).

MS(ESI) [M + H]⁺ calculated for $C_{35}H_{40}O_7Si$: 601.25, found. 601.21.

Truncated MA2, Step 6:

To a solution of **102** (2.7 mg, 4.5 µmol) in THF (1.0 mL) at 0 °C, was added dropwise a solution of hydrogen fluoride pyridine (hydrogen fluoride ~70%, 20 µL) in THF (0.2 mL). The mixture was stirred 4 hours at 0 °C and quenched with saturated NaHCO₃ (0.5 mL). The mixture was then extracted with Et₂O (2.0 mL × 2), and the combined organic layers were washed with brine (1.0 mL), dried over Na₂SO₄, and purified by PTLC (Pentane/Ethyl acetate = 2/8 as eluent) to give **103** (1.0 mg, yield 62%) as a waxy solid. ¹H NMR (500 MHz, CDCl₃) δ 6.28 (d, J = 1.8 Hz, 1H), 6.11 (t, J = 1.2 Hz, 1H), 5.88 (s, 1H), 5.66 (t, J = 1.5 Hz, 1H), 5.14 (dd, J = 9.2, 2.1 Hz, 1H), 5.01 – 4.93 (m, 1H), 4.53 – 4.36 (m, 2H), 3.05 (ddd, J = 11.7, 9.2, 2.4 Hz, 1H), 2.48 – 2.35 (m, 2H), 2.25 – 2.18 (m, 1H), 1.93 (s, 3H), 1.37 (d, J = 6.9 Hz, 3H).

¹³C NMR (126 MHz, CDCl₃) δ 184.29, 133.60, 127.18, 106.81, 80.20, 67.67, 64.25, 54.97, 44.97, 38.31, 29.71, 29.67, 20.59, 18.16, 15.35.

MS(ESI) [M + H]⁺ calculated for $C_{19}H_{22}O_7$: 363.14, found. 363.12.

Truncated MA3, Step 1:

To a solution of **64** (2.0 mg, 3.3 μ mol) in THF (1.0 mL) at 0 °C, was added dropwise a solution of hydrogen fluoride pyridine (hydrogen fluoride ~70%, 20 μ L) in THF (0.2 mL). The mixture was stirred 4 hours at 0 °C and quenched with saturated NaHCO₃ (0.5 mL). The mixture was then extracted with Et₂O (2.0 mL × 2), and the combined organic layers were washed with brine (1.0 mL), dried over Na₂SO₄, and purified by PTLC (Pentane/Ethyl acetate = 2/8 as eluent) to give **104** (0.5 mg, yield 41%) as a waxy solid.

MS(ESI) [M + H]⁺ calculated for $C_{19}H_{20}O_7$: 361.12, found. 361.21.

III.2.10. Goyazensolide diastereoisomer

Step 1:

To a solution of **60** (38 mg, 0.067 mmol), methlacrylic anhydride (15 μ L, 0.10 mmol) and DMAP (0.77 mg, 6.9 μ mol) in CH₂Cl₂ (1 mL) at 0 °C, was added dropwise a solution of Et₃N (23 μ L, 0.17 mmol) in CH₂Cl₂ (0.5 mL). The mixture allowed to warm at room temperature and after 4 hours, HCl 0.1M (1.0 mL) was added. The mixture was extracted with CH₂Cl₂ (2.0 mL × 2), and the combined organic layers were washed with brine (1.0 mL), dried over MgSO₄, and purified by silica gel chromatography (pentane/ethyl acetate = 6/4 as eluent) to give **153** as a yellow oil (22 mg, yield 52%). Yellow oil,

¹H NMR (400 MHz, CDCI₃) δ 7.66 – 7.62 (m, 4H), 7.45 – 7.38 (m, 6H), 6.54 (d, J = 2.2 Hz, 1H), 6.49 (d, J = 3.4 Hz, 1H), 6.08 (t, J = 1.2 Hz, 1H), 5.78 (d, J = 3.0 Hz, 1H), 5.71 – 5.64 (m, 2H), 5.22 (d, J = 1.2 Hz, 1H), 5.16 (s, 1H), 4.95 – 4.86 (m, 1H), 4.46 – 4.37 (m, 1H), 4.24 – 4.16 (m, 2H), 2.74 (dd, J = 16.0, 6.1 Hz, 1H), 2.10 (s, 3H), 2.02 (d, J = 1.2 Hz, 1H), 1.89 (s, 3H), 1.27 (s, 3H), 1.08 (s, 9H).

MS(ESI) [M + H]⁺ calculated for $C_{37}H_{42}O_8Si$: 643.26, found. 643.31.

Steps 2/3:

AcO OH
$$K_2CO_3$$
 HO OH CH_2CI_2 , RT CH_2CI_2 ,

To a solution of **153** (22 mg, 0.034 mmol) in MeOH (2.0 mL) at 0 °C, was added dropwise a solution of K_2CO_3 (17 μ L, 1M in H_2O). The mixture was stirred 20 minutes at 0 °C and quenched with a cold mixture of CH_2CI_2/H_2O (10mL). The reaction was then extracted with CH_2CI_2 (5.0 mL), and the combined organic layers were washed with brine (5.0 mL), dried over MgSO₄, concentrated, and purified by PTLC (pentane/ethyl acetate = 1/1 as eluent) to give the propargyl alcohol **154** as a yellow oil (17 mg, yield 86%). Yellow oil;

To a stirred solution of **154** (17 mg, 28 μ mol) and NaHCO₃ (23 mg, 280 μ mol) in CH₂Cl₂ (1 mL) was added DMP (35 mg, 84 μ mol) and the solution was stirred at room temperature for one night. Reaction diluted with Et₂O and water (10 mL). Organic layer was washed with brine, dried over Na₂SO₄, concentrated and purified by PTLC (pentane/ethyl acetate = 7/3 as eluent) to give ynone **155** as a yellow oil (11.5 mg, yield 71%).

¹H NMR (400 MHz, CDCI₃) δ 7.68 - 7.63 (m, 4H), 7.49 - 7.40 (m, 6H), 6.75 - 6.65 (m, 1H), 6.46 (d, J = 3.1 Hz, 1H), 6.13 - 6.03 (m, 1H), 5.72 (d, J = 2.7 Hz, 1H), 5.62 (t, J = 1.5 Hz, 1H), 5.55 (d, J = 2.0 Hz, 1H), 5.25 - 5.19 (m, 1H), 4.27 (d, J = 2.2 Hz, 2H),

 $3.71 \text{ (d, } J = 3.0 \text{ Hz, } 1\text{H)}, \ 2.56 - 2.39 \text{ (m, } 2\text{H)}, \ 1.89 \text{ (d, } J = 0.6 \text{ Hz, } 3\text{H)}, \ 1.44 \text{ (s, } 3\text{H)}, \ 1.09 \text{ (s, } 9\text{H)}.$

MS(ESI) [M + H]⁺ calculated for $C_{35}H_{38}O_7Si$: 599.24, found. 599.21.

Step 4:

To a stirred solution of **155** (11 mg, 18 μ mol) in THF (1 mL) was added a premix AuClPPh₃ (0.87 mg, 1.8 μ mol) / AgSbF₆ (0.59 mg, 1.8 μ mol) in THF (0.3 mL). The reaction was stirred at room temperature for 15 min diluted with Et₂O and water (10 mL). The organic layer was washed with brine, dried over Na₂SO₄, concentrated and purified by PTLC (pentane/ethyl acetate = 7/3 as eluent) to give furanone **156** as a yellow oil (4.5 mg, yield 68%).

¹H NMR (400 MHz, CDCl₃) δ 7.68 – 7.61 (m, 4H), 7.48 (m, 6H), 6.28 (d, J = 2.7 Hz, 1H), 6.22 – 6.15 (m, 1H), 6.06 (t, J = 1.2 Hz, 1H), 5.72 (s, 1H), 5.63 – 5.55 (m, 2H), 5.48 (d, J = 2.3 Hz, 1H), 5.03 (dd, J = 8.7, 4.8 Hz, 1H), 4.37 (s, 2H), 2.87 (d, J = 2.7 Hz, 1H), 2.37 (dd, J = 14.1, 11.1 Hz, 1H), 2.25 (dd, J = 14.1, 2.4 Hz, 1H), 1.93 – 1.86 (m, 3H), 1.61 (s, 3H), 1.07 (s, 9H).

MS(ESI) [M + H]⁺ calculated for C₃₅H₃₈O₇Si: 599.24, found. 599.28.

Step 5:

To a solution of **156** (4.5 mg, 7.5 μ mol) in THF (0.5 mL) at 0 °C, was added dropwise a solution of HF·pyridine 70% (55 μ L) in THF (1.0 mL). The mixture was stirred 4 hours at 0 °C and quenched with saturated NaHCO₃ (2.0 mL). The quenched mixture was then extracted with Et₂O (5.0 mL × 2), and the combined organic layers were washed with brine (5.0 mL), dried over MgSO₄, and purified by PTLC (Pentane/Ethyl acetate = 2/8 as eluent) to give **157** (1.8 mg, yield 66%).

¹H NMR (400 MHz, CDCl₃) δ 6.35 (s, 1H), 6.27 (d, J = 2.6 Hz, 1H), 6.06 (s, 1H), 5.78 (d, J = 10.3 Hz, 2H), 5.59 (d, J = 2.4 Hz, 1H), 5.49 (d, J = 2.4 Hz, 1H), 5.07 (s, 1H), 4.43 (s, 2H), 3.66 (s, 2H), 2.42 (d, J = 14.3 Hz, 1H), 2.29 (d, J = 2.3 Hz, 1H), 1.89 (d, J = 1.3 Hz, 3H).

MS(ESI) [M + H]⁺ calculated for $C_{19}H_{20}O_7$: 361.12, found. 361.19.

III.2.11. Desthiobiotinylated fluorophore

$$\begin{array}{c} \overset{\circ}{\text{Ho}} \overset{\circ}{\text{NH}} \overset{\overset{\circ}{\text{NH}}} \overset{\circ}{\text{NH}} \overset{\circ}{\text{NH}} \overset{\circ}{\text{NH}} \overset{\circ}{\text{NH}} \overset{\circ}{\text{NH}} \overset{\circ}{\text{NH}} \overset{\circ}{\text{NH}} \overset{\circ}{\text{NH}} \overset{\circ}{\text{NH}} \overset{\circ}{\text{N$$

To a solution of desthiobiotin **147** (100 mg, 0.46 mmol), N-Boc-ethylenediamine **148** (90 mg, 0.56 mmol), HATU (213 mg, 0.56 mmol) in DMF (4.0 mL) was added Et₃N (190 μ L, 1.38 mmol) at 0 °C. The mixture was allowed to warm to room temperature stirred 10 more minutes, and then diluted with ethyl acetate (20 mL) and HCl 0.1N (10 mL). The aquous phase was extracted with ethyl acetate (10 mL × 3) and the combined organic layers were washed with brine (20 mL) dried over MgSO₄, concentrated and purified by silica-gel chromatography (CH₂Cl₂/ ethyl acetate = 8/2) to give the amide as a pale-yellow oil. The crude product was dissolved in dichloromethane (3.0 mL) and cooled down to 0 °C. Trifluoro acetic acid (0.3 mL) was added to the solution and the reaction was carried out for 2 hours at 0 °C. The solvents were evaporated to give **149** as a yellow oil (137 mg, yield 81%).

To a solution of deprotected amine **149** (137 mg, 0.37 mmol), (S)-6-azido-2-(tert-butoxycarbonylamino) hexanoic acid **150** (121 mg, 0.44 mmol), HATU (167 mg, 0.44 mmol) in DMF (4.0 mL) was added Et₃N (153 μ L, 1.11 mmol) at 0 °C. The mixture was allowed to warm to room temperature, stirred for 10 more minutes, and then was diluted with ethyl acetate (20 mL) and HCl 0.1N (10 mL). The solution was extracted with ethyl acetate (10 mL × 3), and the combined organic layers were washed with

brine (20 mL), dried over MgSO₄, concentrated and purified by silica-gel chromatography (CH₂Cl₂/ethyl acetate = 7/3 as eluent) to give the amide **151** as a pale-yellow oil (188 mg, yield 71%).

HRMS(ESI) [M + Na]⁺ calculated for C₂₃H₄₂O₈N₅: 511.3278, found 511.3366.

151 (188 mg, 0.37 mmol) was dissolved in dichloromethane (3.0 mL) and cooled down to 0 °C. Trifluoro acetic acid (0.3 mL) was added to the solution and the reaction was carried out for 2 hours at 0 °C. The solvents were evaporated to give a yellow oil **152** (178 mg, yield 92%).

To a solution of **152** (178 mg, 0.34 mmol), Cy3 **153** (194 mg, 0.34 mmol), HATU (155 mg, 0.41 mmol) in DMF (5.0 mL) was added Et₃N (141 μ L, 1.02 mmol) at 0 °C. The mixture was allowed to warm to room temperature and stirred 10 minutes. The mixture directly purified by reverse chromatography (H₂O/acetonitrile 8/2) followed by lyophilization to give **Desthiobiotinylated Cy3-N**₃ as a pink powder (135 mg, yield 42%).

HRMS(ESI) [M + H]⁺ calculated for $C_{47}H_{67}N_{10}O_4$: 835.5341, found 835.5364.

¹H NMR (400 MHz, DMSO- d_6) δ 7.06 (dd, J = 9.8, 6.3 Hz, 1H), 6.11 (d, J = 9.8 Hz, 1H), 5.59 (d, J = 4.2 Hz, 1H), 4.56 (t, J = 5.4 Hz, 1H), 4.27 (d, J = 13.2 Hz, 1H), 4.12 (dd, J = 13.3, 5.4 Hz, 2H), 3.53 (dd, J = 6.3, 4.2 Hz, 1H), 3.15 (s, 1H), 2.38 (dd, J = 18.0, 13.1 Hz, 1H), 2.15 – 1.94 (m, 5H), 1.91 – 1.67 (m, 3H), 1.65 – 1.51 (m, 2H), 1.25 (s, 7H), 1.17 – 0.98 (m, 3H), 0.90 (d, J = 6.6 Hz, 4H), 0.84 – 0.72 (m, 1H), 0.64 (s, 3H). MS(ESI) [M + H]⁺ calculated for C₂₈H₃₈O₆: 471.27, found. 471.21.

III.2.12. Synthesis of WAPs

To a stirred solution of Withaferin A (3 mg, 6.37 µmol) in THF (0.3 mL) was added Et₃N (2.4 µL, 17 µmol), DMAP (1.5 mg, 12.7 µmol) and withaferin A (1.4 mg, 7.6 µmol) at 0 °C. The reaction mixture was allowed to warm at room temperature and stirred for 1 h. Reaction was then quenched with NaHCO₃ saturated (2 mL), the mixture was extracted with ethyl acetate (5.0 mL), the combined organic layers were dried over Na₂SO₄, then filtered and concentrated *in vacuo*. The residue was purified by HPLC (water/CH₃CN 90/10 to 10/90) to provide WAP-1 (0.6 mg, 20%) and WAP-2 (0.6 mg, 20%).

Analysis of WAP-1:

¹H NMR (500 MHz, DMSO- d_6) δ 7.08 (dd, J = 9.8, 6.3 Hz, 1H), 6.13 (dd, J = 9.8, 1.5 Hz, 1H), 5.60 (dd, J = 4.2, 1.5 Hz, 1H), 4.84 – 4.73 (m, 2H), 4.33 (d, J = 13.1 Hz, 1H), 3.57 – 3.53 (m, 1H), 3.16 (d, J = 1.8 Hz, 1H), 2.39 (s, 1H), 2.18 (t, J = 8.1 Hz, 6H), 2.03 (s, 4H), 1.91 (d, J = 7.2 Hz, 4H), 1.83 – 1.68 (m, 3H), 1.60 – 1.52 (m, 2H), 1.35 – 1.30 (m, 3H), 1.08 (dd, J = 18.8, 10.6 Hz, 3H), 0.91 (dd, J = 6.5, 1.5 Hz, 4H), 0.77 (d, J = 4.1 Hz, 1H), 0.65 (d, J = 1.5 Hz, 3H).

¹³C NMR (126 MHz, DMSO-*d*₆) δ 202.24, 159.57, 145.68, 131.80, 120.65, 78.16, 72.07, 69.13, 59.20, 58.36, 55.73, 51.59, 48.95, 43.88, 42.42, 38.85, 33.07, 29.48, 26.92, 24.48, 21.16, 20.63, 17.70, 16.64, 14.30, 13.50, 11.77.

MS(ESI) [M + H]⁺ calculated for C₃₃H₄₂O₇: 551.29, found. 551.22.

Analysis of WAP-2:

¹H NMR (500 MHz, DMSO- d_6) δ 7.10 (dd, J = 9.8, 6.2 Hz, 1H), 6.31 (d, J = 9.8 Hz, 1H), 4.76 (d, J = 6.1 Hz, 1H), 4.28 (d, J = 13.2 Hz, 1H), 4.21 – 4.07 (m, 2H), 3.40 (s, 1H), 2.35 (dd, J = 7.0, 2.6 Hz, 3H), 2.18 (s, 1H), 2.16 – 2.05 (m, 2H), 2.00 (s, 4H), 1.92 – 1.84 (m, 2H), 1.80 (s, 1H), 1.72 (d, J = 4.4 Hz, 1H), 1.61 – 1.46 (m, 3H), 1.31 (s, 4H), 1.17 (s, 1H), 1.15 – 1.02 (m, 4H), 0.99 – 0.82 (m, 7H), 0.65 (s, 3H).

¹³C NMR (126 MHz, DMSO-*d*₆) δ 201.16, 170.82, 155.21, 140.73, 134.06, 125.91, 78.00, 72.39, 72.22, 59.62, 55.61, 54.99, 51.61, 43.64, 42.37, 38.86, 33.04, 30.90, 29.61, 29.52, 26.95, 24.44, 21.25, 20.37, 15.86, 14.21, 13.54, 11.77.

MS(ESI) [M + H]⁺ calculated for $C_{33}H_{42}O_7$: 551.29, found. 551.34.

III.2.13. Synthesis of FiVe1

Step 1:

3-chloro-2-nitrobenzoyl chloride **140**. To a solution of 2-nitro-3-chlorobenzoic acid (1.00 g, 5 mmol) in dichloromethane (7 mL) was added thionyl chloride (1.82 mL, 25 mmol) followed by DMF (1 drop). The reaction was refluxed 2 hours and evaporated *in vacuo* to give the acid chloride **140** (1.03 g, 94%).

¹H NMR (300 MHz, CDCI₃) δ 8.45 (dt, J = 7.2, 1.0 Hz, 2H), 8.17 (t, J = 8.0 Hz, 1H).

Step 2:

1-(3-chloro-2-nitrophenyl)ethan-1-one **141**. To a suspension of magnesium (258 mg, 10 mmol) in dry THF (15 mL) at 50 °C was added ethanol (1 mL) and carbon tetrachloride (70 μ L). After 30 min. a solution of diethyl malonate (1.68 g, 10 mmol) in ethanol (0.7 mL, 1.72 mmol) was added and the reaction was allowed to stir at 60 °C for 2 hours. The acyl chloride **140** was added (1.0 g, 4.97 mmol) and mixture stirred 1

hour. Quench with 10% sulfuric acid (5 mL). Separate and evaporate the organic layer to give a yellow oil. To the oil was added acetic acid (10 mL), sulfuric acid (1.5 mL) and water (5 mL). This mixture was refluxed 10 hours and the product was extracted with ethyl acetate. The combined extracts were washed with water followed by brine and dried over sodium sulfate and evaporated in vacuo to give the methyketone **141** 650 mg, 72%).

¹H NMR (300 MHz, CDCl₃) δ 7.77 (dd, J = 7.8, 1.3 Hz, 1H), 7.70 (dd, J = 8.0, 1.4 Hz, 1H), 7.56 (t, J = 8.0 Hz, 1H), 2.62 (d, J = 0.8 Hz, 3H).

Step 3:

1-(2-amino-3-chlorophenyl) ethan-1-one **142**. To a solution of 1-(3-chloro-2-nitrophenyl) ethan-1-one **141** (1.0 g, 5 mmol) in glacial acetic acid (7 mL) was added iron powder (877 mg, 15 mmol). The mixture was stirred viguorously at 80 °C for 4 hours. The mixture was cooled, quenched with 10% sodium hydroxide and extracted by ethyl acetate. The combined organic layers were filtered through celite, dry over sodium sulfate and evaporate *in vacuo* to give the aniline **142** (743 mg, 87%).

¹H NMR (300 MHz, CDCl₃) δ 7.68 (dd, J = 8.0, 1.4 Hz, 1H), 7.42 (dd, J = 7.8, 1.4 Hz, 1H), 6.65 – 6.59 (m, 1H), 2.61 (s, 3H).

MS(ESI) [M + H]⁺ calculated for C₈H₈CINO: 170.03, found. 170.21.

Step 4:

8-chlorocinnolin-4-ol **143**. To a suspension of 1-(2-amino-3-chlorophenyl)ethan-1-one **142** (500 mg, 2.95 mmol) in water (3 mL) at 0 °C was added conc. HCl (20 mL). A solution of sodium nitrite (205 mg, 2.97 mmol) in water (0.75 mL) was added dropwise. The reaction was stirred for 1 hour at 0 °C then heated at 65°C for 4 hr. After cooling, the product was collected by filtration. The product was triturated with a minimum of acetone to give the cinnoline **143** (414 mg, 78%).

¹H NMR (400 MHz, CDCl₃) δ 8.20 (dd, J = 8.2, 1.3 Hz, 1H), 7.91 (s, 1H), 7.77 (dd, J = 7.7, 1.3 Hz, 1H), 7.40 – 7.32 (m, 1H).

MS(ESI) [M + H]⁺ calculated for C8H5ClN₂O: 181.01, found. 181.12.

Step 5:

4-bromo-8-chlorocinnoline **144**. Phosphorus tribromide (158 μ L, 1.66 mmol) was added into chloroform (15 mL). To this solution was added 8-chlorocinnolin-4-ol **143** (100 mg, 0.55 mmol) and the reaction was refluxed 2 hours. The mixture was cooled and basified with 10% sodium carbonate. The mixture was filtered through celite and extracted with chloroform. The combined organic layers were dried over sodium sulfate and evaporated to give the product **144** (92 mg, 68%) as a green-brown solid.

¹H NMR (300 MHz, DMSO-*d*₆) δ 9.84 (s, 1H), 8.25 (dd, J = 7.4, 1.2 Hz, 1H), 8.14 (dd, J = 8.6, 1.2 Hz, 1H), 8.05 – 7.99 (m, 1H).

MS(ESI) [M + H]⁺ calculated for C₈H₄BrClN₂: 242.92, found. 242.84.

Step 6:

8-chloro-4-(4-(3-chlorophenyl)piperazin-1-yl)cinnoline **146**. To a solution of 4-bromo-8-chlorocinnoline **144** (10 mg, 0.04 mmol) and 1-(3-chlorophenyl)piperazine HCl **145** (9.6 mg, 0.04 mmol) in dimethylformamide (0.5 mL) was added potassium carbonate (17 mg, 0.123 mmol). The reaction was stirred at 60 °C for 4 hours. Mixture was directly purified by HPLC (water/CH₃CN 95/5 to 10/90) to give **146** (9 mg, 61%).

¹H NMR (400 MHz, DMSO- d_6) δ 9.13 (s, 1H), 8.16 – 8.02 (m, 2H), 7.72 (dd, J = 8.6, 7.5 Hz, 1H), 7.26 (t, J = 8.1 Hz, 1H), 7.07 – 6.93 (m, 2H), 6.83 (dd, J = 7.8, 1.8 Hz, 1H), 3.70 – 3.62 (m, 4H), 3.53 – 3.48 (m, 4H).

¹³C NMR (101 MHz, DMSO-d₆) δ 152.27, 145.37, 136.18, 134.38, 131.61, 131.03, 129.32, 123.74, 120.96, 118.87, 115.09, 114.17, 51.16, 47.75.

MS(ESI) [M + H]⁺ calculated for C₁₈H₁₆Cl₂N₄: 359.08, found. 359.14.

III.3. Computational study (Performed by Dr. Romain Pertschi)

Figure 119 : Gibbs energy reaction profile of the intramolecular Diels-Alder reaction. Energies in kcal.mol⁻¹. B3LYP-D3/6-311+G** (SMD = toluene)

To decipher the stereochemistry of the formed polycyclic compound 18, calculations were carried out at DFT level of theory using Gaussian 09.²⁹⁶ Structures were optimized using the hybrid functional B3LYP including Grimme dispersion model D3 and all the atoms were described by the 6-311+G** basis set. 297-303 To account for the solvation energy the SMD model was used (toluene, $\varepsilon = 2.3741$).³⁰⁴ All reported data are Gibbs free energies given in kcal.mol⁻¹ at 298 K and 1 atm. All optimized structures were characterized by frequency analysis either as energy minima without imaginary frequencies or with only one imaginary frequencies for transition states. A was used as model substrate to avoid possible conformational issues coming from allyl side chain. Figure 119 shows the reaction profile of the intramolecular Diels-Alder reaction. From A, two different approaches of the dienophile to the diene were considered, the endo (TS(A-C)) and the exo (TS(A-B)). The endo approach is highly favoured over the exo by 21.8 kcal.mol⁻¹ and the cycloaddition occurs through an activation barrier of 24.4 kcal.mol⁻¹ via **TS(A-C)**. This approach is favoured thanks to the intramolecular hydrogen bond (in green in Figure 119) between the furane hydroxy group and the carbonyl of the enone moiety. This step yields intermediate C lying at 9.5 kcal.mol⁻¹ which rapidly evolves towards stable product **E** by keto-enol tautomerism. The overall process from reactants to product is exergonic by 11.0 kcal.mol⁻¹. In conclusion, the computational study of the system shows that only the stereoisomer 18 endo should be formed during the intramolecular Diels-Alder.

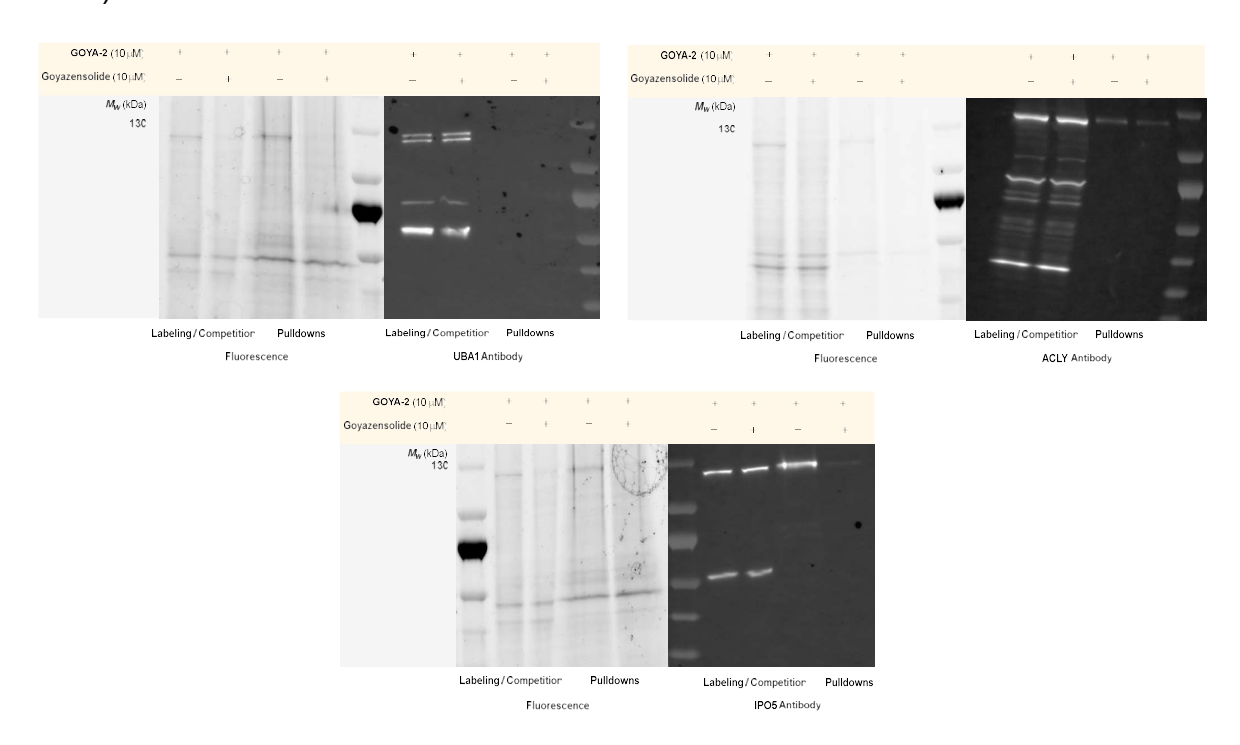
III.4. General information for proteomic/biological part

Biological materials. All materials were purchased from Sigma Aldrich unless otherwise stated. DMEM/High glucose medium, F12-K media, phosphate buffered saline (PBS), MEM Non-Essential Amino Acids, Penicillin-Streptomycin (Pen/Strep) and Trypsin-EDTA were obtained from Life Technologies. Protein concentration was determined using a Q-Bit assay. HeLa cell line (Adenocarcinoma), PC3 cell line (Prostate; derived from metastatic site: bone), HT29 cell line (Colorectal adenocarcinoma), U2OS cell line (Metastatic: lung, other bones), SW620 cell line (Colorectal adenocarcinoma) obtained from ATCC. IPO5 (Sigma-Aldrich, HPA056548) antibody was purchased from Sigma Aldrich. Phospho-AKT (Ser 473) antibody was purchased from Cell signaling. Karyopherin β1, Karyopherin β2, IPO7, IPO8 and IPO12 antibodies were purchased from Santa Cruz biotechnology. UBA1, ACLY, RASAL2, β-actin, anti-rabbit and anti-rabbit Alexa Fluor 488 antibodies were purchased from ABCAM. Images were obtained by image stacking (Confocal microscope Zeiss LSM800). Fluorescence measured with ImageJ software.

Cell culture and preparation of lysates. HeLa, PC3, HT29, U2OS and SW620 cells were maintained in their corresponding media supplemented with 10% (v/v) fetal calf serum (FCS) and Penicillin-Streptomycin 1% (v/v). Cells were grown at 37 °C under 5% CO₂ atmosphere in a humidified incubator. Cells were allowed to grow to confluence and harvested by scraping, centrifuged at 4 °C and resuspended in PBS. Cells were then lysed by sonication in lysis buffer and protein concentration was determined using a Q-Bit assay.

Pull-down experiments. PC3 cells were seeded (350,000 cells/mL) on 10 cm dishes and grown to confluence for 2 days. The cells were harvested and lysates (3 mg/mL, 100 µL each) were prepared as described above. Lysates were treated with DMSO (1 μL) or goyazensolide 10 μM (1 mM, 1 μL) for 30 minutes and then incubated with GOYA-2 10 μM (1 mM, 1 μL) for 30 minutes. Click reaction was achieved by addition of desthiobiotinylated Cy3-N₃ (20 µM, 50X stock in DMSO, Figure S13 for synthesis), TCEP (1 mM, 50X fresh stock in H₂O), TBTA (100 µM, 16X stock in DMSO: tButanol = 1:4), copper (II) sulfate (1 mM, 50X stock in H₂O) and incubated for 1 hour at room temperature in the dark. Proteins were precipitated by adding 450 µL of cold MeOH, 117 μL of cold CHCl₃ and 350 μL of cold H₂O, vortexed and centrifuged for 5 minutes at 14000 g (4 °C). The protein layer was isolated, dried and solubilized in 100 μL of 0.2% SDS in PBS via sonication. Tubes were centrifuged at 4,700 g for 5 minutes, and soluble fractions were transferred to new tubes. Streptavidin agarose beads (25 μL) were added and incubated for 2 hours. Supernatant was discarded and the beads were washed three times with PBS (100 μ L). Then 10 μ L of 2% SDS and 5 μ L of Laemmli buffer were added to the beads and heated 5 minutes at 95°C. Proteins were separated using a 10% SDS-PAGE gel. Gels were visualized at 625 nm using a fluorescence scanner.

Examples of labeling competitions experiments with pulldowns (IPO5, UBA1 and ACLY)



In-Gel tryptic digestion. The bands cutted from the SDS-PAGE were cut in smaller pieces and washed twice with a mixture of 50% NH₄HCO₃ 50 mM in CH₃CN, twice with 200 µL CH₃CN, then twice again with 200 µL NH₄HCO₃ 100 mM and finally twice with 200 µL CH₃CN. The gel fragments were incubated then for 30 minutes at 37 °C with 30 µL of DTT 10mM in H₂O, followed by 30 minutes with 30 µL iodoacetamide 30 mM in H₂O. Gel pieces were washed again twice with CH₃CN, followed by NH₄HCO₃ 100 mM and finally twice with CH₃CN. Then, the in-gel digestion started with 30 µL of a mixture of Trypsin + Glu-C + Chymotrypsin (1.0 µg each in 500 µL of NH₄HCO₃ 50 mM) at 37 °C for 18 hours. 50 µL of NH₄HCO₃ 50 mM were added to the digested mixture and incubate for 10 minutes at room temperature. The supernatant was removed and place into a microtube and the remaining gel fragments were incubated for 10minutes with 50 µL of extraction *buffer 1* (20% CH₃CN, 80% H₂O, 1% formic acid). The supernatant was then collected and the fragments incubate for another 10 minutes with 50 µL of extraction *buffer 2* (95% CH₃CN, 5% H₂O, 1% formic acid). The combined supernatants were lyophilized and summited to MS/MS analysis.

In-Solution Digestion. An IPO5 batch was incubated with one of the natural products (in water) or DMSO control for 45 minutes at room temperature. Solutions were then treated with 10 mM DTT in 10 mM NH₄HCO₃ for 30 minutes at room temperature and then they were treated with the same volume of 50 mM iodoacetamide in Milli-Q water. The solutions were adjusted to 50 μL with NH₄HCO₃ 50 mM. Then the desired protease was added in a relation 1 : 20 to IPO5 (Glu-C or Trypsin, in NH₄HCO₃ 50 mM), overnight at 37 °C. A second Protease addition was done (1 : 100) and the mixture was incubated for 4 hours more at 37 °C. The solutions were lyophilized, resuspended in 20 μL Buffer A (95% H₂O, 5% CH₃CN, 0.1% formic acid) and summited to LC-MS/MS analysis.

Mass spectrometry analysis. MS data were analyzed using Maxquant and ProteomeDiscoverer 2.0 software (Thermo Scientific) and MSMS-spectra were grouped according by fragmentation technique and searched against the homo sapiens Uniprot database using the Sequest and MS-Amanda algorithms. Search against b- and y-ions was specified for HCD and CID spectra and against c- and z-ions for EThcD spectra. A search tolerance of 10 ppm was applied for the precursor and 0.05 Da for fragmen-ions. Oxidation of methionine and modification of cysteines by carbamidomethylation or by Goyazensolide or thiolated Goyazensolide were allowed as variable modifications.

III.5. Experimental procedures for confocal microscopy

Microscopy. Cells (50000/well) were seeded on coverslips in a 12 well plate. After 24 hours, cells were treated with goyazensolide (1) or DMSO for 3 hours. Cells were fixed with PFA 4% for 25 minutes at room temperature. After $3\times$ wash with PBS, cells were blocked using 5% BSA + 0.1% saponin in PBS for 2 hours. Then they were incubated with anti IPO5 antibody (1:100) in 1% BSA in PBS (30 µL/well) for 3 hours at room temperature.

Incubations were performed as followed: the coverslips were taken out of the plate, and place on a drop of antibody solution on parafilm in a humidity chamber, then they were washed 3× with PBS, incubated with anti-rabbit AlexaFluor488 (1: 400), washed 3× with PBS, incubate with Hoechst diluted 2000× in PBS for 10min, washed 3× with PBS, then water and finally the edges were dried. The coverslips were then mounted on a clean slide treated with 5 μ L ProlongDiamond per coverslip for 24 hours at room temperature and finally sealed with nail polish.

Ratio (cytosol/nucleus) caculation of RASAL2.

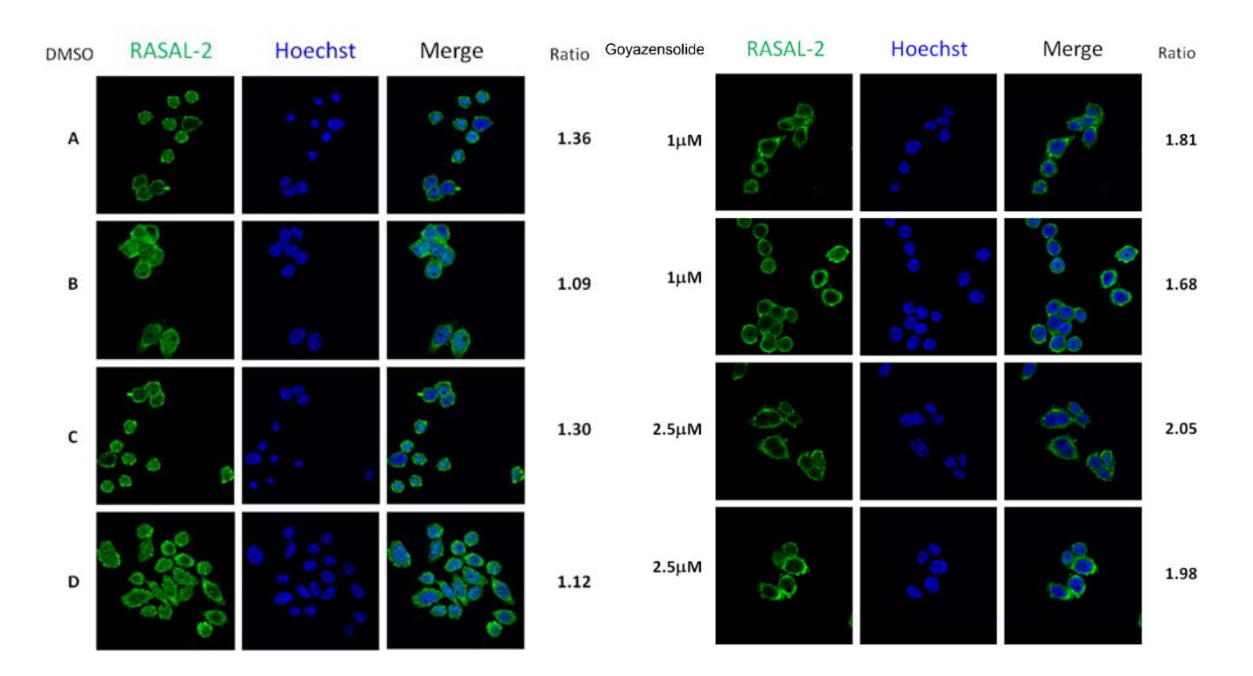
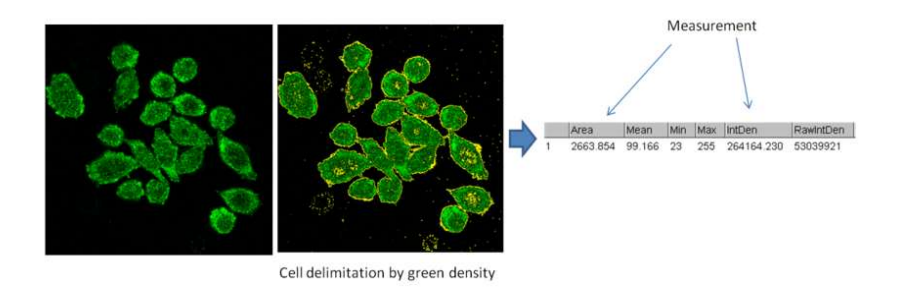


Figure 120 : Confocal microscopy images of SW620 cells after treatment with DMSO or goyazensolide. Ratio of RASAL2 levels in the cytosol and nucleus was calculated applying a threshold mask to quantify fluorescence intensity in the cytosol and in the nucleus

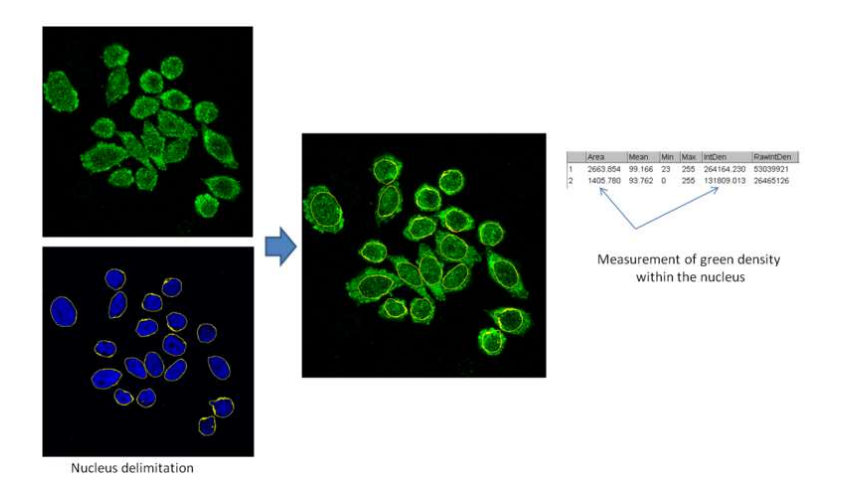
Calculation of fluorescence intensity in the cytosol/nucleus.

Threshold masks were generated in ImageJ software to calculate the integrated density of the signal in the green channel (Alexa488, RASAL2) and blue channel (Hoechst, nuclei).

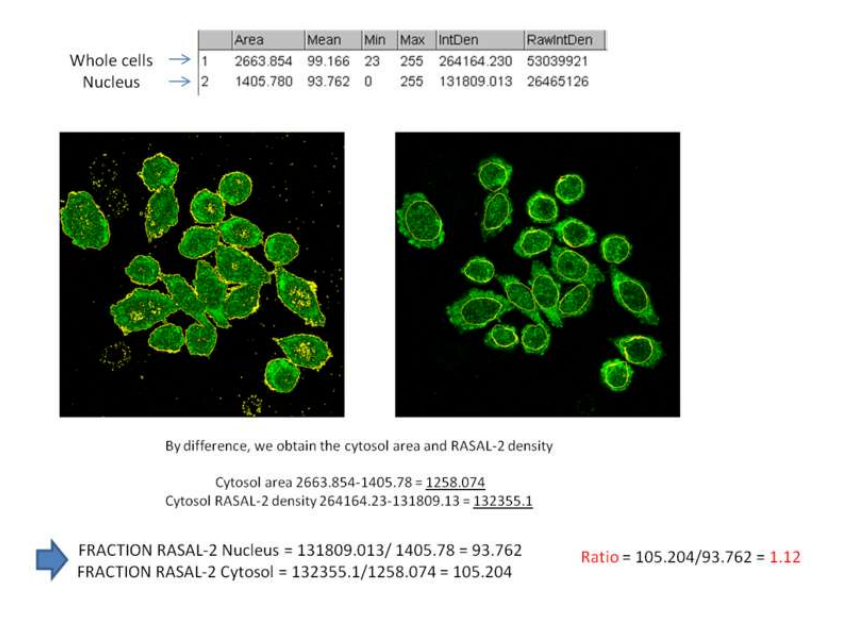
Step 1: Cell surface and green density determination.



Step 2: Determination of the surface and green density within the nucleus



Step 3: Determination of the surface and green density within the cytosol by difference



Step 4: Ratio calculation to all pictures

Table 2: Ratio calculation

DMSO				
	Area	Integrated density	Int/Area	Ratio
No Treatment	Α	,		
Whole cells	999.836	79215.392	79.22839	
Nucleus	524.499	35443.651	67.5762	
Cytosol	475.337	43771.741	92.0857	1.362694
	В			
Whole cells	1326.899	122651.425	92.43464	
Nucleus	726.149	64428.407	88.72615	
Cytosol	600.75	58223.018	96.91722	1.092318
-	С			
Whole cells	1143.299	47116.191	41.21073	
Nucleus	559.298	20005.295	35.76858	
Cytosol	584.001	27110.896	46.42269	1.297862
-	D			
Whole cells	2663.854	264164.23	99.16618	
Nucleus	1405.78	131809.013	93.76219	
Cytosol	1258.074	132355.217	105.2046	1.122037
		Average Ratio DMSO	1.218728	
	<u> </u>			
Goyazensolide				
Coyazonoonao	Area	Integrated density	Int/Area	Ratio
Goyazensolide	1A	milegrated deriety	11147 11 00	1 15115
Whole cells	1036.597	70567.839	68.07645	
Nucleus	383.935	17332.133	45.1434	
Cytosol	652.662	53235.706	81.56704	1.806843
,	1B			
Whole cells	2079.43	142805.488	68.6753	
Nucleus	1030.202	52726.816	51.18105	
Cytosol	1049.228	90078.672	85.85233	1.677424
	25A			
Whole cells	1452.821	70476.786	48.5103	
Nucleus	618.297	18677.594	30.20813	
Cytosol	834.524	51799.192	62.07034	2.054756
,	25B			
Whole cells	890.415	42677.438	47.92983	
Nucleus	405.471	12686.904	31.2893	
Cytosol	484.944	29990.534	61.84329	1.9765
,		Average Ratio 1 µM	1.742134	
		Average Ratio 2.5 µM	2.015628	
		Ratio increasing (%)	65.38786	

Table 3: Raw data

RAW DATA	ImageJ So	oftware	1: Wh	ole cells		
			2: Nuc	cleus		
PICTURE A	Area	Mean	Min	Max	IntDen	RawIntDen
1	999.836	79.228	11	255	79215.392	15905174
2	524.499	67.576	0	255	35443.651	7116514
PICTURE B	Area	Mean	Min	Max	IntDen	RawIntDen
1	1326.899	92.435	19	255	122651.425	24626430
2	726.149	88.726	0	255	64428.407	12936186
PICTURE C	Area	Mean	Min	Max	IntDen	RawIntDen
1	1143.299	41.211	5	255	47116.191	9460172
2	559.298	35.769	0	225	20005.295	4016741
PICTURE D	Area	Mean	Min	Max	IntDen	RawIntDen
1	2663.854	99.166	23	255	264164.23	53039921
2	1405.78	93.762	0	255	131809.013	26465126
PICTURE 1A	Area	Mean	Min	Max	IntDen	RawIntDen
1	1036.597	68.076	12	255	70567.839	14168885
2	383.935	45.143	0	255	17332.133	3480013
PICTURE 1B	Area	Mean	Min	Max	IntDen	RawIntDen
1	2079.43	68.675	6	255	142805.488	28673041
2	1030.202	51.181	0	255	52726.816	10586695
PICTURE 25A	Area	Mean	Min	Max	IntDen	RawIntDen
1	1452.821	48.51	5	255	70476.786	14150603
2	618.297	30.208	0	227	18677.594	3750160
PICTURE 25B	Area	Mean	Min	Max	IntDen	RawIntDen
1	890.415	47.93	6	255	42677.438	8568942
2	405.471	31.289	1	255	12686.904	2547326

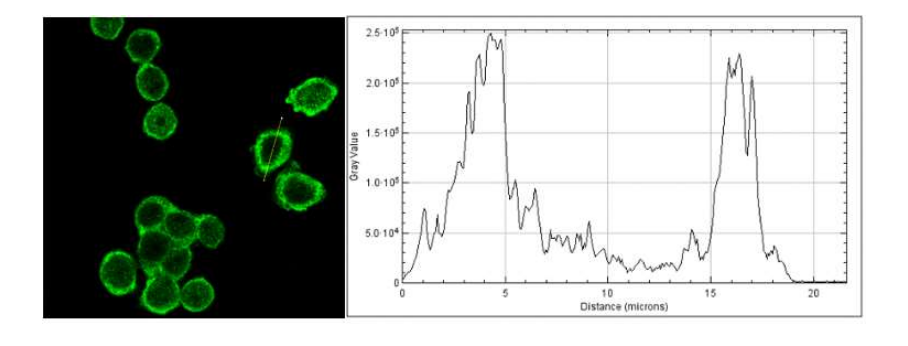


Figure 121: Plot profile determination (Image J software)

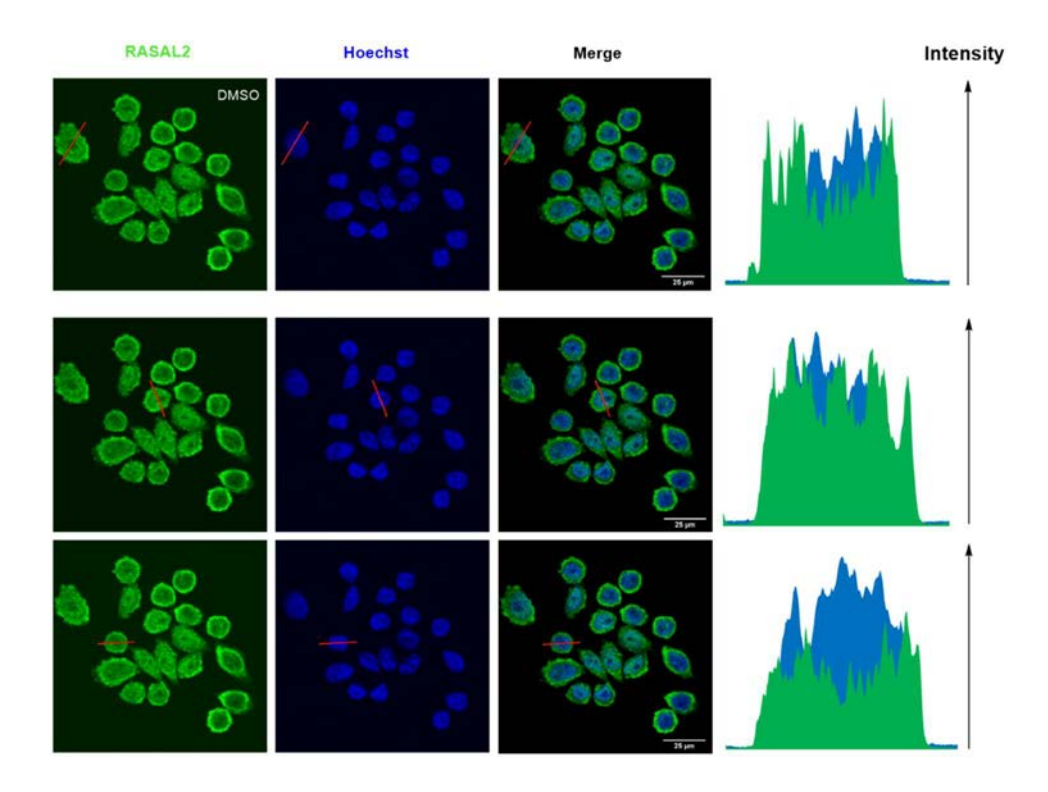


Figure 122 : DMSO treatment

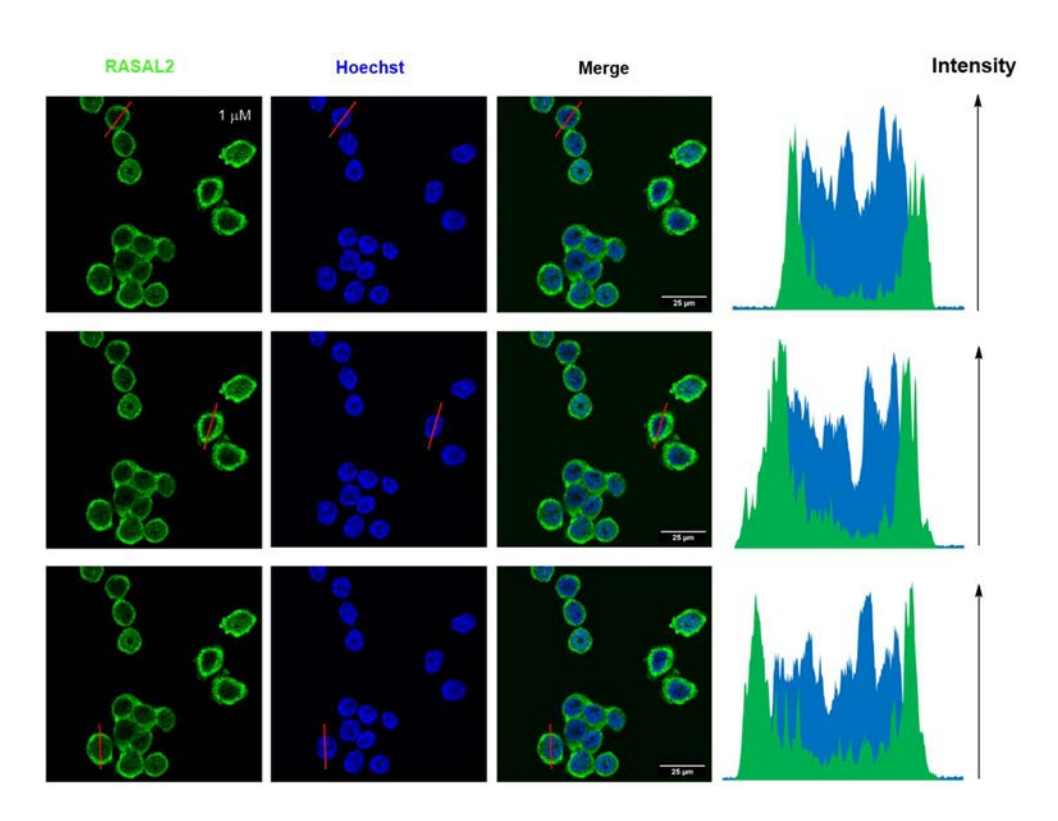


Figure 123: Goyazensolide 1 μM treatment

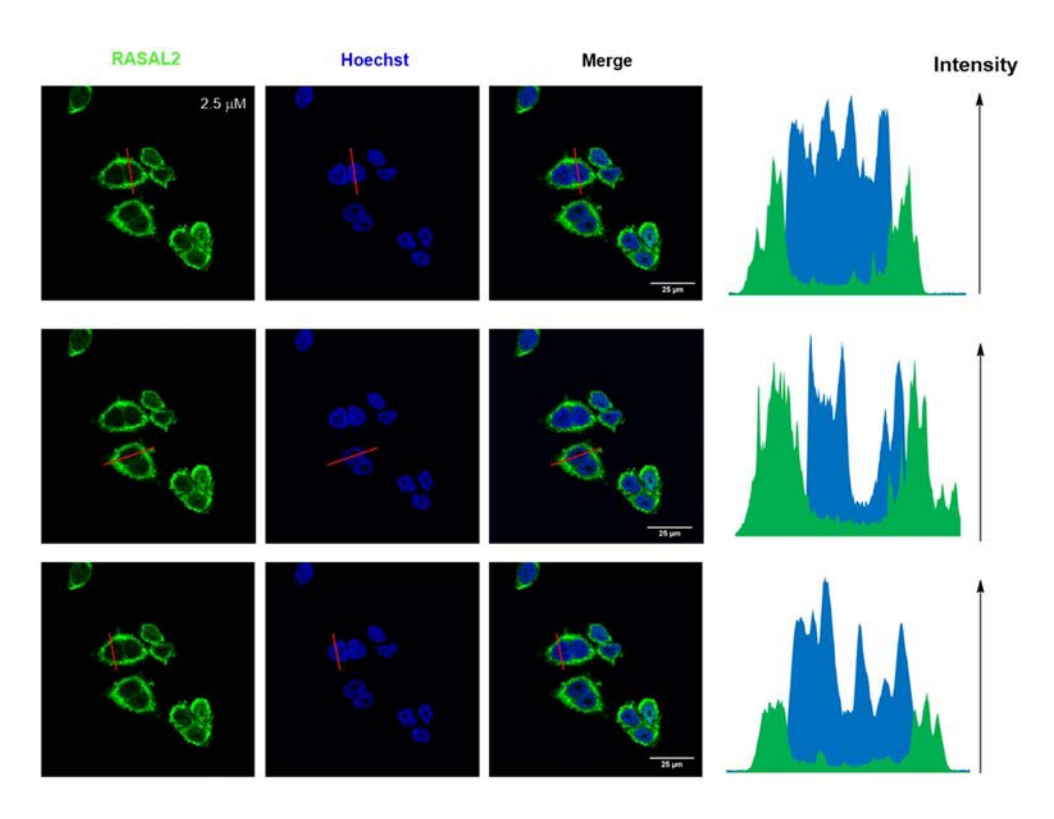


Figure 124: Goyazensolide 2.5 μM treatment

Table 4: Standard deviation (STDEV) and Standard error of mean (SEM)

Ratio	Ratio	Ratio			
DMSO	Goyazens olide 1 µM	Goyazensolide 2.5 µM	Standard de <i>via</i> tion		Standard error of mean
1.362694	1.806843	2.054756	0.132056852	4	0.066028426
1.092318	1.677424	1.9765	0.091513053	2	0.0647095
1.297862			0.055335348	2	0.039128
1.122037					
DMSO	Goyazens olide 1 µM	Goyazensolide 2.5 µM			
1.218728	1.7421335	2.015628			

III.6. Experimental procedures for pAKT assay and NLS pull-down

pAKT assay.

SW620 Cells were seeded (350.000 cells/mL) in a 6 well plate and left two days to attach and grow. Cells were incubated with DMSO or goyazensolide (5 μ M) in a time dependant manner. Cells were lysed and scrapped in the presence of phosphatase inhibitors at 4 °C. Lysates were centrifuge at 14000g for 15 minutes at 4 °C. SDS-PAGE followed by western blot treated with respective antibodies (pAKT and actin).

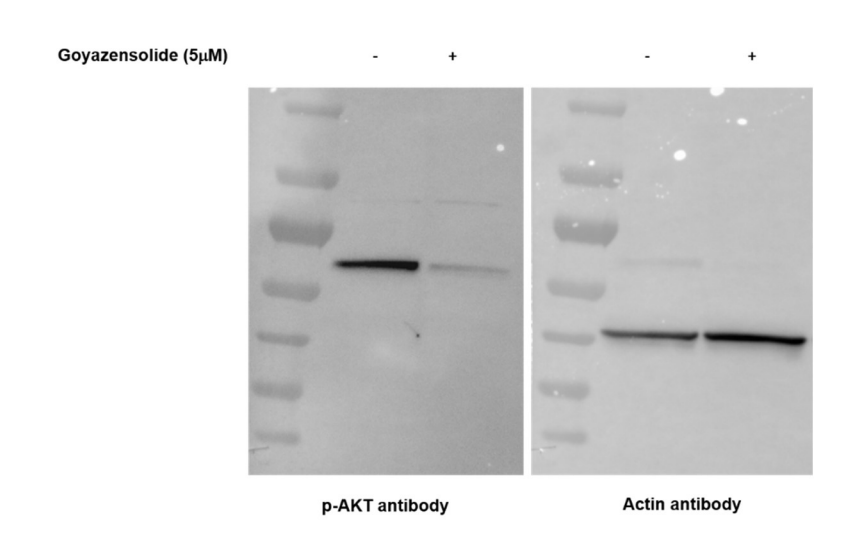


Figure 125 : Full immunoblot of p-AKT (p-AKT Ser473 antibody) expression upon treatment of SW620 cells with DMSO or goyazensolide (5 μ M, 4 h)

Pulldown experiment with viruses NLS. 10μL of 100μM solutions of the corresponding NLS (0.2% SDS in PBS) were added to 30 μL of magnetic streptavidin beads and the suspension was shaken for 1 hour. The supernatant was discarded and the beads were washed $5 \times$ with a solution of 0.2% SDS in PBS. The pre-treated lysates (30 μL of treated lysate (3 mg/mL) with DMSO or goyazensolide 10 μM for 30 min) were added to the beads and shaken 3 hours. The supernatants were discarded and the beads were washed $2 \times$ times (20 μL) with 0.2% SDS in PBS. 15 μL of SDS 5%. For elutions 5 μL of Laemli buffer were added to the beads and the mixtures were shaken and heated at 95°C for 3 minutes followed by SDS-PAGE and western blot. Incubation with IPO5 antibody (1:1000) followed by rabbit secondary antibody (1:1000). Chemoluminescence was used for detection.

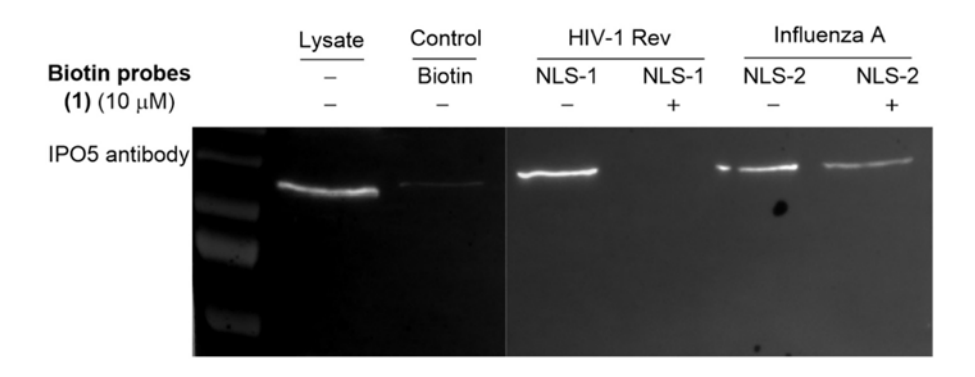


Figure 126: Full immunoblot of competitive interaction between NLS and IPO5. Magnetic streptavidin beads were saturated with corresponding NLS and then incubated for 2 hours with HT29 lysate treated with DMSO or goyazensolide (10 μM, 30 min).

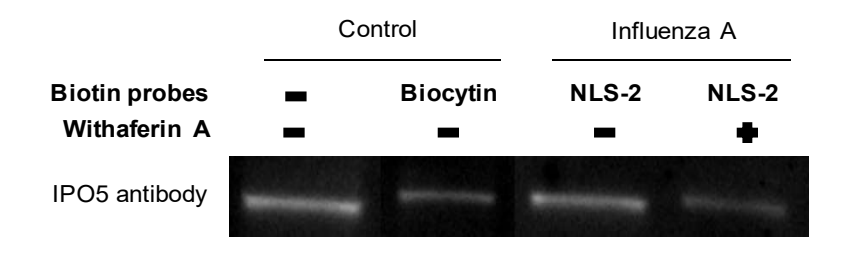


Figure 127: Full immunoblot of competitive interaction between influenza NLS and IPO5. Magnetic streptavidin beads were saturated with biotinylated NLS and then incubated for 2 hours with SW620 lysate treated with DMSO or withaferin A (10 μ M, 30 min).

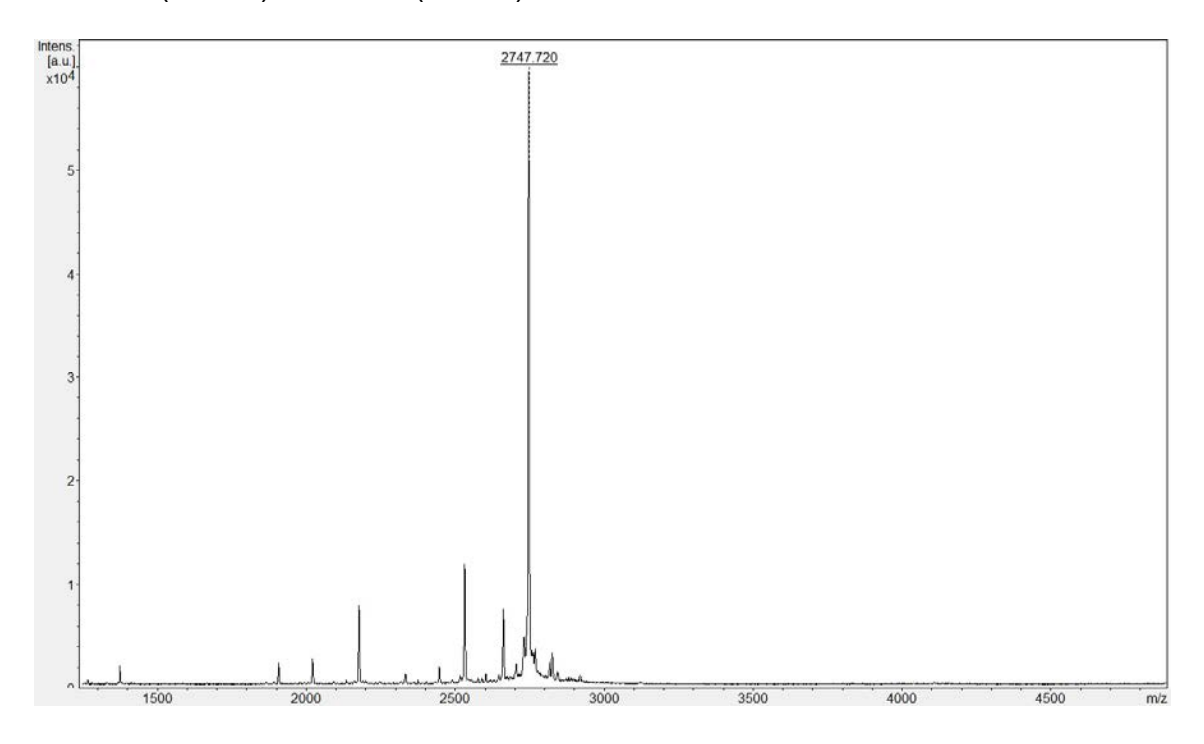
III.7. Preparation of NLS-1 and NLS-2

NLS-1 and **NLS-2** were synthesized using solid-phase synthesis. General procedure described in PLoS One **2020**, *15*, e0238089.

Figure 128: Chemical structures of NLS-1 and NLS-2

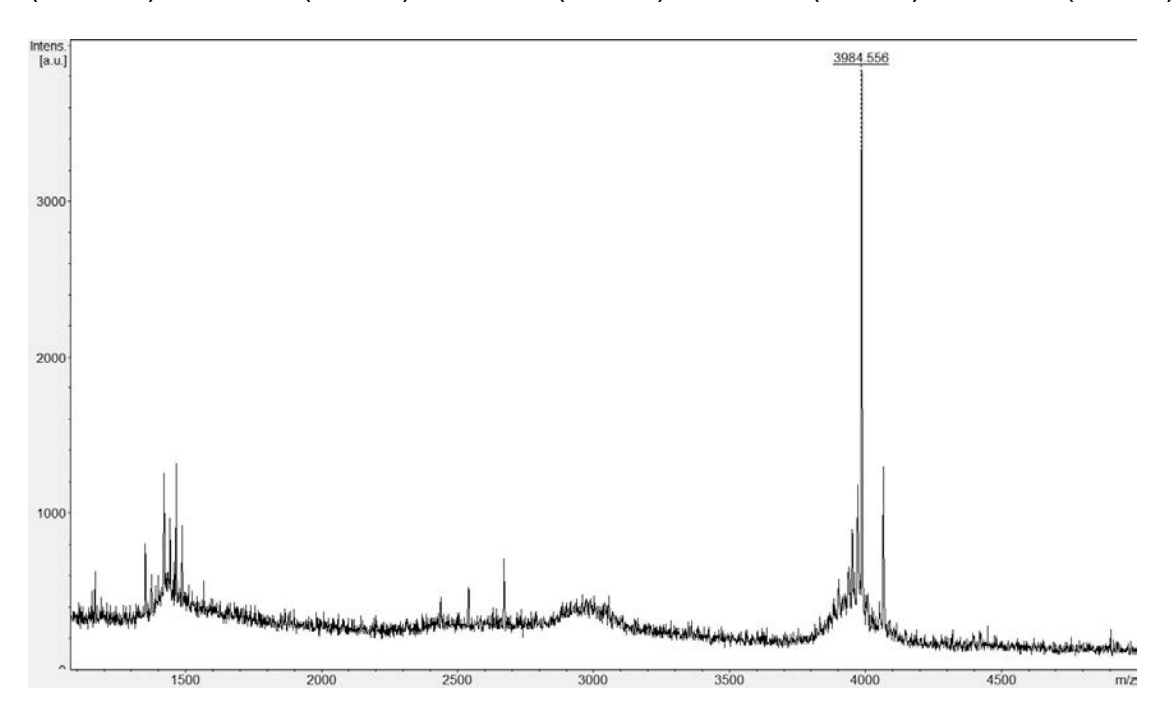
Data of NLS-1:

 $(C_{110}H_{194}N_{56}O_{26}S)$, $[M+H]^+$ isotopic peaks with relative distribution: 2748.53 (100.0%), 2747.53 (84.1%), 2749.54 (35.9%)



Data of NLS-2:

 $(C_{167}H_{299}N_{65}O_{42}S_3)$, $[M+H]^+$ isotopic peaks with relative distribution: 3984.24 (100.0%), 3985.25 (66.1%), 3983.24 (55.4%), 3986.25 (46.9%), 3985.24 (24.0%)



III.8. Quantification of fluorescent bands

Experimental procedures for Figure 76 and Figure 129

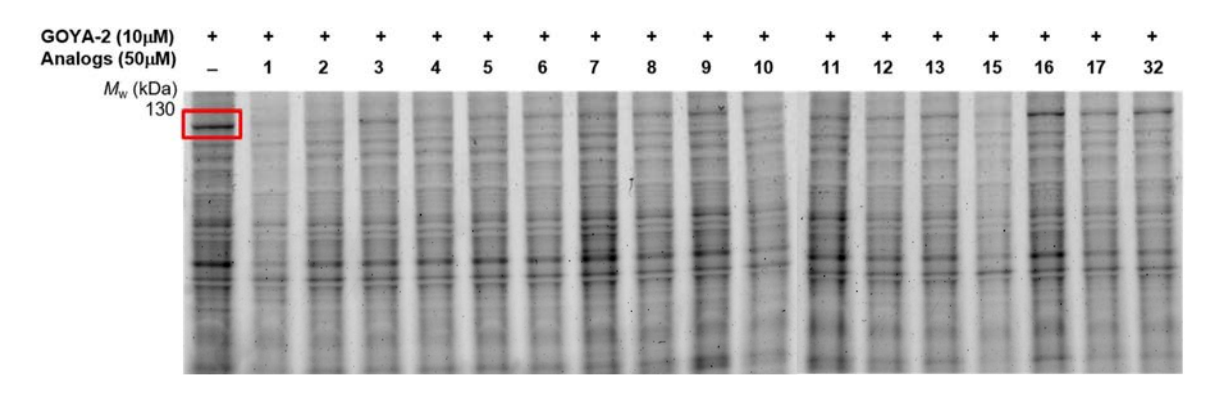


Figure 129: Competition experiment with 50 µM of 1-17 and 32 (correspond to a-p, see Figure 76)

Goyazensolide and atripliciolide selectively bind IPO5 versus other members of the same family of heliangolides. Competition experiment. A SW620 Lysate was incubated for 30 minutes with DMSO or one of the natural products (50 μ M) for 30 min, and then labeled with 10 μ M of **GOYA-2** followed by CuAAC reaction with **Cy3-N₃**. The labeling/competition experiment shows selective binding of goyazensolide (1) and atripliciolide (2) to IPO5 protein.

Quantification (ImageJ software)

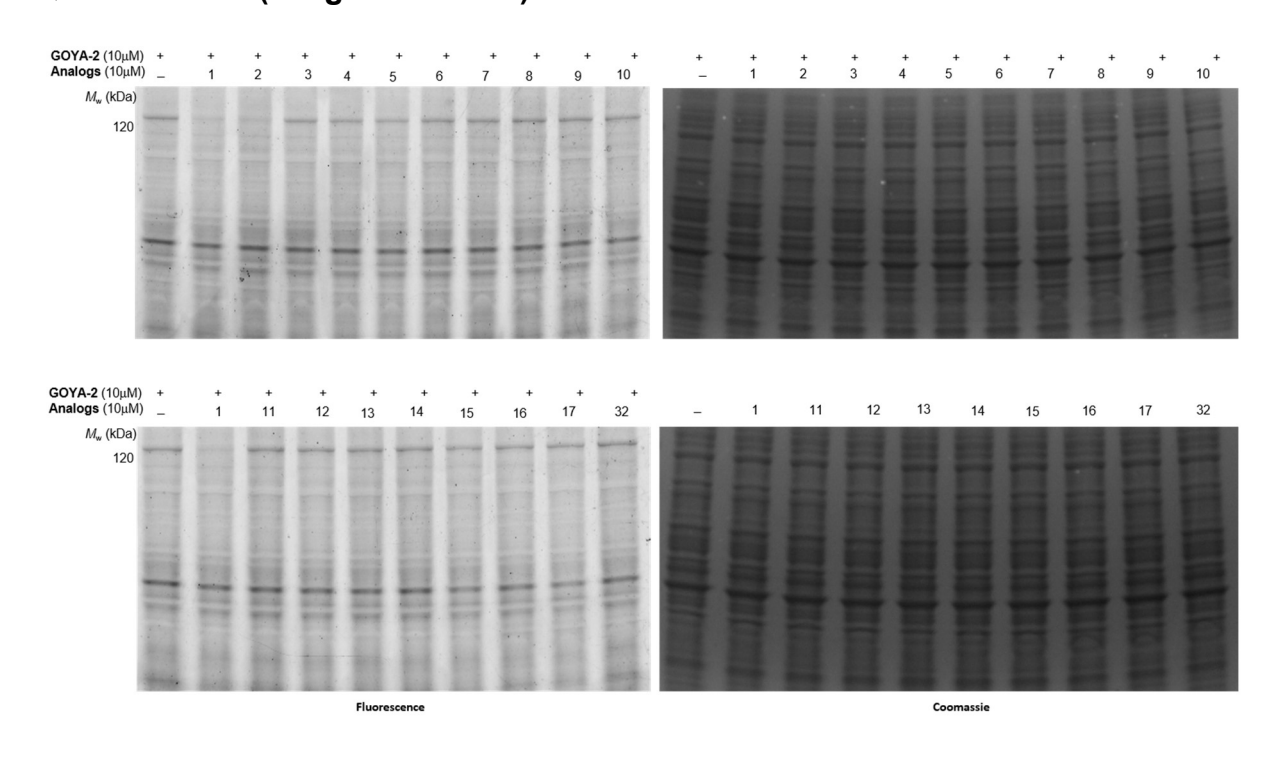


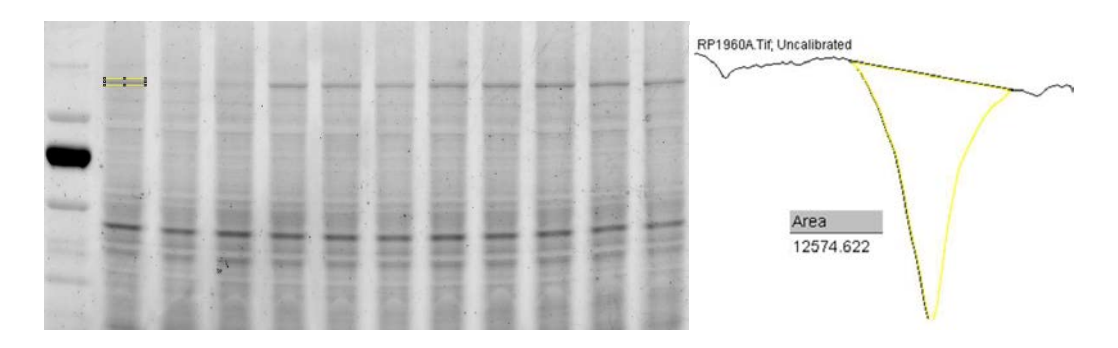
Figure 130 : Competition experiment with 10 µM of analogs 1-17 and 32 (See Figure 76)

PC3 cell lysate were preincubate for 30 min with 10 μ M of DMSO or analogs and then labeled with 10 μ M of **GOYA-2** followed by CuAAC reaction with **Cy3-N**₃. Proteins were separated using a 10% SDS-PAGE gel. Gels were visualized at 625 nm using a fluorescence scanner and then stained with Coomassie brilliant blue.

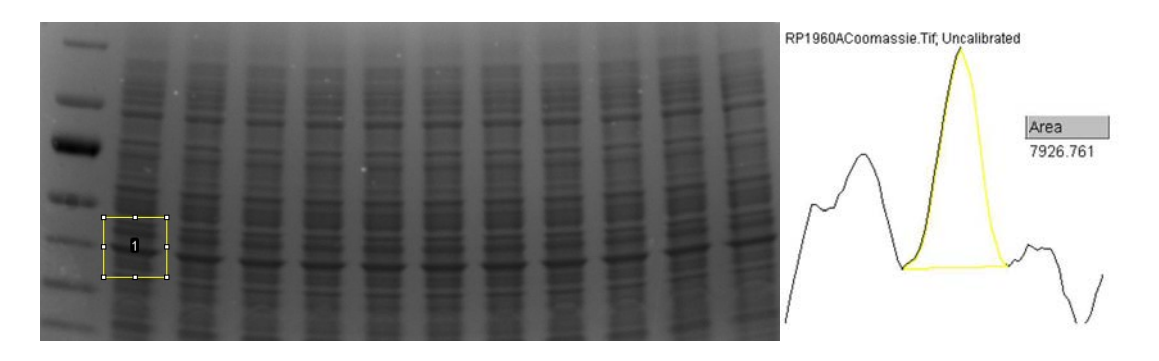
Quantification

Binding efficiency was calculated by density of the fluorescent band. We used Coomassie staining was used as reference.

1) Grey intensity determination for fluorescence



2) Grey intensity determination for Coomassie



3) Calculation

Table 5: Raw data and calculation of Quantification

Analogs	Fluorescence density	Coomassie density (dye)	F/C	Fraction
-	9938.844	5119.347	1.941428	1
1	3166.782	5275.811	0.600246	0.309177
2	2863.225	5417.861	0.528479	0.272211
3	8507.43	5651.154	1.505432	0.775425
4	7714.823	5615.276	1.373899	0.707675
5	6462.045	5792.276	1.115631	0.574645
6	9374.38	5868.276	1.597467	0.822831
7	9108.43	5645.276	1.613461	0.831069
8	10058.309	5812.811	1.730369	0.891287
9	9769.966	5093.296	1.918201	0.988036
10	11011.693	5687.468	1.936133	0.997272
Gel2				
-	11349.67	4811.569	2.35883	1
1	3077.953	4637.569	0.6637	0.281368
11	11662.79	4956.861	2.352859	0.997469
12	10525.38	4756.154	2.213002	0.938178
13	10426.62	4422.326	2.357724	0.999531
14	10538.92	4654.569	2.264209	0.959886
15	8101.48	4933.326	1.642194	0.69619
16	10379.97	4987.983	2.080995	0.882215
17	9482.602	4648.619	2.039875	0.864783
32	11447.21	4881.447	2.345044	0.994156

Binding efficiency representation. We observed a difference of binding efficiency by comparison of compounds **1-6** versus **7-13**. The C8 stereochemistry plays an important role in the binding efficiency.

III.9. Reaction between goyazensolide / atripliciolide / 15-deoxygoyazensolide with glutathione.

Procedure:

1 equivalent of natural product was dissolved in 50 μ L of DMSO^{d6} and 450 μ L of deuterated PBS and placed in an NMR tube. 1 equivalent of glutathione was added

and reaction was monitored by NMR. Once the first binding occurred, a second equivalent of glutathione was added and the reaction was monitored by NMR.

Characterization of atripliciolide by HMBC

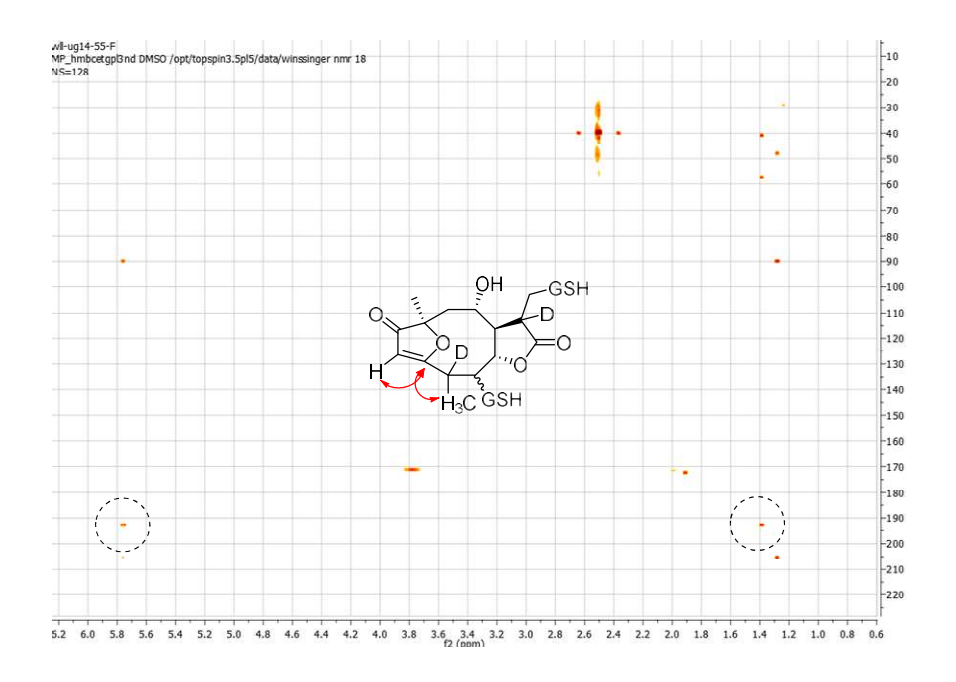


Figure 131: HMBC analysis on the second binding of atripliciolide

III.10. Synthesis of desthiobiotinylated lodoacetamide.

Figure 132: Synthetic route of desthiobiotinylated iodoacetamide

Step 1. DIPEA (325 μ L, 1.79 mmol) was added dropwise to a solution of desthiobiotin (175 mg, 0.717 mmol), amine (186 mg, 0.86 mmol), HATU (327 mg, 0.86 mmol) in

DMF (3 mL) at 0 °C. Mixture stirred 15 min at 0 °C and was used without further purification (315 mg, yield 99%).

Step 2. Compound 2 (315 mg, 0.713 mmol) was treated with 10%TFA in CH₂Cl₂ (2 mL) and stirred 45 min at RT. Solvent removed and purified by HPLC Biotage (Water/ACN 95/5 to 10/90). Lyophilization gave a white powder (188 mg, 58%).

Step 3. Et₃N (18 μ L, 0.128 mmol) was added dropwise to a solution of amine (20 mg, 0.044 mmol) and acyl chloride (18 mg, 0.088 mmol) in CH₂Cl₂ (3 mL) at 0 °C. Mixture stirred 15 min at 0 °C and purified by HPLC ZORBAX (Water/ACN 5/95 to 90/10). Lyophilization gave a white powder (8 mg, 36%).

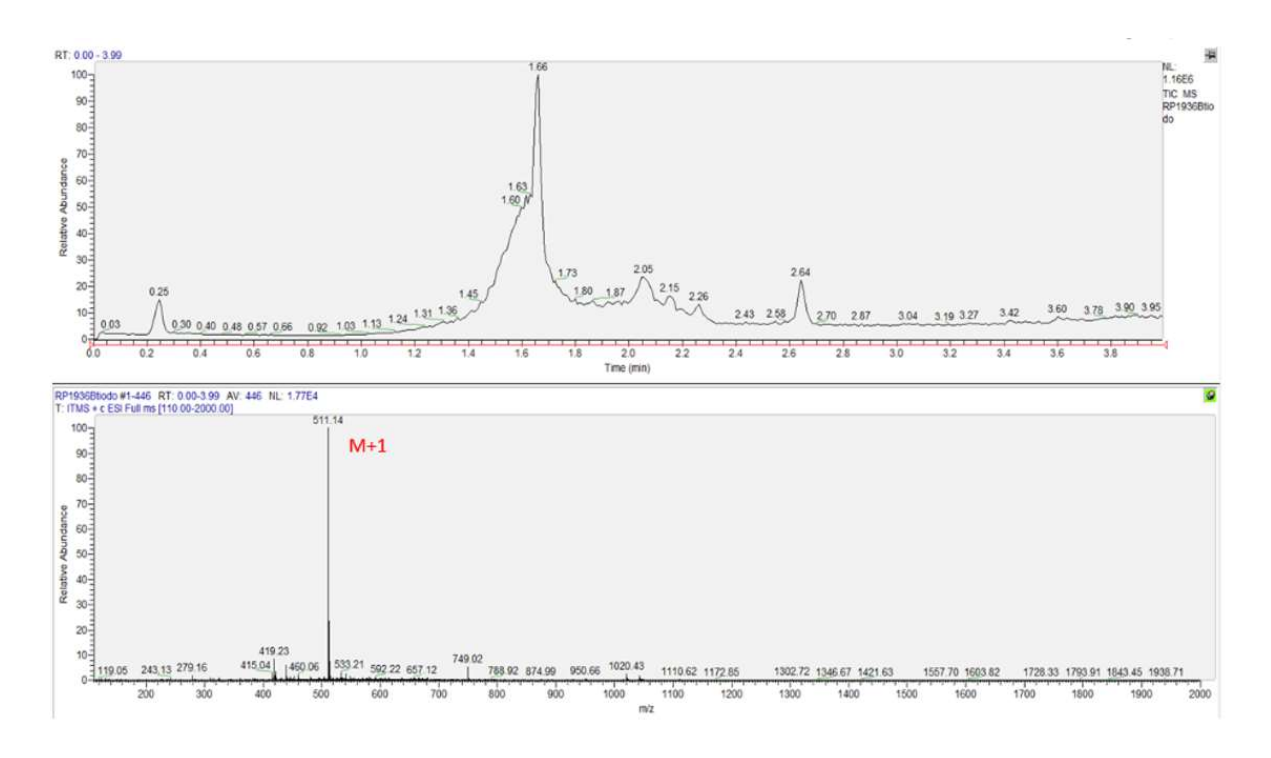


Figure 133: MS analysis of the desthiobiotinylated iodoacetamide

Desthiobiotinylated Iodoacetamide Pull-Down. IPO5-GST (2 μg in 2 μL DPBS, 8 μM) was treated with 10 μL TCEP for 30 minutes at room temperature. 10 μL of desthiobiotinylated iodoacetamide (20 mM) were added, and the mixture incubated 1 hour in the dark at room temperature. Streptavidin enrichment incubating the solution with 20 μL of streptavidin magnetic beads during 2 hours rotation at room temperature. The beads were then washed 2 x PBS/SDS 0.2 % and 3 x NH₄HCO₃ 50 mM and then treated with 20 μL of NH₄HCO₃ 50 mM, 5 μL acetonitrile and 4 μL of trypsin (1 μg in 50 μL NH₄HCO₃ 50 mM) followed by overnight digestion at 37°C under high agitation

(1'500 rpm). The supernatant was removed, and the beads were incubated again with 4 μ L of trypsin during 4 hours at 37 °C. The supernatant was again removed, 30 μ L of NH₄HCO₃ 50 mM was added and the elution was done with a thermal denaturation (5 minutes, 95 °C). The supernatant was placed into a microtube and the remaining beads were incubated for extra 2 minutes under high agitation with 30 μ L of extraction buffer I (20% CH₃CN, 80% H₂O, 1% formic acid). The supernatant was then collected, and the fragments incubate for another 2 minutes with 30 μ L of Extraction Buffer 2 (95% CH₃CN, 5% H₂O, 1% formic acid). The combined supernatants were lyophilized, resuspended in Buffer A (95% H₂O, 5% CH₃CN, 0.1% formic acid) and summited to high-resolution mass spectra. (HRMS, Xevo G2 Tof spectrometer, Ionization mode: ESI positive polarity; Mobile phase: MeOH 100 μ I/min).

III.11. Cell viability / cytotoxicity assays

Procedure cell viability assay

3000 A549 cells per well were seed in a 96 well plates and grow 24h. Cells were incubated with DMSO or compound during 10h. Cells were blocked with PFA 4% during 30 min followed by Hoescht (1 μ g/mL) 30 min. If penetration of Hoescht is not optimal, add saponin 0.01%. Cells were washed with Plate washer, Biotek EL406 (PBS) to remove dead cells. Cells were counted with microscope Whitefield IXM-XL. A total of 25 pictures for each well are taken and give an average per well. Each sample have 6 biological replicates (Total of 125 pictures per samples for a consistent average).

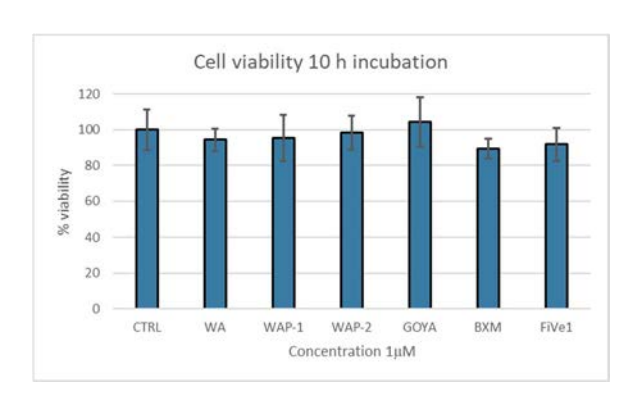
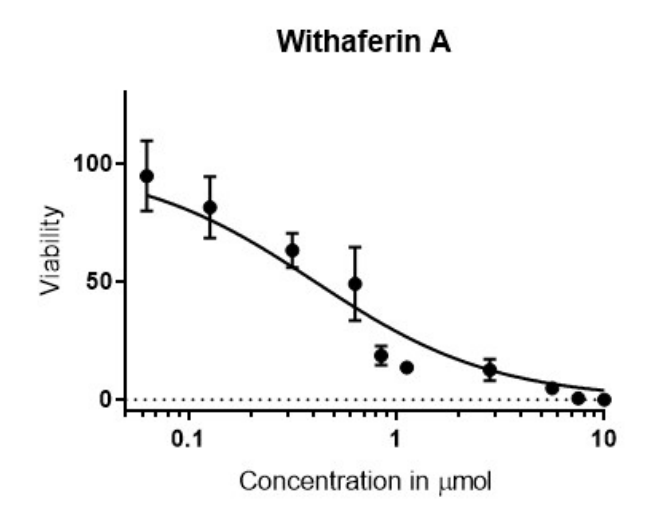


Figure 134: Cell viability assay with all the compounds tested on the plaque assay

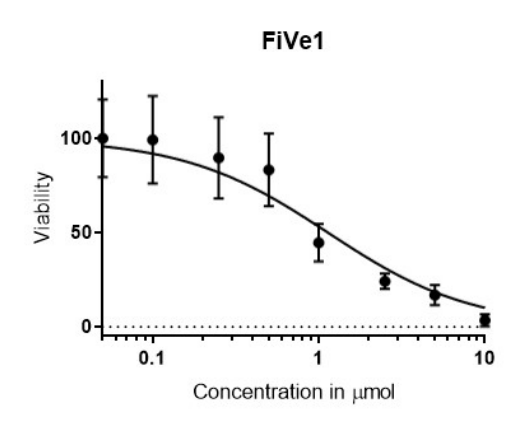
Procedure cytotoxicity assay (cell counting)

Same procedure as cell viability assay. A range of concentration was used and cells were incubated 48h.

Cytotoxicity of withaferin A



Cytotoxicity of FiVe1



III.12. Procedure viral nucleoprotein quantification

In 6 well plates, seed 1.5 10⁵ A549 cells in each wells and let them grow 24h. Cells were preincubated 30 minutes with DMSO or compound. Media removed, cells were washed with PBS and infected at 5 MOI (200 µL) during 40 minutes at 37°C, shake

every 10 minutes. Viral solution removed, washed with infection media (DMEM + BSA 0.2% + TPCK Trypsin Y20000) and add infection media in the presence of DMSO or compound. For each time point, infection media was removed, cells were washed with PBS and Lysis buffer was added. Incubation 3 min then freeze at -80 °C. Lysates were injected in SDS page followed by western blot and nucleoproteins were labeled by the corresponding antibody.

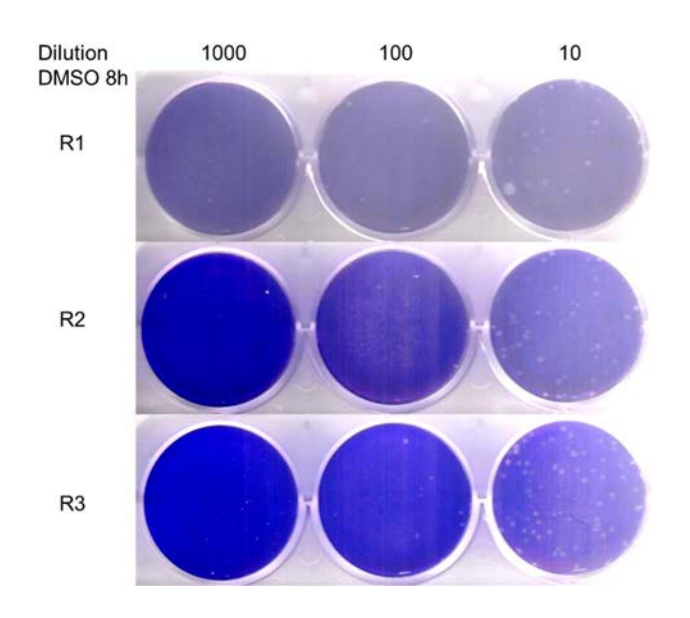
III.13. Procedure plaque assay

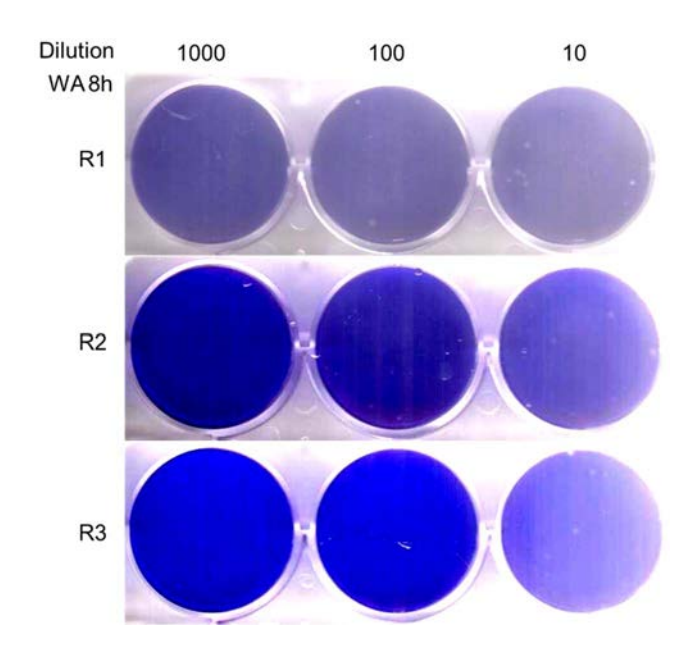
In 6 well plates, seed 1.5 10^5 A549 cells in each wells and let them grow 24h. Media removed and cells were preincubated with DMSO or compound 2h. Media removed, cells were washed with PBS and infected at desired MOI (200 μ L) during 40 minutes at 37°C, shake every 10 minutes. Viral solution removed, washed with infection media (DMEM + BSA 0.2% + TPCK Trypsin Y20000) and add infection media in the presence of DMSO or compound. Take out 100 μ L samples after 8h, 24h, 48h and freeze in a screw cap tube (-80 °C). After 24h, add fresh infection media with DMSO or compound.

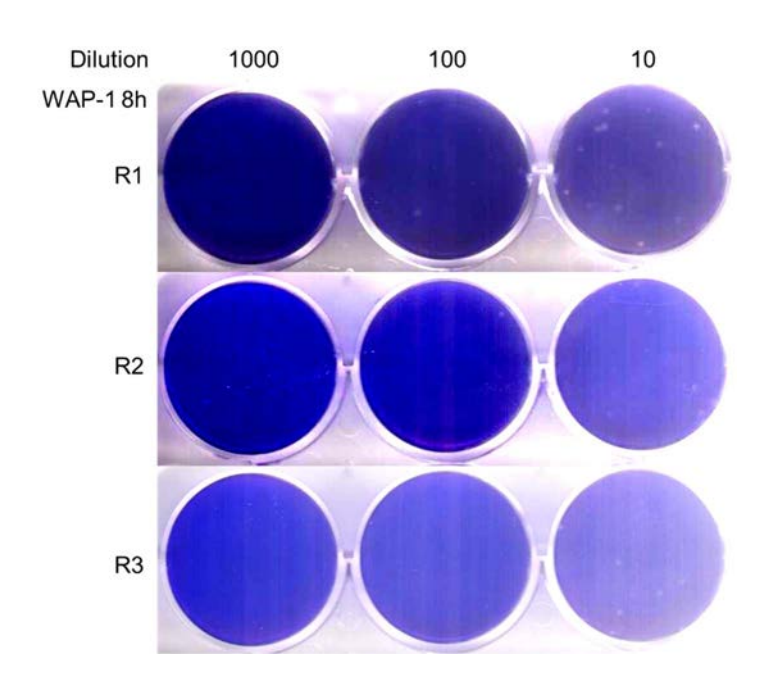
In 6 well plates, seed 10⁶ MDCK cells in each well until confluence (around 24 h). Prepare plaque medium, dilute viral solutions were prepared from 10 to 10⁶.

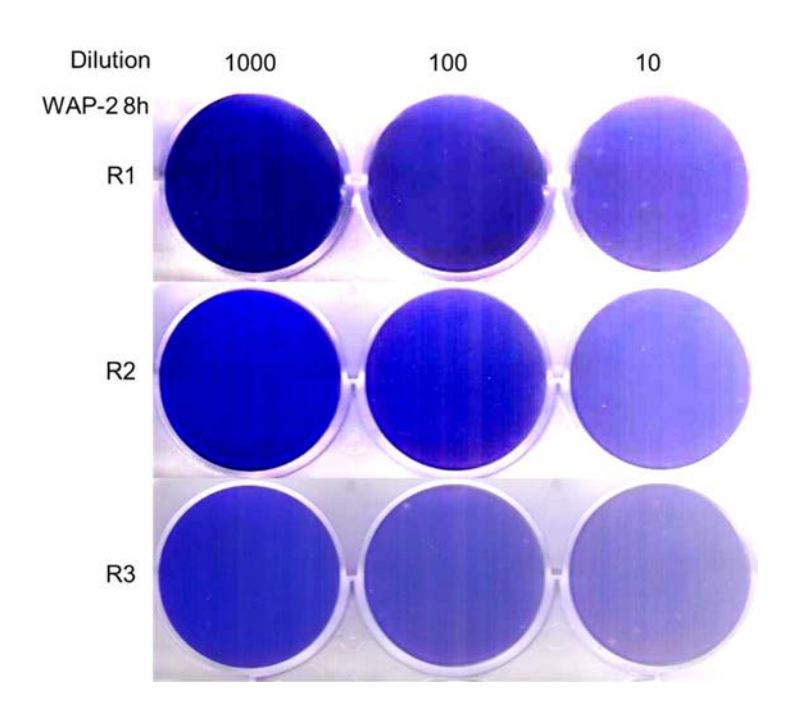
Remove MDCK cells media, wash with PBS and cells were infected with diluted viral solutions (200 μ L, 45 minutes, shake every 10 minutes). Viral solutions were removed, agar plaque medium was added, and plates were placed in the incubator 24-48 hours.

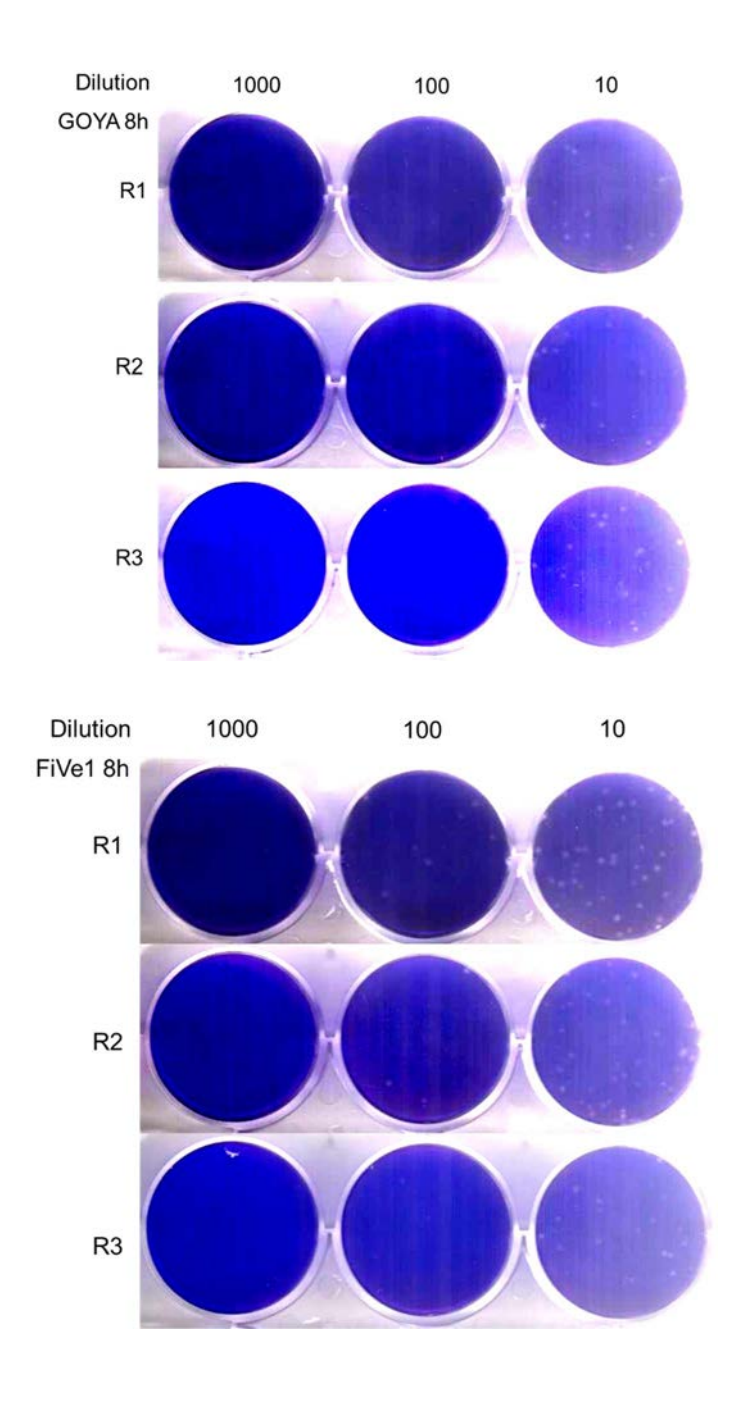
Cells were fixed with PFA 4% and stained with cristal violet. Number of viral plaques were counted.

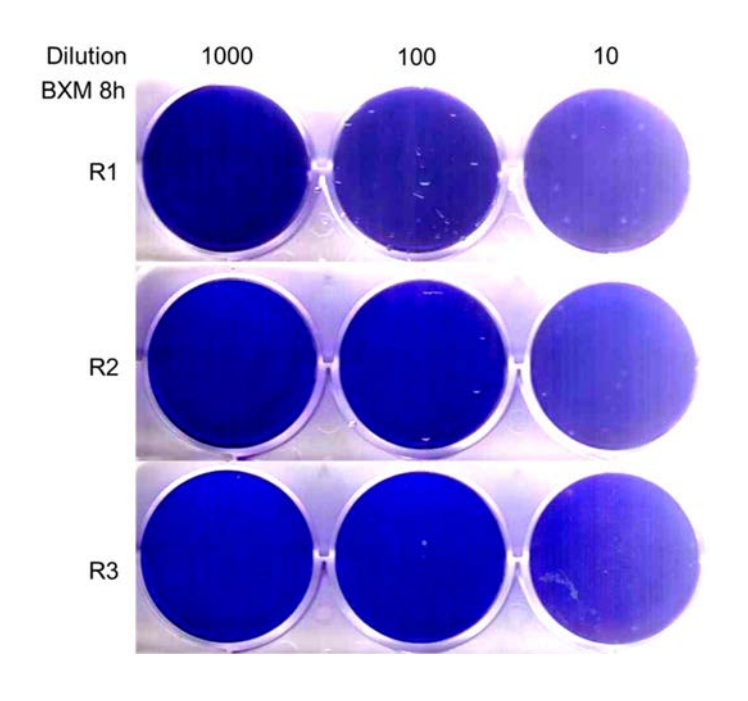






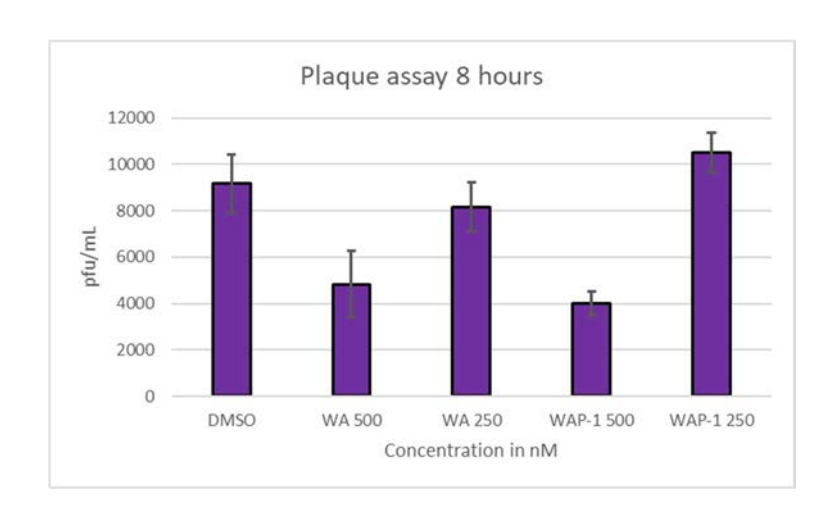




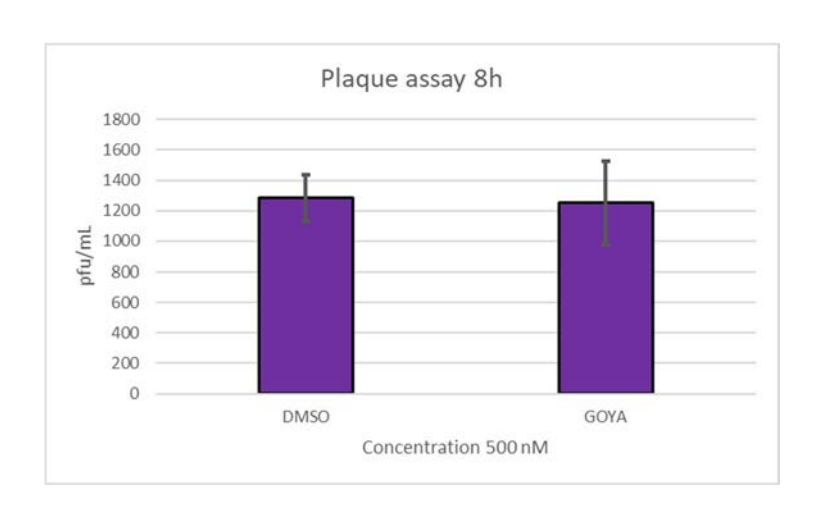


Additional plaque assays

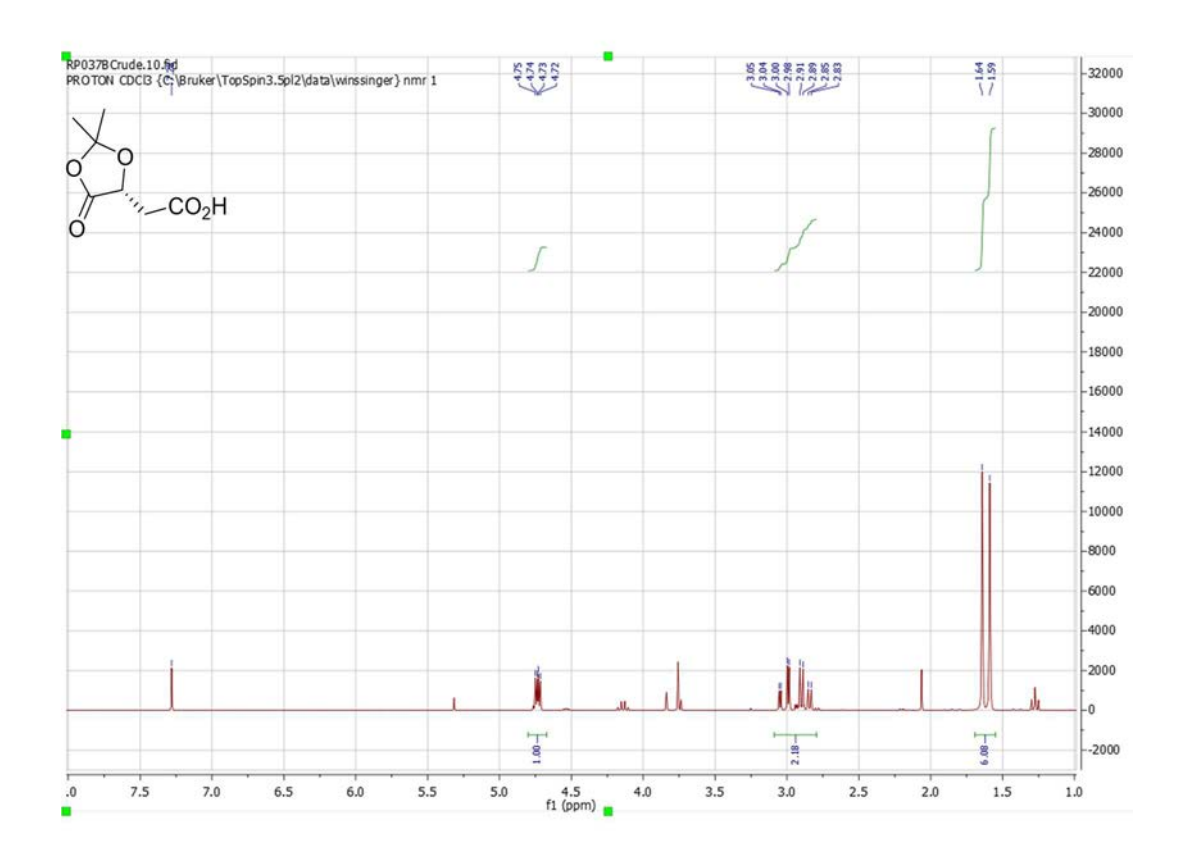
Plaque assay with WA and WAP-1 at 500-250 nM (0.3 MOI)

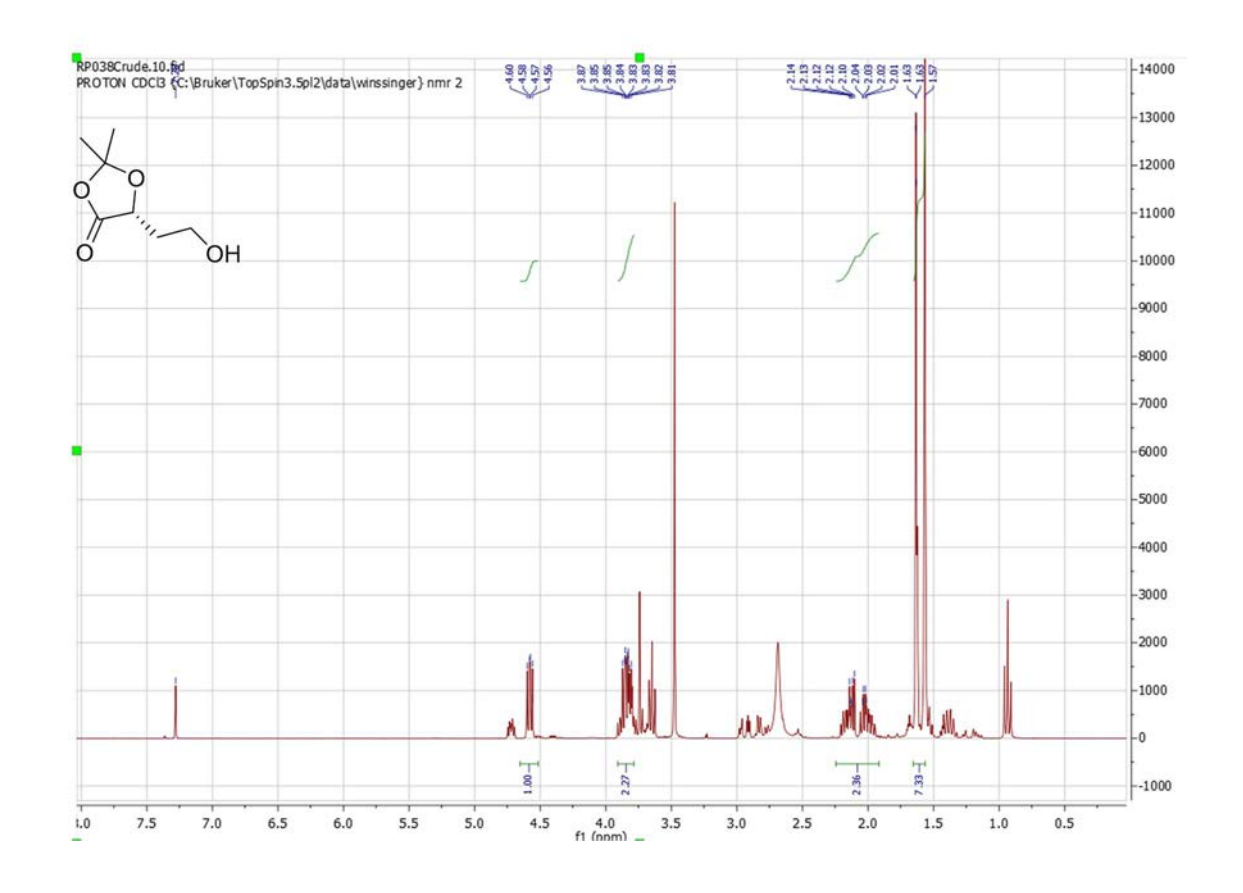


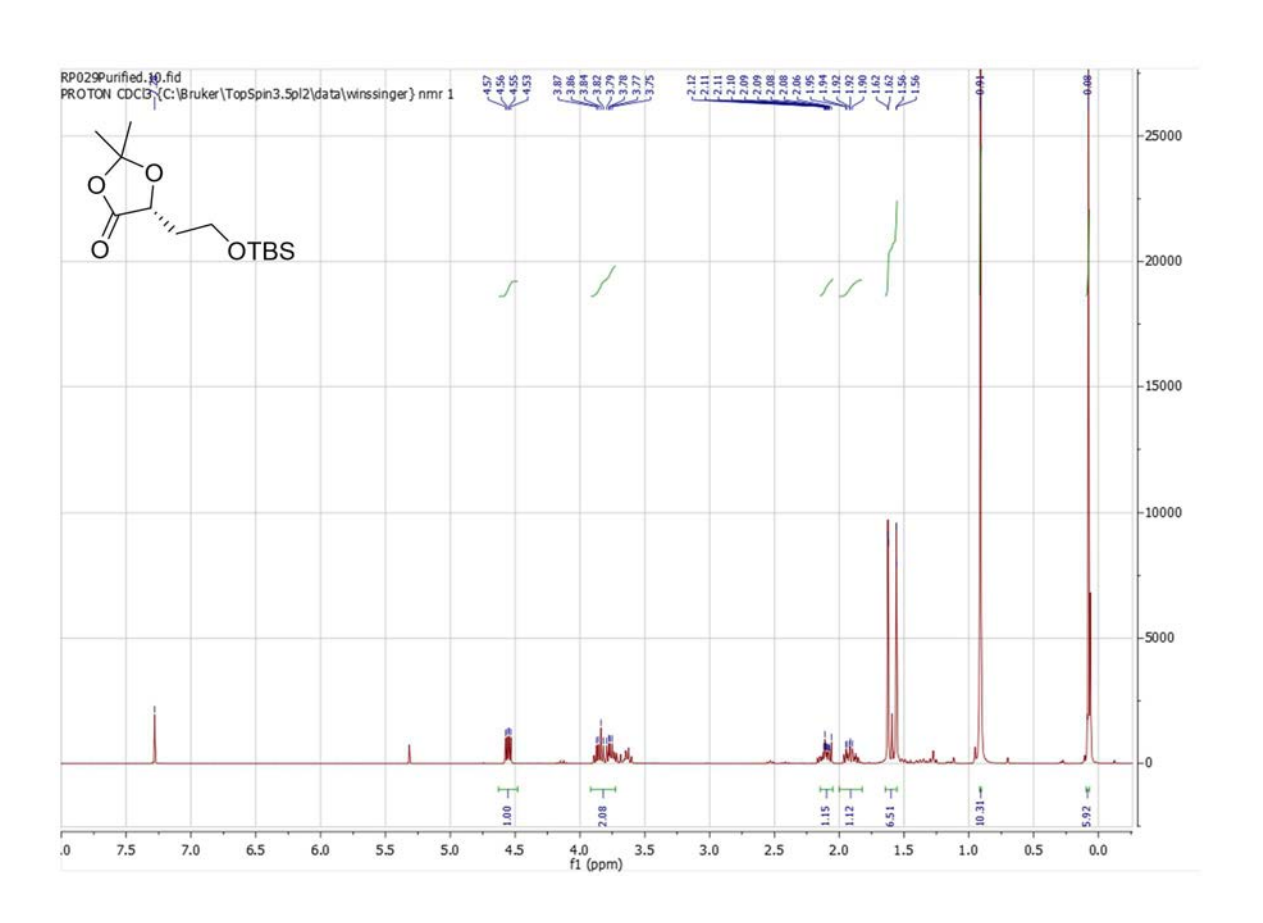
Plaque assay with goyazensolide at 500 nM (0.02 MOI)

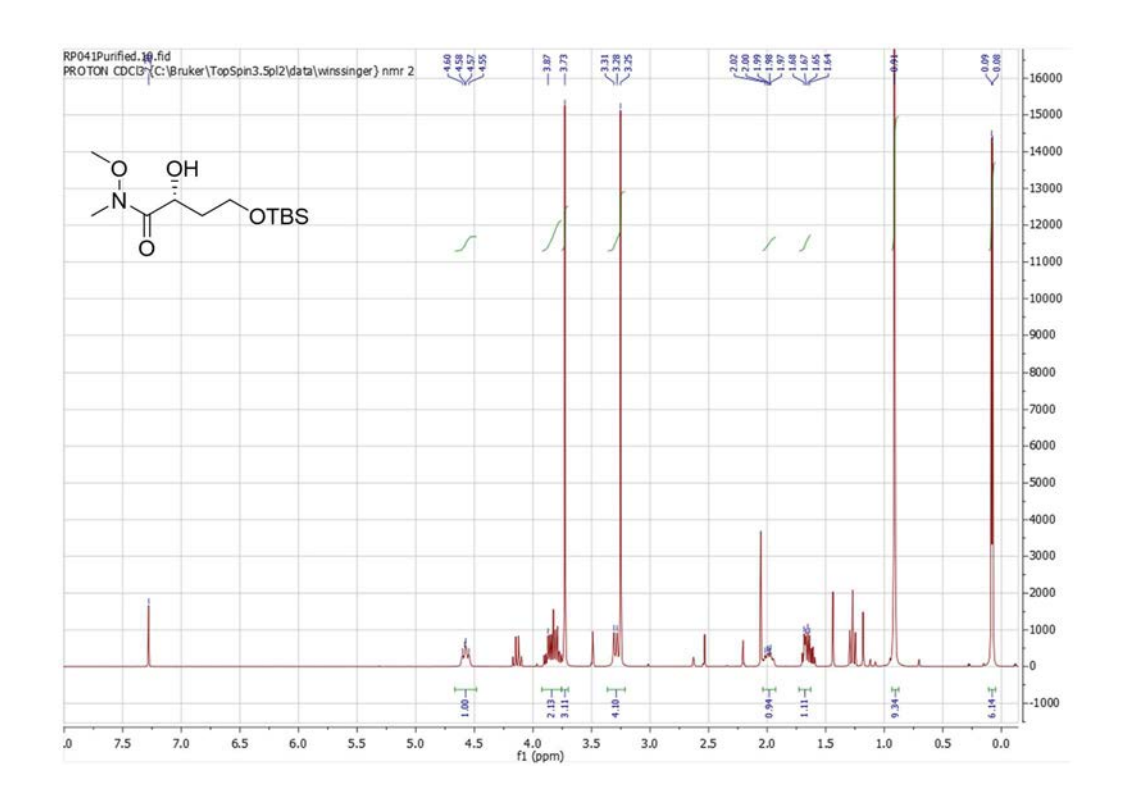


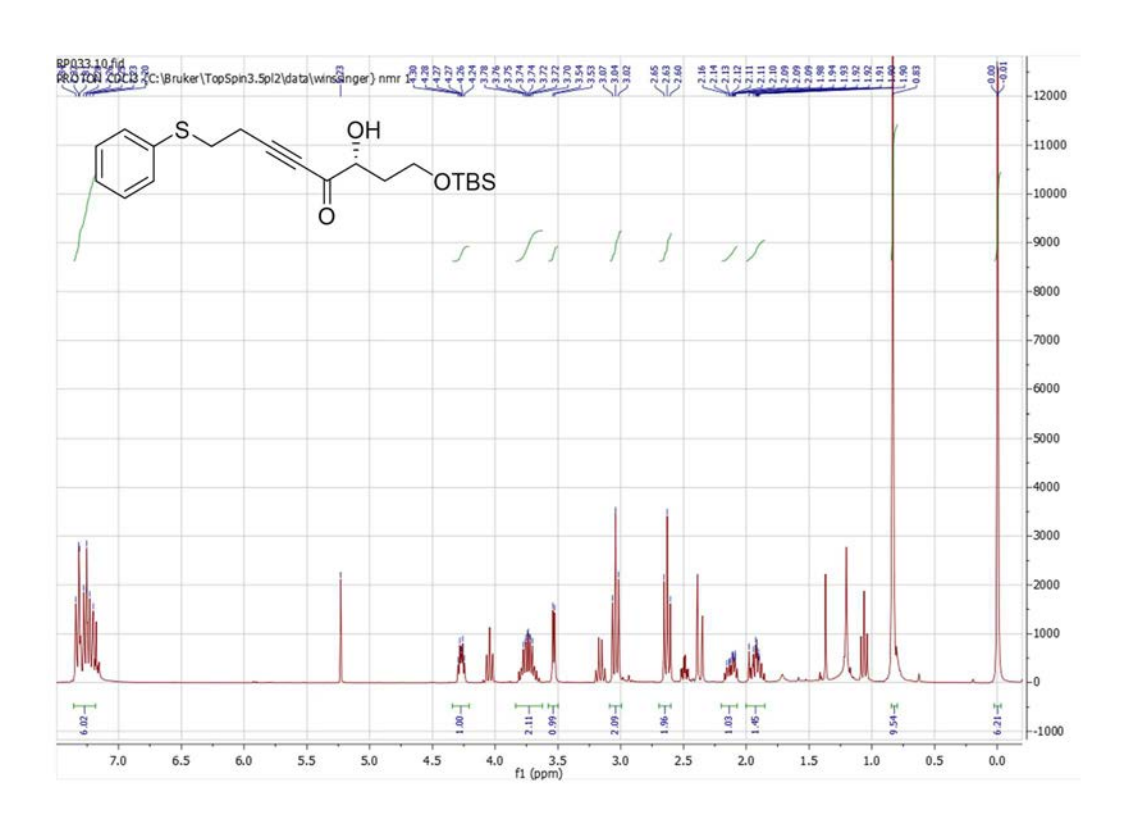
IV.NMR spectrum

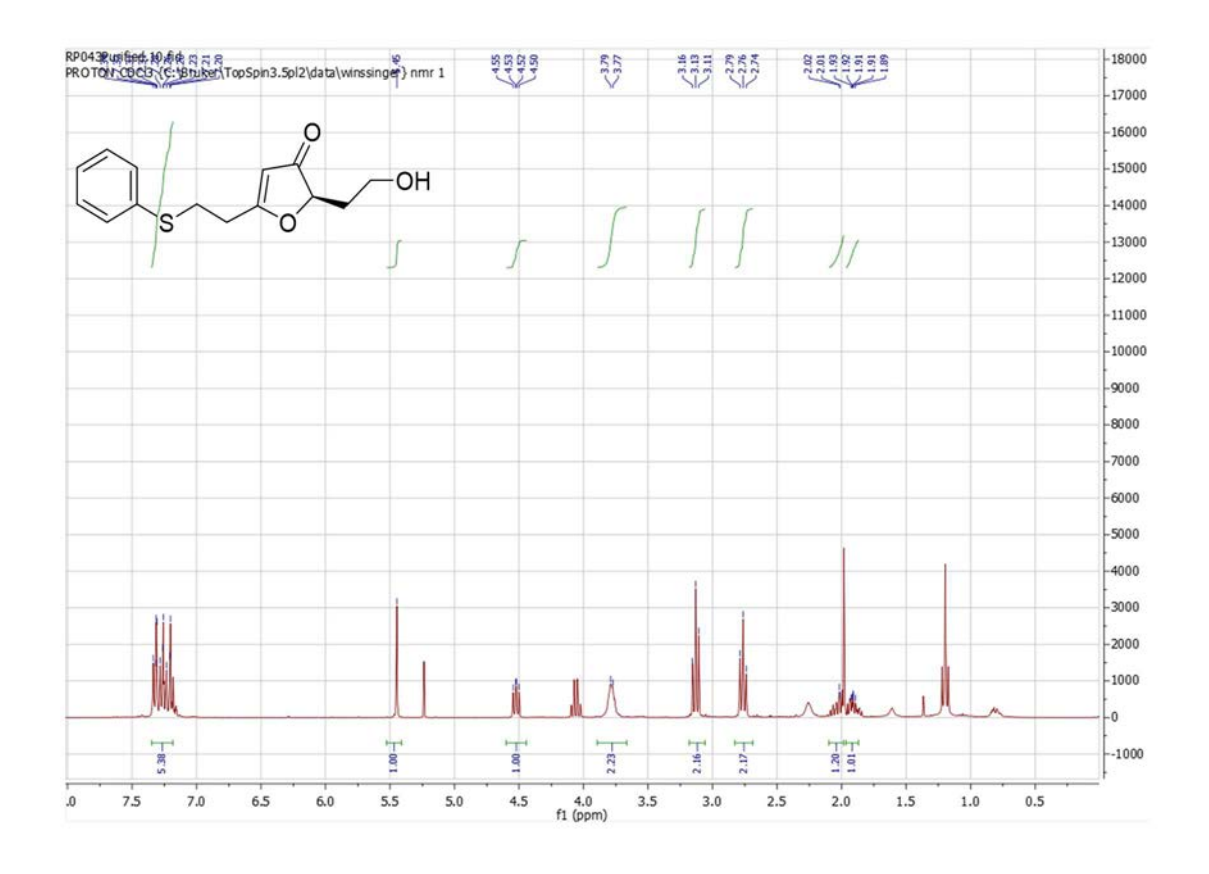


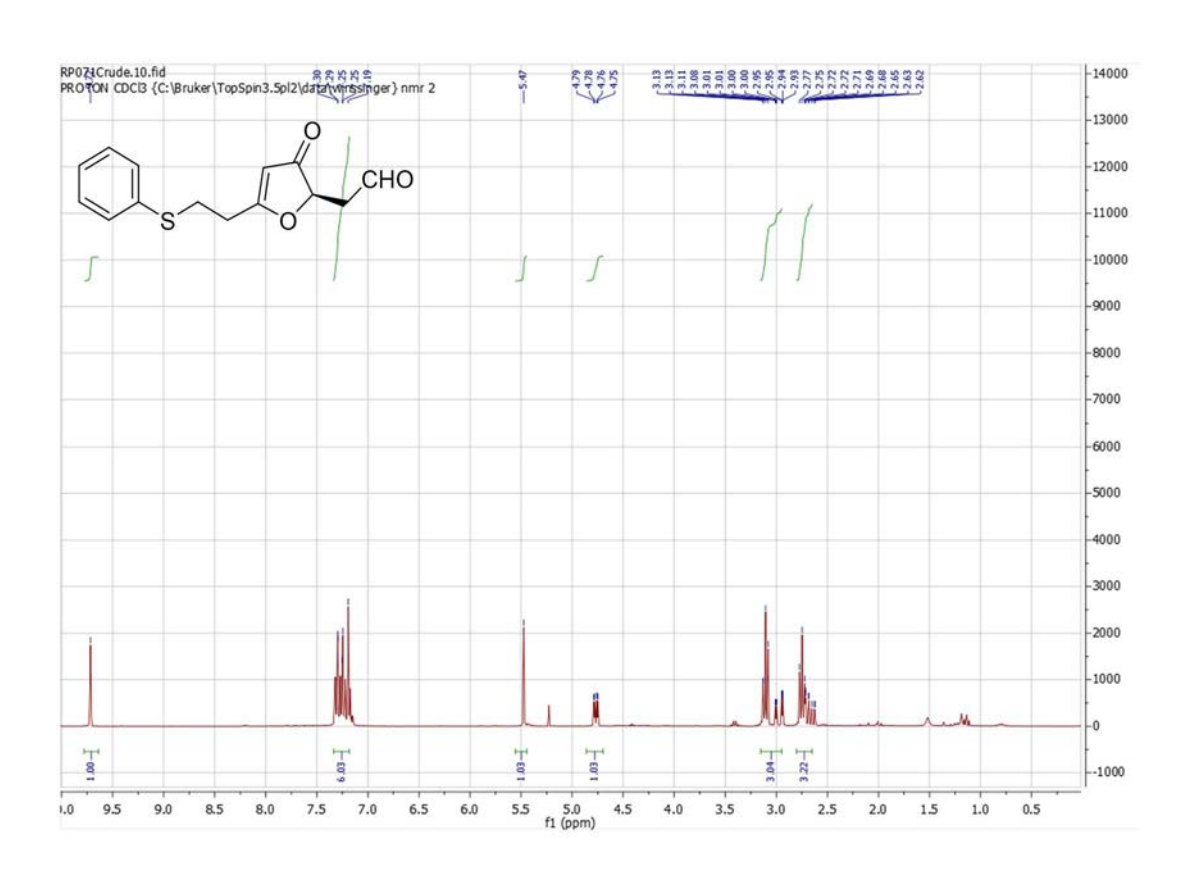


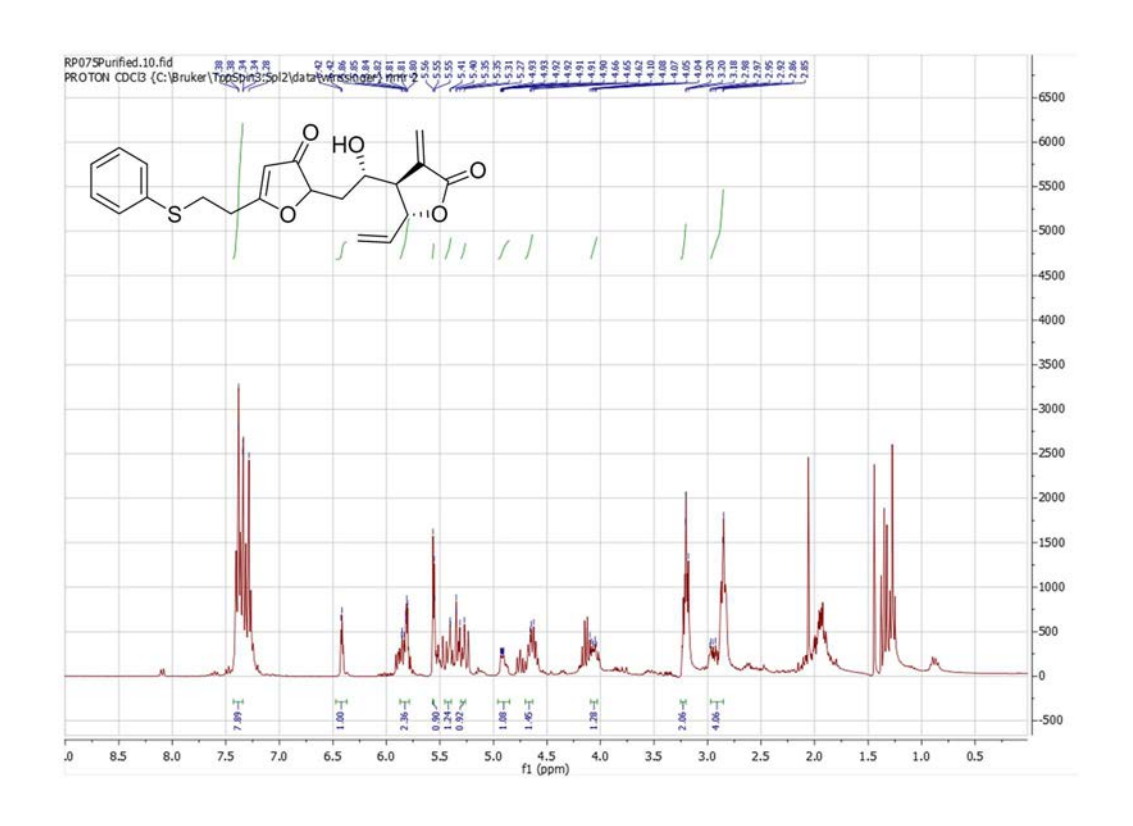


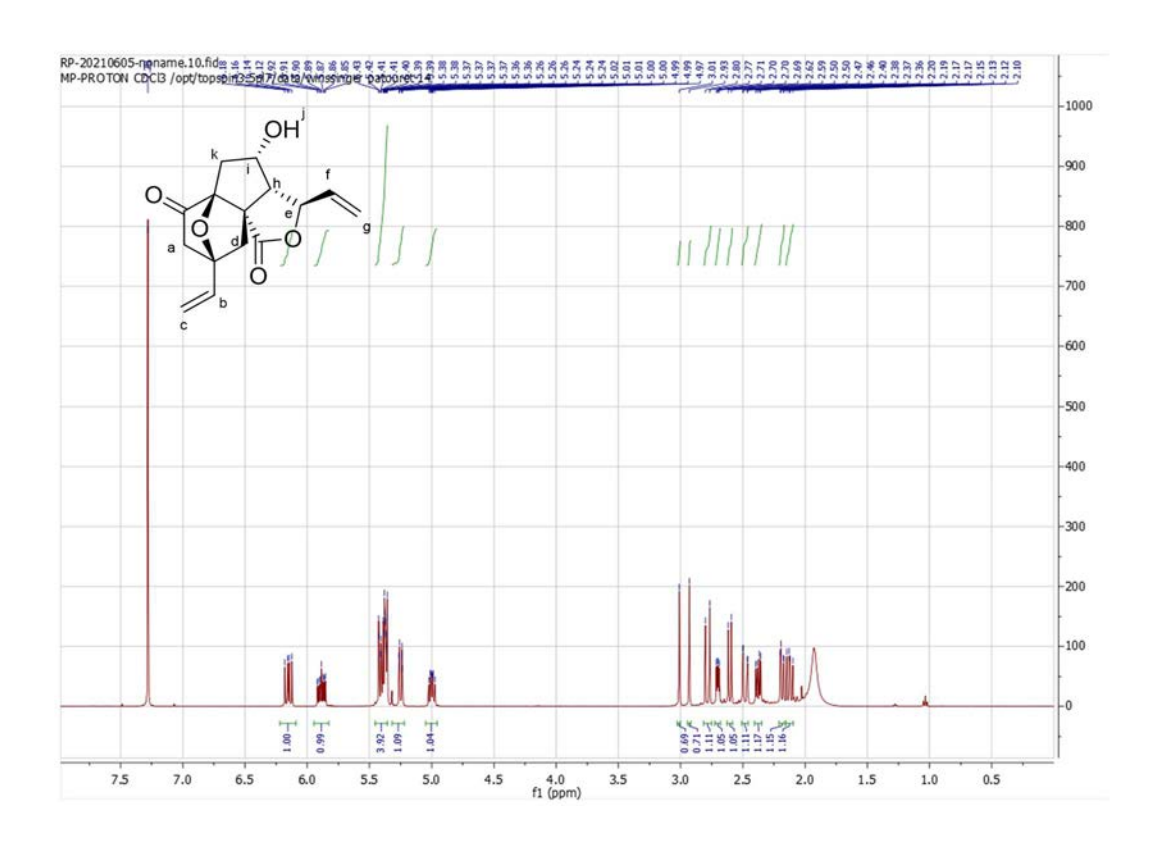


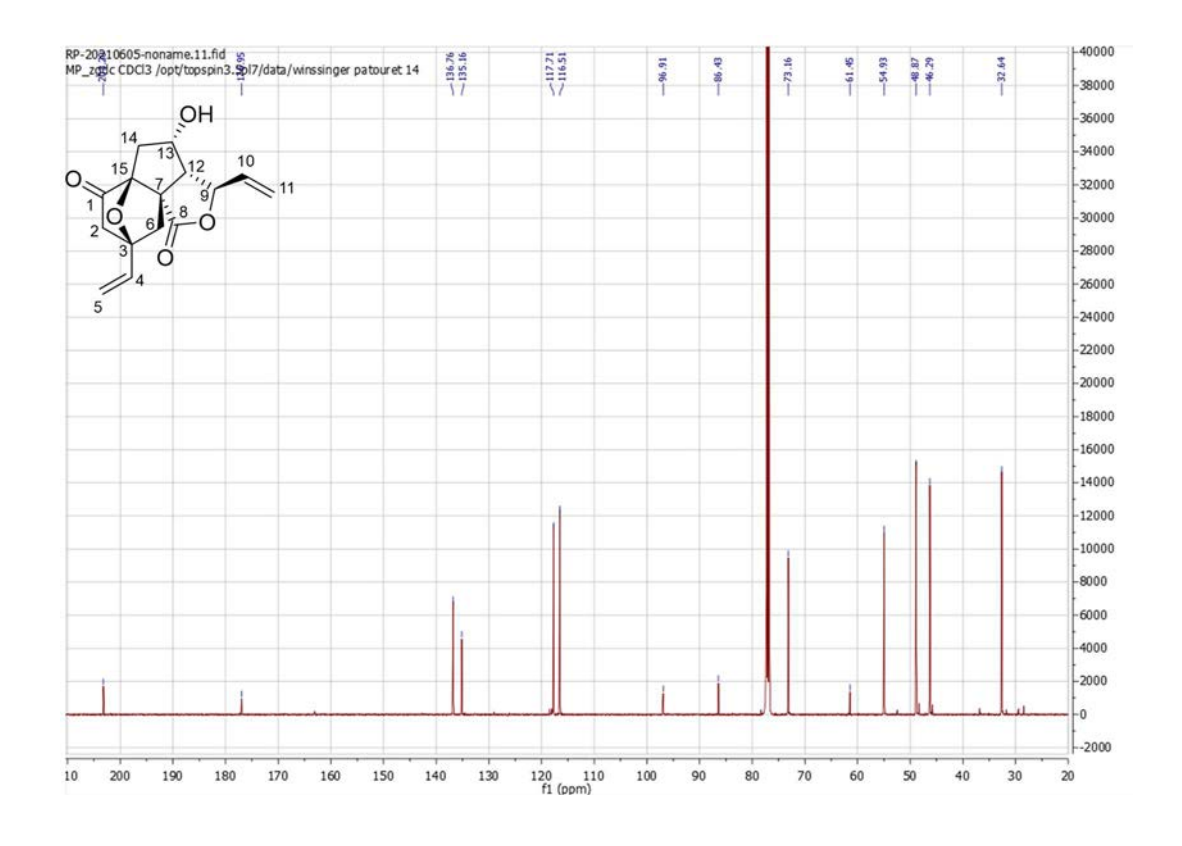


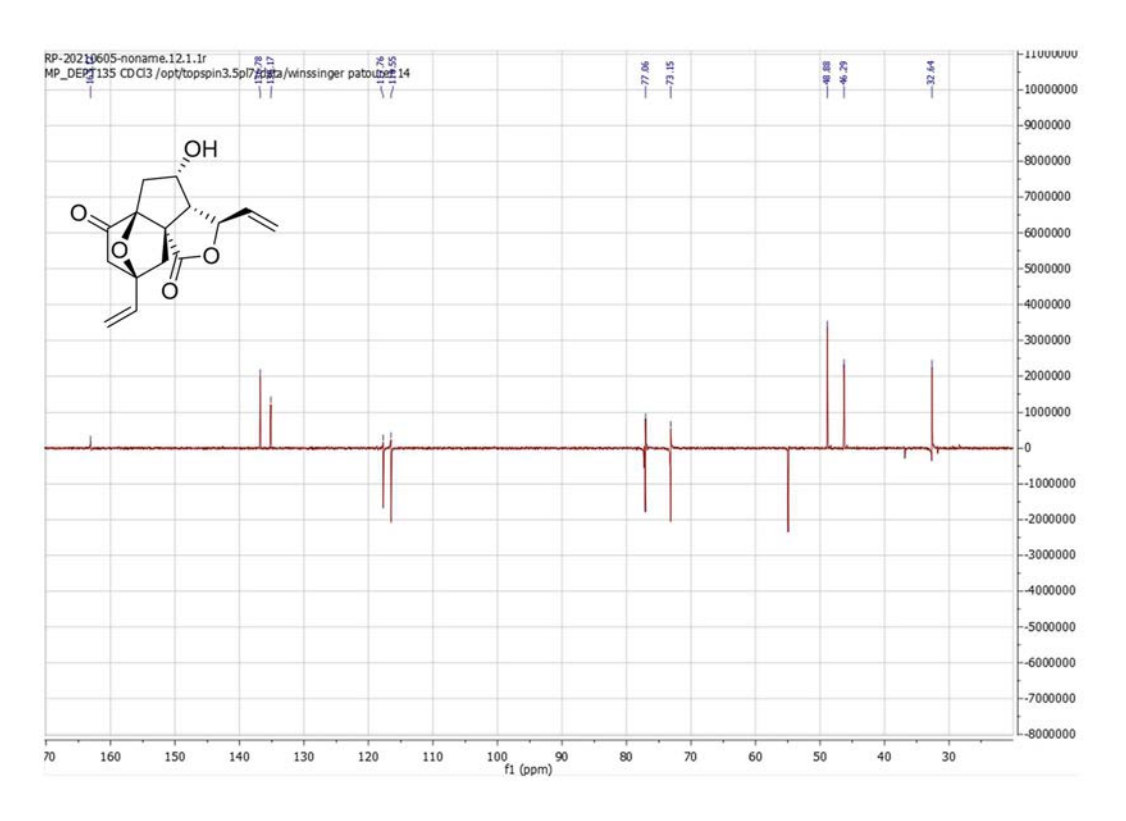


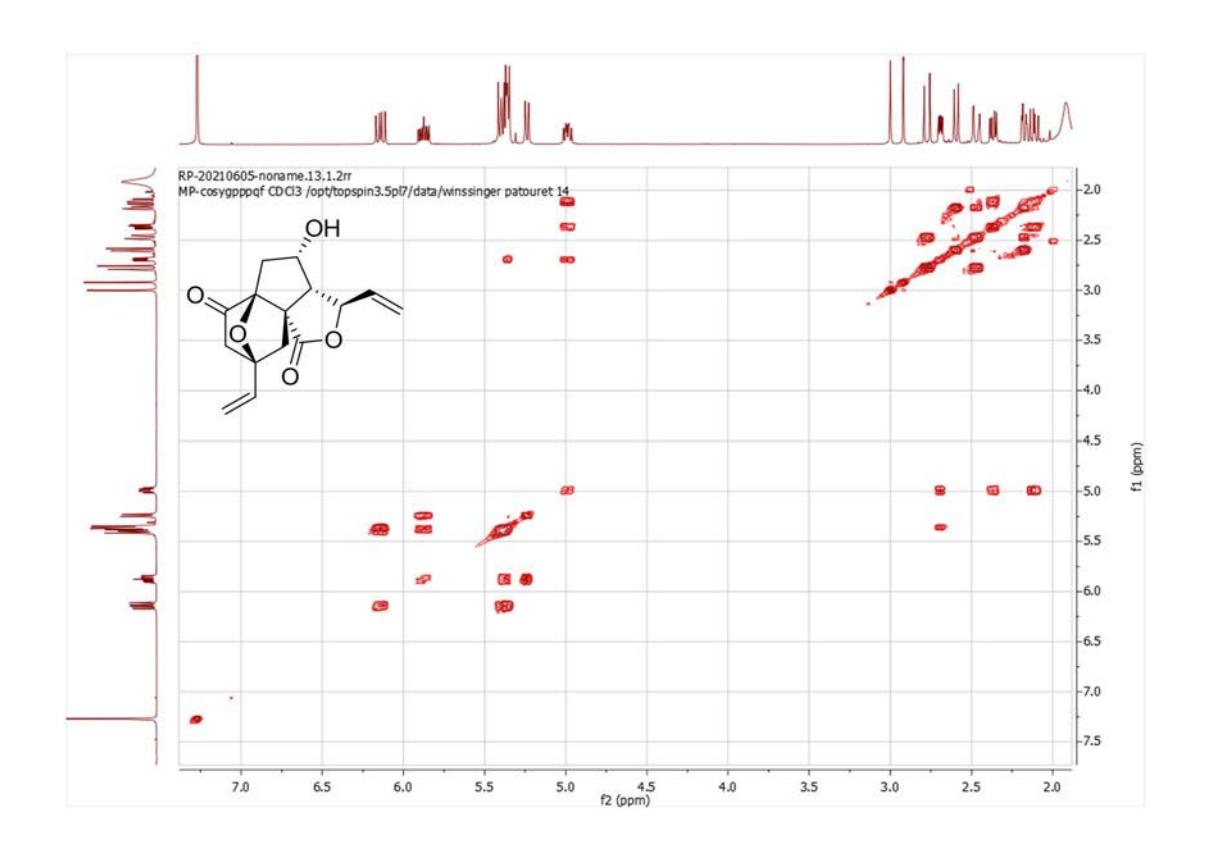


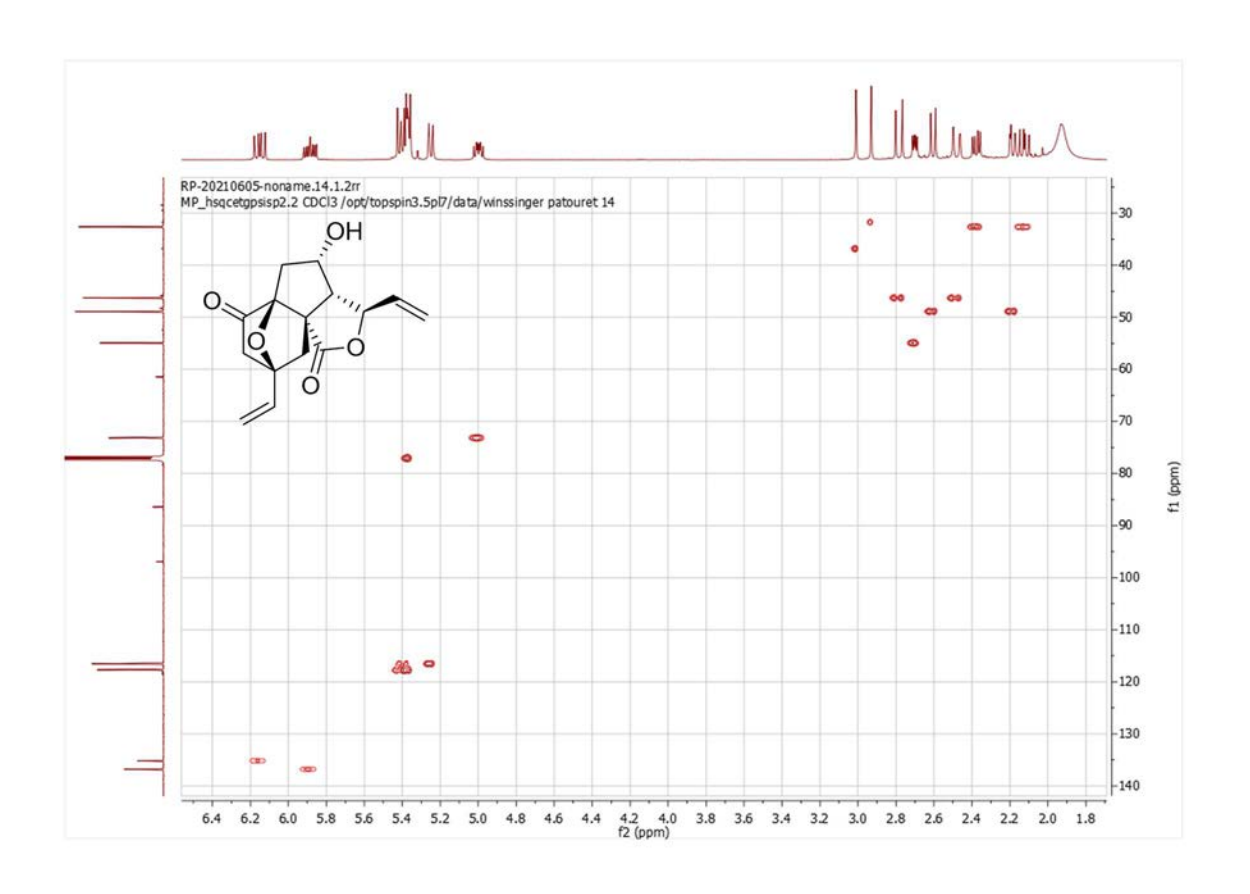


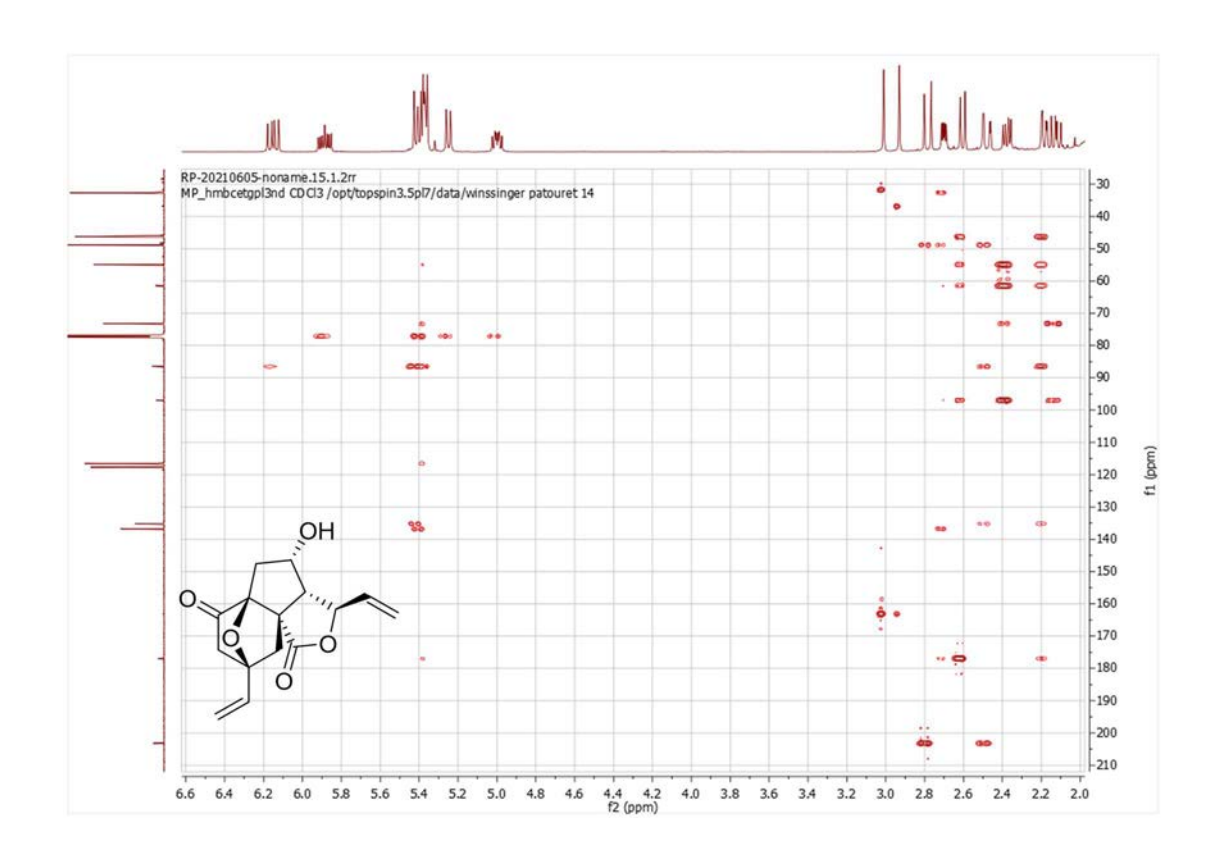


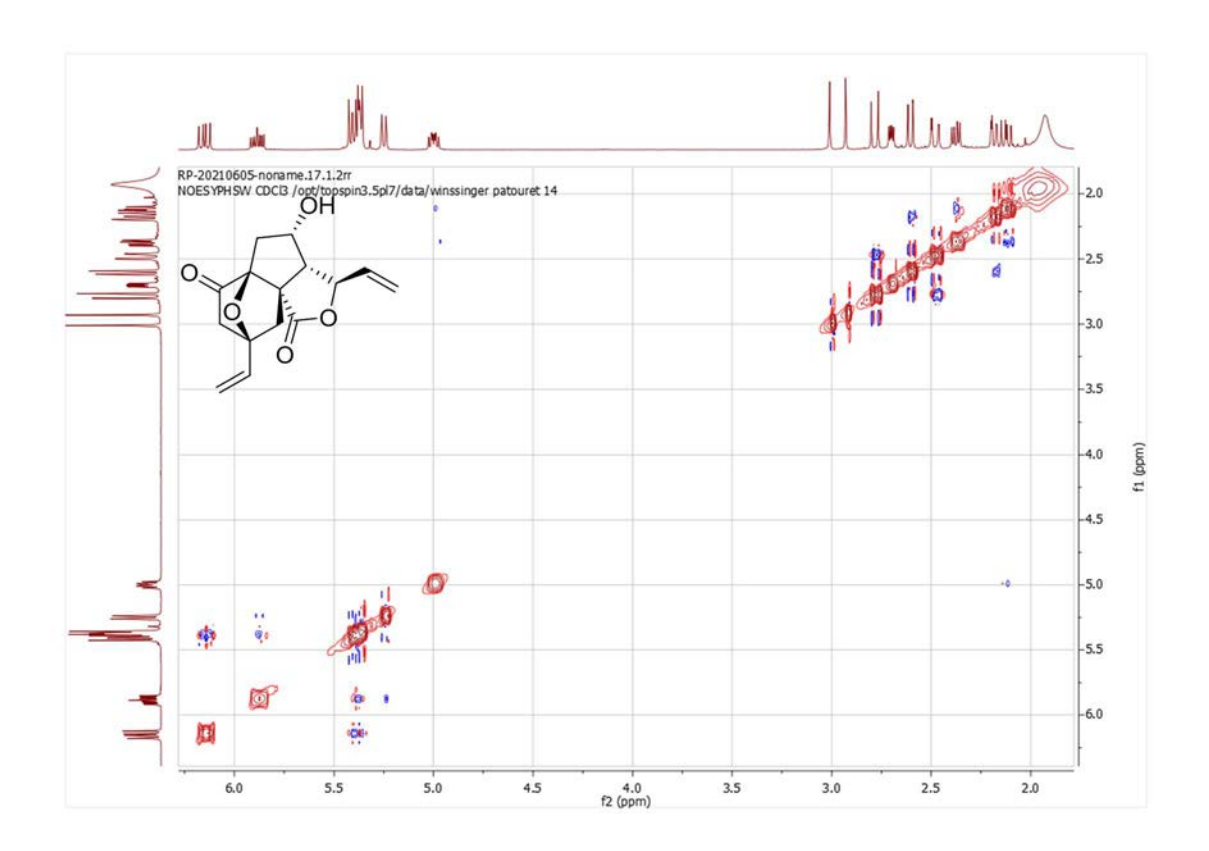


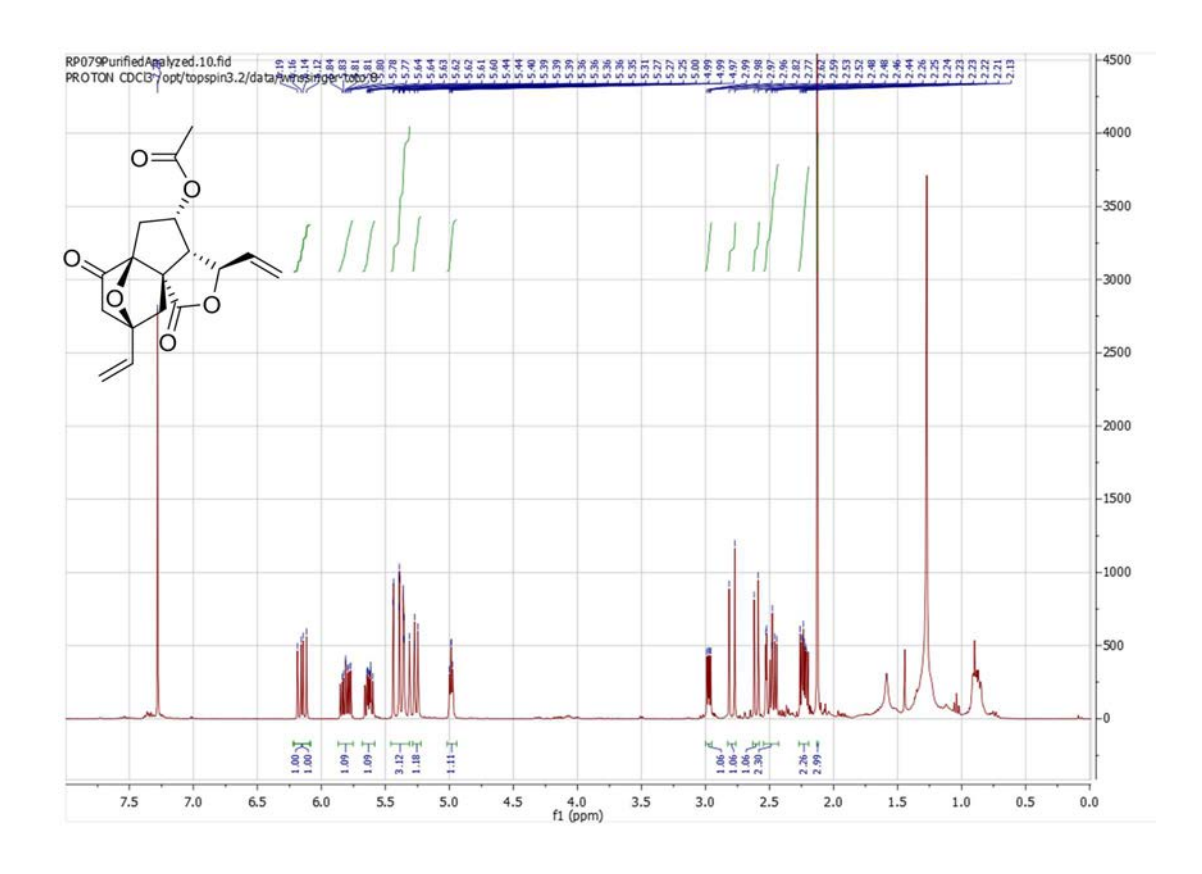


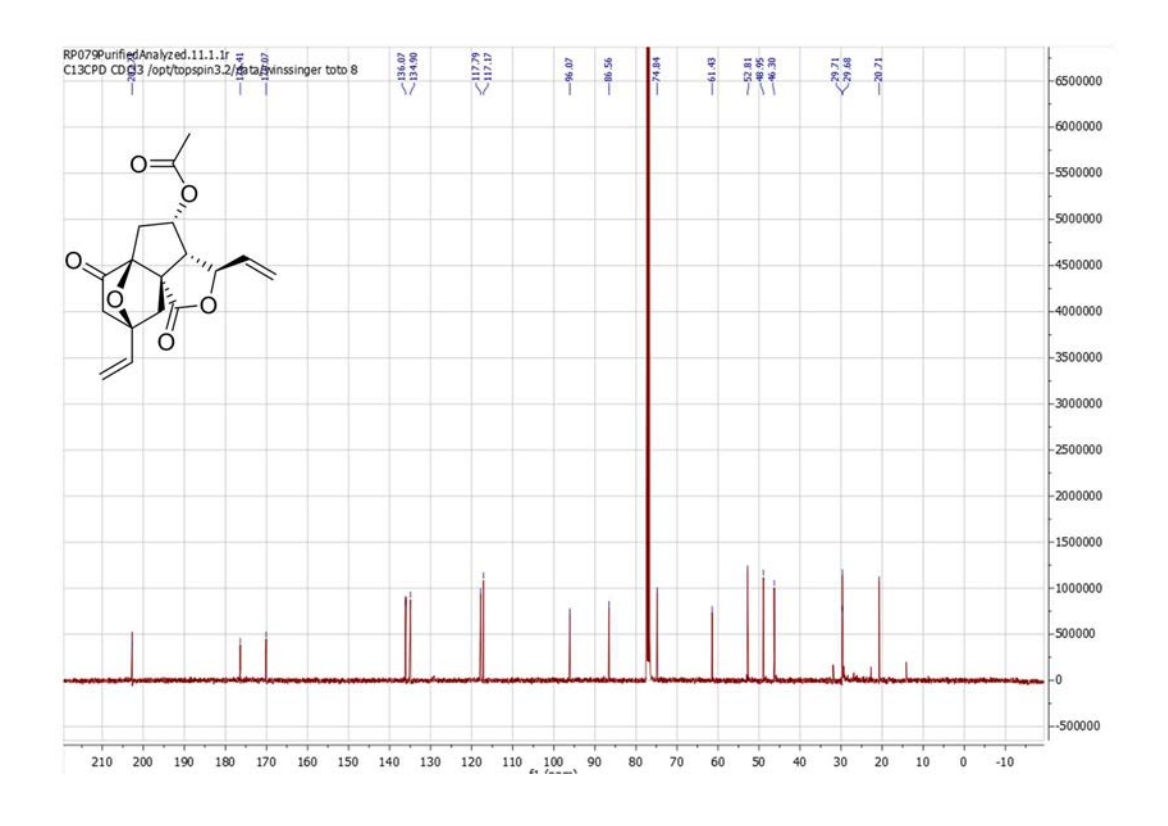


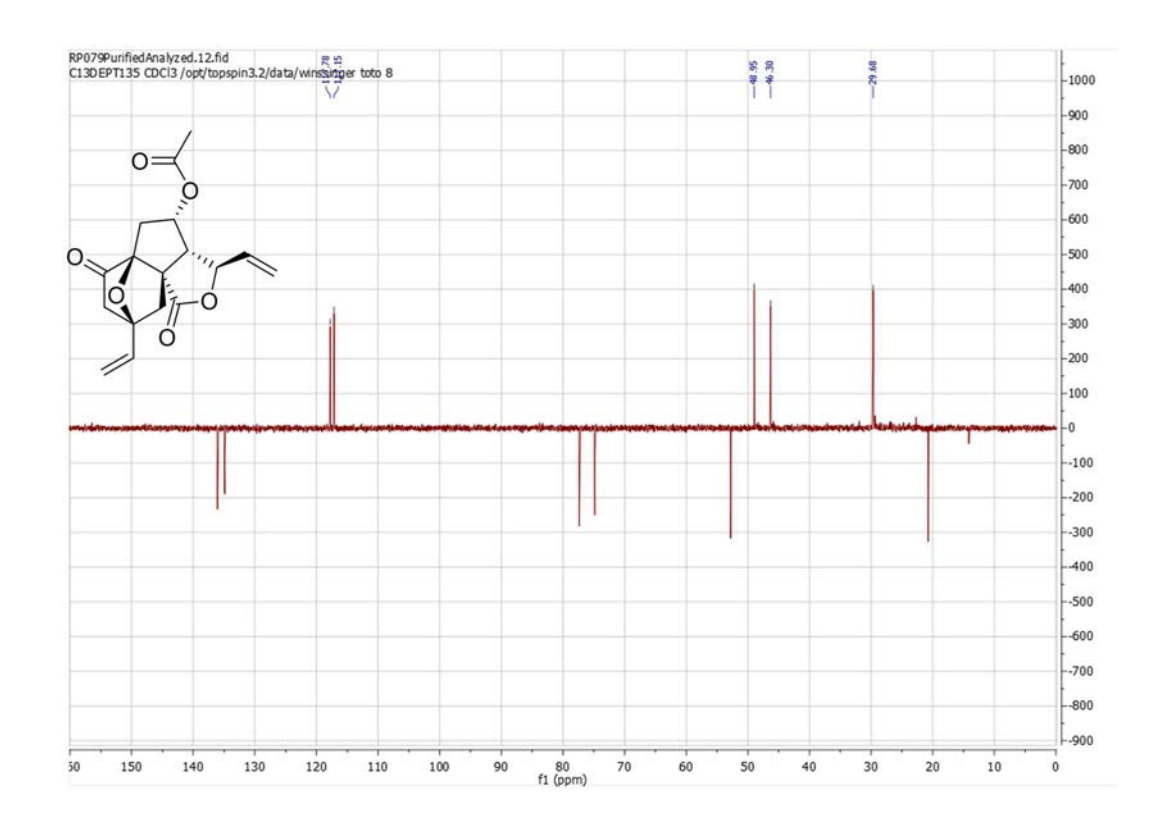


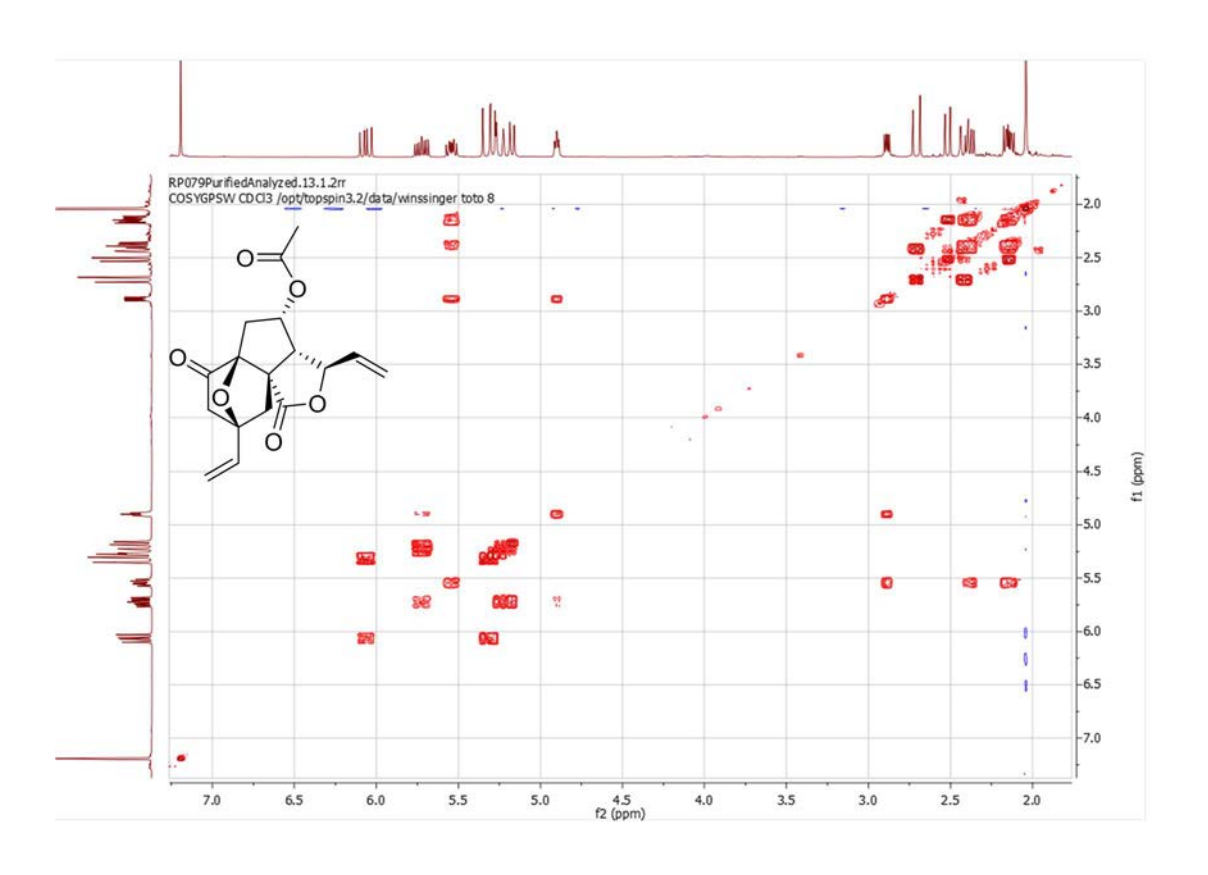


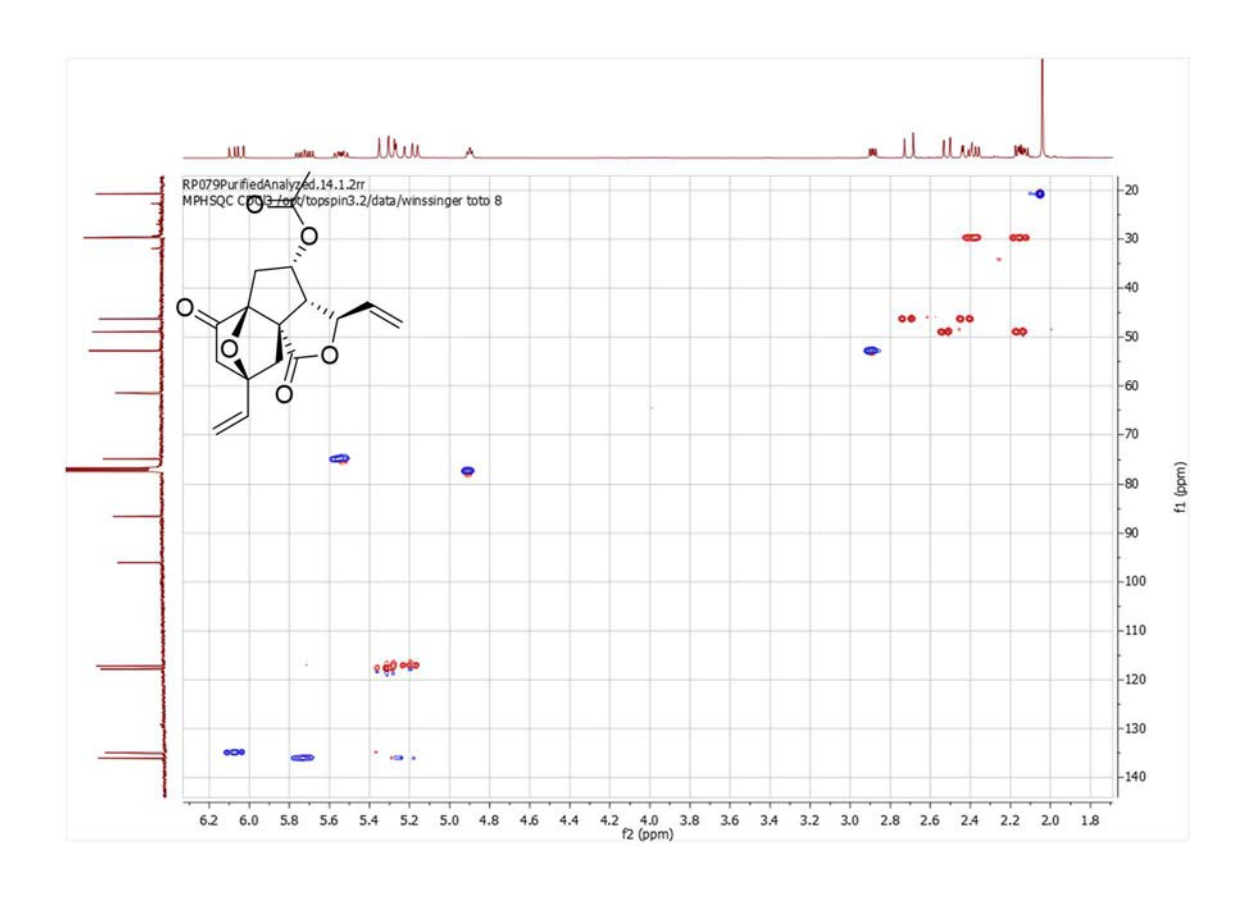


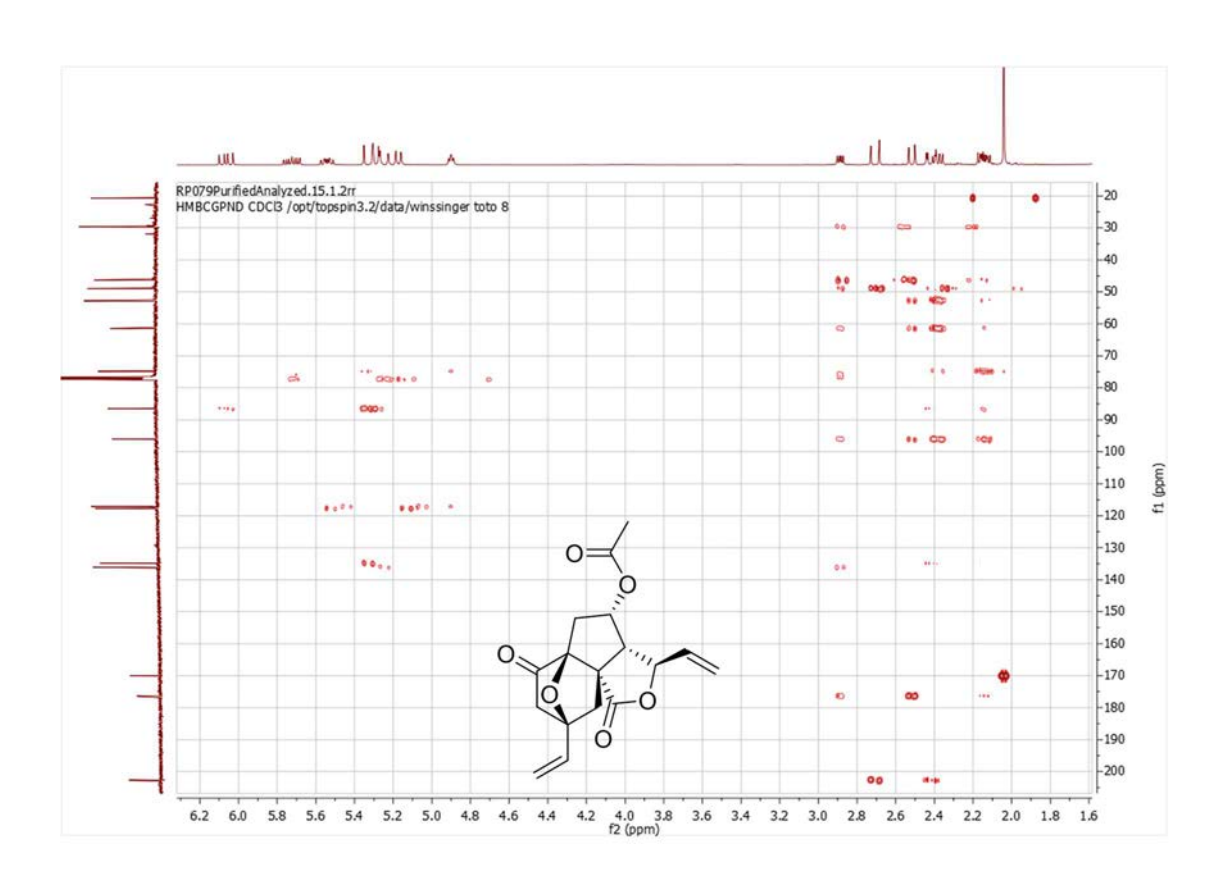


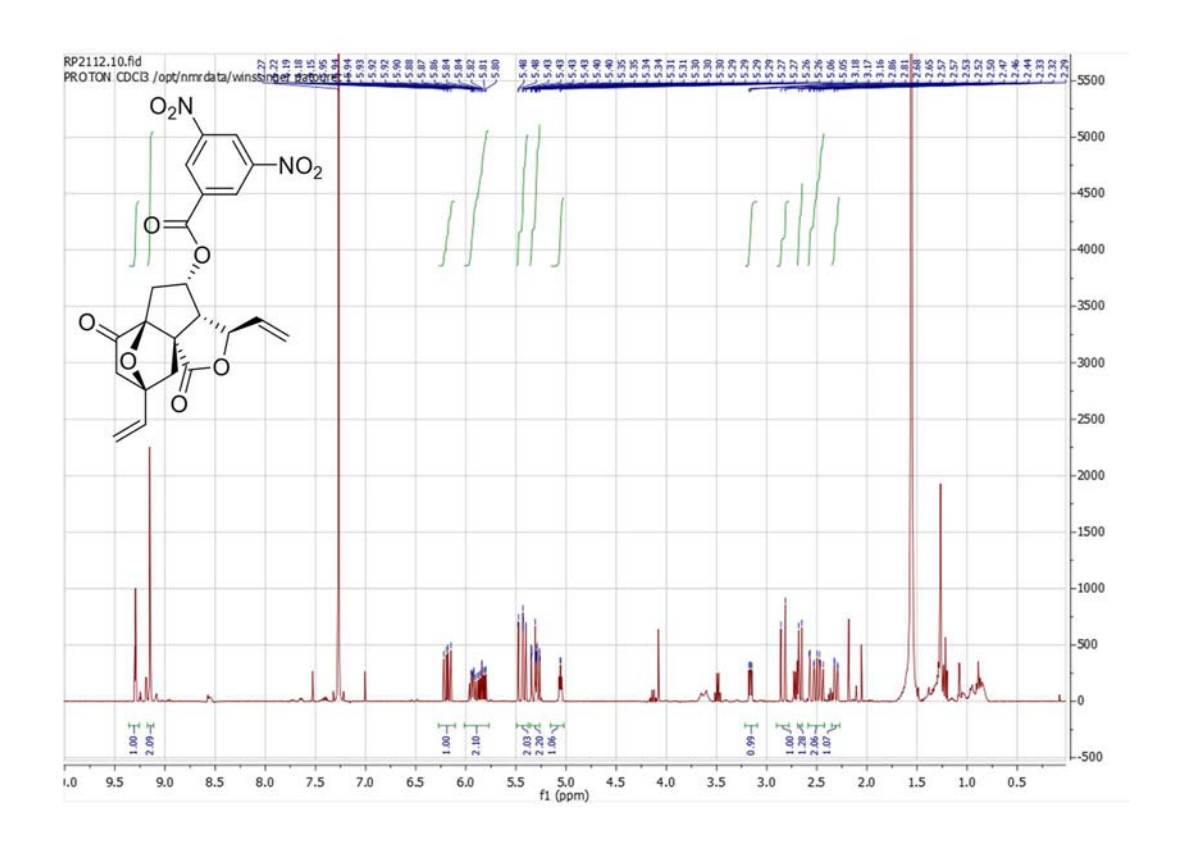


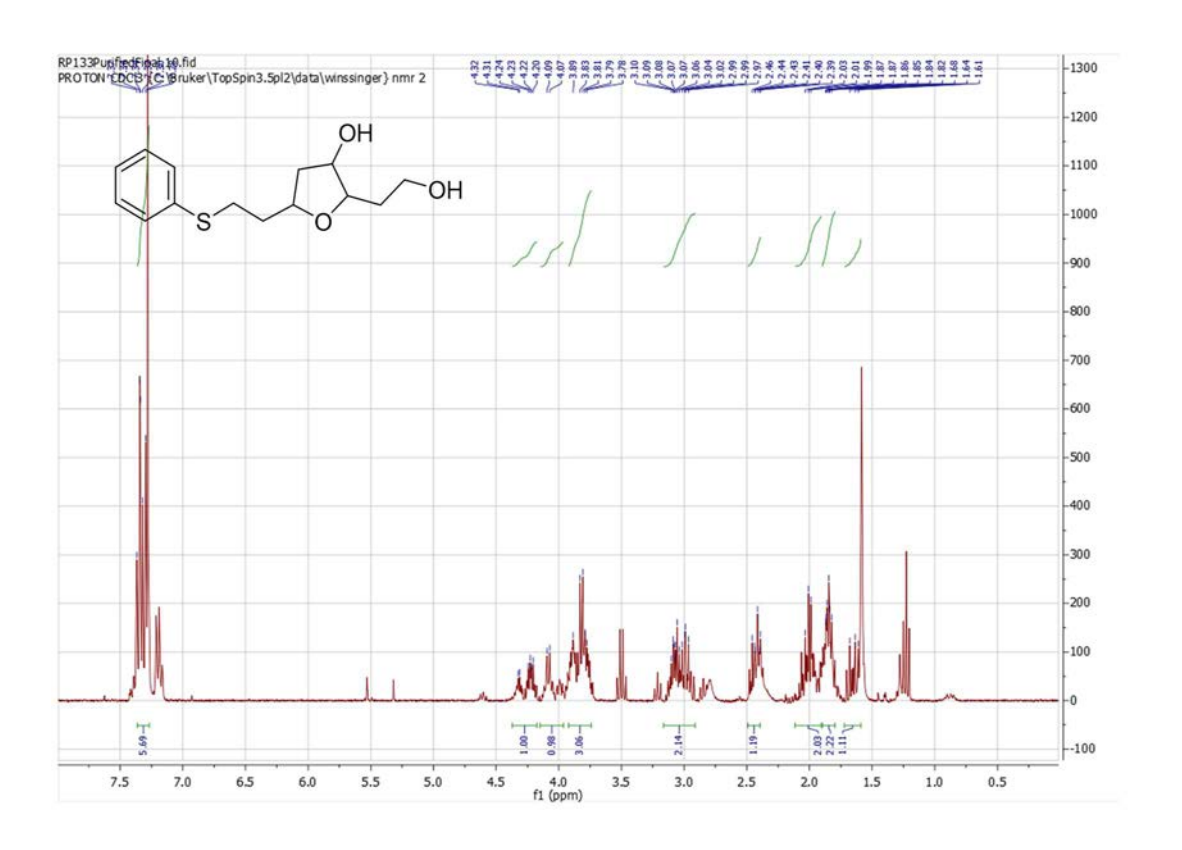


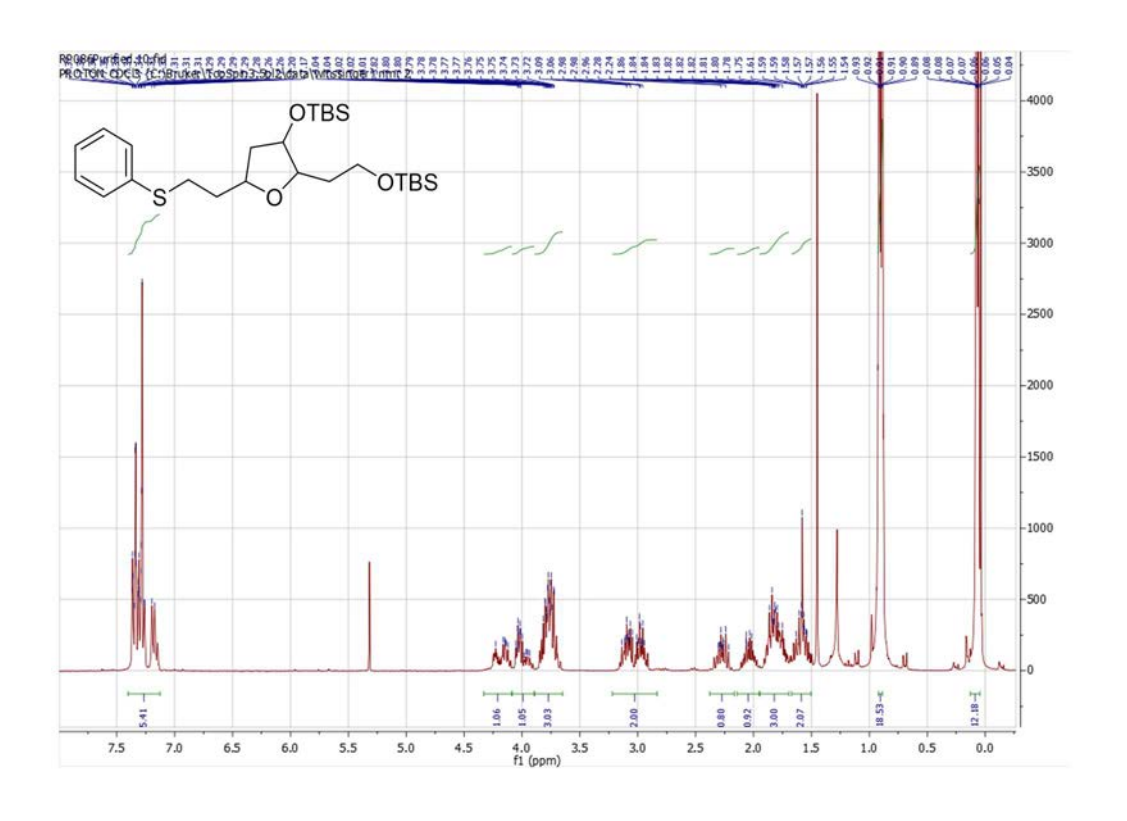


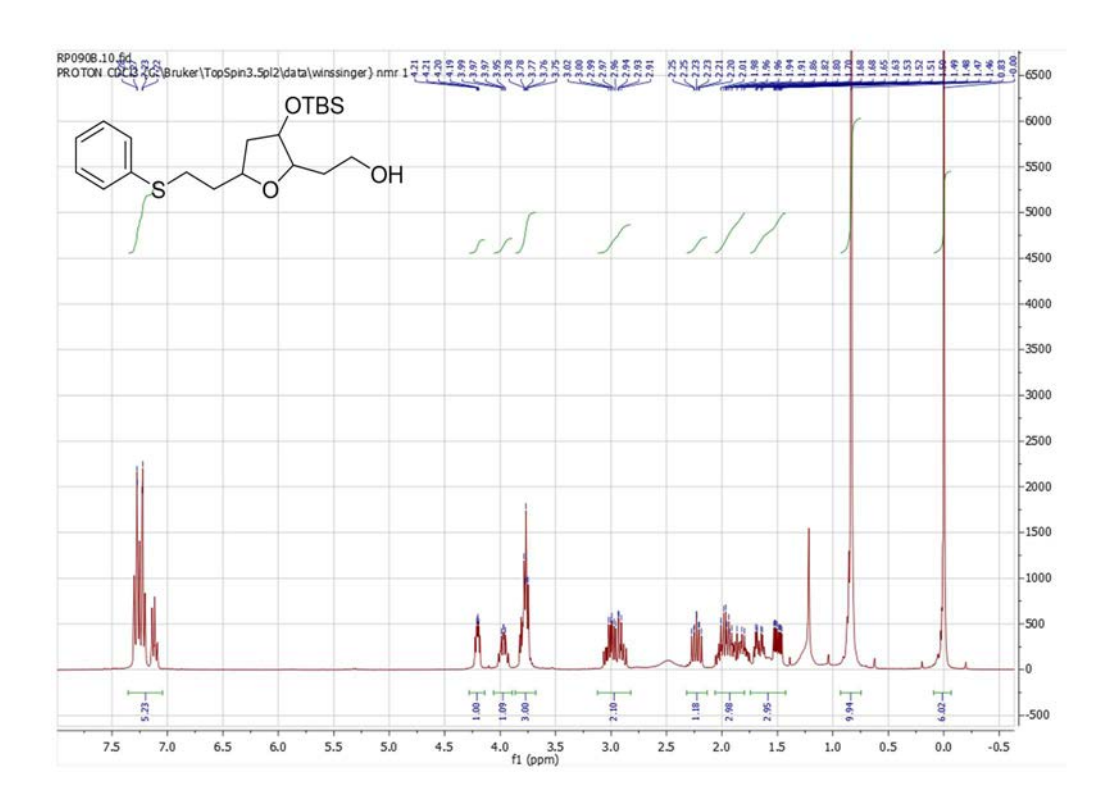


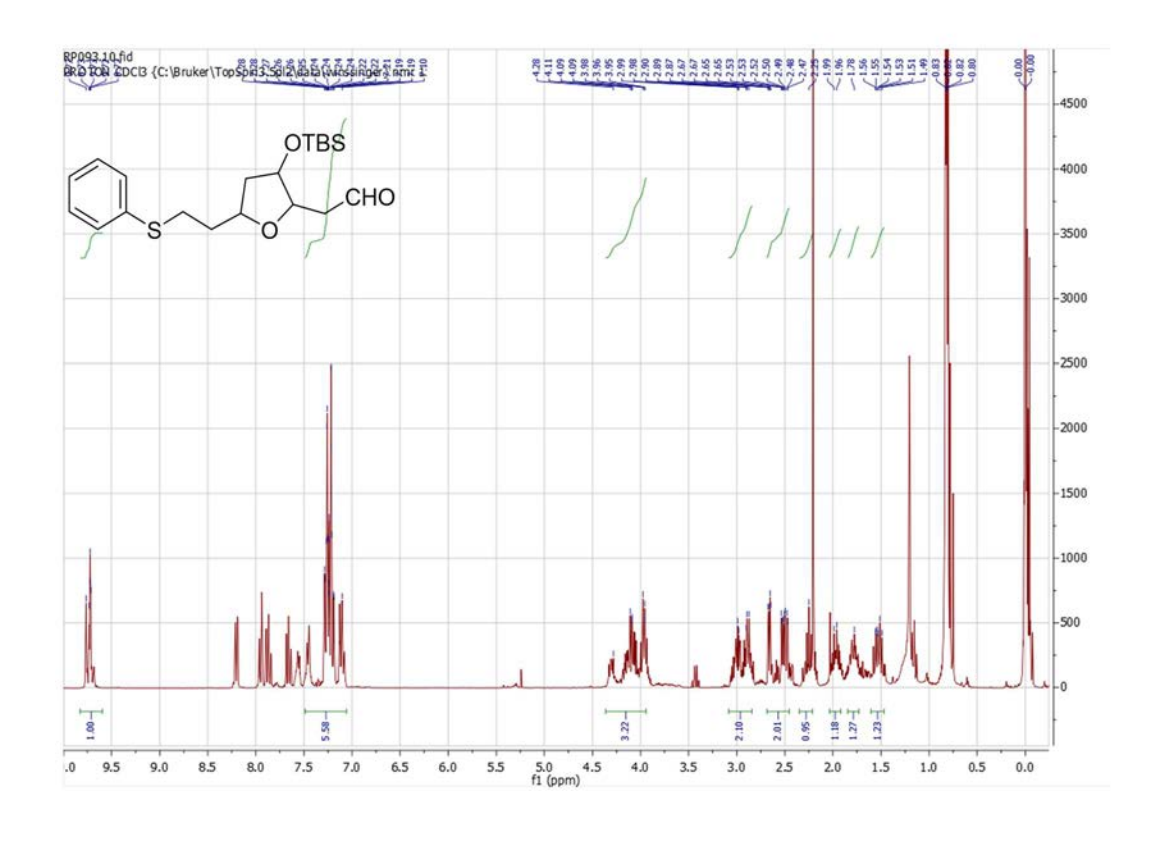


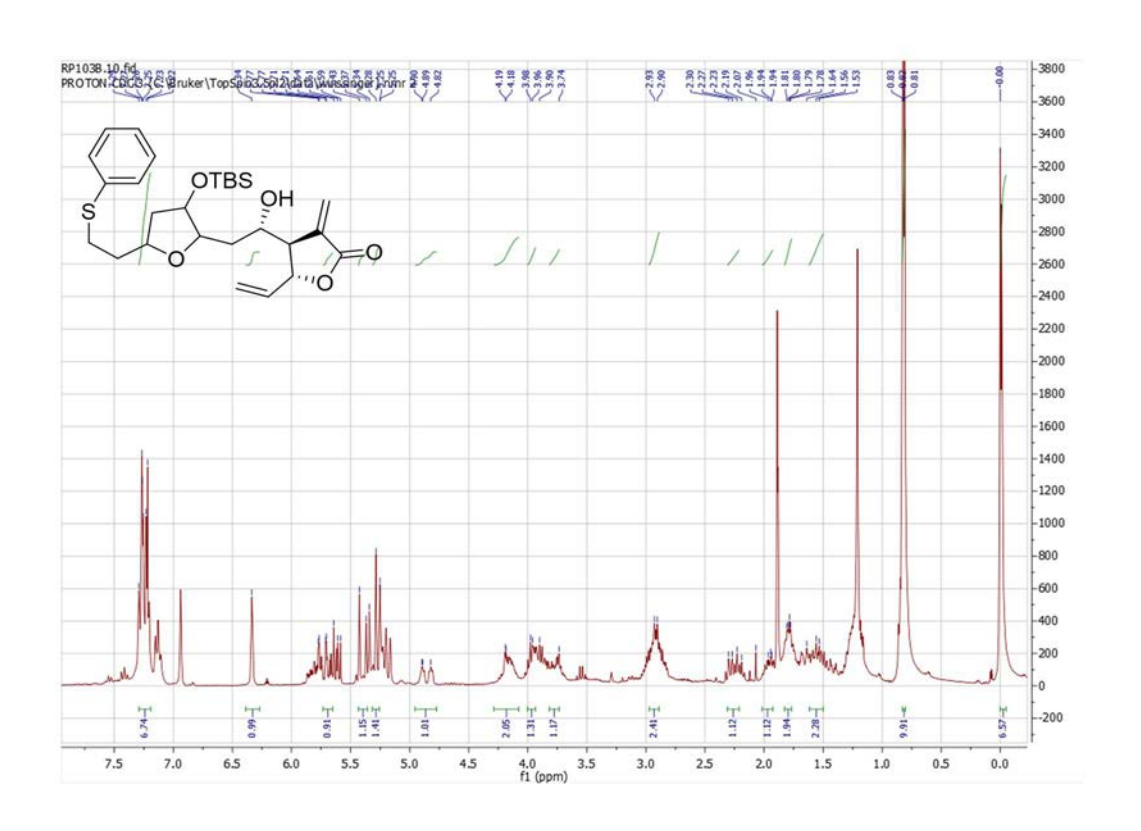


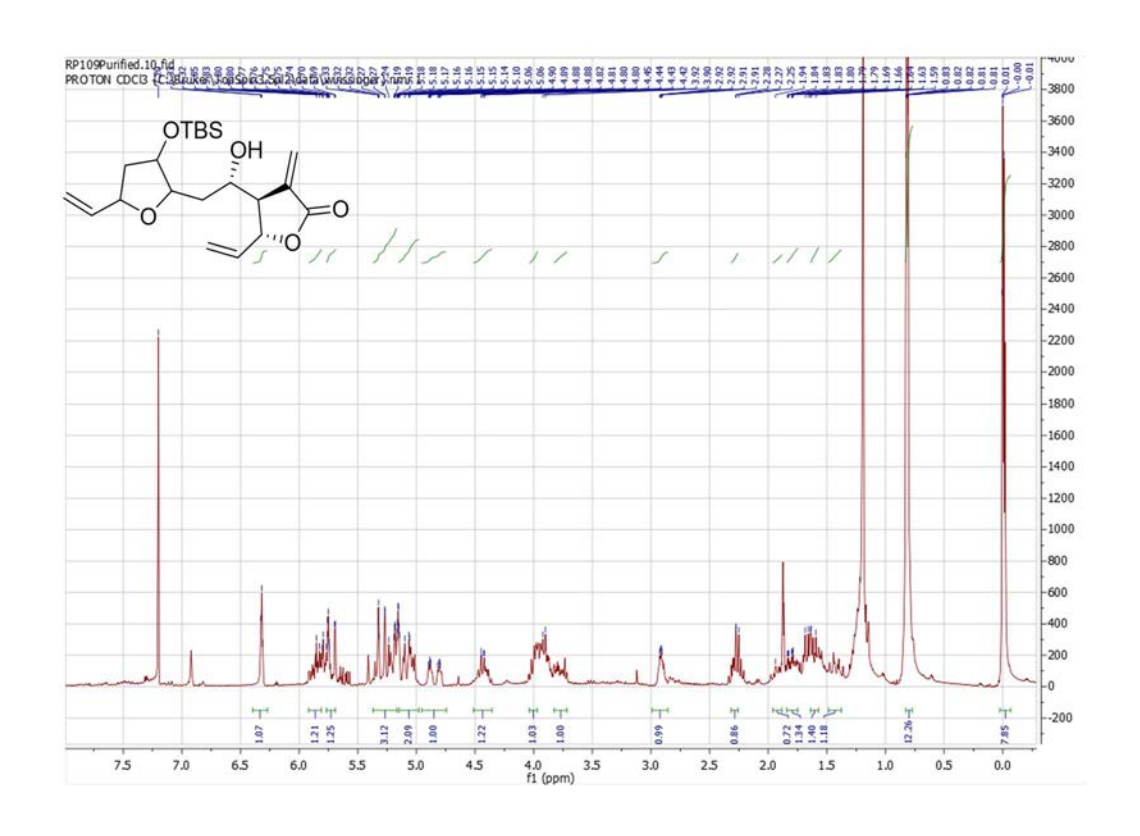


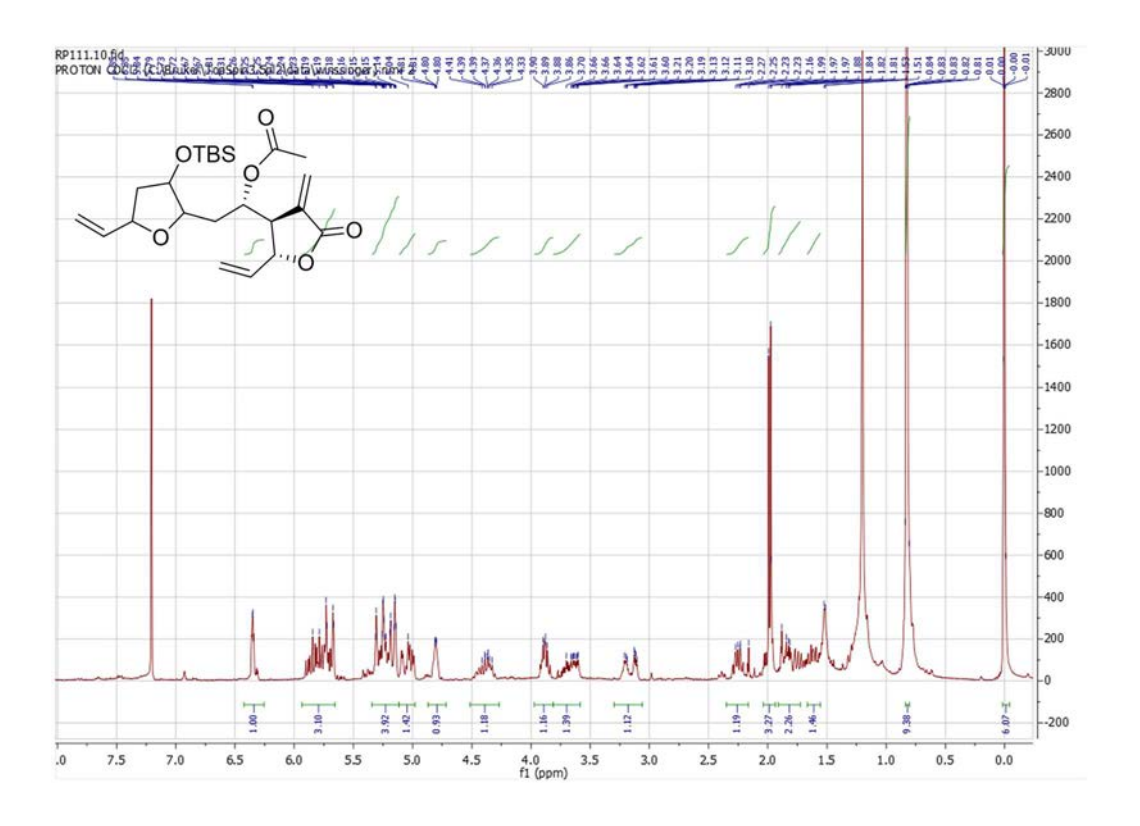


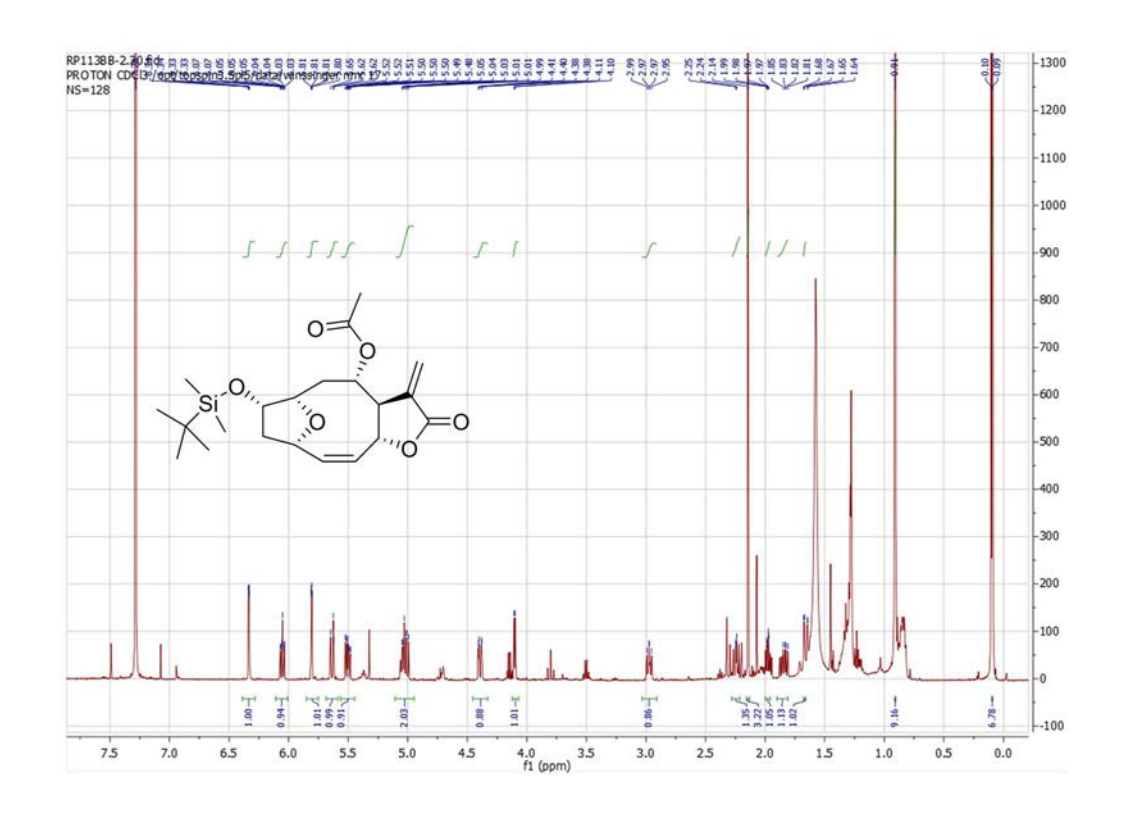


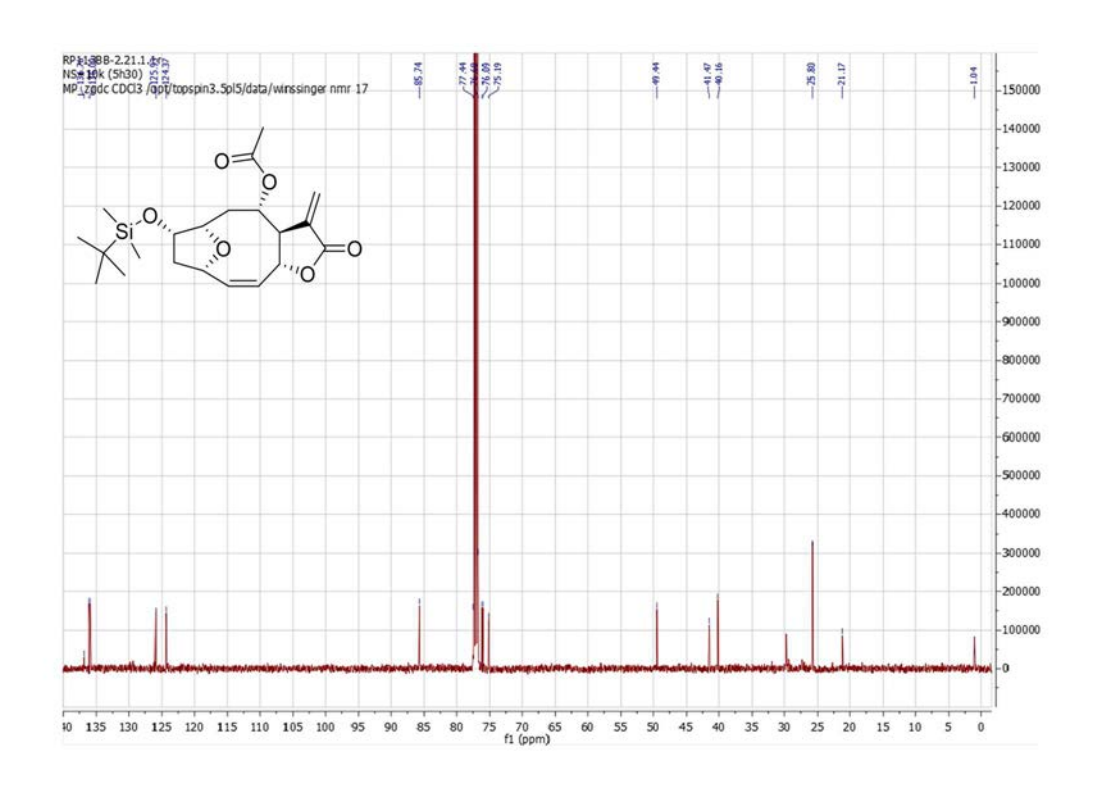


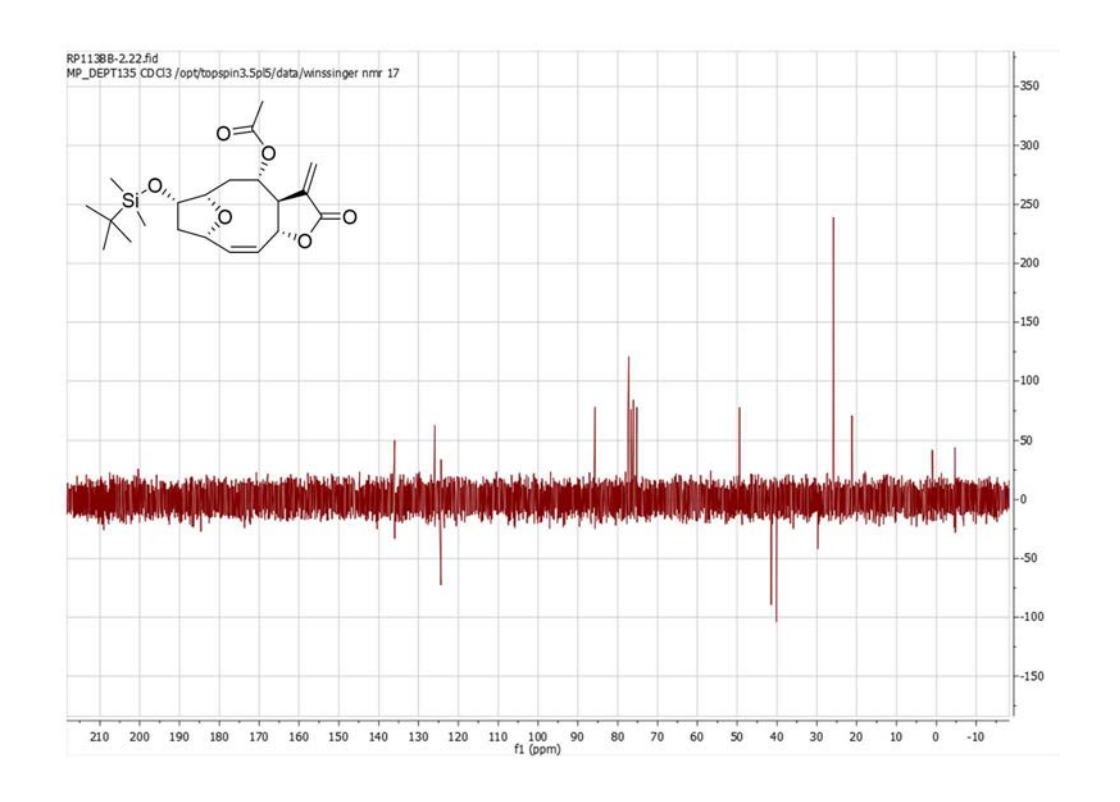


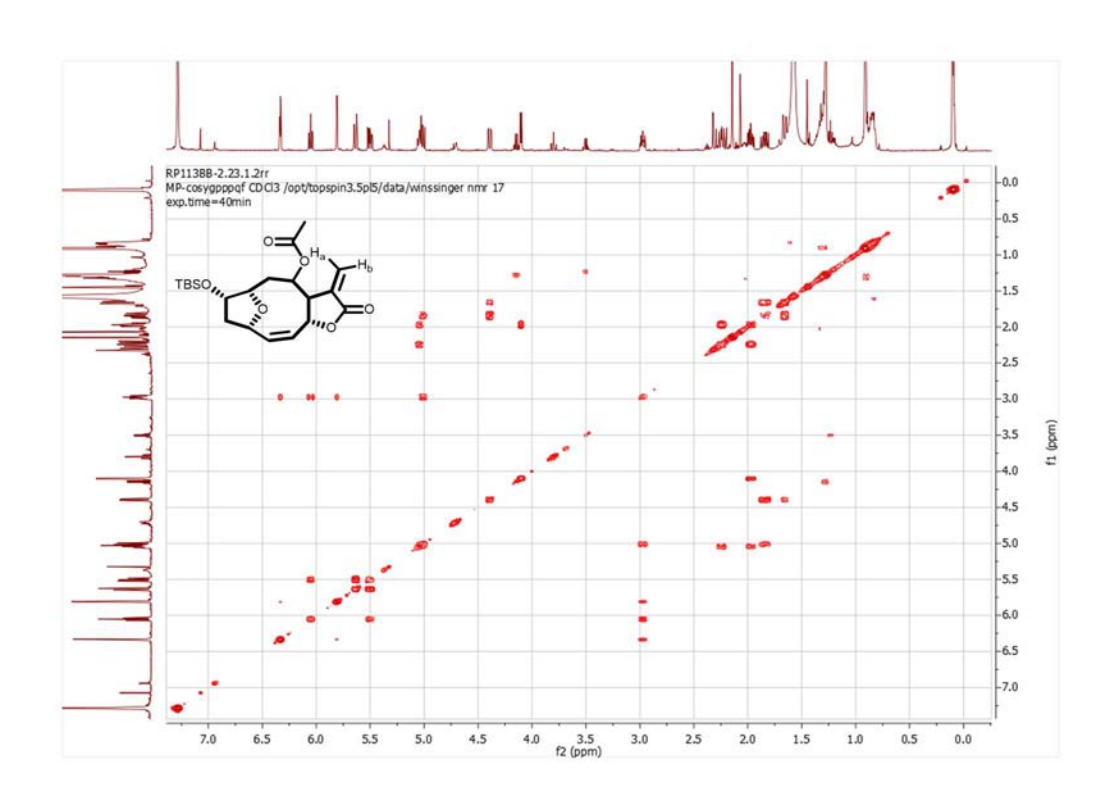


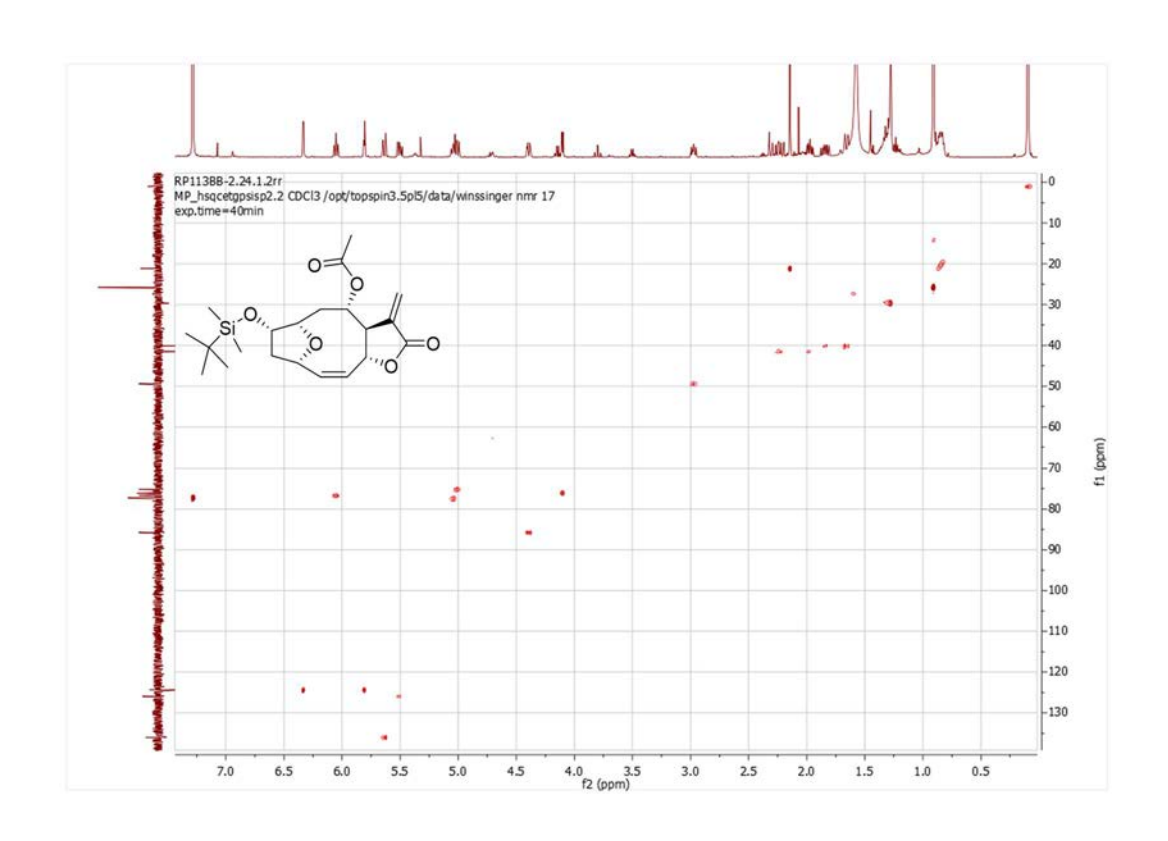


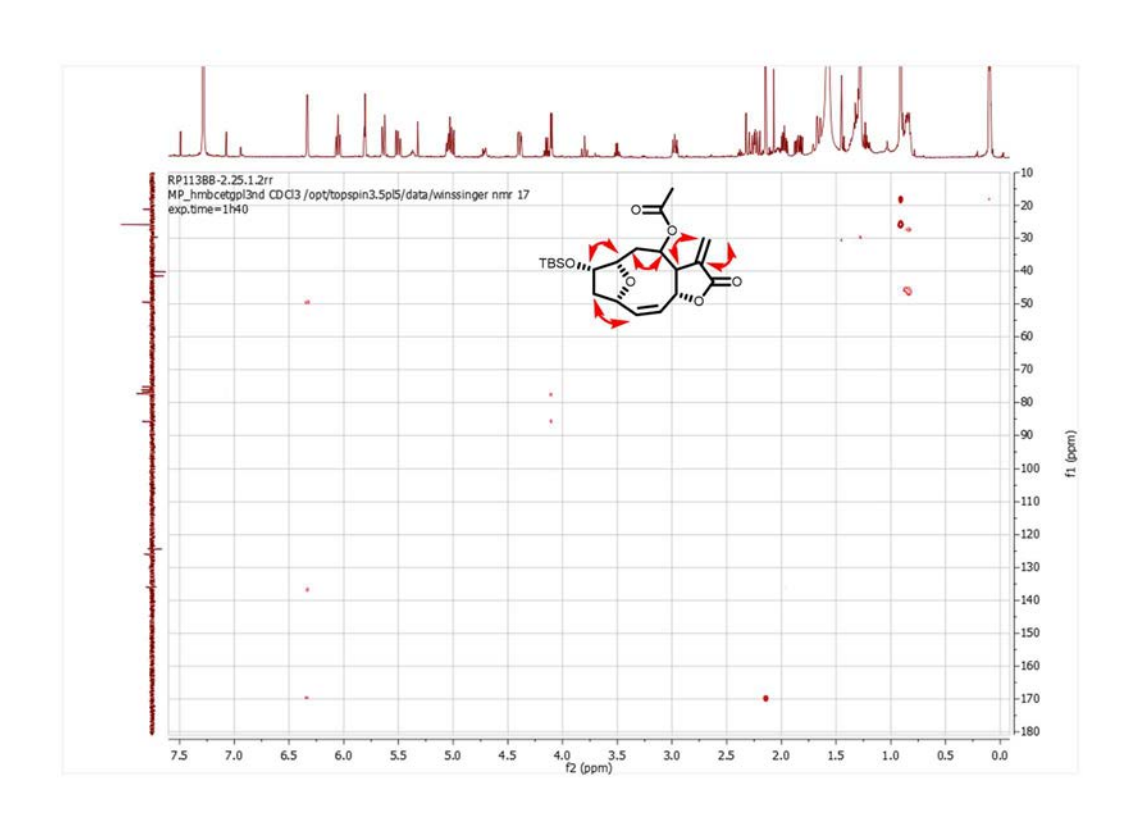


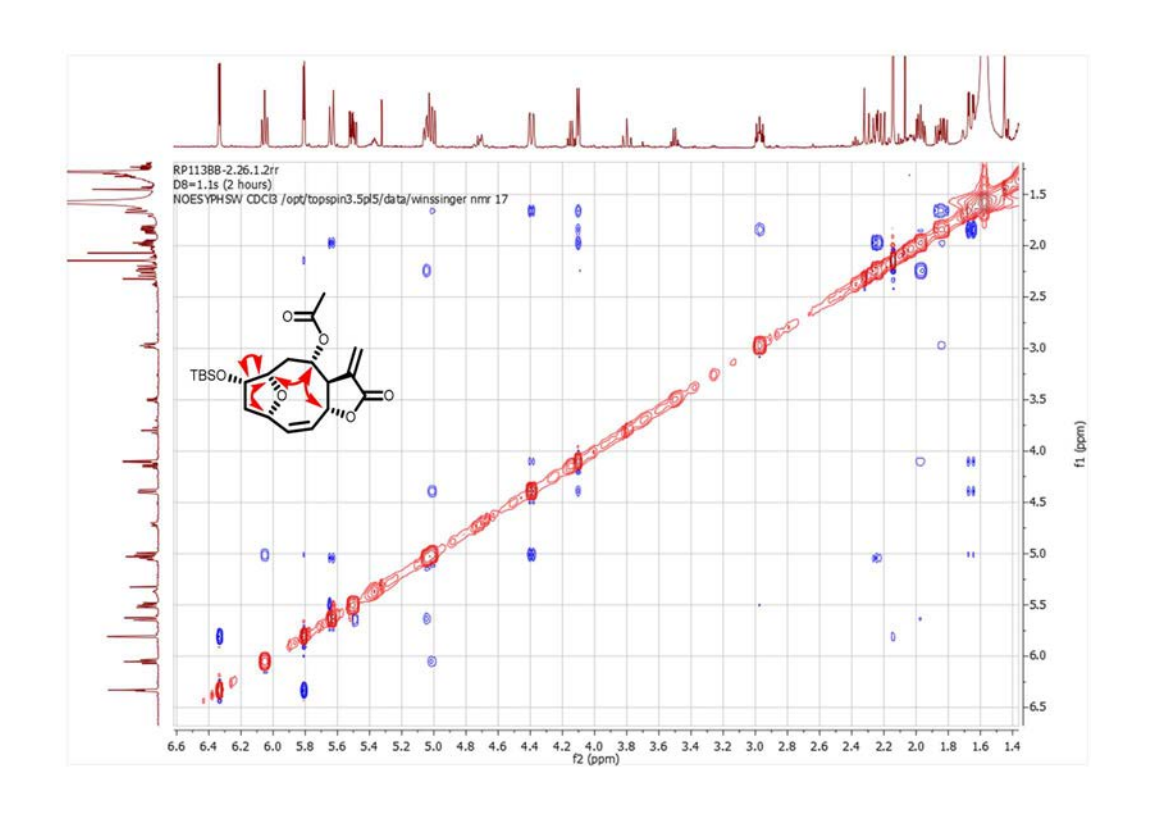


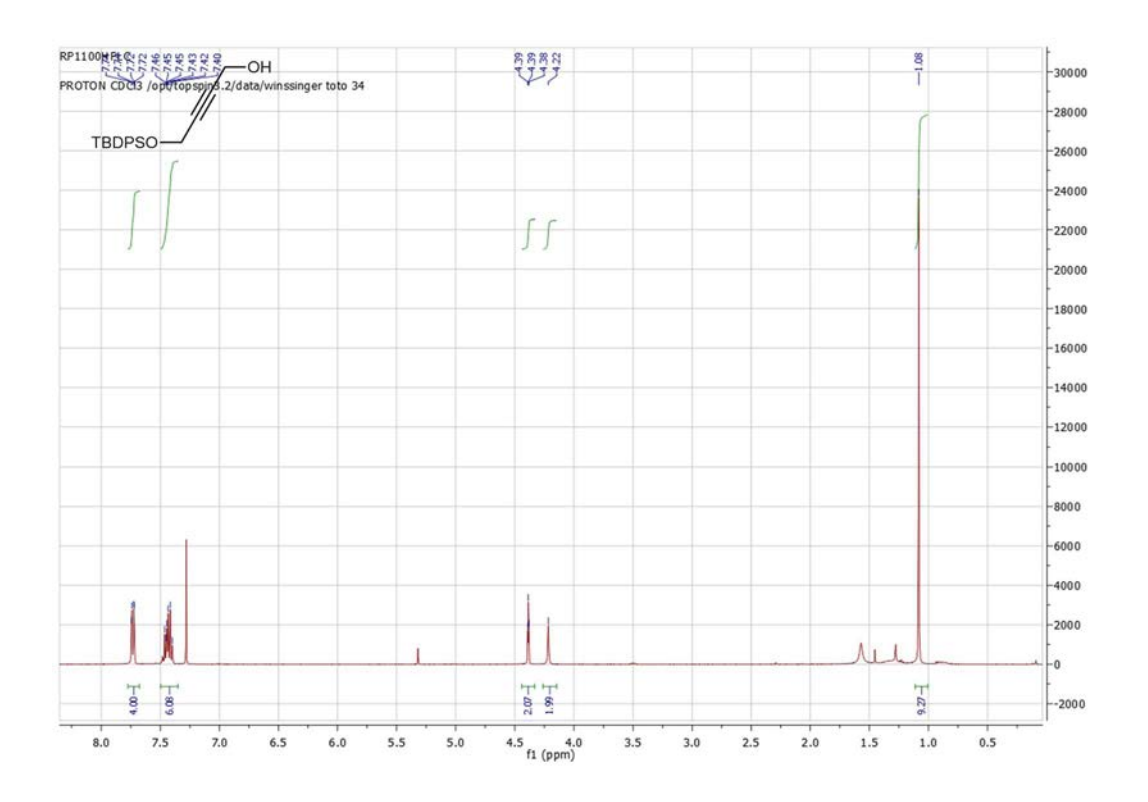


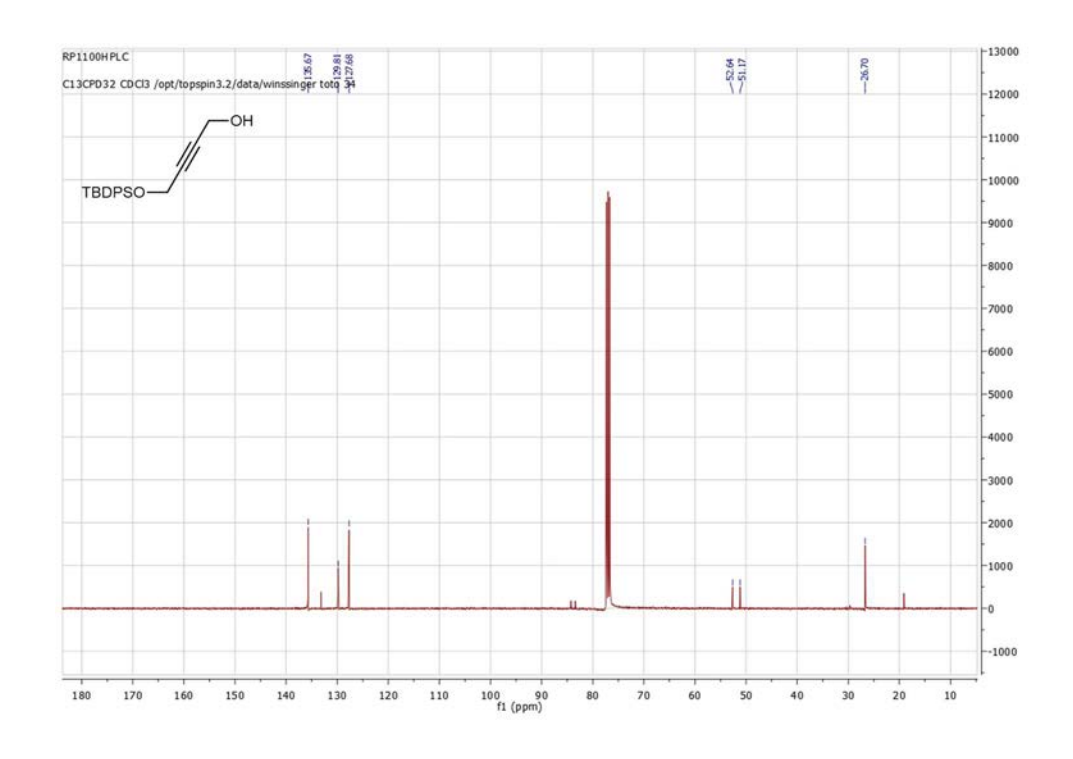


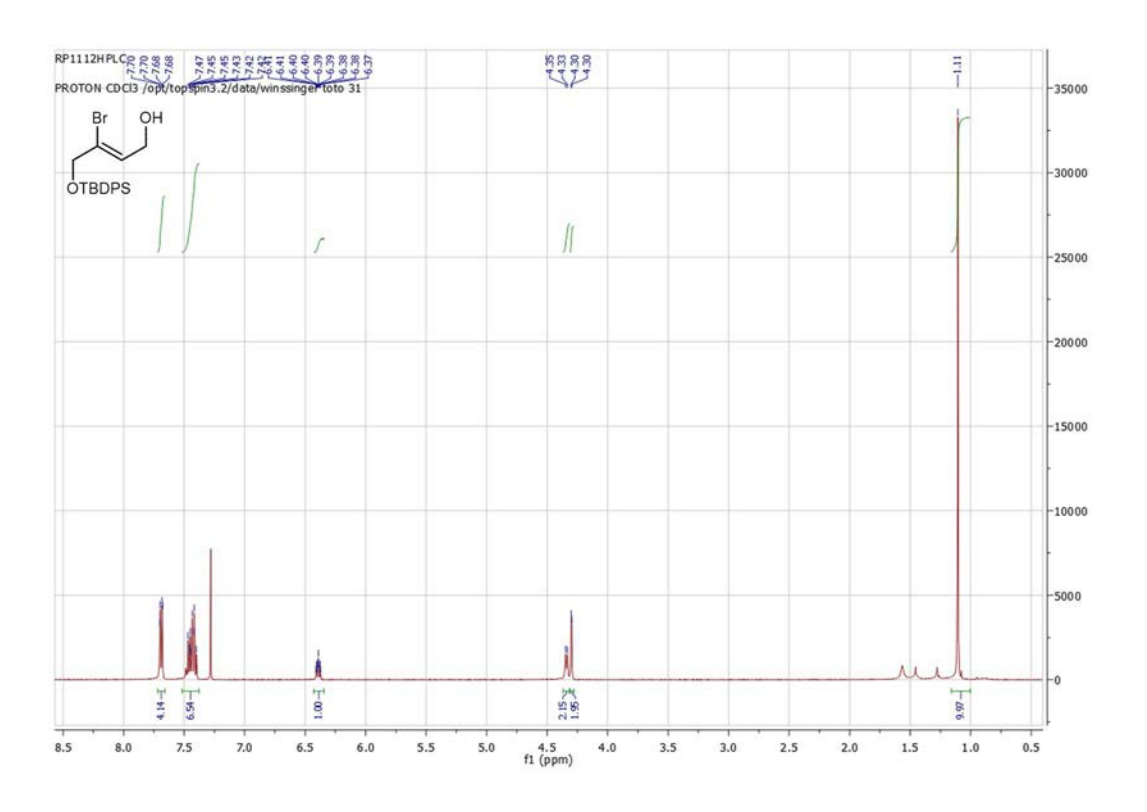


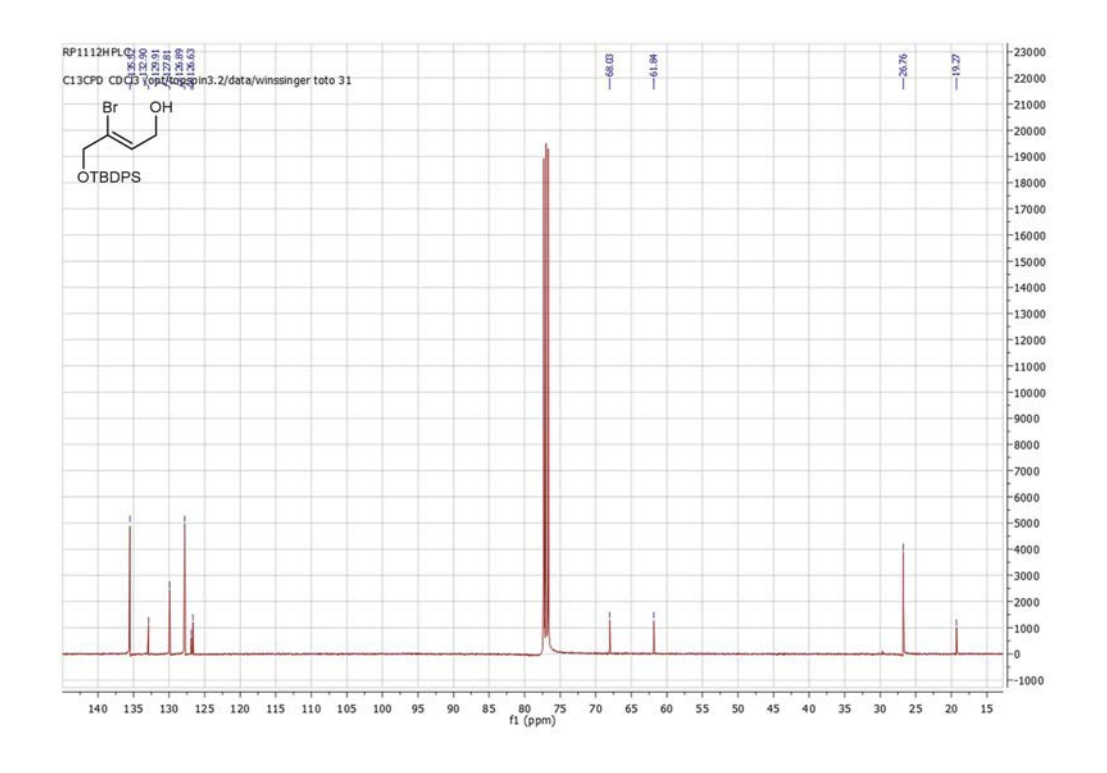


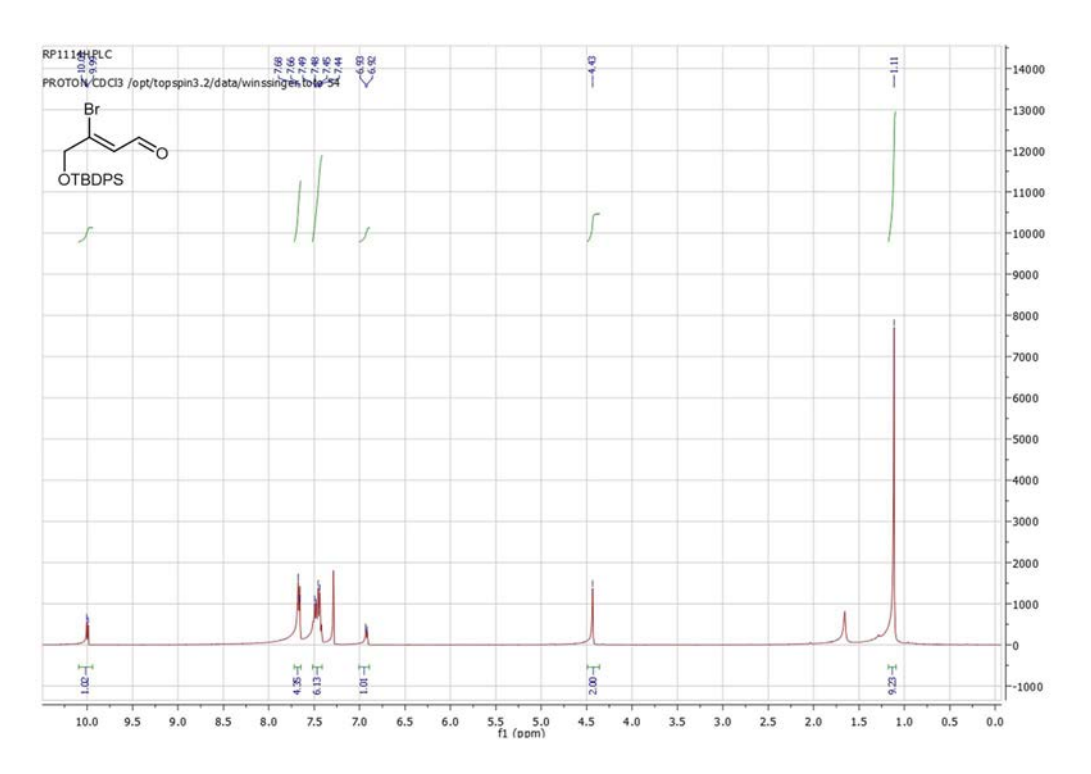


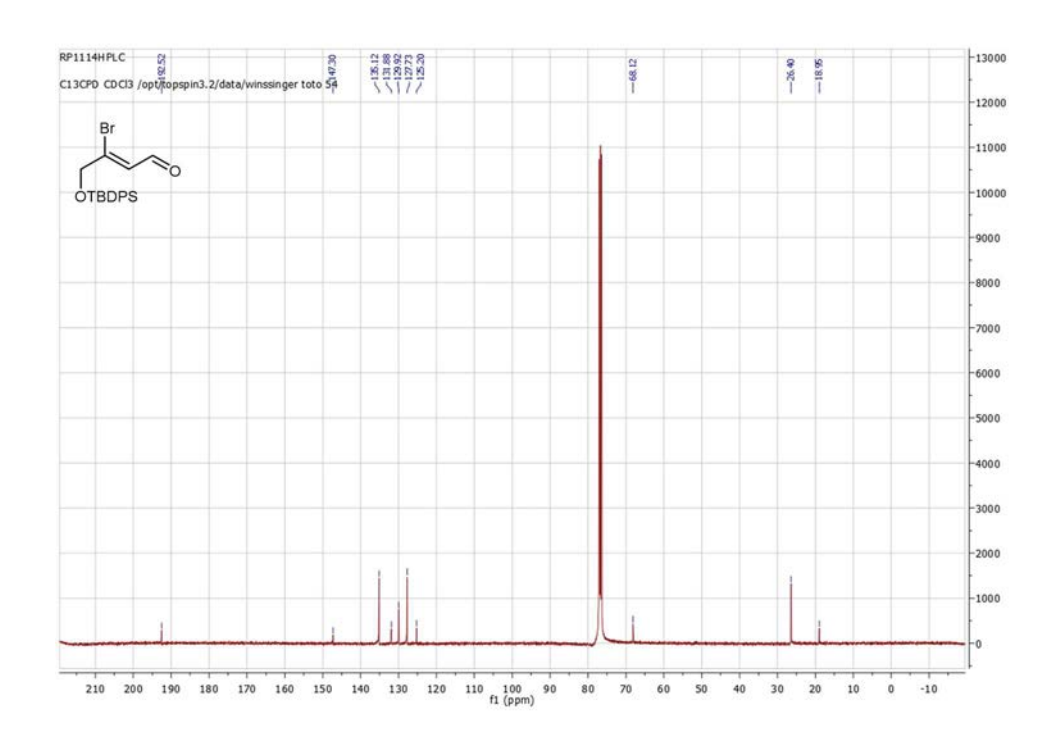


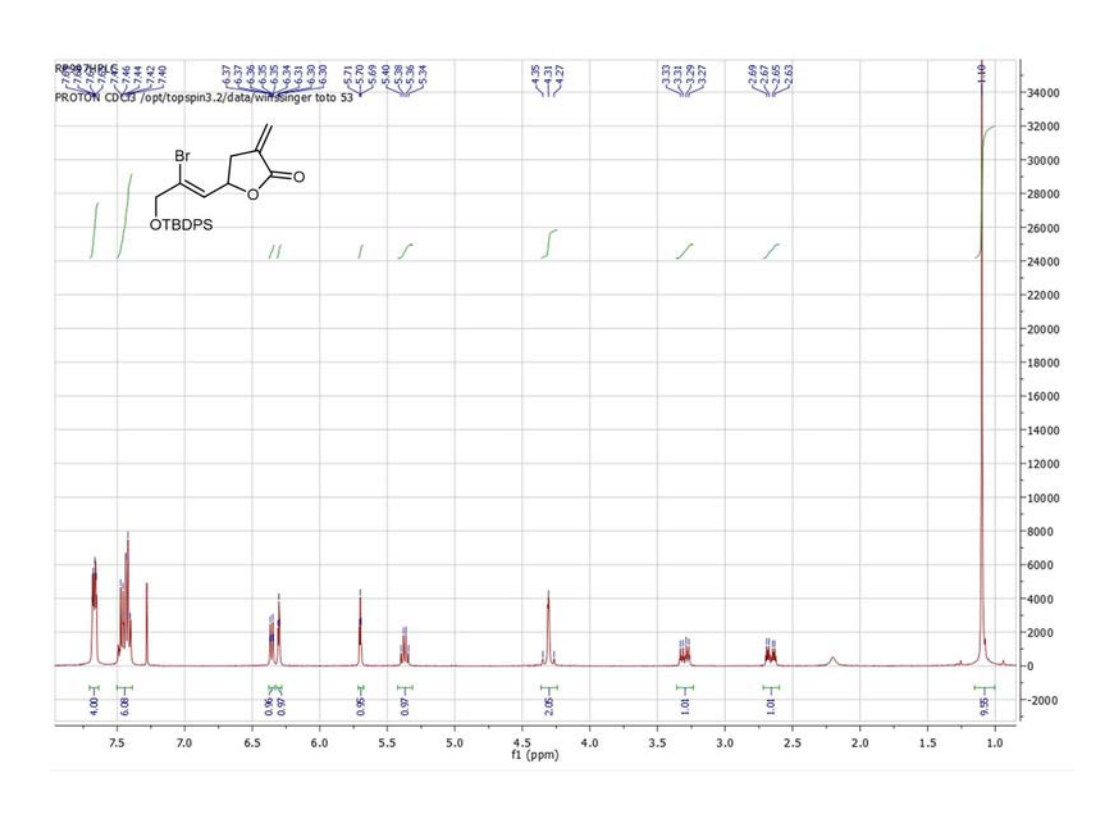


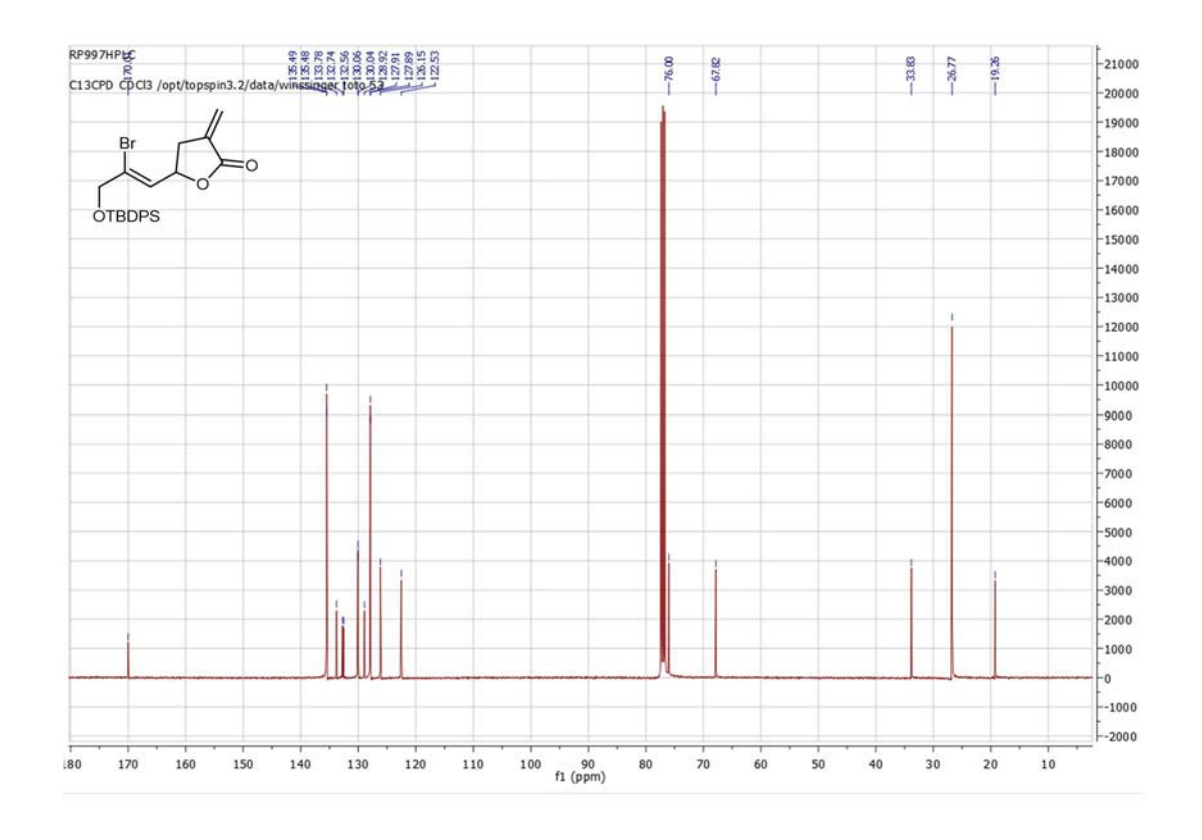


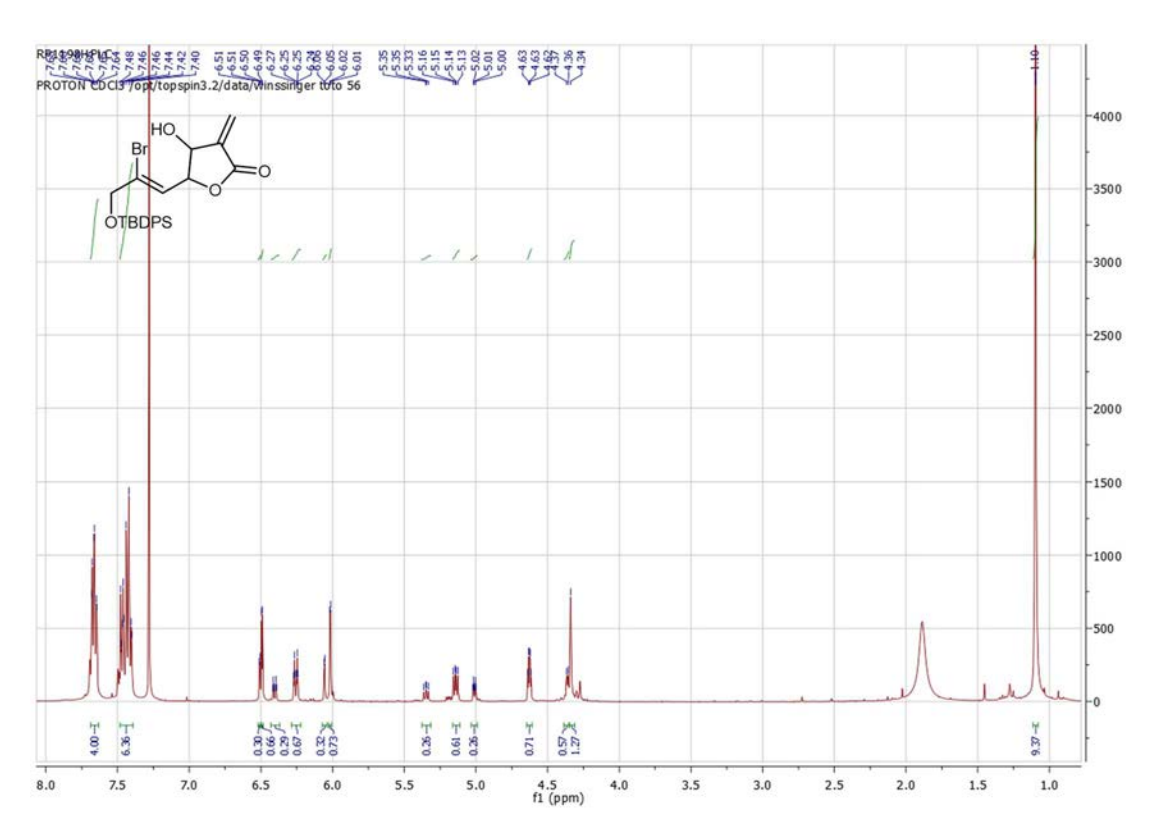


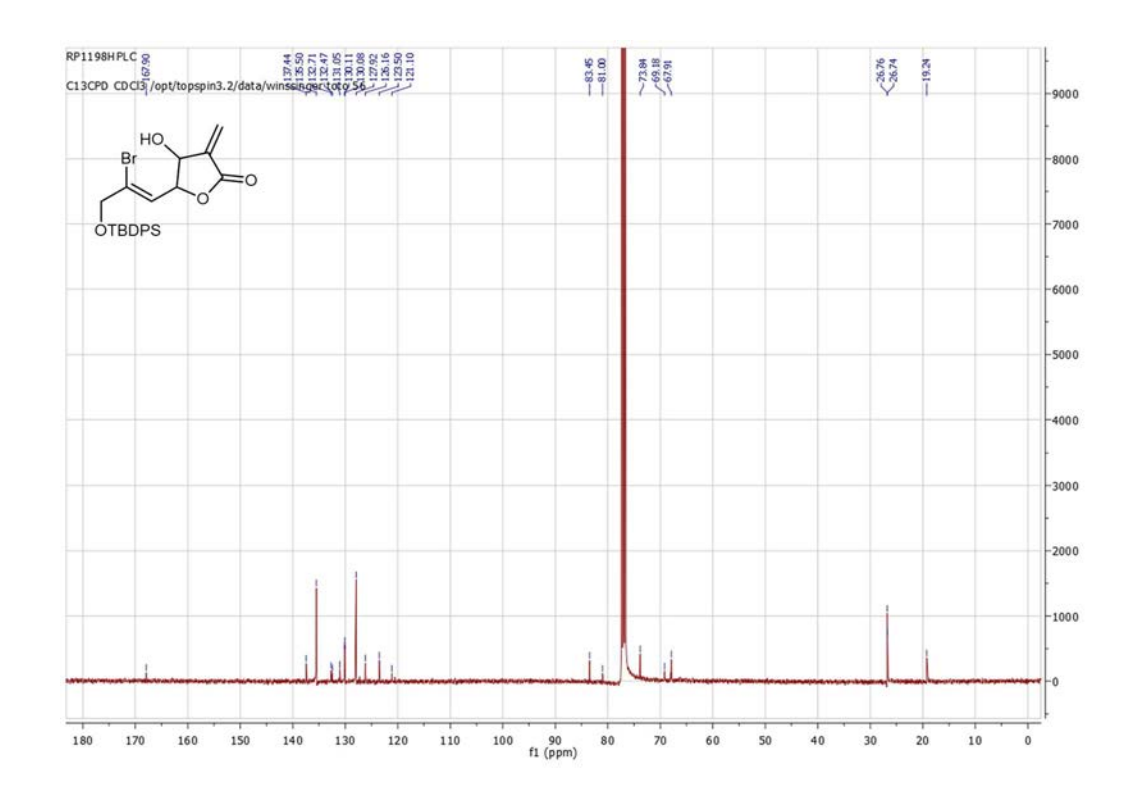


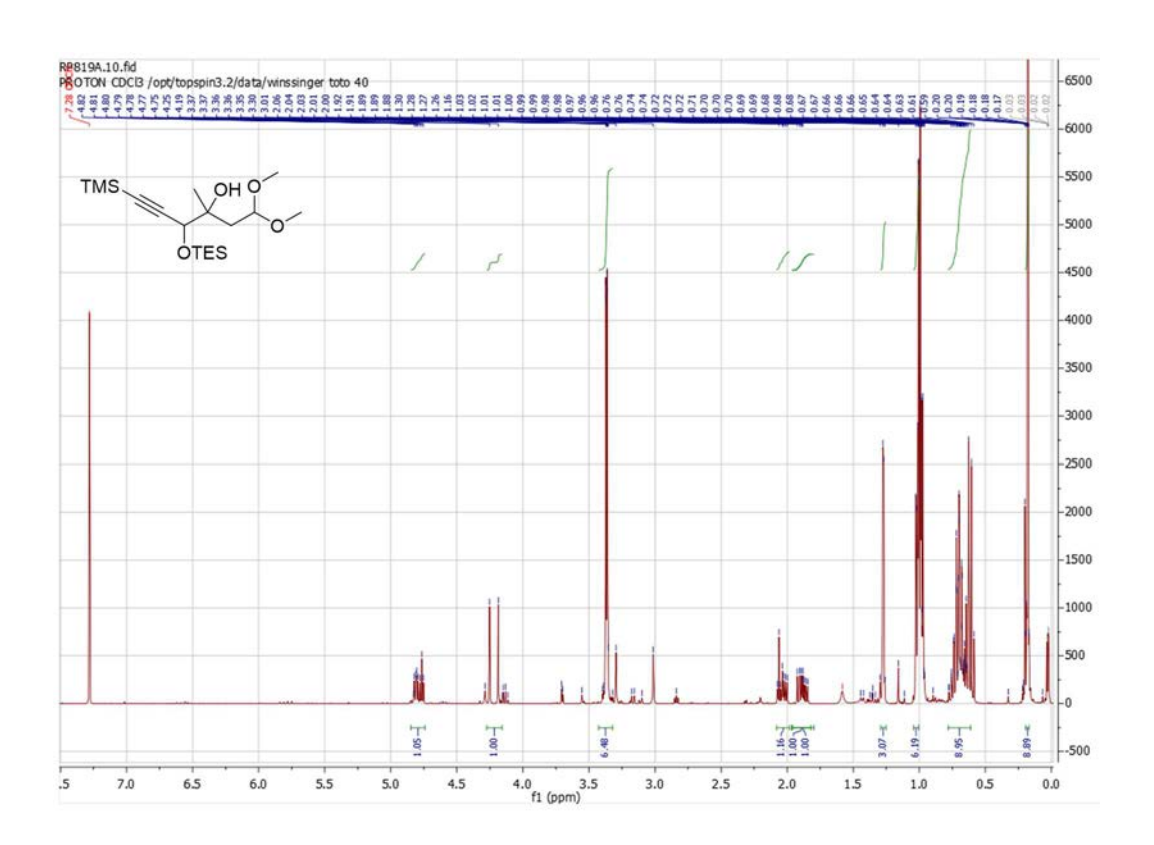


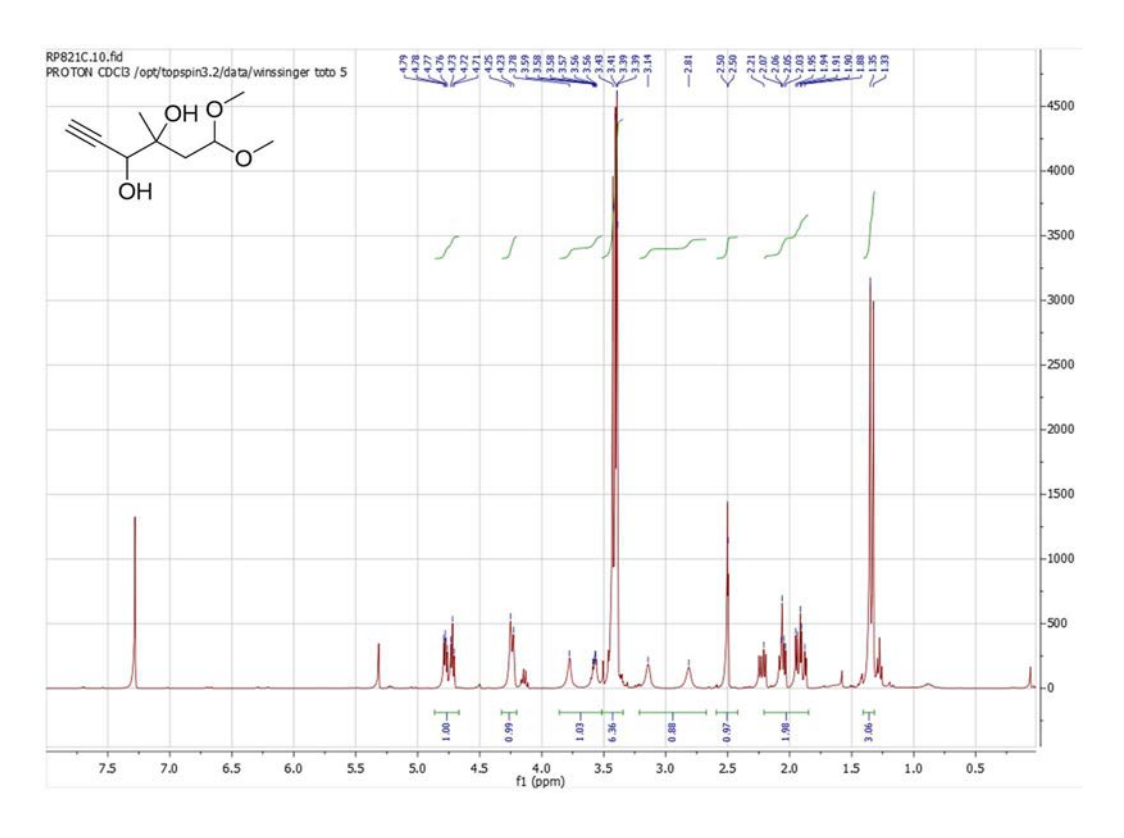


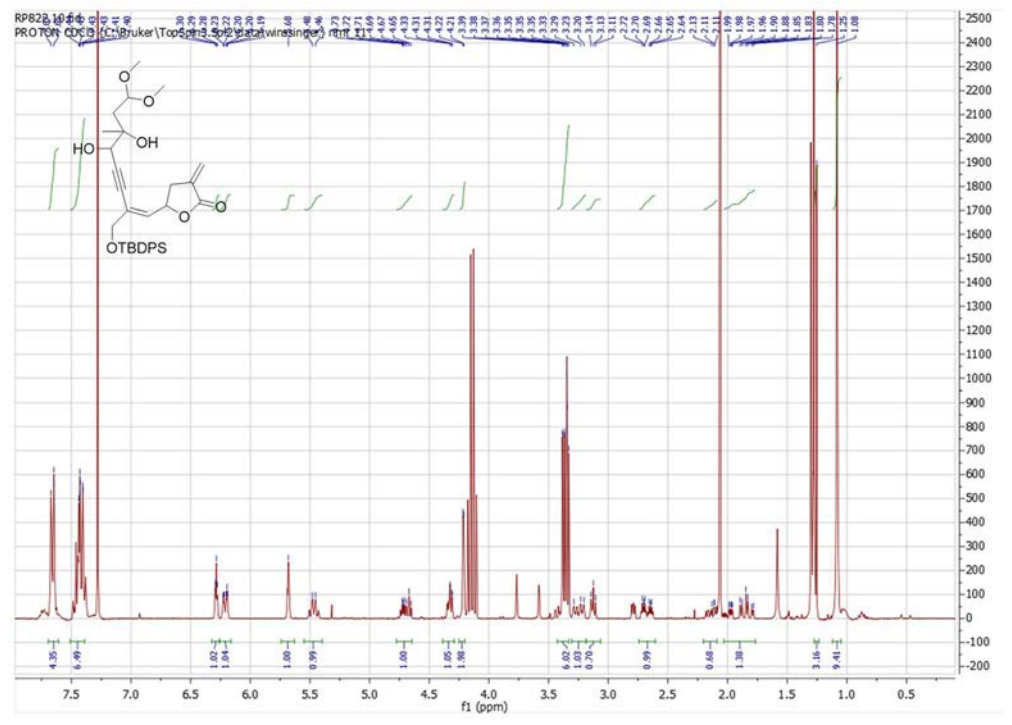


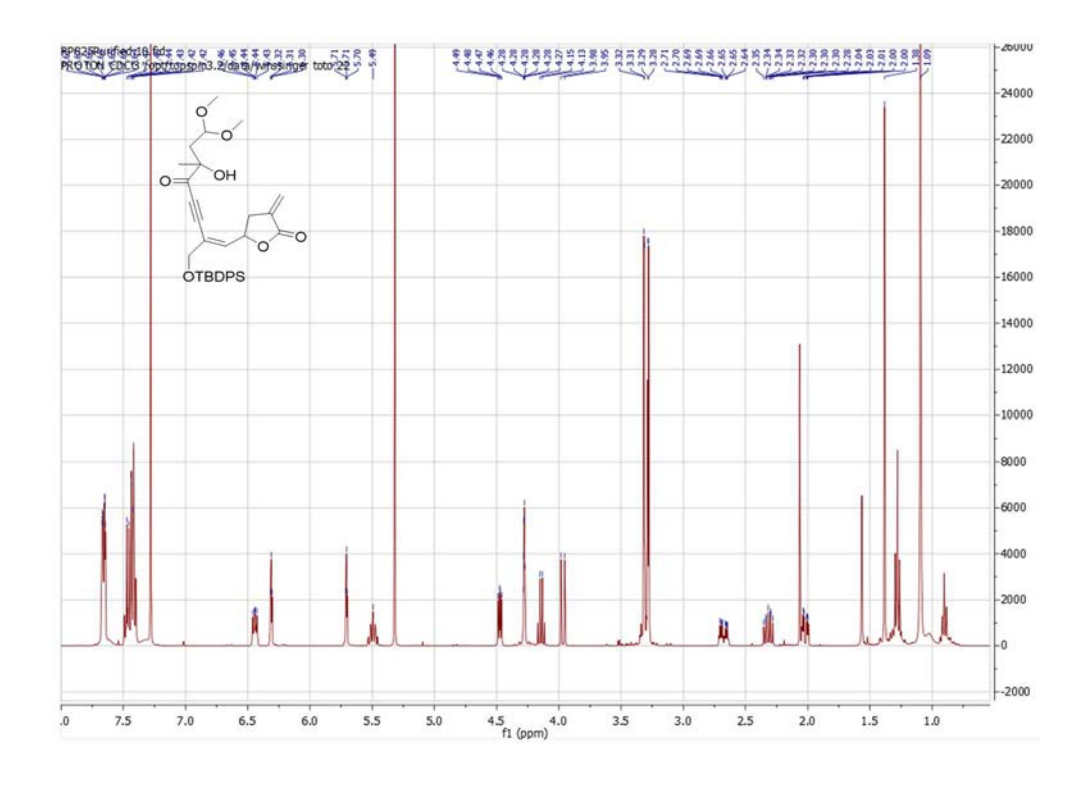


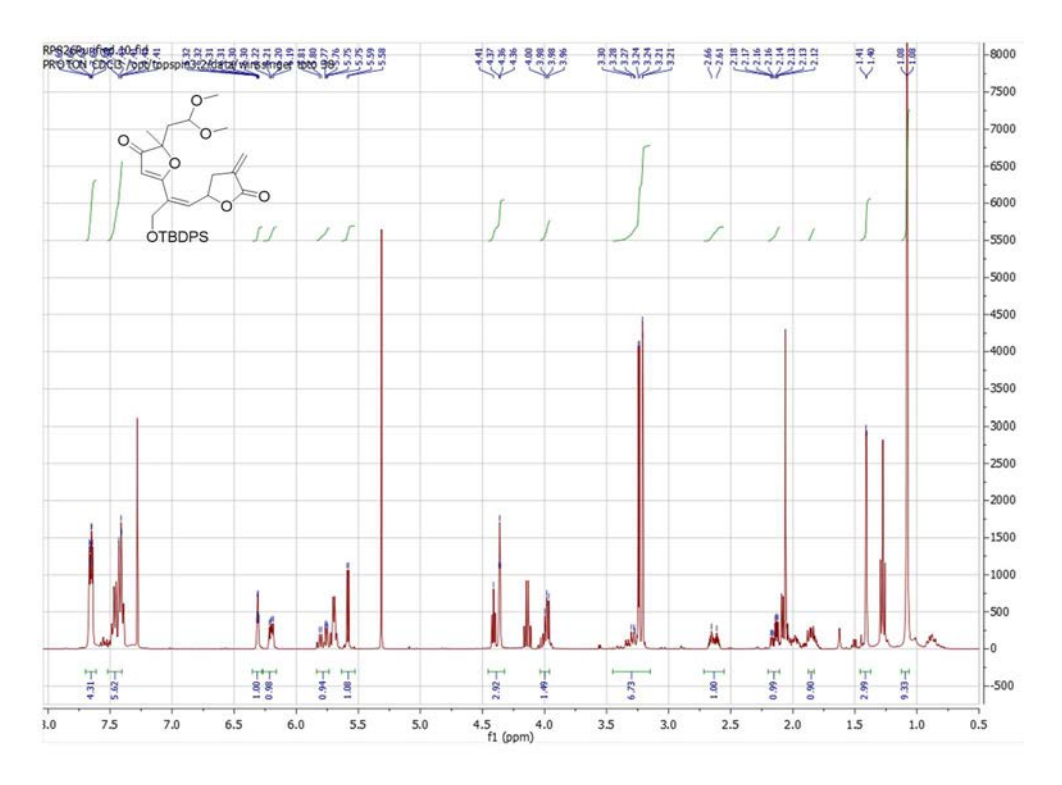


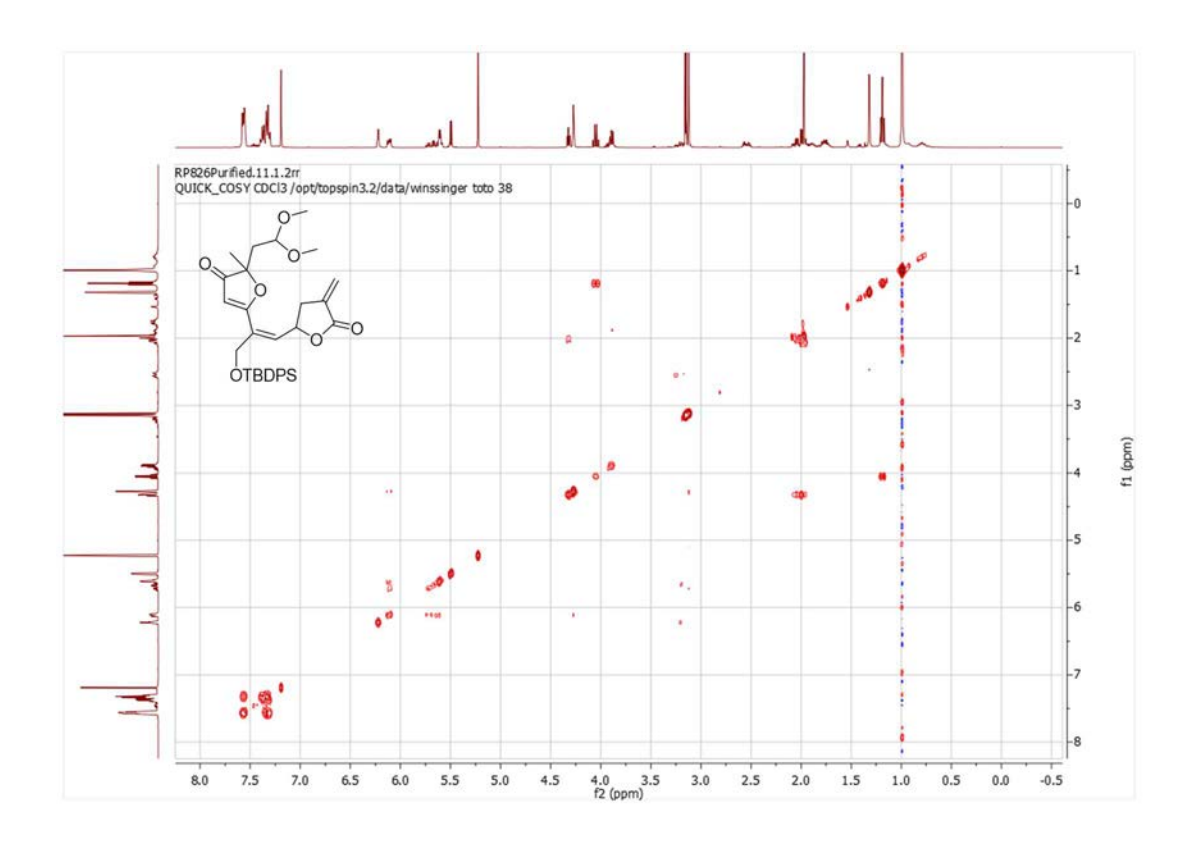


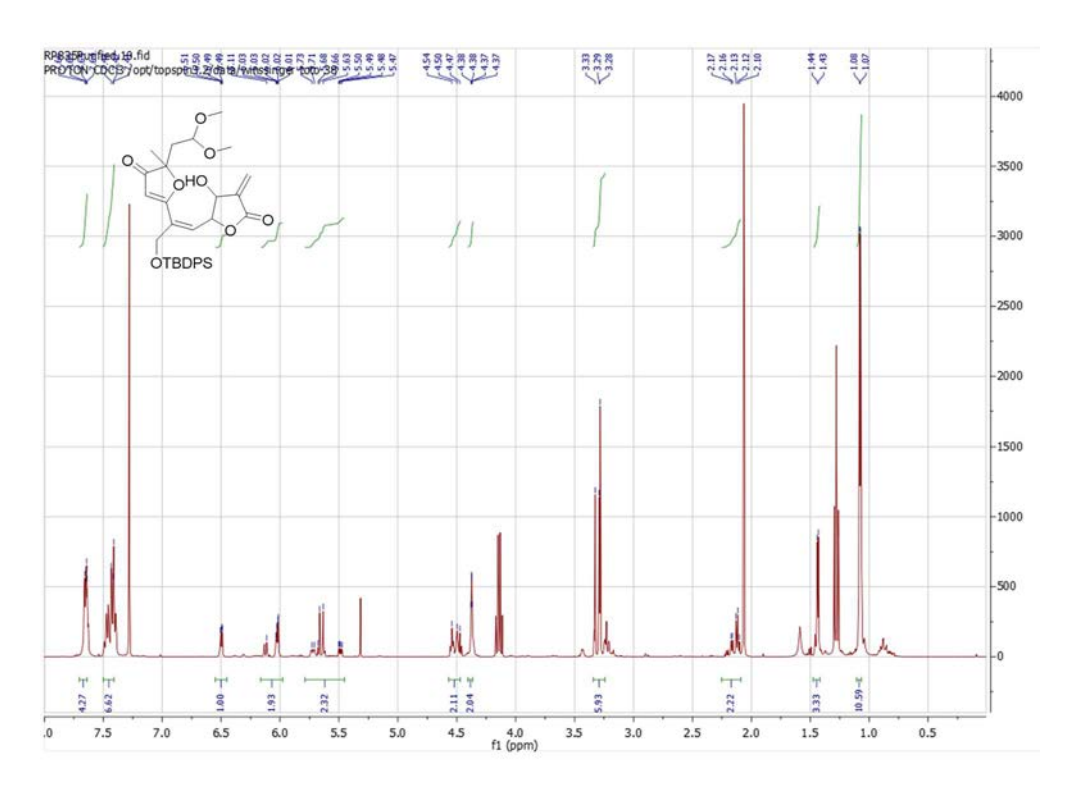


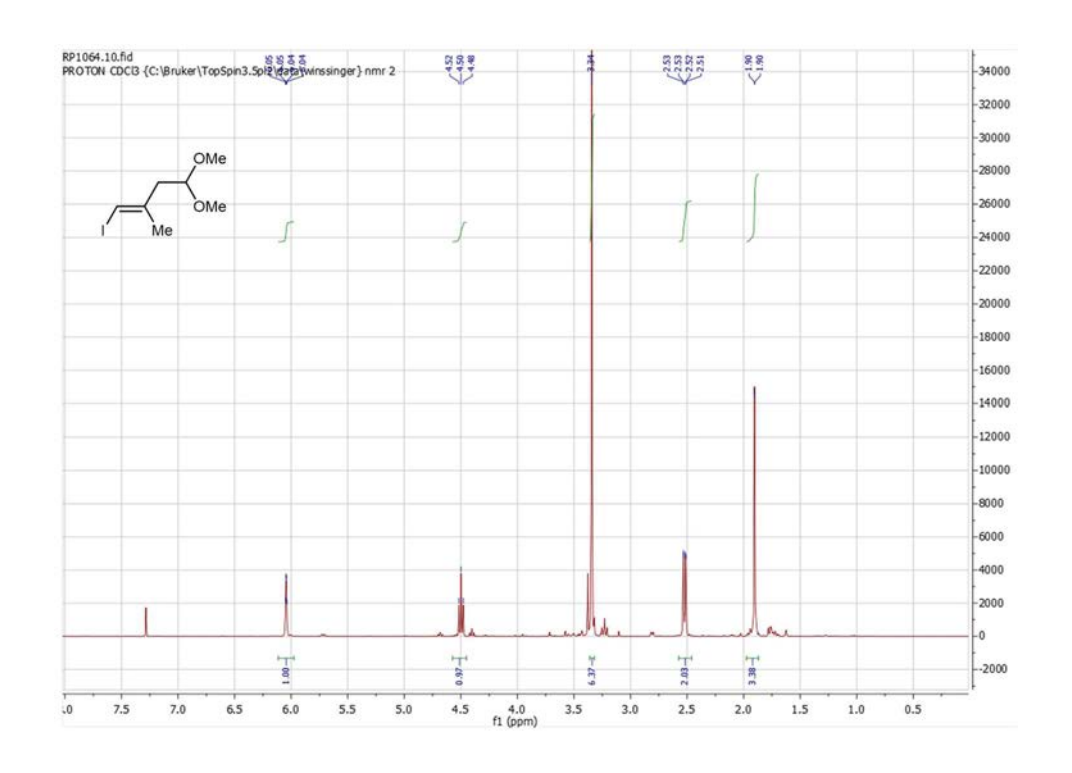


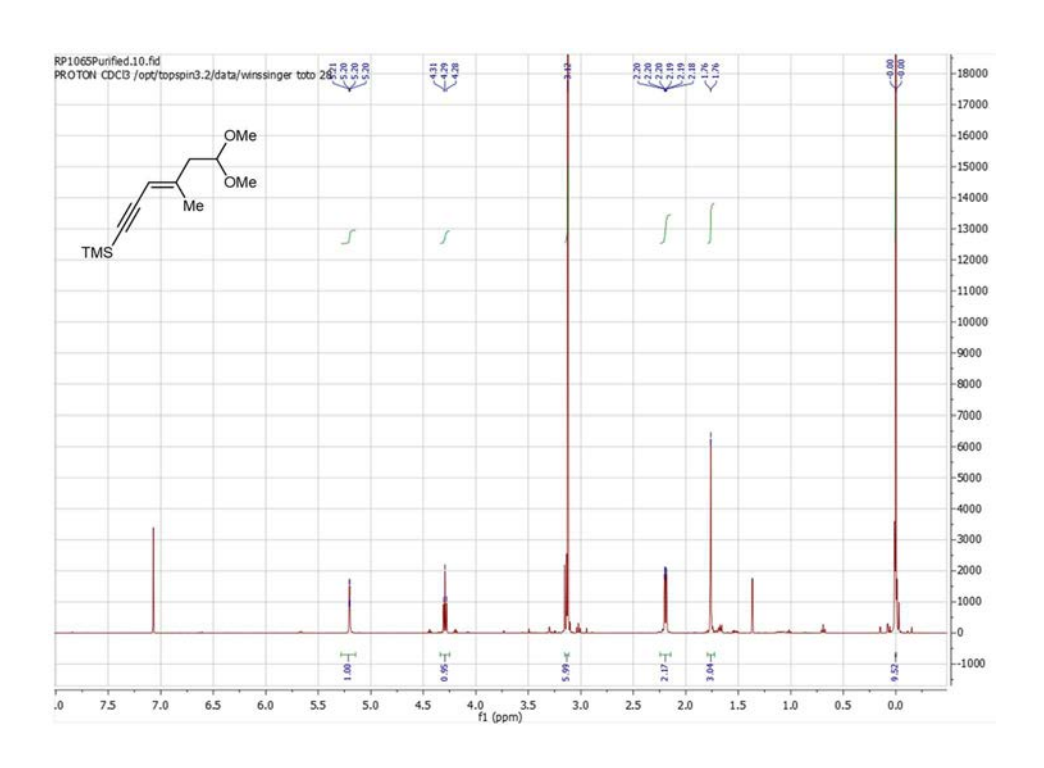


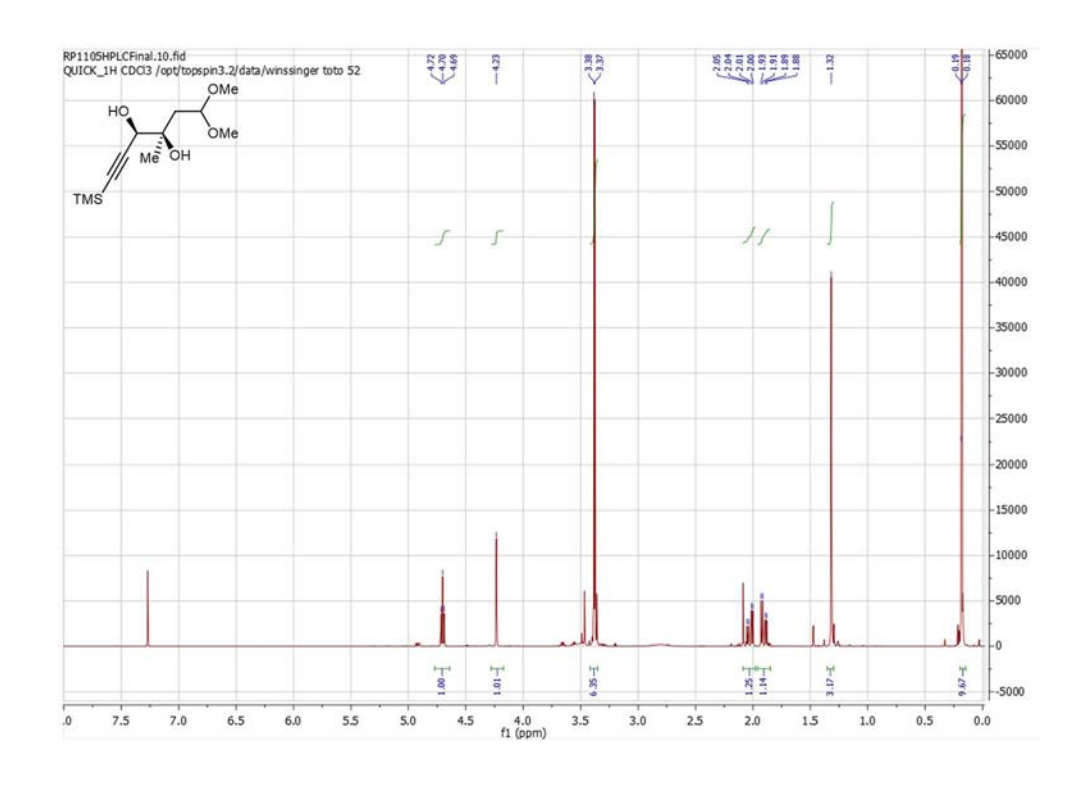


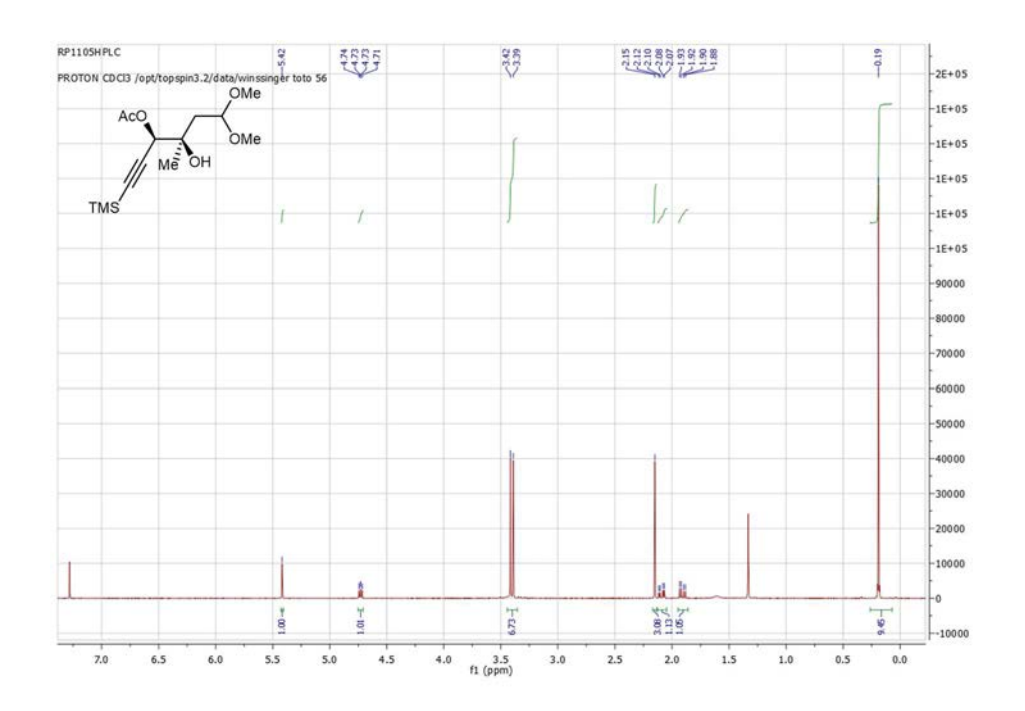


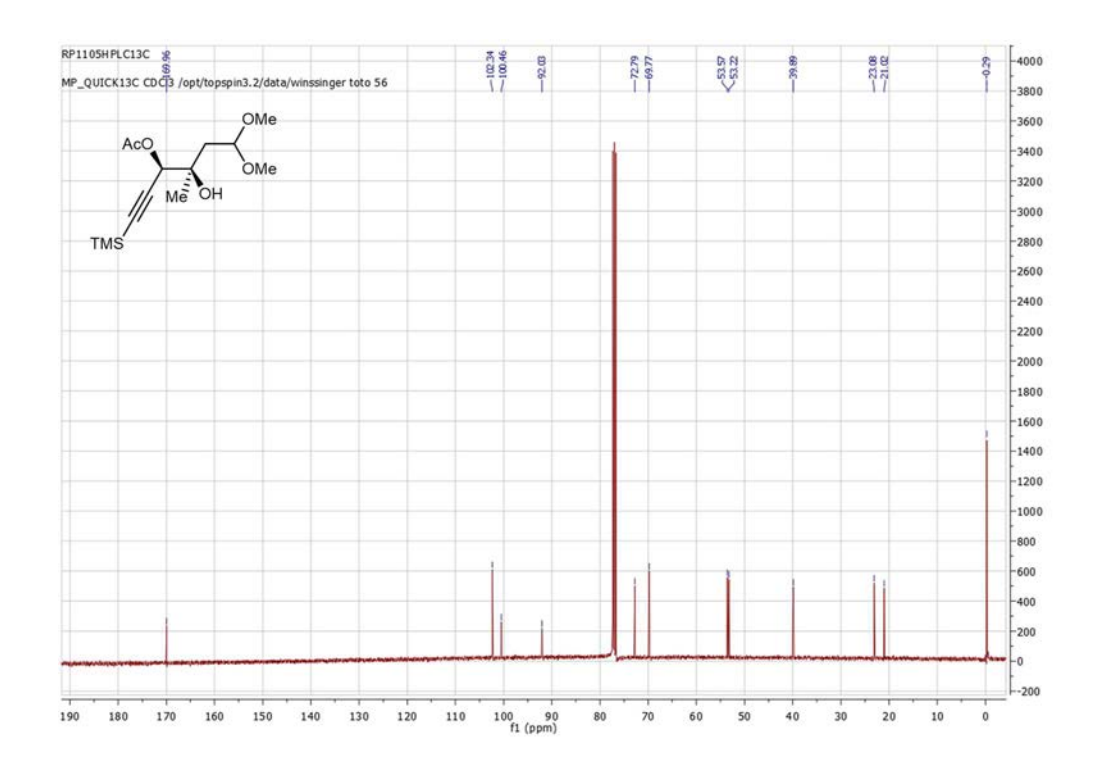


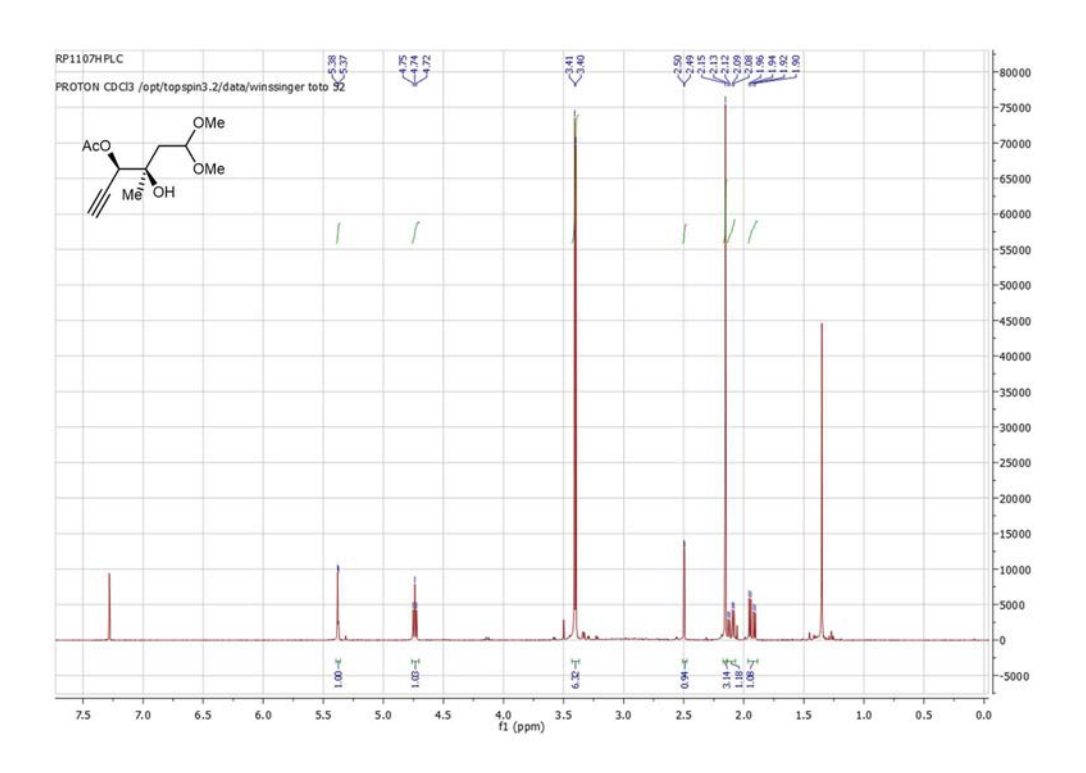


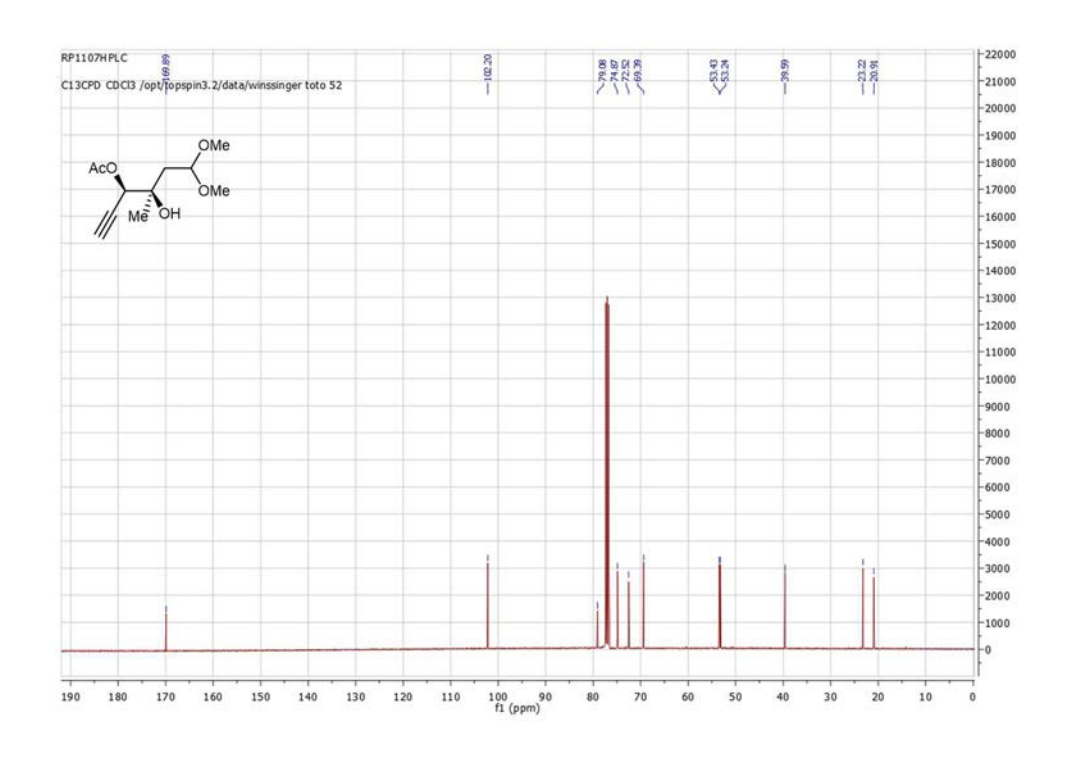


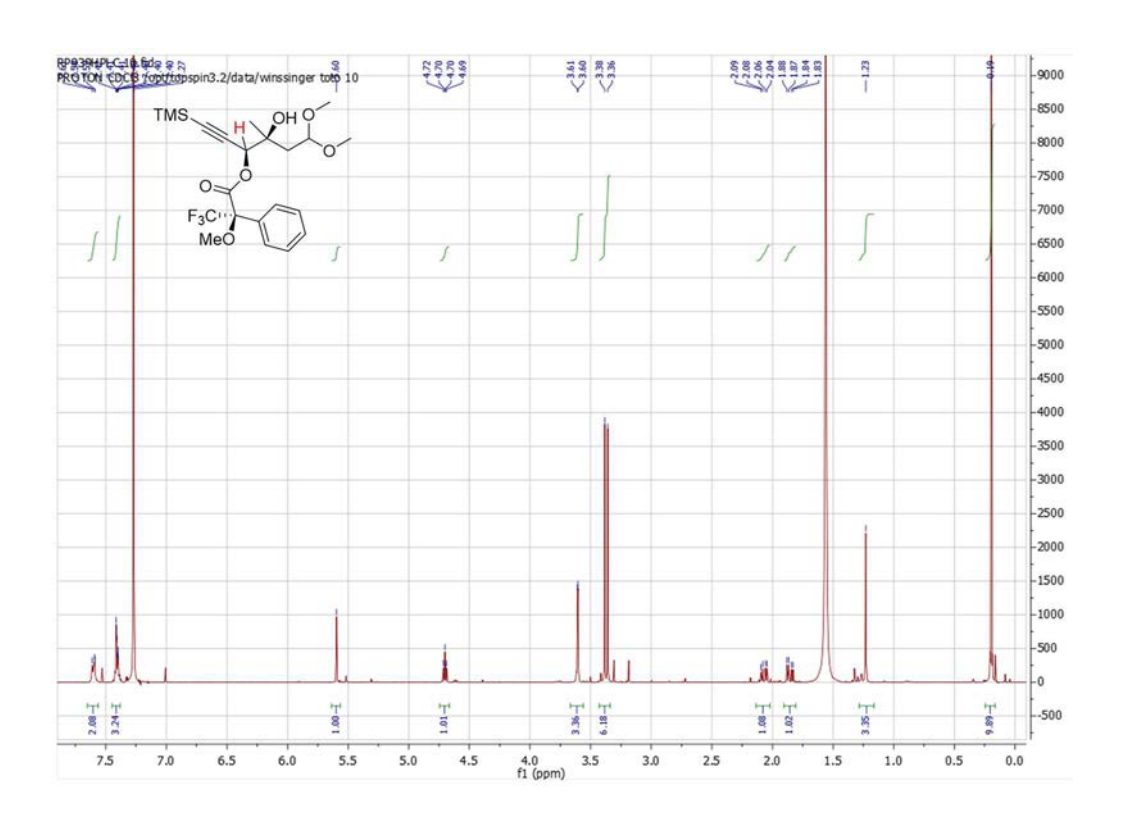


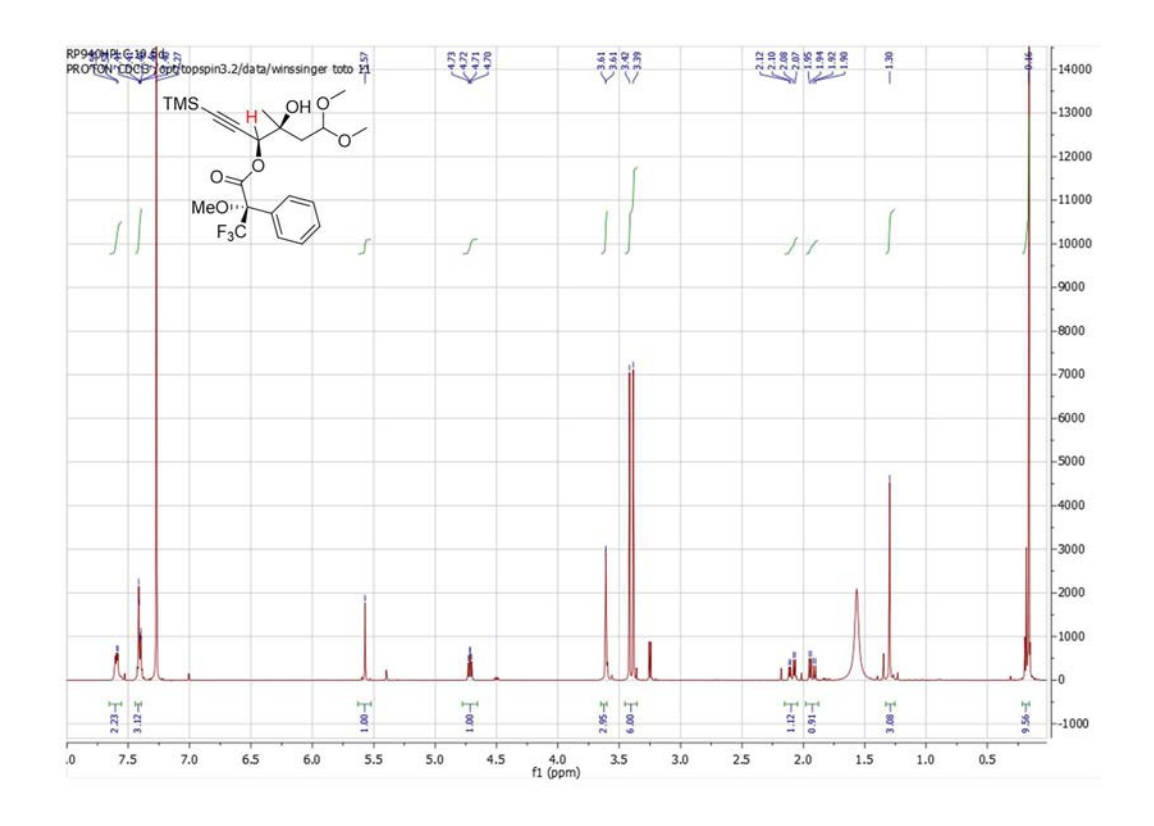


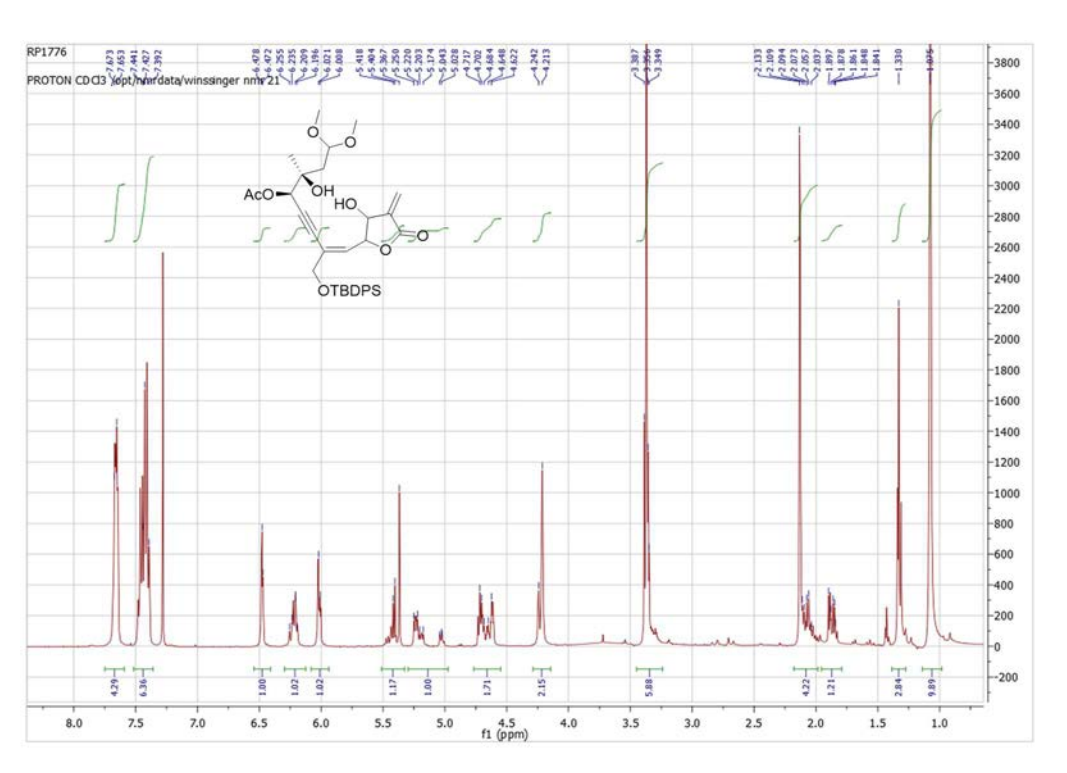


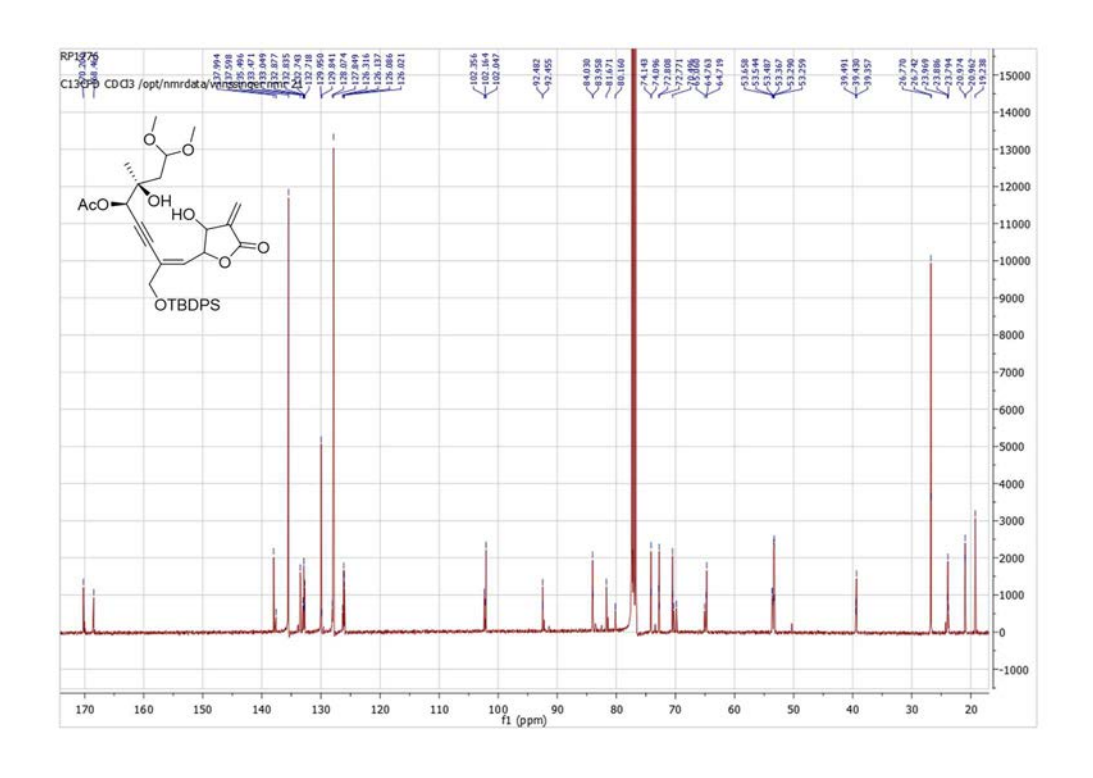


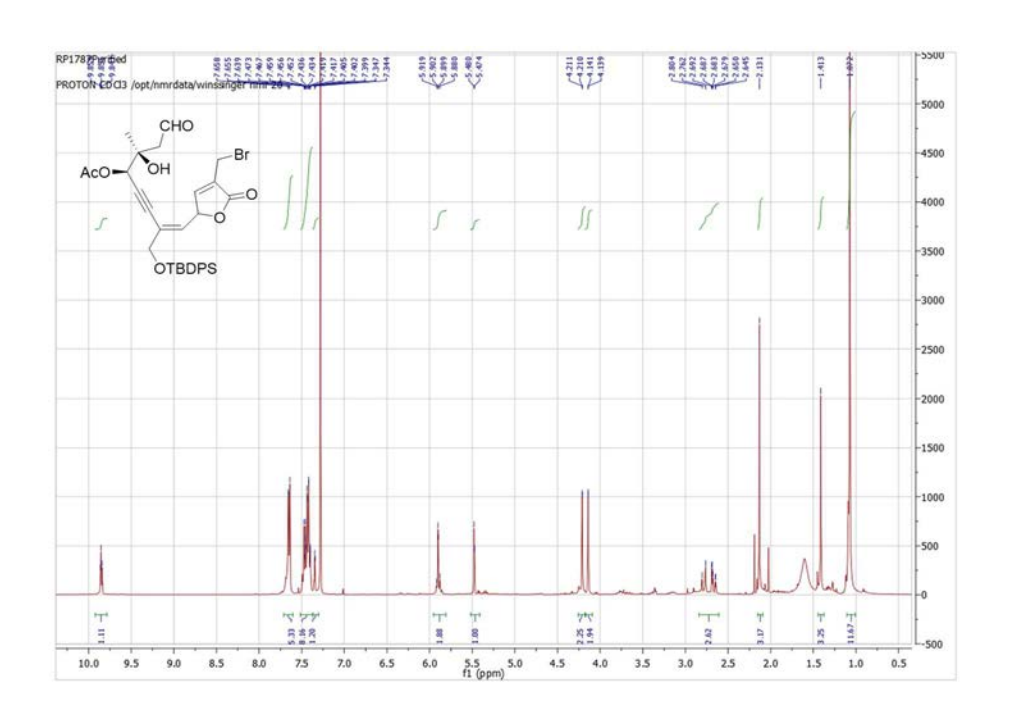


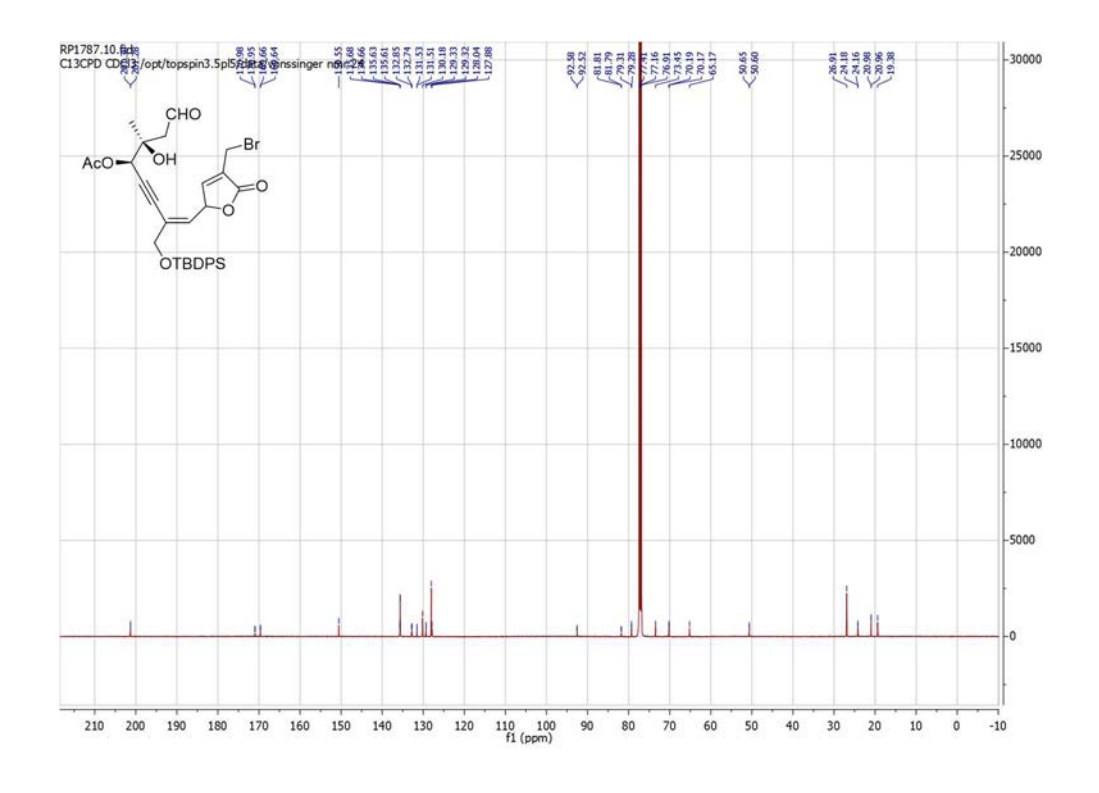


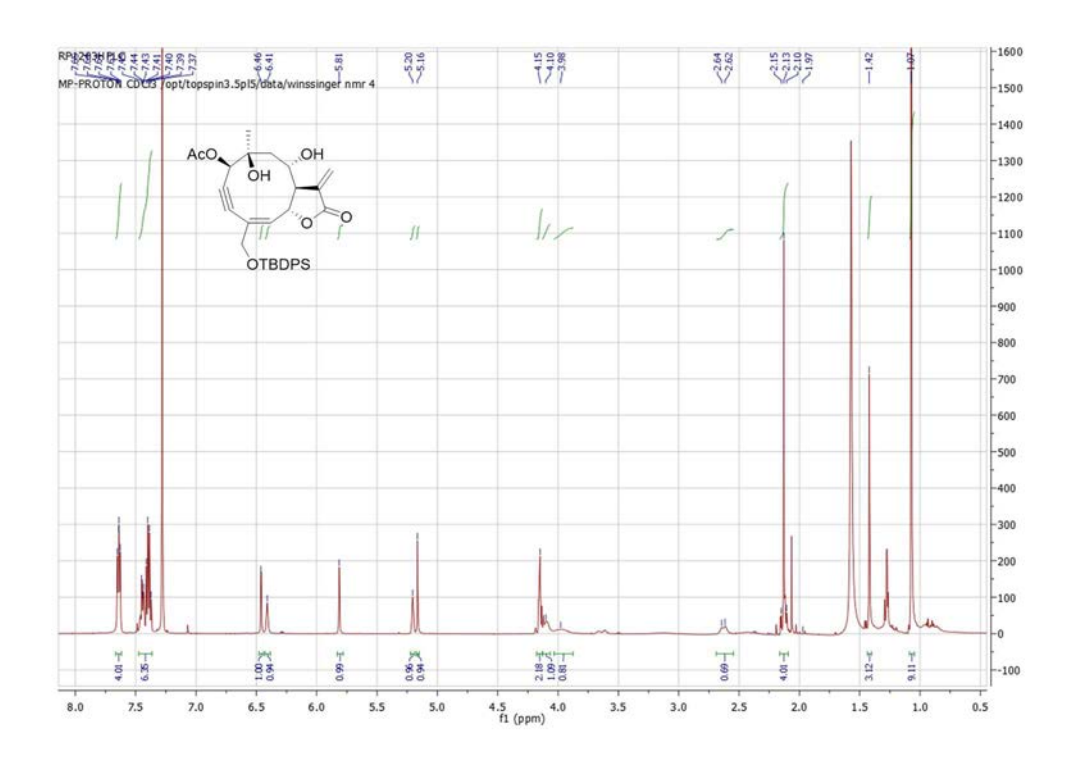


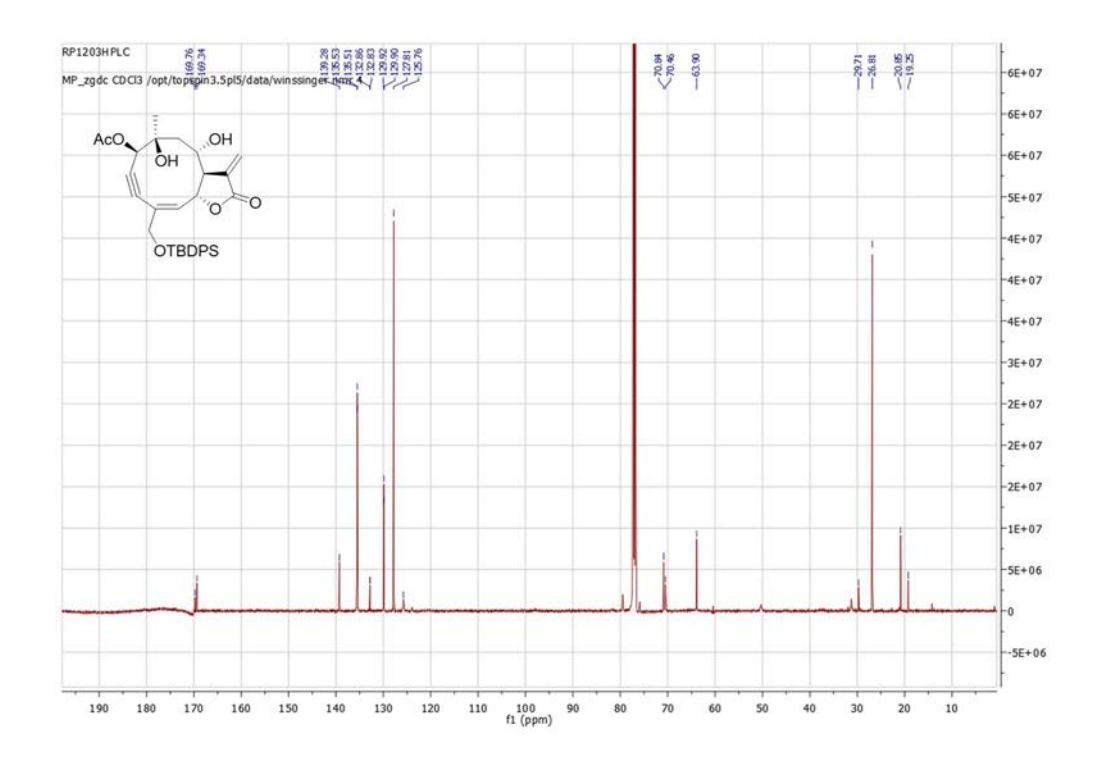


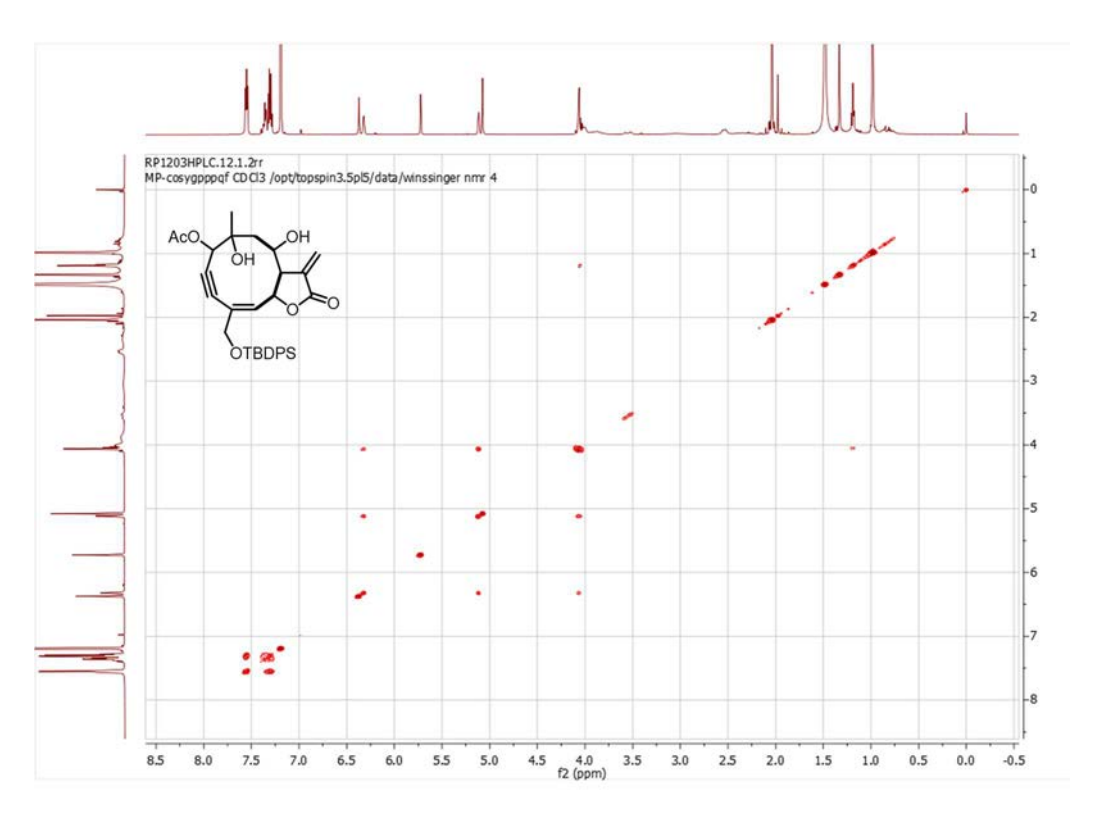


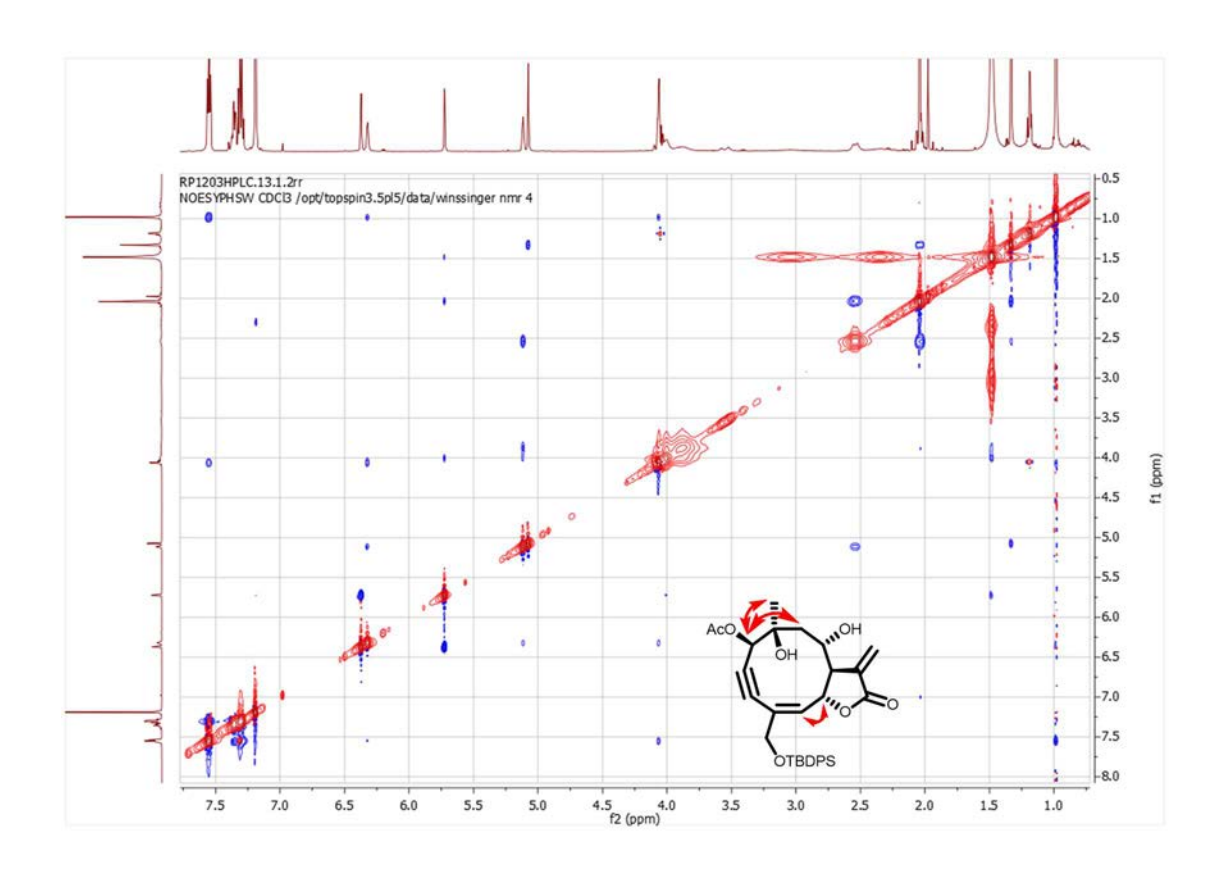


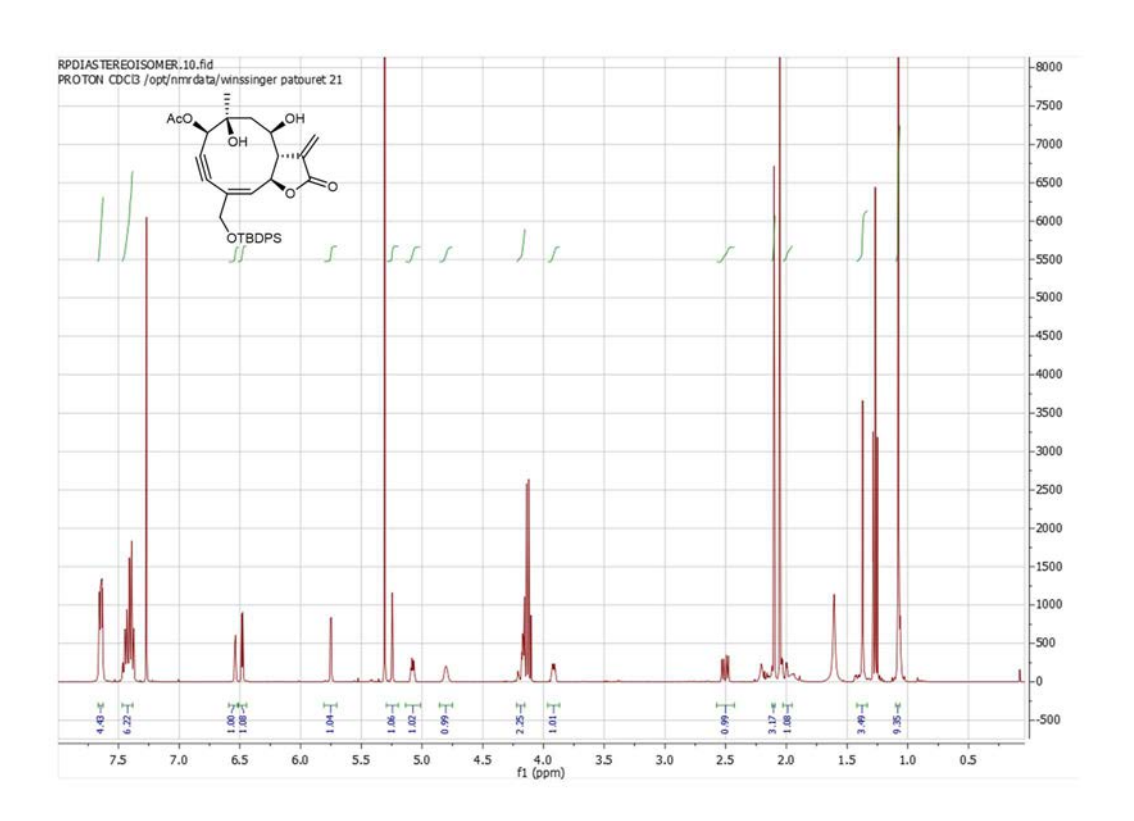


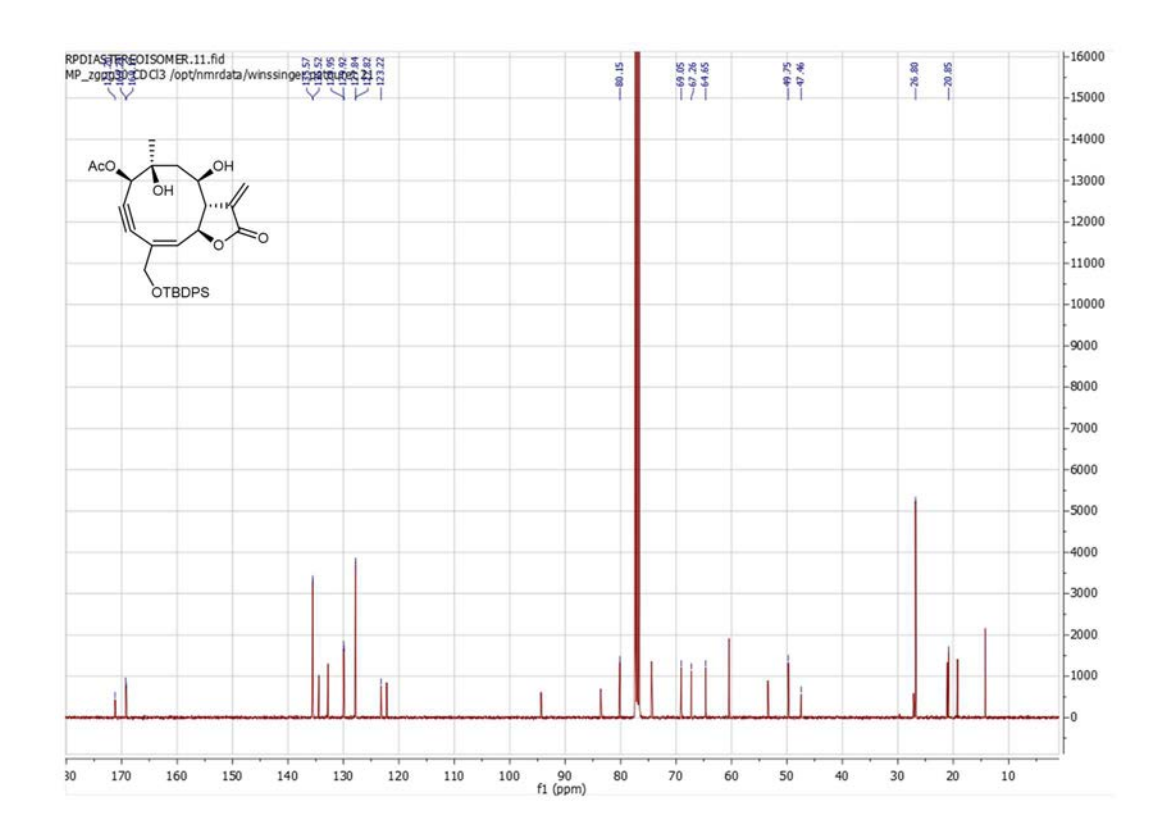


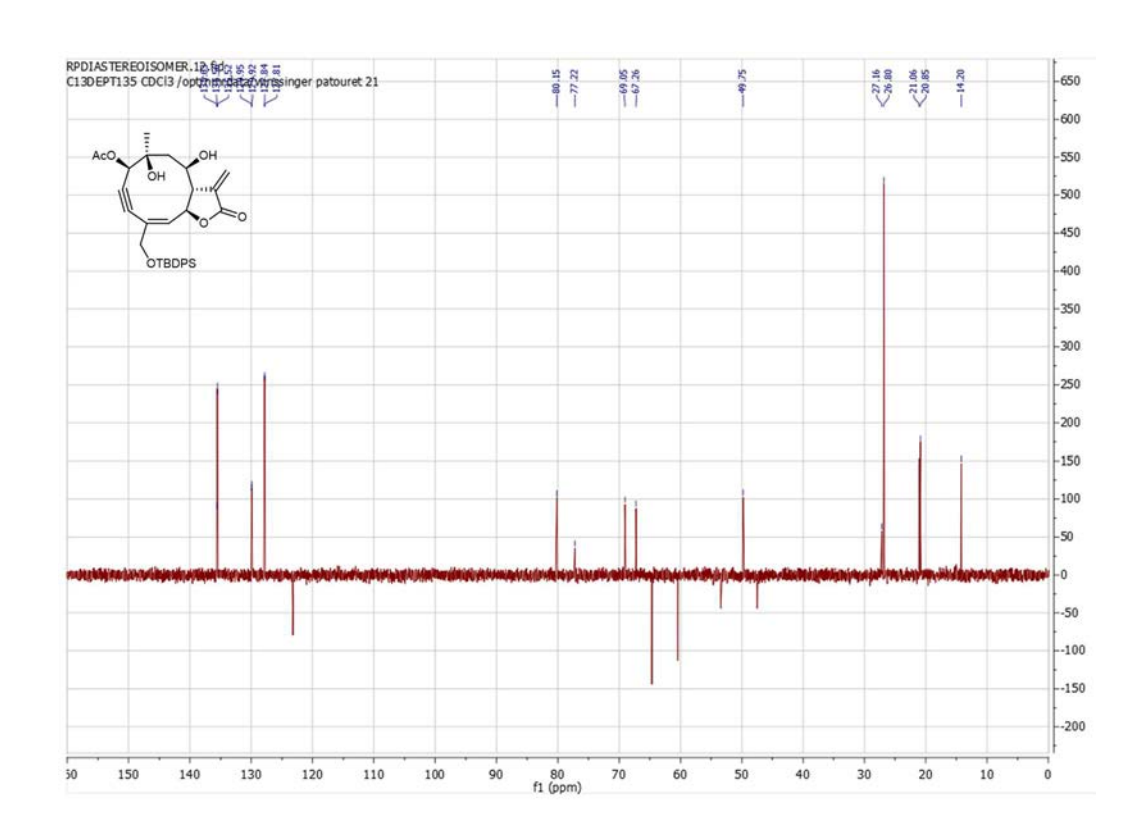


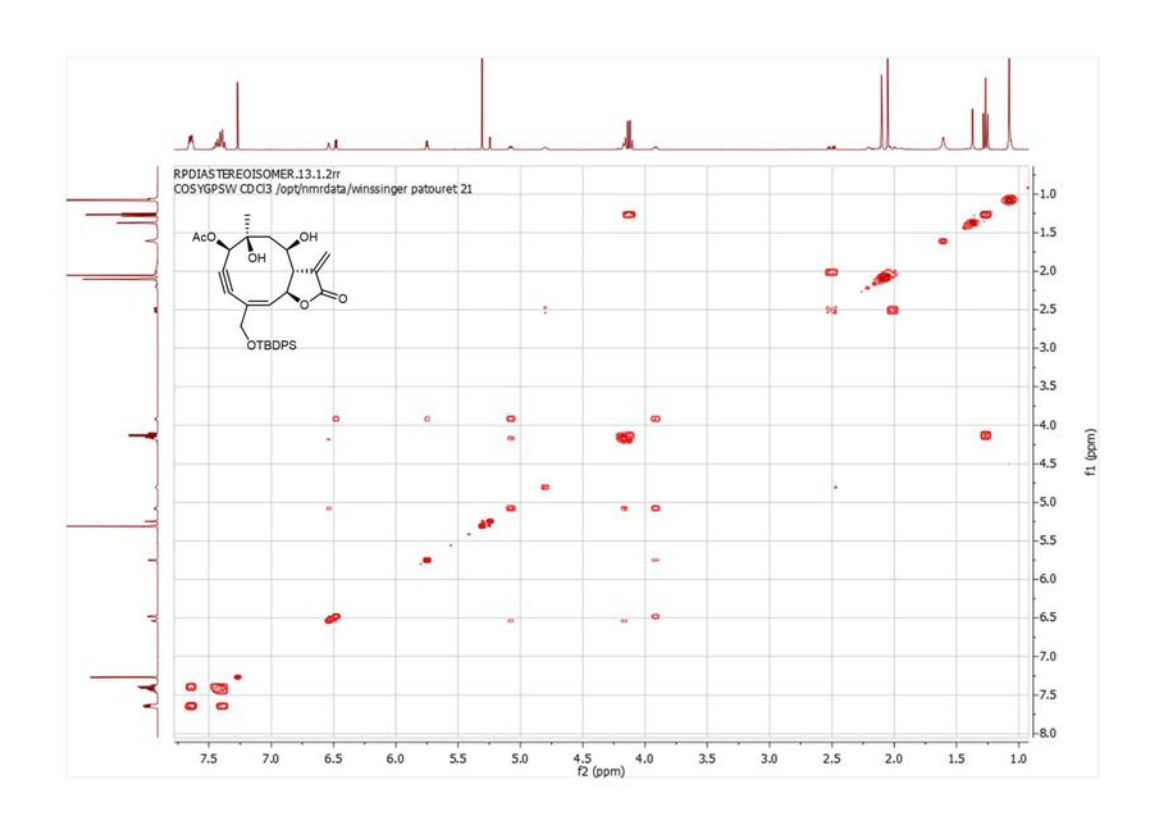


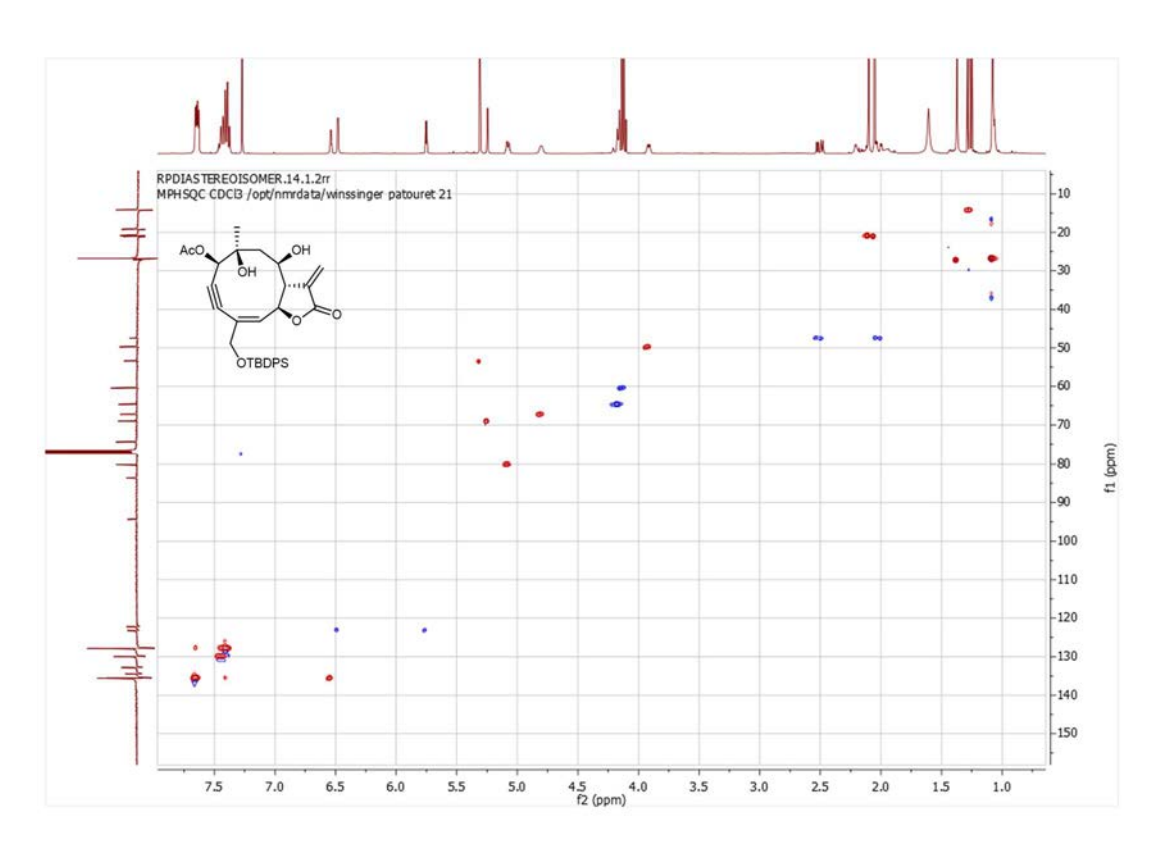


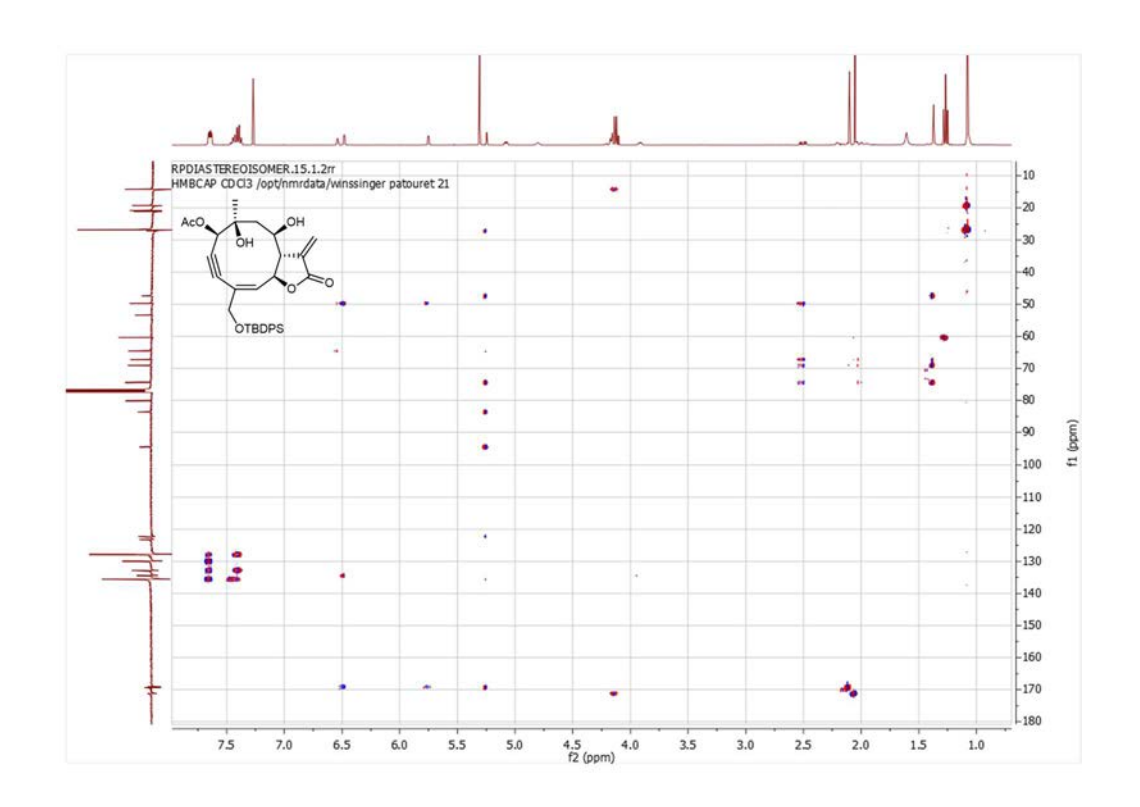


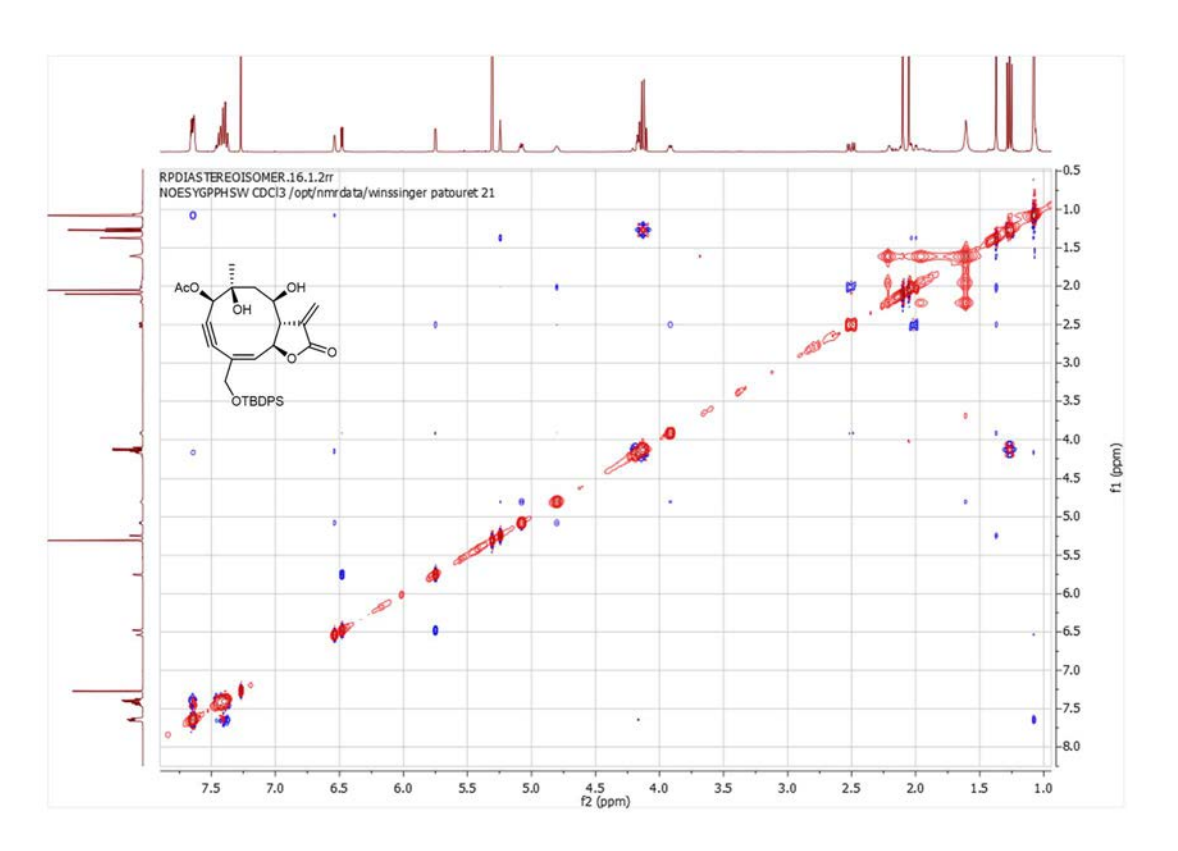


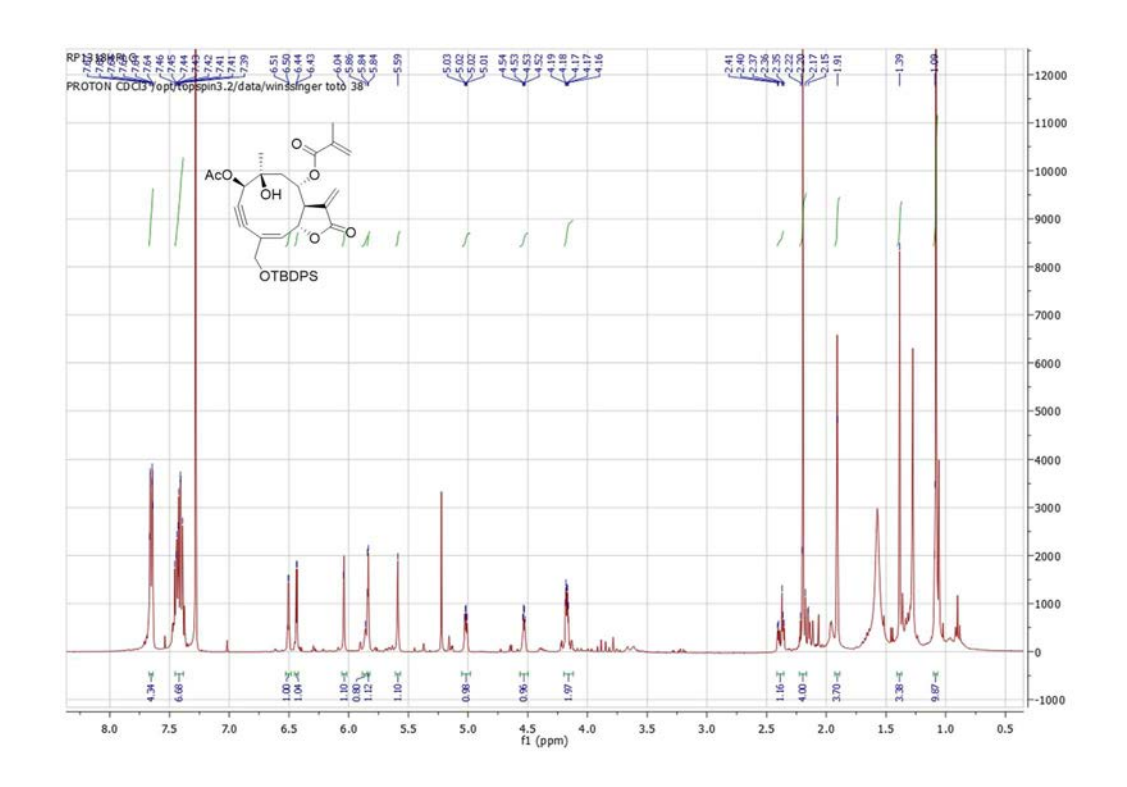


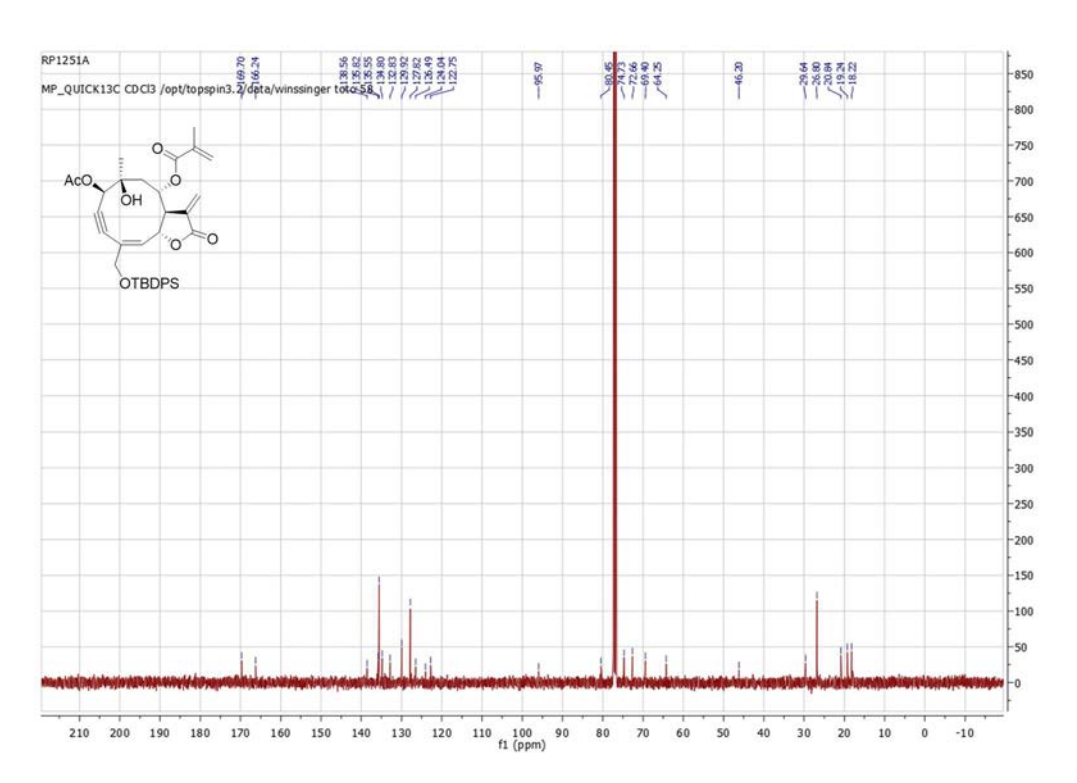


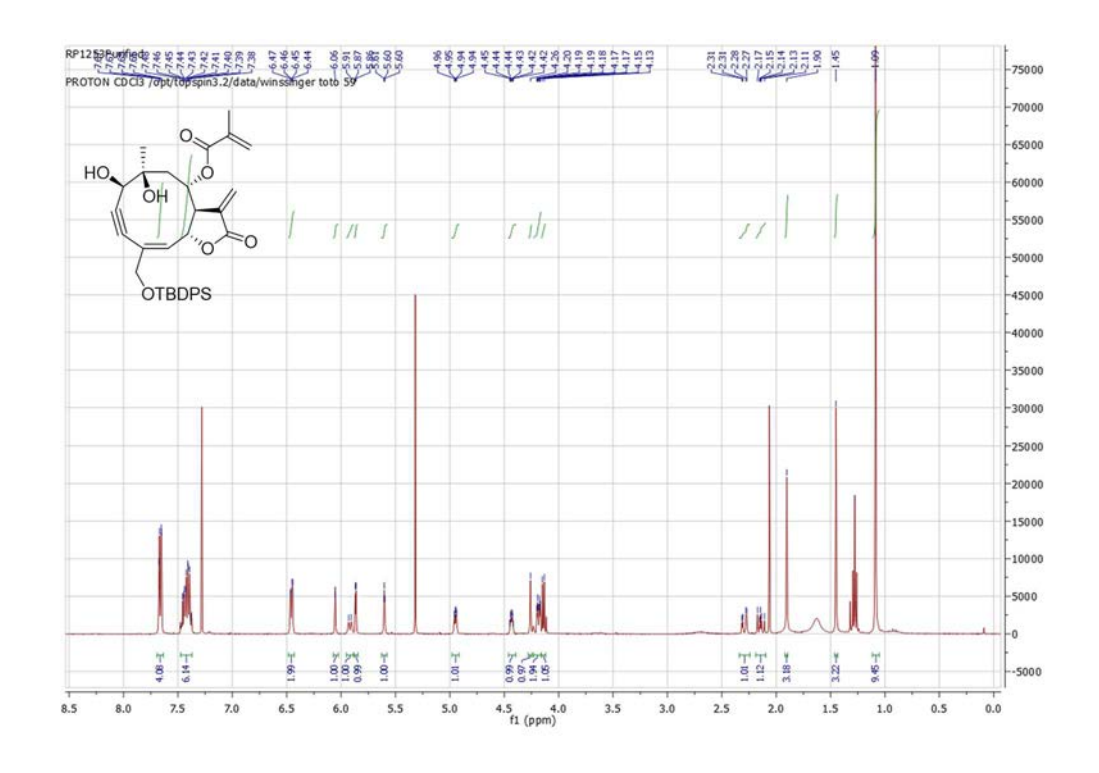


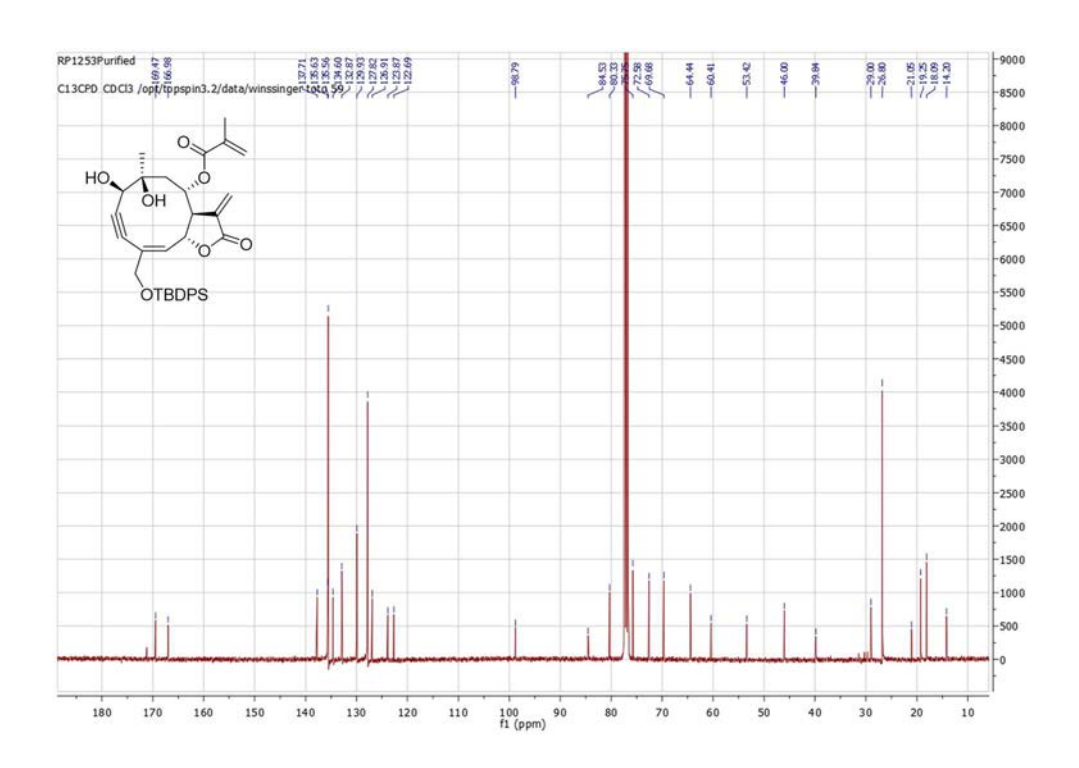


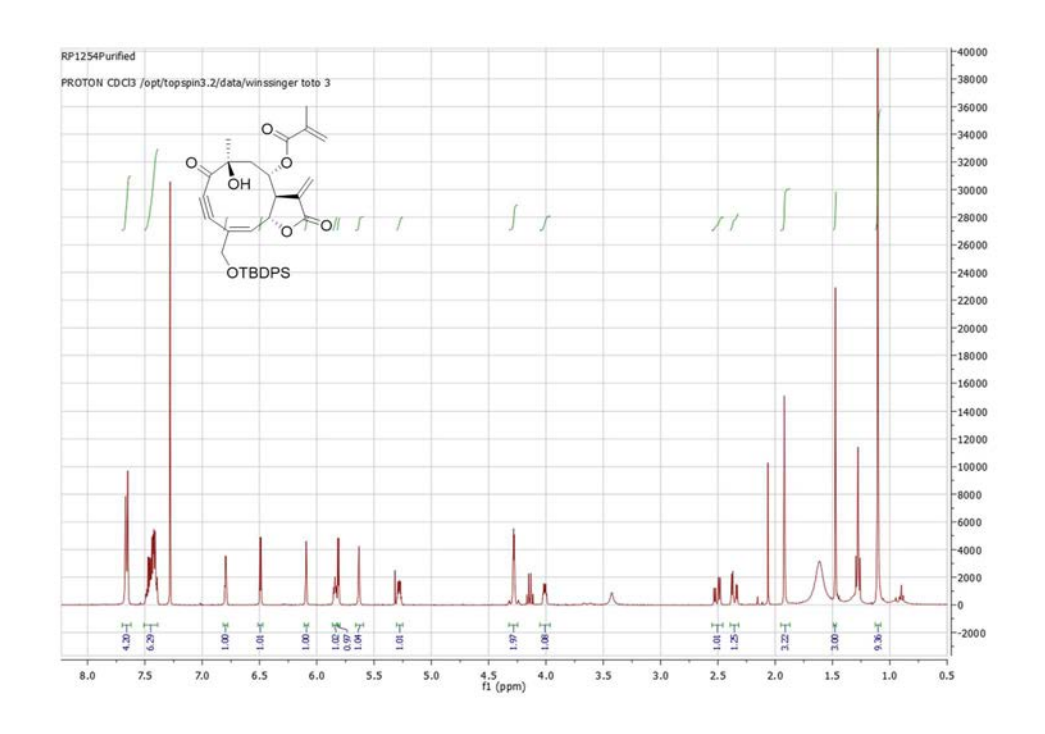


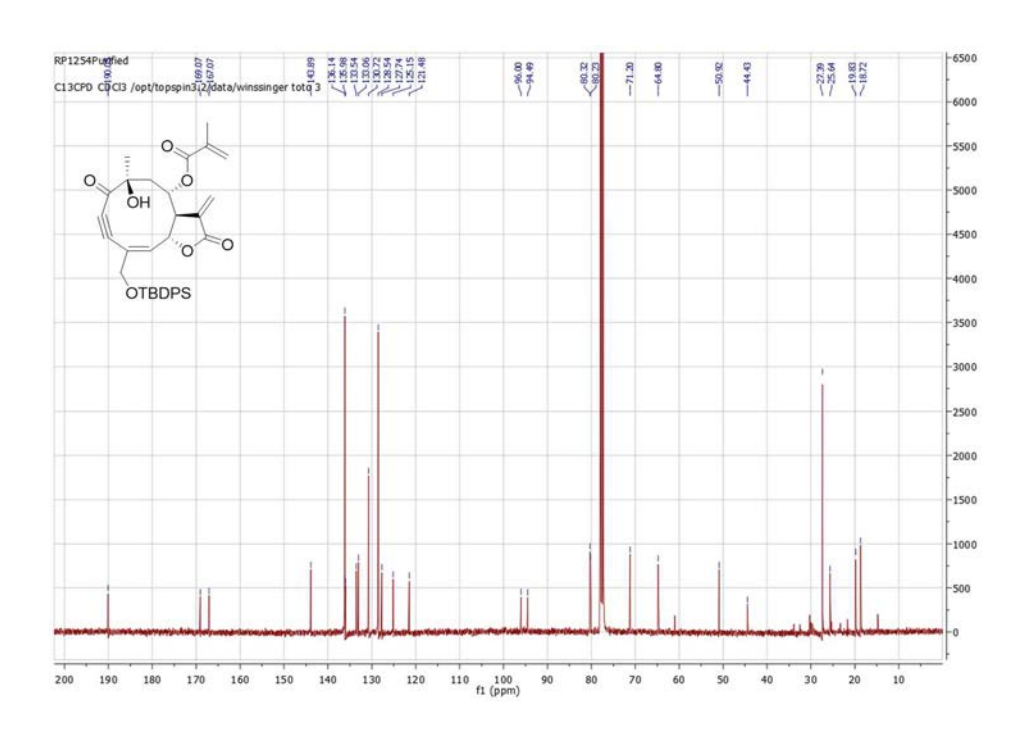


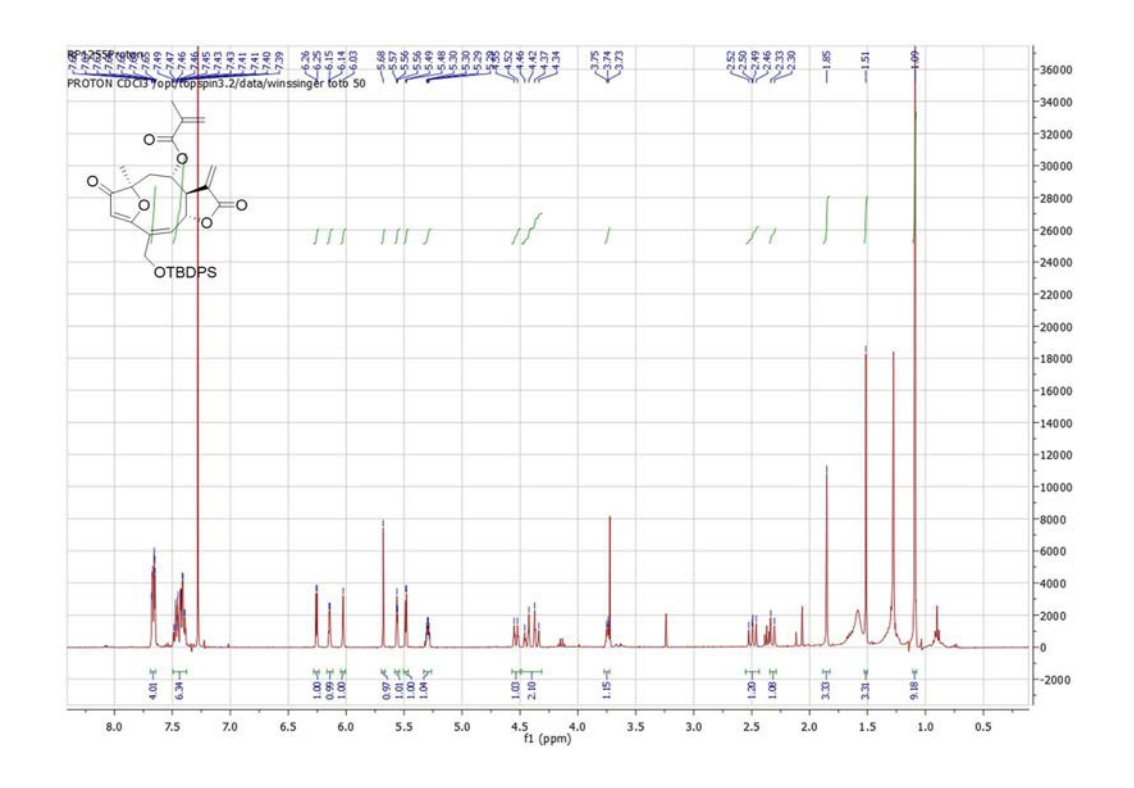


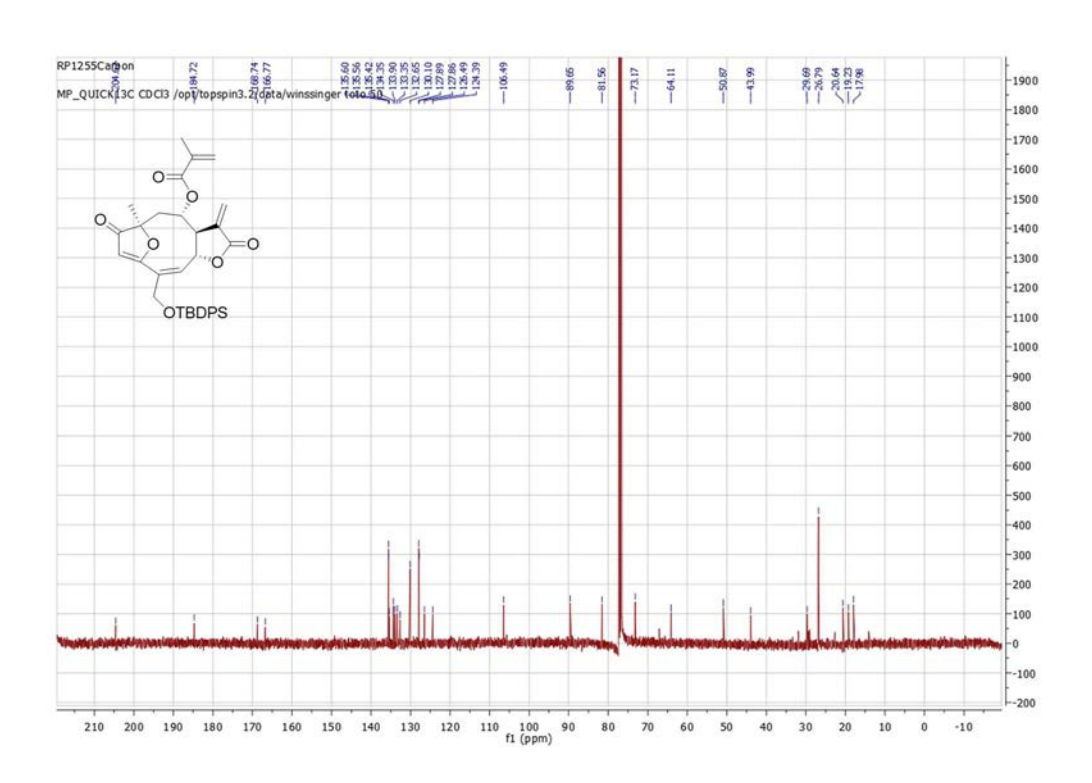


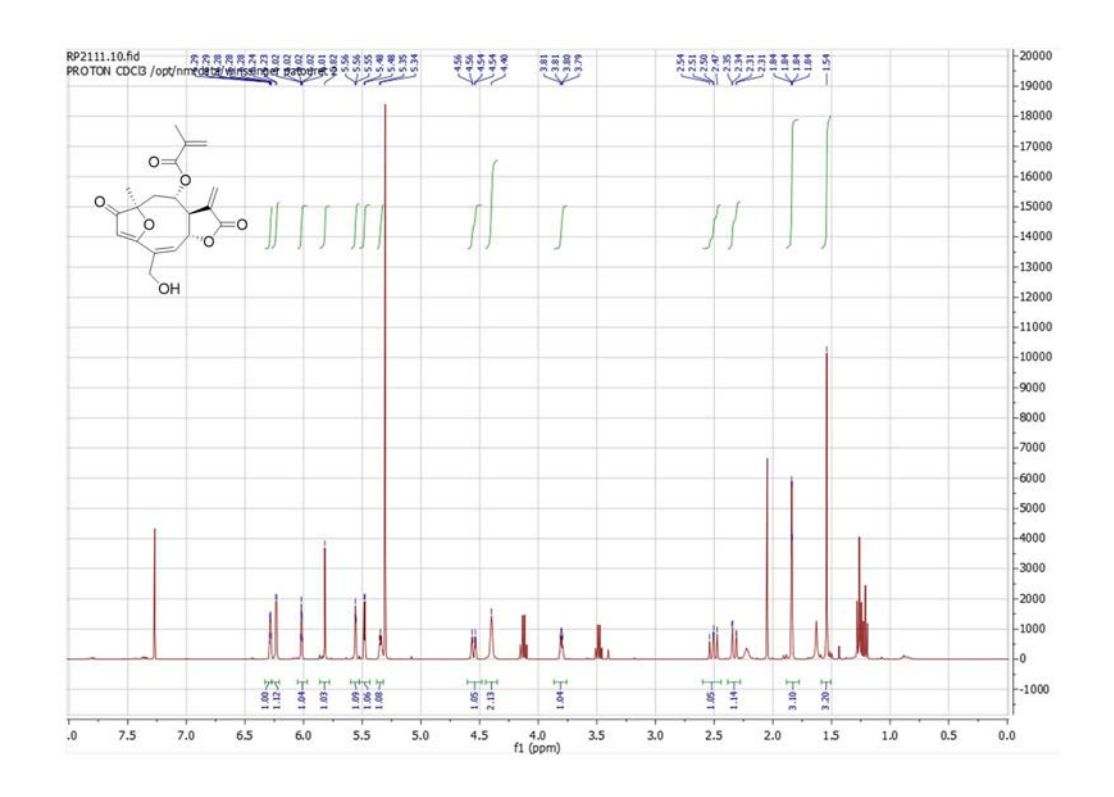


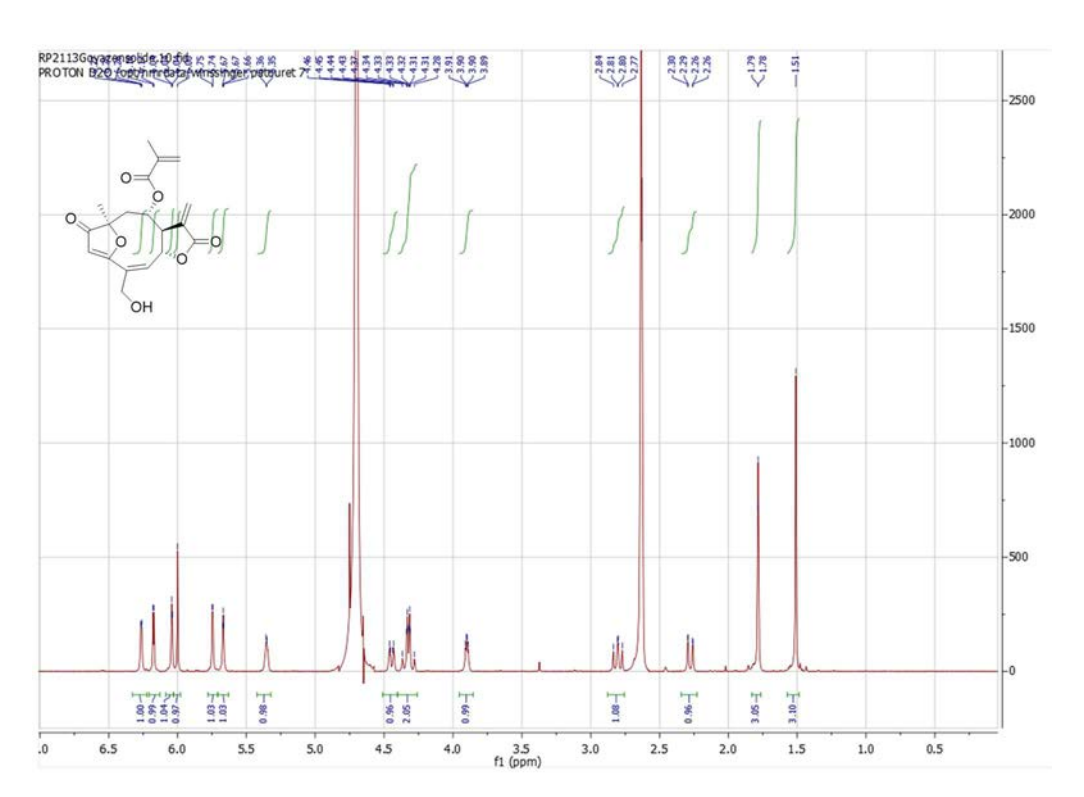


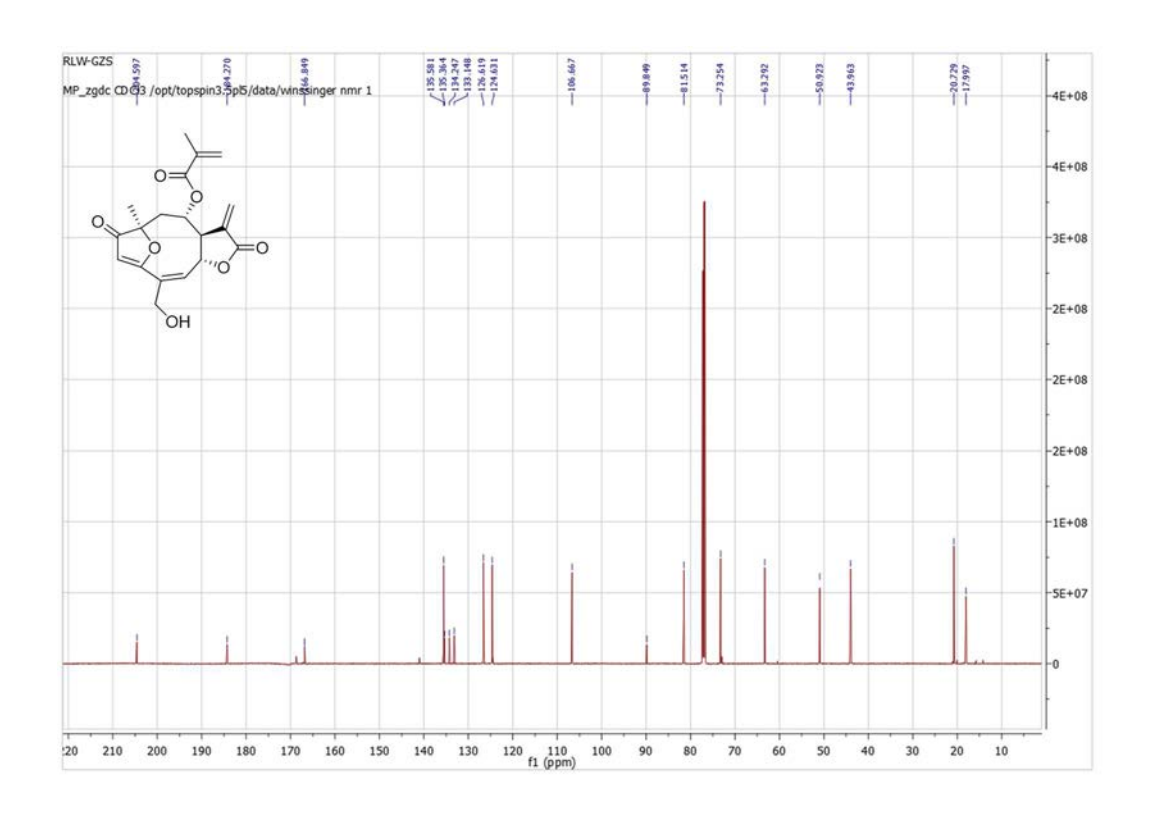


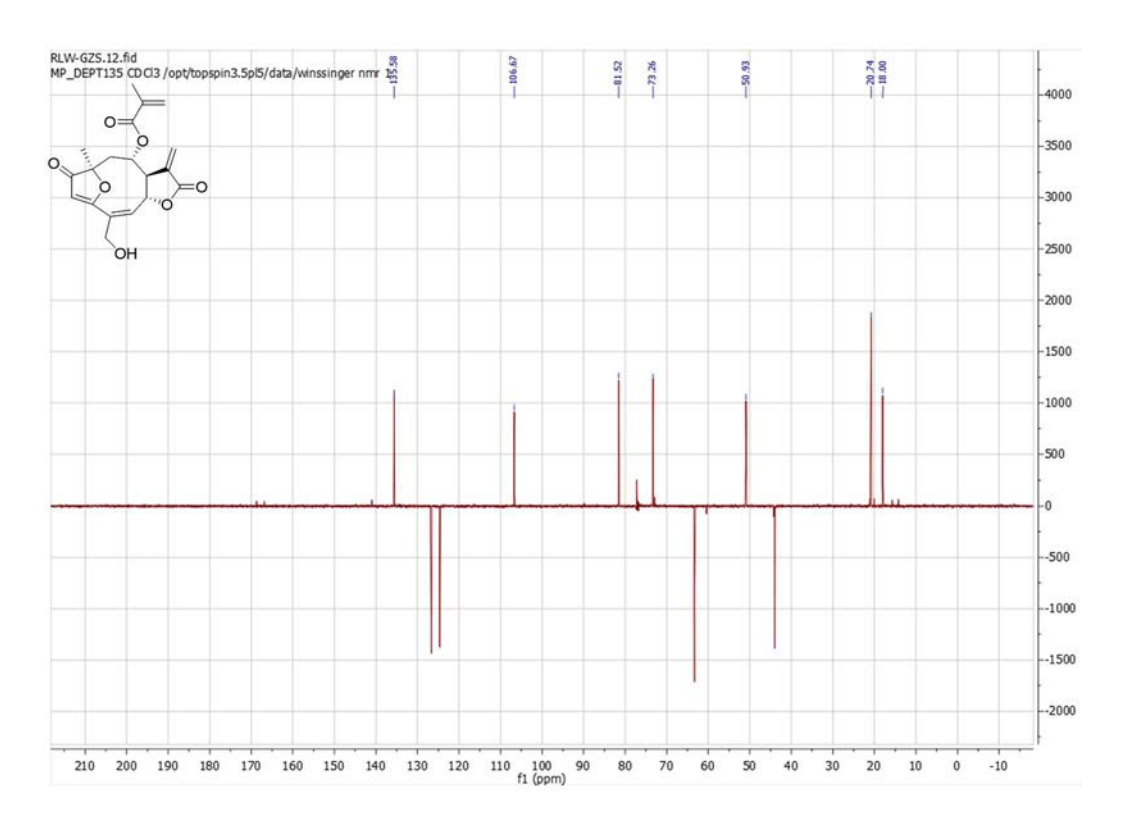


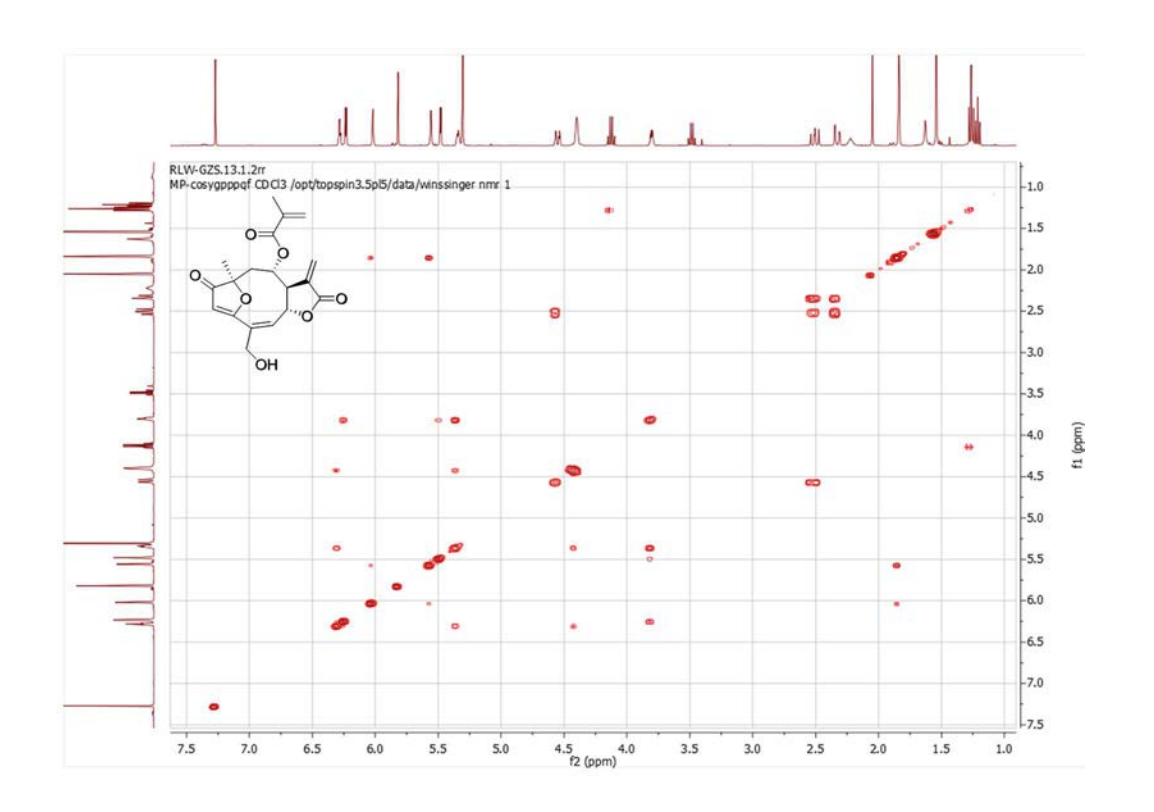


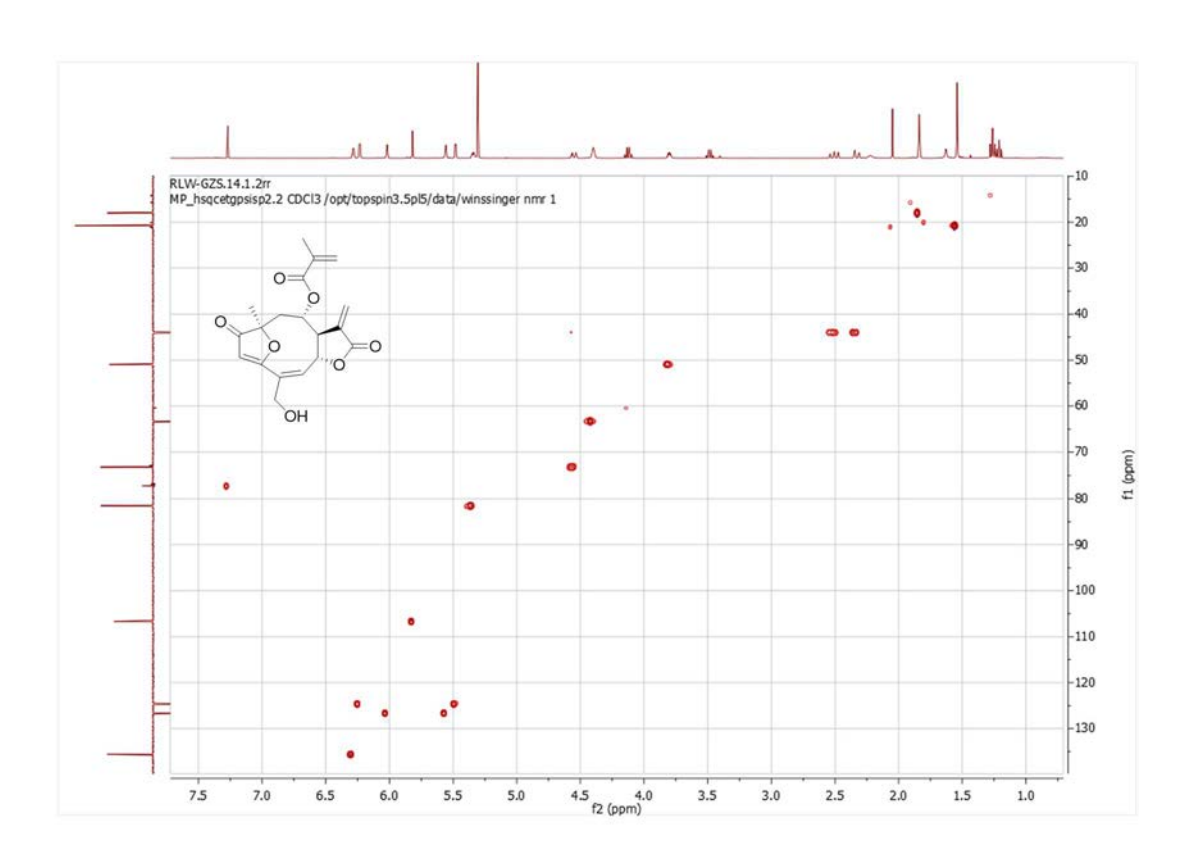


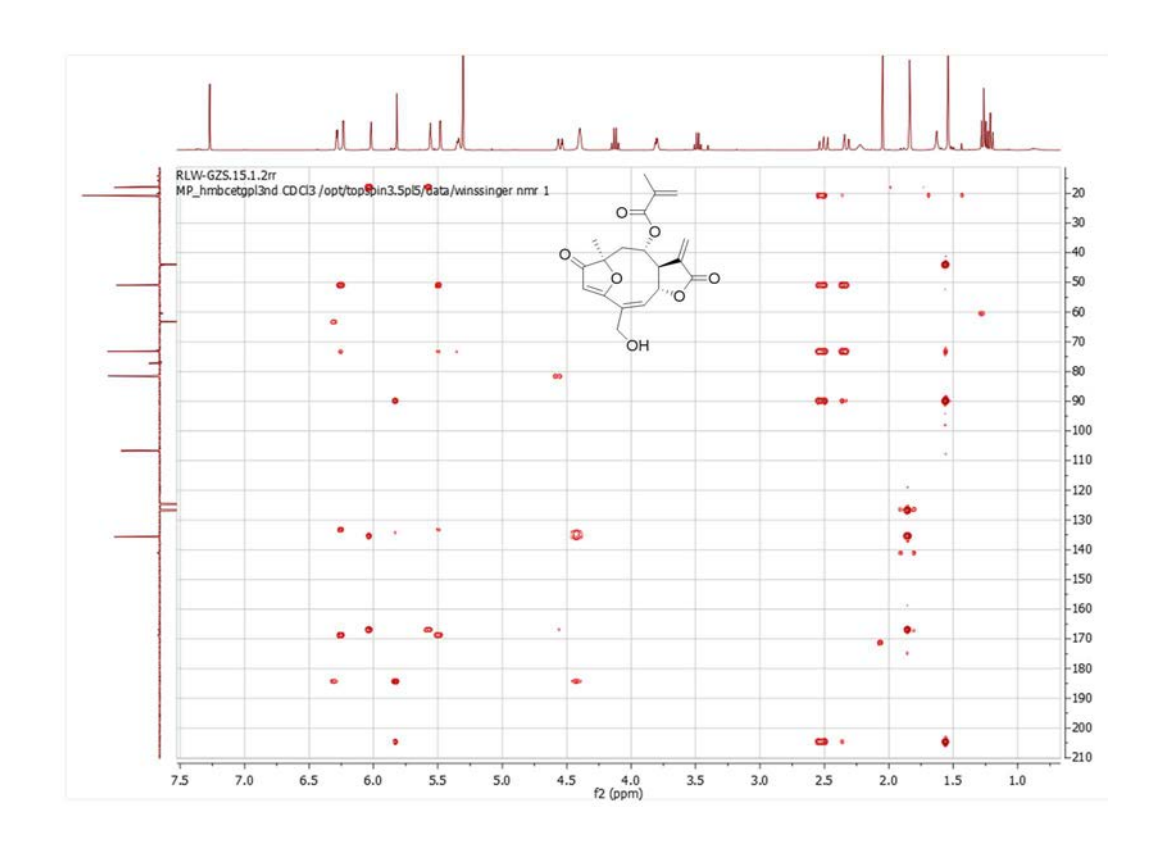


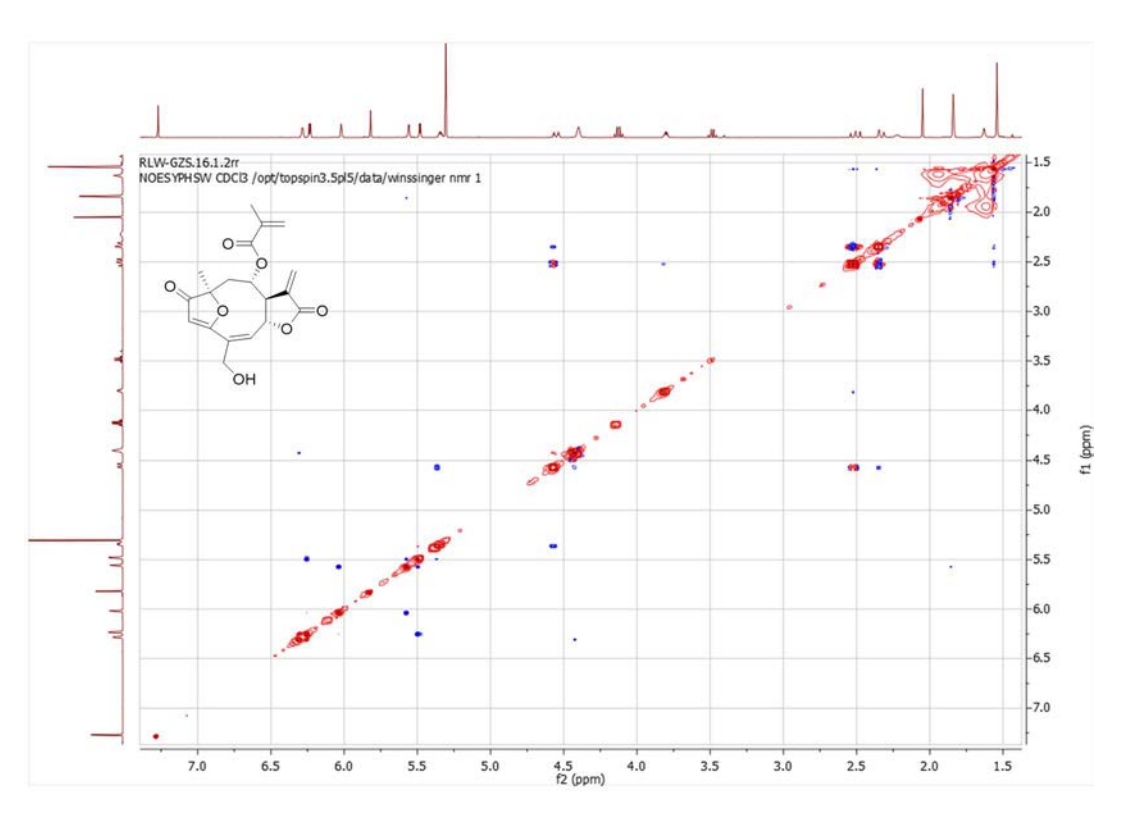


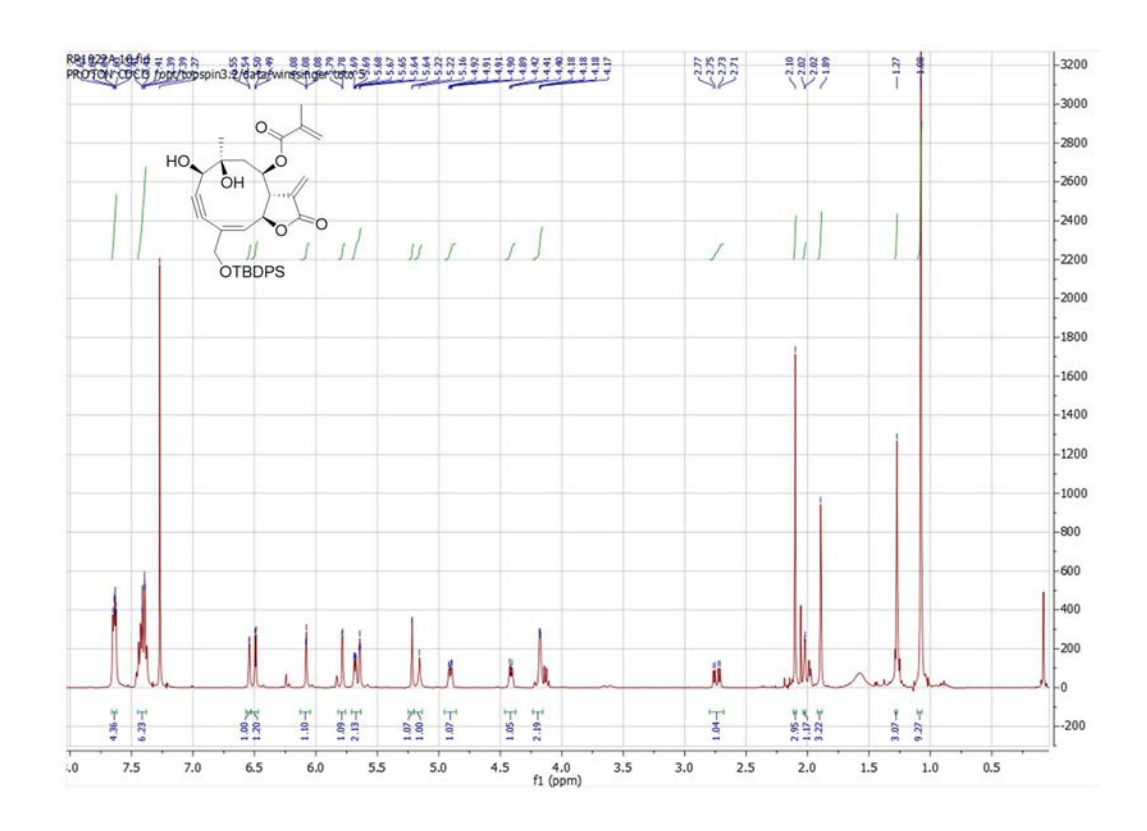


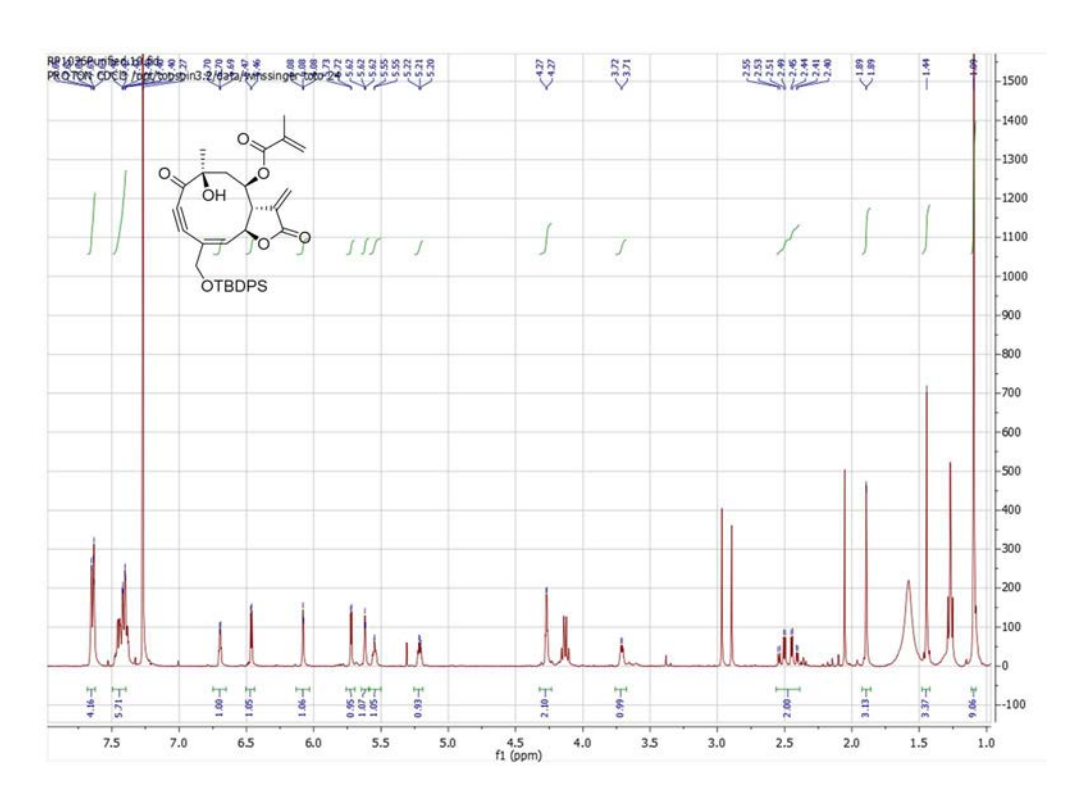


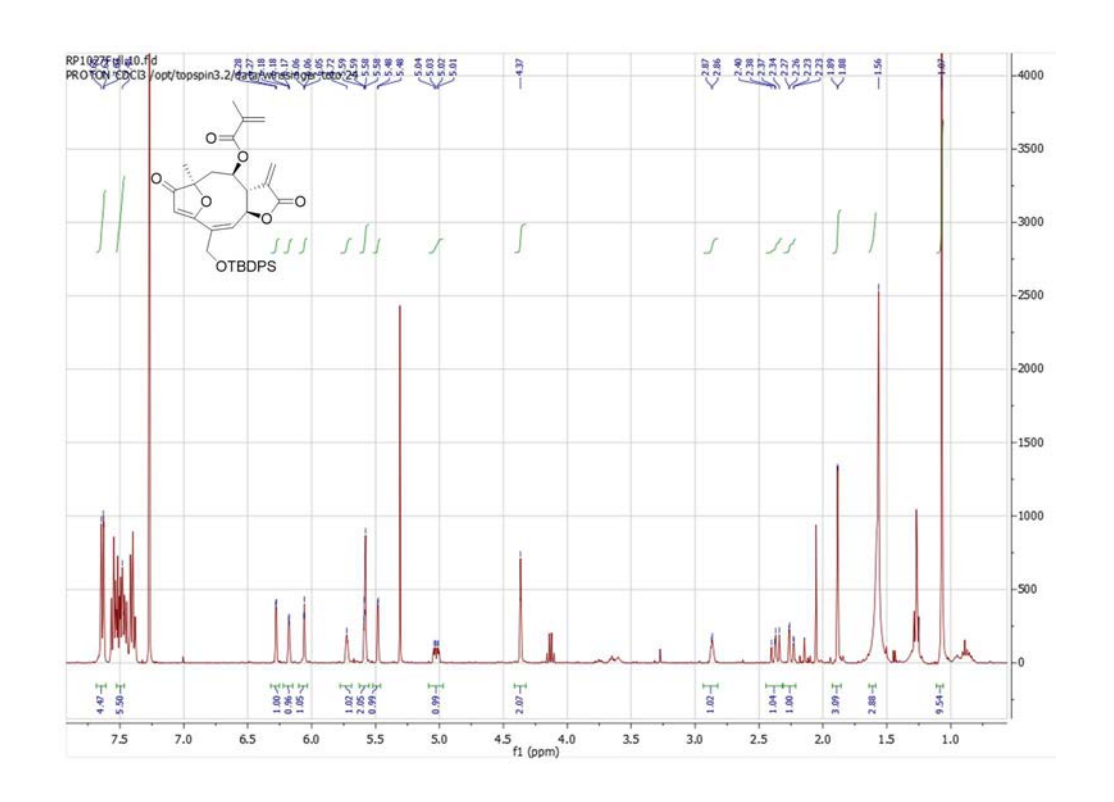


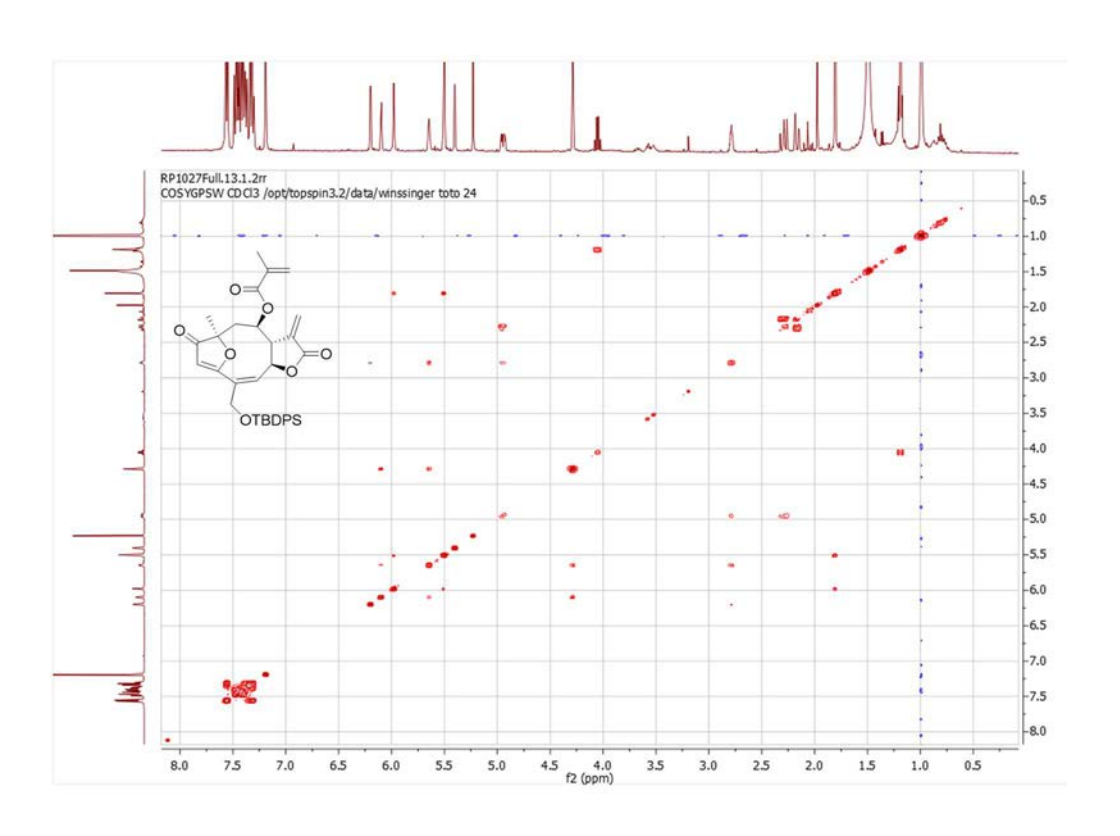


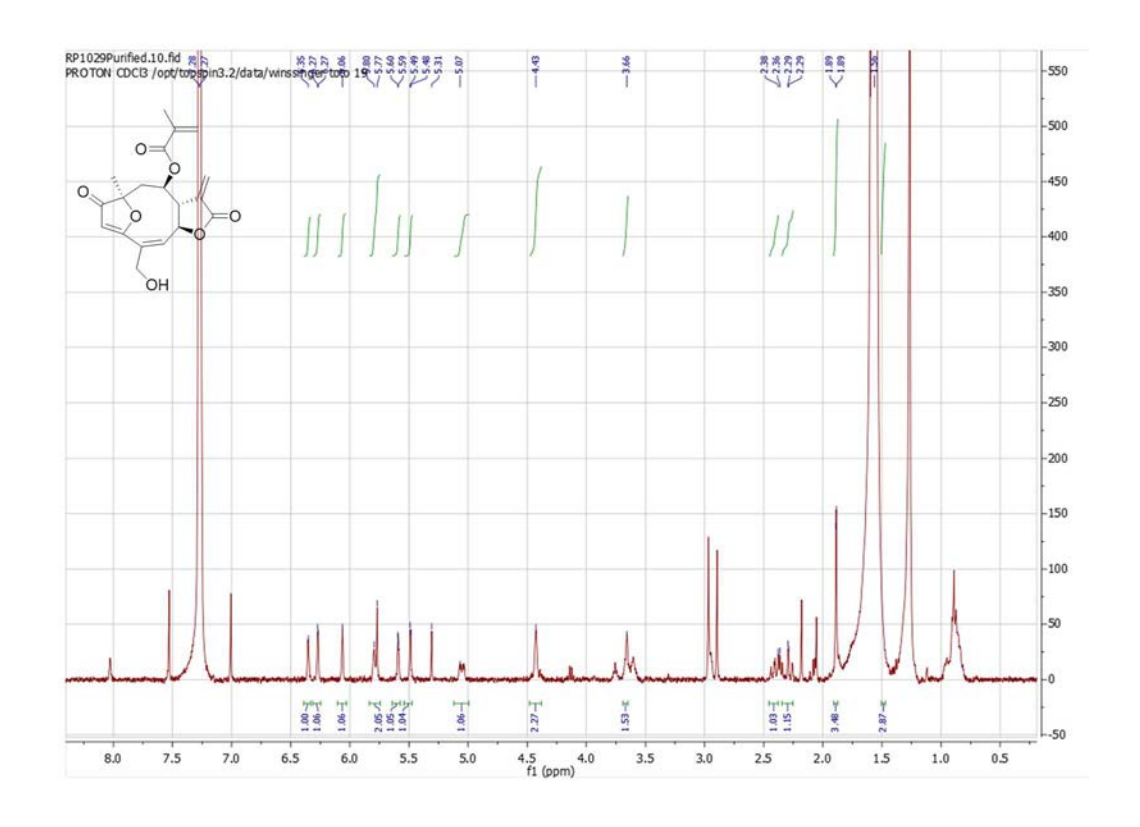


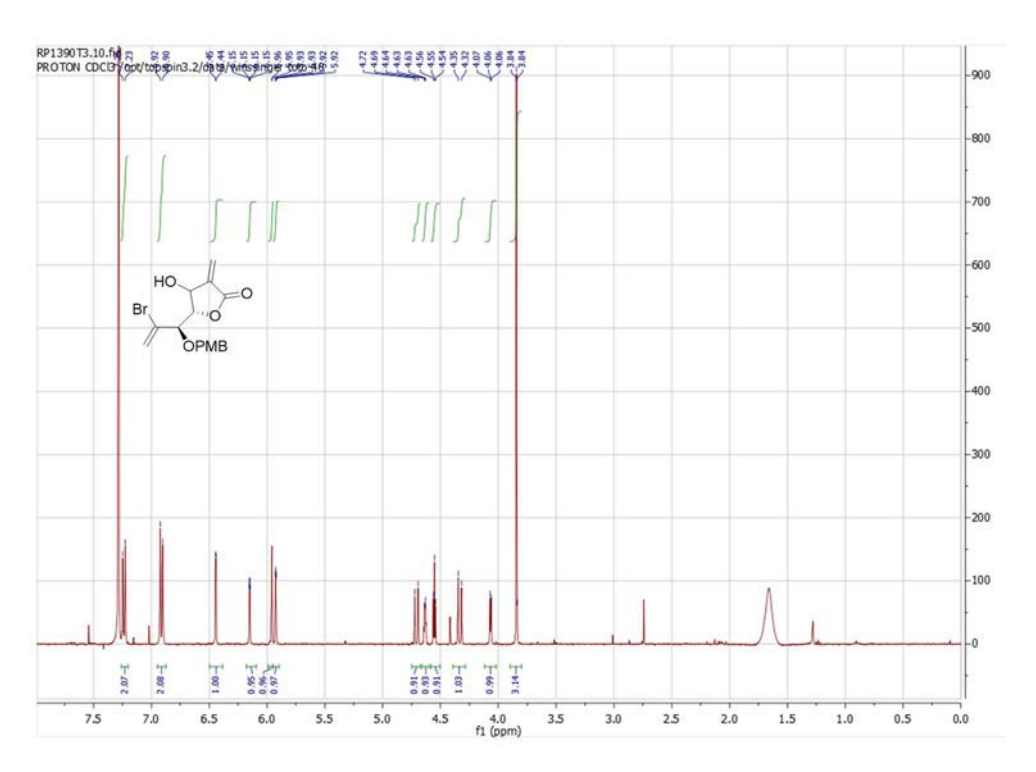


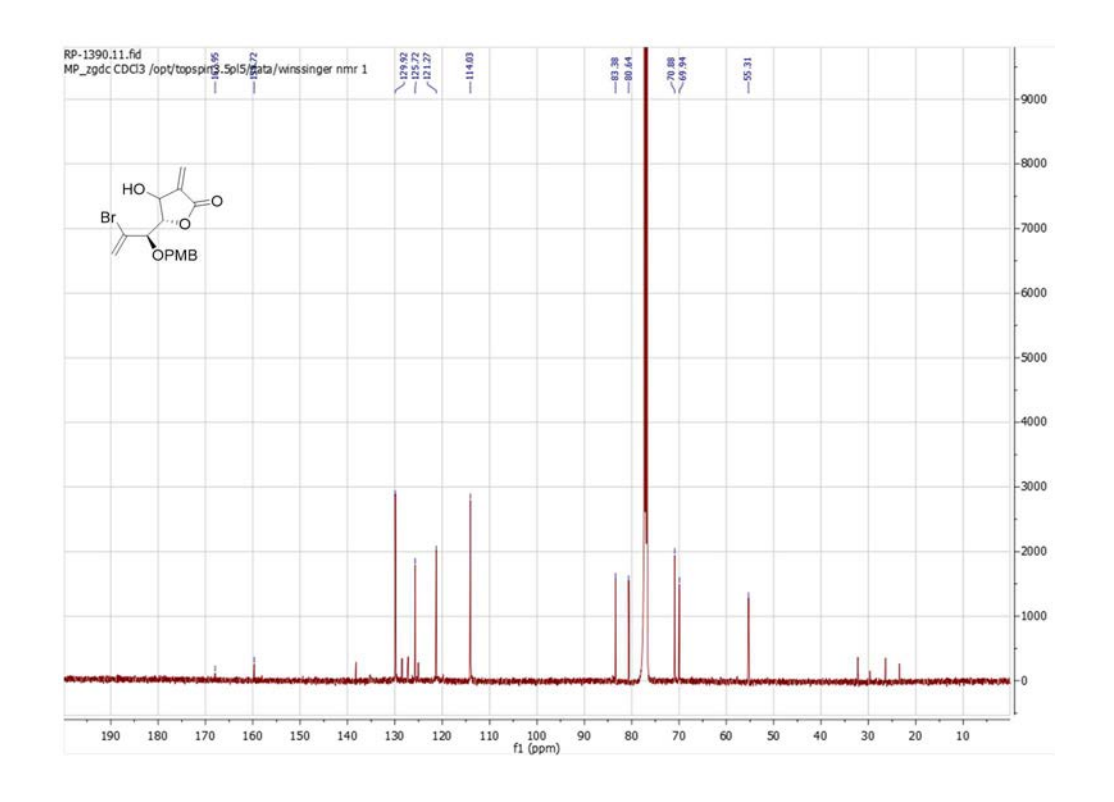


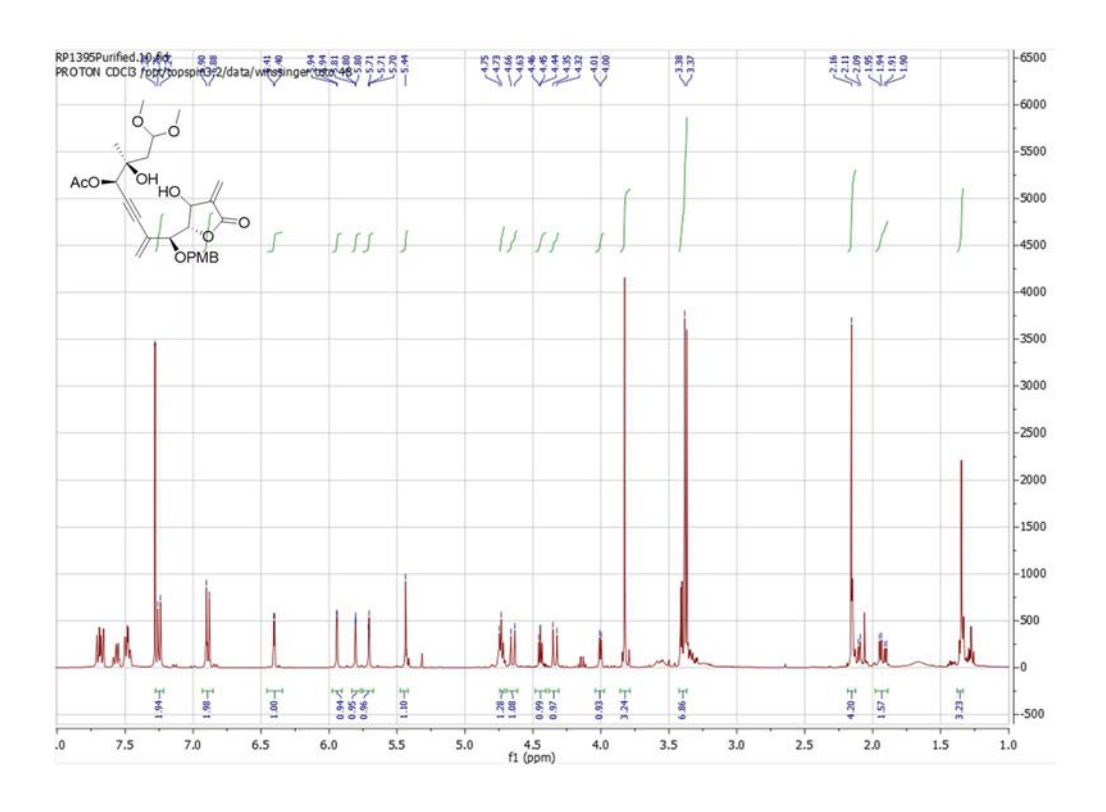


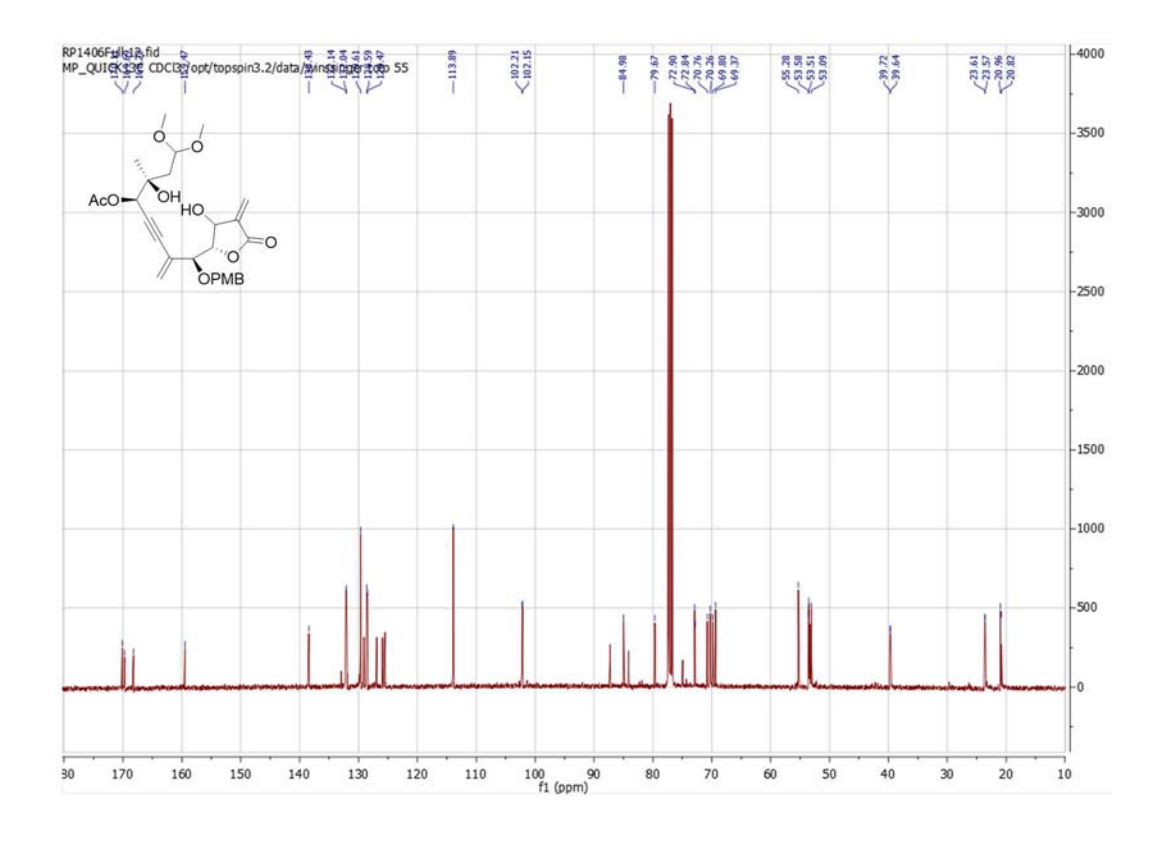


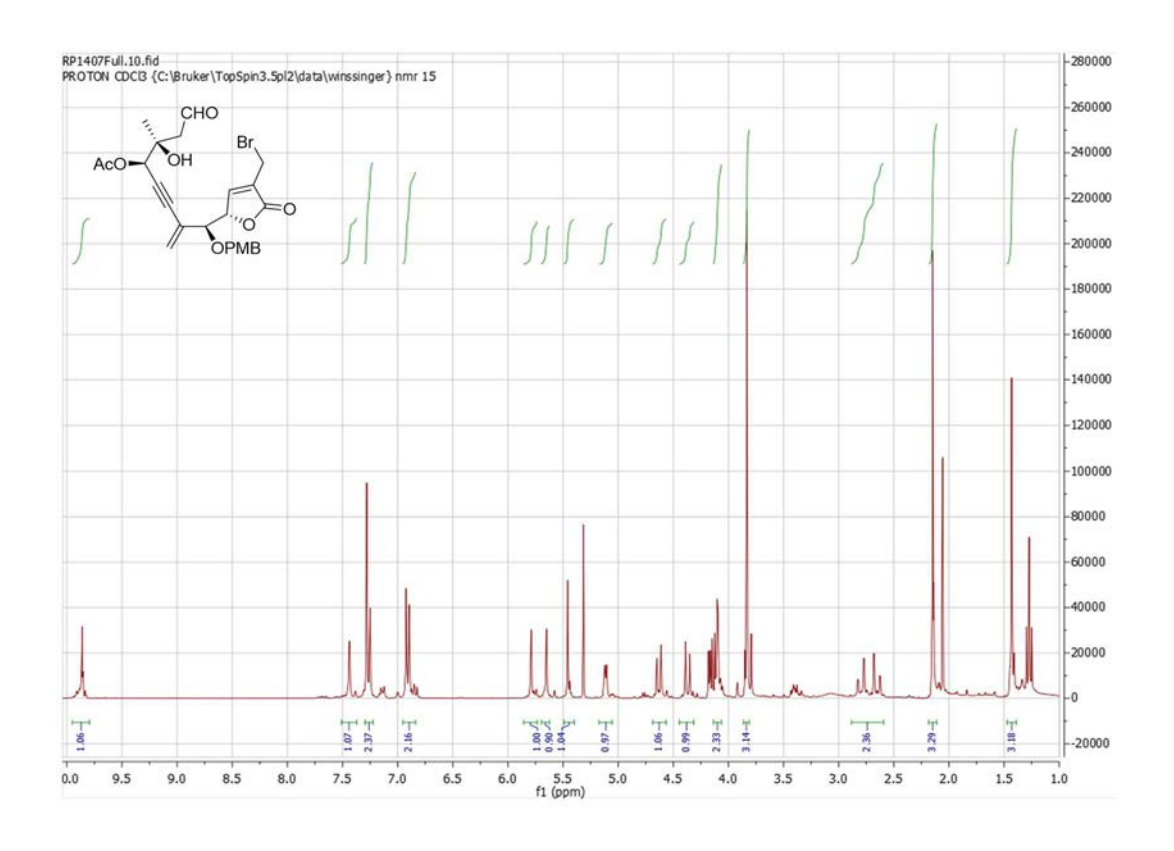


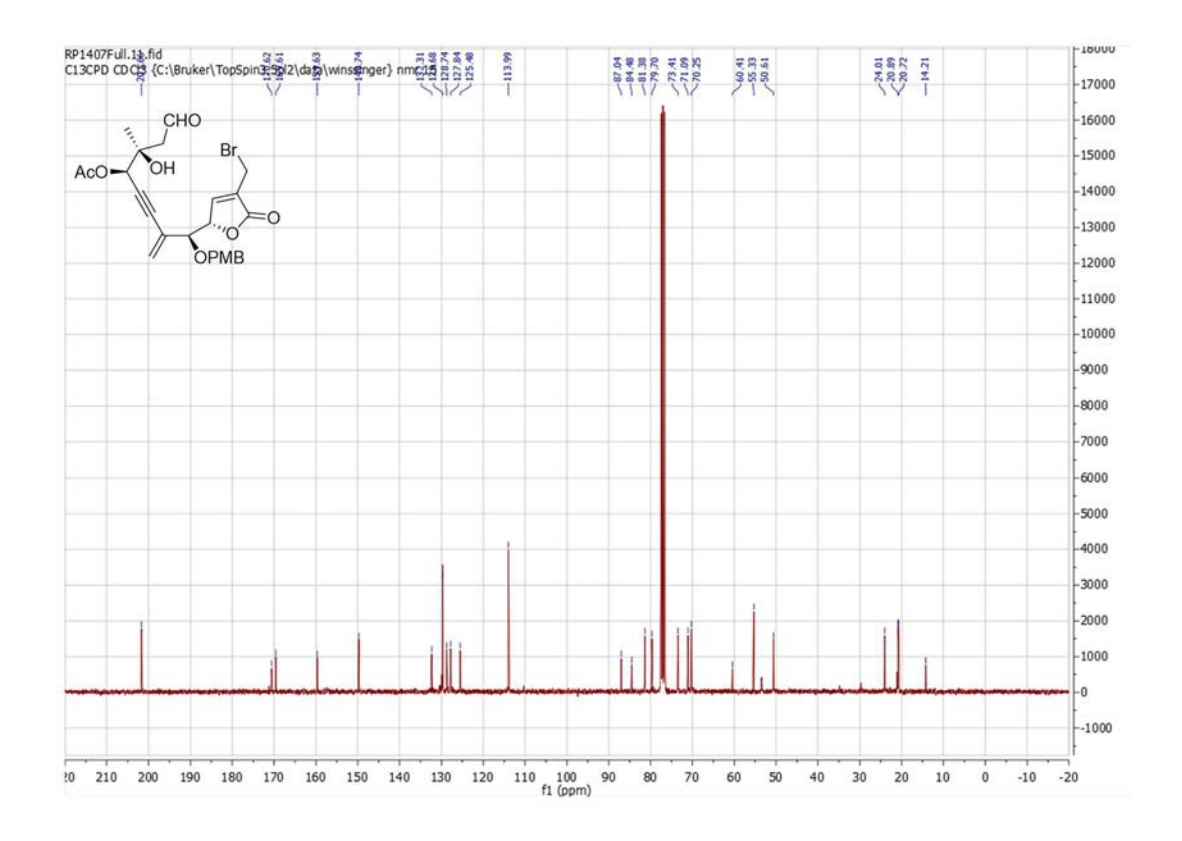


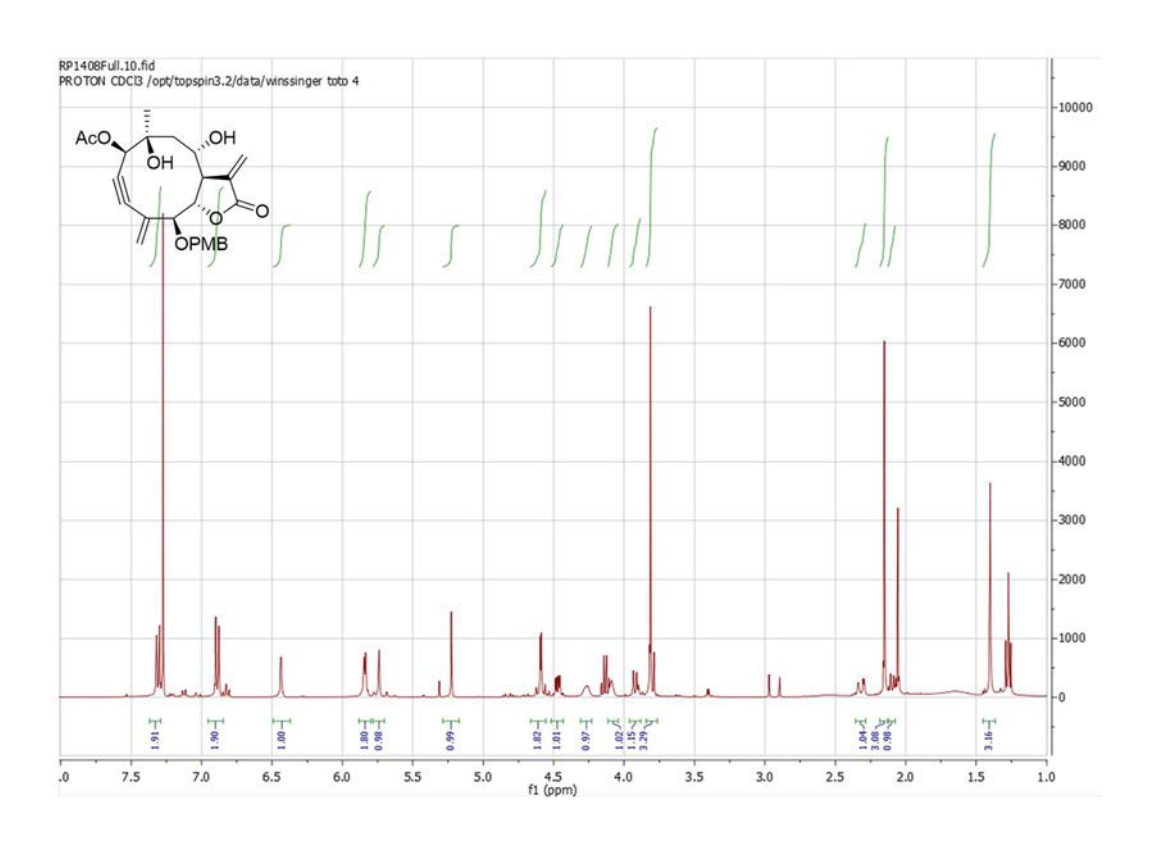


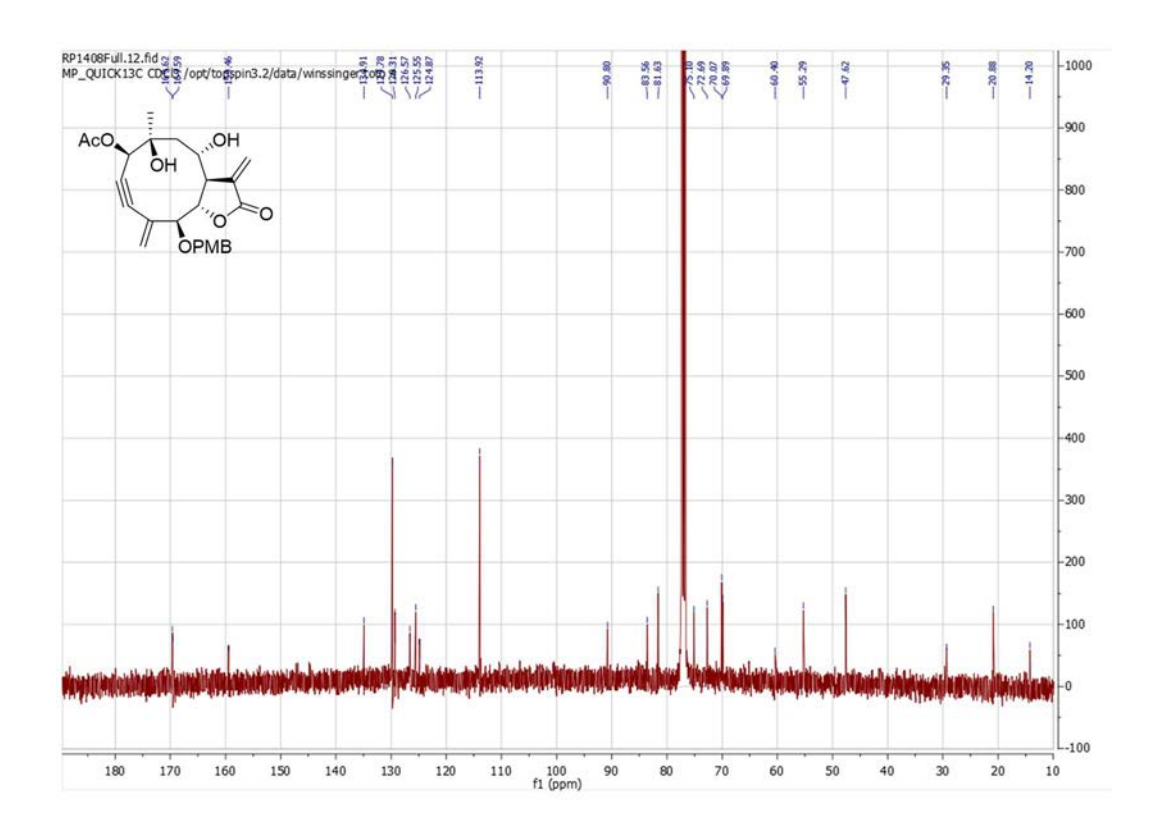


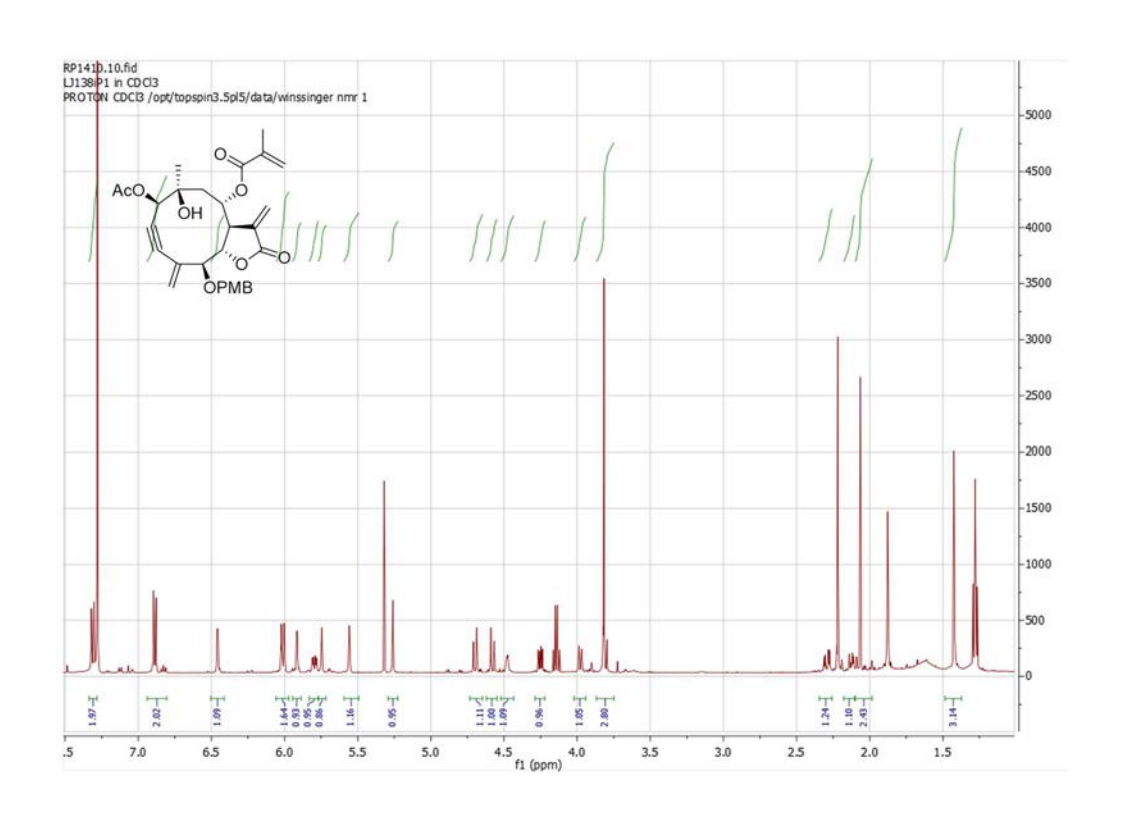


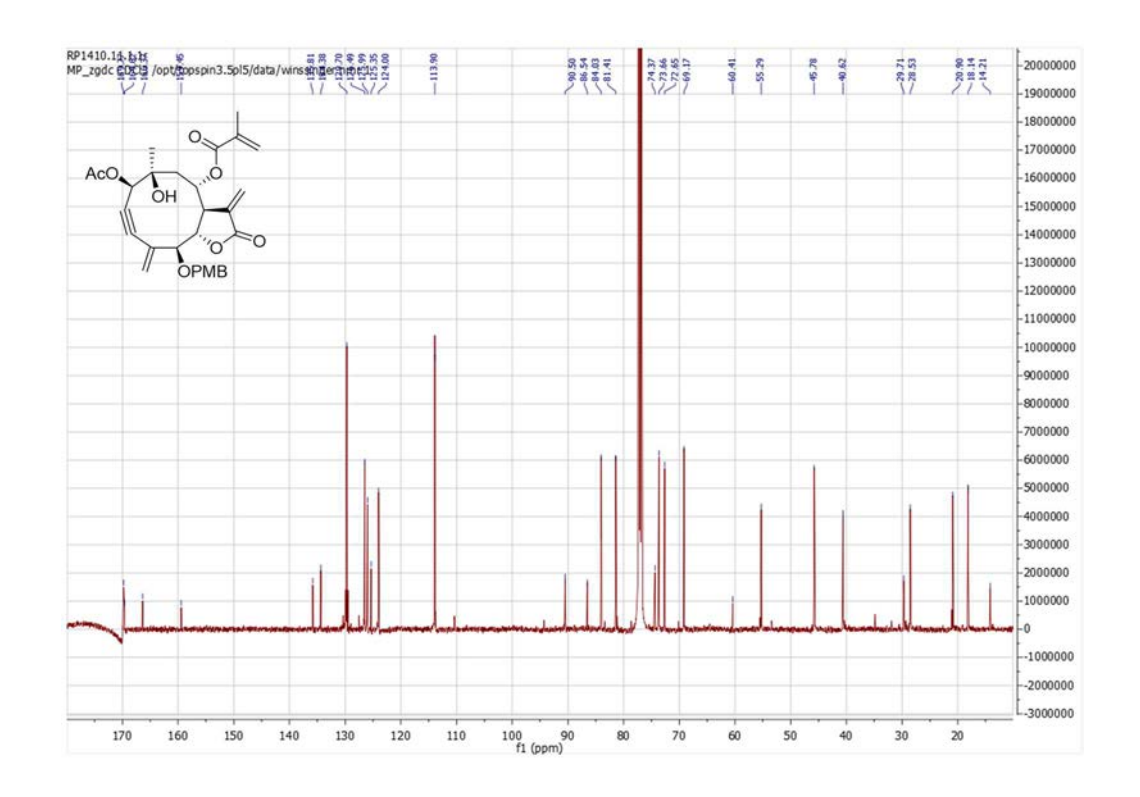


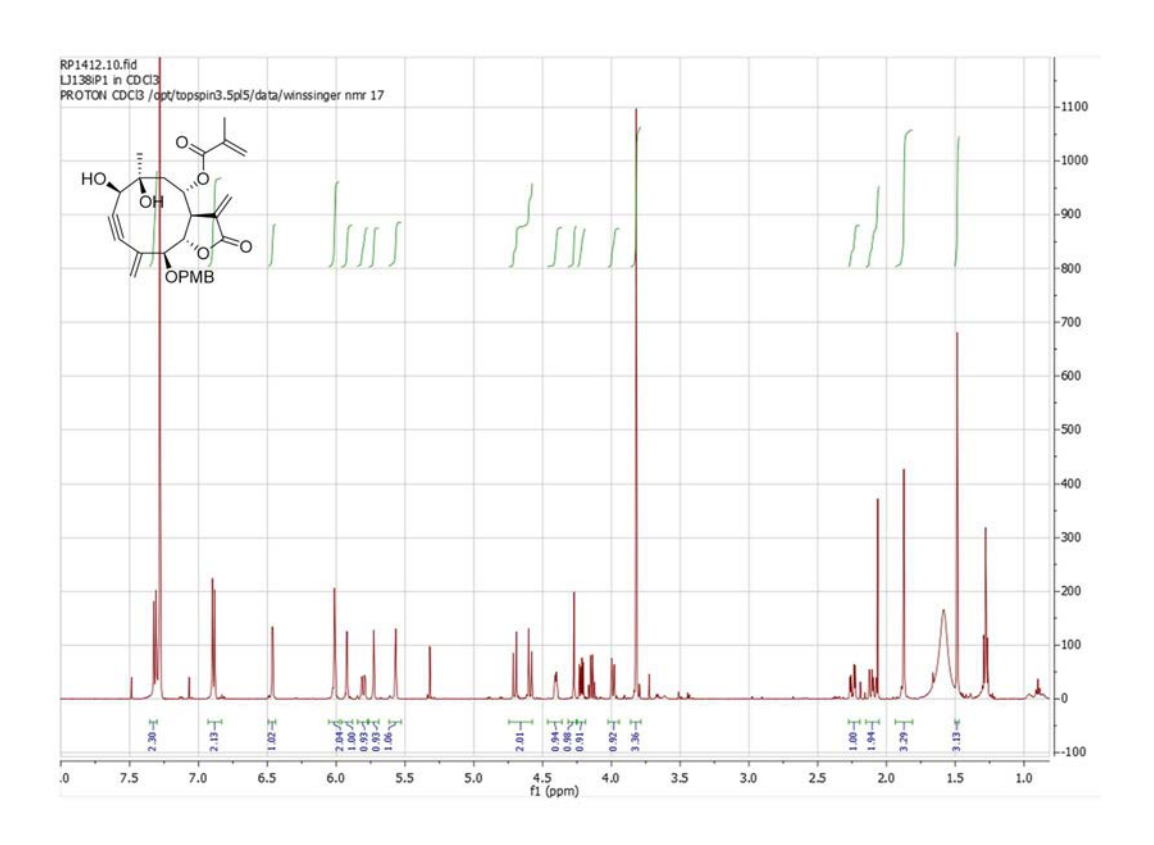


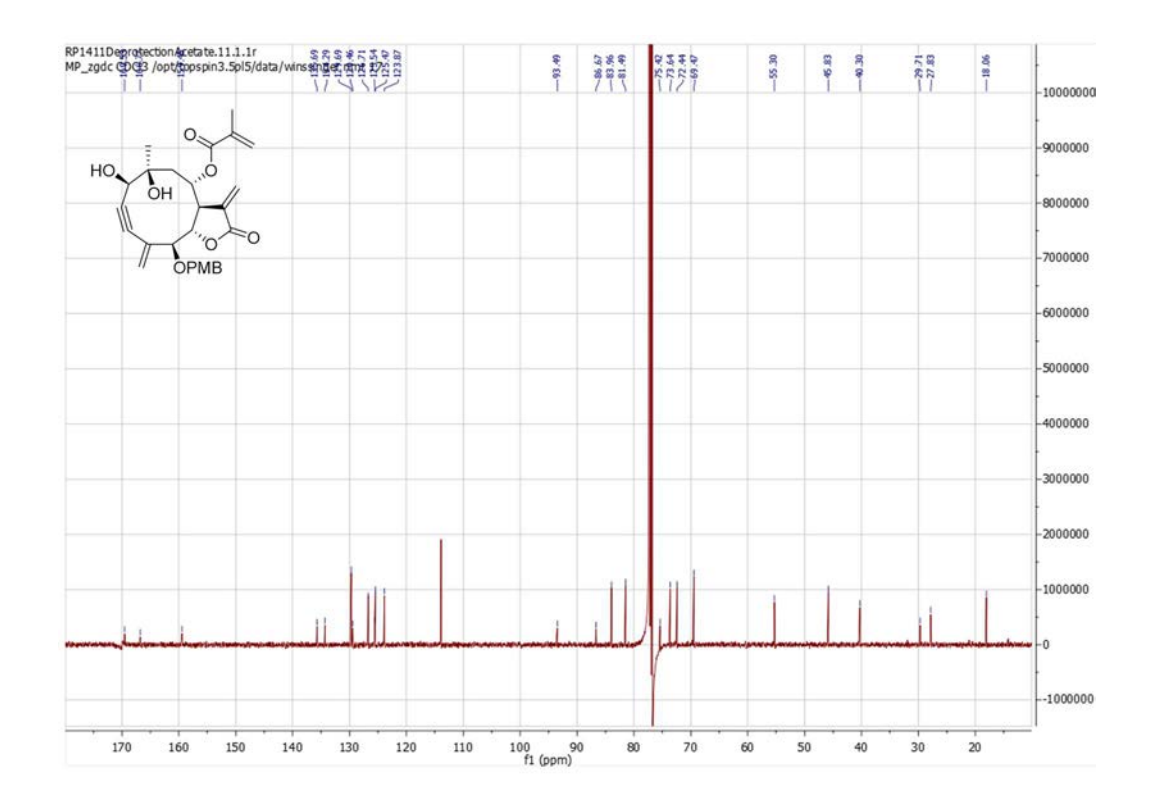


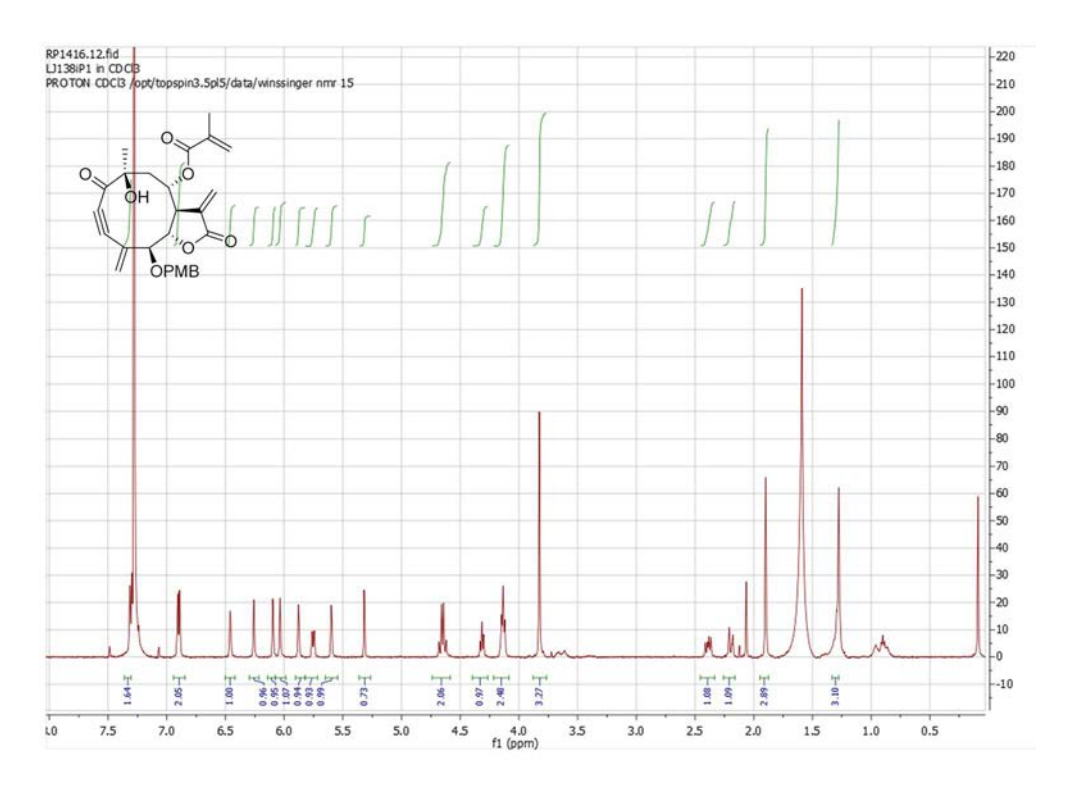


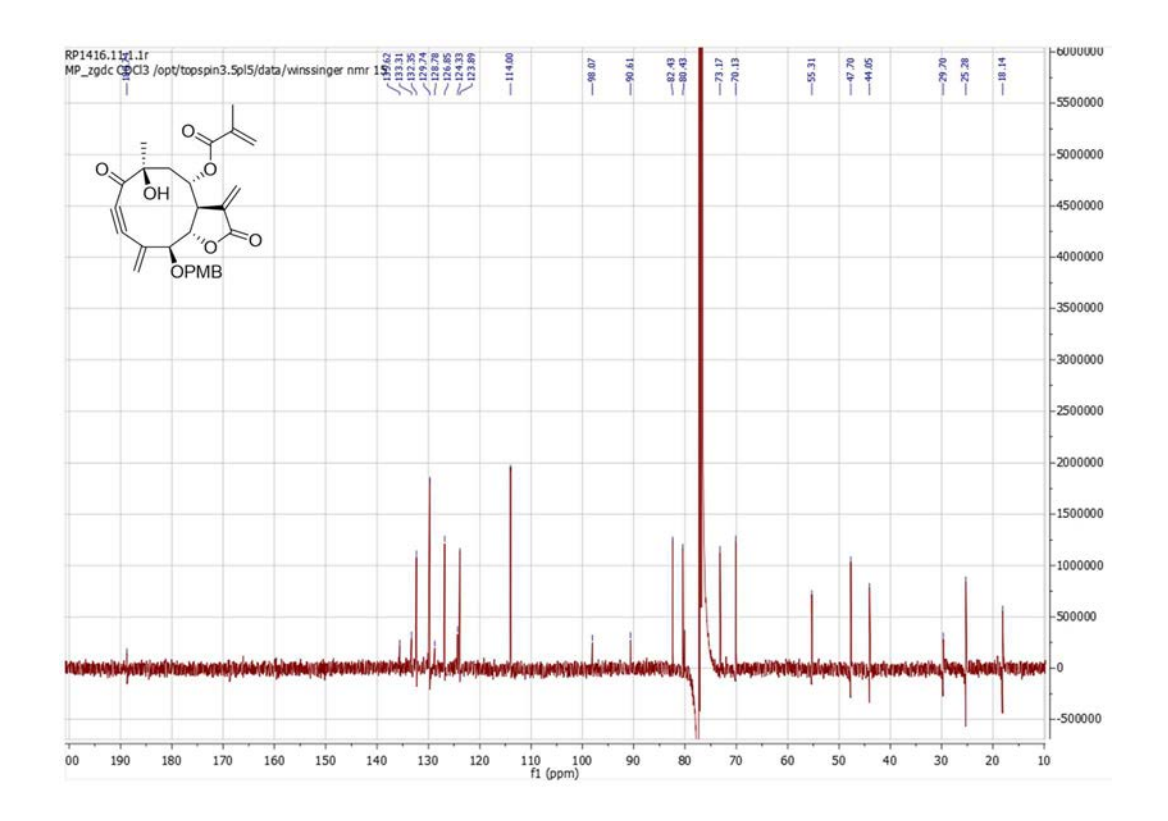


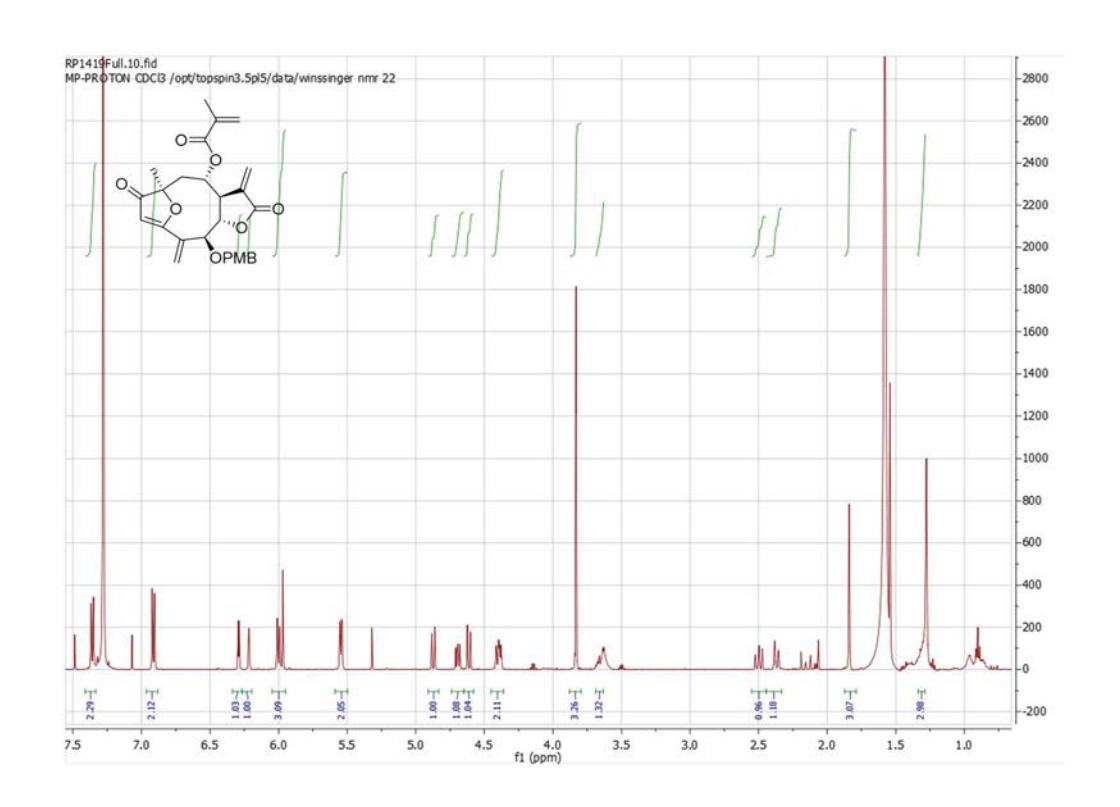


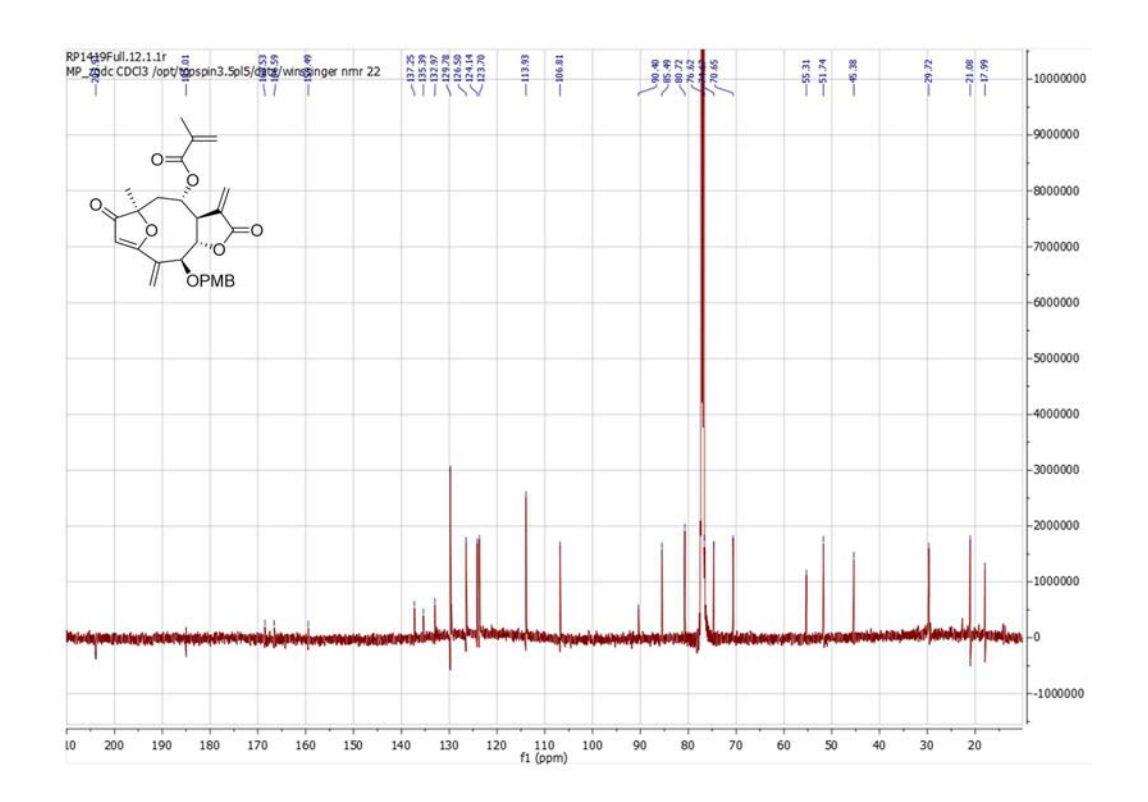


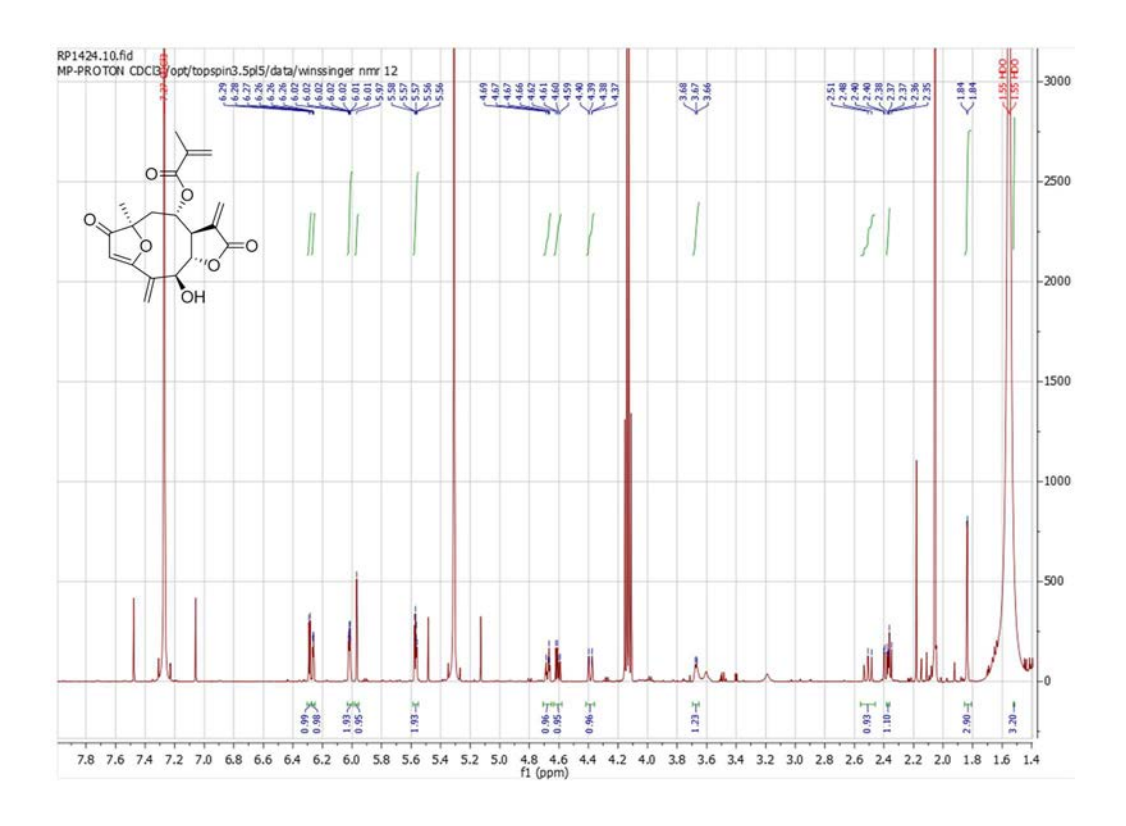


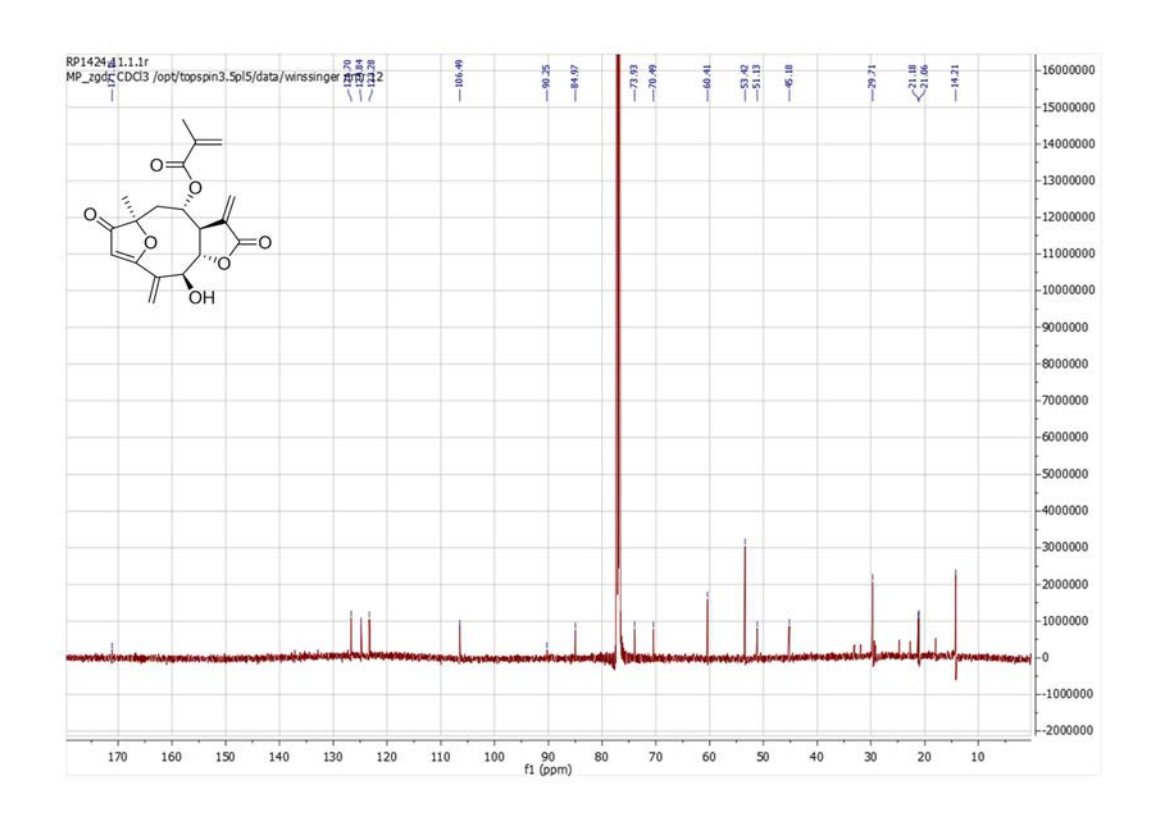


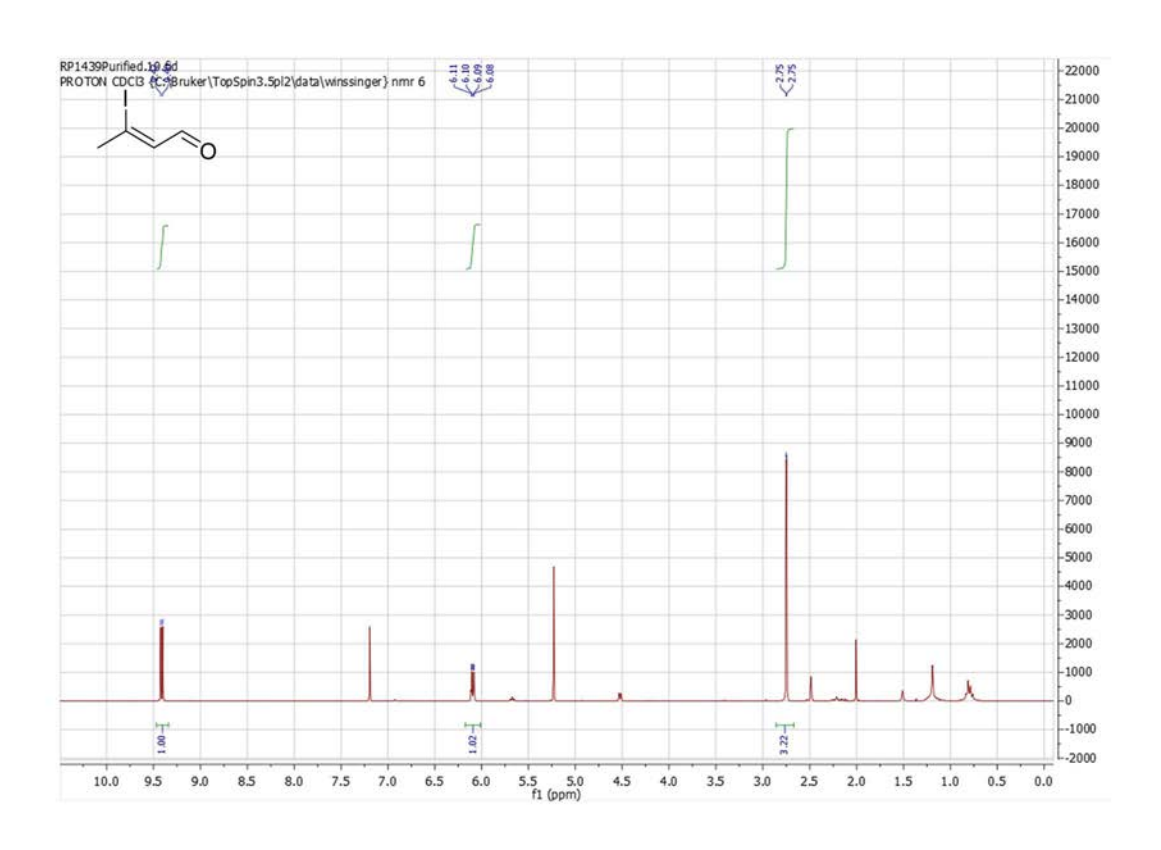


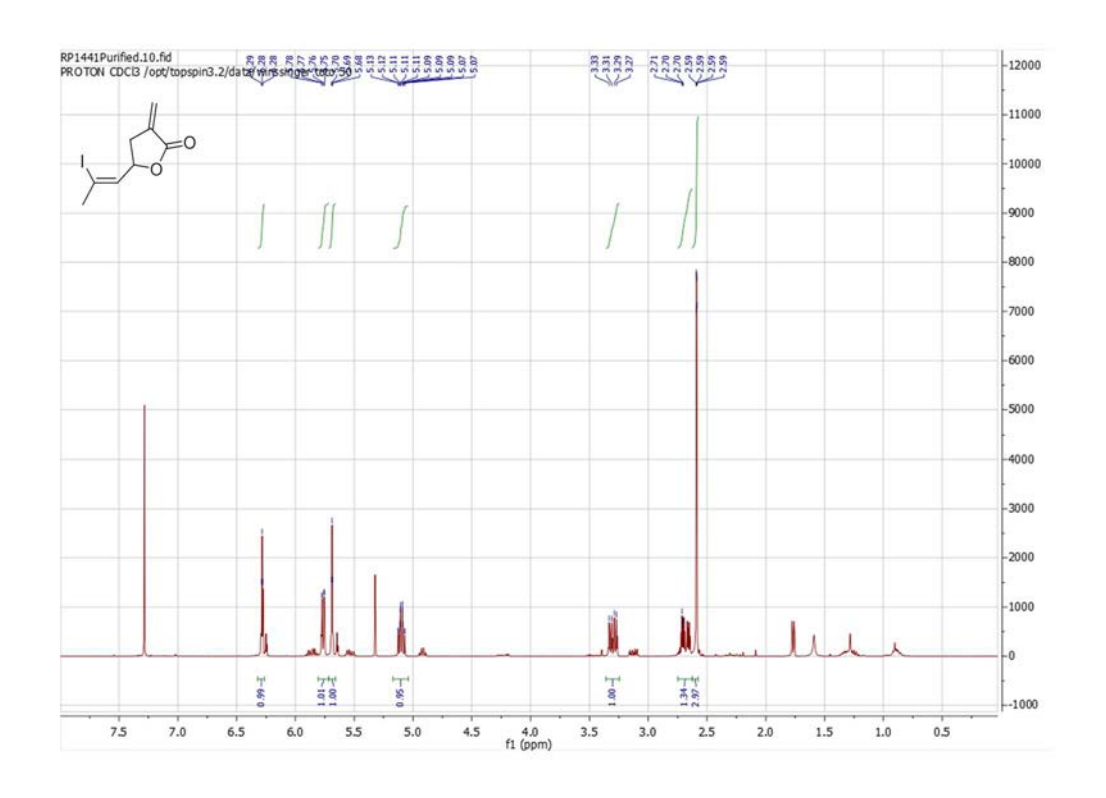


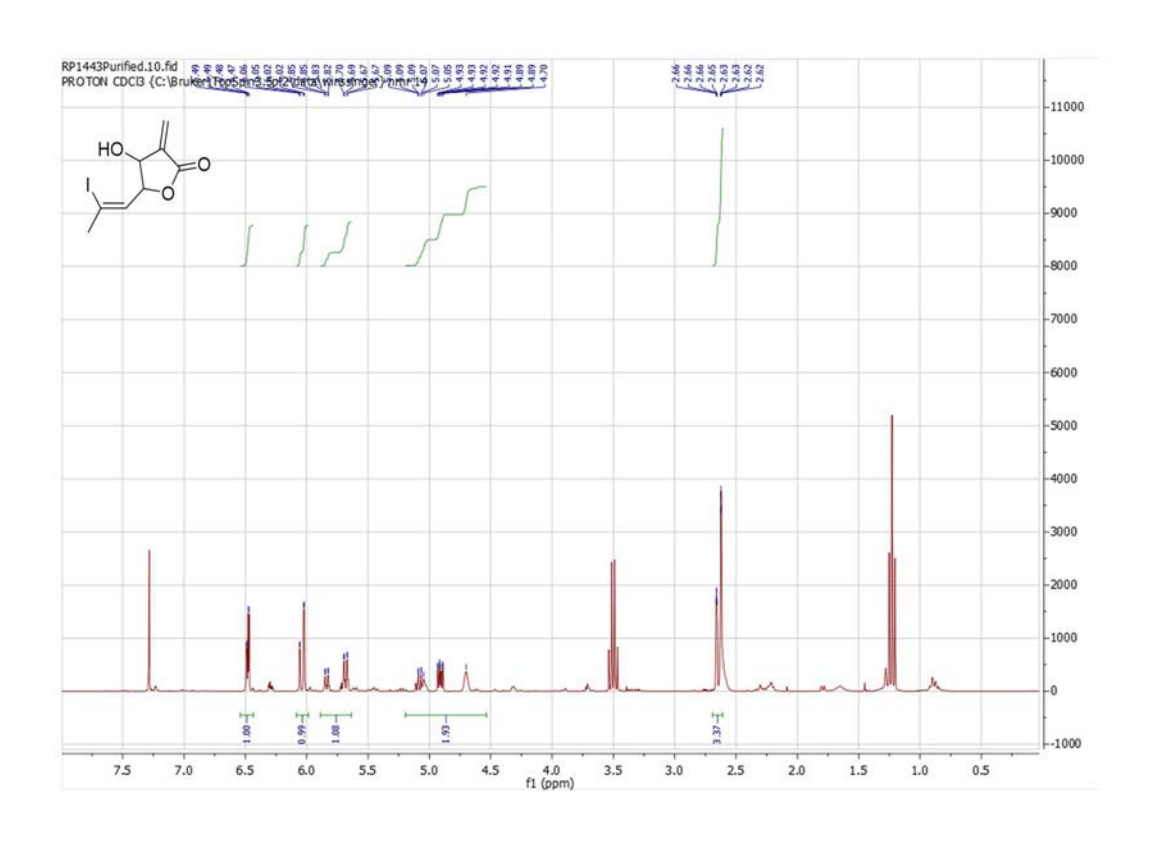


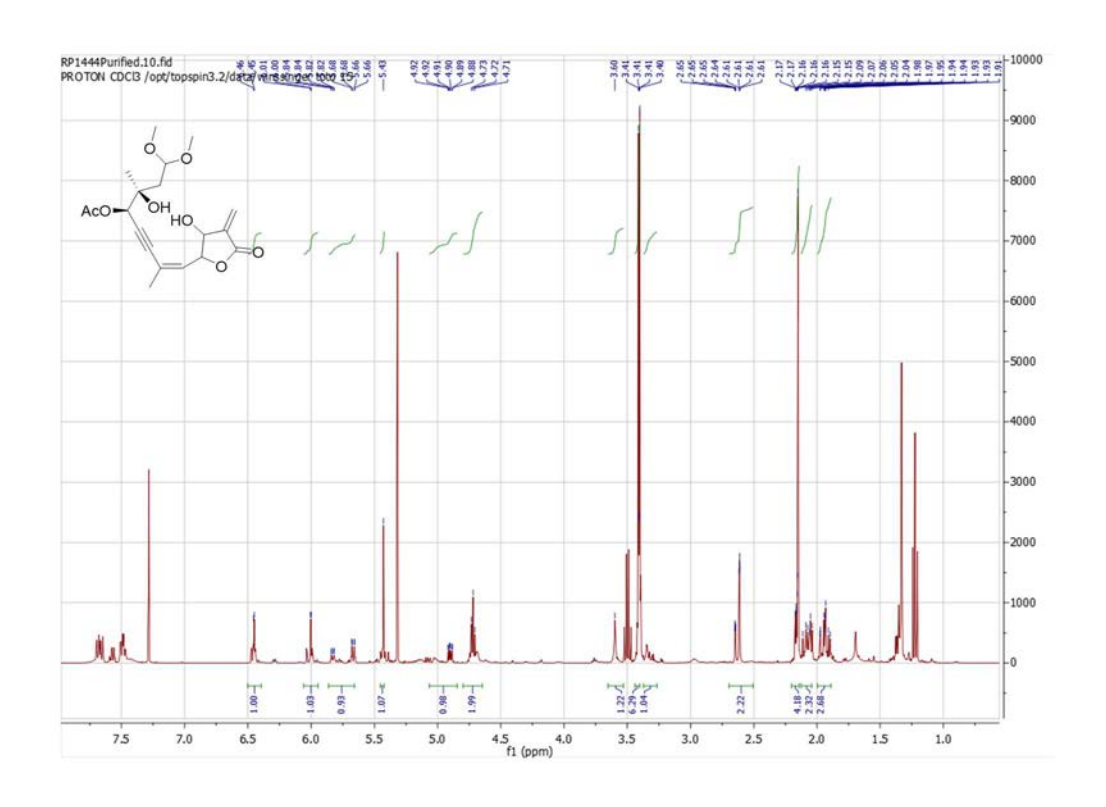


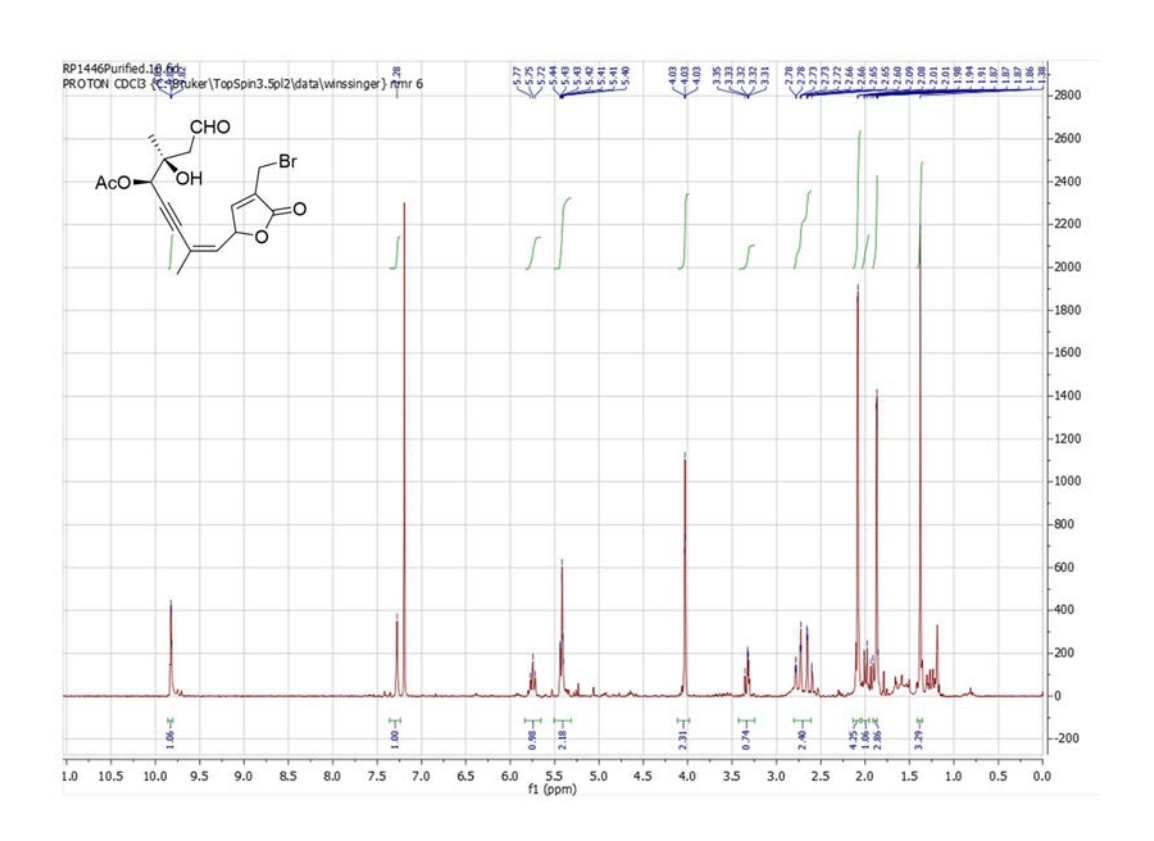


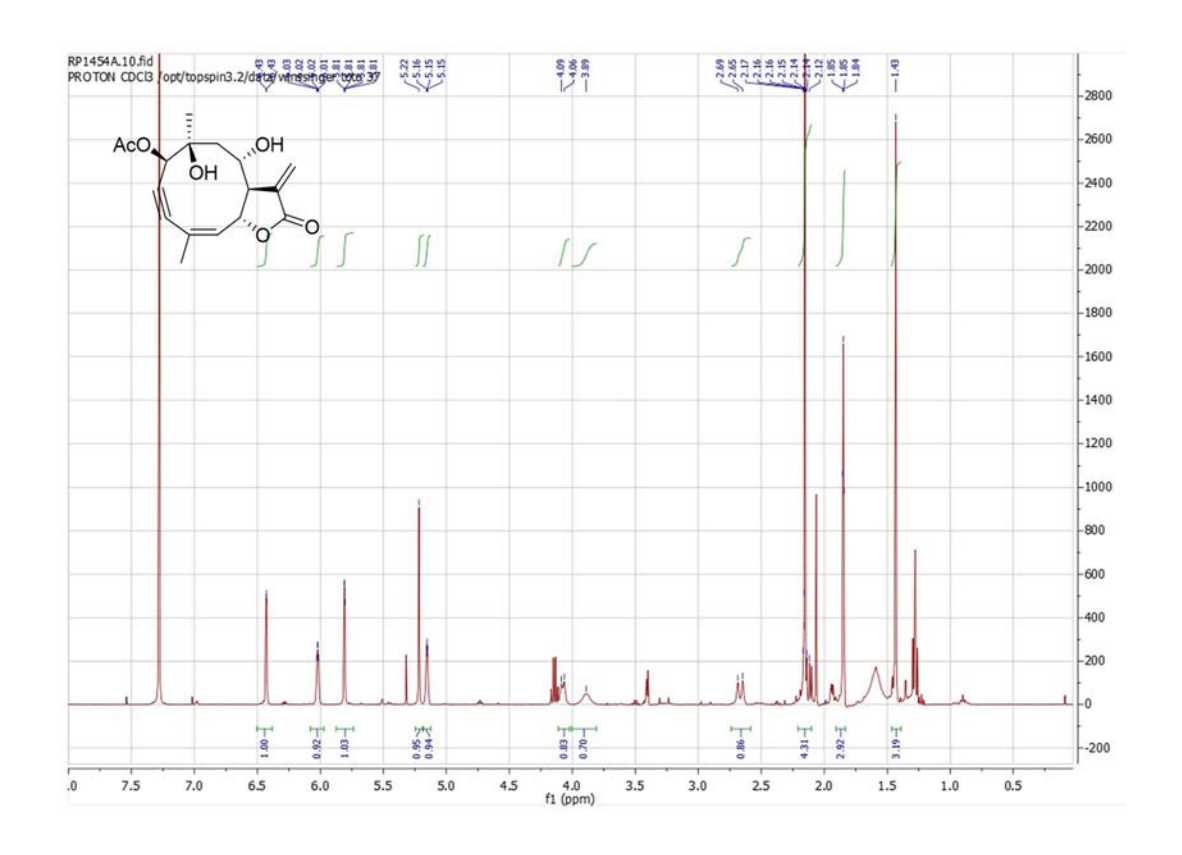


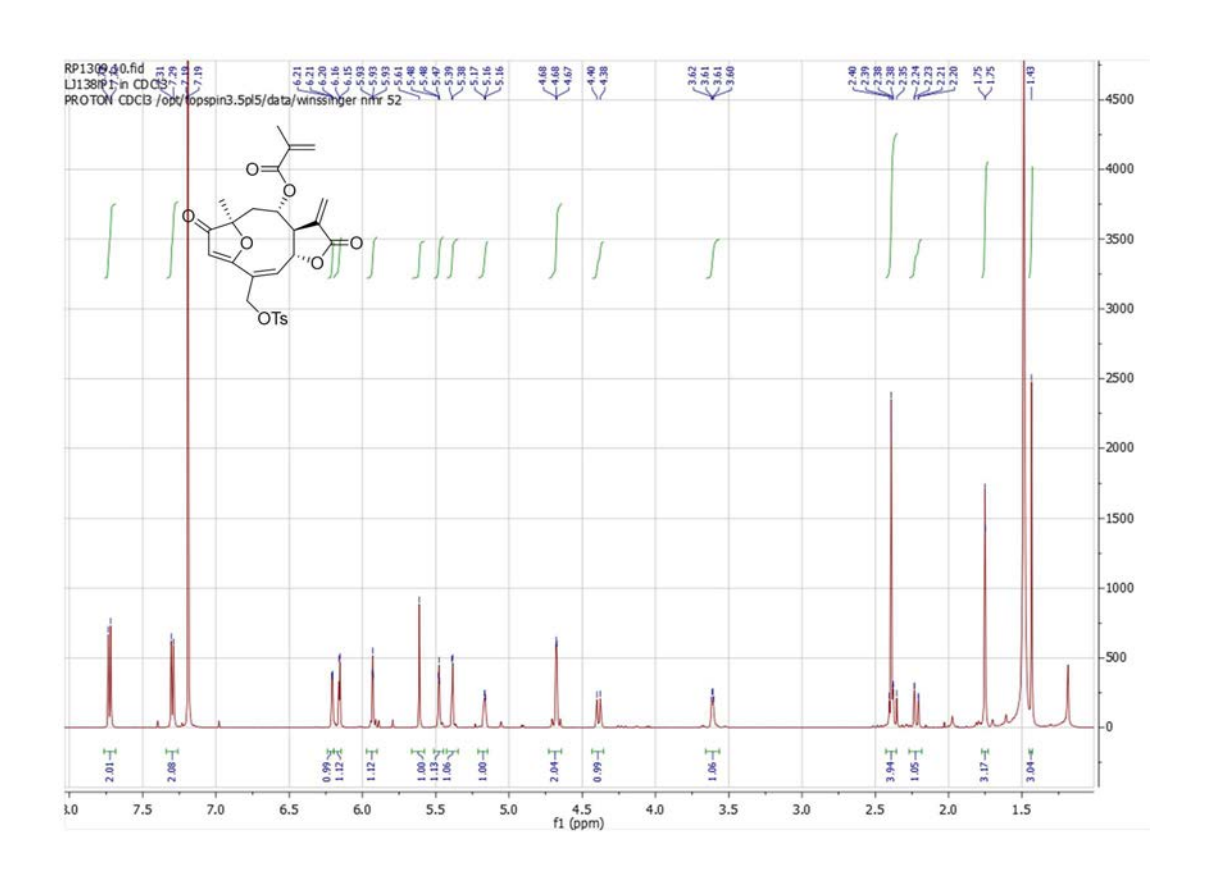


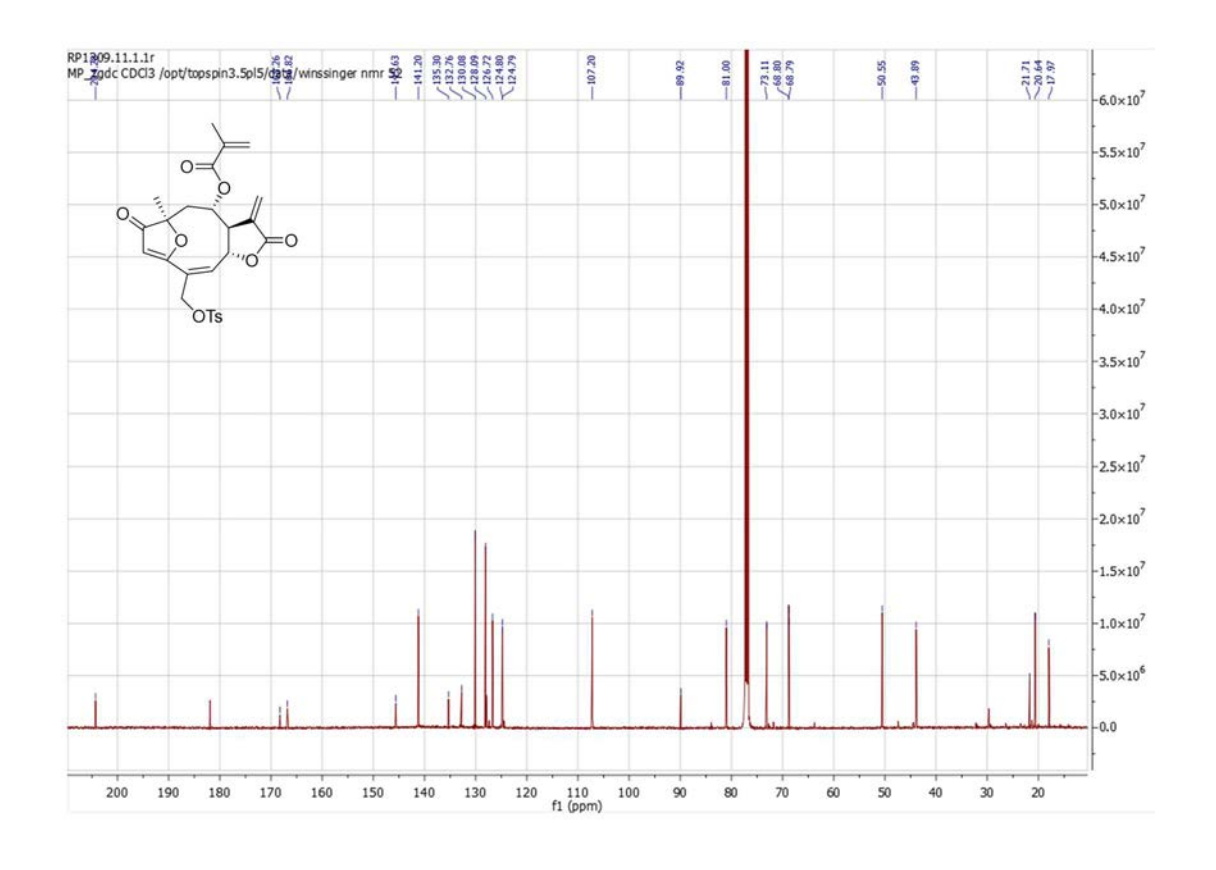


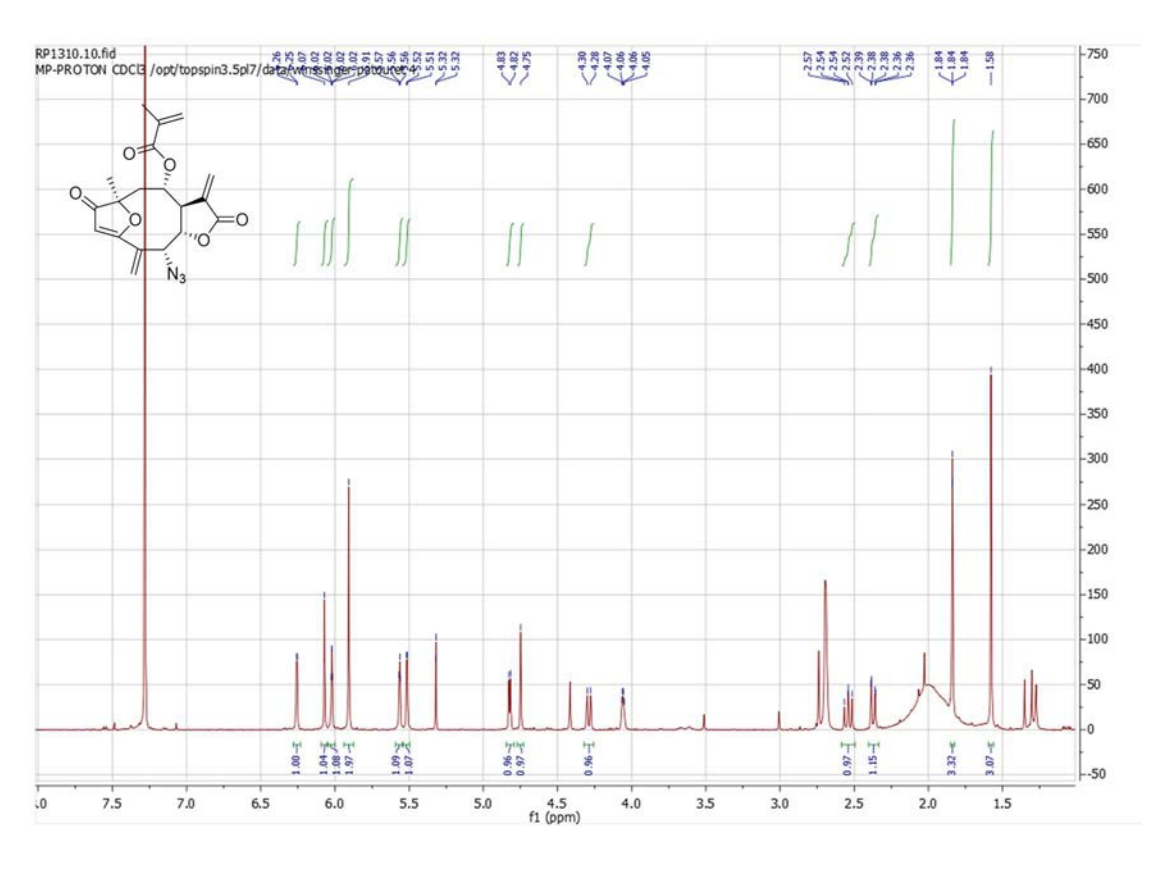


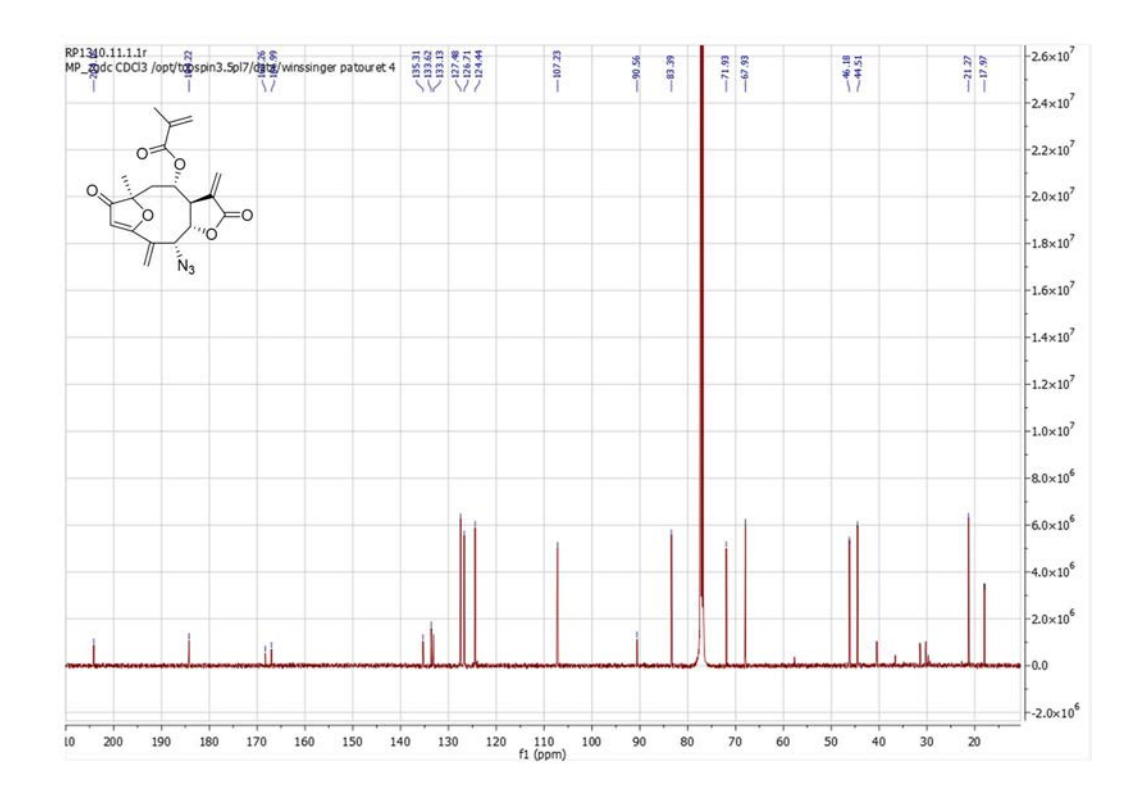


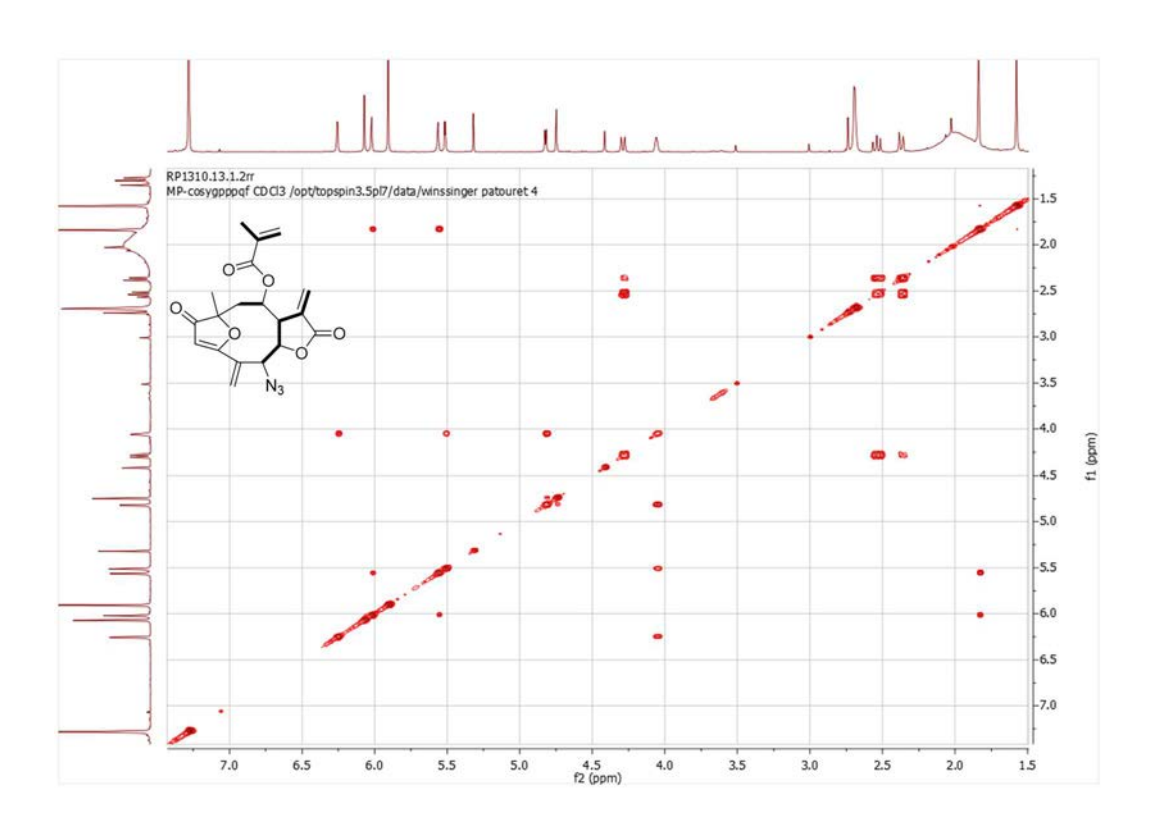


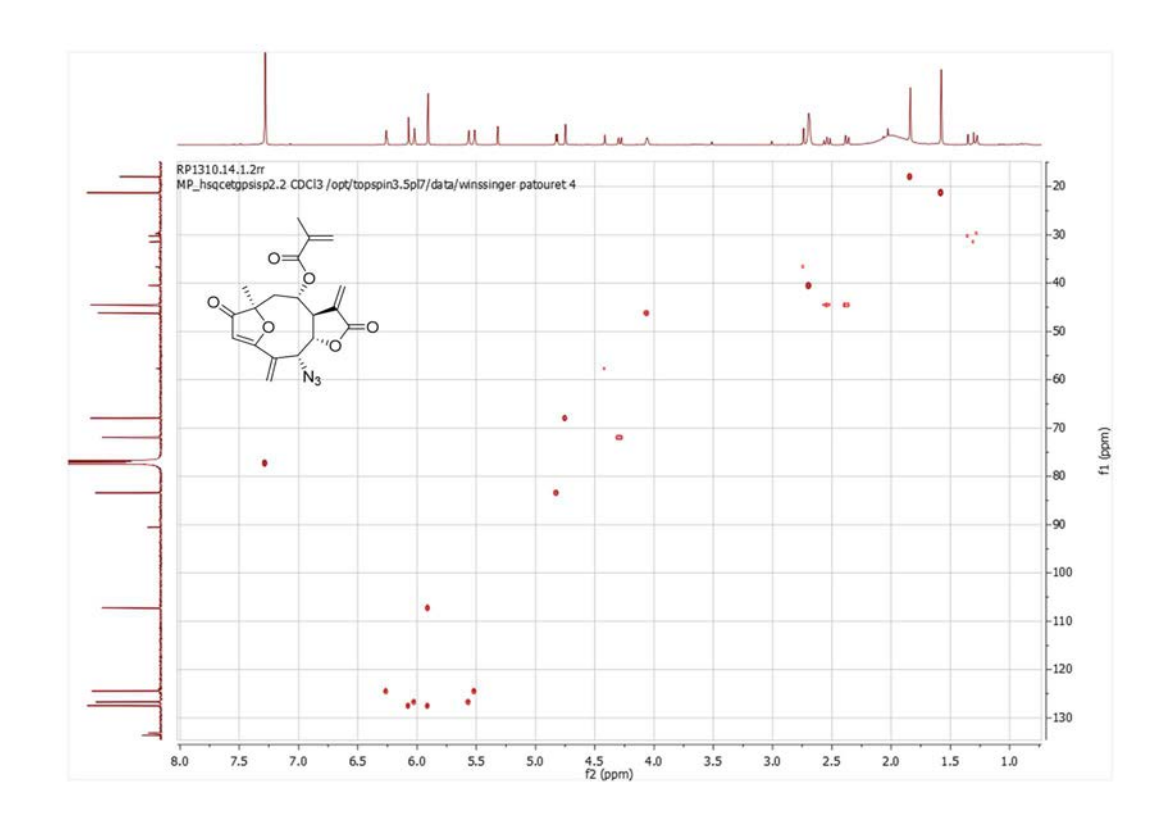


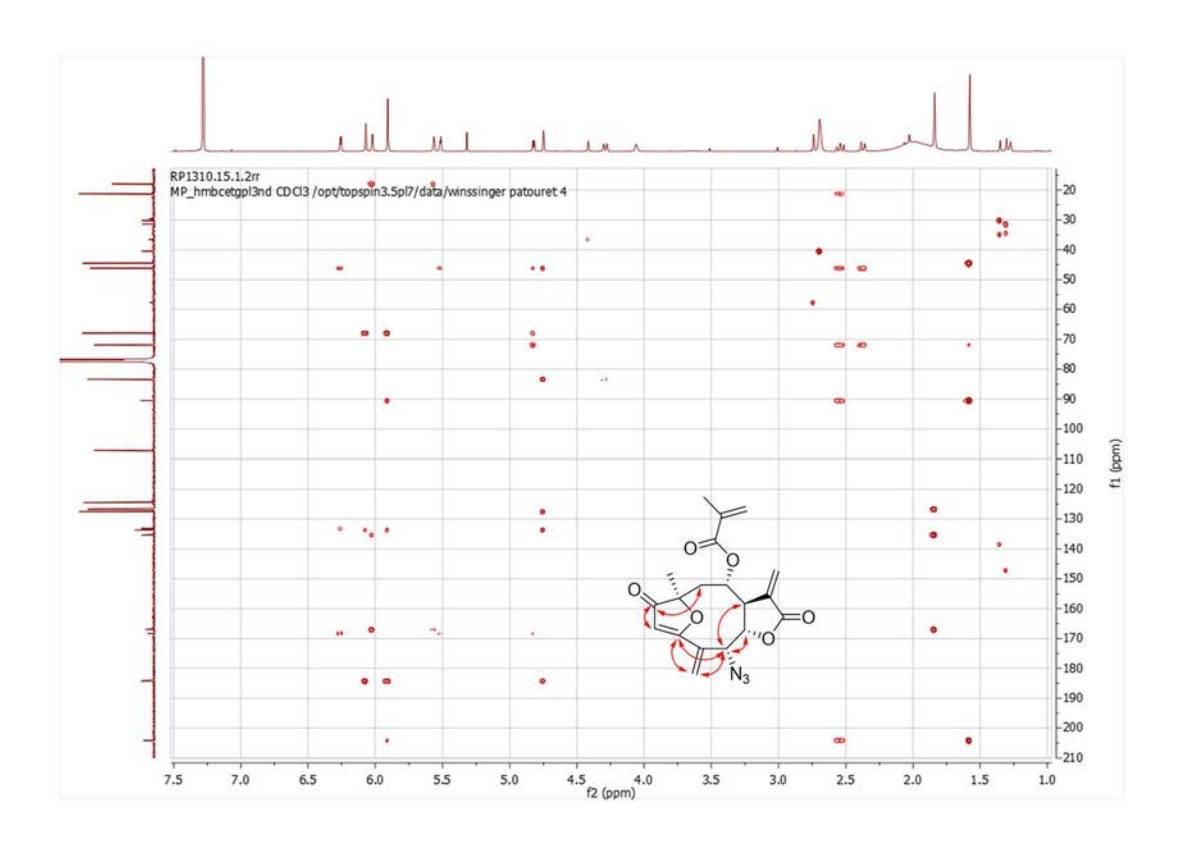


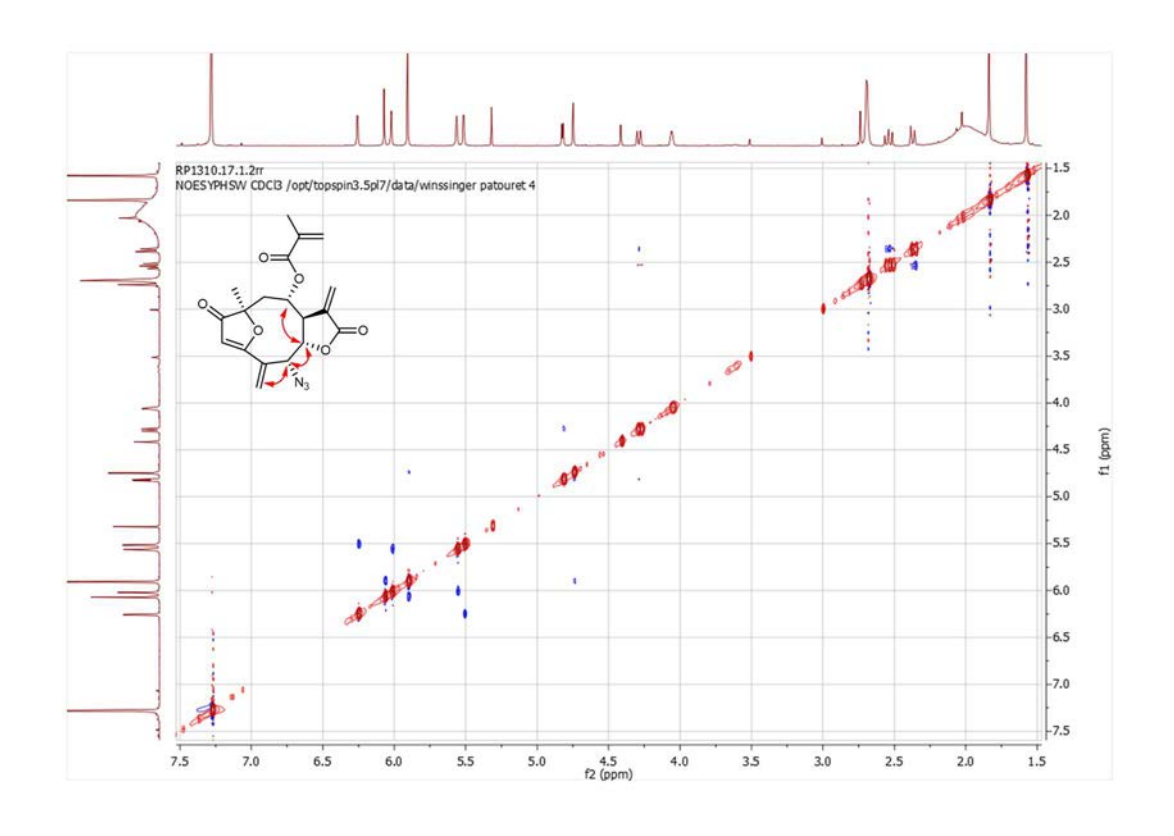


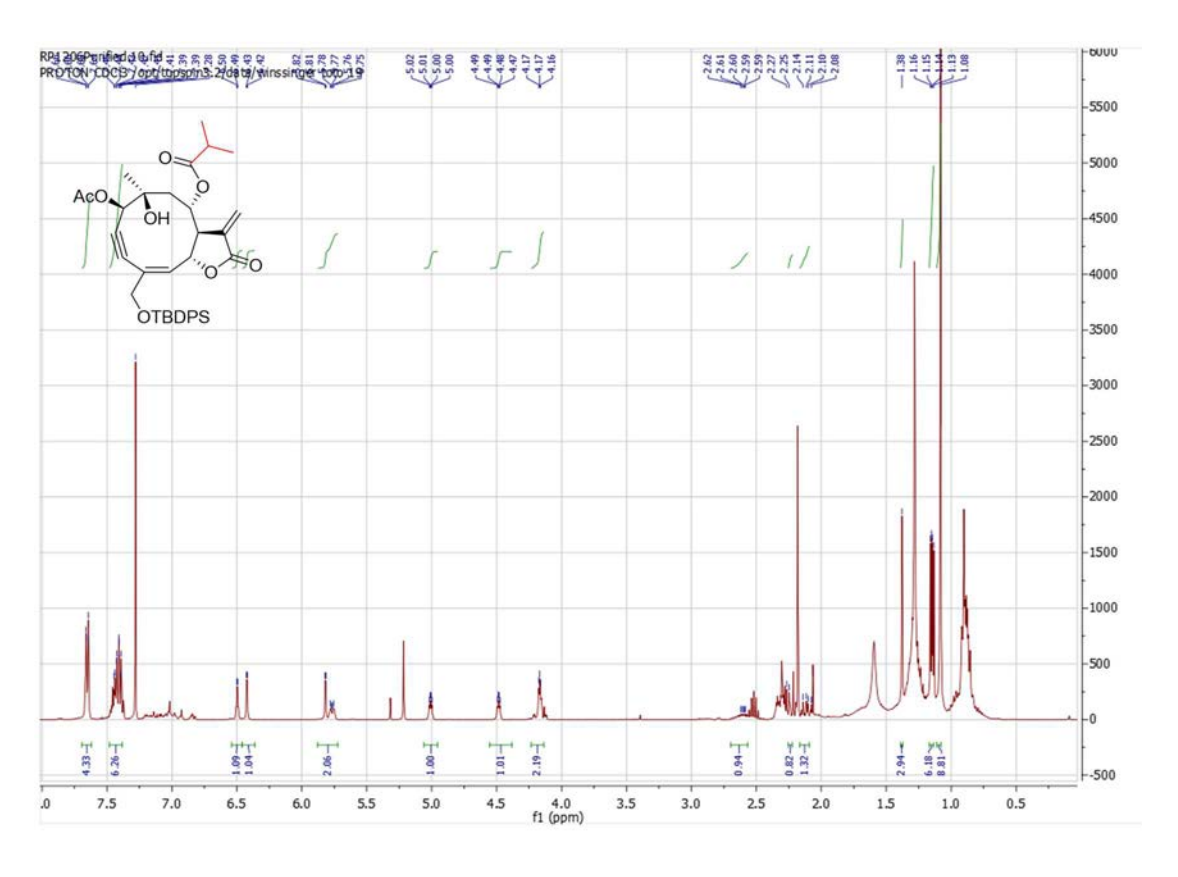


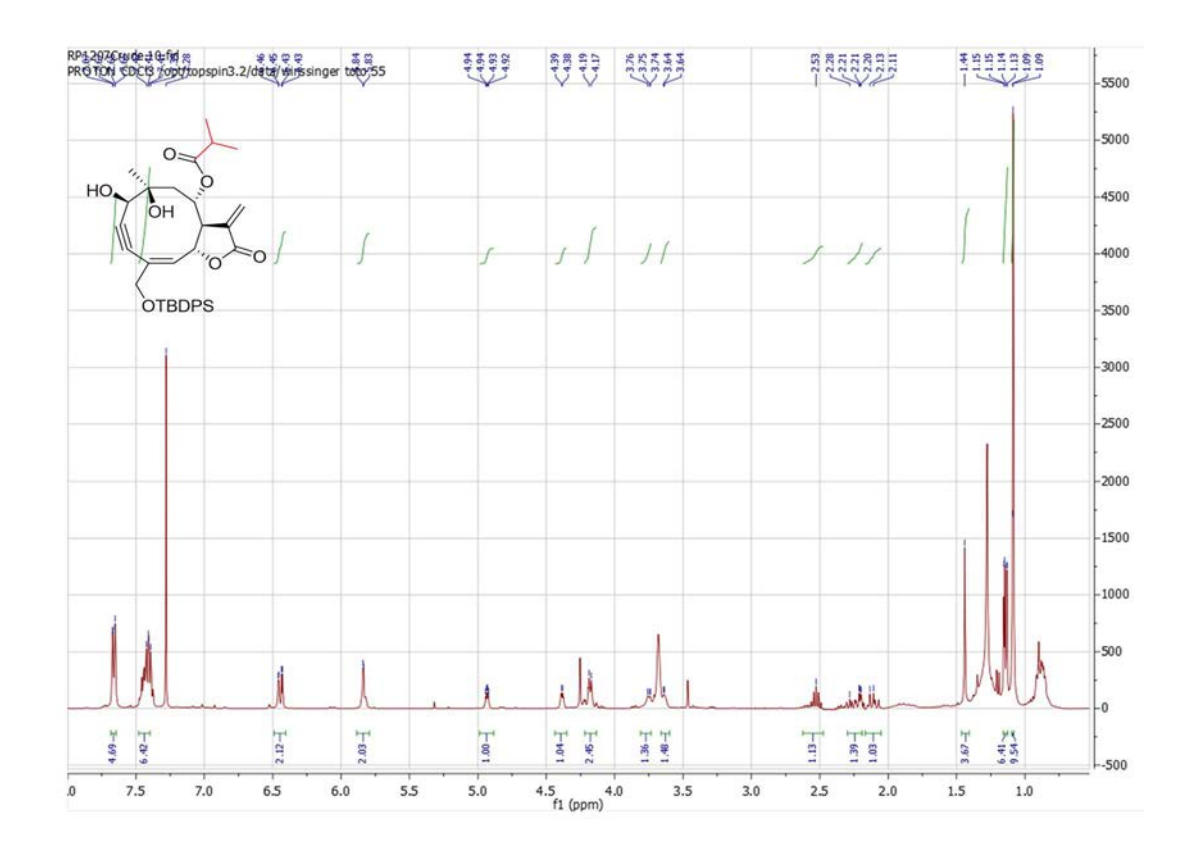


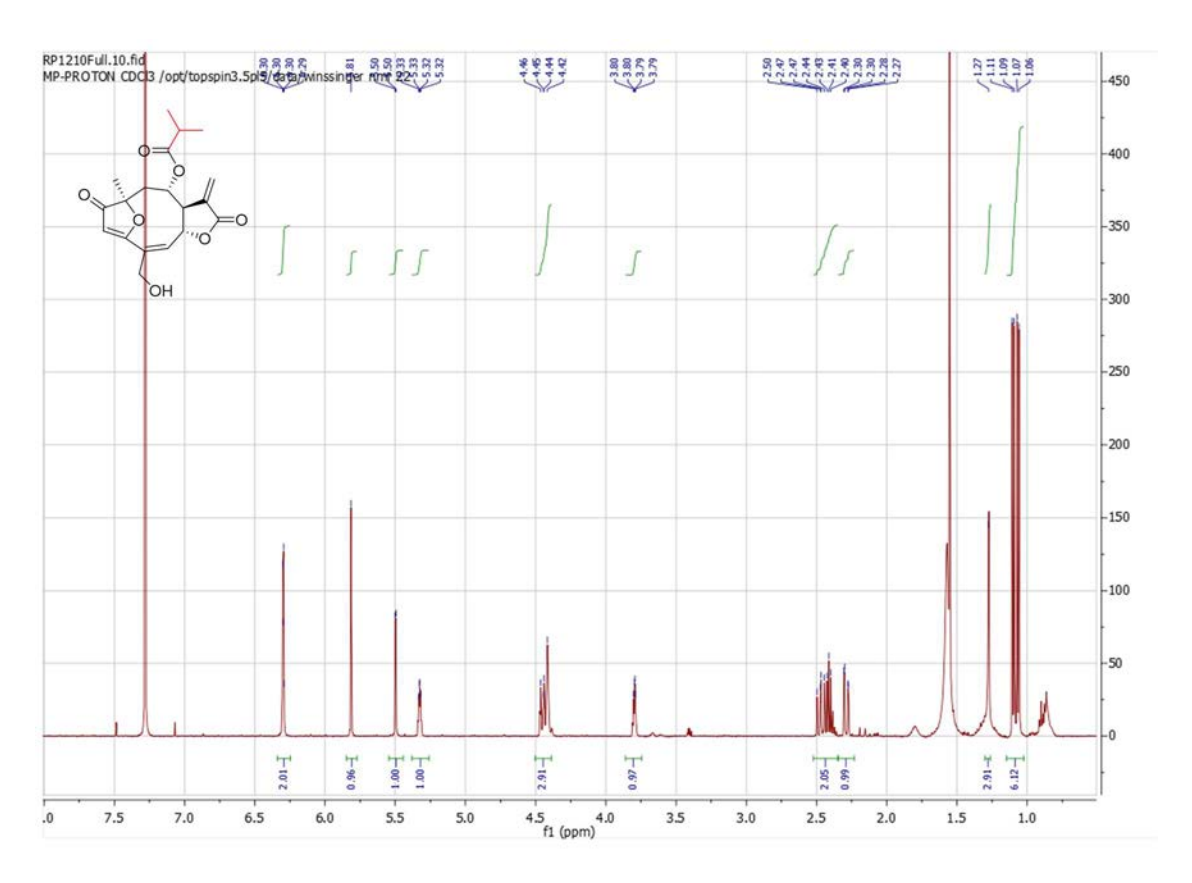


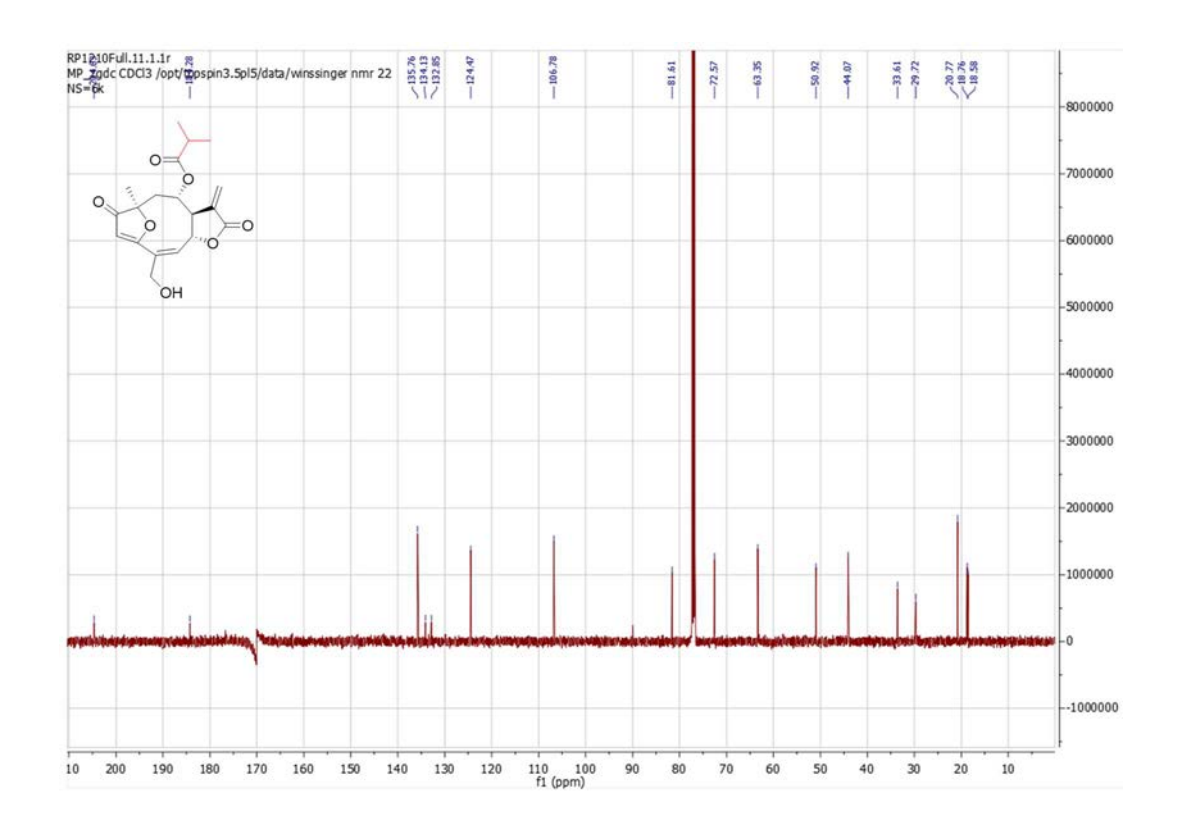


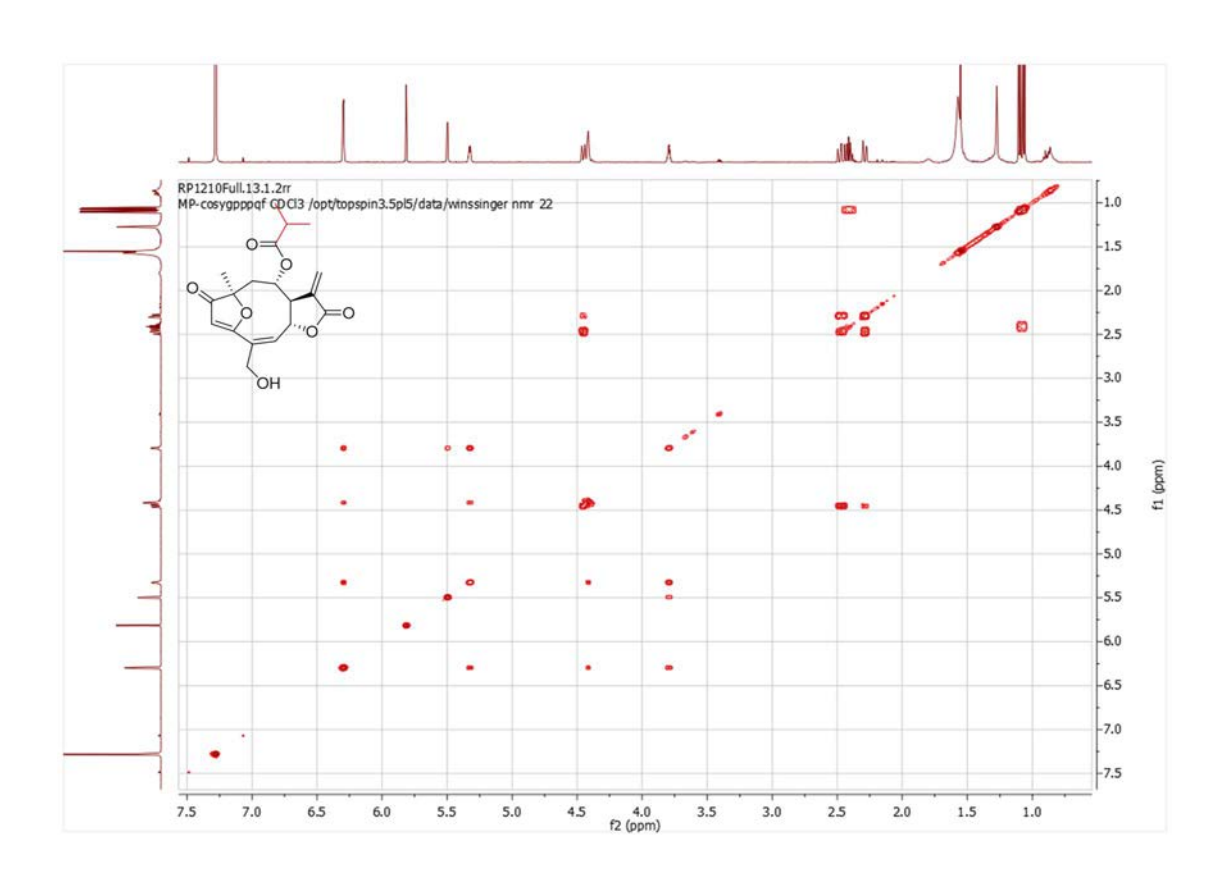


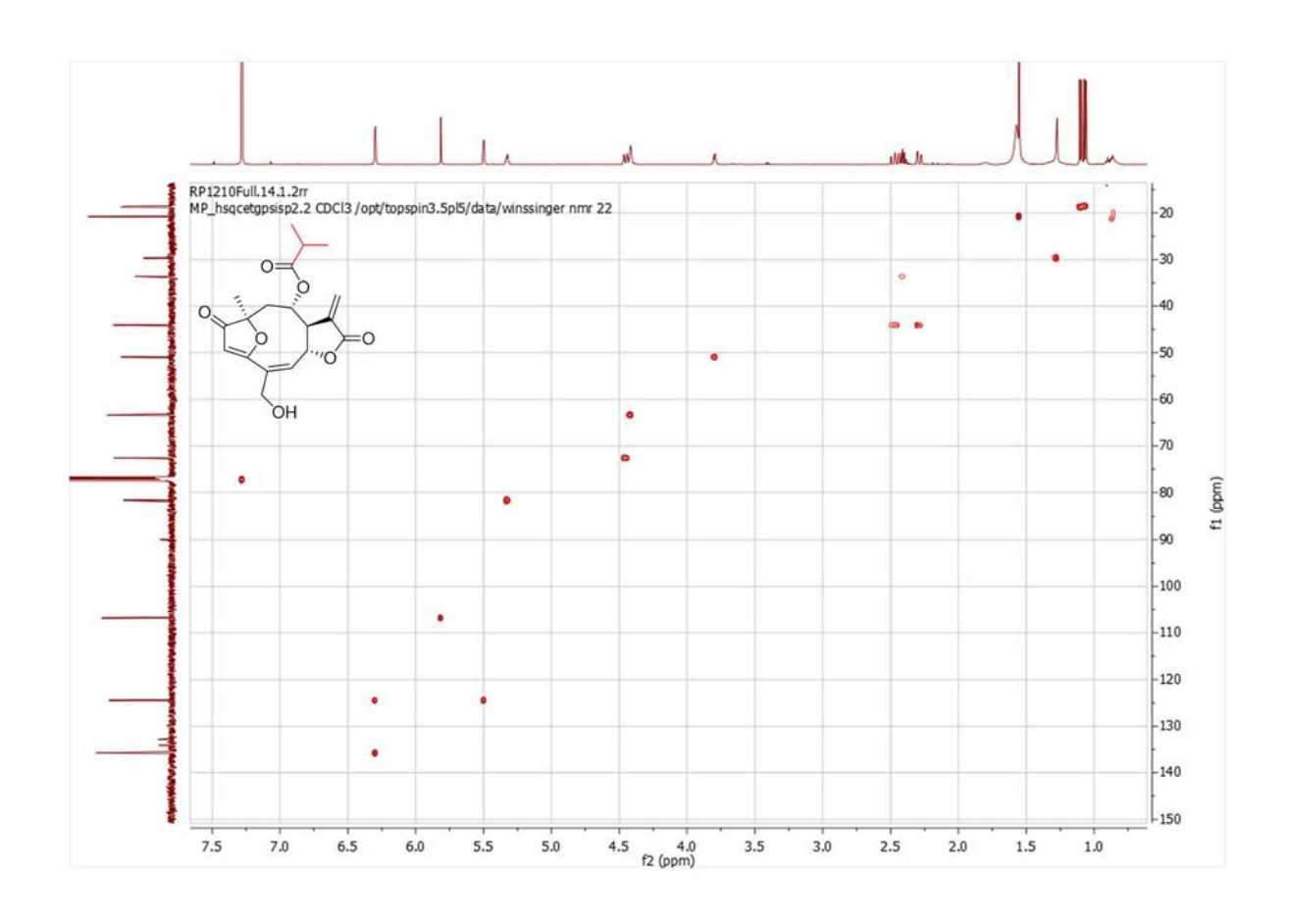


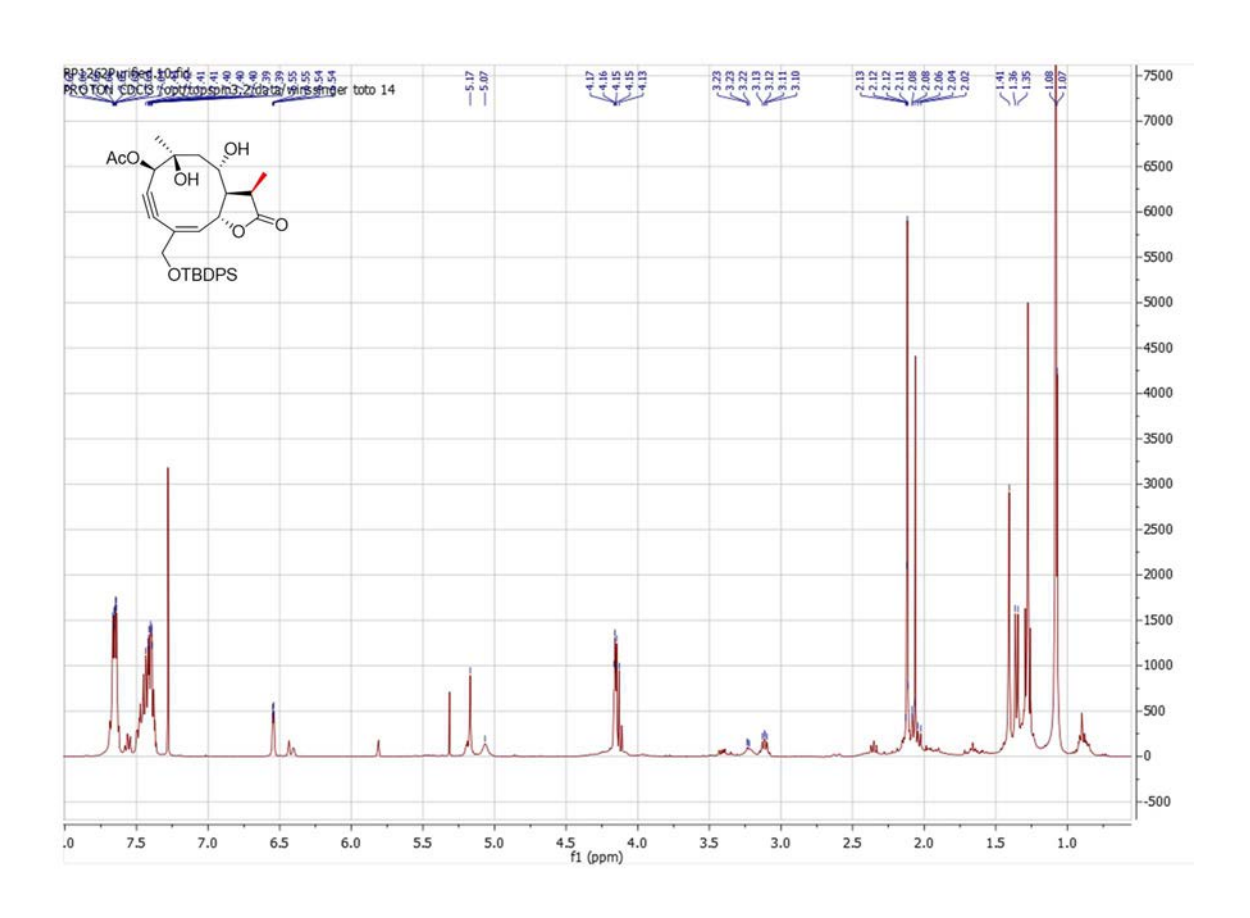


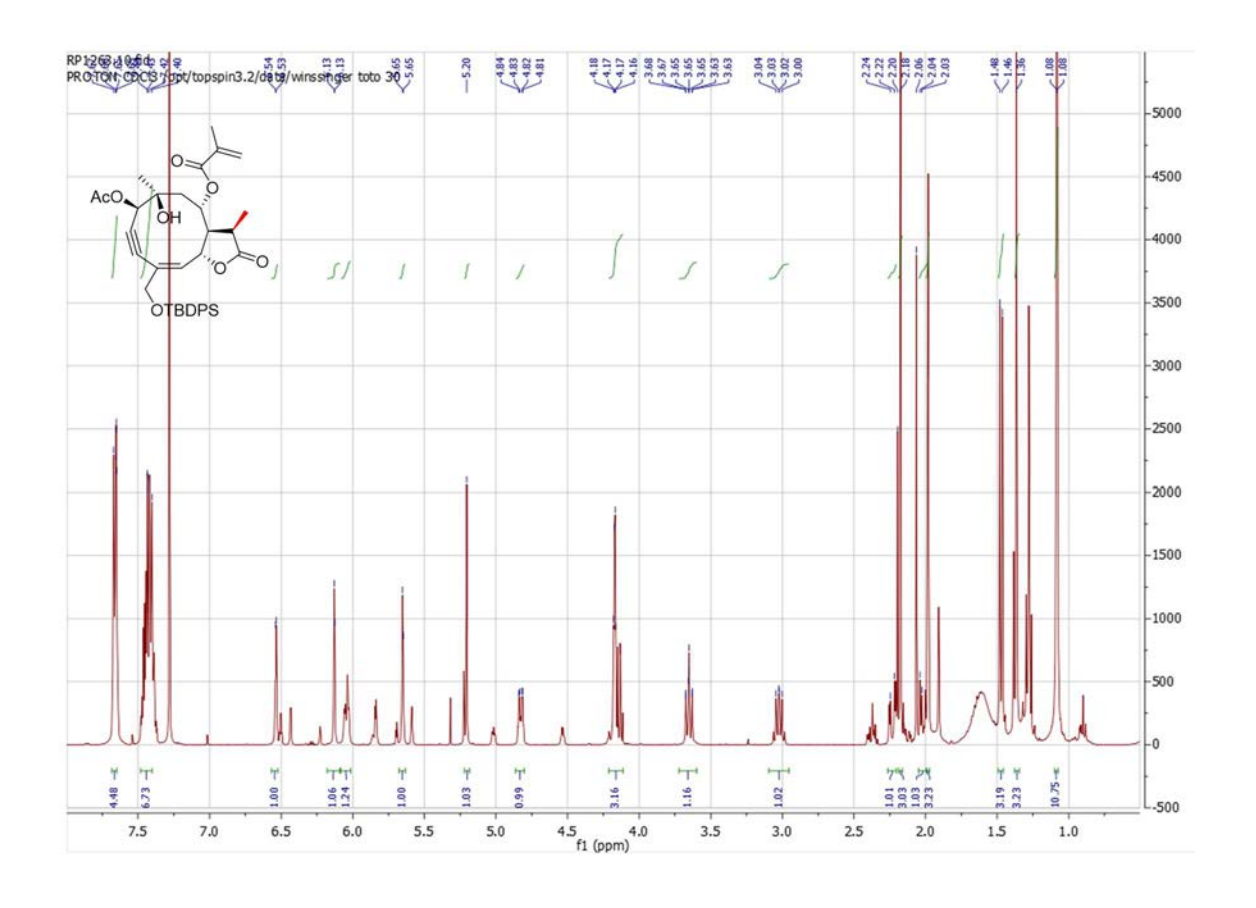


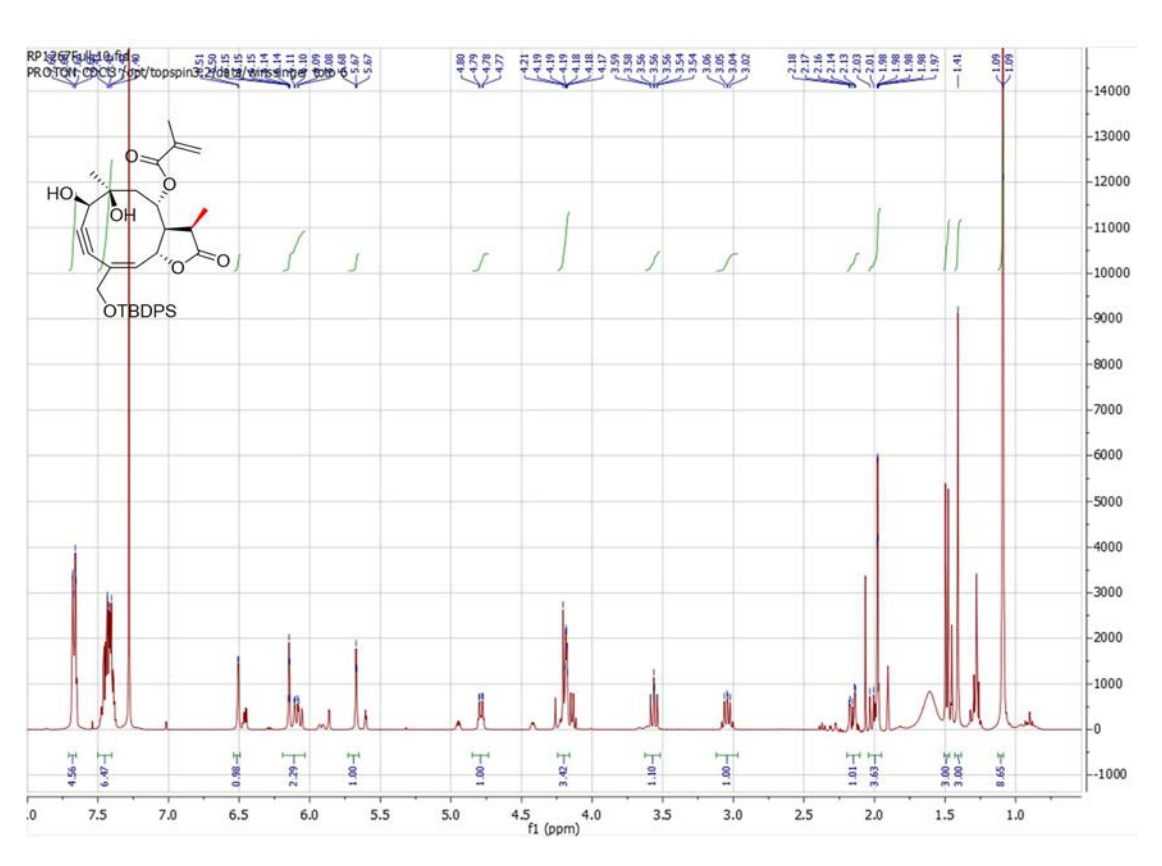


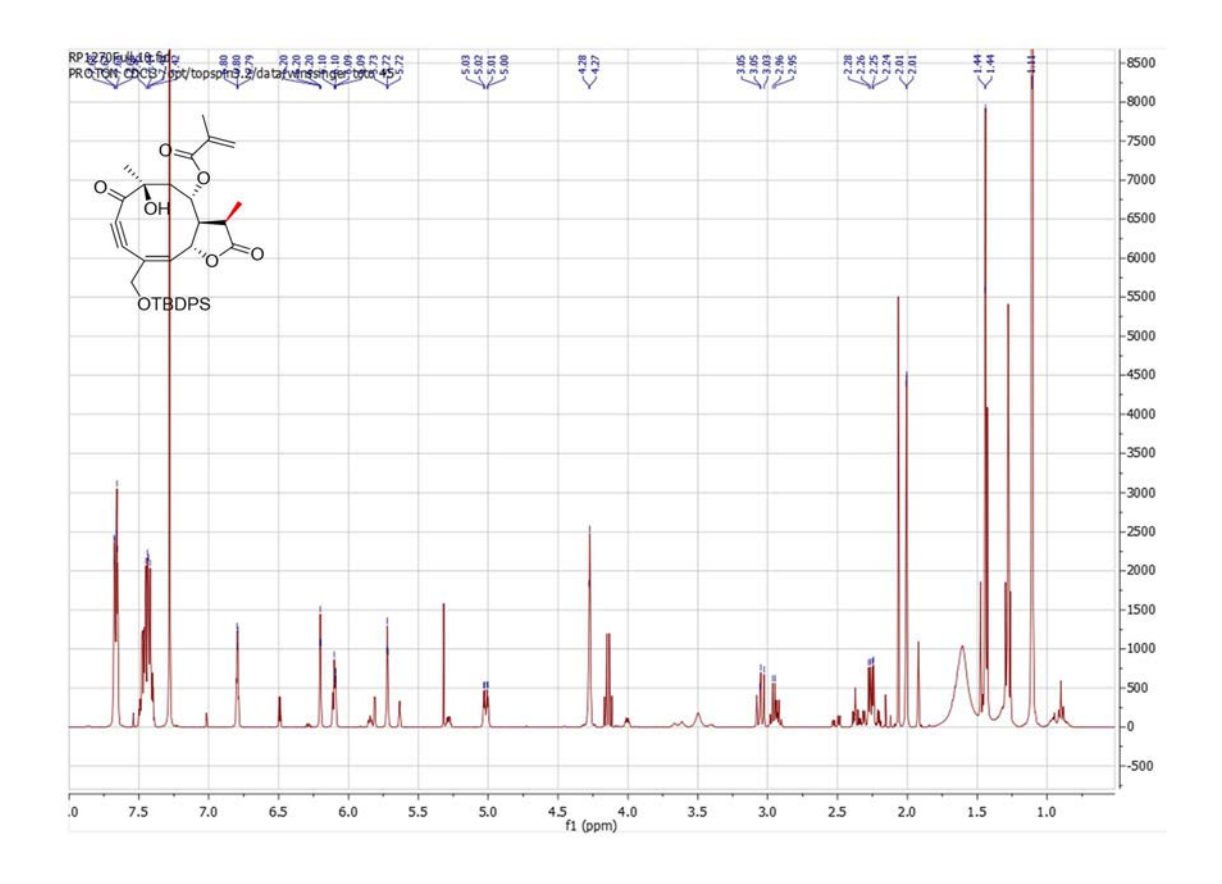


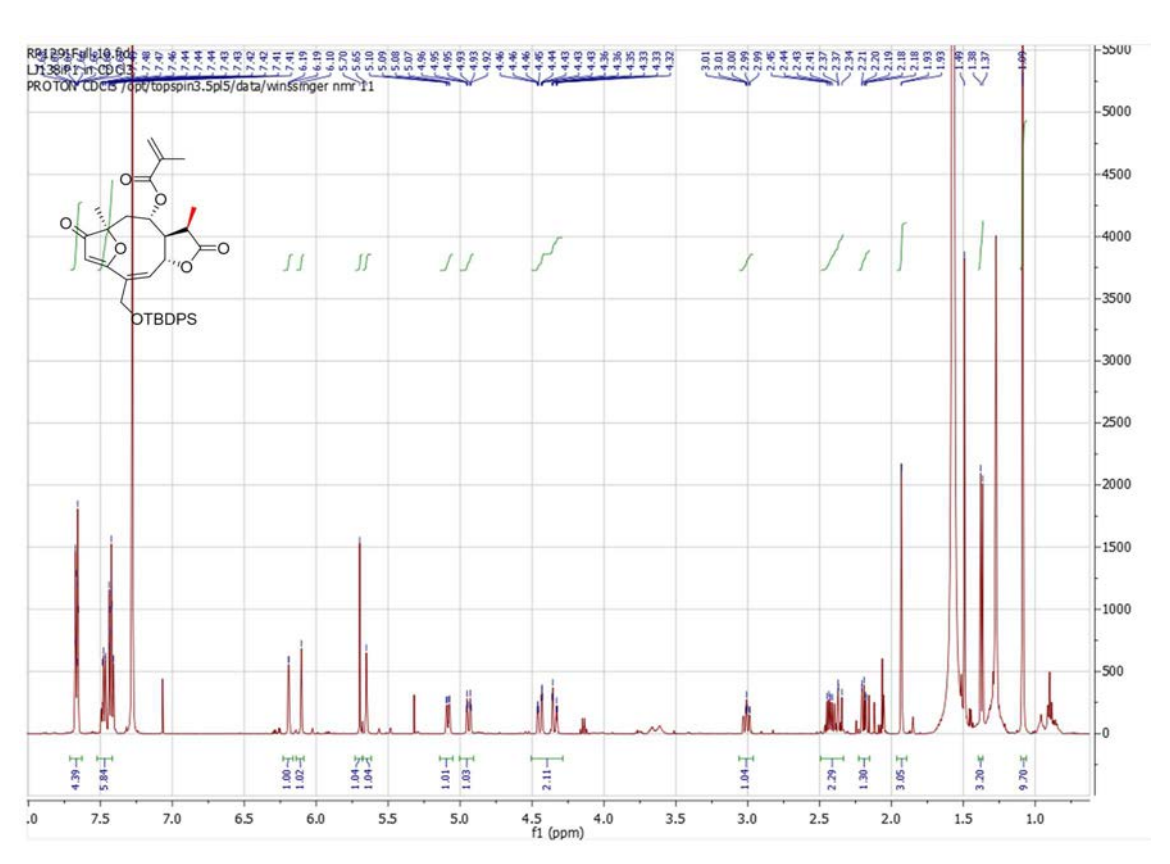


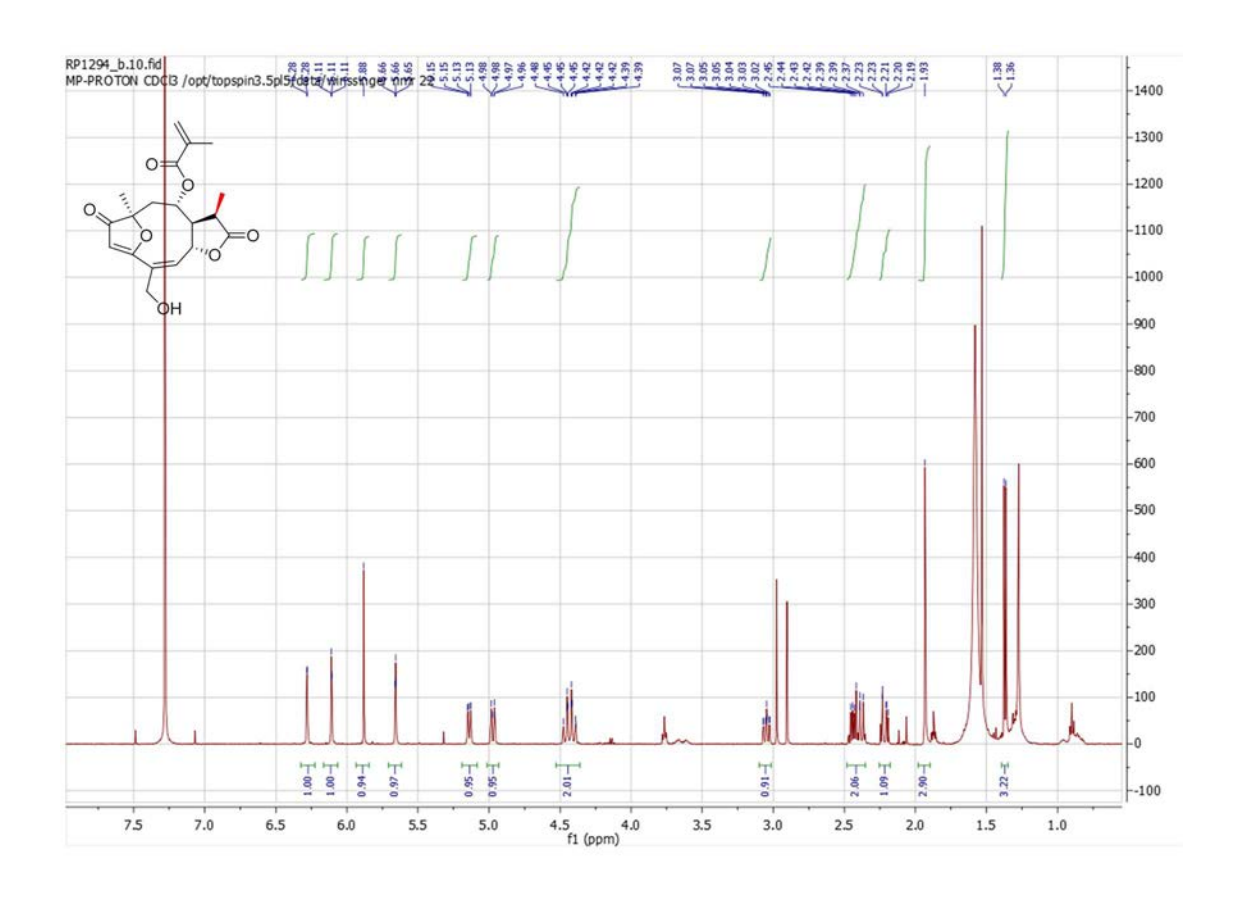


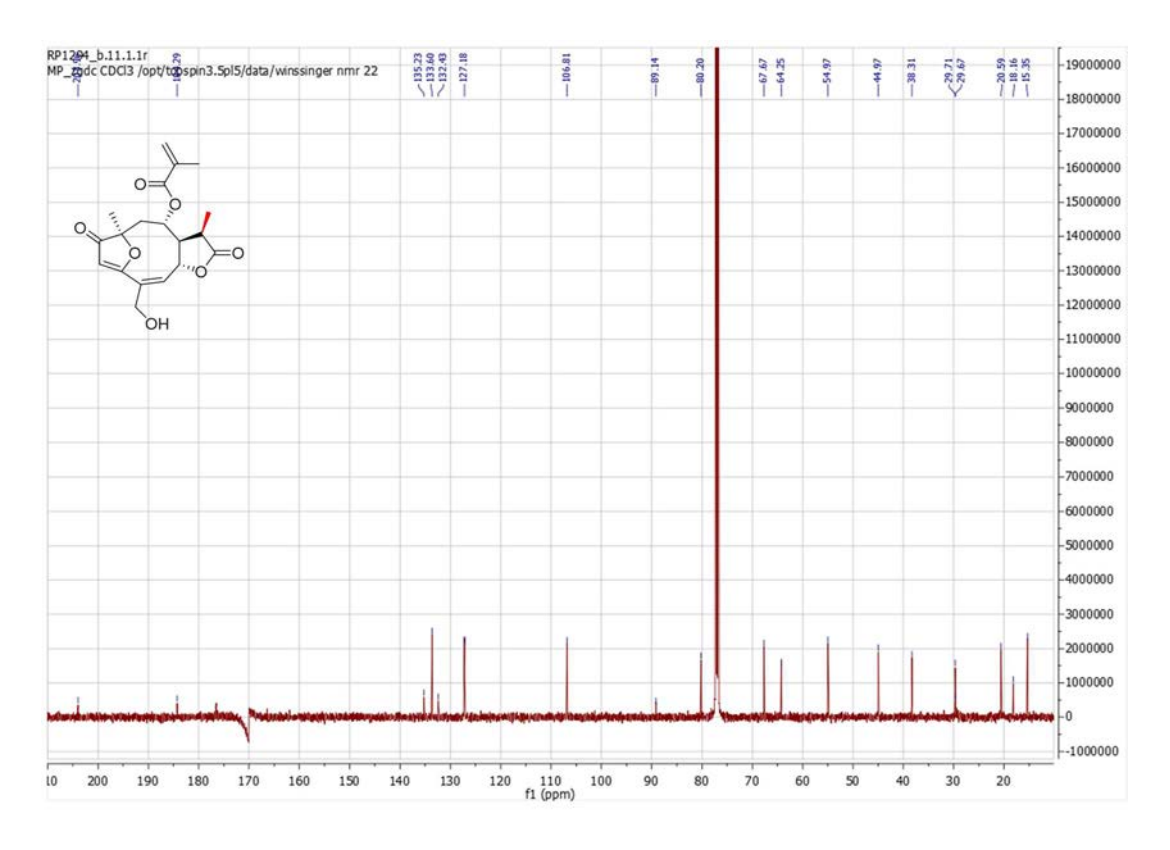


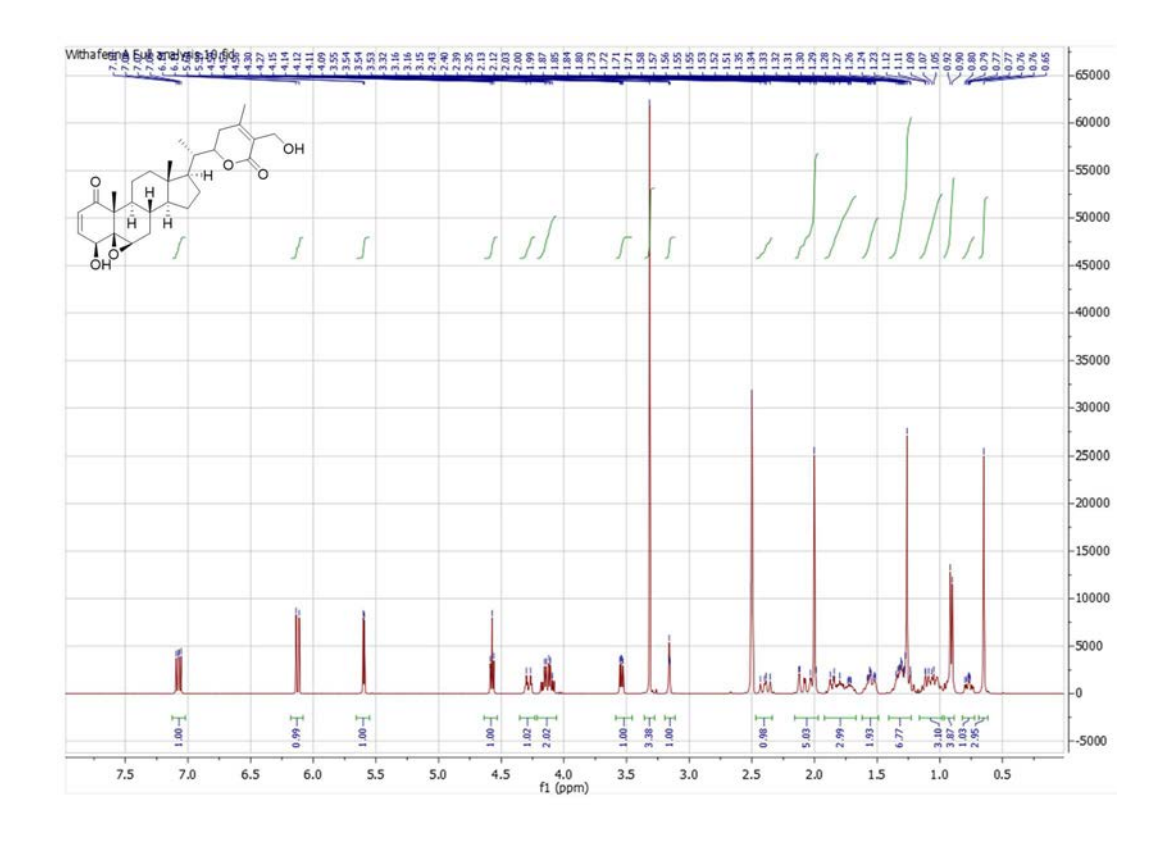


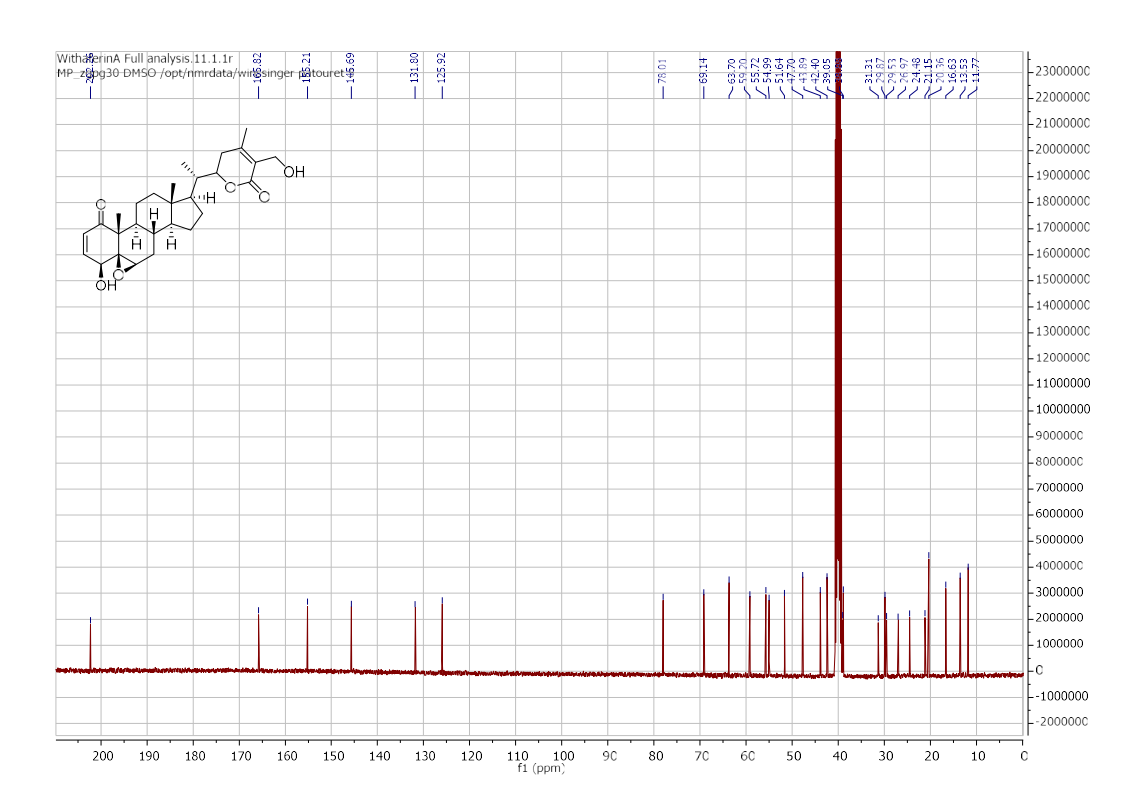


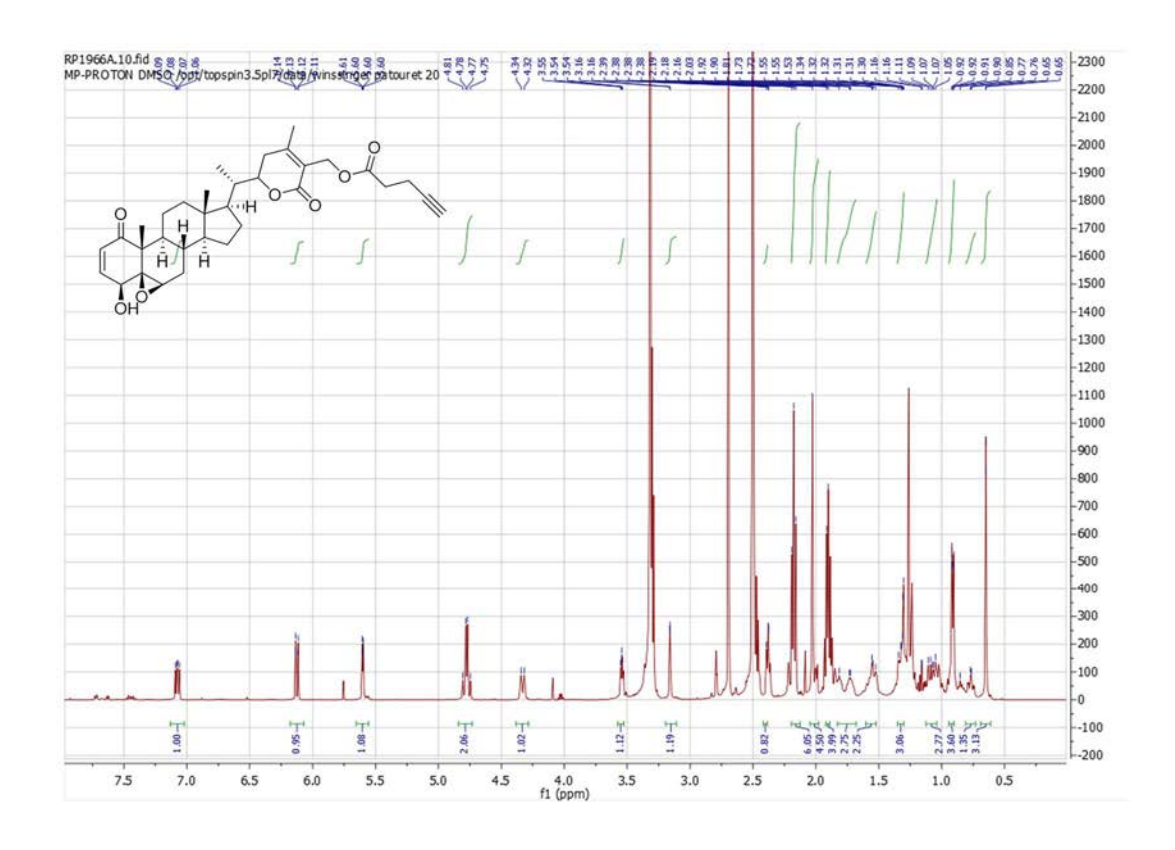


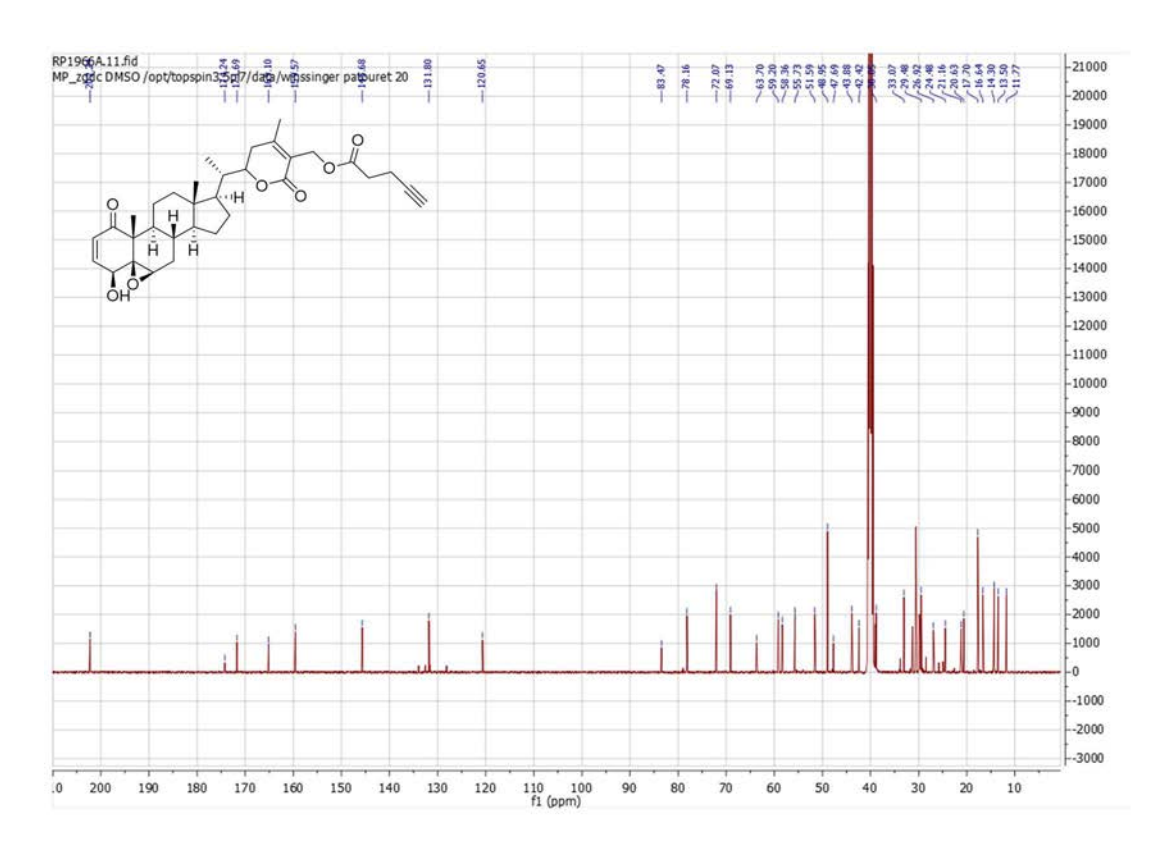


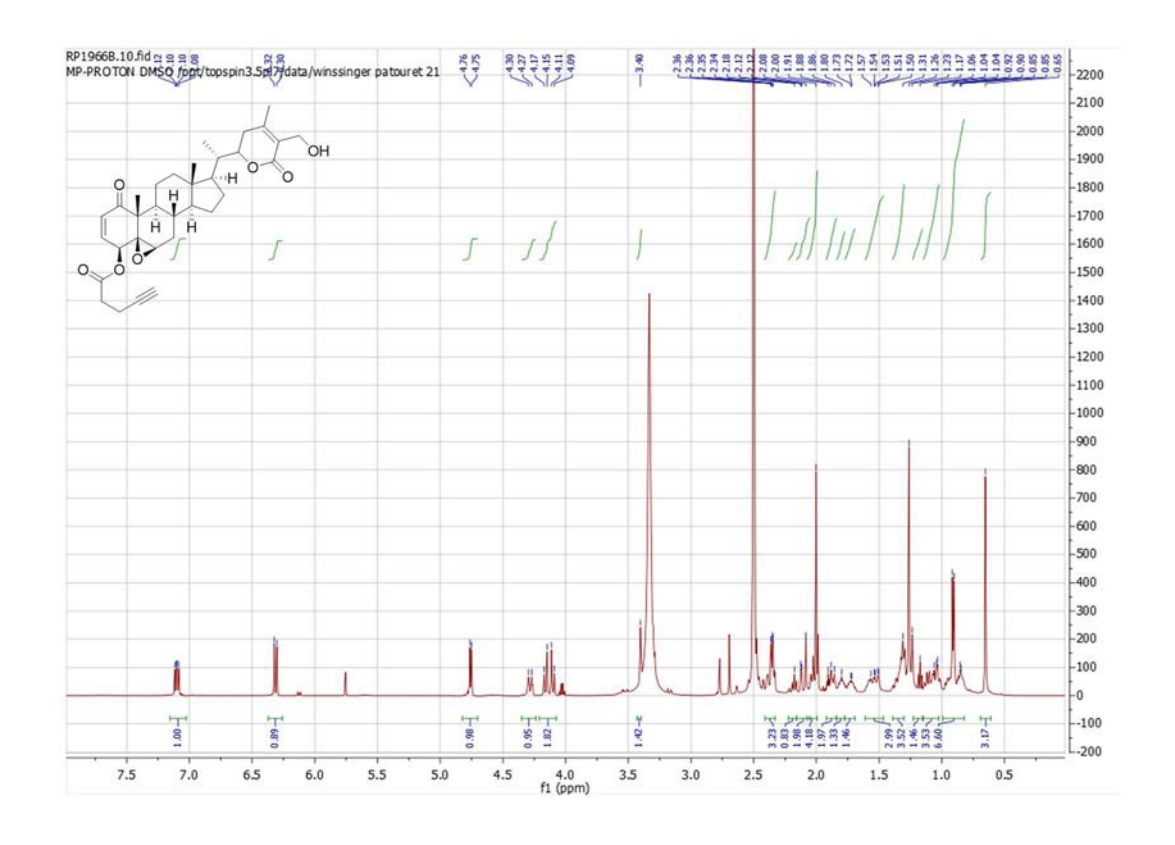


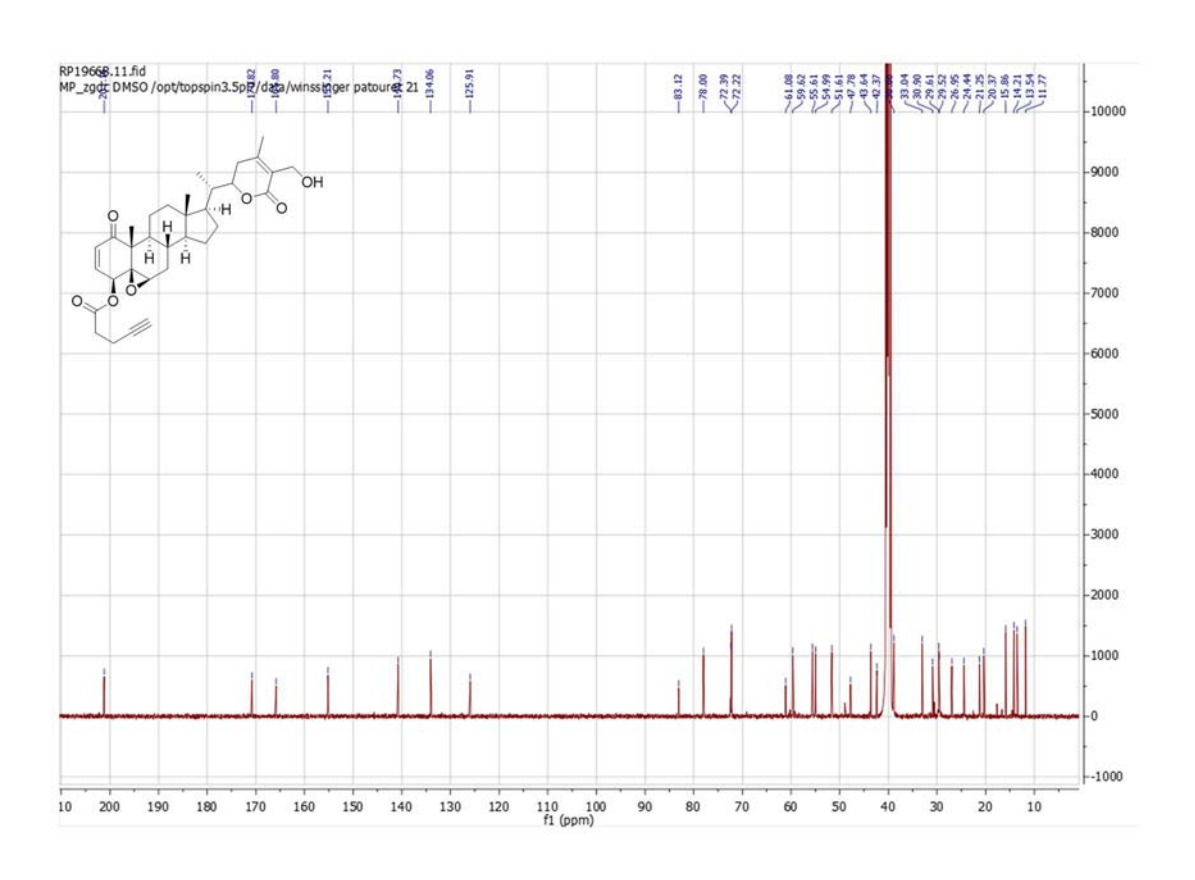


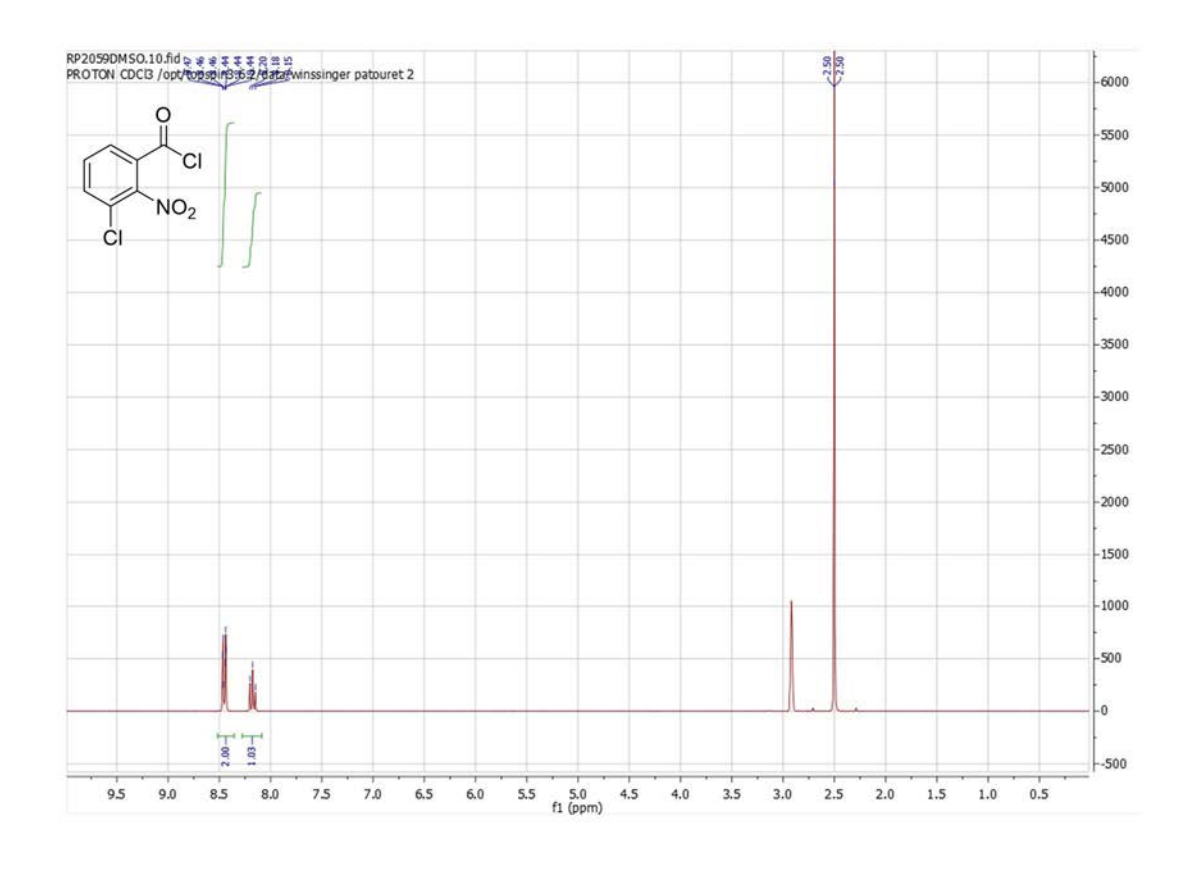


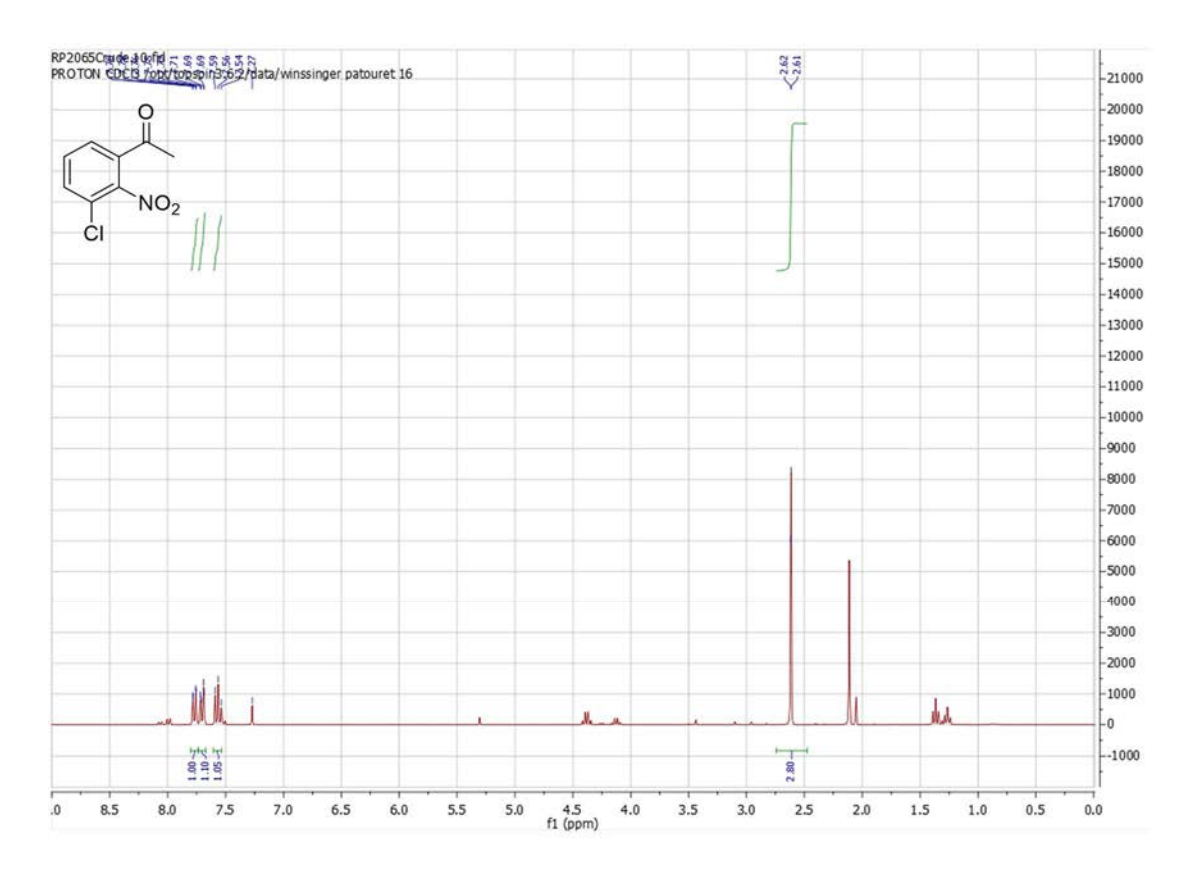


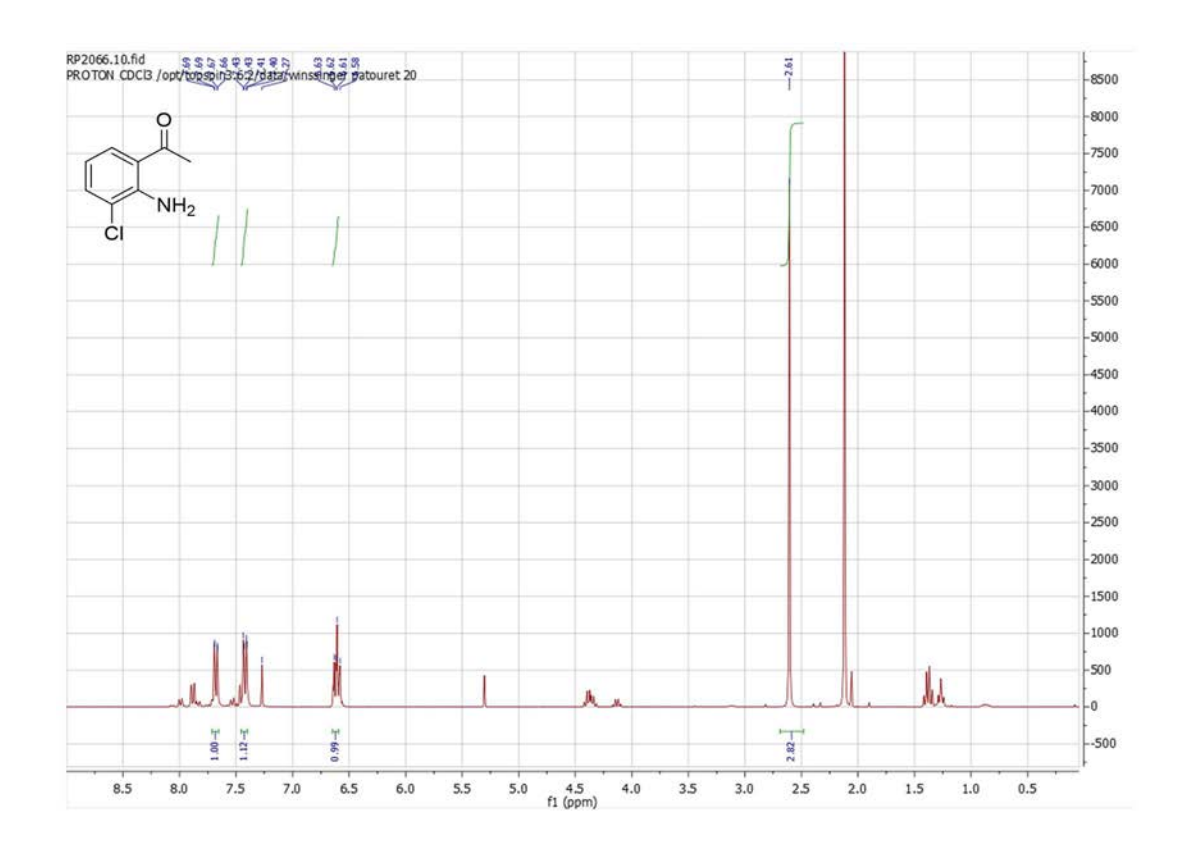


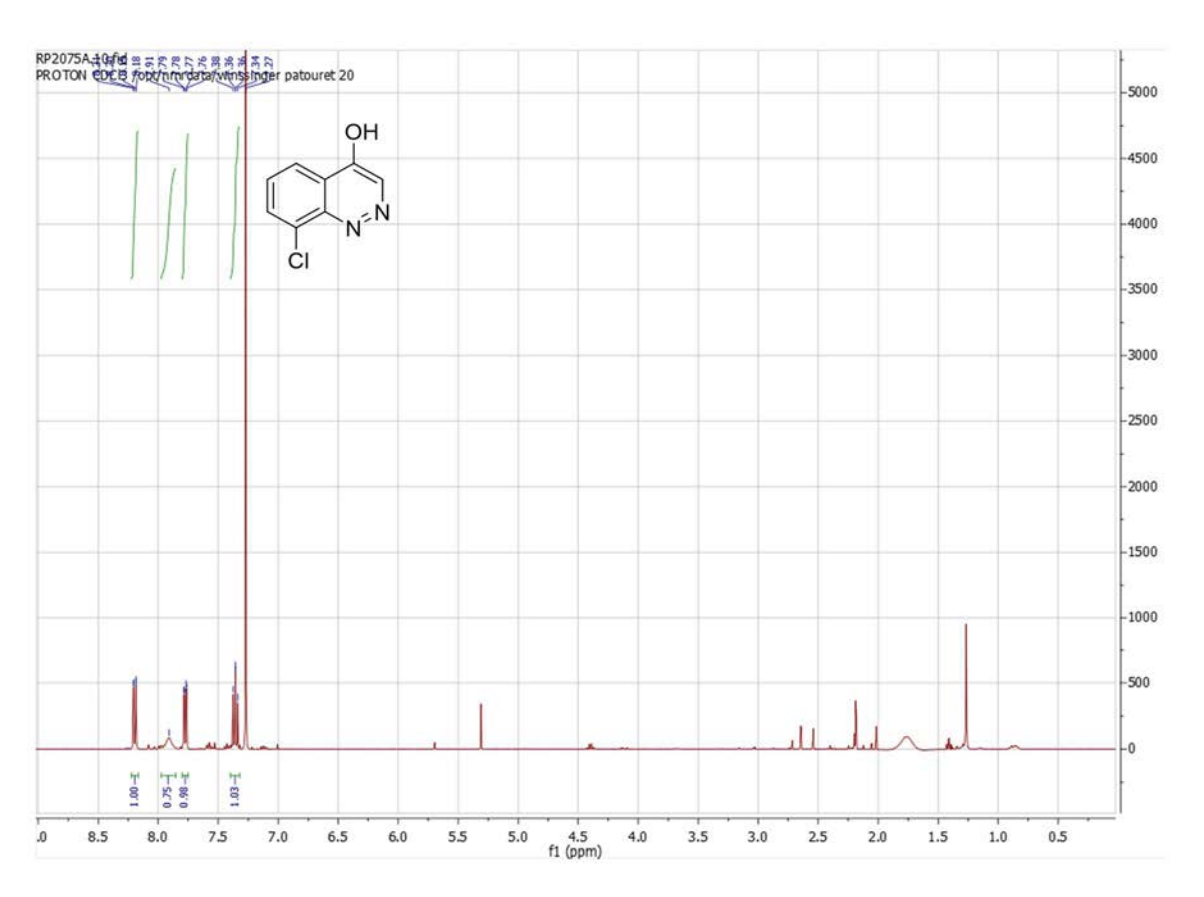


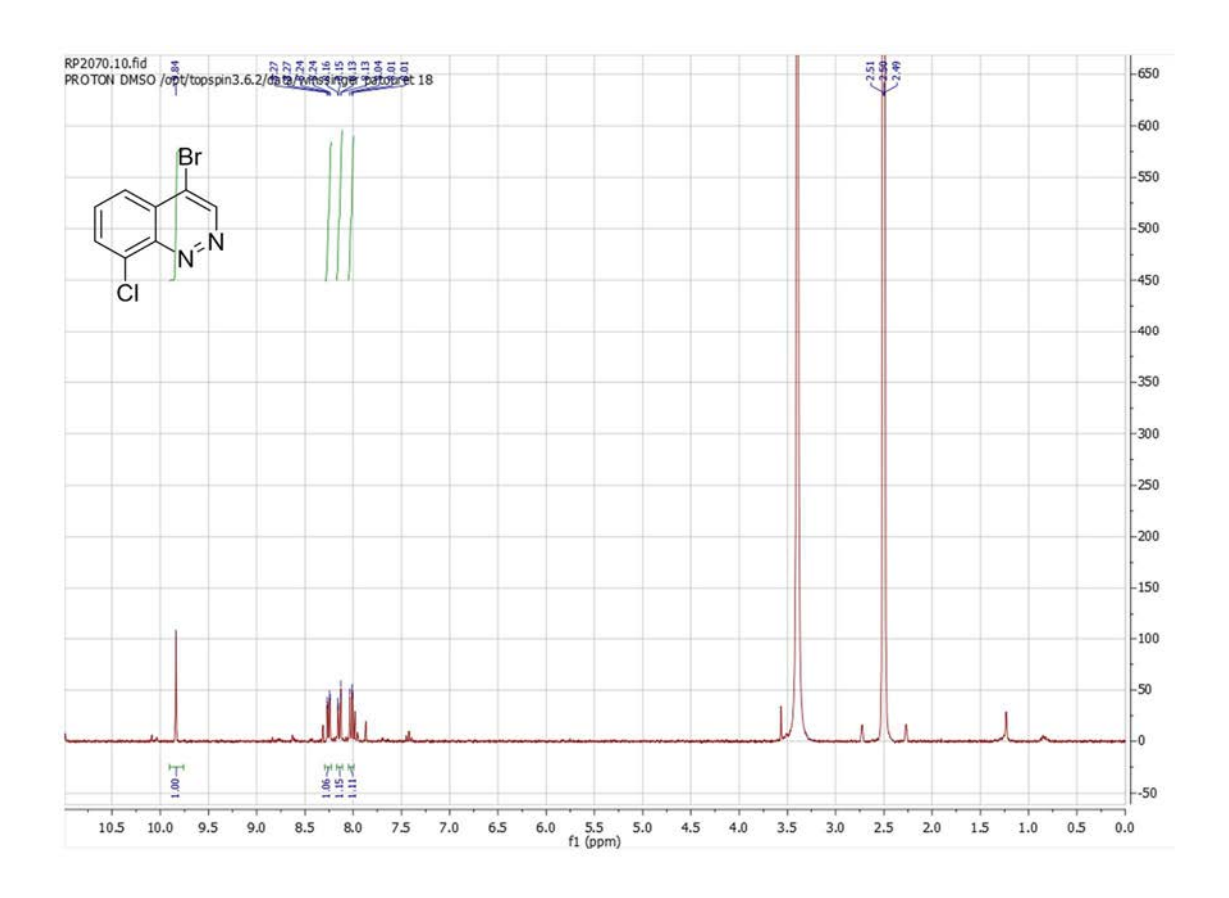


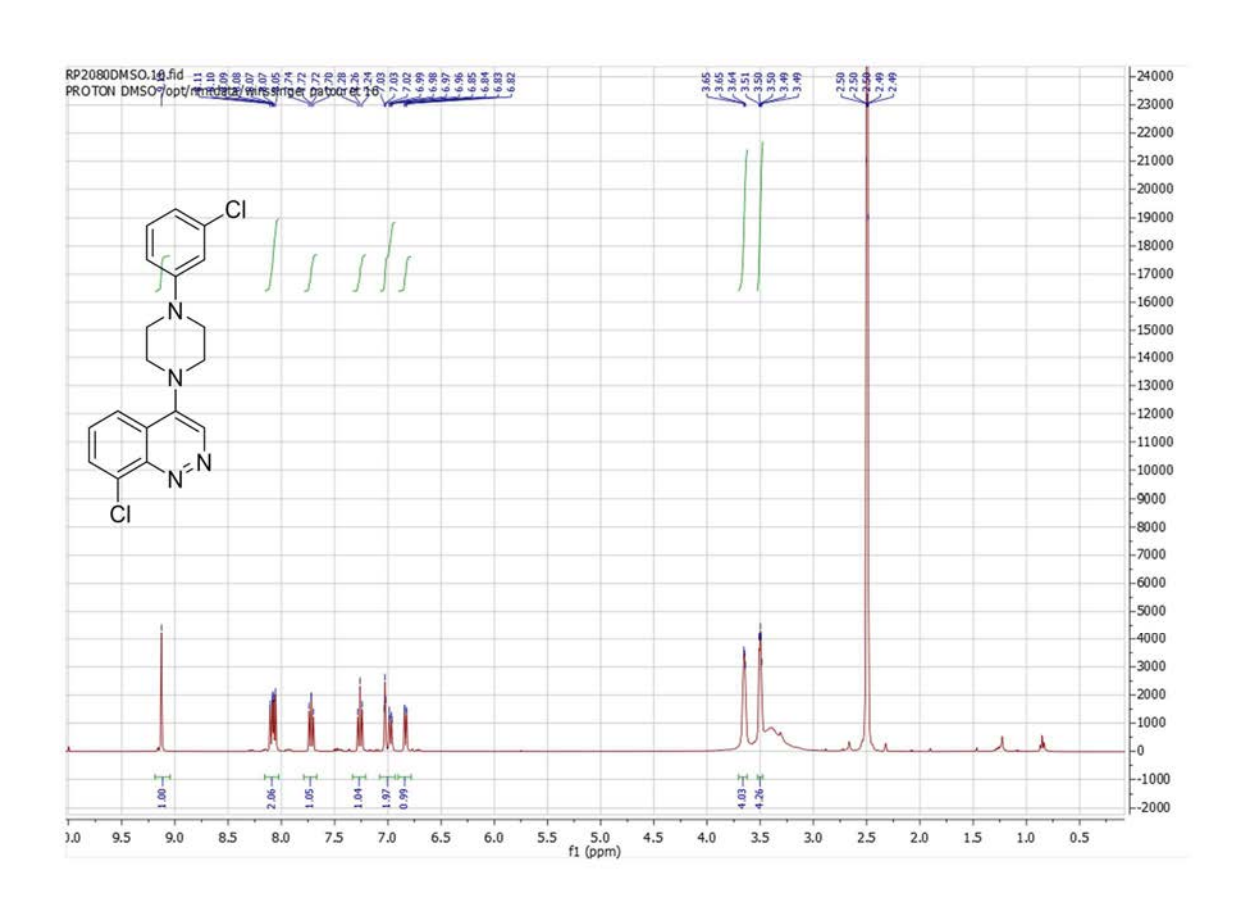


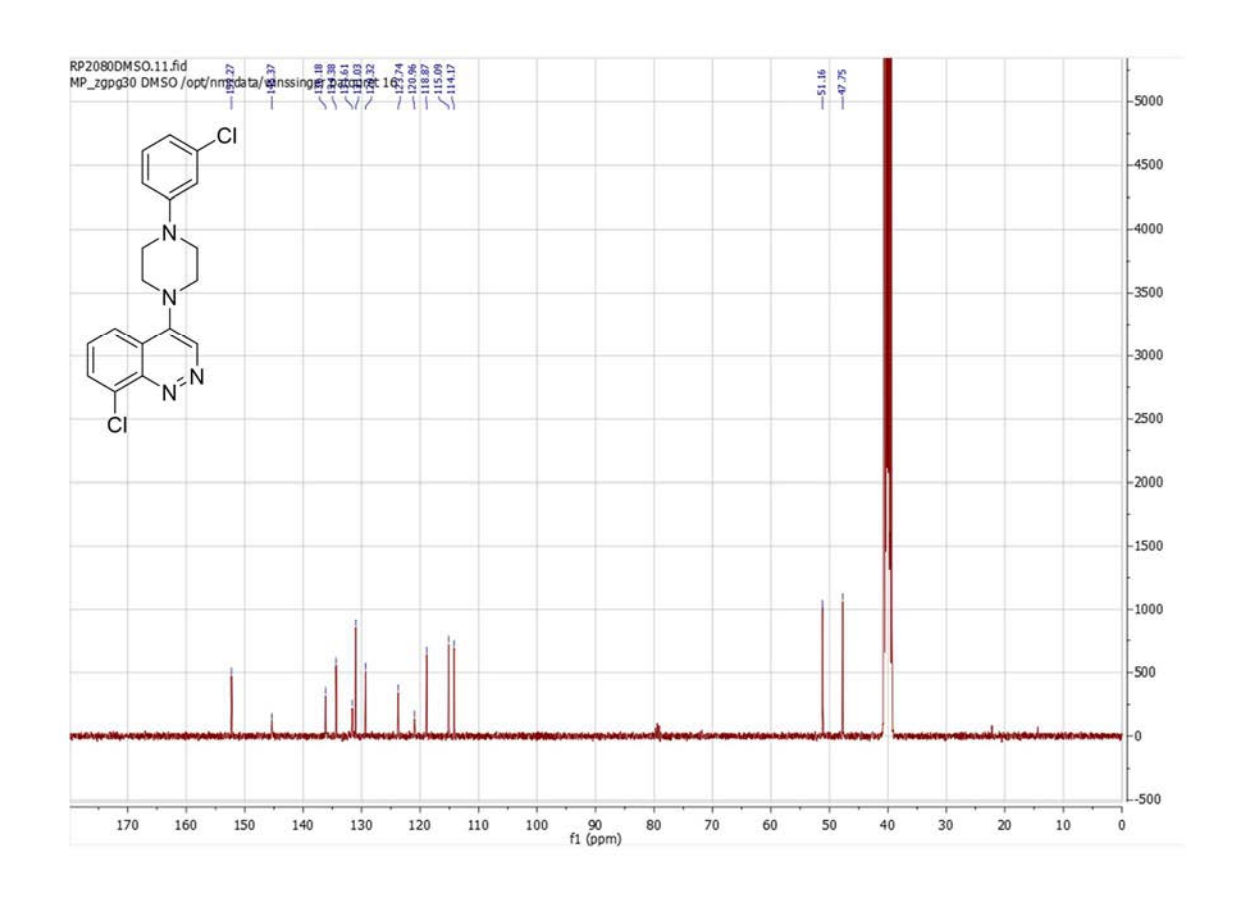












Acknowledgments

I would like to thank Professor Nicolas Winssinger for accepting to host me in his lab in Geneva and allowing me to do a PhD in his group. I had the chance to touch many aspects of chemistry, chemical biology, proteomic and virology. I don't think I would have had this chance anywhere else. I would like to thank all the members past and present of the Winssinger lab, with whom I overlapped over these five years. Thank you for all the moments shared in and out of the lab. Thanks, to those I spent time with Simona, Emma, Jean-Pierre, Bala, Lluc, Mathéo, Pramod, Yev, Heng, Dalu, Mateusz, Miguel, Francesco, Ben, Marcello, Eric, Takuya, Kitae. I want particularly to thank Sofia, without her help and the discussions, this PhD would have been a thousand times more difficult. Thank you Weilong for the amazing work you did in chemistry. Merci Romain pour le super travail en DFT calculations. Thank you Dominic for your help before leaving when I started proteomic. Thanks for the Geneva team (Merck challenge) and congrats to Thomas, Sylvain, Florian, Romain, Kévin, Heng and Elsa; we can be proud to finish in the top 20! Un clin d'œil spécial pour Arthur, Oriane et Milly pour les bons moments du déjeuner ! Un grand merci à Elsa pour avoir rejoint l'équipe et les pauses trop nombreuses mais finalement indispensables! Je me dois de donner une place particulière à Patrick, merci pour ces 5 ans à travailler ensemble avec nos apéros arrosés de superbe vins, charcuteries et fromages! Un grand merci également à Romain Duwald et Kévin Martin qui ont été spécialement présent au bon moment et au bon endroit. Merci encore Kévin, Romain, Pramod et Milly pour m'avoir tant aidé à la rédaction de cette thèse. Merci à Christelle, qui m'a tellement donné, tellement aidé. Merci à Mike, Francky, Fred, Nico, Mumuche, Didie, Yannick d'avoir été toujours là. Mais par-dessus tout, merci à mes parents et à ma sœur (clin d'œil à Ninie !), pour avoir toujours cru en moi, pour m'avoir donné toutes les clefs pour réussir, merci d'avoir fait de moi ce que je suis aujourd'hui.